

NEW EXCAVATIONS OF LATE PLEISTOCENE DEPOSITS AT BONFIRE
SHELTER: A GEOARCHAEOLOGICAL APPROACH TO
DETERMINING THE ORIGINS OF BONE BED 1

by

Sean P. Farrell, B.A.

A thesis submitted to the Graduate Council of
Texas State University in partial fulfillment
of the requirements for the degree of
Master of Arts
with a Major in Anthropology
December 2020

Committee Members:

J. David Kilby, Chair

Stephen L. Black

Charles D. Frederick

COPYRIGHT

by

Sean P. Farrell

2020

FAIR USE AND AUTHOR'S PERMISSION STATEMENT

Fair Use

This work is protected by the Copyright Laws of the United States (Public Law 94-553, section 107). Consistent with fair use as defined in the Copyright Laws, brief quotations from this material are allowed with proper acknowledgment. Use of this material for financial gain without the author's express written permission is not allowed.

Duplication Permission

As the copyright holder of this work I, Sean P. Farrell, authorize duplication of this work, in whole or in part, for educational or scholarly purposes only.

ACKNOWLEDGEMENTS

I would like to take this opportunity to express my sincere thanks to the numerous individuals who have supported this project. When I began this project, I was new to Texas State and the Texas archaeological community. Before classes began, Dr. Steve Black invited me to volunteer at the ASWT's excavations at Eagle Cave and Sayles Adobe, which were nearing completion. This was my first real exposure to the archaeology of the Lower Pecos and I was blown away. Not only by the extraordinary archaeology and exposure to thousands of years of human history, but by the sense of community among the ASWT staff and other volunteers I met over those two weeks. Now, at the completion of this thesis, I feel like a welcomed member of the family. Thank you to Dr. Black, Charles Koenig, Amanda Castaneda, Tori Pagano, and the numerous other volunteers and collaborators for bringing me into the fold.

I would like to thank my advisor, Dr. David Kilby, for inviting me to take on a component of Bonfire Shelter for this thesis. The opportunity to work on such an important site is well beyond what I expected when I was beginning my education at Texas State. I would also like express my gratitude to Dr. Charles Frederick for lending his expertise and hosting me at his laboratory over numerous weekends. His mentorship from the initial conception of this project through its execution and final editing were critical. I also must express my gratefulness to the Skiles family for their ongoing stewardship of Mile Canyon's rich archaeological heritage and incredible hospitality. This thesis, the ongoing work at Bonfire Shelter, and the ASWT's work at Mile Canyon would not have been possible without their support.

A special thank you to the 2017-2018 Bonfire Field Crew, particularly Dr. Marcus Hamilton, Janaka Greene, Ashley Eyeington, John Hedges, Rich McAuliffe, and the Sul Ross field school for your critical support in the field. Thank you to Chris Ringstaff for preparing the experimental lithic assemblage used in this project. Thank you to the TARL staff, particularly MaryBeth Tomka and Lauren Bussiere for your help tracking down records from the Bonfire Shelter collection. Thank you to Dave Robinson and Dan Prykle for sharing your experiences from the 1983-1984 Bonfire expedition and help locating some of the missing maps. Thank you to Brad Jones and Tiffany Osburn at the THC for welcoming me to Texas and introducing me to its extraordinary history. Thank you to my friends and colleagues at SEARCH for encouraging me to earn my Master's Degree and supporting me through the process. In particular, I'd like to thank Dr. Michael Faught for sparking my interest in geoarchaeology and all things Paleoindian.

Finally, I would like to thank my family for supporting my pursuit of archaeology and constant encouragement throughout this project. Thank you Dad, for bringing me along to the lab on weekends and helping me craft overly ambitious science fair projects (and Mom for staying up too late to assemble the posters). A very special thank you to my wife, Megan, for tolerating my caches of dirt all over the apartment, enduring unsolicited training as an archaeologist, and demonstration of extreme patience through the fieldwork, late nights, and long weekends of this project. I couldn't have done this without you.

TABLE OF CONTENTS

	Page
ACKNOWLEDGEMENTS.....	iv
LIST OF TABLES.....	xi
LIST OF FIGURES.....	xiv
ABSTRACT.....	xx
CHAPTER	
1. INTRODUCTION.....	1
1.1 Bonfire Shelter – An Overview.....	1
1.2 Objectives and Justification of Research.....	7
1.2.1 Research Design.....	8
1.2.2 Modeling Expectations.....	10
1.2.3 Minimum Cultural Criteria.....	11
1.2.4 Pre-Clovis Implications.....	13
1.3 Theoretical Framework.....	17
1.4 Thesis Organization.....	21
2. ARCHAEOLOGICAL CONTEXT AND EXCAVATION HISTORY.....	24
2.1 The Museum Phase.....	24
2.2 The Amistad Phase.....	27
2.2.1 Bonfire Shelter and Amistad.....	29
2.2.2 Amistad-Era Stratigraphy.....	32
2.2.3 Amistad Chronology.....	34
2.2.4 A Sign of the Times.....	37
2.3 The University Phase.....	41
2.3.1 The University Phase at Bonfire Shelter.....	42
2.3.2 Results of the University Phase.....	48
2.4 21 st Century Revival.....	50
2.4.1 Prewitt’s Stabilization.....	51

2.4.2	Southern Methodist University	52
2.4.3	The Ancient Southwest Texas Project	55
2.4.4	ASWT and Bonfire Shelter	56
3.	ENVIRONMENTAL CONTEXT	59
3.1	Lower Pecos Canyonlands	59
3.2	Mile Canyon	59
3.3	Climate	61
3.4	Flora	61
3.5	Geology	63
3.6	Fauna	65
3.7	Soils	66
3.8	Flooding and Implications for Archaeological Sites	68
3.8.1	Modern Flooding	69
3.9	Pleistocene Landscape	71
3.9.1	Archaeological Traces of the Pleistocene	73
3.9.2	Friesenhahn Cave	76
4.	ROCKSHELTER FORMATION PROCESSES	80
4.1	How Rockshelters Form	81
4.1.1	Physical Formation Processes	83
4.1.2	Chemical Formation Processes	84
4.1.3	Collapse	87
4.2	Sedimentation	88
4.2.1	Endogenic Sediments	89
4.2.2	Exogenic Sediments	91
4.3	Post-Depositional Modification	96
4.3.1	Cryoturbation	96
4.3.2	Bioturbation	97
4.3.3	Anthroturbation	99
5.	METHODOLOGY	102
5.1	Field Methods	103

5.1.1	Data Recordation	104
5.1.2	Excavation Methods	109
5.1.3	Sampling	113
5.2	Microartifact Methodology	116
5.2.1	Microartifact Background.....	118
5.2.2	Microartifacts at Early Paleoindian Sites.....	121
5.2.3	Criteria for Microartifact Identification.....	122
5.2.4	Field Collection	124
5.2.5	Sample Reduction/Preparation	125
5.2.6	Laboratory Analysis.....	125
5.3	Comparative Sample	126
5.3.1	Edwards Chert Fluorescence	129
5.4	Geoarchaeological Methods.....	131
5.4.1	Geoarchaeological Background and Justification.....	131
5.4.2	Geoarchaeological Sample Preparation	137
5.4.3	Particle Size	138
5.4.4	Carbon Content.....	150
5.4.5	Organic Carbon Content and Stable Isotopic Composition.....	157
5.4.6	X-Ray Diffraction.....	163
5.4.7	Magnetic Susceptibility	168
6.	INTERPRETIVE FRAMEWORK: CLASSIFYING BONE BED 1:.....	173
6.1	Geological Circumstances.....	175
6.2	Ecological Causes	176
6.3	The Elephant in the Shelter.....	178
6.4	Carnivore Activity.....	180
6.5	Human Activity.....	182
6.6	Considerations for Bone Bed 1	187
7.	EXCAVATION RESULTS	189
7.1	Block C Results.....	193
7.1.1	Unit C – Stratum 23.....	194
7.1.2	Unit C – Stratum 24.....	197

7.2	Column Sample 5 (PS06.CS05).....	198
7.3	Block D Results	204
7.4	Faunal Remains.....	211
7.4.1	Faunal Remains – Stratum 23.....	212
7.4.2	Faunal Remains – Stratum 24.....	220
7.4.3	Faunal Remains – 1963-1964	237
7.5	Dating Stratum 24	240
8.	GEOARCHAEOLOGICAL RESULTS.....	248
8.1	Overview.....	250
8.2	Particle Size	255
8.2.1	Coarse Fraction Distribution.....	255
8.2.2	Fine Fraction Distribution.....	256
8.2.3	Distributional Modes	259
8.3	Carbon Content	261
8.4	Gypsum Determination.....	263
8.4.1	Gypsum Sources	265
8.5	Organic Carbon.....	267
8.6	$\delta^{13}\text{C}$ Stable Isotopes	269
8.7	X-Ray Diffraction Mineralogy.....	271
8.7.1	Limestone Control Sample	274
8.8	Magnetic Susceptibility.....	278
8.8.1	Mass Susceptibility	278
8.8.2	Frequency Dependent Susceptibility	279
8.9	Stratigraphic Details.....	283
8.9.1	Stratum 24.....	283
8.9.2	Stratum 23.....	286
8.9.3	Stratum 22.....	288
8.9.4	Stratum 21.....	292
8.9.5	Stratum 20.....	294
8.9.6	Stratum 19.....	298
8.10	Microartifact	303

8.10.1	Limestone	309
8.10.2	Faunal Remains – Bone	310
8.10.3	Faunal Remains – Shell	312
8.10.4	Fossil Shell.....	314
8.10.5	Possible Chert Fragments	315
8.10.6	Quartz Crystal	317
8.10.7	Rounded Gravel.....	318
8.10.8	Gypsum Crystal	319
8.10.9	Gypsum Concretion	321
8.10.10	Botanical Material	322
9.	DISCUSSION & CONCLUSION.....	325
9.1	Stratigraphic Classification	326
9.2	Stratigraphic Narrative	327
9.2.1	Stratum 24.....	327
9.2.2	Stratum 23.....	329
9.2.3	Stratum 22.....	333
9.2.4	Strata 21 & 20.....	335
9.2.5	Stratum 19.....	337
9.3	Post-Mortem	339
9.3.1	Future Research	343
9.3.2	Lessons Learned	345
	APPENDIX SECTION	348
	WORKS CITED	376

LIST OF TABLES

Table	Page
1-1. Select earlier than Clovis-age sites that satisfy one or more of the minimum criteria for consideration for a bona fide human occupation.	17
2-1. Summary of Relevant Museum Phase Studies	26
2-2. 1963-1964 Bonfire Shelter Radiocarbon Dates	35
2-3. Cultural Chronology of the Lower Pecos.	50
3-1. Modern flora of Mile Canyon.....	62
5-1. Microdebitage Attributes, After Fladmark (1982).....	124
5-2. Geoarchaeological sample Field Numbers and Lab Identifiers.....	138
5-3. Geoarchaeological Subsamples	138
5-4. Wentworth Phi Classifications	140
5-5. Hydrometer sampling regimen and equivalent phi values.....	143
5-6. Sorting Classification Scheme after Folk (1980).....	147
5-7. Skewness Classification Scheme after Folk (1980).....	148
5-8. Kurtosis Classification Scheme after Folk and Ward (1957:15)	149
5-9. Bone Bed 1, Bonfire Shelter - XRD Mineral Components	165
6-1. Simplified model explaining the origins of faunal material identified in Bone Bed 1 at Bonfire Shelter	174
7-1. 41VV218 – Main Trench Stratigraphic Alignment.....	192
7-2. Unit Layers and associated Lot FNs for each Block C and Block D excavation Unit	193
7-3. Vertical extent of stratigraphic units documented in CS05	200
7-4. 2017 – 2018 Excavation Results – Stratigraphic Field Descriptions derived from Column Sample 5 (PS06.CS05).....	201

7-5. Summary of faunal remains recovered from each Stratum 23 (E/F/G) provenience	218
7-6. Minimum number of individuals represented in Stratum 23 for each identified taxa	220
7-7. Summary of faunal remains recovered from each Stratum 24 (H) provenience	232
7-8. Minimum number of individuals represented in Stratum 23 for each identified taxa.	234
7-9. Provenience and results for three viable radiocarbon dates recovered from Bone Bed 1.....	243
8-1. Timing of Late Pleistocene interstadials and their correlation to relevant Bonfire Shelter radiocarbon dates.....	252
8-2. Calculated particle size analysis results of <2mm sediment fraction	257
8-3. Modes visually estimated from parabolic distribution peaks in particle size histograms.....	260
8-4. Compiled results of carbon content determinations calculated using differential weight loss methods (LOI), volumetric calcimeter (Chittick), X-ray diffraction - calcite content, and KEPSIL Elemental Analyzer	262
8-5. Comparison of XRD and Differential Weight Loss methods for gypsum determination in Column Sample 5 strata	264
8-6. Comparison of Column Sample 5 organic carbon content as determined vis loss on ignition and KEPSIL Elemental Analyser	267
8-7. Tabularized Column Sample 5 Stable Isotope Ratios	269
8-8. Column Sample 5 sediment mineralogy by stratum, as determined by XRD	273
8-9. Column Sample 5 clay fraction (<4µm) mineralogy as a percentage of total sediment sample mass.....	274
8-10. Limestone and HCl insoluble residual mineralogy.....	276
8-11. Proportion of Endogenic vs. Exogenic <2 mm sediments assuming all calcite, illite/mica, kaolinite, hematite, and 1% of all quartz quartz are derived from limestone parent material	277

8-12. Column Sample 5 Mass Specific Magnetic Susceptibilities and Coefficient of Frequency Dependency.....	281
8-13. Microartifact (1-2mm Fraction) Processing Results.....	306
8-14. Column Sample 5 - Qualitative Microartifact Mircroartifact Results	307
8-15. Summary of rounded gravel recovered from Bone Bed 1 strata.	307
9-1. PS06.CS05 - Bone Bed 1 - Final Classification based on 2017-2018 site data.....	326
A-1. LS001 (S19) Particle Size Distribution: Cumulative Curve Data Tabulation	348
A-2. LS002 (S20) Particle Size Distribution: Cumulative Curve Data Tabulation	350
A-3. LS003 (S21) Particle Size Distribution: Cumulative Curve Data Tabulation	352
A-4. LS004 (S22) Particle Size Distribution: Cumulative Curve Data Tabulation	354
A-5. LS005 (S23) Particle Size Distribution: Cumulative Curve Data Tabulation	356
A-6. LS006 (S24) Particle Size Distribution: Cumulative Curve Data Tabulation	358
B-1. Bone Bed 1: Qualitative Microartifact Results	360
C-1. 1963-1964 Bone Bed 1 Faunal Assemblage - Reconstructed from TARL Records.....	363
C-2. 1983-1984 Faunal Assemblage - Reconstructed from TARL Records and Bement (1986)	366
C-3. 2017-2018 Bonfire Shelter Assemblage - Bone Bed 1	372

LIST OF FIGURES

Figure	Page
1-1. Geographic context of Bonfire Shelter and the Lower Pecos.....	2
1-2. Bonfire Shelter Site Overview and Previous Investigations.....	4
2-1. The 1963-1964 Bonfire Expedition Crew	31
2-2. 1963-1964 illustration of main north-south profile (W50) at Bonfire Shelter extending from the north face of the talus cone to the middle of the shelter.....	36
2-3. 1963-1964 planview exposure of Bone Bed 2 (Units N50 W50 and N50 W60) illustrating the relationship between the large limestone blocks and disarticulated bison remains	39
2-4. 1963-1964 Bone Bed 3 excavation (Unit N80 W42, b) and profile (Unit N50 W70, a) illustrating the repeated pattern of large limestone blocks among disarticulated faunal remains within cultural strata.....	40
2-5. Bement's 1983-1984 profile of record	45
3-1. Geological Map of Langtry Texas illustrating exposed bedrock units in vicinity of Mile Canyon	65
3-2. USDA Soil Series in the vicinity of Bonfire Shelter	67
3-3. High-water mark beneath Pecos River style rock art panel at Skiles Shelter near the confluence of Mile Canyon and the Rio Grande.....	69
3-4. 2014 flooding at Mile Canyon cresting approximately 15 vertical meters (50 ft) below the southern entrance to Bonfire Shelter.....	71
4-1. Water-filled tinaja on the canyon floor below Eagle Cave.....	86
4-2. Honeycomb Tafoni salt weathering along the back wall of the White Shaman site, a rockshelter overlooking the Pecos River	87
5-1. 2017-2018 Bone Bed 1 Excavation Blocks	106
5-2. Platform preparation flakes and shatter from experimental Edwards Plateau chert core	128
5-3. Chert Fluorescence in the Bonfire Shelter lithic assemblage, FN60280	130
5-4. View east towards Bonfire Shelter from the western rim of Mile Canyon	136

5-5. Modern photo of the Bonfire Shelter notch	137
5-6. Fine-fraction sediment samples settling in graduated cylinders during hydrometer-based particle size analysis	143
5-7. Detail photo of sediments settling at base of graduated cylinder	144
5-8. Preparing to remove sediment samples from the muffle furnace after firing at 1,000° C	154
5-9. Chittick Apparatus used to determine calcium carbonate content in sediment	157
7-1. Planview layout of Block C and Block D Bone Bed 1 excavation units	191
7-2. Overview of Stratum 23 excavation in Block C	195
7-3. Exposure of partially excavated mammoth elements in UC1 L1 at the base of 1983-1984 excavations	197
7-4. Profile view of Block C, south wall: PS06.CS05 stratigraphic units prior to column sample excavation	200
7-5. Graphic illustration of the relationship between Bement's Bone Bed 1 stratigraphic units with PS06.CS05	203
7-6. Oblique view east of Block D bench with protective plywood immediately prior to excavation	205
7-7. View south of initial backfill clearing beneath Block D plywood	206
7-8. Oblique view southeast of Block D test units immediately prior to excavation	206
7-9. View east of "spall pavement" exposed across Block D	207
7-10. View east of Sondage excavated beneath the "spall pavement" extending through Unit D8 Layers 6 and 7	210
7-11. Planview illustration of Bone Bed 1 - Stratum 23 (E/F/G) exposed across Block C, Units C1, C2, and C3	213
7-12. Unclassified planview map of Bone Bed 1 - Stratum 23 (E/F/G) highlighting Structure from Motion orthophoto of Units C1, C2, and C3	214
7-13. Mammoth ribs (FN60009 and 60010) and pelvis (FN60011) prior to extration at base of Unit C3 L1, planview - south	216

7-14. In situ plaster-jacketed element (FN60019) in northeast corner of Unit C3 L1	216
7-15. Pedestalled mammoth ribs (FN60112 and 60082) and major elements at Stratum 23/24 interface.....	217
7-16. Graphic comparison of Stratum 23 elements recovered in 1983/84 to the 2017/2018 assemblage	219
7-17. Planview map of Bone Bed 1 - Stratum 24 (H), faunal remains, Block C, Units C1 and C2.....	222
7-18. Unclassified planview map of Bone Bed 1 - Stratum 24 (H) faunal remains, Unit C1 and C2	223
7-19. Bone cluster at base of Unit D4 L3 including scapula (FN60333) and several ribs/fragments (FN60323, 60334 - 60338, 60345), planview - east	224
7-20. Planview map of faunal remains recovered from Bone Bed 1 - Stratum 24 (H), Block D, Unit D4.....	226
7-21. Unclassified planview map of faunal remains recovered from Bone Bed 1 – Stratum 24 (H), Block D, Unit D4.....	227
7-22. Initial exposure of FN60161 (Unconfirmed mammoth element), FN60247 (mammoth rib – center), and FN60292 (mammoth scapula – lower left) at Stratum 23/24 interface.....	228
7-23. Spot samples and fauna remains recovered from Unit C1 L6 and C2 L3	229
7-24. Closing photo of Unit C2 L3 and Unit C1 L6, view south.....	230
7-25. FN60292, mammoth scapula, extending beneath the eastern profile of Unit C2 L3, view east	231
7-26. Partially articulated rodent remains (FN60222) within mammoth element (FN60161), view east.....	231
7-27. Graphic comparison of Stratum 24 elements recovered in 1983/84 to the 2017/2018 assemblage	233
7-28. Planview illustration of superimposed Stratum 23 and 24 faunal assemblages	235
7-29. Unclassified plan map of superimposed Stratum 23 and 24 faunal assemblages.....	236

7-30. Detail photo of FN60295 showing in situ exposure of hackberry seeds (lower – red outline) and context photo illustrating the relationship between FN60295 and mammoth elements (FN60247 and 60161) (upper)	242
7-31. Initial exposure of ¹⁴ C sample FN60312 (upper) and association with cluster of horse remains (lower)	244
7-32. Initial exposure of ¹⁴ C sample FN60329 beneath element FN60282 and FN60283	245
8-1. Column Sample 5 compiled geoarchaeological results and stratigraphic correlations.....	254
8-2. Graphic representation of PS06.CS05 <2mm-fraction USDA sediment texture classification	257
8-3. Proportional sand, silt, and clay components of each PS06.CS05 column sample stratum	258
8-4. Graphic Mean and Standard Deviation of each PS06.CS05 column sample stratum excluding gravel fraction	258
8-5. Gypsum content of Bone Bed 1 strata calculated using the Differential Water Loss method (Artieda et al. 2006)	263
8-6. Gypsum Content: XRD (Anhydrite & Bassanite) vs. Differential Water Loss.....	265
8-7. Example of Tafoni weathering features at the White Shaman Site, Val Verde County, Texas.....	266
8-8. Comparison of Organic Carbon Determination Methods: Elemental Analyzer vs. Loss on Ignition	268
8-9. δ13C versus Vienna Pee Dee Belemnite (parts per thousand (‰)) as determined by the University of Kansas KEPSIL for each PS06.CS05 stratum	270
8-10. Column Sample 5 mineralogy by stratum, as determined by XRD.....	273
8-11. Column Sample 5 clay fraction (<4µm) mineralogy as a percentage of total sediment sample by mass.....	274
8-12. Limestone Mineralogy pre- and post-dissolution in HCl	276
8-13. Proportion of Endogenic vs. Exogenic <2.0 mm sediment	277
8-14. Column Sample 5 Mass Specific Magnetic Susceptibilities (χ _{lf} & χ _{hf})	280

8-15. Column Sample 5 Mass Corrected/Frequency Dependent Magnetic Susceptibilities (χ_{fd})	280
8-16. Column Sample 5 Mass Corrected Susceptibility versus Volumetric Calcimeter Calcium Carbonate Content (calcium carbonate equivalent)	281
8-17. Column Sample 5 Mass Susceptibility versus Sorting and Composition.....	282
8-18. Higher resolution comparison of Column Sample 5 χ_{FD} , <2mm particle size and sorting, and feldspar content.....	282
8-19. Column Sample 5: Round Gravel Count and Frequency vs. Exogenic Sediment.....	308
8-20. Limestone gravel was the primary component of all analyzed microartifact samples	310
8-21. Examples of osseous material recovered from FN60092	311
8-22. Bone fragments recovered from FN60092	312
8-23. Snail shell fragments recovered from FN60092.....	314
8-24. Examples of fossil shell fragments recovered from FN60092	315
8-25. Possible chert fragments observed in spot sample FN60092, Unit C2 L1	316
8-26. Quartz crystal fragments recovered from FN60092	317
8-27. Examples of rounded gravel observed in FN 60299.....	319
8-28. Crystalline gypsum fragments observed in FN60092.....	320
8-29. Rounded gypsum nodules observed in FN60092	322
8-30. Nearly intact hackberry (Celtis sp.) seeds and hemispheres recovered from FN60299	323
8-31. Hackberry (Celtis sp.) seed fragments recovered from FN60299	324
A-1. LS001 (S19) Particle Size Distribution with Gravel: Histogram and Cumulative Curve.....	349
A-2. LS001 (S19) Particle Size Distribution without Gravel: Histogram and Cumulative Curve.....	349
A-3. LS002 (S20) Particle Size Distribution with Gravel: Histogram and Cumulative Curve.....	351

A-4. LS002 (S20) Particle Size Distribution without Gravel: Histogram and Cumulative Curve	351
A-5. LS003 (S21) Particle Size Distribution with Gravel: Histogram and Cumulative Curve	353
A-6. LS003 (S21) Particle Size Distribution without Gravel: Histogram and Cumulative Curve	353
A-7. LS004 (S22) Particle Size Distribution with Gravel: Histogram and Cumulative Curve	355
A-8. LS004 (S22) Particle Size Distribution without Gravel: Histogram and Cumulative Curve	355
A-9. LS005 (S23) Particle Size Distribution with Gravel: Histogram and Cumulative Curve	357
A-10. LS005 (S23) Particle Size Distribution without Gravel: Histogram and Cumulative Curve	357
A-11. LS006 (S24) Particle Size Distribution with Gravel: Histogram and Cumulative Curve	359
A-12. LS006 (S24) Particle Size Distribution without Gravel: Histogram and Cumulative Curve	359

ABSTRACT

Bonfire Shelter is a stratified rockshelter site in Val Verde County, Texas with Multiple archaeological components spanning the Paleoindian through Late Prehistoric Periods. The shelter is primarily known as the site of two well-documented bison kills: one in the Archaic (Bone Bed 3) and one in the Late Pleistocene (Bone Bed 2). Excavators in the 1960s and 1980s argued that a third bone bed, designated Bone Bed 1, comprised entirely of extinct Pleistocene megafauna, is also the result of human activity. If unambiguous evidence of human activity is identified, Bone Bed 1 may predate the appearance of Clovis or related Early Paleoindian traditions in the region. This thesis presents the results of new excavations and geoarchaeological analyses conducted to evaluate the formation processes associated with Bone Bed 1 and their implications for potential archaeological deposits.

In the summer of 2017, Texas State University's Ancient Southwest Texas Project initiated new excavations of Bone Bed 1. Intact portions of the Bone Bed 1 substrata with in situ faunal remains were identified at the base of test units dating to the 1960s and 1980s. A series of 11 test units and one column sample excavated in this area reidentified and confirmed the Bone Bed 1 stratigraphy and faunal assemblage reported by Bement (1986).

Sediment from each column sample strata, including three strata related to Bone Bed 2, was evaluated with a suite of geoarchaeological analyses to better understand the formation processes contributing to the Late Pleistocene deposits at Bonfire Shelter. Targeted microartifact sampling was conducted to identify ephemeral traces of human activity potentially overlooked by previous investigators.

A functional model exploring plausible scenarios that could account for the presence of the Pleistocene faunal assemblage at Bonfire Shelter was developed based ethnoarchaeological accounts, modern proxy studies, and known archaeological sites of similar antiquity. Geological, faunal, and potentially cultural evidence was synthesized using this model to identify the “best fit” scenario for each Bone Bed 1 stratum. While no conclusive evidence of human activity was identified, this thesis provides valuable insight into the dynamic conditions at Bonfire Shelter in the Late Pleistocene and refines the chronology of Bone Bed 1 by over 1,000 years, providing critical context for newly identified Early Paleoindian activity elsewhere in Mile Canyon.

1. INTRODUCTION

Bonfire Shelter is a stratified rockshelter site in Val Verde County, Texas with multiple archaeological components spanning the Paleoindian through Late Prehistoric periods. The shelter is primarily known as the site of two well-documented bison kills: one in the Archaic (Bone Bed 3) and one in the Late Pleistocene (Bone Bed 2). Previous excavators argued that a third bone bed, designated Bone Bed 1, comprised entirely of extinct Pleistocene megafauna is also the result of human activity. If unambiguous evidence of human activity is identified, Bone Bed 1 may predate the appearance of Clovis or related Early Paleoindian traditions in the region. This thesis presents the results of new excavations and geoarchaeological analyses conducted to evaluate the formation processes associated with Bone Bed 1 and their implications for potential archaeological deposits.

1.1 Bonfire Shelter – An Overview

Bonfire Shelter is one of six major rockshelters within the Mile Canyon National Register of Historic Places District near Langtry, Texas (Bell and Dibble 1970). Illustrated in **Figure 1-1**, the site is located near the head of Mile Canyon, approximately one kilometer upstream from its confluence with the Rio Grande. Also referred to as Eagle Nest Canyon, the deeply incised box canyon forms the lower reaches of Eagle Nest Creek, an ephemeral tributary to the Rio Grande. Mile Canyon measures approximately 90 meters (m) (300 feet (ft)) from rim to rim at its maximum width with depths ranging from approximately 24 m (80 ft) to 61 m (200 ft) from canyon rim to canyon floor. The elevation of the canyon floor varies with periodic fluvial scouring and sedimentation driven by massive flash floods along Eagle Nest Creek and overbank flooding from the Rio Grande.

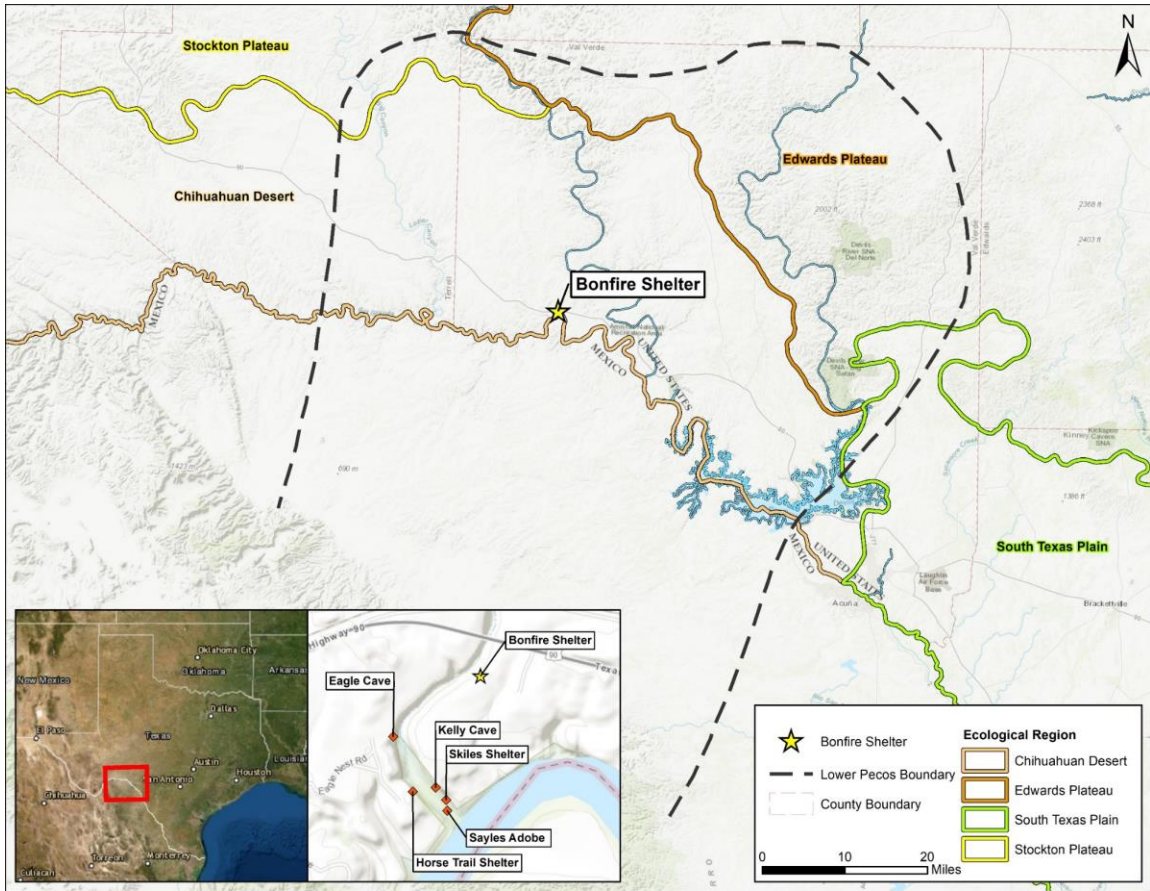


Figure 1-1. Geographic context of Bonfire Shelter and the Lower Pecos.

Bonfire Shelter is weathered into the eastern wall of the canyon approximately 18 m (59 ft) above the modern canyon floor (Byerly et al. 2005:624). The crescent-shaped shelter interior encompasses approximately 1,750 square m (19,000 square ft). Ceiling height varies from approximately 4 m (13 ft) to 10 m (39 ft) above to modern shelter floor. The long axis of the shelters is oriented roughly north-south and extends approximately 97 m (320 ft) from end to end and extends approximately 18 m (60 ft) east-west into the Cretaceous Devils River Formation limestone bedrock that characterizes Mile Canyon. (Frederick 2017b; Freeman 1964; Kilby et al. 2020).

A massive colluvial boulder field obscures the shelter’s mouth, making it nearly undetectable from the opposite canyon rim. The collapse event responsible for the boulder field appears to pre-date human use of the shelter but plays a critical role in the site’s depositional

history. The obstruction functions as a retaining wall trapping endogenic and exogenic sediments as well as Bonfire Shelter's rich archaeological record. In addition to inhibiting erosion, the obstructed entrance and northern orientation restricts direct sunlight to the shelter interior to narrow bands as the sun passes overhead of the narrow gap between the boulders and the canyon rim.

Access to the shelter is limited to narrow passages behind the boulders at the extreme northern and southern ends of the shelter. A distinct notch weathered into canyon rim above the southern shelter entrance channels upland sheetwash and debris into the shelter interior, accumulating in 5 m (17 ft) "talus cone". The talus cone area marks the densest concentrations of archaeological material and bone within Bonfire Shelter.

The deeply stratified deposits span over 12,000 years of human history. Excavations at Bonfire Shelter conducted in 1963-1964 (Dibble and Lorrain 1968) and 1983-1984 (Bement 1986a) documented three significant bone deposits: Bone Beds 1, 2, and 3 numbered from oldest to youngest. Bone Bed 3, the youngest bone bed, represents the remains of a large Late Archaic Period *Bison bison* kill which excavator David Dibble argued was the result of a jump-kill event from the canyon rim. The dense deposit and associated Castroville and Montell projectile points are heavily burned provide the namesake for Bonfire Shelter (Dibble and Lorrain 1968:42-48).

Figure 1-2 illustrates the extent of previous excavations relative to areas excavated in 2017-2018. Note the talus cone on the southern margin of the site where the densest portions of Bone Beds 2 and 3 are located.

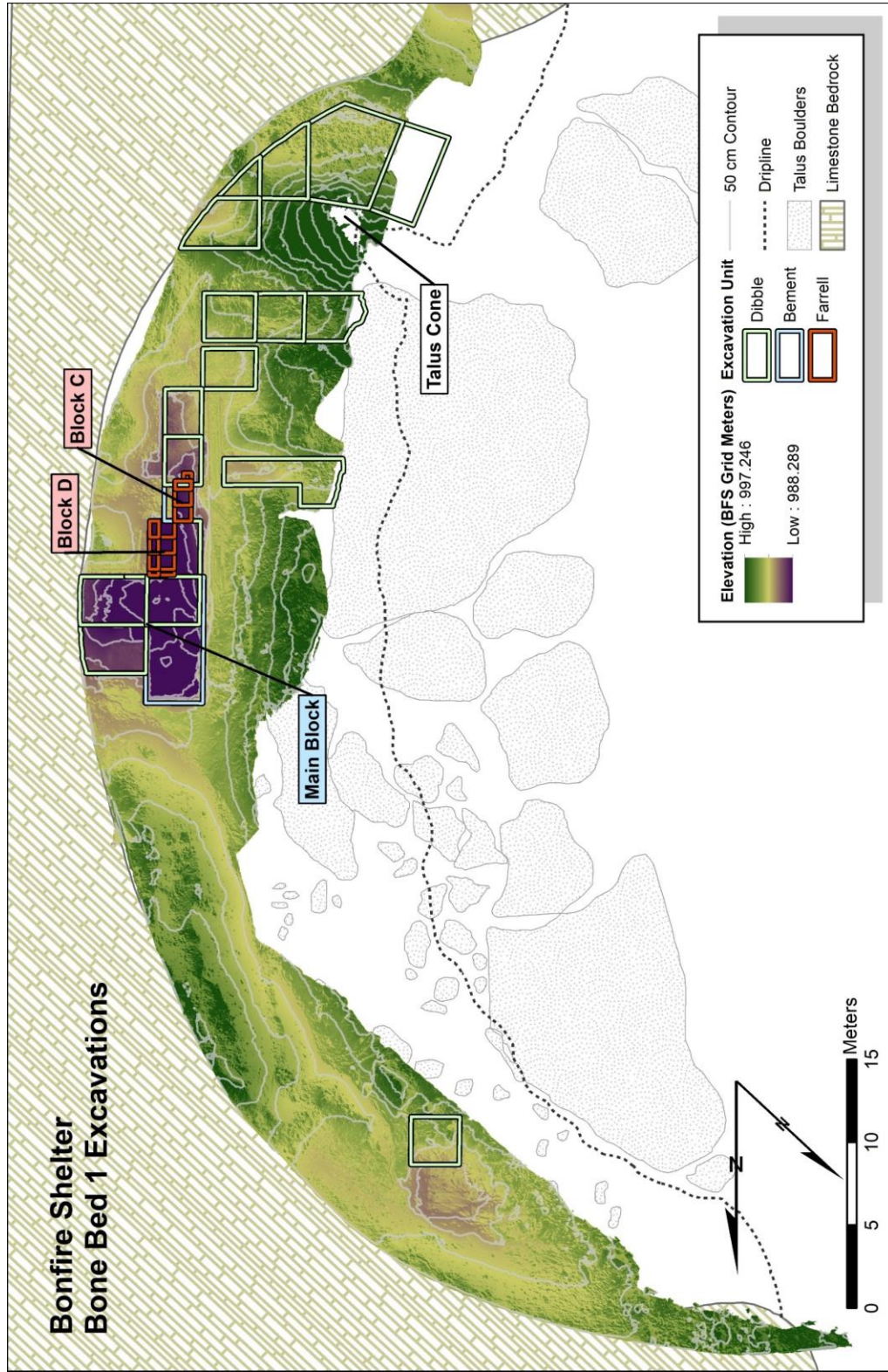


Figure 1-2. Bonfire Shelter Site Overview and Previous Investigations. Digital elevation model derived from Structure from Motion photogrammetry rendered at 3.0 cm raster resolution overlaid with 50.0 cm contours. Talus boulders, dripline, and excavation units digitized from Bement 1986. Elevation model provided courtesy of ASWT, 2015

Bone Bed 2 is Paleoindian bone deposit separated from Bone Bed 3 by approximately one meter of sediment bearing limited evidence of human exploitation of Bonfire Shelter. Bone Bed 2 is characterized by the presence of Folsom and Plainview or Plainview-like projectile points as well as the remains of numerous *Bison antiquus* or *occidentalis*. Both Dibble and Bement argue that Bone Bed 2 also represents the remains of a jump-kill, making it the oldest and southern-most bison jump in North America (Bement 1986a:33; Dibble and Lorrain 1968:29-40). Differential burning across Bone Bed 2's three substrata suggest multiple kill events may be represented. Questions regarding the number of individual bison and the number kill events represented in both Bone Beds 2 and 3 remain outstanding (Bement 2007; Byerly, Cooper, et al. 2007).

Subsequent reevaluations of the Bone Bed 2 assemblage and stratigraphy have questioned this hypothesis, suggesting that the deposit resembles a secondary processing locality from a single event with far fewer individuals represented rather than a primary kill locus derived from three events. Similar arguments have been extended to Bone Bed 3, though the Archaic deposits appear to be more consistent with a jump kill (Bement 2007; Byerly, Cooper, et al. 2007; Byerly et al. 2005; Byerly, Meltzer, et al. 2007; Prewitt 2007).

Bone Bed 1 is a series of six bone-bearing substrata in some places less than 10 cm beneath Bone Bed 2. Unlike Bone Beds 2 and 3, Bone Bed 1 is confined to the shelter interior and has not been identified on the talus cone; the extent of the deposits in the northern portions of the shelter is unknown. Bone Bed 1 is characterized by the presence of Rancholabrean Pleistocene megafauna and the notable absence of stone tools. The stratum was initially identified during the 1963-1964 excavations, where Dibble noted the presence of Pleistocene horse (*Equus francisci*), mammoth (*Mammuthus sp.*), bison (*Bison antiquus*), camel (*Camelops hesternus*) and antelope (*Capromeryx sp.*). Dibble argued the bone fracture patterns combined with the presence of anomalously large limestone cobbles, trace charcoal, and the absence of a clear introductory

vector suggested human agents may be responsible for the accumulation (Dibble and Lorrain 1968:28). While no radiocarbon dates were obtained from Bone Bed 1 during the 1963-1964 excavations, the deposit's stratigraphic position below the Folsom – Plainview aged Bone Bed 2 suggested an Early Paleoindian temporal association.

The 1983-1984 expedition specifically targeted Bone Bed 1, evaluating the nature of the deposits and the extent of human involvement. Bement defined six substrata within Dibble's Bone Bed 1: Stratum E-F, H1, H2, and I. Strata A – C were assigned to the three Bone Bed 2 substrata and Stratum D was assigned to the intermediate Zone 2 separating the Bone Bed 1 and Bone Bed 2 strata (Bement 1986a:8). Stratum H-1 yielded a single radiocarbon date of 12,460 +/- 490 RCYBP (AA-344) (Bement 1986a:9); potentially older than the commonly accepted age of Clovis (Haynes et al. 2007; Waters and Stafford 2007).

Bement drew similar conclusions as Dibble: the distribution of faunal remains with spiral fractures and green-breaks around anomalous limestone blocks resembled "butchering stations" observed in Bone Beds 2 and 3, possibly modified elements that resembled improvised bone tools, elements exhibiting V-shaped incisions, and the presence of small amounts of charcoal all suggest humans contributed to the accumulation of the Bone Bed 1 strata (Bement 1986a:63). No stone tools or debitage were recovered; arguments for human actors primarily hinge on similarities drawn between Bone Bed 1 and the unambiguously cultural Bone Bed 2.

Bement also identified a complicating factor. Parabolic u-shaped incisions generally associated with carnivore tooth marks were identified on several elements, including specimens that also exhibited V-shaped incisions interpreted as cut marks. Puncture marks consistent with *Homotherium serum*, a sabretooth cat species, were identified on a mammoth long bone fragment. Carnivore remains themselves have not been recovered from the Bone Bed 1 strata, but these modifications imply their presence and contribution to the bone accumulations (Bement

1986a:51-54). The presence of these carnivore modifications complicates the attribution of Bone Bed 1 to human agents, casting doubt on the interpretation of other supporting evidence.

Neither the 1963-1964 nor the 1983-1984 excavation yielded unequivocal evidence of human activity associated with Bone Bed 1. These arguments for human activity and the specific supporting evidence put forth by Dibble and Bement are discussed in detail in **Chapter 2**. The chapter evaluates criticisms and alternative interpretations of the Bone Beds and additional laboratory studies derived from the major Bonfire Shelter expeditions.

1.2 Objectives and Justification of Research

This thesis evaluates the six substrata that comprise Bone Bed 1 using geoarchaeological methods to determine if natural formation processes can account for the presence of Pleistocene faunal remains and the absence of cultural material in Bone Bed 1. In the summer of 2017, Texas State University's Ancient Southwest Texas project (ASWT) initiated new excavations of Bone Bed 1 at Bonfire Shelter. This undertaking primarily seeks an understanding of these ambiguous Pleistocene bone deposits and the taphonomic processes that entombed them beneath three meters of intact rockshelter archaeology. If Bone Bed 1 is derived from human activity, it provides a unique opportunity to understand the role of static landscape features, such as rockshelters, in Early Paleoindian settlement patterns and subsistence strategies.

Geoarchaeological methods are employed to identify environmental changes during the Late Pleistocene that impact the suitability of Bonfire Shelter for human activities or the visibility of cultural material. This research is imperative due to ongoing destabilization and erosion at Bonfire Shelter and impending remediation efforts that will render intact portions of Bone Bed 1 inaccessible without large-scale excavations.

1.2.1 *Research Design*

To date, the Bone Bed 1 strata have yielded no definitive artifacts. Arguments that humans are at least partially responsible for the accumulation of Bone Bed 1 hinge on the identification of isolated cut marks and ambiguous improvised bone tools. The identification of stone tools or lithic debitage associated with the Pleistocene faunal remains in sound geological context would provide unequivocal evidence that humans are responsible for the bone accumulations.

The new excavations initiated by the ASWT are designed to collect three primary data series supporting the evaluation of Bone Bed 1:

1. Geoarchaeological data evaluating the depositional processes contributing sediment to Bone Bed 1 and the composition of those sediments.
2. Targeted sampling for microartifacts in association with Pleistocene faunal remains
3. Preliminary analysis of faunal remains for evidence of human modification and spatial patterning that may provide additional insight into the bone bed taphonomy.

This research design expands upon David Robinson's pilot study "Stratigraphic Analysis of Bonfire Shelter, Southwest Texas" (Robinson 1997). Robinson correlated the results of a sedimentological analysis and a palynological analysis conducted by Linda Scott Cummings to reconstruct the environmental setting surrounding the three major bone beds at Bonfire Shelter. Robinson's analysis broadly reviewed the entire stratigraphic sequence of the shelter. This thesis specifically targets three accessible Bone Bed 1 strata and three immediately overlying strata, including portions of the Late Paleoindian age Bone Bed 2.

The geoarchaeological component of this thesis includes eight analyses: X-ray diffraction and particle size analysis, the primary methods employed by Robinson (1997), provide key data characterizing the composition, size profile, and sorting of each stratum. A multifaceted

approach was implemented to assess the impact of exogenic deposition in each stratum. Loss-on-ignition provides a proxy measure for organic carbon and calcium carbonate (CaCO₃). A volumetric calcimeter method (Chittick apparatus) was used to directly verify anomalous loss-on-ignition CaCO₃ results. Organic carbon samples were verified using the Elemental Analyzer (EA) services at the University of Kansas. This analysis includes carbon and nitrogen stable isotope fractionations, providing additional insight into the environmental conditions at the time of deposition. Gypsum content was assessed using a differential weight loss method similar to loss-on-ignition; gypsum was thought to contribute to the unexpected loss-on-ignition results. Magnetic susceptibility assessed the presence of magnetic minerals in the deposits. Due to the Devils River limestone's low inherent magnetic susceptibility, elevated susceptibilities suggest exogenic deposition. Together, these data form a profile of the major formation processes contributing to the Bone Bed 1 contextualizing the faunal remains and any archaeological material recovered.

The goal of this geoarchaeological methods is to determine if exogenic processes could have introduced faunal remains into the shelter, scoured away associated artifacts, or include chemical signatures of human occupation. The geological and taphonomic processes that contribute to the formation of rockshelters and the present state of Bone Bed 1 are outlined in **Chapter 4**. The specific methods for assays used to evaluate those processes will be discussed in detail in **Chapter 5.4**.

Microartifact analysis was conducted to identify lithic debitage in the 1-2 mm sediment fraction. Previous fieldwork sampled for >0.25 in (6.35 mm) artifacts. Detailed microfauna and sedimentological analysis was conducted in the laboratory, but microartifacts were not considered. By frequency, microdebitage is the most abundant by-product of stone tool production, representing over 99% of all debitage fragments (Fladmark 1982). In highly raw-material conservative Paleoindian subsistence models, curated tools may be removed from the

site after use (Kelly and Todd 1988; Kilby 2008:13-21). The residual debris from resharpening tools may remain in place becoming integrated with the local sediment and subjected to the same post-depositional processes (Sherwood 2001). If human exploitation of Bonfire Shelter was ephemeral, microartifacts provide the highest probability for detection (Schiffer 1987:269). (Homsey-Messer et al. 2016) Methodologies for microartifact processing and sorting will be discussed in greater detail in **Chapter 5.2**.

At present, faunal remains are the primary source of evidence for human activity associated with Bone Bed 1. This thesis includes the preliminary field identifications of remains recovered during the 2017 – 2018 Bone Bed 1 excavations. A formal zooarchaeological analysis was beyond the scope of this project. Many of the elements recovered remain classified as “Unidentified” due to their fragmentary and highly deteriorated nature. Preliminary analysis suggests that the newly excavated remains are consistent with the composition of the 1980s Bonfire assemblage. Significant research opportunities remain for future zooarchaeologists. Methods employed to extract and evaluate faunal remains will be discussed in **Chapter 5**.

1.2.2 *Modeling Expectations*

A comparative model was developed to better synthesize these data. Outlined in detail in **Chapter 6**, this model integrates ethnoarchaeological accounts, modern proxy studies, and archaeological data from other Late Pleistocene sites to identify scenarios that could account for the Bone Bed 1. The model presents the geological, faunal, and cultural attributes expected in each of the four scenarios. Field and laboratory data collected from Bone Bed 1 was compared against the expected values to identify the “best fit” scenario for each Bone Bed 1 stratum.

The null hypothesis for this thesis is that the Bone Bed 1 assemblage is the result of geological redeposition; no cognizant actors were involved. Alternative hypotheses include: Bone Bed 1 is the result of carnivore activity; Bone Bed 1 is the result of fauna dying in Bonfire Shelter

of natural causes; and Bone Bed 1 is the result of human activity. **Table 6-1** (Chapter 6) presents the criteria that must be satisfied accept these hypotheses.

The experimental results were not expected to align with any one hypothesis with 100% accuracy. Countless formation processes contribute to the observable conditions at any archaeological site. These hypotheses represent “likely” scenarios derived from similar sites and that can be measured archaeologically. The goal of this model is to identify diagnostic archaeological signatures that confirm/preclude each potential scenario.

1.2.3 *Minimum Cultural Criteria*

With the discovery of a chert projectile point lodged in the ribs of a *Bison antiquus* at the Folsom site in 1927 (Figgins 1927; Meltzer 2006a:5), stone tools became the “smoking gun” evidence unambiguously placing humans in North America during Late Pleistocene. The formal description of Clovis at Blackwater Draw, NM corroborated these findings soon after (Cotter 1937). The high-profile finds quickly linked what would become Paleoindian archaeology to the identification of Pleistocene mega-mammal remains. Due to their relatively high-visibility on the landscape, the faunal remains were often the key to identifying the presence of very early archaeological site. In many cases, the associated stone tools were identified only after the faunal remains were investigated (Meltzer 2006b:115). Prior to these discoveries, the Pleistocene presence of humans in North America was considered a speculative hypothesis (Meltzer 1983).

Outside of North America, human history extends hundreds of thousands of years into the past beyond the Pleistocene. Lower Paleolithic studies and paleoanthropology take place on a geological timescale (Schick and Toth 1994a:78-92). As such, the materials and geological contexts have been subjected to tens of thousands of years of weathering that must be differentiated from cultural activity. The scientific community does not consider fossil hominid finds credible until they can be proven legitimate beyond a reasonable doubt (Schick and Toth 1994a:93-99). The same rigorous standards are applied to sites that challenge the archaeological

status quo, and should be used to evaluate all archaeological sites in general. A plethora of “Pre-Clovis” sites have been reported across the Americas, but few have withstood scientific scrutiny (Haynes 2015). The criteria employed by Paleoanthropologists to assess the validity of Lower Paleolithic and early hominid sites in Africa’s Great Rift Valley are also applicable to the evaluation of North American sites (Meltzer 2009a; Schick and Toth 1994b:100-102). At a minimum, sites must include:

- Unambiguously and reliably identifiable cultural artifacts, preferably in the form of stone tools
- Temporal control verified with multiple chronometric methods
- Well documented and uncontaminated provenience

A site without definitive artifacts or features remains equivocal. The insinuation of human activity through cut marks, bone breakage patterns, or chemical signatures is valuable, but circumstantial, evidence (Meltzer 2009a). Experimental studies have demonstrated that environmental processes can result in patterns that “mimic” human modification patterns (Haynes 1988, 1991a, 1991b; Haynes and Klimowicz 2015; Haynes and Krasinski 2010; Holen et al. 2017). A single flake among hundreds of otherwise naturally fractured stones or a single cut-mark among dozens of carnivore toothmarks cannot be reliably attributed to human activity. If human behavior *is* the source of these patterns, then additional by-products of those actions should be present.

If the Bone Bed 1 faunal remains are the result of human activity, the implements and by-products of the tools used to process them should still be present. The preservation of bone and organic materials is a hallmark of Lower Pecos rockshelter archaeology (Turpin 2004:266). If perishable tools were used in the shelter, they may still be preserved with identifiable wear patterns. However, the cumulative effects of over 10,000 years of trampling, spalling, freezing,

thawing, and gnawing can yield similar results. The recovery of stone implements and/or associated debris would link the faunal remains to human activity.

Chronometric verification is an essential component of any archaeological investigation; particularly so at sites of great antiquity. The presence of mammoth, horse, and camel in Bone Bed 1 places it comfortably in the Pleistocene. In North America, the cohabitation of modern humans with these fauna is restricted to a relatively narrow window at the end of the epoch typically characterized by the presence of Clovis technology. The single radiocarbon date (12,460±490 BP) recovered from Bone Bed 1 in the 1980s suggests that Bone Bed 1 predates Clovis, which conservatively dates to 13,250 – 12,800 cal BP (Haynes et al. 2007; Rasmussen et al. 2014; Waters and Stafford 2007). If validated, may be the only confirmed earlier than Clovis site in the Lower Pecos (McCue 2019:164-168). Without additional samples, it is impossible to assess the accuracy of the chronometric results or identify potential contamination effects. Dating material from multiple sources (i.e.: charcoal, macrobotanical material, bone collagen, etc.) using multiple laboratories would further validate these findings.

1.2.4 *Pre-Clovis Implications*

At nearly 13,000 RCYBP, Bone Bed 1 predates the traditionally accepted timeline for modern human presence in North America. Clovis, characterized by distinct fluted lanceolate projectile points, has long been considered the oldest cultural horizon on the continent 13,250 – 12,800 cal BP (Haynes et al. 2007; Rasmussen et al. 2014; Waters and Stafford 2007). A growing body of evidence suggests that humans were present in North America before the appearance of Clovis technology and possibly into the Full-Glacial Pleistocene. The nature of these peoples as precursors to Clovis or as independent traditions remains a point of debate (Haynes 2015).

Table 1-1 summarizes several notable North American sites reporting an earlier than Clovis component. Each site has encountered substantial criticism, ranging from healthy skepticism to blanket rejection. Unaccounted for contaminants, nascent technologies, and

unacceptably large radiocarbon date standard deviations all have the potential to undermine a site's credibility. Researcher bias including the discriminant inclusion or reject of apparent outlier radiocarbon dates and other archaeological evidence can have similarly detrimental impacts. Limited reproducibility and lack of independent verification further preclude the acceptance of evidence that might outwardly appear to satisfy Schlick and Toth's criteria.

Grayson and Meltzer (2002, 2015) evaluate the credibility of Early Paleoindian megafauna kill sites across North America, including Bone Bed 1 at Bonfire shelter, using criteria similar to Schlick and Toth. They concur with Wyckoff (1999:349) that the paucity of cut-marks, the absence of lithic tools and debitage, and the unknown extent of carnivore activity excludes Bone Bed 1 from consideration as a human occupation. Haynes (2015) assess the evidence and unresolved complications at possible earlier than Clovis sites and compares them against modern Clovis subsistence models and technological adaptations to identify evidence of cultural continuity. The collective evidence was ambiguous, with few commonalities among the early sites that would suggest a progression towards Clovis.

The diversity among earlier than Clovis sites highlights a key point of friction. Pre-Clovis implies a linear relationship between the well-defined, wide-spread, fluted-point, Clovis and the sites that pre-date them, suggesting observable technological and/or cultural continuity (Haynes 2015). "Earlier than Clovis" or "Older than Clovis" has been adopted as the preferred terminology by other investigators to avoid implying a direct relationship between Clovis and the preceding groups (Collins and Bradley 2008; Collins et al. 2014).

Some in the earlier than Clovis camp suggest that the technological differences are derived from multiple migratory pulses (Beck and Jones 2010). In this model, the Clovis toolkit is a unique adaptation brought onto the continent by a group with little relationship to the peoples already there. At Gault and Paisley Caves, two generally well-accepted Earlier than Clovis sites, the lithic assemblage is distinctly non-Clovis (Collins and Bradley 2008; Jenkins et al. 2012;

Williams et al. 2018). Projectile points recovered from the earlier than Clovis horizons at both locations are technologically distinct stemmed projectile points lacking the hallmark fluted lanceolate formats of later Paleoindians.

The search for Clovis antecedents has dominated much of Paleoindian, and Northern American in general, archaeology for much to the 20th century (Meltzer 1983). The fluted points, polyhedral cores, curated bifaces, and overshot flakes that characterize the Clovis toolkit are ubiquitous across vast swaths of the United States. The highest incidence of Clovis points (often identified as isolated finds) occurs in the Eastern United States. In the west, fewer points have been identified but the specimens are more frequently found in site contexts that can provide more insight into subsistence strategies (Anderson et al. 2010).

The extant body of evidence renders Bone Bed 1 at Bonfire Shelter equivocal under the criteria outlined above. The single radiocarbon date collected in the 1980s is insufficient by modern standards and was unverified prior to the present ASWT excavations. No formal artifacts have been recovered; faunal elements bear the burden of proof. However, the weight and credibility of the evidence is compromised by co-occurring evidence of carnivore scavenging activity in the same strata (Bement 1986b:54-58; Johnson 1989:437-438, 443).

Subsequent studies addressing the early formation of Bonfire Shelter are geared towards paleoenvironmental reconstruction (Bryant and Holloway 1985; Robinson 1997; Scott-Cummings 1992). Representative samples from each major stratum have been processed for fossil pollen, microfauna, and sediment particle size but microartifacts were not considered. Samples were collected from continuous column samples, but the intermittent levels remain unanalyzed and in storage at the Texas Archeological Research Laboratory (TARL). The stratigraphic components of Bone Bed 1 appear to be contextually sound, but the substrata identified by Turpin and Bement have not been scrutinized beyond their initial description.

For these reasons, Bone Bed 1 is referenced in intentionally vague terms regarding cultural affinity; “potentially” and “possible” modify “earlier than Clovis or “very early Paleoindian”. The Bone Bed 1 strata underlie confirmed Late Paleoindian deposits (Bement 1986a), but lack of cultural material precludes our ability to ascribe Bone Bed 1 to any specific archaeological culture. Statements regarding the specific temporal association of Bone Bed 1 remain circumspect due to the original radiocarbon date’s 1000-year range. New data reported in this thesis provide additional temporal context for Bone Bed 1, but care is taken to avoid descriptors with specific cultural connotations.

The North American sites presented in **Table 1-1** yielded evidence sufficient to merit serious consideration as earlier than Clovis occupations. Page-Ladson, Paisley Caves, Gault, and Debra L. Friedkin are generally well regarded and satisfy multiple cultural criteria, though they are not without issue. Others, including the Manis mastodon, the Schaefer mammoth, and the Hebior mammoth, are more ambiguous. The date ranges below are provided in the format published by original authors, except where marked with an “*”. These dates were calibrated independently using OxCal Online v.4.3 (Bronk Ramsey 2009) against the IntCal13 calibration curve (Reimer et al. 2013) and are present as a 2σ range.

^{14}C radiocarbon years BP (RCYBP) dates are uncalibrated radiocarbon years before present. Calibrated years before present (cal yr BP) are calibrated against a geological standard to account for variation in atmospheric carbon isotopes over time (see site-specific source for specific details regarding calibration variables). Calibrated dates from the Late Pleistocene sometimes exhibit significant deviations due to the radical climatic shifts that characterize the epoch. The “Methods” field refers to the dating method and/or source of the chronometric date. ^{14}C indicates a standard AMS radiocarbon date. Average ^{14}C indicates that the reported dates include results from multiple samples. OSL indicates an Optically Stimulate Luminescence date derived from quartz grains. OSL dating is a relatively new technology; early dates and sites

argued on unverified OSL dates have been met with skepticism. IRSL indicates Infrared Stimulated Luminescence dating, a method similar to OSL that does not rely on quartz grains. Collagen dates are derived from carbon extracted from bones recovered in archaeological context. Modern purification and processing techniques address contaminants that previously compromised dates derived from faunal remains.

Table 1-1. Select earlier than Clovis-age sites that satisfy one or more of the minimum criteria for consideration as bona fide human occupation. None of the sites listed below are without criticism and issue. Dates marked with an “*” were calibrated independently using OxCal v.4.3 and the IntCal13 calibration curve.

Site	Location	¹⁴ C yr BP	Calibrated (cal) yr BP	Method	Citation
Page-Ladson	Florida	12,175±40 – 12,465±40	14,475	Average ¹⁴ C	(Halligan et al. 2016)
Paisley Caves	Oregon	12,265±25, 12,260±30	14,305-14,048* 14,310-14,035*	¹⁴ C	(Jenkins et al. 2012)
Meadowcroft Rockshelter	Pennsylvania	12,800±870 – 16,175±975	~13,000-22,000	¹⁴ C	(Adovasio et al. 1990; Adovasio et al. 1977)
Topper	South Carolina	-	15,200±1,500	OSL	(Goodyear and Steffy 2003; Goodyear 2005; Smallwood 2011)
Gault	Texas	-	13,230±760, 13,650±790	IRSL	(Collins and Bradley 2008; Williams et al. 2018)
Debra L. Friedkin	Texas	-	14,080±920 – 16,515±1,075	OSL	(Michael R. Waters et al. 2011; Waters et al. 2018)
Cactus Hill	Virginia	15,070±70	~ 18,200	¹⁴ C	(McAvoy and McAvoy 1997)
Manis	Washington	11,960±17	13,860-13,763	Average ¹⁴ C – Bone Collagen	(Gustafson et al. 1979; M. R. Waters et al. 2011)
Schaefer	Wisconsin	12,290±60 – 12,570±45	14,628-14,030* 15,152-14,629*	Purified Bone Collagen	(Joyce 2006)
Hebior	Wisconsin	12,480±60 – 12,590±50	15,041-14,269* 15,174-14,669*	Purified Bone Collagen	(Overstreet and Kolb 2003)

1.3 Theoretical Framework

Due to the paucity of artifacts, a primarily geoarchaeological approach was implemented to evaluate Bone Bed 1 at Bonfire Shelter. Geoarchaeology emphasizes understanding the natural

geological processes impacting an archaeological site and the implications of those processes for cultural material. Geoarchaeology has played a key role in establishing the “antiquity of man” in North America and continues to feature prominently in Paleoindian research (Holliday 1997; Meltzer 2006b). Paleoindian sites are often deeply buried, well stratified, and include diverse Pleistocene faunal assemblages. A multi-disciplinary approach provides much needed interpretational context for the foreign depositional environments of extinct glacial landscape. Integrating methods and mindsets from quaternary geosciences and paleontology is an essential component of Late Pleistocene archaeology (Holliday 2009).

Schiffer’s (1987) *Formation Processes in the Archaeological Record* was used to contextualize the faunal remains and taphonomic processes identified in Bone Bed 1. In Schiffer’s model, “primary refuse” includes objects utilized by humans and discarded at the same location where they were used. Whereas “secondary refuse” are removed from their use-area and discarded at a secondary location (Schiffer 1987:58-59). The conspicuous absence of artifacts in Bone Bed 1 begs the question: are we digging the wrong place? Overall low artifact densities in the Pleistocene strata reported by previous excavators and the experimental back-dirt sampling conducted in the early 2000s (Byerly, Meltzer, et al. 2007:128-134) suggest that this may be a possibility. The 1983 expedition did not recover a single stone artifact from Bone Bed 1 or the unequivocally cultural Bone Bed 2.

Laville et al. (1980), Farrand (2001), and Meltzer (2017) provide a geoarchaeological framework for assessing the Bone Bed 1 sediments. The diverse transport mechanisms that contribute sediment to any visibly discernable stratigraphic unit and the similarly complex systems of post-depositional modification can result in a palimpsest of geological, faunal, and cultural material. Disentangling the relevant processes through granulometric and compositional analysis can elucidate the archaeological/systemic context of recovered materials or their absence.

Archaeological and systemic contexts are terms coined by Schiffer (1972) to describe the use-life of cultural materials. Systemic context refers to the entire use-life of an object within a behavioral system from initial procurement and manufacture to permanent discard, including various recycling and rejuvenation mechanisms (Schiffer 1972:158). Archaeological context refers to the history of an object after it has been permanently discarded or has otherwise exited a behavioral system (Schiffer 1972:159-160). It is possible that materials that have been discarded in the past are recovered and reutilized well into the future (i.e.: Paleoindian tools recovered and repurposed in the Archaic, wood from a prehistoric structure scavenged and repurposed in an early Colonial structure, etc.). Lateral cycling, where an object transitions between archaeological and systemic contexts or is repurposed within systemic context, can occur any number of times (Schiffer 1972:159).

The point where an object exits systemic context and enters archaeological context is particularly relevant to this thesis. As noted above, tools may be curated and removed from the site to be discarded elsewhere. Tools discarded with substantial apparent use-life remaining due to inadvertent loss or otherwise unplanned abandonment are considered *de facto* refuse (Schiffer 1972:160). Residual primary refuse, including lithic debitage derived from tool maintenance and manufacture, is unobtrusive enough to remain in the vicinity of an activity even after an area is cleaned and larger debris removed to a secondary location (Schiffer 1987:65-72).

In resource-conservative subsistence models, “residual” lithic debitage or *de facto* expedient tools (lithic or bone) might be expected to enter archaeological context at rockshelter kill/processing localities (Schiffer 1987:93-94). Johnson (1982:145-146) describes expedient bone tools identified in the Bonfire Shelter (Bone Bed 2) assemblage as tools crafted at a kill site from elements of the animal being processed and discarded at the use-site when processing is complete. Possible expedient bone tools represent the only potential artifacts recovered from Bone Bed 1 to date (Bement 1986b). Each of these could be considered primary refuse that

entered the archaeological record at the use-site unless clear discard areas or geological impacts are identified. (Schiffer 1987:62-64, 90-91).

Lithic debitage, especially very small fragments (<2mm microdebitage), occur in large quantities during manufacture or retooling and are more likely to be left behind due to their limited salvage value (Binford 1978a:355-356; Schiffer 1987:94, 267-268). Microdebitage is readily incorporated into the local sediment matrix, increasing the likelihood that they will remain in the vicinity of their initial deposition. As integrated components of the sediment matrix, microdebitage are susceptible to post-depositional geological processes that can disperse them according to their size (Farrand 2001; Fladmark 1982). Despite their initial deposition at the use/manufacture site, artifacts impacted by geological activity may be redeposited as secondary refuse. This can skew the archaeological visibility of an occupation, especially where high-energy processes completely remove sediment from its primary context.

The Bone Bed 1 assemblage is expected to include small debitage intentionally left behind or expedient tools with limited recyclability deposited as primary refuse; intact formal tools would likely have been removed from the site and curated for future use (Kelly and Todd 1988). With no evidence of long-term exploitation, there is little reason to expect intentional waste removal activity at Bone Bed 1. Even if moderate clean up activity occurred and larger refuse was deposited along the perimeter of the site, microartifact residues should remain (Schiffer 1987:62-68). Geological processes may hinder the differentiation of primary and secondary contexts. Geoarchaeological sampling of surrounding sediment matrix can help control for many of these otherwise unknown variables. Methods outline by Folk (1980); Folk and Ward (1957); Gale and Hoare (1991) comprise the primary geological framework established for this thesis. Goldberg et al. (2001), Nordt (2001), Waters (1992), and Weiner (2010d) provide additional analytical insight.

1.4 Thesis Organization

This thesis is divided into nine chapters. This chapter, **Chapter 1**, has outlined this project's main research goals: identifying evidence of cultural activity in Bonfire Shelter's Bone Bed 1 strata and elucidating geological formation processes that may preclude the validation of these data. **Chapter 1** also contextualizes this project within Paleoindian and geoarchaeological research, providing a theoretical framework grounded in Schiffer's Behavioral Archaeology and an understanding of systematic formation processes (Schiffer 1987, 1995).

Chapter 2 contextualizes the 2017-2018 Bonfire Shelter Expedition within the broader history of archaeological inquiry in the Lower Pecos, Mile Canyon, and Bonfire Shelter. The exquisite preservation and archaeological diversity of the region's sites have attracted professional archaeologists since the 1930s. Nearly 40 years have elapsed since the last large-scale excavations at Bonfire Shelter. **Chapter 2** reviews the archaeological background of Bone Bed 1 that provides a foundation for this thesis.

Chapter 3 provides a geographic and environmental context for the Lower Pecos, Mile Canyon, and Bonfire Shelter. This information was used to establish the geological processes and preservation conditions expected to contribute to Bone Bed 1. **Chapter 3** also reviews local floral and faunal communities found in the modern Lower Pecos and their potential impact on archaeological. The role of changing climatic conditions through the Late Pleistocene-Holocene transition is also addressed.

Chapter 4 provides a detailed overview of rockshelter formation processes and sedimentation. Understanding these processes was critical to the development of the geoarchaeological testing methodology for this thesis, translating geoarchaeological data into real-world processes, and assessing the implications of those processes for associated archaeological deposits.

Chapter 5 is divided into three subsections describing the methods employed to evaluate Bone Bed 1 including: field methods, microartifact processing methods, and geoarchaeological methods. In addition to outlining the execution of each analysis, a brief discussion of interpretative criteria and research applications is provided. Notes regarding deviations from the original workplan and published methodologies are also addressed.

Chapter 6 outlines the interpretative model used to evaluate each Bone Bed 1 stratum, reiterating hypotheses explaining the potential origins of the faunal material and exploring the criteria established to accept or reject each one. This model functions as the translation between raw field observations and geoarchaeological data and the real world processes that contributed to the formation of Bonfire Shelter. The case studies, modern proxies, and ethnoarchaeological studies that form the foundation of this model are reviewed here.

Chapters 7 and 8 report the results of fieldwork and lab work respectively. **Chapter 7** highlights the results of field excavations, including descriptions of each test unit and stratigraphic unit as well as a summary of the recovered faunal remains. These results are compared to findings from the 1963-1964 and 1983-1984 expeditions. **Chapter 7** concludes with the results of new radiometric dating efforts and their implications for Bone Bed 1.

Chapter 8 reports geoarchaeological data derived from Column Sample 5 (CS05) including a discussion of materials identified during microartifact sampling. Results from each analysis are discussed stratigraphically, constructing an increasingly detailed picture of the changing conditions at Bonfire Shelter in the Terminal Pleistocene. Results are supplemented with figures illustrating trends and correlations between various datasets.

Chapter 9 synthesizes field and laboratory data to construct narrative descriptions of each stratum. These statements regarding natural and/or cultural formation processes are used to argue the primary depositional agents responsible for the accumulation of Bone Bed 1 within the

context of the model outlined in **Chapter 6**. Each stratum was evaluated independently to determine if some, all, or none of the Bone Bed 1 strata can be attributed to human agents. The chapter concludes with a debriefing assessing the effectiveness of the model, anomalies in the data, implications for Paleoindian and Lower Pecos Archaeology as well as opportunities for future research.

Three appendices present supplemental data in a long-form format. **Appendix A: Particle Size Distributions** includes tabularized particle size data and histogram/cumulative curves for each Column Sample 5 stratum. **Appendix B: Raw Microartifact** presents the raw weights and counts from the microartifact analysis in a tabular format. **Appendix C: Faunal Assemblage** includes the Bone Bed 1 faunal assemblages from the 1963-1964 (reconstructed from TARL records), 1983-1984 (aggregated from Bement 1986, with supplemental data from TARL records), and the 2017-2018 excavations.

2. ARCHAEOLOGICAL CONTEXT AND EXCAVATION HISTORY

Archaeological inquiry in the Lower Pecos Canyonlands can be classified into three major periods: The Museum phase of the 1930s, the Amistad Salvage Project, and the University phase. Each period had unique catalysts, but all were drawn to the unsurpassed preservation of the region's dry rockshelters. This section provides an overview of major excavations, key players, and the scientific motivations of each phase. For additional detail regarding the archaeological history of the Lower Pecos, see Turpin (2004) and (Black 2013). Rodriguez (2015) provides a detailed narrative history of archaeological investigations specifically at Mile Canyon. This thesis emphasizes the excavation history of Bonfire Shelter with additional discussion allotted of nearby sites with Paleoindian components and/or Pleistocene fauna.

2.1 *The Museum Phase*

In the 1930s, a flourish of archaeological activity commenced in the Lower Pecos Canyonlands (Black 2013:142-144). Expeditions from the newly established Witte Museum of San Antonio (Davenport 1938; Martin 1933), the Smithsonian (Setzler 1934), the University of Texas (Pearce and Jackson 1933; Taylor 1948, 1949), and several other organizations (Kelley 1932; Mear 1949; Sayles 1935) including privately funded endeavors (Martin and Dorchester 1941), descended on the Lower Pecos seeking the perishable artifacts preserved in the region's ubiquitous dry rockshelters. While no excavations were conducted at Bonfire Shelter, these early expeditions laid the archaeological groundwork to facilitate future excavations in the region.

In 1932, E. B. Sayles and J. Charles Kelley, of the Arizona-based Gila Pueblo Foundation, conducted a reconnaissance of Mile Canyon, mapping the location of Eagle Cave, Kelley Cave, Skiles Shelter, and terrace that would become known as Sayles Adobe (Sayles 1935). Their work at Eagle Cave and Kelley Cave became the first formal excavations conducted in Mile Canyon (Kelley 1932; Rodriguez 2015:19). Based on their findings, Sayles and Kelley expanded upon G.

C. Martin's early chronology of the "Texas Cave Dwellers" (Martin 1932) to include the "Pecos River Focus", characterized by intensive rockshelter occupations with well-preserved perishable artifacts, sotol roasting pits (both in the shelters and on the surrounding uplands), and the unique polychrome rock art panels (Kelley et al. 1940; Sayles 1935; Taylor 1948:75-77; 1949:73-88).

From 1935 to 1936, the Witte Museum returned to Eagle Cave, conducting extensive excavations at Eagle Cave under the supervision of Walter Davenport and Harding Black (Davenport 1938). The team opened expansive trenches bisecting the deepest deposits and extending across the rear shelter wall (Black 2013:142). Davenport provided the earliest stratigraphic documentation of the Mile Canyon shelters, reporting five major zones and intervening layers of exogenic sand (Davenport 1938:23-24). Davenport's main trench was left open following the 1936 excavations and became the starting point for subsequent work in Eagle Cave.

Following Davenport's work at Eagle Cave and the outbreak of World War II, the pace of archaeological inquiry in the Lower Pecos slowed. Several smaller expeditions at Mile Canyon, noted in **Table 2-1**, were conducted in the decades preceding the Amistad operations. Gene Mear's 1949 work at Kelley Cave (Mear 1949) is noteworthy with regard to Paleoindian research in the Lower Pecos. The University of Texas graduate student specifically set out to identify evidence of Pleistocene fauna associated with archaeological material, excavating a series of large units over a week-long period (Nielsen 2017:29; Rodriguez 2015:28). Extending to nearly six feet below surface, no evidence of Pleistocene fauna or Paleoindian material was recovered.

Museum exhibits derived from these expeditions brought the dry shelters of the Lower Pecos Canyonlands into the media spotlight, drawing a host of "relic hunters" and private collectors (Black 2013:143). Collecting intensity varied but was typically correlated with shelter size and accessibility. The archaeological integrity of many of the region's larger rockshelters was compromised (Turpin 1992:10). In many cases, the perishable items and projectile points

from the near-surface deposits placated collectors, leaving the earlier cultural horizons intact (Mear 1949).

Despite the extensive excavations at Mile Canyon in the 1930s and 1940s, no work was conducted at Bonfire Shelter. It is unclear if Bonfire Shelter was known to the early excavators. The shelter does not appear on the 1932 Sayles map (Rodriguez 2015:13) and extensive archival research has not yielded other documentation from this period (Black 2013; Rodriguez 2015). It is possible that Bonfire Shelter was known but not considered an archaeological site due to the paucity of visible artifacts, especially contrasted against the rich assemblages at Eagle Cave and other shelters visited during the Museum phase. The shelter's concealed entrance and relatively remote location may have gone unnoticed by visiting archaeologists and relic hunters alike, sparing Bonfire Shelter from the worst impacts.

Table 2-1. Summary of Relevant Museum Phase Studies

Year	Location	Sites	Investigator	Affiliation	Notes
1932	Seminole Canyon	Fate Bell Shelter	J. Pearce & A. T. Jackson (Pearce and Jackson 1933)	University of Texas	Major excavations at Fate Bell Shelter within modern Seminole Canyon State Park. Documented extensive looting.
1932	Mile Canyon	Eagle Cave, Mile Springs, Kelley Cave, Skiles Shelter, "Sandy Adobe"	E. B. Sayles	Gila Pueblo	Mile Canyon Reconnaissance marking Eagle Cave and Kelley Cave for further excavation.
1932	Mile Canyon	Kelley Cave, Eagle Cave	J. Charles Kelley E. B. Sayles (Kelley 1932; Sayles 1935:63-66)	Gila Pueblo	Exploratory trenches at Eagle Cave and Kelley Cave. Expanded Martin's (1932) chronology of the "Big Bend Basket Makers" to include a "Pecos River Focus" (Martin 1932; Sayles 1935:63-66)
1933	Rio Grande	Shumla Caves	G. C. Martin (Martin 1933)	Witte Museum	
1933	Pecos River	Goat Cave, Moorehead Cave	F. Setzler (Setzler 1934)	Smithsonian	

Table 2-1. Continued

Year	Location	Sites	Investigator	Affiliation	Notes
1935	Mile Canyon	Eagle Cave	J. W. Davenport, H. Black (Davenport 1935; 1938)	Witte Museum	Extensive excavations at Eagle Cave, first stratigraphic documentation. Identified four cultural horizons overlying a culturally sterile zone (Davenport 1938:23-24)
1935	Mile Canyon	Eagle Cave, Kelley Cave, Skiles Shelter	F. Kirkland (Kirkland 1937, 1938, 1939)	Private	Extensive survey and vibrant water-color reproduction of over 200 rock art panels across the Lower Pecos and West Texas. Reported a correlation between Pecos River Style rock art, perishable artifacts and expansive burned rock middens. See also Jackson's (1938) study of Texas rock art, including numerous sites in Val Verde county.
1939-1940	Mile Canyon, Val Verde County	Kelley Cave	G. C. Martin (Martin and Dorchester 1941; Rodriguez 2015:25-27)	Private	Poorly documented excavations across Val Verde County, including Kelley Cave and possibly Skiles Shelter.
1947 - 1948	"Mouth of the Pecos" - Texas and Northern Coahuila	Mile Spring	H. C. Taylor (Taylor 1948, 1949)	University of Texas	Reconnaissance of 48 sites in the vicinity of the Pecos-Rio Grande confluence including excavations at *Skiles Shelter. *Archival work conducted by Rodriguez (2015) determined excavations actually occurred at Mile Spring Shelter, which led to the site's formal documentation in 2012 (Rodriguez et al. 2012).
1949	Mile Canyon	Kelley Cave	G. Mear (Mear 1949; Rodriguez and Black 2017:58)	Texas Memorial Museum	Extensive excavations at Kelley Cave seeking evidence of Pleistocene fauna associated with archaeological material. No Paleoindian deposits identified.

2.2 *The Amistad Phase*

The large-scale development projects of the post-World War II era, including the proposed construction of Amistad International Reservoir, triggered a period of renewed

archaeological activity in Southwestern Texas. The work was contracted through the National Park Service's Interagency Archeological Salvage Program under the Reservoir Salvage Act of 1960 (Story and Bryant 1966:3; Team 2001). Under the direction of Dr. Edward Jelks, the Texas Archeological Salvage Project (TASP) documented 251 archaeological sites in an initial survey of the Diablo Reservoir (subsequently renamed the Amistad International Reservoir) impact zone, 188 of which were located within the United States (Dering 2002:3.15; González Rul 1990). Graham and Davis recommended funding to excavate 32 sites (including 3 large rockshelters, 10 intermediate rockshelters, and 8 small rockshelters) threatened by inundation or increased exposure to looting (Graham and Davis 1958:3). Despite its location above the high-water mark, Bonfire Shelter¹ became a priority of the TASP (Dibble and Lorrain 1968)

The Amistad era excavations emphasized refining regional and site-specific cultural chronologies, implementing the relatively new ¹⁴C radiometric dating technology (Black 2013:144). The excavators defined major stratigraphic units and developed broad models of social organization and subsistence spanning over 10,000 years (Story and Bryant 1966:8-9). Basic paleoenvironmental reconstructions backed by a National Science Foundation grant helped to contextualize the dramatic changes observed over the long cultural sequences (Black 2013:147; Story and Bryant 1966).

Extremely high artifact densities and deep sedimentation combined with a limited timeframe in the face of imminent destruction often forced the archaeologists to make methodological compromises. Excavators passed over lithic debitage and small or disarticulated faunal remains in favor of diagnostic projectile points and articulated megafauna configurations (Dibble and Lorrain 1968:19). The thin laminations that characterize rockshelter deposits were

¹Other large-scale TASP undertakings during this period included excavations at Arenosa Shelter (Dibble 1967), Eagle Cave (Ross 1965), Fate Bell (Story and Bryant 1966), Devil's Mouth (Johnson 1964), Devil's Rockshelter (Story and Bryant 1966), Coontail Spin and Zopilote Cave (Nunley et al 1965), among numerous other sites.

often lumped together, providing limited information regarding variation within these temporal periods (Ross 1965). At Bonfire Shelter, screening was largely restricted to bone-bearing strata while “intermediate horizons” were removed *en masse*, with only cursory inspection (Dibble and Lorrain 1968:18-20).

These compromises facilitated the movement of massive volumes of earth. At Arenosa Shelter, a now inundated site at the confluence of the Pecos River and the Rio Grande, a massive 42 ft (nearly 13 m) profile representing 11,000 years of periodic human occupation was cut deep into the alluvium (Dibble 1967). While much of the earth-moving at Arenosa was aided by heavy machinery, the scale of the excavations is staggering; rappelling equipment was necessary to fully document the exposed faces (Whelan and Black 2008b). The Amistad excavations yielded enormous amounts of data and decades of laboratory analysis, research, and follow-up excavations (Black 2013:148).

The Amistad excavations allowed archaeologists to explore farther into the past than ever before. With the identification of Late Paleoindian projectile points at Bonfire Shelter and Devil’s Mouth, TASP’s excavations were the first to unequivocally confirm the presence of Late Pleistocene hunter-gathers in the Lower Pecos; confirming the speculation of archaeologists and paleontologists dating back to the 1940s and extending the regions cultural history by thousands of years (Chadderdon 1983; Word and Douglas 1970:3). The identification of Late Pleistocene fauna beneath these Paleoindian strata laid the foundation for entirely new research trajectories which the next phase of archaeological inquiry would set out to address.

2.2.1 *Bonfire Shelter and Amistad*

Prior to the Amistad excavations, Lower Pecos expeditions passed over Bonfire Shelter in favor of the rich, easily accessible cultural deposits and enchanting rock art at Eagle Cave and other nearby sites. Bonfire’s entrance is obscured by massive talus debris and brush. Access from the south canyon requires visitors to traverse a narrow “goat trail” less than one-foot wide high on

the canyon's north wall or scramble through a boulder-field periodically rendered impassable by standing water. Access from the north requires the installation of ladders and a vertical scramble from the canyon rim. The logistical challenges of moving people and equipment into the shelter and the limited amount of outwardly visible cultural material left Bonfire Shelter's archaeological deposits largely intact until the Amistad excavations.

The first reports of potentially significant archaeological deposits at Bonfire Shelter surfaced in 1958. As a teenager exploring Bonfire with the Skiles family, Dr. Michael Collins identified substantial quantities of burned bone shallowly buried near the shelter's southern entrance (Black 2001c). Collins brought a sample to Midland Geologist Glen Evans, who identified the specimen as a prehistoric *Bison bison* mandible. Jack Skiles, the owner of the ranch encompassing Mile Canyon, enthusiastically reported the find to University of Texas archaeologists who were in the planning phases of the Amistad project.

In 1962, TASP archaeologist Mark Parsons was dispatched to evaluate sites in the vicinity of Langtry, TX for the allocation of Amistad mitigation resources (Dibble and Lorrain 1968:10). At Bonfire Shelter, Parsons relocated and expanded Collins' pit from four years earlier identifying a Late Archaic Montell projectile point associated with the burned bison bone. He formally recorded Bonfire Shelter (referred to at the time as "Ice Box Cave" and subsequently as "Bone Cave") as archaeological site 41VV218 (Parsons 1962). The possibility of a minimally disturbed Archaic bison-kill moved Ice Box Cave to the TASP priority list; excavations were slated to coincide with major undertakings at Eagle Cave the following fall (Black 2001c).

Concurrent excavations at Bonfire Shelter and Eagle Cave were initiated in 1963. The Bonfire Shelter excavations were conducted under the supervision of David Dibble (Dibble and Lorrain 1968), while Richard Ross and Mark Parsons led the excavations at Eagle Cave (Ross 1965). Dibble earned his BA from the University of Utah in the late 1950s and had extensive experience in large-scale reservoir salvage operations across the American west (Black 2001b).

His work on deeply stratified rockshelters in Utah and Wyoming helped secure him a supervisory position on the Amistad project (Black 2013:146).

In addition to Dibble, the 1963 expedition included a core crew of 10 archaeologists pictured in **Figure 2-1**. Several staff were recruited from nearby Del Rio and Comstock, including the Hinojosa brothers whose family name is inscribed on the shelter wall. Elton Prewitt, a well-known Cultural Resource Management professional and active member of the Texas archaeological community, got his start on Dibble's crew in the Bonfire Shelter trenches (Black 2001b).

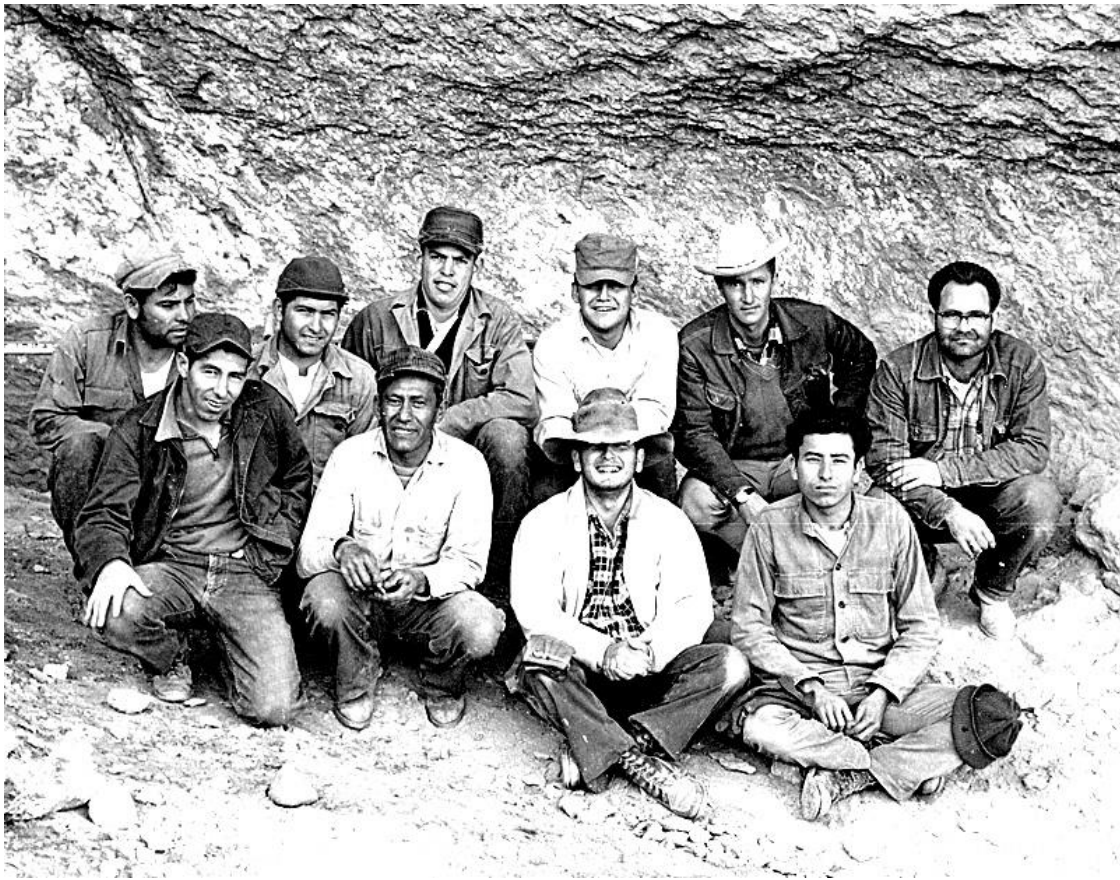


Figure 2-1. The 1963-1964 Bonfire Expedition Crew. Photo courtesy of Texas Beyond History and the Texas Archeological Research Laboratory. Featured in the back row: Emilio Hinojosa, Florencio Hinojosa, Salmoe Cantu, Carlos Guerrero, David Dibble and Bill Harrison; In the front row: Richard Lugo, Reyes Magallanes, Elton Prewitt, and Cosme Hinojosa. https://www.texasbeyondhistory.net/bonfire/images/1963-64_crew.html

2.2.2 *Amistad-Era Stratigraphy*

Excavations at Bonfire Shelter commenced in September 1963 and extended through February 1964. Dibble's excavation units were concentrated in the southern portion of the shelter on the margins of the talus cone. As the extent of the Archaic-aged burned bone horizon (Bone Bed 3) became apparent, additional units were opened to the north extending into the shelter interior. In the fall of 1963, a lanceolate projectile point was recovered from a second, deeply buried *Bison antiquus* bone bed (Bone Bed 2). The find confirmed the presence of a Paleoindian at Bonfire Shelter. That winter, the crew encountered a third bone bed deep in the deposits of the shelter interior: Bone Bed 1.

In five months, the Bonfire team opened 18 excavation units each extending three meters or more into the shelter substrate (Dibble and Lorrain 1968:17-20). Three bone beds and an organic fiber layer were identified. Each bone bed was separated by an ostensibly sterile fill horizon which Dibble referred to as Intermediate zones. **Figure 2-2** illustrates the stratigraphic relationship between these horizons. This profile (view west along the W50 grid-line) spans three excavation blocks from the north face of the talus cone nearly to the shelter mid-point. Unit W40 N100-N120, the rightmost panel in **Figure 2-2**, is the only figure from the 1968 report that captures Bone Bed 1 (Dibble and Lorrain 1968:21). Bone Bed 1 appears to be discontinuous, present only in the deepest portion of the shelter. It has not been identified on the talus cone (Dibble and Lorrain 1968:25).

Dibble describes Bone Bed 1 as a sparse, horizontally bedded cluster of Pleistocene *Bison*, *Camelops*, *Equus*, and *Mammuthus* remains approximately 2.5 m (8 ft) below the modern shelter floor (Dibble and Lorrain 1968:24). From Dibble's profile drawings, Bone Bed 1 appears to be approximately 10 cm (3.94 in) thick. However, narrative descriptions indicate that small clusters of bones and isolated bone fragments were observed up to 1.0 m (3.28 ft) below the

mapped extent of the bone bed. Despite the deposit's thickness, overall faunal densities in Bone Bed 1 were significantly lower than in Bone Beds 2 or 3 (Dibble and Lorrain 1968:30,42).

Most of the Bone Bed 1 faunal remains were recovered from a band of silty brown laminations and dense limestone spall accumulating in a trough-like depression near the center of the shelter (Dibble and Lorrain 1968:28). Dibble suggests that the silts represent localized waterborne deposits lacking sufficient energy to redeposit the large elements. Fractured elements retained rough edges bearing no evidence of the rounding associated with alluvial processes (Fernandez-Jalvo and Andrews 2016:168-177). Large limestone cobbles up to 30.5 cm (1.0 ft) wide were identified across Bone Bed 1 (Dibble and Lorrain 1968:28). At least one cobble was associated with a cluster of fragmentary bone, a pattern observed only in the overlying bone beds.

Excavations continued approximately 1.2 m (3.75 ft) beneath the mapped extent of Bone Bed 1 into Zone 1 (Dibble and Lorrain 1968:21). Dibble describes Zone 1 as a dense accumulation of angular limestone spalls interbedded with a small amount of very fine light gray silty sediment (estimated at <5% of the stratum matrix). The limestone spalls ranged from 2.5 cm (1.0 in) to 30.5 cm (1.0 ft) in diameter. Zone 1 spalls observed in southern excavation units were slightly rounded and associated with an increased proportion of fine-fraction matrix. Dibble attributed the rounding to increased runoff exposure from the canyon rim (Dibble and Lorrain 1968:24). The specific location of isolated bone concentrations attributed to Bone Bed 1 within the spall zone is not described or mapped (Dibble and Lorrain 1968:28).

Zone 2a, a "culturally sterile" stratum similar to Zone 1, directly overlies Bone Bed 1. Zone 2a is an accumulation of light brown silt with abundant relatively small, slightly rounded limestone spall inclusions (Dibble and Lorrain 1968:26). Dibble notes an increased proportion of fine-fraction matrix in Zone 2a compared to Zone 1. He suggests this may be a function of increased exogenic deposition driven by the aridizing climate approaching the end of the Pleistocene (Dibble and Lorrain 1968:27). Zone 2a slopes upward against the eastern shelter wall

to form a “bench”, tapering from nearly 75.0 cm (2.5 ft) thick on the northern slopes of the talus cone to only 10.0 cm (3.90 in) thick in the central shelter where it forms the contact plane between Bone Beds 1 and 2 (Dibble and Lorrain 1968:24).

Excavations terminated among a series of massive boulders uncovered in the deepest portions of Zone 1 (Dibble and Lorrain 1968:27). The boulders proved impassable and true bedrock was never reached, in part due to the time and funding constraints of the Amistad operations. Dibble left the deepest excavation units open with the hope that future archaeologists would return to evaluate the oldest deposits at Bonfire Shelter.

Despite the absence of lithic artifacts, Dibble cautiously suggests that humans contributed to the accumulation of Bone Bed 1 (Dibble and Lorrain 1968:28). The shattered bone fragments and trace charcoal associated with large limestone “anvils” bore a striking similarity to distributions observed in Bone Beds 2 and 3 (Dibble and Lorrain 1968:30, 32, 48). No taphonomic processes or depositional agents that might account for the features could be identified (1968:28). The charcoal and organic material observed in Bone Bed 1 proved to be insufficient for the radiocarbon dating technologies of the 1960s. However, the superposition of Pleistocene fauna beneath the Folsom and Plainview-aged Bone Bed 2 suggested that Bone Bed 1 was very old (Dibble and Lorrain 1968:20). In the 1960s, Clovis-first was archaeological dogma. Dibble was very cautious in describing the oldest Bonfire deposits, but subtly implied that they may be older than Clovis (Dibble and Lorrain 1968:24-28).

2.2.3 *Amistad Chronology*

The Amistad Salvage Project marked the first widespread application of radiocarbon dating in the Lower Pecos (Black 2013:144). Ten viable dates, presented in **Table 2-2**, were recovered during the 1963-1964 Bonfire Shelter expedition (Dibble and Lorrain 1968:50-51). These dates were published prior to the development of modern calibration curves and fractionation correction (Taylor and Bar-Yosef 2014:155-157). The ranges presented here were

calibrated using OxCal v.4.3 against the modern IntCal13 curve to facilitate comparison with later Bonfire Shelter dates and against other sites.

Despite the vast quantity of bone recovered, most specimens were not included in the Bonfire Shelter radiocarbon series. Dates from bone processed in the early decades of radiocarbon dating are generally considered unreliable due to unaccounted for contaminants in the inorganic fraction (Dibble and Lorrain 1968:33; Taylor and Bar-Yosef 2014:75). Only two charred bone specimens from Bone Bed 3 (TX-46 and TX-47) contribute to the published Bonfire Shelter chronology (Dibble and Lorrain 1968:50; Tamers et al. 1964). These dates were recovered from an otherwise well-dated provenience and could be crosschecked against other samples. The contamination problem associated with bone dating was documented even in the 1960s. 13 additional Bonfire Shelter bone samples recovered from Bone Bed 2 were utilized in a study developing effective pretreatment methods for archaeological bone specimens (Tamers and Pearson 1965).

Table 2-2. 1963-1964 Bonfire Shelter Radiocarbon Dates

Sample ID	Stratum	RCYBP	Deviation (+/-)	Cal Median Probability	Cal BP (2σ)	Material
TX-151	Fiber Layer, Hearth 7	1,400	130	1,298	AD 406-894; AD 925-936	Charcoal
TX-194	Fiber Layer, Hearth 6	1,690	80	1,578	AD 132-541	Charcoal
TX-046	Bone Bed 3	2,310	210	-	-	Burned Bone
TX-047	Bone Bed 3	2,810	110	-	-	Burned Bone
TX-106	Bone Bed 3	2,780	110	1,221-788 BC; 1,260-1,229 BC	2,867	Charcoal
TX-131	Bone Bed 3	2,510	100	833-392 BC	2,680	Charcoal
TX-152	Intermediate Zone, Hearth 2	7,240	220	6,472-5,710 BC; 5,680-5,671 BC	8,066	Charcoal
TX-153	Bone Bed 2, Hearth 1	10,230	160	11,398-12,565	12,006	Charcoal
TX-657*	Bone Bed 2, Hearth 1	9,920	150	11,010-12,088	11,516	Charcoal
TX-658*	Bone Bed 2, Hearth 1	10,100	300	10,860-12,705	11,805	Charcoal
Table derived from Dibble and Lorrain (1968:50) and Dibble (1970)*						
Dates initially published in <i>Radiocarbon</i> : Tamers et al. (1964) and Pearson et al. (1965)						

BONFIRE SHELTER

41 VV 218

NORTH-SOUTH PROFILE ALONG WEST 50

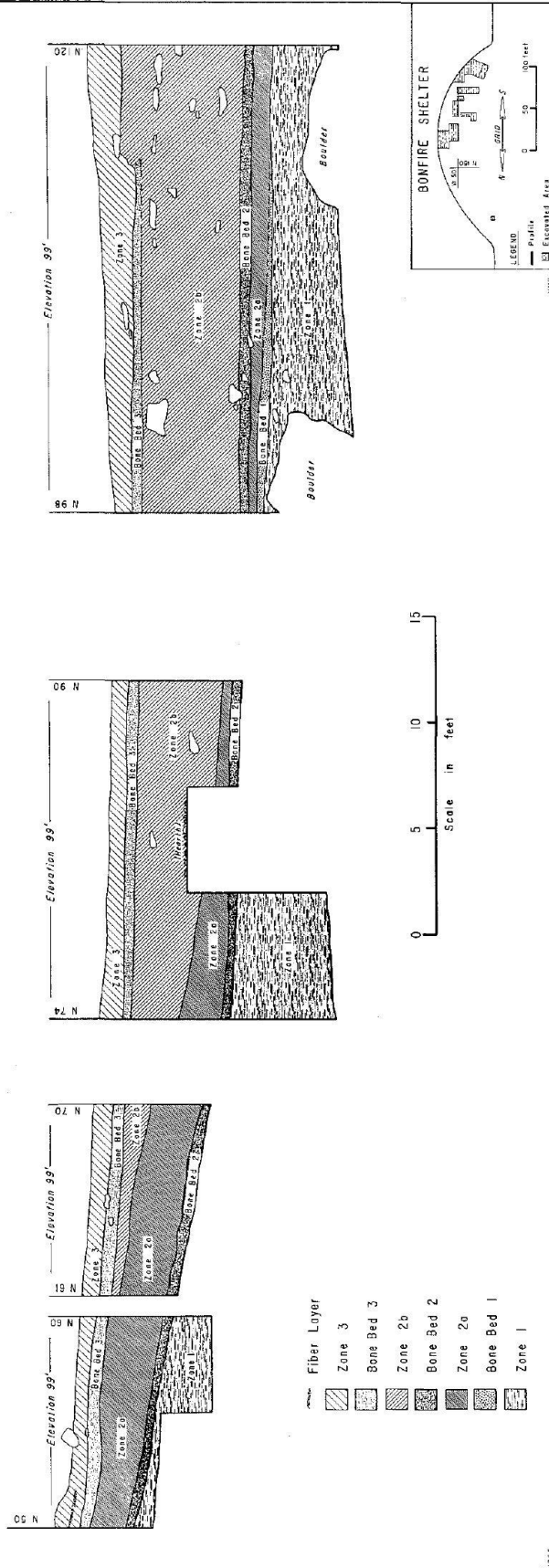


Figure 2-2. 1963-1964 illustration of main north-south profile (W50) at Bonfire Shelter extending from the north face of the talus cone to the middle of the shelter. Note that Bone Bed 1 was only observed in the northern-most excavation block. Reproduced here from Dibble and Lorrain (1968:21).

2.2.4 *A Sign of the Times*

As noted above, the Amistad era methodologies were primarily designed to resolve the cultural chronology of the Lower Pecos. (Black 2013:144). Excavated fill from the bone beds was selectively screen through ¼” or ½” mesh. Fill from the intermittent zones was generally not processed (Dibble and Lorrain 1968:20). However, excavations proceeded with enough caution for the crew to document several hearth features between the bone beds, suggesting Bonfire Shelter was at least intermittently exploited between major kill events (Dibble and Lorrain 1968:40). Photography and mapping was similarly limited due to their low yield of “archeologically useful information” (Dibble and Lorrain 1968:19-20). As such, the lithic and faunal assemblages and documentation heavily biased temporally diagnostic projectile points, stone tools, and articulated remains.

Charcoal and bone specimens collected for radiocarbon dating were a mixed success. The viable charcoal samples often yielded deviations exceeding modern error tolerances (McCuiestion 2019:84-87). The recovery of datable material and diagnostic artifacts (in the case of Bone Bed 1) from the deeper strata at Bonfire Shelter was limited (Dibble and Lorrain 1968:28,33,40) restricting chronological interpretations to relative stratigraphic position. As noted above, accurate methods for dating bone had not yet been developed (Tamers and Pearson 1965). Bulk soil and palynological samples were collected from each context, but with limited provenience control. Despite these shortfalls, the environmental record and radiocarbon data from Bonfire Shelter was essential to constructing the cultural chronology and paleoecology of Lower Pecos (Bryant 1969; Bryant and Holloway 1985; Lorrain 1965, 1966; Story and Bryant 1966).

Dibble’s bone bed interpretations have not been without criticism. The rounded limestone blocks (examples from Bone Beds 2 and 3 are illustrated in **Figure 2-3** and **Figure 2-4** below) identified among shattered Bone Bed 1 fauna were cited as evidence of human activity (Dibble and Lorrain 1968:28). The assertion is based on the repetition of this pattern in the definitively

cultural Bone Beds 2 and 3 and its conspicuous absence from the intermediate zones. Dibble's correlation has been interpreted as a false equivalence (Meltzer et al. 2007). The events of one period cannot be assumed to influence past or future events, especially where other variables are not held constant across strata. The intermediate zones lack the faunal densities observed in the bone beds and depositional circumstances appear to vary greatly over time. The environmental conditions that sustained the unique animal (and human, in the case of Bone Beds 2 and 3) populations during the bone bed periods cannot be ruled out as a block-source. Inconsistent excavation methodologies and implied biases further inhibit direct comparisons between strata; even Dibble's sterile zones yielded artifacts and features negating the perceived relationship of cobbles and humans (Dibble and Lorrain 1968:40-42).

Unfortunately, the limestone blocks in question were only illustrated in Bone Bed 2 (Dibble and Lorrain 1968:24, Figure 13) and Bone Bed 3 (Dibble and Lorrain 1968:43, Figure 18). The photographs are reproduced in **Figure 2-3** and **Figure 2-4** (Dibble and Lorrain 1968:24, 43). No photographs or plan maps illustrating the continuation of this pattern, or spatial patterning of any kind, in Bone Bed 1 were published in 1968.

Bone Bed 1 remained ambiguous despite Dibble's confident interpretations of Bone Beds 2 and 3. Limited time and funding prevented a thorough evaluation of the deposits. Lack of lithic artifacts in the deposits left faunal evidence equivocal. Broader questions regarding the role of Bonfire Shelter in early Paleoindian subsistence strategies remained unuttered due to the uncertainty surrounding Bone Bed 1.



Fig. 13. Vertical view of top of Bone Bed 2 as uncovered in portions of Squares N50 W50 and N50 W60. Note general disarticulation of bones and association with large limestone boulders. Scale is 1.5 feet in length.

Figure 2-3. 1963-1964 planview exposure of Bone Bed 2 (Units N50 W50 and N50 W60) illustrating the relationship between the large limestone blocks and disarticulated bison remains. Figure reproduced from (Dibble and Lorrain 1968:24)



a



b

Fig. 18. Views of Bone Bed 3. (a) Closeups of section of bone layer as it appeared in profile of north wall of Square N50 W70. Note closely packed, burned, and fragmented nature of bone and association of large limestone spalls. Tape drawn out to one foot. (b) Excavating to top of Bone Bed 3 in Square N80 W42. In this area the deposit was thin and unburned.

Figure 2-4. 1963-1964 Bone Bed 3 excavation (Unit N80 W42, b) and profile (Unit N50 W70, a) illustrating the repeated pattern of large limestone blocks among disarticulated faunal remains within cultural strata. Figure reproduced from (Dibble and Lorrain 1968:43)

2.3 *The University Phase*

A relative lull in archaeological activity fell over the Lower Pecos following the Amistad Salvage excavations at Bonfire Shelter and Eagle Cave as data was processed and collections were analyzed. TASP, rebranded as the Texas Archeological Survey (TAS), leadership turned their attention to sites across the region that were not threatened by the imminent construction of the reservoir (Story 2010). Dibble became the organization's director in 1970s after earning his Ph.D at Washington State University publishing his dissertation on the Amistad work at Bonfire Shelter (Black 2001b; Dibble 1975). Under Dibble, TAS affiliated archaeologists carried out Cultural Resource Management contracts across Texas.

The Center for Archaeological Research (CAR-UTSA) was founded at the University of Texas at San Antonio in 1974 (Hester 2010). The center's mission included public outreach, training new archaeologists, connecting citizens and agencies to archaeological resources, and conducting state and federally mandated archaeological investigations. Thomas Hester, the CAR's first director, supervised excavations at Baker Cave, Val Verde County beginning in the summer of 1976 (Chadderdon 1983; Shafer and Bryant Jr 1977). Located along a tributary of the Devils River, this follow up to the intermittent excavations of the 1960s yielded additional evidence supporting a diverse Late Paleoindian presence in the Lower Pecos (Word and Douglas 1970).

In 1975 and 1976, Harry Shafer and Vaughn Bryant supervised Texas A&M University's extensive excavations at Hinds Cave; a dry rockshelter on a narrow box canyon tributary to the Pecos River (Dering 1979; Shafer and Bryant Jr. 1977, 1988). The excavations yielded abundant perishable artifacts and a detailed paleoenvironmental record. Samples from Hinds Cave and Bonfire Shelter (among other sites) contributed significant data to Bryant and Holloway's 1985 synthesis of the Southwest Texas Post-Glacial environment (Bryant and Holloway 1985:56-58). The Hinds Cave assemblage continues to yield valuable insight into paleoethnobotany and human

ecology of the Lower Pecos well into the 21st century (Dean 2006). The excavations at Hinds Cave and Baker Cave highlight a significant methodological shift from the Amistad-era. Emphasis shifted from chronology to more nuanced questions of human interaction with a changing landscape. Without the pressured impoundment timeline, excavations could proceed in a more controlled manner (Black 2013:147-148).

In the early 1980s, Solveig Turpin, Dibble's successor at TAS, conducted several archaeological surveys and data recovery projects in the Lower Pecos (Black 2001b). Turpin and a team of TAS archaeologists surveyed over 2,100 acres acquired by the Texas Parks and Wildlife Department for the development of Seminole Canyon State Historic Park (Turpin 1982). The survey included the first systematic survey of Lower Pecos rock art since the Jackson and Kirkland expeditions of the 1930s. Excavations at Seminole Sink, a 7.0 m (23.0 ft) deep vertical shaft cave within the proposed park boundary, provided unique insight into the social organization and mortuary practices of the Archaic Lower Pecos after the remains of at least 22 individuals were identified in the cavern depths (Turpin et al. 1988).

2.3.1 *The University Phase at Bonfire Shelter*

In 1983-1984, Turpin led the second major excavation at Bonfire Shelter, supported by grants from The Potts and Sibley Foundation (Midland, TX), The University of Texas at Austin, the Wenner-Gren Foundation for Anthropological Research, and The Moody Foundation (Galveston, TX) (Bement 1986a:ii). The expedition's primary objectives included gathering additional data resolving the nature of Bone Bed 1 and ultimately reaching bedrock. The excavations expounded upon Dibble's stratigraphic and chronological framework while collecting a wealth of additional zooarchaeological, paleoenvironmental, and chronometric data (Bement 1986a, 1986b). Turpin's operation introduced new technologies and increasingly modern methods at Bonfire Shelter. Systematic column samples, advances in radiocarbon dating, and more controlled excavation techniques significantly increased the resolution of their findings.

The archaeologists further increased their capacity by engineering an elaborate system of scaffolding, mine carts, cranes, water works, and generators facilitated round-the-clock excavations and sediment processing (Black 2001c).

The 1963-1964 site datum was reestablished using a metric coordinate system and a 4.0 x 3.0 m (13.12 x 9.84 ft) excavation block was opened immediately north of Dibble's deep pit (Bement 1986a:5-6). Illustrated in **Figure 2-5**, six strata (D – I) were defined beneath Dibble's Bone Bed 2 (Strata A, B, and C), encompassing Zone 2a, Bone Bed 1, and Zone 1 before excavation was again impeded by large impenetrable boulders (Bement 1986a:8,19-22). Several column samples were excavated around the block's perimeter for subsequent paleoenvironmental (Bement 1986a:4).

Strata A, B, and C are correlated with Dibble's Late Paleoindian *Bison antiquus* kill horizon, Bone Bed 2. These strata appear to be consistent with Dibble's three Bone Bed 2 sub-strata documented on the southern slopes of the talus cone, which he interpreted as three kill events (Dibble and Lorrain 1968:30). Regardless of subsequent debate regarding the number of associated events and specific bone bed taphonomy (Byerly et al. 2005; Byerly, Meltzer, et al. 2007), the strata are traceable across all excavated portions of the shelter and serve as valuable stratigraphic markers. Stratum D corresponds with Dibble's Zone 2a: an intermediate, culturally sterile horizon stratigraphically separating Bone Beds 1 and 2 (Dibble and Lorrain 1968:26). The bone-bearing units beneath Stratum D classify the "sparse bone fragments" Dibble observed within Zone 1, the intermediate horizon beneath the formally mapped extent of Bone Bed 1 (Bement 1986a:20; Dibble and Lorrain 1968:24).

Stratum E, F, and G reflect arbitrary subdivisions within a massive deposit of brown silty clay (Bement 1986a:6). For the purposes of this thesis, these strata will generally be referenced as a single unit: Stratum E/F/G. Stratum E/F/G contained primarily Pleistocene *Bison*, *Camelops*, *Equus*, and *Mammuthus* leg skeletal elements (Bement 1986a:33-38). The bones were largely

fragmentary and clustered around a series of large limestone blocks. Bement argues that the blocks served as anvil stones for processing the bone, noting helical fractures sometimes associated marrow extraction on several specimens. Other *Camelops* specimens exhibited use-wear and surface polish, which Bement suggests reflect use as expedient tools (Bement 1986a:36). Geologically, Bement describes Stratum E/F/G as complex, composite, undulating, and variably thick suggesting depositional instability and turbulence (Bement 1986a:20).

Trace charcoal collected from the Stratum H-1 yielded a radiocarbon date of 12,460±490 BP (AA344). Prior to 2019, this date represented the only chronometric reference point available for any Bone Bed 1 strata. In addition to being unverified, the date was derived from charcoal grains collected from across the stratum, contributing to the very large standard deviation (Bement 1986a:54). New radiocarbon dates recovered during the 2017-2018 excavations are presented in **Section 7.5**, verifying the 1983-1984 age of Stratum H-1. No further Bone Bed 1 dates were recovered in the 1980s. However, the *Capromeryx* observed in Stratum H-2 is generally diagnostic to the Late Pleistocene; consistent with the Stratum H-1 assay (Bement 1986b:11).

Very limited information regarding the nature of the two Stratum H subdivisions, illustrated in **Figure 2-5**, was reported. Stratum H-2 is geologically distinguishable from Stratum H-1 by increasing spall size and density (Bement 1986a:22) and a dramatic shift in the faunal assemblage from large megafauna to isolated *Capromeryx* mandible fragments (Bement 1986b:58). No information beyond stratigraphic position was reported for Stratum H-3.

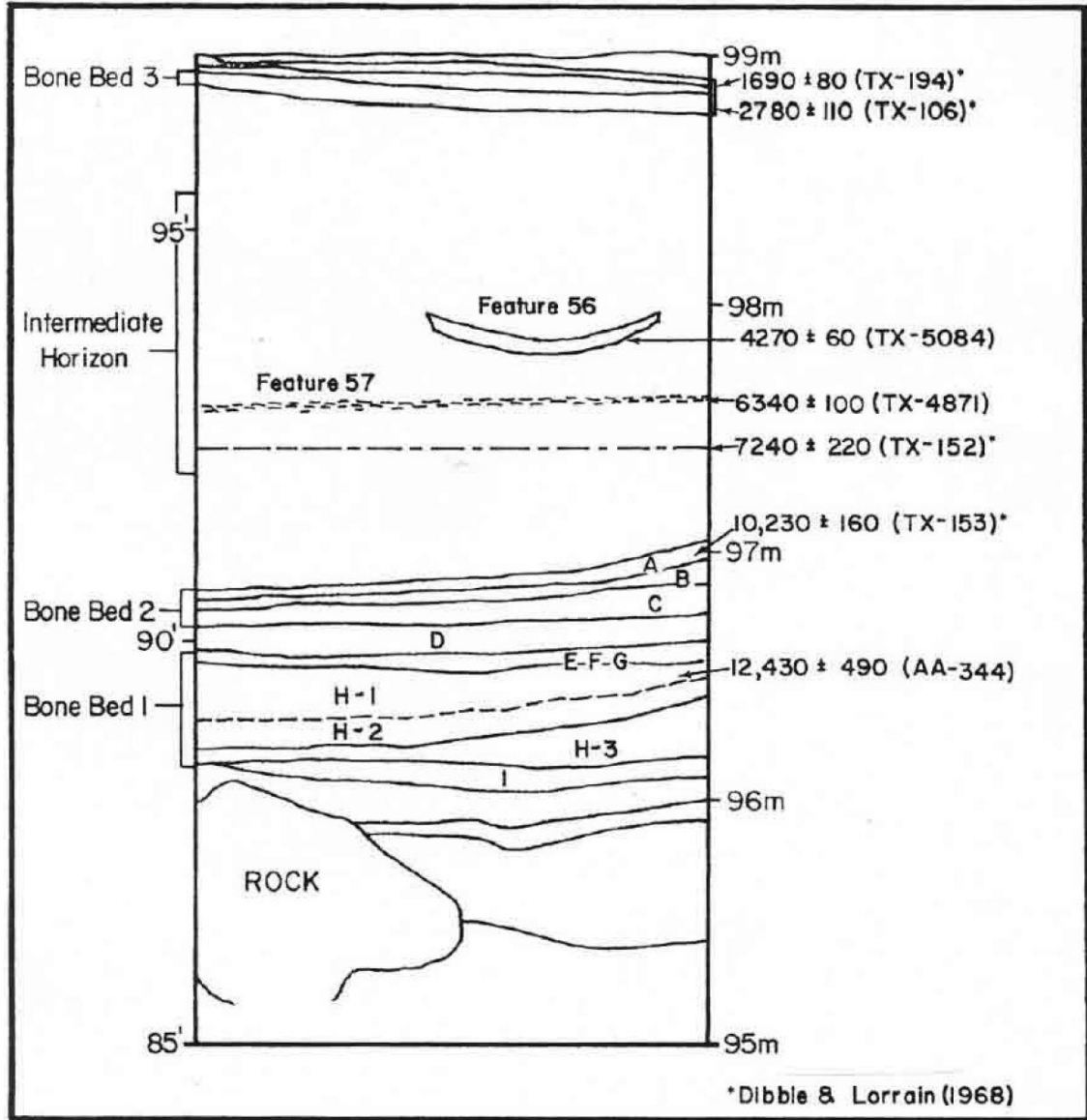


Figure 2-5. Bement's 1983-1984 profile of record: Northernmost face of the main excavation block at Bonfire Shelter. Figure reproduced from (Bement 1986a)

Bison hindquarter elements, horse mandibles, and horse vertebra were recovered from Stratum I (Bement 1986a:55-59). The remains were identified in close association with large limestone boulders, which dominate the stratum. Numerous V-shaped incisions were observed on multiple bison elements, evocative of lithic tool cut-marks incurred during butchering. Based on patterns observed elsewhere in the shelter, Bement argues that the initial disarticulation of the bison and horse was cultural. Subsequent skeletal scattering was likely the result of carnivore

scavenging activity likely attributable to *Homotherium*. Puncture marks consistent with the conical canines of this “scimitar-toothed” Pleistocene cat were observed on mammoth elements recovered from Stratum H-1. Further evidence of carnivore activity in Stratum I and the other Bone Bed 1 deposits is incidental; no predator remains were observed in the assemblage (Bement 1986a:51-54, 55-59).

The 1983-1984 expedition successfully evaluated and radiometrically dated the deepest deposits at Bonfire Shelter. Bement’s analysis is a detailed follow-up study to Dibble’s initial cultural assessment of Bone Bed 1, adding to the potential human modifications in the faunal assemblage. Despite this, every cut mark or distribution pattern documented in Bone Bed 1 could be accounted for by an equally plausible environmental scenario. No unambiguous cultural material that was recovered from Bone Bed 1. The geoarchaeological component of this thesis evaluates the environmental processes contributing to these strata and their implications for faunal taphonomy described by Dibble and Bement.

Notably, Bone Bed 2 also yielded no new artifacts during the excavation. While not conclusive by any means, this pattern opens the possibility that the 1983-1984 excavation methods may have overlooked some category of evidence. Even during the 1960s, it was clear that artifact distributions varied across the site with higher densities recovered near the talus cone (insufficient screening methods notwithstanding). Based on this information, the potential for artifact recovery in unexcavated portions of Bone Bed 1 cannot be ruled out. Especially so if the deposits extend into unevaluated portions of the shelter. The microartifact sampling strategy implement in this thesis aims to test the possibility that <6.35 mm (0.25 in) artifacts were systematically excluded from analysis by comparing samples from Bone Bed 1, Bone Bed 2, and Zone 2a.

Several problems remain outstanding in addition to the absence of artifacts from Bone Bed 1. Many of the original documents related to the Bonfire Shelter expeditions are missing or

otherwise not available from the TARL archives. David Robinson, a member of the 1983-1984 Bonfire team, located several original profile maps during the background research phase of this thesis. Detailed plan maps illustrating Bone Bed organization have not been found. Original maps from the 1963-1964 excavations are also unavailable at TARL and could not be located. Plan maps published in Bement's reports (Bement 1986a, 1986b) are simplified, only including centroid points for the elements identified in each stratum. Without size, orientation, and similar metrics it is difficult to draw independent conclusions regarding the distribution of faunal remains.

Each major excavation at Bonfire Shelter has implemented a new mapping coordinate system. The 1963-1964 expedition described locations in terms of northing and easting feet. The 1983-1984 expedition implemented a system of northing and westing meters. Current excavations at Bonfire Shelter utilize a canyon-wide mapping system ultimately tied to UTM coordinates. Matters are further complicated by the inconsistent application of old and new stratum designations, variable stratigraphic resolution, and missing primary documents. Directly comparing spatial data across projects becomes a cumbersome process.

Despite careful bone bed excavation in the 1980s, the "culturally sterile" levels identified in the 1960s (where extremely limited screening was employed) were excavated in bulk. The excavated sediments were used as fill for slumping units (Bement 1986a:4). Bement reports that the absence of cultural material from these levels was "reaffirmed", but the methods used to sample or otherwise verify this assertion are unclear from published accounts.

While radiocarbon technology had improved since the Amistad excavations, dating the Pleistocene strata at Bonfire Shelter continued to be problematic. One viable sample was recovered during the extensive Bone Bed 1 excavations in the 1980s, yielding a date of $12,460 \pm 490$ RCYBP (AA-344) (Bement 1986a:9). The date was based on "charcoal flecks" collected from the matrix surrounding Stratum H-1 faunal remains. A communication between

Turpin and the University of Arizona Department of Physics radiocarbon lab processing the samples indicates that two additional samples from Bone Bed 1 were submitted for analysis but did not survive pretreatment (Jull 1983). The previously unverified date and large deviation did not fully satiate questions regarding the range of dates represented in the newly identified Bone Bed 1 strata or the potential that AA-344 was an outlier. Modern AMS pretreatment techniques yield high precision dates from milligram quantities of carbon (Taylor and Bar-Yosef 2014:121). Combined with advances in bone collagen purification (Sealy et al. 2014; Taylor and Bar-Yosef 2014:77-82), viable alternatives have emerged to date sites with a paucity of traditionally assayed materials, including Bone Bed 1.

2.3.2 *Results of the University Phase*

Turpin aggregated data from the extensive surveys and large-scale excavations of the Amistad and University eras to develop a five-phase cultural sequence of the Lower Pecos (Turpin and Bement 1988). Bonfire Shelter's relatively well-dated, undisturbed, and continuous 12,000+ year depositional sequence became the cornerstone of this chronology. Unifying paleoenvironmental records with clearly defined diagnostic artifact horizons, Turpin's chronology became a stable comparative benchmark for contextualizing incomplete or chaotic sequences from other regional sites.

The chronology has since been updated, integrating data from the burgeoning Lower Pecos archaeological revival of the early 21st century (Turpin 2004). Summarized in **Table 2-3**, Turpin's model integrates over 300 radiocarbon dates from across the region. The oldest cultural horizons, the *Aurora Phase* (14,500 – 11,900 RCYBP) and the *Bonfire Phase* (10,700 – 9,800 RCYBP), are primarily based on the 1963-1964 and 1983-1984 excavations at Bonfire Shelter.

The Aurora Phase is characterized by the presence of extinct Pleistocene fauna, burned and fragmented bone, and a conspicuous absence of stone tools (Turpin 2004:268-269). The culturally ambiguous spiral-fractures and possible improvised bone tools of Bone Bed 1 at

Bonfire Shelter provide the best example of this poorly defined period. Diagnostic fauna and rounded cobble associations attributable to Aurora Phase strata were also documented at Cueva Quebrada and Arenosa Shelter (described above) (Dibble 1967; Lundelius 1984). Like Bone Bed 1, the complicity of humans has not been firmly established in these deposits. The limited number of radiocarbon dates associated with the Aurora Phase overlap with the earliest dates for Clovis and Earlier than Clovis components elsewhere in North America (Haynes 2015). Aurora Phase sites can generally be attributed to the very early Paleoindian period.

The Bonfire Phase is defined almost exclusively by Bone Bed 2 at Bonfire Shelter (Turpin 2004:269). Radiocarbon dates associated with Plainview and Folsom projectile points place the Bonfire Phase in the early to middle portions of the Late Pleistocene Paleoindian period (Bousman et al. 2004:16). Smaller accumulations of *Bison antiquus* were identified in the deep deposits at Cueva Quebrada and Arenosa Shelter (Dibble 1967; Lundelius 1984; Whelan and Black 2008a).

The Oriente Phase marks a shift in environmental conditions and subsistence behavior in the Terminal Pleistocene and Early Holocene (Turpin 2004:269). The adaptations manifest in lithic technology as Golondrina and Angostura projectile points, as identified at the Devil's Mouth site (Johnson 1964). The Oriente Phase is typically associated with the Late Paleoindian period and is not represented at Bonfire Shelter.

Table 2-3. Cultural Chronology of the Lower Pecos.
 Recreated after Turpin 2004:268.

Cultural Chronology of the Lower Pecos (2004)		
Period	Sub-Phase	RCYBP
Historic	Historic	350-1
Late Prehistoric	Infierno	450-250
	Flecha	1,320-450
Late Archaic	Blue Hills	2,300-1,300
	Flanders	2,300-?
	Cibola	3,150-2,300
Middle Archaic	San Felipe	4,100-3,200
	Eagle Nest	5,500-4,100
Early Archaic	Viejo	8,900-5,500
Late Paleoindian	Oriente	9,400-8,800
Paleoindian	Bonfire	10,700-9,800
	Aurora	14,500-11,900

2.4 21st Century Revival

The pace of excavation slowed in the 1990s through the first decade of the 21st century, but the stage was being set for a resurgence of non-profit and university-backed undertakings. In 1991, Turpin and Jim Zintgraff established the Rock Art Foundation (RAF) at the Witte Museum, San Antonio. The RAF continues to document and preserve the perpetually deteriorating pictographs of the Lower Pecos (Boyd and Cox 2016c:3). Decades of intensive excavation combined with the ongoing rock art studies led to new theories on the culture and ideology of the Archaic Lower Pecos (Boyd 1996, 2003; Boyd and Dering 1996; Turpin 1990, 1992, 1994b, 1996, 2004; Turpin et al. 1986).

In 1998, Dr. Carolyn Boyd founded the Shumla Archaeological Research and Education Center (SHUMLA (Boyd and Cox 2016a:9). The non-profit, based in Comstock, TX, is

committed to documenting and interpreting the rock art of the Lower Pecos, conducting extensive outreach campaigns raising public awareness and accessibility. In addition to developing state-of-the-art photographic and chemical analytical methods, Shumla integrates the ethnohistories of the Huichol and other indigenous populations to develop compelling narrative interpretations of the region's rock art panels (Boyd 2003; Boyd and Cox 2016c). Shumla's establishment marks the start of the contemporary period of archaeological research in the Lower Pecos.

2.4.1 *Prewitt's Stabilization*

In the early 1990s, Elton Prewitt, a member of Dibble's original 1963-1964 Bonfire team, returned to Bonfire Shelter to mitigate significant erosion to the talus cone and damage to Bone Bed 3 (Black 2001c). The measures, partially funded by the Texas Archeological Society, included a base layer of burlap overlaid with plastic safety fencing staked to the surface of the cone to diffuse run-off from the canyon rim. This procedure slowed damage and temporarily stabilized the underlying deposits. In the 30 intervening years, the burlap and fencing have nearly disintegrated or had become dislodged leaving the densest portions of the bone beds exposed and susceptible to erosion (Prewitt 2007:157).

Unfortunately, the measures did not address the significant damage to the main block, which had remained opened since Dibble's work in the 1960s. Meters-long sections of intact deposits had collapsed along the western wall, precariously suspending enormous boulders over any would-be visitor's head. Column samples cut into other profiles functioned as rain chutes, funneling water into the main block and further incising the profiles. These adverse effects in the shelter interior posed a clear and present danger for Bone Beds 1 and 2, which lose archaeological context and structural integrity with every passing year. Despite this, Prewitt's stabilization efforts laid the groundwork for more permanent conservation efforts.

2.4.2 *Southern Methodist University*

From 2003 to 2005, a team of SMU archaeologists headed by David Meltzer returned to Bonfire Shelter (Byerly et al. 2005; Byerly, Meltzer, et al. 2007). Their work was designed to test alternative hypotheses regarding the nature of Bone Bed 2. Specifically, Lewis Binford's 1978 assertion that Bone Bed 2 represented a secondary processing locus rather than the jump-kill originally argued by Dibble in 1968 (Binford 1978b:475; Dibble and Lorrain 1968).

As alluded to in **Section 1.2.4**, Meltzer's team did not specifically test Bone Bed 1. Turpin and Bement's work in the 1980s failed to yield unambiguous evidence supporting human intervention in Bone Bed 1. Reviews of the growing number of potentially Older than Clovis sites in North America published in the 1990s and early 2000s excluded Bone Bed 1 on the basis of equivocal faunal evidence, lack of stone tools, and limited radiometric verification (Grayson and Meltzer 2002, 2015; Wyckoff 1999:349). The SMU team concluded that further work on Bone Bed 1 would likely yield results redundant with Dibble and Bement (Byerly et al. 2005:595). Instead, they concentrated their efforts on Bone Bed 2, where little new work had been conducted since the Amistad era². However, their experimental design yields several important insights relevant to Bone Bed 1.

Ryan Byerly, a SMU graduate student and primary author of the 2005 and 2007 Bonfire articles (Byerly, Cooper, et al. 2007; Byerly et al. 2005), employed a three-pronged experimental approach to evaluate Bone Bed 2. The study included a GIS suitability model to identify potential bison drive-lines on the Mile Canyon uplands, a detailed analysis of the Bonfire Shelter faunal

² Paleoenvironmental studies were conducted during the intervening years utilizing samples derived from the 1960s and 1980s excavations (Bryant and Holloway 1985; Robinson 1997; Scott-Cummings 1992). While the studies included overviews of the *Bonfire Phase* strata, Bone Bed 2 was not the primary focus of the research. Similarly, Bement's work in the 1980s included data from Bone Bed 2, but his research questions squarely targeted Bone Bed 1.

assemblage held in trust at TARL, and limited sampling of the Amistad-period spoil piles to evaluate excavator sampling biases.

Dibble explicitly states in the original Bonfire report that screening methods were implemented in an ad hoc manner (Dibble and Lorrain 1968:19-20); intermediate “culturally sterile” zones received little attention and only the more robust faunal elements were stable enough to extract for Lorrain’s analysis. To quantify excavator bias and determine if a significant number of artifacts were overlooked, the SMU team excavated a series of auger probes and small test pits into Dibble’s spoil piles along the rear wall of the shelter. The fill was then screened through 1/16th inch hardware cloth. The probes yielded five pieces of unmodified debitage in just over one cubic meter of excavated sediment. Because of the sediment’s unknown provenience, the expected Amistad artifact density was calculated by estimating the total volume of all excavated strata divided by the total number of unmodified flakes recovered from all strata (Byerly, Meltzer, et al. 2007).

The spoil sample contained a significantly higher artifact frequency per 1 m³ than reported in 1968, suggesting that a large number of artifacts were overlooked (Byerly, Meltzer, et al. 2007:128-130). With a sample size slightly more than 1 m³, the results may not be statistically robust. However, they provide proof of concept, confirming that biases capable of skewing site interpretations are at play in both the lithic and faunal assemblages. These effects are reinforced with Byerly’s observation that all five of the spoil-pile flakes were large enough to be recovered on Dibble’s ¼ in (if not ½ in) screens (Byerly et al. 2005:624).

Byerly’s findings in the spoil pile study are directly applicable to Bone Bed 1. The SMU team notes that artifact densities observed in the spoil piles cannot be directly extrapolated across the site nor can they be expected to occur in a normally distributed manner (Byerly, Cooper, et al. 2007:129). The presence of debitage in ostensibly evaluated sediments indicates that notable quantities of artifacts from some portion of the shelter were overlooked. Bement’s work in the

1980s yielded no lithic artifacts (from the definitively cultural Bone Bed 2 or otherwise) despite their intensive flotation and waterscreening procedures (Bement 1986a). Further study is needed to evaluate the impact of selection bias on a stratum by stratum basis. The methods described in **Chapter 5** were designed to facilitate artifact recovery particularly in size classes that may have eluded previous excavators. Field and lab workflows included intensive screening of all sediment excavated from Bone Bed 1 (up to 3.2 mm [0.125 in]) and microartifact sampling (up to 1.0 mm [0.04 in]).

The other components of Byerly's study yielded seemingly contradictory findings. The least-cost path spatial analysis identified several routes terminating at Bonfire Shelter that could serve as efficient bison drivelines to Mile Canyon. The routes had topography reminiscent of the well known Northern Plains bison jumps at Head-Smashed-In (Reeves 1978) and Big-Goose-Creek ((Byerly et al. 2005:600; Frison 1991). The faunal reanalysis identified a bias for heavily disarticulated, high-yield bison sections with a high proportion of long bone green-breaks. Byerly argued that the Bone Bed 2 assemblage represents a secondary processing site rather than a primary kill locus, consistent with Lewis Binford's 1978 hypothesis (Binford 1978b:475-476; Byerly, Meltzer, et al. 2007:126-127, 135-142).

Byerly's 2005 and 2007 publications elicited strong responses from Bement and Prewitt, both of whom worked extensively at Bonfire Shelter and supported Dibble's Bone Bed 2 jump-kill hypothesis. For the full exchange, see Bement (2007), Byerly, Cooper, et al. (2007), and Prewitt (2007). Key arguments from the exchange are summarized below.

Bement asserts that Byerly had conflated site-type with butchering practices, suggesting that the act of butchering itself may destroy clear evidence of the employed hunting methods (Bement 2007:371). Byerly responds that the preponderance of high-utility limb sections suggest secondary introduction to the shelter, despite the potential effects of differential taphonomy and excavator bias across the site (Byerly, Cooper, et al. 2007:378-379). Prewitt argues in favor of the

original jump-kill hypothesis, with Bone Bed 2 representing a minimum of three events spanning a 1,000 year period each of which were processed in-situ. He notes that the differential burning and discrete stratigraphy that he observed in the field bore little resemblance to redeposited or otherwise modified stratigraphic units (Holliday 2000; Prewitt 2007:156-157). The SMU team offers the final response in the exchange, arguing that site use changes over time and that the events of Bone Bed 3 cannot be used to make direct inferences about the events of Bone Bed 2 thousands of years earlier (Meltzer et al. 2007:159). Ultimately, the authors conceded that additional evidence is still needed to resolve competing interpretations of Bonfire Shelter.

2.4.3 *The Ancient Southwest Texas Project*

The Ancient Southwest Texas Project (ASWT), a research program within the Department of Anthropology at Texas State University in San Marcos, Texas, has conducted extensive research in the Lower Pecos since its establishment in 2009. Founded by Dr. Stephen Black, the ASWT conducted reconnaissance surveys and minor excavations on several ranches in the region from 2010 to 2012. In 2013, ASWT excavations began in Mile Canyon. Many of the methodologies implemented at Bonfire Shelter were initially developed for use at Mile Canyon's other rockshelters.

The 2013 Texas State Field School included a formal survey of the canyon uplands (which led to the formal recordation of Mile Spring Shelter, among other sites) and documentation of the canyon's rock art (Basham 2015; Rodriguez 2015). Major excavations at Eagle Cave, Kelley Cave, and Skiles Shelter as well as limited testing at Horse Trail Shelter began in 2014 (Heisinger 2019; Nielsen 2017). An extended field season was launched in January 2015 focusing exclusively on the main trench at Eagle Cave. Work at Eagle Cave was ultimately catalyzed by the need to conserve the collapsing deposits along the main trench, portions of which had been open since the Davenport excavations in the 1930s. The work followed the ASWT's "low impact, high resolution" motto, primarily focusing on intensive sampling along

main trench profiles. Additional excavations were conducted in the summer of 2015 by the Texas State University archaeological field school in coordination with the ASWT.

In 2016, excavations continued at Eagle Cave and at Sayles Adobe, a deeply stratified alluvial terrace site near the mouth of the canyon (Black 2017:7-8; Pagano 2019). The 2016 Eagle Cave expedition continued below Ross's base of excavation, identifying lithic artifacts and culturally modified bone in Late Pleistocene deposits previously considered archaeologically sterile (Koenig, Nielsen, et al. 2017:86-91). Further analysis of this material may have significant implications for Bone Bed 1 at Bonfire Shelter, particularly so if the strata are determined to be contemporary.

In 2017, final samples were collected from Eagle Cave and the main trench was backfilled, stabilizing the intact archaeological deposits and returning the shelter to pre-1963 conditions. The effort required over 225 yd³ (172 m³) of sterile sand, the "archaeo-engineering" of an 50+ foot (15.2 m) chute over the canyon rim, and hundreds of man-hours of labor (Black and Koenig 2018). The Eagle Cave conservation effort was conducted in tandem with the 2017 Bonfire expedition. Dr. David Kilby joined the ASWT team as Co-Principle Investigator in 2017, spearheading the new research at Bonfire Shelter.

2.4.4 *ASWT and Bonfire Shelter*

A Texas Preservation Trust Fund grant from the Texas Historical Commission facilitated a tripartite mitigation strategy at Bonfire: stabilize and backfill the collapsing excavation blocks from the 1960s and 1980s; develop a water management system to minimize erosion on the talus cone and replace Prewitt's deteriorating mechanism; and to conduct minimally invasive new excavations in the existing excavation blocks prior to restoring the shelter to its original state.

Several significant questions remained outstanding after 50 years of research: (1) how many kill events are represented in Bone Beds 2 and 3?; (2) does Bone Bed 2 actually represent a

jump-kill; (3) is Bone Bed 1 the result of human activity? Since the conclusion of the Turpin and Bement's work in the 1980s, Bone Bed 1 has been treated with a justifiable degree of skepticism with limited research potential (Byerly et al. 2005; Byerly, Meltzer, et al. 2007). The imminent backfilling of Bonfire Shelter will render the currently exposed portions of Bone Bed 1 inaccessible to new data collection. This thesis reports the results of Bone Bed 1 excavations conducted in the main trench in 2017 and 2018, prior to the initiation of intensive backfilling efforts initiated in 2020.

In the winter of 2017, an advance team of graduate students and volunteers from Texas State University mobilized to Bonfire Shelter to conduct a preliminary field view. The goal of the visit was to evaluate potential excavation locations and develop a sampling strategy that maximized data collection in the at-risk areas. Ground was broken removing significant quantities of slump that had accumulated in the main trench and around the talus cone.

Under the direction of Dr. David Kilby, the first full season of fieldwork began in the summer of 2017. The work included intensive sampling on the reexcavated north face of the talus cone and new excavations into Bone Bed 1. The 2017 session marked the first major excavations at Bonfire Shelter in over 30 years (Black 2001c). Major efforts to stabilize the talus cone were conducted by Charles Koenig and Amanda Castaneda and the Eagle Cave restoration crew under the supervision of Dr. Stephen Black. Protective measures included: the construction of a retention wall along the southern margin of the talus cone; the installation of a rock-filled breakwater at the apex of the talus cone to disperse sheet-wash from the notch; and the excavation of drainage ditches lined with coconut-fiber buffers to redirect runoff away from the heavily eroded main trench profile (Black and Koenig 2018).

Work at Bonfire Shelter continued in the summer of 2018, including intensive sampling on the south face of the reexcavated talus cone and resumed excavations in Bone Bed 1. Column samples spanning the full height of the main trench's western and northern (Bement's profile of

record) profiles were excavated, documenting all observable stratigraphic units. A smaller column sample (CS05) directly targeting the Bone Bed 1 strata was excavated along the southern margin of the main block. Geoarchaeological results derived from CS05 are presented **Chapter 8** below. With the assistance of the Sul Ross University field school, a new excavation block was opened in the central portion of the shelter, approximately 50 meters north of the main trench.

In the summer of 2019, Texas State University hosted cooperative field school between the ASWT and Shumla. The field school included data recovery excavations at Langtry Rock Midden (41VV168) on the uplands near the head of Mile Canyon (incidentally, the closest recorded site to Bonfire Shelter), survey of another property owned by the Skiles family north of Mile Canyon, rock art documentation modules facilitated by Shumla, and additional sampling on the talus cone and main trench profiles at Bonfire Shelter. In January of 2020, a series of micromorphology samples on the talus cone and the western profile of the main trench were impregnated with resin and left to cure. Volunteers also began backfilling the deepest portions of the main trench using the large spoil piles north of the block. Backfilling operations and final sample collections are scheduled to continue through the summer of 2020, restoring Bonfire Shelter to pre-Amistad surface conditions.

3. ENVIRONMENTAL CONTEXT

3.1 *Lower Pecos Canyonlands*

The Lower Pecos Canyonlands encompasses approximately 300 square kilometers (km) (115 square miles (mi)) across southwestern Texas and northern Mexico. The region extends northward approximately 65 km (40 mi) from the Rio Grande towards the Val Verde County Line and southward towards the Serranías del Burro range of Northern Coahuila, Mexico (Turpin 2004:266-267). Historically, research south of the Rio Grande has been limited and the southern boundary is poorly defined (Taylor 1948). The eastern and western boundaries of the region encompass large swaths of the lower Pecos and Devils River watersheds extending west towards Dreyden, TX and east to the confluence of the Devils River with the modern Amistad Reservoir (Turpin 2004:266-267).

The region's boundaries are roughly defined by the presence of Pecos River style rock art., a Middle to Late Archaic polychrome pictograph tradition found in the caves and dry rockshelters surrounding the confluences of the Pecos River and the Devils River with the Rio Grande **Figure 1-1** (Bates et al. 2015; Boyd and Cox 2016b:15-16, 24; Turpin 2004). Pecos River style pictographs are frequently accompanied by expansive burned rock middens and bedrock mortars; evidence of repeated utilization as desert succulent processing and roasting sites (Boyd and Cox 2016b:15-16). The semi-arid environment and protected conditions within the shelters preserved perishable fiber artifacts including intricately woven baskets and matting, sandals, cordage, and the remains of foodstuffs (Davis 1990). The abundance and pristine condition of the artifacts attracted generations of archaeologists, and artifact hunters, to the region.

3.2 *Mile Canyon*

Box canyon tributaries to the Pecos River, Devils River, and the Rio Grande are ubiquitous across the Lower Pecos. As previously mentioned, Mile Canyon is an ephemeral tributary to the

Rio Grande located approximately 43.0 km (26.7 mi) up stream from the confluence of the Rio Grande with the Pecos River near Langtry, Texas. The head of the canyon is marked by a vertical limestone face where seasonal floodwaters abruptly plunge over 18.0 m (59.1 ft) from the uplands to the modern canyon floor. A deep plunge pool is weathered into the limestone bedrock immediately below the fall line, approximately 350.0 m (1148.3 ft) upstream from Bonfire Shelter. Giant boulders line the much of the canyon floor, the result of millennia of karstic erosion, undercutting, and subsequent collapse along the canyon rim. Since the construction of Amistad Reservoir, Mile Canyon has been subjected to periodic slack-water flooding, as the reservoir swells and backs up into its neighboring tributaries (Frederick 2017b:14-18).

Like many of the region's other canyons, Mile Canyon hosts a gallery of dry rockshelters. Six major dry rockshelters are located along Mile Canyon: Eagle Cave (Nielsen 2017), Horse Trail Shelter (Castañeda et al. 2017), Mile Springs (Rodriguez 2015:27-28), Kelley Cave (Rodriguez 2015), Skiles Shelter (Heisinger 2019), and Bonfire Shelter (Bement 1986a; Dibble and Lorrain 1968). Numerous smaller terraces, overhangs, and crevices along the canyon and surrounding uplands contain also contain archaeological material (Basham 2015, 2017; Pagano 2019). In 1970, Mile Canyon was listed in the National Register of Historic Places as a Historic District (Bell and Dibble 1970). Additional details regarding the excavation history and archaeological setting at Mile Canyon are discussed in **Chapter 2**.

The rich archaeological resources at Mile Canyon are protected under the active stewardship of the Skiles family. Guy Skiles, the family patriarch, purchased the canyon and surrounding ranchland in the early 1940s. The property remains under the care of Jack and Wilmuth Skiles and their three children: Raymond, Russel, and Peggy. Their active advocacy for history and science has facilitated decades of archaeological research, training scores of archaeologists, and preserved the irreplaceable resources for future generations.

3.3 *Climate*

The Lower Pecos is located within an ecotone at the intersection of the Chihuahuan Desert to the south and west and the Edwards and Stockton Plateaus to the North and East (**Figure 1-1**) Blair 1950). This unique intersection of plant and animal communities derived from the arid desert of the Trans-Pecos, the humid South Texas Plains, and the karstic landscape of the Edwards Plateau has played a key role in the preservation of the pictographs and archaeological deposits that have drawn generations of archaeologists (Blair 1950:95; Turpin 2004:268). The resulting ecological diversity has sustained the region's human occupants for millennia (Turpin 2004:268).

Langtry, TX has a mean annual temperature of 69.3°F (20.7°C), however daily summer temperatures can exceed well over 100°F (37.8°C); winter temperatures below 32°F (0°C) are not uncommon (NOAA and NWS 2019). Langtry receives an average of 15.6 inches of rain per year. Rainfall increases through the summer with peak rainfalls typically occurring in September and continuing through the fall rainy season. Violent thunderstorms are not uncommon, and are exacerbated by tropical weather events blowing inland from the Gulf of Mexico (Pagano 2019:19; Patton and Dibble 1982:97). Sustained rainfall during these events result in the massive flash flood events that shape the canyon landscape. The implications of these flood events are discussed in greater detail in **Section 3.8**. Snow is rare, but occasional short-lived dusting averaging <0.1 inches occur (Golden et al. 1982:2; NOAA and NWS 2019). Prevailing winds shift from southeasterly in the summer to northeasterly in the winter, introducing higher intra-day temperature variability (Golden et al. 1982:11).

3.4 *Flora*

The intersectional environment of the Lower Pecos supports a diverse floral community consisting of arid desert agaves and scrub brush native to the Chihuahuan desert and the more temperate savannah and grassland biota of the Edwards Plateau and South Texas Plain (Blair

1950:97). The Pecos River is an arbitrary demarcation between eastern and western ecologies. The canyons and waterways within this transitional zone are a unique refugia for species of the plateau, while the wind-swept uplands foster comingled communities of the plains and desert west (Blair 1950:97). The increased humidity, intermittent flooding, and deposition of alluvial sediments along the of the Rio Grande host a unique mix of hydrophytic plants (Tiner 1991).

A paleoethnobotanical survey identified multiple microclimate zones within Mile Canyon and the surrounding area (Bush 2015). **Table 3-1** outlines the species associated with each of these zones. The canyon uplands are sparsely populated with a variety of Chihuahuan and South Texas Plains taxa including lechugilla, sotol, yucca, and cacti among other succulents. Stands of creosote, cenizo, ocotillo, and other thorny savannah and desert scrub are also common. The canyon floor is comparatively lush, especially approaching the Rio Grande to the south. Mesquite, hackberry, Texas persimmon, juniper and live oak trees are common (Bush and Hanselka 2017; Dering 2002:2.3-2.4). The canyon’s steep walls and limestone outcrops provide partial shade, fostering species poorly suited for the harsh uplands including the slenderlobe passionflower which grows only in the immediate vicinity of Bonfire Shelter (Dering 2002:2.3-2.4).

Table 3-1. Modern flora of Mile Canyon. Adapted from Bush and Hanselka 2017:23-24. Passiflora identification reported in Rodriguez 2015:198-205 – Appendix A – Plants Observed in Eagle Nest Canyon.

Native Habitat	Common Name	Scientific Name	Notes
Chihuahuan Desert	Creosote	<i>Larrea tridentata</i>	Semi-arid Desert
	Ocotillo	<i>Fouquieria splendens</i>	
	Lechugilla	<i>Agave lechugilla</i>	
	Sotol	<i>Dasyilirion texanum</i>	
	Yuccas	<i>Yucca torreyi</i> , <i>Y. Thompsoniana</i>	
	Chollas	<i>Cylindropuntia sp.</i>	
	Passion Flower	<i>Passiflora tenuiloba</i>	Only identified in vicinity of Bonfire Shelter

Table 3-1. Continued

Native Habitat	Common Name	Scientific Name	Notes
Edwards Plateau	Oak	<i>Quercus sp.</i>	Savannah Grassland
	Hackberry	<i>Celtis sp.</i>	
	Juniper	<i>Juniperus sp.</i>	
	Mesquite	<i>Prosopis glandulosa</i>	
	Roundflower Catclaw	<i>Senegalia roemeriana</i>	
	Assorted grasses		
South Texas Plain	Brasil Grass	<i>Condalia sp.</i>	Brushland Shrubbery
	Guajillo	<i>Senegalia berlandieri</i>	
	Catclaw	<i>Senegalia greggii</i>	
	Huisache	<i>Vachellia farnesiana</i>	
	Cenizo	<i>Leucophyllum frutescens</i>	
	Prickly pear	<i>Opuntia sp.</i>	
Rio Grande Valley	Common reed	<i>Phragmites australis</i>	
	Willow	<i>Salix sp.</i>	
	Tree tobacco	<i>Nicotiana glauca</i>	Invasive
	Giant reed	<i>Arundo donax</i>	Invasive
	Salt cedar	<i>Tamarix sp.</i>	Invasive

3.5 Geology

Mile Canyon is eroded through three Cretaceous bedrock formations: The Devils River Formation (also known as the Georgetown Formation); the Buda Formation; and the Boquillas Flags (or Eagle Ford Shale) (Barnes et al. 1977; Frederick 2017b:10). The combined weathering of these bedrock units contributes sediments directly to Bonfire Shelter. Derivative minerals, such as gypsum, have a significant effect on regional rockshelter formation and post-depositional processes.

The fossiliferous Devils River limestone is the most apparent in Mile Canyon. The canyon's major rockshelters are formed directly in the exposed faces of this Lower Cretaceous unit (Dibble and Lorrain 1968:13). Fossil bivalves, particularly *Hippuritoidea* (also known as

rudistids), are abundant throughout the boulders and limestone faces of the formation (Barnes et al. 1977). Rudistid fossils are temporally diagnostic to the Late Jurassic through the Cretaceous geological epochs and provide a glimpse into the region's distant past as a massive reef in a warm, shallow, saline sea (Steuber 2002). The road cuts along US 90 and the Pecos River crossing are the type-sites for several rudistid species (Scott 2002). The accumulation, sedimentation, and lithification of these shells on the ocean floor is a major source of calcium carbonate in Devils River limestone, and subsequently, the sediments accumulating in the region's rockshelters. Chert nodules and outcrops found in the Devils River and, less frequently, Buda formation may have provided a local source of raw material for stone tool production (Freeman 1964). The karstic processes that play a critical role in the formation of the Lower Pecos rockshelters are described in greater detail in **Chapter 4**.

The Buda Formation, an Upper Cretaceous sedimentary limestone deposit, overlays the Devils River Formation (Barnes et al. 1977) In the vicinity of Mile Canyon (**Figure 3-1**), Buda Formation limestone is primarily located on the upland margin approximately 10 m above the canyon rim (Frederick 2017b). The Buda Formation is significantly thinner than the underlying Devils River Formation with limited fossil content and chert outcrops (Freeman 1964).

The Boquillas Flags is a major target of the oil and gas plays of South Texas (Lock et al. 2010). This Upper Cretaceous formation expands considerably to the north and west of the Lower Pecos (Barnes et al. 1977). The Eagle Ford formation caps the Buda and Devils River Formation in the upland areas surrounding mile canyon (Texas Water Science Center 2014). The Boquillas typically manifests as relatively thin, black bands of shale and limestone that weather to tan and reddish brown due to the oxidation of pyrite (FeS_2) to iron oxides (Barnes et al. 1977; Frederick 2017b:10). The weathering processes leads to an excess of sulfur, which binds with dissolved calcium from the weathering of the abundant limestone (largely CaCO_3) to form gypsum ($\text{CaSO}_4 \cdot 2\text{H}_2\text{O}$) (Bain 1990; Frederick 2017b:13).

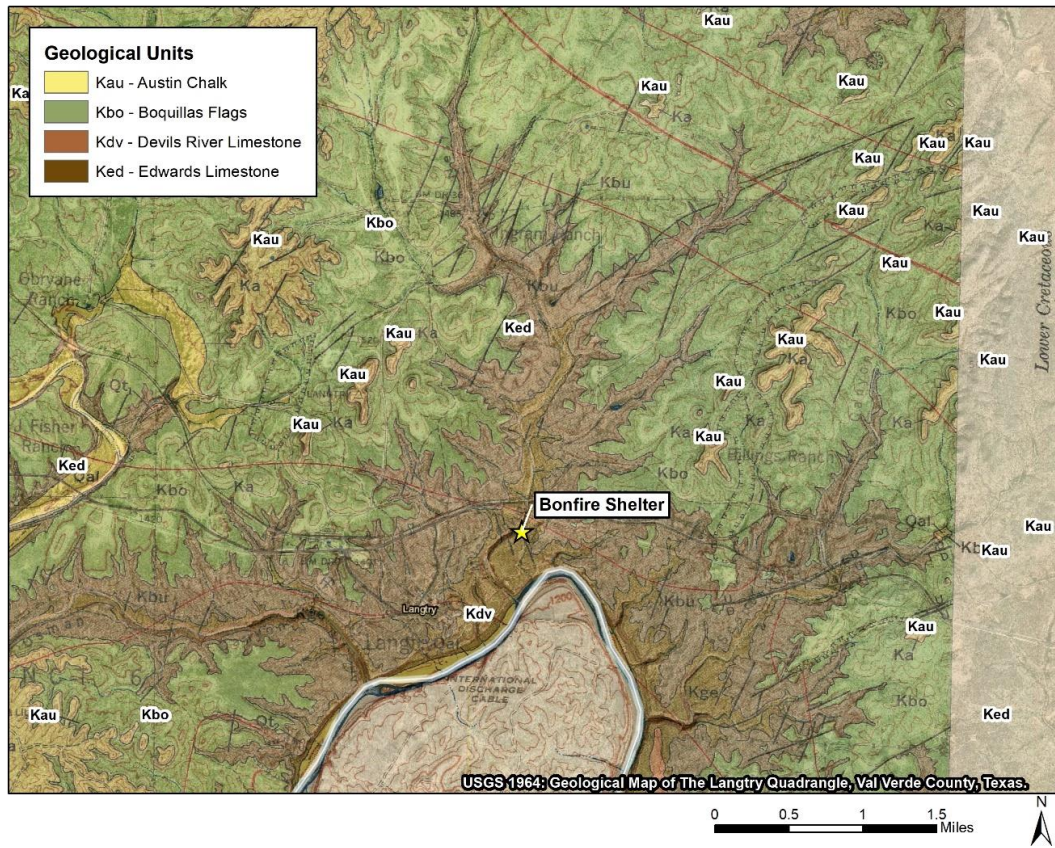


Figure 3-1. Geological Map of Langtry Texas illustrating exposed bedrock units in the vicinity of Mile Canyon. Data derived from Freeman 1964: Geological Map of the Langtry Quadrangle, Val Verde County, Texas

3.6 Fauna

The Lower Pecos’s unique climate and associated floral communities host a similarly diverse array of animal life. In general, the modern faunal community is dominated by species well adapted to the rocky outcrops and scrub-brush that dominates the landscape (Bahm and Mueller 2011). Smaller omnivorous and herbivore mammalian taxa including jackrabbit hare, cotton-tail rabbit, squirrel, raccoon, possum, skunk, porcupine, and a variety of mice are abundant. Larger mammals observed in the region include white-tailed deer, barbary sheep (non-native), and javelina. Predators include mountain lion, coyote, and gray fox (Bahm and Mueller 2011:15-26). A variety of snakes, lizards, and amphibians, largely of Chihuahuan affinity, are common (Blair 1950:108,115). The region’s river systems are home to a variety of fish and fresh-

water bivalves. Avian species in the vicinity of Amistad Reservoir and Mile Canyon include the canyon- and cactus wren, raven, eagles (the namesake of Eagle Nest Canyon), and hawks (Blair 1950; Nielsen 2017) as well as at least 16 species of bat (Bahm and Mueller 2011:13). Modern domesticated animals, primarily sheep and goats, are common; the rocky landscape typically cannot fodder cattle or larger grazing livestock (Golden et al. 1982:24, 60-51).

3.7 Soils

Soils surrounding Mile Canyon are typically very shallow and deflated, composed primarily of sediments weathering from the underlying limestone bedrock (Golden et al. 1982:5-7). **Figure 3-2** illustrates the USDA NRCS Soil Series in the vicinity of the canyon and the vast extent of exposed rock outcrops and steep slopes. The paucity of upland soils has been exacerbated by the region's historic use as range land. During the 1982 soil survey, over 98% of Val Verde county was utilized as rangeland, primarily producing sheep and goats (Golden et al. 1982:1,60-62). Over-grazing has stripped the uplands of grasses and understory vegetation. Without consolidating root systems, wind and water readily entrain the soils and in many cases leave only exposed bedrock at the surface (Bush and Hanselka 2017:24; Turpin 2004:266).

The Rio Grande floodplain is an exception to this pattern. A relatively narrow band of silty to fine sandy loams flanks the river, forming terraces ranging from one to six meters high (Golden et al. 1982:13-14). Sediment accumulation is most pronounced on the concave interior of river bends, where the water velocity is slightly lower. This reduced velocity allows sediments to drop out of transport and accumulate along the banks as point bars (Waters 1992:120-126). Bend exteriors are exposed to the highest water velocities and subjected to increased erosion forming steep cut banks (Waters 1992:129-132).

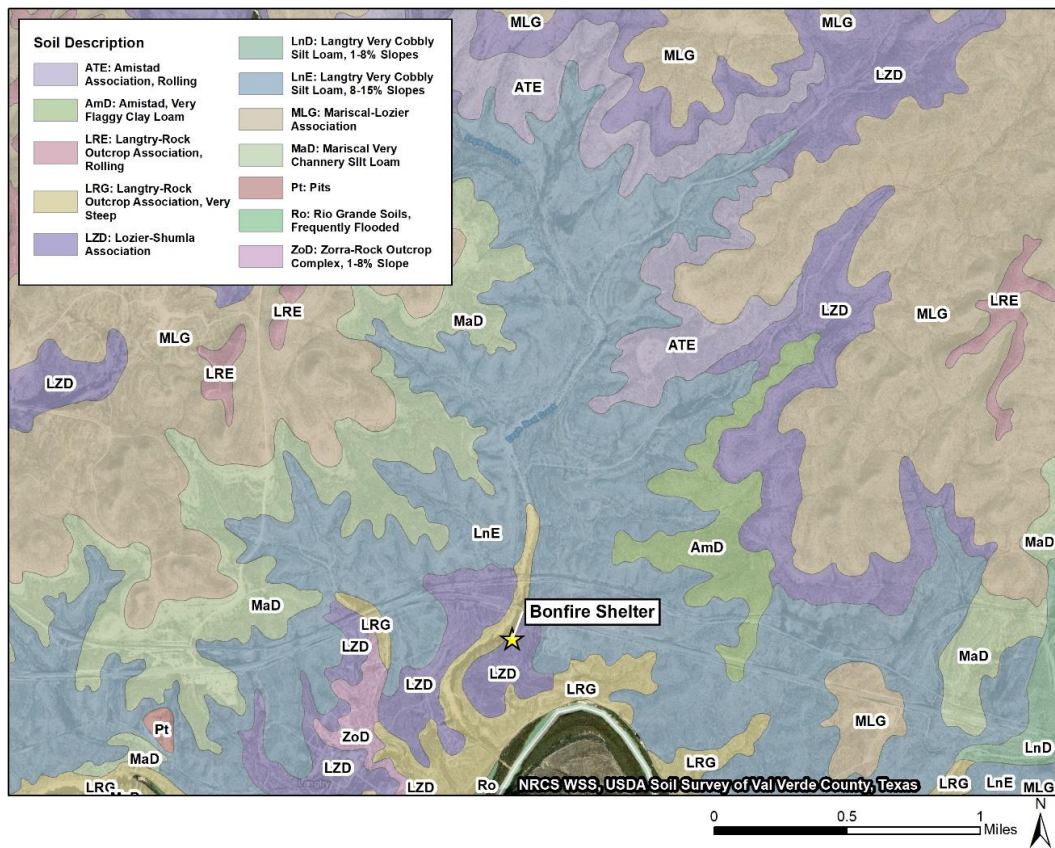


Figure 3-2. USDA Soil Series in the vicinity of Bonfire Shelter. Data derived from NRCS Web Soil Survey, USDA Soil Survey of Val Verde County, Texas (Golden et al. 1982).

The remnants of two Pleistocene strath terraces and one Middle-Late Holocene alluvial terrace flank the Rio Grande's northern margins near Mile Canyon (Frederick 2017b:11). Periodic downcutting of the Rio Grande incised the terraces into the underlying bedrock (Brown 1997:150-151). Downcutting occurs as rivers erode sediments and bedrock to reach a state of equilibrium with its discharge base level, typically sea level. As sea levels fluctuate and the overall gradient of a system shifts, the incising rate may increase or decrease reflecting broader environmental trends. Lower base levels may result in more rapid incising, while elevated base levels may decrease the rate or exacerbate horizontal erosion. Alluvial, or depositional terraces, are the result of overbank flooding and the accumulation of entrained sediments forming a floodplain and subsequent incising through that floodplain (Waters 1992:149).

3.8 *Flooding and Implications for Archaeological Sites*

The 2014 ASWT excavations at Horse Trail Shelter, located along the western wall of Mile Canyon approximately 300 m (984 ft) upstream from the confluence with the Rio Grande, revealed a deeply stratified alluvial profile. An OSL date recovered from a reddish brown band approximately 1.5 m (4.9 ft) below the excavation surface yielded a date of 22,010±1700 BP; well into the Late Pleistocene (Castañeda et al. 2017:67-69). No artifacts were recovered from these deeply buried strata. However, the elevation of the deposits above the canyon floor provide a shocking glimpse of the scale of flooding events that influenced Mile Canyon's prehistoric filling and scouring cycles.

Evidence of prehistoric flooding is visible at several Mile Canyon sites. Thick alluvial deposits dated to approximately 610 BP (1340 AD) form a stratigraphic correlation between Skiles Shelter and the neighboring Kelley Cave (Koenig, Black, et al. 2017:43). At Sayles Adobe, discreet flood-drapes mark the tempo of flood events over 9,000 years and seal intact cultural features (Pagano 2019:164-165).

Geoarchaeological analyses at Eagle Cave identified significant amounts of Rio Grande alluvium comingled with anthropogenic and endogenic rockshelter sediments (Nielsen 2017:125). Nielsen hypothesizes that significant quantities of sediment derived from the Rio Grande were intentionally imported to cap the shelter's abundant earth ovens. Hydrological modeling suggests floods breaching Eagle Cave, in excess of 32 m (106 ft), are possible and may have occurred during the Holocene (Koenig, Nielsen, et al. 2017:96). However, the repeated utilization of earth ovens has disrupted any in situ stratigraphic evidence of alluvial deposition such as the massive deposits observed in the lower canyon shelters. Particle size distributions indicate aeolian processes also redeposited Rio Grande sediments at in Eagle Cave, but the significant quantities of exogenic material observed suggest other processes simultaneously contributed sediment (Frederick 2017a; Nielsen 2017:160).

3.8.1 *Modern Flooding*

The construction of Amistad International Reservoir significantly altered the Rio Grande's flooding patterns. Seasonal rains cause the reservoir to back up and the ensuing slack-water floods continue to deposit alluvium along its banks (Golden et al. 1982:14, 45). However, violent high-energy floods periodically impact upstream waterways and tributaries.



Figure 3-3. High-water mark beneath Pecos River style rock art panel at Skiles Shelter near the confluence of Mile Canyon and the Rio Grande.

In 2014, a record 29.46 cm (11.6 in) of rain fell in under eight hours interrupting ASWT excavations in Mile Canyon. (Koenig and Black 2014a). The subsequent flash flooding deposited gravel bars and dunes over 5 m (15 ft) tall, stripped small vegetation, and permanently bent trees near the mouth of the canyon at 45° angles (Koenig and Black 2014b). Illustrated in **Figure 3-3**, the high-water mark from a 2010 flood event remains visible precariously close to the Skiles Shelter rock art panels, permanently highlighting the massive volumes of water which move through the canyon. The dynamic elevation of the canyon floor may have influenced prehistoric site usage as shelters were rendered more or less accessible by the shifting sediments.

Canyon floor topography is particularly relevant at Bonfire Shelter. Byerly's argument for the post-kill introduction of the bison comprising Bone Bed 2 to the shelter leans heavily on higher canyon floor elevations (Byerly et al. 2005:624). The modern shelter configuration would require individuals to drag *Bison antiquus* carcasses (or large carcass segments) 18 m (59 ft) up a very steep incline to access the shelter interior. Opponents of this hypothesis argue that this process is unrealistic, especially considering the number of bison required to amass Bone Bed 2 (Prewitt 2007). A higher elevation canyon floor would render this a much less strenuous exercise. A higher canyon floor during Bone Bed 1 times would similarly facilitate the introduction of megafauna, either under their own power, by humans, or by other predators (Byerly et al. 2005:624-625). However, indications of the Late Glacial elevation of the Mile Canyon floor are circumstantial.

Unlike other shelters in the Mile Canyon, the intensive plant-baking industry driving stratigraphic disruption and possible artificial sediment introduction is not present. No massive alluvial deposits have been identified at Bonfire Shelter, suggesting that floodwaters have not breached the site. **Figure 3-4** courtesy of Dr. Charles Frederick, captures the crest of the 2014 floodwaters approximately 15 m (49 ft) below the southern entrance to Bonfire Shelter. Flooding on a much larger scale would be required to directly introduce alluvial sediments. However, exogenic materials still appear to play a significant role in Bonfire Shelter's depositional history.

Runoff from heavy rains is funneled through the notch and (to a lesser degree) the northern shelter entrance, redepositing upland sediments on the talus cone and across the shelter interior (Byerly et al. 2005:613). The talus cone and massive boulders obscuring the mouth of the shelter limit air circulation, channeling aeolian-entrained sediments through the narrow northern and southern entrances. The thesis explores the mechanisms that introduced and modified the Bone Bed 1 faunal remains, including fluvial action, human and carnivore activity, or natural expiration.

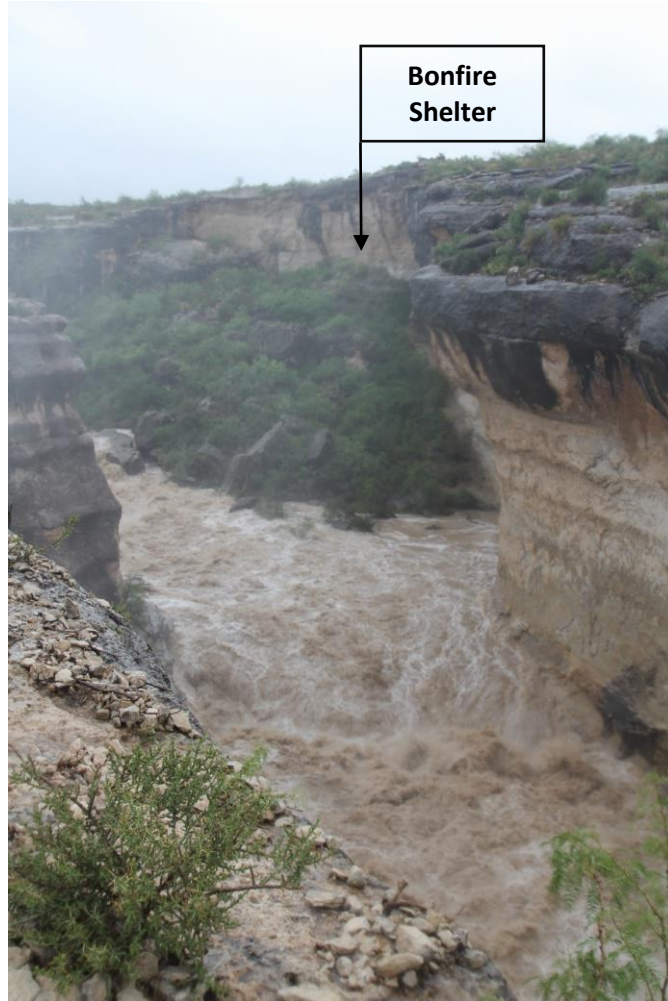


Figure 3-4. 2014 flooding at Mile Canyon cresting approximately 15 vertical meters (50 ft) below the southern entrance to Bonfire Shelter. Photo courtesy of Dr. Charles Frederick, ASWT.

3.9 Pleistocene Landscape

In 1985, Vaughn Bryant and Richard Holloway of Texas A&M University published a paleoenvironmental overview of the Texas Quaternary based on fossil pollen analysis (palynology) (Bryant and Holloway 1985). Samples from Bonfire Shelter collected during the Amistad-Era excavations comprise the bulk of their Southwestern Texas evidence. Their results were initially published in the 1966 Amistad Reservoir Salvage report (Hevly 1966) and in Bryant's 1969 doctoral research at the University of Texas (Bryant 1969). Samples were collected from three profiles (A: N110, W42; B: N98, W47.5; and C: N30, W67; Dibble's coordinates).

Sample volume and frequency were discontinuous and uncontrolled between profiles. Samples from Bone Bed 3 and Zone 1 were poorly preserved, leaving gaps in the palynological sequence.

Bryant and Holloway describe three primary temporal periods: The Wisconsin Full-Glacial Period from 22,500 – 14,000 BP (Bryant and Holloway 1985:47), the Late Glacial Period from 14,000 - 10,000 BP (Bryant and Holloway 1985:51-52), and the Post-Glacial Period from 10,000 BP – Present (Bryant and Holloway 1985:56-58). The Full-Glacial Period was characterized by much cooler and wetter conditions than the present marked by high pine pollen concentrations. A gradual trend towards aridity followed, marked by increasing ephedra and grass pollens with decreasing pine pollen in the Late-Glacial Period. Semi-arid scrub and desert species such as agave, yucca, and sotol begin to replace the grasslands during the Post-Glacial Period.

In 1992, PaleoResearch Laboratory processed the palynology column sample collected during the 1983 expedition (Scott-Cummings 1992). Linda Scott-Cummings reported an environmental sequence consistent with Bryant and Holloway's profile but sampled at a much higher resolution. The column sample encompassed 550 sequential centimeters and 18,000 years of Bonfire Shelter sedimentation (Scott-Cummings 1992:1-2). Limited chronological control and pollen degradation continued to hinder interpretations, particularly in the Full and Late Glacial strata (Scott-Cummings 1992:5).

In the early 1990s, David Robinson conducted a sedimentological analysis of a second column sample excavated during the 1983 expedition (Robinson 1997). Consistent 2 cm sequential levels were excavated through both sediment and palynology columns, allowing his results to be directly correlated with Scott-Cummings' palynological data. Robinson's geoarchaeological analysis included particle size and mineralogy analysis. Particle size was measured through a reductive three-step process: 2cm coarse sorting, nested dry sieving, and hydrometer fine-fraction sampling. Fine fraction mineralogy was then assessed using X-ray diffraction (Robinson 1997:36).

Robinson argued that composition and particle size variation within the column is attributable to climate variation and human activity within Bonfire Shelter. Late Pleistocene deposits were characterized by concentrations of platy frost spalls, while Holocene deposits were marked by accumulations of finer dusts (Robinson 1997:41). When correlated with pollen data, bone-bearing strata were found to occur in periods of thinning woodlands and temperate winters. Robinson's key thesis is that Bison migration patterns shifted south into the expanding grasslands during temperate interludes. Bison hunters from the Plains tracked the migrations southward and comingled with the indigenous population of the Lower Pecos (Robinson 1997:42-43).

3.9.1 *Archaeological Traces of the Pleistocene*

Bonfire Shelter is one of the few sites in the Lower Pecos where scientists and geologists have identified intact Pleistocene deposits (Turpin 2004:268-269). The remains of extinct Pleistocene fauna are uncommon, even in ideal dry rockshelter conditions; confirmed Paleoindian sites associated with these remains are even more uncommon (Bousman et al. 2004). The paucity of these sites on the landscape, in the Lower Pecos and across the world, may be a function of preservation bias as well as human behavioral ecology (Collins 1991). Pleistocene sites have been exposed to environmental processes for thousands of years longer than their Archaic and Late Prehistoric counterparts. The landforms where the sites occur can become deeply buried, heavily eroded, or otherwise obscured greatly reducing visibility and accessibility to archeologists.

In North America, human population density was much lower during this time period, resulting in fewer total sites (Amick 2017; Buchanan et al. 2019; Waguespack 2012). The high mobility of these hunter-gatherer groups often yields ephemeral archaeological deposits; limited refuse can accumulate in any one place when occupation is limited and sites are continuously rotated (Kelly and Todd 1988). The scarcity of Pleistocene sites and the allure of studying a very different world from our own has attracted the attention of generations of archaeologists and geologists (Meltzer 2009b:233-236).

Recent ASWT excavations at Eagle Cave and Sayles Adobe have confirmed the presence of Paleoindian occupations in Mile Canyon beyond Bonfire Shelter (Koenig, Nielsen, et al. 2017; Pagano 2019). Excavations at Eagle Cave in the 1960s identified Pleistocene-age geological deposits beneath the rich Archaic horizons, but no cultural material was identified (Nielsen 2017:29-23; Ross 1965). In 2017, the ASWT extended the Eagle Cave trench into the Pleistocene deposits beneath Ross's base of excavations (Koenig, Nielsen, et al. 2017). Within the spall and limestone dust, excavators identified Paleoindian material including a small surface hearth surrounded by fragmentary bison bone and a small amount of lithic debitage. Deeper still, a juvenile mammoth mandible was recovered that exhibited cut marks consistent with stone-tool disarticulation (Koenig, Nielsen, et al. 2017).

At Sayles Adobe, excavations extending deep into the alluvial deposits along the Rio Grande yielded two Late Paleoindian radiocarbon dates (Pagano 2019:108). Auger probes excavated at the base of excavation blocks already extending over 4.0 m (13.1 ft) deep yielded two dates from macrobotanical samples associated with a small quantity of debitage (Pagano 2019:297-304). While limited cultural material was associated with these dates, the findings illustrate broader patterns of site use across Mile Canyon beyond rockshelter contexts.

The Devil's Mouth site (named for its location at the mouth of the Devils River) (Johnson 1964) and Arenosa Shelter (located at the confluence of the Pecos River and the Rio Grande) (Dibble 1967) are two of the very few other confirmed Paleoindian sites in the Lower Pecos. The alluvial setting of both sites resulted in extremely deep stratification and the preservation of detailed cultural sequences. Golondrina and Angostura projectile points recovered from the Devil's Mouth are associated with the Late Paleoindian period, approximately 10,000 years ago during the last gasps of the Pleistocene (Johnson 1964:46-58). Golondrina points were initially considered a variant of Plainview projectile point, similar to the lanceolate points recovered from Bone Bed 2 at Bonfire Shelter (Bousman et al. 2004:60-61).

Two Paleoindian-age deposits were identified near the base of a massive profile exposed at Arenosa Shelter extending over 12.8 m (42.0 ft) (Dibble 1967). Zone 5 included uniface tools and lithic debitage associated with a small amount of charcoal that dated to approximately 10,990 cal BP (Whelan and Black 2008a:5). Zone 6, the deepest series of strata excavated at Arenosa, yielded the disarticulated remains of two *Bison antiquus* associated with intrusive limestone cobbles and a radiocarbon date of 11,400 cal BP (Whelan and Black 2008a:6). Much like Bonfire Shelter, no stone tools or definitive cut marks were observed with these Pleistocene remains. The active deposition of fine alluvial sediments at Arenosa Shelter is very different than the dense ebbolis and gravels of Bonfire Shelter; the cobbles at Arenosa stand out much more prominently against the fine-grained sedimentary background. Despite these differences, the association of large, intrusive cobbles with extinct megafauna is reminiscent of Bone Beds 1 and 2 at Bonfire Shelter (Whelan and Black 2008a, 2008b).

Cueva Quebrada, a small annex shelter associated with Conejo Shelter, is located along a minor tributary canyon to the Rio Grande north of its confluence with the Pecos River (Lundelius 1984). Excavations yielded an assemblage similar to Bonfire Shelter, including suspiciously burned and fragmented bone and an *Equus* femur bearing a possible cut-mark (Lundelius 1984:461. 464). Lithic debitage and a stone adze were recovered from similar contexts associated with radiocarbon dates ranging from 12,000 – 14,300 RCYBP. However, the stratigraphic relationship between the artifacts, the potentially modified remains, and the dated material is uncertain (Black and Dering 2008). Like Bone Bed 1 at Bonfire Shelter, the evidence is evocative of human agents. Possible contamination from carnivore activity and lack of a preponderance of evidence relegates the Pleistocene deposits at Cueva Quebrada to the list of “possible archaeological sites”.

3.9.2 *Friesenhahn Cave*

Approximately 20 miles southwest of San Antonio, Friesenhahn Cave is among the densest concentrations of *Homotherium serum*, the scimitar-toothed cat, remains in the world (Graham et al. 2013:26). Puncture marks consistent with *Homotherium* upper-canine dentition were identified in mammoth elements recovered from Bone Bed 1 at Bonfire Shelter (Bement 1986b:56); Bement specifically cites a Friesenhahn Cave specimen as a comparative sample. The temporal and geographic proximity of Friesenhahn Cave to Bonfire Shelter affords a unique comparative assemblage to explore the *Homotherium* denning and predation behavior in the Late Pleistocene. The site was first excavated from 1949-1951 by the Texas Memorial Museum under the direction of geologist Glen Evans (Evans and Meade 1961). Russel Graham returned to Friesenhahn in the mid-1970s to conduct doctoral research in vertebrate paleontology through the University of Texas at Austin (Graham 1976).

During the Late Pleistocene, Friesenhahn Cave was subjected to significant exogenic sedimentation via sheet-wash from a sinkhole in the northern portion of the cavern roof. Debris accumulated to form a talus cone immediately below the opening. Lenses of variably reduced and oxidized clay suggest pooling water periodically persisted in the southern end of the cave. The growing talus cone eventually obstructed the northern entrance, limiting deposition and restricting access to smaller taxa. Early in the Holocene, a portion of the cave ceiling collapsed to form the modern shelter entrance making the shelter once again accessible to larger fauna and exogenic sedimentation (Graham et al. 2013:24-26).

The majority of the large vertebrate fossils was recovered from Evans' Zones 2 and 3, a series of clayey laminations derived from cyclical ponding and drying along the toe-slopes of the talus cone and southern shelter (Evans and Meade 1961:17). Over 50 taxa were represented in Friesenhahn Cave, but the assemblage is dominated by mammoth and *Homotherium serum*. Other large herbivores and ungulates including Pleistocene horse, camel, bison, tapir, deer, and isolated examples of mastodon were present in limited numbers. Notably, all of these species were likely

too large to enter the cave of their own accord. The vertical-shaft entrance to the cave may have contributed to the taxonomic diversity of the assemblage, trapping individuals straying too close to the obscured sink (Graham 1976:196). The assemblage also includes limited examples of other carnivores including *Smilodon* (the dirk-tooth cat), *Canis dirus* (dire wolf), and *Arctodus* (short-faced bear), however their presence in the shelter was fleeting and may have been limited to secondary scavenging activity.

At least 30 individual *Homotherium* are represented in the assemblage, exhibiting a bimodal distribution of adults and juveniles (Graham 1976:197). Three nearly complete, articulated *Homotherium serum* skeletons were identified on the muddy slopes of the talus cone: two juveniles and one adult. Graham argues that this is consistent with denning behavior observed among other big cats (Graham et al. 2013:24).

Nearly all of the mammoth identified in the cave appeared to be juveniles, <2.5 years old (based on modern elephant proxy) and still nursing (Graham et al. 2013:27). Calculations for total number of mammoth vary wildly, ranging from up to 400 (Rawn-Schatzinger 1992:68) to 34 (Marean and Ehrhardt 1995:520). Regardless of the specific MNI, mammoth is the most frequently observed taxa. The discrepancy is a function of the intense disarticulation and scattering of all herbivore and ungulate remains in the cave.

Significant quantities of crania and low-utility elements led Graham to believe that juvenile mammoth were brought to the cave as complete units; a task requiring large predators, even considering the immaturity of the prey (Graham 1976:189). Modern big cats, such as leopards and jaguars, exhibit similar behavior, dragging whole antelope into trees for secure consumption (Graham et al. 2013:27). Subsequent analyses show that limb long bones are better represented than foot bones, suggesting at least some selection bias and disarticulation by predators (Marean and Ehrhardt 1995:525-526). Unlike hoofed ungulates, elephant feet contain significant quantities of fat and meat, raising their caloric value and making their presence in the

cave less anomalous (Haynes 1991a). The significant proportion of mammoth cranial anatomy in the cave leaves questions regarding disarticulation unresolved.

Carnivore damage to bone was common but did not appear pervasive enough to account for the mammoth discrepancies via total element deletion. Striations and other cortical tooth marks consistent with defleshing were much more common than crushing or gnawing associated with scavenger marrow extraction (Haynes 1988:144-146). Marean and Ehrhart argue that *Homotherium* dentition may have prevented the intense gnawing required for marrow extraction (Marean and Ehrhardt 1995:529).

Early reports suggested that polished surfaces and sheared faces on several elements might be attributable to humans (Evans and Meade 1961:21). Subsequent analysis indicates this damage is more consistent with tooth marks and partial bone digestion. Chert nodules within the limestone parent material further complicated the search for human activity (Evans and Meade 1961:21). The site's active hydrology and ongoing animal trampling resulted in numerous geofacts that could not be unambiguously attributed to humans (Graham 1976:198-200). Subsequent excavations and analysis have not identified further evidence of human activity at Friesenhahn Cave; the faunal accumulations are generally attributed to *Homotherium* denning behavior (Graham 1976; Graham et al. 2013; Marean and Ehrhardt 1995; Martin 1968).

Friesenhahn Cave is a unique case study in *Homotherium* predation and denning behavior providing valuable insight into other Pleistocene bone beds across Texas. Graham (Graham 1976) and Marean's (Marean and Ehrhardt 1995) analyses demonstrate that the taphonomy of *Homotherium* denning behavior may be very distinct from the modern wolf and hyena dens described by Binford (Binford 1981). Bias towards juvenile mammoth, broad range of elements returned to the den, and limited crushing and gnawing damage provide a clear profile for differentiating *Homotherium* assemblages from other Pleistocene predators (Graham et al. 2013; Marean et al. 1992).

Bone Bed 1 exhibits several attributes of the Friesenhahn den assemblage, but is not a perfect match. Bone Bed 1 is not skewed as intensely towards mammoth; *Equus* dominates the Bonfire assemblage. Mammoth is well represented at Bone Bed 1. The remains appear to be juvenile and gnawing or other tooth damage is limited. Bone Bed 1 bone surface modifications include several striations tentatively attributed to tooth marks as well as the clear *Homotherium*-punctured mammoth long bone fragment. The Bone Bed 1 assemblage includes low utility elements not necessarily expected at a secondary consumption site including pelvis, scapula, vertebra, and cranial fragments in addition to high-yield limb bones. However, Friesenhahn illustrates that a broader spectrum of material may be returned to consumption sites. No carnivore remains have been identified in the Bonfire Shelter bone beds; a clear deviation from Friesenhahn where carnivore are the second most abundant taxa.

4. ROCKSHELTER FORMATION PROCESSES

On a landscape densely pocketed with caves, crevices, canyons, and rockshelters, Bonfire Shelter is unique. The shelter's isolated location, obscured entrance, precariously notched brow, and proximity to the Rio Grande coalesce to form a setting that has been exploited by the region's inhabitants for thousands of years. The geographic set and cultural setting have influenced how people have interacted with Bonfire within the context of Mile Canyon's rockshelter ensemble over time.

At a time when most of the region's shelters were conscripted into service as earth oven industrial facilities, entire herds of Bison were slaughtered at Bonfire Shelter (by way of the canyon rim or otherwise). Relative lulls in the archaeological record at Bonfire Shelter with limited evidence of human occupation are a stark counterpoint to the dense human exploitation of a contemporary Eagle Cave. A detailed understanding of rockshelter formation processes may provide insight into these site use patterns and help explain the differential preservation of Late Pleistocene deposits between the upper and lower Mile Canyon rockshelters.

This chapter explores the geological mechanisms that form rockshelters and contribute to their dynamic morphology over time. These processes have direct implications for the accessibility of a shelter to humans, plants, and animals; the suitability of a shelter for various cultural activities; the accumulation and preservation of sediments and refuse; and the accessibility of deposits to modern scientists. The geological signatures associated with these processes can be detected using geoarchaeological methods and leveraged to infer the environmental setting at specific points in the past. With these data in mind, patterns of stability, accessibility, and suitability for various activities can be assessed.

Bonfire Shelter's unique morphology has significant implications for sedimentation and formation processes, potentially causing deviations from the expected formation profiles. The massive boulders and brow-collapse debris that obscure the shelter deflect water and sediment

towards the interior rather than diffusing it across toe-slopes and talus fields. These boulders further restrict sediment erosion, limiting the periodic fluvial scouring observed at downstream Mile Canyon shelters and contributing to aeolian sediment trap effects. Limited erosion and increased sediment retention capacity has resulted in a long, mostly continuous sediment sequence highlighted in previous paleoenvironmental reconstructions (Bryant and Holloway 1985; Robinson 1997; Scott-Cummings 1992). The processes outlined in this chapter provide context for the geoarchaeological analyses used to assess the Bone Bed 1 strata. An understanding of the processes that form geological deposits and their interactions with Bonfire Shelter's unique geography can inform expectations for their appearance in the lab.

4.1 How Rockshelters Form

Rockshelters are natural recesses and overhangs formed in exposed bedrock faces through a perpetual cycle of incising, sedimentation, and collapse driven by ongoing physical and chemical erosion (Mentzer 2017). Caves are similar but unique geographic features characterized by enclosed voids that may extend significant distances into a bedrock formation, portions of which are in perpetual darkness. (Mentzer 2017:726; Straus 1990:256). Rockshelters typically extend only short distance into the bedrock and receive at least partial sunlight throughout the day. These recessed cavities offer natural protection from the elements, making them ideal habitation sites for a variety of fauna, including humans. Geoarchaeological methods can be used to evaluate the changing conditions within a cave or shelter over time and assess their suitability for human exploitation.

On a geological time scale, caves and rockshelters are in constant motion (Straus 1990:257).. Mechanical attrition and chemical dissolution work in tandem to incise crevasses into soft or soluble bedrock formations. Differential weathering along faults, fissures, bedding planes, and other bedrock imperfections gradually expand to form caves and the characteristic rockshelter overhangs. These features are more likely to form where erosion susceptible strata are

“sandwiched” between erosion resistant strata through the process of differential weathering (Mentzer 2017:730). The size and scale of the feature is determined by the intensity of the formation processes and the variable susceptibility of bedrock units to weathering. In addition to direct weathering, rockshelters can form where larger cave systems collapse to expose the internal facies of previously sealed passages.

Modern, observable rockshelter morphologies may vary significantly from their appearance in the Pleistocene, Early Holocene, or other points in the geological past (Laville et al. 1980:50-52). The rockshelter cycle of weathering, sedimentation, and collapse form “steps” of geological and archaeological deposits as a shelter recedes into the bedrock unit, perpetually burying older strata beneath newer sediments and talus debris from collapse events.

The resulting talus slopes may bury earlier archaeological deposits or obscure shelter entrances, rendering them inaccessible (Collins 1991:158). In a study of the limestone rockshelters of the Périgord in southwestern France, archaeologist Henry Laville estimated that up to 25% of shelters are rendered inaccessible or otherwise obscured from the landscape over a 10,000-year period. That number rises to 50% over a 15,000-year period (Collins 1991:161-163; Laville et al. 1980:48-51). The massive collapse event that currently obstructs Bonfire Shelter at a minimum pre-dates Bone Bed 2 (over 10,000 years ago) but has not been directly dated (Dibble and Lorrain 1968:13,26). The area beneath the debris was once functional space protected beneath the brow. It is possible that archaeological or paleontological materials that pre-date the collapse are sealed beneath the boulder field.

The processes outlined below drive the rockshelter cycle of undercutting, infilling, and collapse. The environmental conditions associated with each process have significant implications for a shelter’s suitability for habitation or other subsistence purposes. The combined environmental conditions can often be inferred from the derivative sediments through geoarchaeological methods.

4.1.1 *Physical Formation Processes*

Mechanical processes driven by broader climatic trends are primary weathering agents capable of eroding significant quantities of material from bedrock. Cryoclastic, fluvial, and aeolian activity contribute to the shelters of the Lower Pecos. The extent and efficiency of any one process is a function of duration, intensity, and differential bedrock susceptibility (Black 2001a; Dibble and Lorrain 1968; Robinson 1997).

Cryoclastic weathering, or frost spalling, appears to be the dominant mode of sedimentation contributing to Bone Bed 1 (Robinson 1997). The crystallization and expansion of water molecules contained in bedrock pores and crevices below 32° F (0° C) drives tabular spalls (eboulis) from the interior surfaces of the shelter (Laville et al. 1980:51). Water may expand up to 9% by volume during freeze episodes, creating tensile forces exceeding 200 pounds per square inch (PSI). During colder, wetter intervals (such as the Pleistocene), bedrock exfoliation drives rapid incision into the parent material and causing the formation of overhanging shelter brows. This significant force impacts all scales of the landscape, from fracturing small cobbles to triggering massive collapse events (Mentzer 2017:728-730). The significant quantities of eboulis in Zone 1 and Bone Bed 1 suggest that the Late Pleistocene was a time of relatively rapid expansion and instability at Bonfire Shelter (Dibble and Lorrain 1968:28; Robinson 1997:41).

The relative proportion of coarse frost spalls to finer-grained sediments accumulating within the shelter can provide a generalized indication of paleoclimatic conditions (Laville et al. 1980:48-51). Large quantities of eboulis are indicative of cold wet conditions; a preponderance of fine-grained sediments suggest warmer drier intervals. Increased stability marked by reduced quantities of debris falling from the ceiling may make shelters more suitable for habitation and exploitation by a variety of species (Bement 1986a:61; Robinson 1997:41).

Sediment particles entrained in fluid systems, including both wind and water, can scour and abrade exposed rockfaces to form shelters. The intensity of the abrasive force, the size and quantity of entrained sediment particles, and exposure duration ultimately determine the extent of

erosion (Waters 1992:208-210). Over a long enough interval, the repetitive impact of entrained particles and direct fluid action can etch cavities into even the most resistant rock formations. Locations where fluid velocity increases, rapidly changes direction, or is continuous over long periods of time (such as the bend of a canyon or narrowing of a river) are more susceptible to abrasive erosion (Waters 1992:208-210).

Fluvial action can entrain a broad spectrum of sediment particles from fine silts and clays to massive boulders (Waters 1992:120-122). Entrained sediment loads have significant abrasive potential, but erosion requires direct contact with the moving water source. Fluvial processes do not appear to play a significant role in formation of Bonfire Shelter.

In contrast, aeolian processes transport a relatively narrow band of particles ranging from fine sands to coarse silts (Waters 1992:186-187). Arid landscapes with sparse vegetation to hold sediments in place are often susceptible to aeolian erosion. Unlike cryoclastic weathering, aeolian erosion tends to scour smaller individual grains and clasts away from exposed bedrock surfaces, resulting in an abraded or sand-blasted appearance and rounded, elongate alcoves (Mentzer 2017:729-732). Aeolian erosion is most efficient at lower altitudes where the coarsest sediment load is concentrated forming undercut landforms such as “balanced rocks” and zeugen (Pelletier et al. 2018). Fine-grained aeolian sediment loads can be transported vast distances from the source. Rockshelters acting as sediment traps can provide unique insight into regional environmental trends. Bonfire’s obscured entrance may cause an increased capacity for aeolian sediment retention (Straus 1990:259).

4.1.2 *Chemical Formation Processes*

Karstic landscapes are systems of caves, springs, sinkholes, and faults formed through the chemical dissolution of limestone, dolomite, and other water-soluble bedrocks (Karkanis and Goldberg 2017:108-118). Rainwater becomes slightly acidic as it absorbs atmospheric CO₂ to form carbonic acid, making it a more effective solvent. Networks of these features facilitate the

subterranean movement of water through local aquifers (Ford 2004). The deeply incised canyons and rockshelters of the Lower Pecos are indicative of an active karstic environment.

Karstic landscape features range considerably in size, many of which are visible in the vicinity of Bonfire Shelter (Gines 2004:1010-1016). Centimeter-thick rillenkarren flutes are visible along the rim and upland margins of Mile Canyon. Illustrated in **Figure 4-1**, meter-wide dissolution pans, referred to locally as tinaja, pocket the canyon floor and retain water for a short time following rain. While not documented at Mile Canyon, cenotes and sinkholes several meters wide can form where subterranean dissolution caverns collapse. The resulting void may extend from the surface deep into the bedrock and aquifer, perpetually replenishing the cavern with water. The plunge pool at the head of Mile Canyon evokes these water-filled cisterns, but torrents of water pouring over the vertical face during major precipitation events likely contributed to its formation as much as chemical dissolution. Some have argued the Mile Canyon itself is a collapsed karstic cave system (Gines 2004; Williams 2004:17-18). The massive boulder fields through the upper canyon may represent the remnants of the cavern's roof (Frederick 2017b:17-18).

Dissolved minerals precipitate as crystalline solids when the water-carbonate solution becomes supersaturated, often due to a drop in CO₂ levels. Depressed CO₂ levels are common in caves where atmospheric air exchange is limited (Dreybrodt 2004; Hill and Forti 2004). The deposited minerals form speleothems including highly variable dripstones (i.e.: stalactites and stalagmites) and flow stones (i.e.: travertine and tufa). Dripstones are more common in true caves than in rockshelters, but flowstones are present in the Mile Canyon rockshelters. At Skiles Shelter, a two-meter accumulation of tufa demarks the boundary between the northern and southern shelter lobes. Tufa forms where dissolved carbonates precipitate at spring heads as supersaturated water is vented from the aquifer back to the surface (Smart and Worthington 2004:1503). Because they incorporate atmospheric CO₂, speleothems can be directly dated to

contextualize geological and archaeological deposits (Haynes and Agogino 1986; Pentecost 2005).



Figure 4-1. Water-filled tinaja on the canyon floor below Eagle Cave. View northeast towards Bonfire Shelter.

Tafoni, or surface weathering driven by salt crystallization, form through a bedrock exfoliation process similar to cryoclastic weathering (Mentzer 2017:728-730). Illustrated in

Figure 4-2, salt weathering results in the distinct honeycomb surface texture visible at numerous Lower Pecos shelters including the White Shaman and Skiles Shelter. Salts, frequently gypsum, form as dissolved minerals react in solution and precipitate through evaporation (Forti and Hill 2004). Crystal growth within bedrock pores can fracture rock and drive tabular spalls from exposed surfaces with the same force as frozen water. Significant quantities of gypsum detected in Bone Bed 1 and across Mile Canyon suggest that salt weathering plays a significant role in local shelter formation (Koenig, Nielsen, et al. 2017:96-100).



Figure 4-2. Honeycomb Tafoni salt weathering along the back wall of the White Shaman site, a rockshelter overlooking the Pecos River.

4.1.3 *Collapse*

As shelters expand, they may begin to undercut the overlying geological formations to the point where the overhanging brow cannot support itself and collapses (Laville et al. 1980:48-51). Mass wasting events occur as weathering processes continue to weaken joints, fracture planes, and other imperfections in the brow to the point that abrupt climate changes, frost wedging, seismic activity (in susceptible regions), or general attrition cause a catastrophic failure. The

resulting colluvial debris, referred to as talus, accumulates near the mouth of the shelter. Collapse events may completely change the functional space of a shelter (Straus 1990:279). Primary activity areas near what was previously the drip line can be rendered inaccessible to inhabitants and subsequent archaeologists beneath massive debris fields. The obstructions and receding brow-line force occupants to utilize deeper interior portions of the shelter, resulting in terrace-like archaeological deposits with younger deposits theoretically concentrated closer to the rear shelter wall. As weathering continues, cycles of undercutting and collapse may entirely obscure shelter entrances (Waters 1992:244-246). It appears that the large collapse event at Bonfire Shelter occurred well before the earliest evidence of human occupation (Dibble and Lorrain 1968:24). This changing in the shelter's morphology played a critical role in subsequent site-use and sedimentation patterns (Bement 1986a:2.; Dibble and Lorrain 1968).

4.2 *Sedimentation*

Once formed, rockshelters function as sediment traps, accumulating material through a complex array of environmental processes (Jonathan and Paul 2010:261-262; Waters 1992:242). The same processes that initially create the shelters also drive their sedimentation. Rockshelter sediments accumulate from endogenic sources including the bedrock parent material and derivative minerals, and exogenic materials originating outside the shelter. Once deposited within the shelter, bioturbation, freeze thaw cycling, chemical alteration, and anthropogenic activity (among other processes) continue to modify sediments. (Laville et al. 1980:61-73). In the shelters of the Lower Pecos, formal pedogenesis is often limited due to the sheltered setting, arid conditions, limited sunlight, and stunted microbial activity (Davis 1990; Mentzer 2017:735). Despite this, active post-depositional processes can still have the potential to move, damage, or destroy archaeological materials accumulating within these strata. Geoarchaeological analysis of rockshelter sediments can help to disentangle the relationship between environmental conditions, sediment sources, and archaeological materials (Farrand 2001).

The structure of archaeological deposits in rockshelter contexts is influenced by these formation processes (Straus 1990:264-266). Materials deposited on rapidly aggrading surfaces may be more likely to remain in primary, well-stratified context. Surfaces exposed for long periods with limited deposition are more likely to suffer from a palimpsest effect, where material from multiple events become unintelligibly comingled and superimposed as a result of ongoing activities within the shelter. Dense eboulis may indicate a period of environmental instability where regular spall detachments rendered the shelter hazardous with falling debris. Coarse sediments can abrade or incise materials incorporated into the matrix, creating patterns resembling use-wear and modification (Laville et al. 1980:61-63).

4.2.1 *Endogenic Sediments*

Endogenic sediments derived from the shelter's bedrock parent material accumulate as byproducts of the weathering processes described above (Waters 1992:242). Endogenic particle size distributions vary greatly as functions of parent material grain-size, environmental conditions at the time of weathering, the mode of particle detachment, and post-depositional modification processes. Large tabular spalls (eboulis) and massive boulders may be driven off in great quantities via intensive cryoclastic action during cold, wet periods (Laville et al. 1980).

Controlled experiments suggest that the frequency of the freeze-thaw cycles, rather than the intensity of temperature extreme variation, has a greater impact on spall size and morphology (Farrand 2001:552-555). Farrand argues that more frequent freeze-thaw cycles in wetter environments will ultimately result in smaller, more abundant debris in the sediment column (Farrand 1975:19; Lautridou and Ozouf 1982). The weathering processes that drive spall exfoliation do not cease once the material is deposited and spalls will continue to fracture and break down in situ. By volume, frost spalls of varying sizes are the most abundant component of the Pleistocene strata at Bonfire Shelter.

Smaller particles are released as spalls exfoliate from the bedrock but represent a small proportion of the cold-climate sediment matrix compared to larger eboulis. During more

temperate intervals, the ratio of smaller grains may be higher (Laville et al. 1980:52-53).

Attrition, or granular disintegration, from wind/water weathering and less intense (but potentially more frequent) freeze-thaw cycles releases individual grains from the bedrock which continually accumulate across the shelter interior (Donahue and Adovasio 1990:240-242; Laville et al. 1980:53).

Excavators at Meadowcroft Shelter, a rockshelter with a reported earlier than Clovis component incised into the Morgantown-Connellsville Sandstone of Southwestern Pennsylvania, quantified bedrock attrition over a five year period in the 1970s (Adovasio et al. 1990; Donahue and Adovasio 1990:240-242). Over a 25m² area, between 2 and 50 grams of material exfoliated from the shelter ceiling each day, averaging 10-15 grams with higher rates during colder months. The investigators calculated that this would result in the accumulation of 1.1 – 27.4 cm of sediment over 1000 years. Parent material grain-size and lithology ultimately determines the attributes of the exfoliated material. Meadowcroft attrition sediments were fine-grained sands with a normal grain-size distribution derived from the Morgantown-Connellsville sandstone (Donahue and Adovasio 1990:242). Mean particle size, morphology, and rate of attrition will vary between parent materials, but similar patterns might be expected.

The accumulation of karstic precipitates (i.e.: gypsum or calcium carbonate) is secondary source of endogenic sediment (Farrand 2001:539). In addition to speleothems, dissolved minerals can percolate through the sediment column and recrystallize (Karkanas 2017:132). The precipitates may fill voids within the sediment matrix or adhere to surface of individual grains, gravel, bone, or artifacts (Farrand 1975:12). Ongoing precipitation can form nodules or mineral “shells” several millimeters thick. Porous bone may be more susceptible to his effect, providing ample surface area for mineral accumulation. While moisture is required for minerals to move through the sediment column, precipitation may be more abundant in arid environments driven by rapid evaporation (Karkanas 2017:133).

4.2.2 *Exogenic Sediments*

Exogenic sediments originate from sources other than the shelter parent material. The hollowed alcoves and partially obscured entrances of rockshelters function as natural sediment traps, retaining wind-blown, water-borne, and colluvial sediments. Sediments protected beneath the overhanging brow are less susceptible to erosion and pedogenic activity. The resulting stratigraphic sequences are valuable sources of geological data, providing insight into changing sediment transport vectors, sediment sources, regional flora and fauna, and cultural patterns over time (Bryant and Holloway 1985; Scott-Cummings 1992; Waters 1992).

4.2.2.1 *Aeolian Transport*

Aeolian processes can transport fine-grained particles significant distances from their source as suspended sediment load (constantly elevated) or through saltation (periodically elevated) (Waters 1992). In addition to persistent winds, aeolian transport requires significant sources of unconsolidated sediment, a common feature of sparsely vegetated arid environments. The particle size bands lifted by wind are narrow and consistent, resulting in well sorted deposits and an inverse correlation between particle size and distance transported.

Sand particles between 0.84 – 0.11 mm are readily entrained in air currents (Waters 1992:185-186). Fine silts and clays can remaining aloft over significant distances but require higher initial entrainment velocities to overcome electrostatic charges that cause them cling to one another (Huggett 2015). Coarser particles travel shorter distances or may only creep across the ground surface. This winnowing effect results in relatively homogenous sediments at any given distance from the sediment source (Waters 1992:186-187). Aeolian-entrained sediments are redeposited as particle velocity decreases due to reduced wind speeds or obstructions. Rockshelters act as eddies, allowing sediments to enter but blocking the shifts in wind speed and direction needed to re-entrain particles (Waters 1992:242).

Previous geoarchaeological studies at the Mile Canyon shelters identified the Rio Grande as a significant exogenic sediment source (Heisinger 2019; Rodriguez 2015). Massive alluvial deposits observed within features at Skiles Shelter (Rodriguez 2015:71-72) and (to a lesser degree) Kelley Cave (Rodriguez 2015:88, 160-161) are the remnants of prehistoric flood events that breached the shelters. Compositional analysis and grain-size studies at Bonfire Shelter and Eagle Cave identified anomalous magnetic minerals in the fine sediment bands similar to the alluvium, but no evidence of direct flooding has been documented (Nielsen 2017; Robinson 1997). At Eagle Cave, anthropogenic sediment introduction to support the massive Archaic earth oven industry appears to account for much of the alluvial sediment identified in the Archaic horizons (Nielsen 2017:160). No comparable anthropogenic mechanism has been identified at Bonfire Shelter, let alone Bone Bed 1. Aeolian redeposition of Rio Grande alluvium may account for the presence of at least some of the fine-grained exogenic material.

From its headwaters in the San Juan Mountains of Colorado and the Sierra Madre Oriental in Northern Mexico, the Rio Grande accumulates an enormous sediment load laden with heavy, iron-rich, minerals with high magnetic susceptibilities as it traverses the volcanic landscape of the Trans-Pecos (Pagano 2019:86-87; Schmidt 2010). Over-bank flooding downstream redeposits these mineral-rich sediments across the broad floodplains of the South Texas, contributing to the Lower Rio Grande Valley's reputation as fertile agricultural land (Johnson 2010).

In Val Verde County, the Rio Grande is deeply incised into the limestone bedrock. Despite this, sediments continue to accumulate along narrow terraces and point bars (Golden et al. 1982). Relict Pleistocene strath terraces and alluvial sediment packages high on the canyon margins are indicative of a long-term cycle of flooding, sediment deposition, erosion, and down-cutting in the immediate vicinity of Mile Canyon throughout prehistory (Frederick 2017b; Pagano 2019). The relative aridity of the Lower Pecos and limited vegetation cover leaves floodplain sediments susceptible to secondary aeolian erosion (Golden et al. 1982).

4.2.2.2 *Fluvial Transport*

Aside from mass wasting processes, fluvial action has the potential to transport the largest volume and largest individual sediment clasts (Waters 1992:120-121). Rockshelters located on active riverine landforms or in the associated flood zones are especially susceptible to fluvial sedimentation. Chronic or intermittent flooding can introduce massive sediment deposits if water levels breach the mouth of the shelter.

The structure, sorting, and morphology of water-borne sediment deposits can provide insight into the relative velocity and energy of a depositional environment (Ferring 2017:5). The transport and subsequent deposition of water-borne sediments is governed by Stokes Law: more energy is required to entrain and suspend larger particles than smaller particles (Waters 1992:36-40, 121-124). Smaller particles will remain suspended for longer periods of time. Typically, sediments are deposited sequentially as water velocity decreases; large particles are deposited first followed by the gradual settling of smaller particles. This often results in the characteristic well-sorted fining upward and fining outward sequences of alluvial deposits (Collinson 1996). Deviations from this model are not uncommon. Analysis of sediments at Arenosa shelter identified inverted fining sequences attributed to slack-water flooding (Patton and Dibble 1982:108). High energy and turbulent environments can result in poorly sorted deposits with comingled particle sizes (Collinson 1996:38-40).

The massive alluvial deposits identified at the lower Mile Canyon sites are not present at Bonfire Shelter (Rodriguez 2015). However, fluvial action can occur on a smaller scale if sediment-laden runoff enters via the canyon rim or accumulates and redeposits additional sediment from within the shelter itself. Waterborne deposits from any source may result in distinguishable fining sequences. The “silty trough” described by Dibble and Bement in Bone Bed 1 may be the result of such an event (Dibble and Lorrain 1968:28).

Exogenic water-borne material can often be identified from macroscopic attributes (Waters 1992:26-28). Fluvial sediments often have distinct rounded morphologies and larger

maximum clast sizes than aeolian or attrition sediments. Constant impacts with other entrained sediments and channel debris while in transit abraded and polished particle surfaces. Chemical dissolution can further round the surfaces of entrained soluble materials. This rock-tumbler effect is visible in particles of all sizes, from the largest boulders to individual fine sand grains. The sampling interval implemented for particle size studies could preclude the detection of intra-stratum fining sequences (Ferring 2017:10). In these instances, particle morphology is a valuable marker for fluvial activity.

4.2.2.3 *Colluvial Transport*

Sheet wash, landslides, and rockfall events have significant implications for shelter morphology and sedimentation (Mentzer 2017:739-740). These gravity-mobilized sediments and rocky debris often accumulate at the base of cliffs or other steep slopes. In rockshelter settings, colluvium accumulates along the dripline as sheetwash over the overhanging brow and talus debris from roof collapse events (Farrand 2001:549). Water containing sediment derived from the uplands outside the shelter can enter through cracks, crevices, and spring events in the bedrock (Karkanis and Goldberg 2017:112). These high energy transport vectors often result in poorly sorted and heterogenous deposits (Waters 1992:232, 241). Deposits that extend beyond the shelter brow are susceptible to secondary erosion and down-slope movement due to their steep angle of repose, unconsolidated composition, and increased exposure to the element. Collapse debris, eroded sediments, and anthropogenic refuse removed from internal activity areas often accumulate in middens beneath the main shelter area (Straus 1990:259).

The accumulation of large volumes of colluvium can dramatically change sedimentation patterns (Mentzer 2017:735, 739-740). Large roof-collapse events can inhibit erosion from the shelter interior and exacerbate the accumulation of aeolian and/or alluvial sediments. The accumulation of alluvium behind large collapse debris directly contributed to the massive stratigraphic profiles visible at Arenosa Shelter and Sayles Adobe (Dibble 1967; Pagano 2019). At Bonfire Shelter, the massive rockfalls obstructing the mouth of the shelter redirect sheetwash

spilling from the canyon rim back into the shelter interior (Bement 1986a:2). The notch in the canyon rim funnels upland sediments and debris directly into the shelter where it accumulates on the talus cone. Variable sediment accretion and erosion rates contribute to stratigraphic discontinuities across the shelter (Farrand 2001:547). The tripartite stratigraphy of Bone Bed 2 visible on the talus cone becomes increasingly undifferentiated as it tapers across the shelter interior (Dibble and Lorrain 1968:29). Bone Bed 1 is not visible on the talus cone at all.

4.2.2.4 *Manuports and Non-Local Material*

The presence of non-local materials is a critical signal that external processes are influencing the development of a rockshelter ecosystem. Dissecting the contributing processes can provide critical context towards determining the provenience and post-depositional history of associated objects (Farrand 2001:543). Manuports are unmodified objects identified in a geological context where they would not be expected in nature. Especially within the context rockshelters and archaeological sites, non-local materials that cannot be accounted for within the working formation model may be attributable to human activity and classified as manuports (Farrand 2001:242).

Dibble and Bement argue that the rounded cobbles observed in Bone Bed 1 are manuports based on their inconsistent morphology compared to the surrounding spall-laden matrix (Bement 1986a; Dibble and Lorrain 1968). A well-developed geological model that accounts for many of the observed formation processes can strengthen the argument for a manuport. Without supporting evidence, manuports are equivocal and are insufficient for the classification of an archaeological site or horizon.

Rounded pebbles recovered from burned rock horizons at Eagle Cave and other Mile Canyon shelters well above typical flood levels and devoid of other contextual evidence that would explain their presence have been classified as manuports (Nielsen 2017:152). It is unlikely that such gravels could have entered the shelter without human or animal assistance. The coincident identification of painted pebbles with similar morphologies suggest that these stones

were introduced intentionally for some unknown purpose; possibly to make more painted pebbles or as painted pebbles with no extant pigments.

4.3 Post-Depositional Modification

Once deposited, rockshelter sediments do not remain static. Formal pedogenesis may be limited in rockshelter settings (Davis 1990), but the accumulated sediments remain susceptible to taphonomic processes that alter their geological profile and impact the preservation of associated cultural material (Laville et al. 1980:52-63; Mentzer 2017:735). Primary post-depositional impacts relevant to the Lower Pecos include cryoturbation, bioturbation, and anthroturbation each with unique geoarchaeologically detectable geological profiles. The impact of post-depositional processes on Bone Bed 1 has been acknowledged, but not fully addressed. The volume of spall accumulating in deep Bonfire strata suggests conditions were suitable for cryoclastic action. Bement notes evidence of carnivore scavenging on several of the Bone Bed 1 remains (Bement 1986a:62), but the implications for archaeological evidence and the displacement of faunal remains have not been fully studied. The impact of burrowing rodents and smaller fauna is similarly deficient.

4.3.1 Cryoturbation

In addition to contributing to shelter expansion, freeze-thaw cycles churn in situ sediments through the repeated expansion and contraction of water within the matrix (Farrand 2001:554). Extended freeze-thaw cycling and increased sediment moisture content increases cryoturbation intensity and effects. Cryoturbation causes post-depositional eboulis fracturing, abrasion, and rounding through the repetitive churning processes, resulting in additional fine-fraction sediment accumulation and smaller average spall size (Lautridou and Ozouf 1982; Laville et al. 1980:51). Artifacts and bone within the matrix suffer the same post-depositional effects of cryoclastism. The resulting abrasions and fracturing may superficially resemble use-wear or modification (Laville et al. 1980:61-63). The cryoclastic displacement of artifacts,

sediments, and other materials of interest can cause significant interpretative complications (Texier et al. 1998).

4.3.2 *Bioturbation*

Cool, shaded rockshelter interiors offer protection from the elements and host potential sources of food and water. These resources draw the attention of animals of all sizes and dispositions, including humans. The combined effects of this ecosystem can influence the structure composition of actively accumulating surfaces and buried deposits (Farrand 2001:539-542). Biological displacement of in situ artifacts, faunal remains, and datable material complicates stratigraphic interpretation and can compromise the integrity of associated data.

Accurately identifying evidence of animal activity is critical to the interpretation of Bone Bed 1 at Bonfire Shelter. Regardless of the origins of the Bone Bed 1 faunal assemblage, at present there is no explanation for the observed fragmentation patterns. Like cryoturbation, post-depositional trampling and/or gnawing causes taphonomic “artifacts” which can be difficult to differentiate from human butchering practices and can contribute to the horizontal displacement of remains (Fernandez-Jalvo and Andrews 2016; Haynes 1988; Texier et al. 1998). Vertical displacement can result in mismatches between datable material and stratum of origin, leading to the mischaracterization of associated materials. Accounting for these potential sources of error can strengthen arguments for the role of human agents.

Rodents and other small mammals burrow through soft cultural deposits, displacing artifacts and sediments (Johnson 2002). Burrow infilling creates intrusive pockets of younger material, sometimes referred to as krotovina. Specimens unknowingly collected from these disturbed contexts can result in anomalously young dates, skewing the chronologies of entire sites (Goldberg and Macphail 2013:59). Packrat middens are well documented features in Lower Pecos rockshelters. Despite disturbing in situ deposits, packrats actively collect small vertebrate bone, seeds, insect remains, and cultural material in their nests, which subsequently provides a superb cross-section of the environmental conditions of a time period (Rogers et al. 2008:18-19).

The activities of larger animals can be similarly detrimental. Hoofed animals can churn the upper centimeters of the shelter floor and may create deeper ruts or wallows susceptible to infilling. In addition to displacement, artifacts and bones within the impacted zone can be directly damaged. In highly abrasive sediments, trampling effects on bone can be misconstrued as evidence of cultural modification (Rogers et al. 2008:293, 307-308).

The introduction of domesticated sheep and goats to the Lower Pecos in the 19th century is visible in the archaeological record, marked by the appearance of goat and sheep dung in excavated samples (Nielsen 2017:161). These droppings function as cultural markers and evidence of churned or disturbed contexts. Some ranchers used the rockshelters as livestock pens, stabling dozens of animals at a time. The constant abrasion of wool and fur creates a distinct polish on the interior walls of the shelter and may contribute to bedrock attrition (Mentzer 2017:727, 738).

Insects are also valuable paleoenvironmental indicators with populations rapidly shifting in tandem with environmental conditions (Panagiotakopulu and Buckland 2017). Insect burrowing can cause displacement effects and obscure stratigraphy in the same manner as burrowing mammals, albeit on a smaller scale (Goldberg and Macphail 2013:59). Insect disturbances are especially prevalent in previously excavated or otherwise disturbed contexts (Nielsen 2017:184). At Bonfire Shelter, insects including giant foot-long centipedes capable of displacing large amounts of sediment, were observed burrowing into the slumping faces of the 1960/1980 excavation block. Small beetles were regularly observed burrowing directly into recently exposed faunal remains, contributing to their rapid deterioration. Beyond sediment impacts, human activity within the shelter can significantly alter the local insect population (Panagiotakopulu et al. 2010). Humans may inadvertently introduce insects, pests, and parasites to shelter settings on their person, as hosts, or on materials that are introduced to the shelter.

4.3.3 *Anthroturbation*

Humans have a unique capacity to modify landscape features to suit their subsistence needs (Straus 1990). Passive impacts, such as trampling and minor surface disturbances, may be indistinguishable from other animals (unless associated artifacts are identified) but have the potential to entirely obscure underlying deposits (Goldberg and Macphail 2013:59; Patton and Dibble 1982:108). Passive introduction of exogenic sediments on a person or their belongings may be detectable, but difficult to differentiate from other mechanisms (Farrand 2001:542). Unlike other visitors, humans intentionally modify rockshelters, actively introducing large amounts of foreign material to facilitate subsistence activities. Anthroturbation may not be directly relevant to the interpretation of Bone Bed 1 but is a critical factor in the development of many rockshelters.

Humans have exploited the rockshelters of the Lower Pecos for millennia. Pit excavation for cooking, burying the dead, latrines, or caching tools displaces large amounts of sediment (Farrand 2001:542). Much like the bioturbations described above, these features can be intrusive to underlying strata, altering the vertical position of artifacts and causing stratigraphic discontinuities across the site. The impact is clearly visible in the main trench profile at Eagle Cave. Pleistocene stratigraphy composed primarily of endogenic roof spall and limestone dust abruptly gives way to a palimpsest of earth-oven refuse, clearing debris, and associated cultural material. The shift marks a dramatic transition towards the desert plant based subsistence strategies of the Holocene Archaic (Koenig, Nielsen, et al. 2017:85; Nielsen 2017:17).

4.3.3.1 *Archaeological Impacts to the Archaeological Record*

Excavation and archaeological inquiry itself can be considered a form of anthroturbation. The highly variable methodologies implemented across the Lower Pecos have had serious adverse consequences for the remaining intact deposits. In addition to professional archaeologists,

the region's reputation for stunning artifacts has attracted private collectors and illicit excavations for over a century.

As early as the 1930s, professional archaeologists noted looter's trenches at the shelters that they visited (A.T. Jackson went as far as noting that the pot-hunters were "angels" compared to the "egotistical asses" that vandalize rock art panels) (Jackson 1938:xxi). Several shelters on private property (including Fate Bell) were operated as "Pay-to-Dig" attractions for many years before conservation-minded organizations subsumed management. Relic hunters were often placated by the stone and woven artifacts of later occupants, leaving underlying early Archaic and Paleoindian strata relatively intact (Turpin 1992:10; 1994a:73). Bonfire remained relatively undisturbed by pothunters due to its limited visibility and notable lack of cultural material on the surface.

The Amistad investigators factored future vandalism susceptibility into their triage strategy, but often failed to implement conservation measures once their own excavations were complete (Koenig, Nielsen, et al. 2017:76). The excavation blocks at Eagle Cave and Bonfire Shelter remained open well into the 21st century (Black 2001c). Dibble intentionally left his excavations open to encourage future research in the deeply buried strata of Bonfire Shelter. He also strategically placed spoil piles over the deepest portion of the shelter, which he believed would yield the densest concentrations of archaeological material, to discourage excavation by unprepared archaeologists and illicit prodders. Since Amistad, the blocks have yielded significant new data. After nearly 60 years, erosion has rendered the blocks unstable threatening the integrity of the entire site.

Archaeological priorities have also changed since the first excavations in the Lower Pecos (Black 2013). Early expeditions sought the acquisition of artifacts as oddities and art pieces, followed by basic questions of chronology. Modern methods target specific nuances of human behavior. Future archaeologists may have entirely different priorities. In many cases, it is difficult to ask new questions of old datasets. The undocumented or poorly provenienced removal

of artifacts from archaeological sites biases the assemblage and can skew interpretations. As an inherently destructive science, it is impossible to reconstruct the provenience of artifacts once they are extracted. Even if every privately held artifact were recovered, the relationships between them would be circumstantial and incomplete at best.

Without Dibble's open block, the University of Texas, Southern Methodist University, and Texas State University's access to Bone Beds 1 and 2 at Bonfire Shelter would have been greatly hindered. Direct access to these profiles has facilitated the ASWT's "Low Impact, High Resolution" strategy, integrating 60 years of technological and methodological advances to collect the maximum amount of data using the least invasive excavations possible.

The current excavations at Bonfire Shelter and the ASWT's Eagle Cave expedition include restoration clauses designed to leave the sites in better condition than they were encountered. The main trench at Eagle Cave has been backfilled, minimizing the potential for additional collapse. At Bonfire, the talus cone was stabilized and a water runoff management system was implemented. Backfilling the main block began in January of 2020 following the completion of the 2019 field season. This conservation minded approach was implemented with the goal of protecting the remaining intact deposits for the next generation.

5. METHODOLOGY

This chapter describes the field and laboratory methods used to evaluate Bone Bed 1. Rockshelter settings, and Bonfire Shelter in particular, present unique challenges. Deep stratigraphy, unconsolidated sediments, poor visibility, and sheer volume of material (among other factors) influenced by the dynamic site formation processes described in **Chapter 4** result in an environment unlike most open air sites. The excavation methods and documentation procedures implemented during the 2017 and 2018 field seasons at Bonfire Shelter were adapted from the ASWT Project's Eagle Nest Canyon Expeditions (2014 – 2017) to overcome these challenges (Koenig and Black 2015). Without their refinement of the specialized excavation techniques and data collection workflows at Eagle Cave and across the Lower Pecos, the current undertakings would not be possible. The theses of ASWT alumni were critical resources in this process (Castañeda 2015; Heisinger 2019; Nielsen 2017; Pagano 2019; Rodriguez 2015).

The integration of Structure from Motion photogrammetry into the Bonfire Expedition workflows is a direct result of the ASWT's extensive field testing and development (Koenig, Willis, et al. 2017). This 3D mapping technology facilitates data collection at an unprecedented resolution, embodying "Low Impact, High Resolution" mantra. The geoarchaeological methods implemented in this thesis were developed in consultation with ASWT co-principle investigator Dr. Charles Frederick. The methods (Nielsen 2017; Pagano 2019) utilized at Eagle Cave (Nielsen 2017), Kelley Cave (Rodriguez 2015), Skiles Shelter (Heisinger 2019; Rodriguez 2015), and Sayles Adobe (Pagano 2019) provided a solid foundation for the Bone Bed 1 analytical framework. The Pleistocene deposits at Bonfire Shelter were very different from the Archaic strata assessed by these researchers; extremely coarse sediments and elevated gypsum levels necessitated the modification of previous analytical strategies to suit the unique Bone Bed 1 environment.

5.1 *Field Methods*

Two primary testing areas, Block C and Block D illustrated in **Figure 5-1**, were identified as viable Bone Bed 1 excavation areas during preliminary field visits to Bonfire Shelter in January of 2017. These areas represent the only unimpeded access to Bone Bed 1 remaining in the shelter. Access to other portions of Bone Bed 1 would require large-scale excavation through at least 2.0 m (6.6 ft) of intact archaeological deposits. During this reconnaissance, all open excavation blocks from the 1960s and 1980s main trench were mapped and assigned arbitrary sequential letter identifiers (Salvage Blocks A through H). Bone Bed 1 excavation Blocks C and D take their names from these designations. Both excavation areas are near the center of the shelter, roughly 5.0 m (16.4 ft) west of the rear shelter wall and 20.0 m (65.6 ft) northeast of the talus cone apex.

Block C measures approximately 3.0 x 1.5 m (9.8 x 4.9 ft), extending north from Dibble's (Dibble and Lorrain 1968)s grid (N90-100 ft/E 45-50 ft) line. Block D measures approximately 3.5 x 1.5m (11.5 x 4.9 ft), extending south from Dibble's grid (N 98-110, E 40-45 ft) line. Both excavation blocks are within or abut the 1983-1984 southernmost excavation unit; an excavated baulk between two of Dibble's interior blocks. Block C spans the width of the main southern entrance to the block. Block D is immediately northeast of Block C parallel to the main walkway.

Block D was partially excavated in the 1980s, terminating at the Bone Bed 1-Zone 2a interface (Bement's Stratum D-E/F/G interface). The base of excavation was covered with a layer of geotextile cloth and capped with a layer of screened back-dirt. A sheet of plywood was later placed over the block for further protection. In Bement's northern "large block" (Block H), Bone Bed 1 was fully excavated.

Three main data series were collected in addition to potential cultural and faunal specimens: geoarchaeological samples for compositional and sedimentological analysis, strategic spot samples targeting microartifact recovery, and high-resolution spatial data. Exposed elements were mapped and photographed in situ. The bone surface morphology of each element was inspected for evidence of modification in the field. This strategy was designed to identify minute traces of cultural activity and explore the taphonomic environment at Bonfire Shelter in the Late Pleistocene.

5.1.1 *Data Recordation*

A master Field Number (FN) Log was implemented to consolidate field specimen, lot, element, and other special sample logs into a single accession sequence. This tracking method eliminated duplicate numbers and provided a quick provenience reference for each entry. Each sampled provenience received a unique FN that functioned as a Lot Number. All subsequent specimens recovered from that provenience received the same Lot FN Number, as well as a unique FN identifier functioning as a Field Specimen or Bag Number. Items that received FNs include: Profile Sections (PS), Strata, Unit Layers, archaeological features, point provenienced artifacts, in situ faunal remains, geological samples, ¹⁴C samples, other special samples, and screen lots.

Each Excavation Unit received a unique identifier following a block-unit number convention. The block prefix indicates the unit's location within the main trench (Block C or Block D) as well as a consecutive number identifying the unit within that block. For example: Unit C1 was the first new unit excavated in Block C while Unit D4 was the fourth new unit opened in Block D.

Profile Sections were designated to specify vertical unit facies and trench walls targeted for sampling or mapping. Profile Sections were numbered continuously across the whole shelter, integrating previously excavated profiles on the talus cone and in the Main Trench. Profile

Sections and their associated FNs tracked the provenience of samples collected directly from profiles (i.e.: no associated unit-layer), the location of Ground Control Points, and the provenience of associated spatial data.

5.1.1.1 Total Station

A Sokkia Total Station paired with an external data collector running SurvCE software was used to measure the location of every sample or provenience FN at precisions up to .001 m (1.0 mm, 0.039 in). Three primary survey datums established by the ASWT in 2014 were used to map Bone Bed 1. Each measurement was recorded on a continuous Total Station Log, which included the shot number, subject (i.e.: FN 60001, GCP-001, etc.), and coordinates. Because each FN was measured with the total station, the total station log proved to be a valuable cross-reference for data quality assurance.

All measurements were recorded on an arbitrary coordinate plane based on Easting and Northing meters ultimately tied to the ASWT Eagle Nest Canyon-Wide grid and UTM coordinates. All total station measurements, 3D Models, orthophotos, and GIS data reference this grid, ensuring compatibility with other ASWT data. Integrating older survey measurements and associated data sets was problematic due to the use of independently defined grids described in **Section 2.3.1**.

The Sokkia's reflectorless mapping capability was extensively utilized across the shelter. This function records measurements without the use of a stadia rod and prism, ideal for mapping Bone Bed 1's delicate faunal remains and unconsolidated stratigraphy. A 5.0 cm (2.0 in), 25 cm (9.8 in), or 3 m (9.8 ft) (extendible to 6.0 m [19.5 ft]) stadia rod paired with interchangeable 25 mm (1.0 in) and 62 mm (2.4 in) prism assemblies was used to map points without a direct line of sight from the survey datum. The precise elevation of stadia-prism assembly was measured and accounted for when mapping without the reflectorless function.

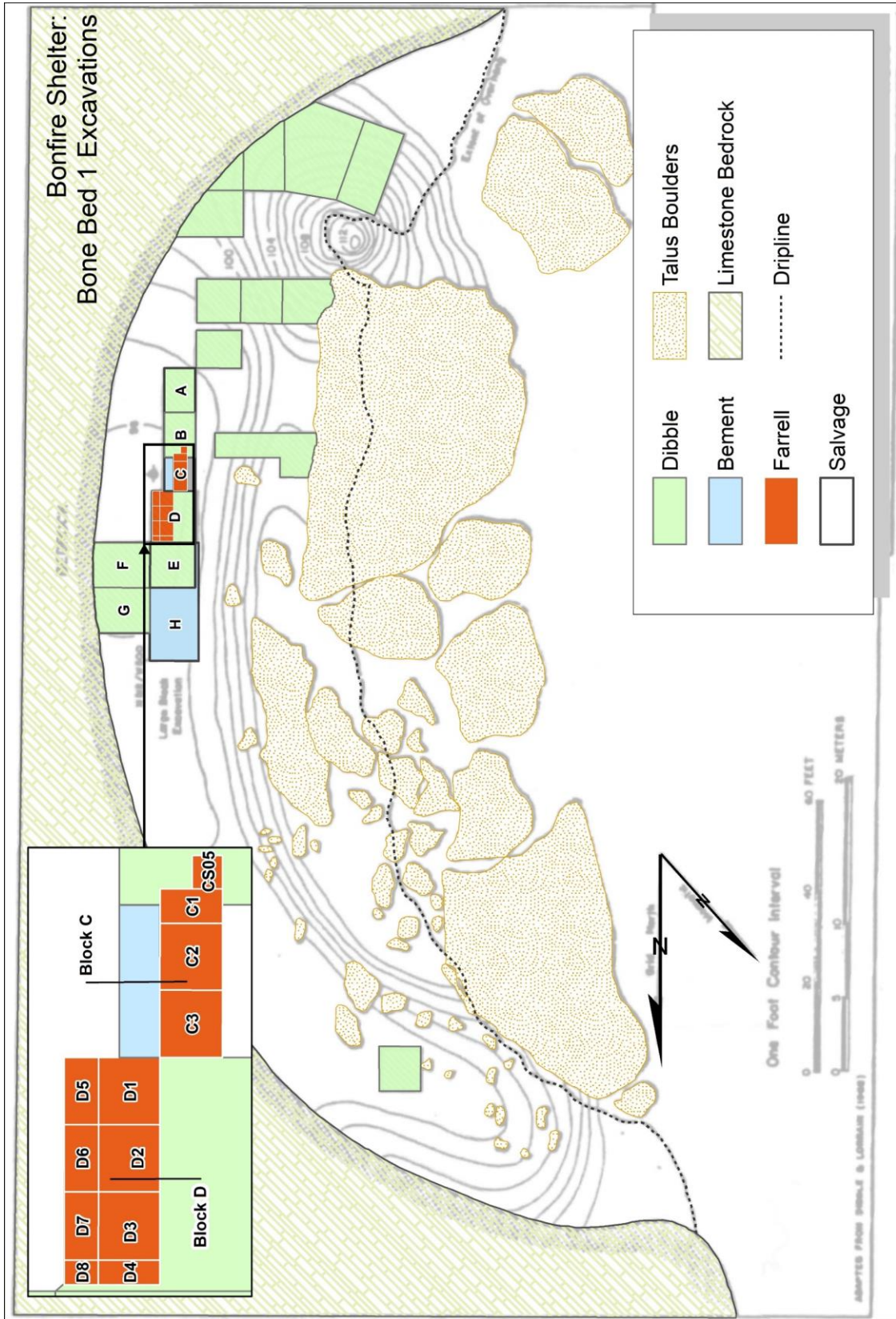


Figure 5-1. 2017-2018 Bone Bed 1 Excavation Blocks

5.1.1.2 *Structure from Motion*

Structure from Motion photogrammetry was used to create 3D models of each excavated unit layer and sampled profile section. The Bonfire Shelter methodology was adapted from the ASWT's process developed for the Eagle Nest Canyon expedition (Koenig, Willis, et al. 2017). Models are constructed from a series of overlapping high-resolution photographs of the target surface and associated GCPs. Photographs were taken in a regular grid-like pattern with 30-80% overlap between each frame. Settings including focal length, ISO, shutter speed, and white balance as well as camera elevation above the subject were maintained throughout each photo series.

Maintaining consistent lighting and minimizing shadows was problematic in the main excavation blocks. Portions of the block were cast in constant shadow by angle of the shelter's mouth, talus debris, and tall profiles. Sets of tripod-mounted 10,000 Lumen LED shop lights were configured overhead and at oblique angles to illuminate workspaces and minimize shadows in photosets and final 3D models. Larger exposures were modeled in "chunks" due to the limited number of available light fixtures. Shadows cast by the photographer were nearly unavoidable when lighting surfaces from multiple angles. Many shadows could be removed during Metashape image post-processing, but persisted as a logistical challenge throughout the excavations.

Photogrammetry photosets were processed using AgiSoft MetaShape (previously AgiSoft PhotoScan) to create 3D models with photorealistic textured overlays, Digital Elevation Models (DEMs), and composite orthophotos. The derived datasets were used natively in MetaShape for measurements and to map faunal remains or exported to ESRI ArcMap/ArcGIS Pro to produce figures and perform other calculations. All spatial data was backed up to secure off-site servers hosted by Texas State University.

5.1.1.3 Ground Control Points

Ground Control Points (GCPs) are semi-permanent spatial markers with known X, Y, and Z coordinates used to georeference 3D models (Koenig, Willis, et al. 2017). To minimize error, five to eight GCPs were included in each Bone Bed 1 model. GCPs were inscribed on prominent boulders, spalls, sample markers/nails, and other stable features as an “X” with permanent marker. Each GCP was photographed to provide context and mapped with the total station. GCPs were tracked by a unique identifier in the Total Station Log as a site-wide sequence of continuous three-digit numbers (i.e.: GCP-123). If a GCP was disturbed, eroded, or destroyed during excavation, a new GCP was established to replace it to ensure a sufficient number of control points were visible in each model.

Accurate measurement of each GCP, consistent georeferencing during MetaShape processing, and precise total station balancing in the field directly impact the accuracy of derivative 3D models and maps. Model accuracy is calculated as Root-Mean Square (RMS) error or, the average difference between the expected coordinates of each GCP in the model and their actual placement (Agisoft 2020:56).

Model accuracy is calculated as Root-Mean Square (RMS) error or, the average difference between the expected coordinates of each GCP in the model and their actual placement (Agisoft 2020:56). Human errors were among the most significant issues encountered. Accidental shifts or bumps to the survey instrument, unaccounted for adjustments to stadia height, dislodged GCPs, and typographical inconsistencies introduce serious errors that may not be noticed until data is returned from the field. In many cases, this may be well after the subject was excavated. Uncorrected errors carried into the analysis process, inconsistent georeferencing, or further typographical errors influence the overall reliability of a 3D model or derivative map. Minimizing human error through mindfulness, both in the field and in the lab, and a robust quality assurance process is critical.

5.1.2 *Excavation Methods*

5.1.2.1 *Unit Placement*

Contiguous 1.0 x 1.0 m (3.28 x 3.28 ft) excavation units were established in Block C and Block D to sample the intact portions of Bone Bed 1 initially exposed during the 1980s expeditions. Three units (UC1, UC2, and UC3) were established in Block C. The northern 50.0 cm (19.7 in) of UC1 was excavated concurrently with UC2 and UC3. The southern 50.0 cm (19.7 in) of the unit provided the most complete (and feasibly excavated) vertical cross-section of Bone Bed 1 in the block and was retained as an intact baulk. After carefully documenting the profile (assigned PS06), a 50.0 x 50.0 cm (19.7 x 19.7 in) sampling column (CS05) was excavated through the baulk.

Eight units were established in Block D (UD1 – UD8), a 3.5 x 1.5 m (11.5 x 4.9 ft) bench immediately northeast of Block C. Units included three full 1.0 x 1.0 m (3.28 x 3.28 ft) units (UD1 – UD3) and five approximately 1.0 x 0.5 m (3.28 x 1.64 ft) partial units (UD4 – UD8). Partial units were placed along the northern and eastern margins of Block D to capture all accessible portions of Bone Bed 1. A 1.0 x 0.5 m (3.28 x 1.64 ft) sondage was excavated across Units D4 and D8 to explore the stratigraphy below the Block D base of excavation. In addition to **Figure 5-1**, **Figure 1-2** and **Figure 7-1** illustrate the placement of these units in the main block and their relationship to other topographic features within the shelter.

5.1.2.2 *Excavation Strategy*

Unit layers were excavated by natural stratigraphy, except where strata exceeded 10.0 cm (3.94 in) in thickness. Thicker strata were arbitrarily subdivided at 10.0 cm (3.94 in) to more accurately describe specimen provenience. In Block D, faunal remains were recovered from multiple layers within Stratum H. The excavation interval was reduced from 10.0 cm (3.94 in) to 5.0 cm (1.97 in) in layers where remains were encountered.

A standardized layer form was completed for each level excavated from each unit. Layer forms were modified from the ASWT Eagle Cave excavations to meet the conditions at Bonfire Shelter. Layer forms included fields for: detailed sediment matrix descriptions; presence/absence of cultural material, faunal remains, botanical material/charcoal; excavation techniques; FN numbers of all faunal elements, artifacts, or samples recovered; associated 3D models; associated photo numbers; and other relevant notes. Each completed layer was photographed, mapped, and modeled in plan-view prior to the removal of in situ faunal remains, large spalls and cobbles, and artifacts (if present).

Sediments were excavated using a combination of trowels, brushes, wooden picks, and scoops. Excavated material was transported by five-gallon bucket to designated screening stations located south of the talus cone or in Dibble's northern-most open excavation unit. Small camera lens "poofers" were used to clear sediment around delicate specimens while minimizing physical contact. Battery operated leaf-blowers were used to clear settling cave dust from profiles and excavation exposures prior to photographing.

Sediments excavated from each provenience were screened separately. All sediments were processed through a set of three approximately 1.0 x 0.5 m (3.28 x 1.64 ft) rectangular nested sieves lined with increasingly fine hardware cloth; 12.7 mm (0.5 in), 6.35 mm (0.25 in), and 3.175 mm (0.125 in) respectively. This method quickly separated the substantial coarse-fraction gravels, improving fine fraction processing efficiency and roughly size grading recovered materials. The sub-3.175 mm sediment fraction was not screened for cultural material in the field. However, point-provenienced geological samples were collected from each unit layer for laboratory analysis.

Materials recovered on the screen were assigned a single Screen Lot FN and bagged together. Botanical material, faunal material larger than 2.0 cm (0.79 in), and diagnostic/potentially modified faunal remains were retained. Potential artifacts, exogenic lithic

materials, and evidence of disturbed contexts (modern flagging tape, pin flags, metal tools, and other residual debris from previous archaeological investigations) were also retained in the screen lot.

5.1.2.3 *Faunal Remains*

Faunal remains were recovered from every excavated Bone Bed 1 stratum. Each element was assigned an FN, photographed in place, and measured at its center point with the total station. Scaled sketch maps of the bone beds were recorded in field notes to track the assigned FNs. Elements were left in situ until the unit layer was fully excavated. Excavation around faunal material was conducted with brushes and wooden tools to minimize damage that could be mistaken for or obscure prehistoric cut-marks.

After mapping, individual elements were wrapped in a layer of aluminum foil. A spray foam jacket was then applied to the aluminum foil to protect the layers during transport. After the foam was set, elements were undercut using wooden implements, supported underneath with multiple trowels, and inverted. The bottom of the jacket was then closed with a layer of aluminum foil and sealed with a final layer of spray foam. Provenience information, including FN, was transcribed directly on the spray foam jacket as well as on the interior aluminum foil. This spray foam method was adapted from a technique used by Leland Bement to facilitate the recovery of human remains from the Seminole Sink site (approximately 20 mi east of Bonfire Shelter), where traditional plaster jackets would not set in the humid cave environment (Bement 1985). Like Seminole Sink, the light-weight foam jackets were logistically advantageous at Bonfire Shelter, where materials were ultimately extracted via a crane with limited capacity on the canyon rim.

The adapted foil and spray foam method implemented during the current Bonfire expedition was largely successful. However, several of the highly deteriorated mammoth ribs recovered from Bone Bed 1 did not survive extraction intact. The deteriorating elements were treated with an Acryloid B-72 resin and acetone consolidant solution prior to extraction but

remained extremely unstable. As the elements were inverted for extraction, B-72-treated cortical surfaces remained fairly intact while the interior cancellous bone that could not be directly treated disintegrated and fell away. Larger fragments were refitted and packed in the foam case with the intact bone where possible. Smaller fragments and bone dust were retained as supplemental material with an associated FN.

Remains in Block D were significantly more stable than those recovered from Block C and required minimal stabilization (see **Chapter 7** discussion of differential preservation in the main trench). Block D elements were wrapped in aluminum foil and/or gauze and transferred to a large artifact bag packed with a piece of 0.64 cm (0.25 in) foam-board to provide support in transit. Foam jackets were generally reserved for very large or very unstable elements. Stable elements, and elements with well-preserved cortical surfaces, were specifically not treated with B-72 to facilitate future bone collagen dating.

The original excavation strategy called for the concurrent excavation of all units across each block, creating a single mappable surface. This method quickly proved to be problematic as more faunal remains were exposed. The cramped quarters of Block C allowed only one person to excavate at a time. Excavating the southern units required the excavator to physically stand on the surface of an adjacent unit. The exposure of each new element reduced the safe positions for the excavator to stand without compromising the integrity of underlying deposits or unintentionally trampling previously exposed areas and remains.

The comingled nature of the bone bed caused a domino effect of destabilization. As one element deteriorated, others shifted sometimes causing further fragmentation. Despite stabilization efforts and minimized contact, many elements immediately exfoliated their cortical surfaces, and disintegrated upon exposure. Burrowing insects immediately descended on the exposed bone, further compromising their integrity.

In Block C, excavation was shifted to the exposure of one unit-layer at a time, minimizing exposure time for any one element. Upon reaching the Bone Bed 1 strata in Unit C1, Units C1 and C2 could be excavated concurrently as extra space opened north of the C1 baulk. Block D yielded fewer remains and was logistically easier to excavate, allowing larger surfaces to be exposed across the block. Field maps and 3D models were used to reconstruct partial exposures in the laboratory.

Differential preservation between Blocks C and D may be a function of their position within the shelter. Both units were partially excavated in the 1980s. However Block C spanned the main entry path into Bement's "Deep Block", receiving significantly more foot traffic than Block D over intervening 40 years. One plaster jacketed element and drips of plaster observed on the initially exposed Unit C3 floor suggest that at least some of the remains in the upper layers of Block C were at one point completely exposed and subsequently reburied. It is unclear if other elements were removed from this area, as published maps only illustrate the northern "Deep Block" (Bement 1986a). The massive blowouts and slump along the western profile of the main block suggest elevated moisture content and erosional impacts in the vicinity of Block C further exacerbated damage to the buried remains. Block D was at a higher elevation within the shelter and protected beneath geotextile fabric and a plywood board, avoiding the worst erosional effects. Block D was also set away from the high foot traffic entryway, reducing wear-and-tear on the underlying deposits.

5.1.3 *Sampling*

Three primary sample types were collected from each excavated layer: geomatrix samples, spot samples, and ^{14}C samples. All samples were collected using a combination of trowels, brushes, and bamboo (for non- ^{14}C samples) picks. Forceps were used in place of trowels to collect particularly small or fragile specimens for ^{14}C dating. Samples were not pre-screened or processed in the field. All coarse fraction gravels, faunal material, and other inclusions were

separated out and retained in the lab prior to analysis. Each sample received a unique FN and was mapped with the total station prior to removal. Spot samples and ^{14}C samples were typically photographed and plotted on sketch maps for later reference.

Geomatrix samples were bulk sediment samples collected specifically for matrix compositional studies. The goal of these analyses was to develop a geological profile of each natural stratum observed in excavation units or profiles. Geomatrix samples were collected using large 6-mil, 4+ liter, tie-off geological specimen bags. A minimum of two liters of matrix was retained en masse for each sample, except where prohibited by thin stratigraphy. Judgmental matrix samples were collected from potential cultural features and within bone concentrations.

Spot samples were smaller, judgmental sediment samples collected to retain examples of stratigraphic anomalies and other areas of interest. Spot samples were extensively used to collect sediment for microartifact analysis. Microartifact samples targeted the margins and articular surfaces of faunal remains as well as between and beneath bone concentrations. Spot samples ranged in size from approximately 200 grams up to 1 kilogram, and generally only included particles < 2.5 cm (1.0 in).

^{14}C Samples were collected specifically for chronometric dating purposes. The majority of the ^{14}C samples consisted of charcoal observed during excavation, however several macrobotanical and faunal specimens were also retained. Only material recovered in situ with unambiguous provenience was collected for ^{14}C analysis. Charcoal samples varied from very small trace charcoal flecks observed within the sediment matrix to centimeter fragments of wood-charcoal encountered in column samples. Bone retained for collagen and/or apatite dating was not treated with B-72 consolidant and was specifically flagged for dating purposes to avoid unintentional contamination. Individual charcoal and botanical specimens were packed inside small aluminum foil envelopes inscribed with the appropriate FN number which was placed inside a 4-mil artifact bag tagged with all appropriate provenience information. Faunal remains

selected for dating were packed in a similar manner. Larger elements were directly wrapped with aluminum foil. Fragile or otherwise unstable elements were stored in artifact bags with a piece of foam board for additional support.

5.1.3.1 Column Samples

A 50.0 x 50.0 cm (19.7 x 19.7 in) column sample (CS05) was excavated in the southwestern corner of Profile Section 6 (PS06); the UC1 baulk. Column samples were excavated by natural stratigraphy as observed in the cleaned profile section. Each stratum was assigned a unique Stratum Number correlated with PS01, Bement's profile of record, prior to excavation. Stratum numbers tracked continuous surfaces across the shelter interior wherever they could be positively identified. Major stratigraphic units can be clearly traced around the perimeter of the open excavation blocks; a fortunate result of the limited prehistoric ground disturbing activity within the shelter and a stark contrast to the massive earth-oven palimpsests in the other Mile Canyon shelters.

All sediment excavated from each column sample stratum was retained as a bulk geomatrix sample including all spall, gravel, and faunal remains. This collection procedure provides a representative sample of the inclusions and the entire particle size spectrum for each stratigraphic unit. Potentially diagnostic faunal remains and artifacts encountered in situ within the column samples were assigned a unique FN, mapped, and collected separately for later identification to prevent damage. Due to the variable depths and significant coarse fraction, many samples required multiple bags and were quite large. Aliquots from each column sample were used for the geoarchaeological analyses described in **Section 5.4** including: particle size distribution, compositional studies, and microartifact analysis.

5.2 *Microartifact Methodology*

The paucity of macro-lithic material from the Paleoindian strata at Bonfire Shelter is well documented (Byerly et al. 2005; Byerly, Meltzer, et al. 2007). The competing interpretations of Bone Bed 2 as a primary kill site and as a secondary processing location provide potential explanations for this scarcity (Bement 2007; Byerly, Cooper, et al. 2007; Byerly et al. 2005; Meltzer et al. 2007; Prewitt 2007). Based on the excavations of other Late Paleoindian sites on the Great Plains, Byerly reports that kill-site lithic assemblages are composed primarily of formal tools that were lost or broken during the hunt. In contrast, processing locality assemblages were defined by a variety of expedient flake tools, resharpening debitage, and other butchery implements (Byerly, Meltzer, et al. 2007:138). Potential improvised bone tools have been identified at several processing sites, including the Colby Mammoth site, the Lang-Ferguson site, and both Paleoindian Bonfire Shelter bone beds (Frison and Todd 1986; Hannus et al. 2018; Johnson 1982). The validity of improvised bone tools has been heatedly debated and will not be used as a defining criterion (Bonnichsen 1979; Johnson 1982).

Byerly and Meltzer's 2005 sampling of Dibble's back dirt yielded five unmodified flakes recovered from limited hand-auger and small trench excavations (a total excavated volume of 1.38m³, approximately 0.5% of Dibble's total excavation volume) (Byerly, Meltzer, et al. 2007:129-132). Extrapolated from these findings, Dibble's limited 12.7 mm (0.5 in) and 6.35 mm (0.25 in) screening methodology was categorically biased against lithic artifact recovery (Byerly, Meltzer, et al. 2007:130). Byerly notes that even using this calculated correction factor the lithic assemblage appears small for a bison processing site. The 2005 study recognizes that it is impossible to differentiate the stratigraphic association of the resampled back dirt artifact, assessing the ratio of total artifacts recovered to total volume of sediment excavated from each unit.

Sediments excavated in 1980s were screened through 6.35 mm (0.25 in) hardware cloth, with portions floated and analyzed for microfauna and botanical materials (Bement 1986a:4). Byerly argues that these high-resolution analyses should minimize the likelihood of artifacts being overlooked (Byerly, Meltzer, et al. 2007:130). The fact that artifacts were observed in neither Bone Bed 1 nor Bone Bed 2 supports this hypothesis. However, microdebitage was not an analytical priority during these analyses and, if present, may have gone unnoticed (Robinson 2016: Personal Communication).

Byerly presents three hypotheses that could account for the absence of lithic material in the shelter interior: geological scouring processes, culturally prescribed clean-up processes, or that artifacts were never deposited in these areas (Byerly, Meltzer, et al. 2007:129-132). From the base of the Talus Cone to the central excavation units, the shelter floor loses over 1.8 m (6.0 ft) in elevation (over 3.7 m [12.0 ft] from to talus cone apex) (Byerly, Meltzer, et al. 2007:131). Runoff moving across this northward gradient could displace surface artifacts, redepositing them in the largely unexcavated northern portion of the shelter where the topography begins to regain elevation towards the northern exit. Geological evidence of such scouring has been limited. However, Byerly suggests it may account for the two flakes recovered from Dibble's northernmost N225/W95 block. Cleaning up living spaces could similarly bias artifact distributions. Discarding debitage in the northern or southern ends of the shelter could also account for the observed patterns. Alternatively, if debitage-producing activities never occurred in the shelter interior, debitage would simply not be a significant component of the Bone Bed 2 assemblage. This potentiality has significant implications for the interpretation as a primary kill site or secondary processing site.

Traditional excavations and sampling at Bonfire Shelter have been extensive. Tons of sediment have been excavated and over 12.0 m (nearly 40.0 ft) of column samples have been collected. Despite this, methodological deficiencies appear to have biased the lithic assemblage.

Detailed microfauna and palynology studies have been conducted, but artifacts smaller than 6.35 mm (0.25 in) have been consistently overlooked – particularly with regards to Bone Bed 1.

The identification of cut marks on Bone Bed 1 faunal remains suggests that, if cultural, at least some level of processing with stone tools occurred (Bement 1986a:39). If processing occurred, especially of large Pleistocene fauna, debitage derived from tool resharpening or utilization should be present.

5.2.1 *Microartifact Background*

Microartifact analysis is a powerful tool for assessing the relative intensity of an activity and variation in those activities over time and space, yielding nuanced reconstructions of intra-site activity patterns (Sherwood 2001:329-330). Differential patterning of cultural material, including pottery, pigments, lithic material, macro-botanical remains, or charcoal can provide insight into *who* was using a space in addition to what activities were occurring (Homsey-Messer and Ortmann 2016). The simple presence or absence of microartifacts can be used to differentiate cultural from geological strata, suggesting broader patterns of site use, abandonment, and reuse (Kilby 1998:9).

Human behaviors such as cleaning living surfaces, tool curation, abandonment, and material scavenging can obscure potentially significant cultural features or modify the archaeological context of traditional macro-artifacts (Hull 1987:773; Schiffer 1972). Traditional archaeological sampling methods and excavator biases can systematically overlook artifacts in smaller size classes. Microartifact cultural signatures may be exempt from these preservation and detection biases, remaining identifiable where other evidence has been destroyed or modified (Fladmark 1982:208).

Because of their small size, microscopic cultural particles become integrated with the surrounding sediment matrix, entering the archaeological record through different vectors than

their larger counterparts (Sherwood 2001:329). Silica dust and small shatter fragments are unlikely to be cleaned up after a stone tool is manufactured or modified (Schiffer 1983). Even if the work area is swept up or larger flakes retained, a “cultural residue” indicative of past human activity is likely to remain at the site (Fladmark 1982). Microartifacts are also introduced to secondary locations on the person or belongings of individuals working in (or even passing through) a primary activity area. However, residue is likely to be densest where the actual activity occurred.

Microartifacts are subject to the same taphonomic processes as the surrounding soils (Homsey-Messer et al. 2016). At <2.0 mm (0.08 in), the size cut-off differentiating fine gravels from coarse sands, microartifacts are functionally the same as naturally occurring sand, silt, and clay particles. Artifacts within the particle transport threshold may be entrained in wind or water and redeposited along with geological sediments (Hull 1987:773-774). However, the mass differential between artifacts and geological sediments may bias what materials are entrained and how far they are transported compared to lighter weight particles of the same size (Fladmark 1982:208).

Experimental studies suggest that sub-2.0 mm (0.08 in) artifacts are more susceptible to redeposition while artifacts between 2.0 and 6.35 mm (0.08 – 0.25 in) have enough mass to remain in place when trampled or otherwise embedded in a sediment substrate (Homsey-Messer and Ortmann 2016:4). It is conceivable that <2.0 mm (0.08 in) microartifacts could contaminate a location if comingled with sediments redeposited from an external site (Homsey-Messer et al. 2016). This effect could be exacerbated in rockshelter settings, which function as natural sediment traps. Larger, heavier microartifacts are less susceptible to transport and more likely to be derived from activity occurring within the shelter itself, reducing the chance of error due to contamination.

Microartifact's archaeological, systemic, and geological context should be considered in broader interpretations of site function and formation processes. Rooted in Binford's Binford (1978a) and Schiffer's (1983, 1995) behavioral conceptions of the archaeological record, Kathleen Hull outlines three criteria for evaluating the context of microartifacts: *Primary Refuse* identified by the presence of corresponding micro- and macro-artifacts; *Secondary Refuse* identified as macro-artifacts with no microartifacts present; and *De Facto Refuse* identified as high microartifact density in the presence of large reduction flakes and/or formal tools (Hull 1987:773).

Primary refuse suggests that the artifacts were deposited at the same location where they were produced (Schiffer 1972:159-160; 1995:27-29). Secondary refuse indicates that the artifacts were moved away from the location where they were produced, through environmental processes or anthropogenic agents. De Facto refuse represents "unintentionally" deposited materials. De Facto refuse includes waste by-products from all stages of lithic reduction, from large cortex removal and platform preparation flakes to shatter and silica dust derived finishing pressure flaking.

Particles of charcoal, bone, botanical and other exogenic materials often associated with human activity found in "out-of-place" contexts have been considered microartifacts in cases where their presence cannot be attributed to natural environmental or depositional agents (Sherwood 2001:330). Even if subjected to significant post-depositional processes, the presence of microartifacts within a stratum suggests at the very least that cultural activity occurred in the spatial and temporal vicinity of the sampling location.

By frequency, microdebitage is the most abundant lithic artifact class produced during all stages of lithic reduction (Fladmark 1982). By count, 99% of all artifacts derived from hard hammer percussion may be <1.0 mm (0.04 in). By mass, the ratio of micro to macro debitage varies by manufacturing technique. Hard hammer percussion may yield 99% macrodebitage and

only 1% microdebitage by mass. In contrast, soft hammer techniques may yield a higher proportion <2.0 mm (0.08 in) debris with 80% macrodebitage and 20% microdebitage by mass (Fladmark 1982:207). Fladmark's study demonstrates that enormous proportions of residual debitage should remain detectable in the vicinity of a lithic reduction event, regardless of the manufacture technique and secondary refuse clean-up.

5.2.2 *Microartifacts at Early Paleoindian Sites*

The resource-conservative subsistence and lithic procurement strategy of Early Paleoindians may have significant implications for the distribution of artifacts and microartifacts in Bone Bed 1. Biface-based toolkits require significant time and energy investment, including travel to raw material sources, manufacture, and maintenance (Kelly 1988). Highly mobile Pleistocene hunter-gatherers developed toolkits that minimized the amount of raw material carried while maximizing the flexibility and reliability of those tools, utilizing large biface cores and conservative maintenance strategies (Kelly and Todd 1988). The significant distances between raw material sources on the landscape and preference for high-quality lithic material reinforces/necessitates curatorial behavior (Kilby 2008:13-16; 2014). These behavioral patterns are detectable in the diverse lithic assemblages observed at different types of Clovis sites (Kilby 2014:202).

Clovis projectile points and tools recovered from kill sites are often broken, extensively retouched, or nearly new with limited retouch but recovered in contexts suggesting that they were unintentionally lost (Kilby 2008:17-18). Clovis camp site assemblages consist of debitage associated with tool rejuvenation and maintenance (discarding broken projectile points, retouching worn tools) and discard of non-projectile point tools associated with food preparation and other domestic activities (Kilby 2008:19-20). At quarry locations, projectile points retouched seemingly beyond their functional limit are often discarded only when the acquisition of a suitable replacement was ensured. Somewhat counter-intuitively, the tools discarded at quarry

sites are often crafted from far flung raw materials reinforcing the long-range mobility and conservative subsistence strategies of Clovis hunter-gatherers (Kilby 2008:20-21). Unless tools are lost or at the end of their useful life, they are unlikely to be recovered at Early Paleoindian sites. Debitage is more frequently encountered, especially considering the curatorial behavior observed on Early Paleoindian tools and extensive utilization of biface cores.

If the incisions reported in the (Bement) 1986 Bone Bed 1 faunal assemblage are in fact cut marks, some evidence of the tools that did the cutting should be present. If Bone Bed 1 at Bonfire Shelter represents an Early Paleoindian kill site, the absence of tools is not necessarily anomalous. Traces of expedient tool production and biface tool rejuvenation should be detectable. If some manner of primary disarticulation took place at the site of the kill, but the material density may be lower than at other types of sites. If the shelter was utilized as a secondary processing location or extensive disarticulation occurred at the site of the kill, larger quantities ofdebitage and residual debris should be present; especially considering the robust nature of the faunal assemblage. If Bone Bed 1 represents a camp site, a more diverse array of tools and tool fragments might be expected in addition to charcoal and botanical material preserved in the arid shelter conditions. Even if usable material was scavenged, tool fragments anddebitage should remain.

5.2.3 *Criteria for Microartifact Identification*

Within the context of this thesis, *microartifact* specifically refers to lithicdebitage derived from the manufacture, use, and re-honing of stone tools smaller than 2.0 mm (0.08 in). This analysis specifically targets artifacts between 1.0 and 2.0 mm (0.04 – 0.08 in), the smallest fraction where diagnostic conchoidal fracture patterns observed on macro-debitage remain identifiable (Fladmark 1982:205). Bone and perishable artifact fragments are similarly unlikely to remain identifiable below this scale. Prehistoric pottery may be identifiable at 1.0 mm (0.04 in) but is not expected in Late Pleistocene contexts. Charcoal observed during sample processing was

quantified but not considered an artifact, though some authors considered it a marker of human activity (Hassan 1978). The diagnostic criteria used to classify microartifacts in this thesis have been adapted from Fladmark's 1982 experimental study, outlined in **Table 5-1** below.

The first phase of the laboratory analysis evaluated the presence or absence of microartifacts in each sample based on the criteria listed in **Table 5-1**. If identified, the microartifacts were to be quantified and, to the extent possible, classified using a lithic analysis schema modeled after Andrefsky (2005). The identification of flake attributes including platforms, percussion bulbs, dorsal flake scars, and terminations were considered diagnostic.

In addition to morphology, lithic raw material type was a key identification attribute. At 1.0 mm (0.04 in), typical flake attributes may not be expressed on culturally derived fragments (Sherwood 2001; Shott 1994)}. Cryptocrystalline silicates are common materials used in stone tool manufacture for their ability to form and hold a sharp edge, controllable conical fracture mechanics, and relative abundance across the landscape. Potential cryptocrystalline fragments, ambiguous non-limestone material, and examples of atypical angular material were assessed under higher-power magnification. If identified, angular shatter and ambiguous debris from tool sharpening or use were expected to outnumber identifiable flakes by a significant margin.

In the context of Bonfire Shelter, the background sediment matrix was composed primarily of endogenic limestone. Non-limestone particles were considered exogenic and potentially indicative of broader site formation processes that could redeposit cultural material. Due to their small size, microartifacts are particularly susceptible to transport processes. Determining the source of exogenic materials can highlight sources of contamination from secondary locations.

Table 5-1. Microdebitage Attributes, After Fladmark (1982)

Attribute	Notes
Highly Angular	Especially notable in the otherwise blocky limestone matrix
Transparent/Translucent	Very thin; opaque particles unlikely to be cryptocrystalline material
Larger than Mean Particle Size	Thin profile and elongate form readily pass through sieve
Geometric Shapes	Sub-rectangular, sub-triangular, trapezoidal, semi-lunate
Conchoidal Fracture Attributes	Diagnostic flake features similar to macro-artifacts: Percussion bulb/Hertzian cone, striking platform, flake scars/facets, concentric ripples. Difficult to discern below 1.0 mm and on coarser materials
Lies near surface of sample	Primarily applicable to 0.5 - 0.25 mm slide-mounted samples
Lithic Material	Cryptocrystalline stone or other knappable non-limestone lithic material

5.2.4 *Field Collection*

Using the methods outlined in **Section 5.1.3** Spot Samples were collected judgmentally from the margins of faunal remains and within bone concentrations specifically for microartifact processing. At least one spot sample was collected from every excavated unit-layer. No pre-screening or processing was conducted in the field; all collected sediment was retained for laboratory analysis. In addition to Spot Samples, subsamples from each CS05 bulk matrix sample were allocated for microartifact analysis. These samples were drawn from the same lots as the geoarchaeological samples to facilitate the direct comparison of sedimentological and microartifact results.

The judgmental sampling strategy was designed to maximize the likelihood of recovering cultural material. Given the small study area accessible in Bone Bed 1, a systematic sampling method afforded little opportunity to differentiate activity areas across the site. This strategy yielded discrete data points rather than a continuous artifact density surface. However, the sampling density may be great enough to make generalized statements regarding artifact and inclusion distributions within the immediate study area (Sherwood 2001:337)

5.2.5 *Sample Reduction/Preparation*

Microartifact samples were screened through a series of nested geological sieves to separate coarse gravels (>2 mm, 0.08 in) from sands, silts, and clays (<2.0 mm, 0.08 in). The <2 mm (0.08 in) fraction was floated to separate organic matter for ¹⁴C dating from the sediments. The heavy fraction was water-screened through a 1.0 mm (0.04 in) geological sieve, air-dried, and retained. Approximately 50 g of un-floated bulk <2.0 mm (0.08 in) fraction was retained as a geomatrix sample for curation/further analysis. The 1.0 mm (0.04 in) fraction was air-dried and retained with the separated light fraction for detailed inspection. The retained geomatrix samples provided an opportunity to evaluate the presence of microartifacts across the full particle size spectrum if cultural material was identified during 1.0 mm (0.04 in) processing.

The 1.0 - 2.0 mm (0.04 – 0.08 in) fraction was selected for microartifact analysis to balance analytical resolution and time investment. 2.0 mm (0.08 in) was the cut-off for separating the gravel fraction from the sand/silt/clay fraction used for the geoarchaeological analyses described in **Section 5.4.2**, below. Below 1.0 mm (0.04 in), the time required to identify cultural material would increase significantly while the confidence with which they could be identified simultaneously decreases. Below 0.5 mm (0.02 in), approaching the fine sand particle size threshold, artifacts become difficult to physically separate from the sediment matrix. At these scales, micromorphological thin sections are considered more efficient than hand picking to identify the target lithic materials (Sherwood 2001:327-329). The 2.0 mm (0.08 in) fraction integrated seamlessly with other geoarchaeological workflows and provided a functional analytical resolution.

5.2.6 *Laboratory Analysis*

A 20.0 g subsample was drawn from the 1.0 mm (0.04 in) fraction of each microartifact sample for preliminary screening. The air-dried 1.0 mm (0.04 in) fraction was manually agitated and homogenized to minimize sampling biases before each subsample was drawn. The sample

was spread evenly across a flat, well-lit surface and visually inspected under 10x and 20x magnification. A Celestron hand-held USB microscope with 20x-200x magnification was used to inspect materials in more detail and to record digital photographs. Forceps and/or wooden picks were used to sort and manipulate materials during processing.

Samples were sorted into classes of their constituent components³: limestone, bone fragments, shell fragments, fossiliferous limestone, botanical material (further differentiated where possible), charcoal, non-limestone material, gypsum nodules, crystalline gypsum, crystal quartz grains, rounded gravel, other non-limestone lithic material, and possible microartifact. Particles of non-limestone (exogenic) material with angular facets or otherwise abnormal morphology were separated for microscopic inspection and identification.

The mass of each sorted material class was recorded to the nearest 0.01 g and as a percentage of the total analyzed sample mass. Mass was selected over count data due to sheer volume of material in each sample and to normalize the comparison of different sized samples. The total volume of each spot sample collected in the field varied significantly, from multiple liters (>1.0 kg) to several milliliters (<100.0 g). Only a small amount of material remained for microartifact analysis after processing, floatation, and retaining a geomatrix sample.

5.3 Comparative Sample

To create a baseline comparative sample for the identification of microartifacts, an experimental sample was knapped by archaeologist Christopher Ringstaff. The sample consisted of a nodule of dark gray Edwards Plateau chert (approximately 750 g) reduced to create a large biface core (335 g) and a round biface scraper (42.4 g). Debitage derived from various reduction stages including large cortex removal flakes, platform preparation flakes, retouch debris, and several pressure flakes were retained. Platform preparation and retouch debris are of critical

³ Listed in order of abundance by mass

interest to this study. If tools were curated and removed from the site (or simply not excavated), this material should remain in situ. The comparative assemblage was assessed under magnification to determine the range of attribute variation that might be expected in Bone Bed 1.

Retouch debitage was nearly all <2.0 mm (0.08 in) and translucent. The degree of transparency was directly proportional to the flake's thickness. Conchoidal fracture attributes including striking platforms, percussion bulbs, dorsal flake scars, rippling, and feather terminations (among other typical flake attributes) were present on many examples. Flakes were extremely angular, taking on generally rectangular or triangular forms. **Figure 5-2** illustrates examples of platform preparation debris derived from the Edwards Plateau chert comparative sample.

Larger retouch flakes (<1.0 cm, 0.4 in) were thicker and less transparent, often featuring a tapering profile (from platform to termination thickness) and more overall convexity. Flake attributes were more pronounced and readily identifiable, particularly platforms and dorsal flake scars. Smaller debitage was much thinner and of more consistent thickness through individual flakes. Flake attributes were more subtle, but still identifiable. Complete micro-flakes were less common, often observed as medial-distal sections. This may be a function of their thin profiles and increased susceptibility to breakage during manufacture, transport, or storage.

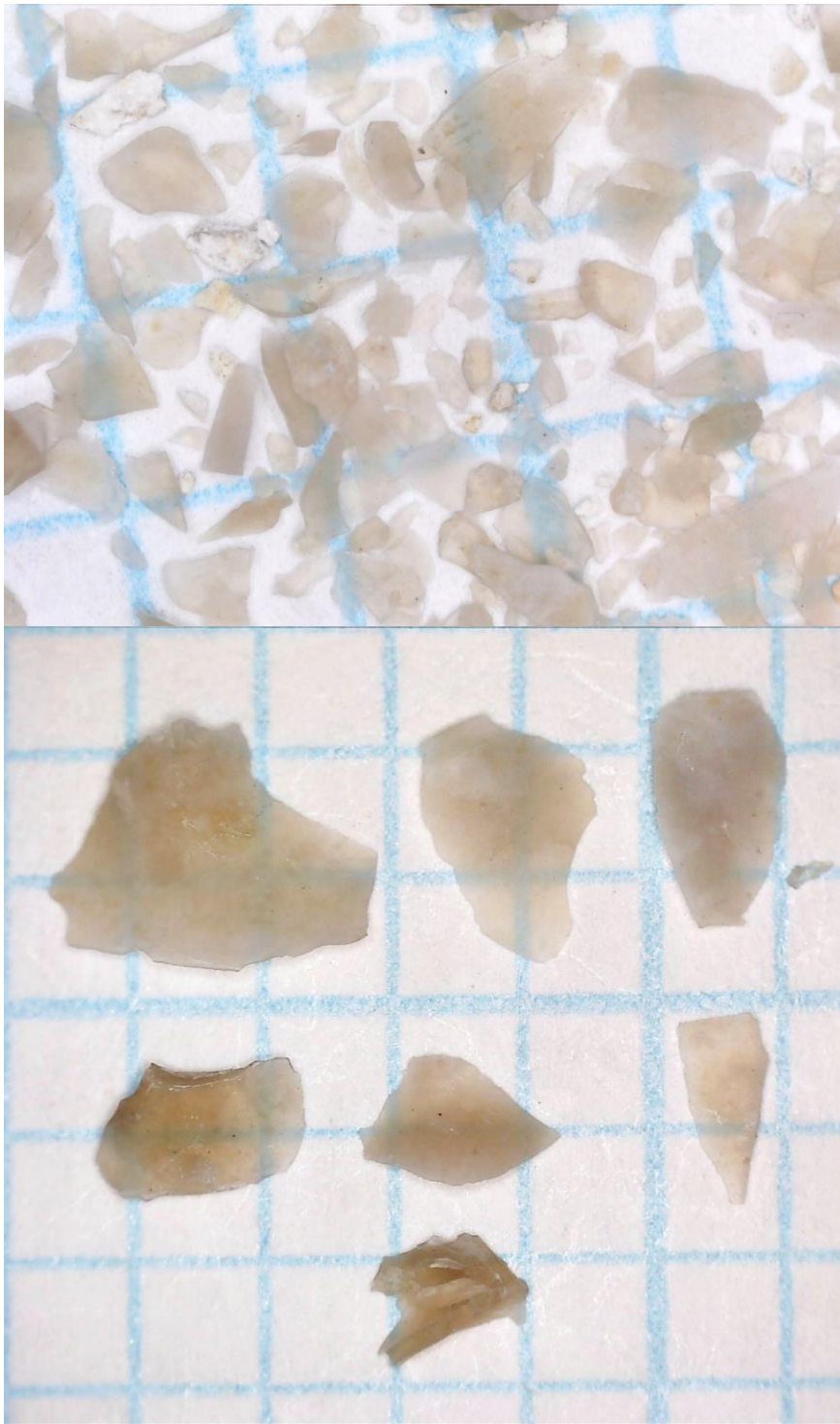


Figure 5-2. Platform preparation flakes and shatter from experimental Edwards Plateau chert core. 1 cell = 2.5 mm (0.1 in). Upper panel: roughly 50x magnification; Lower panel: roughly 30x magnification.

5.3.1 *Edwards Chert Fluorescence*

Edwards Plateau chert fluoresces a unique orange color when exposed to ultraviolet (UV) light (Hofman et al. 1991). This phenomenon is an effect of the incorporation of fluorophores during lithic material formation. Upon exposure to specific wavelengths of light, fluorophores emit a secondary wavelength causing the material to glow a distinct color (Frederick 2020, Personal Communication). Fluorescence color and intensity is a function of the type fluorophores present, fluorophore concentration, and the wavelength and intensity of the light source. As such, fluorescence has been utilized to differentiate lithic source materials (Collins and Headrick 1990; Frederick et al. 1994; Gonzalez et al. 2014).

The orange glow of Edwards Plateau chert is distinctive but highly variable, even within single outcrops (Hofman et al. 1991). Because of this, UV fluorescence is useful for differentiating superficially similar materials but not necessarily sourcing artifacts to specific quarries. Other Texas lithic materials including Alibates and Tecovas chert and Ogallala quartzites have unique fluorescent properties distinct from the orange hues of Edwards Plateau chert that are similarly useful.

To test the suitability of UV fluorescence to aid in the identification of microartifacts from Bonfire Shelter, the experimental sample of Edwards Plateau chert (described above) was exposed to long wavelength (365nm) UV light using a small hand-held UV flashlight in a darkened room. All illuminated cores, tools, and debitage fluoresced the diagnostic Edwards Plateau orange, consistent with Hofman et al.'s (1989) and Collins and Headrick's (1990) descriptions. The fluorescent effect was more pronounced in thicker specimens, likely due to increased concentrations of the reactive fluorophores.

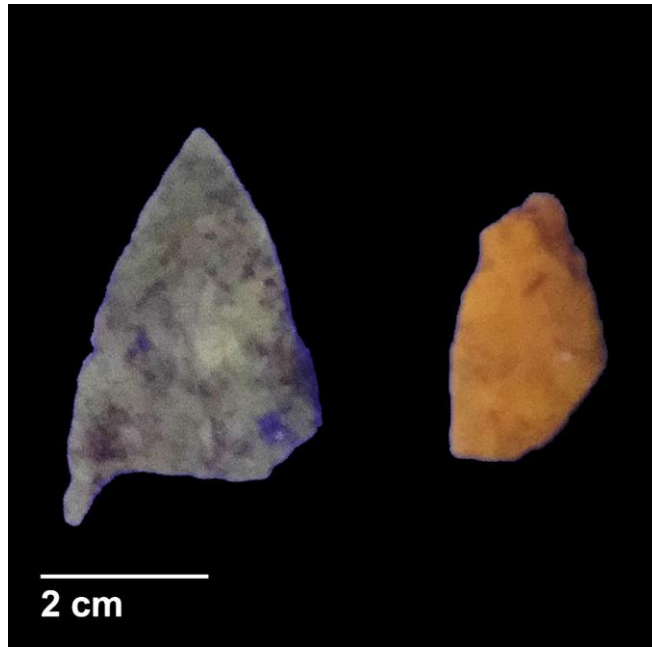


Figure 5-3. Chert Fluorescence in the Bonfire Shelter lithic assemblage, FN60280. Note the bright orange Fluorescence of the Edwards Plateau chert specimen on the right. Both specimens recovered from disturbed contexts on the talus cone; neither are associated with Bone Bed 1.

In another control trial illustrated in **Figure 5-3**, projectile point fragments associated with Bonfire Shelter Bone Beds 2 and 3⁴ were illuminated with UV light. One specimen fluoresced bright orange, confirming the presence of Edwards Plateau chert in the Bonfire Shelter assemblage. The other specimen had a more ambiguous signature, exhibiting a very pale orange glow that, based on the patterns observed in other known specimens, could not be confidently attributed to Edwards Plateau chert.

With the success of these tests, UV fluorescence was incorporated into the microartifact processing workflow to aid in the identification of potential lithic artifacts. While each sample was spread out across the processing surface, it was illuminated with 365nm light and inspected for fluorescing material. Due to the variability of ultraviolet fluorescence and analyst subjectivity, no attempt was made to quantify the effect during this study. As a qualitative measure, this method aided in the differentiation of cherts and non-limestone material during inspection. White

⁴ FN 60280: Projectile Point Fragments recovered from disturbed contexts on the talus cone

shells, fossil limestone, bone, and the underlying sorting surface reflected the bright blue light, potentially obscuring the fluorescence of small chert fragments. The technique proved particularly valuable for spot-checking individual fragments.

5.4 *Geoarchaeological Methods*

The entirety of each Column Sample 5 (UC1.PS06.CS05) stratum was retained as bulk matrix samples for geoarchaeological analysis. The suite of analyses was designed to determine what transport mechanisms contributed to the sedimentation of Bone Bed 1 and if those mechanisms carried enough energy to introduce the large megafauna elements observed in the deposits. If high energy deposits are present, evidence of human intervention must be robust evidence due to the potential for external contamination of the shelter.

CS05 geoarchaeological samples were excavated near the end of the 2017 field sessions after the full extent of Profile Section 6 (PS06) was exposed and mapped. Processing and analysis of these samples was conducted under the supervision of Dr. Charles Frederick in Dublin, Texas using the methods outlined below. The results of these analyses are reported in **Chapter 8: Geoarchaeological Results**.

5.4.1 *Geoarchaeological Background and Justification*

This thesis leverages geoarchaeological methods to identify and evaluate artifact-bearing strata in Bone Bed 1 at Bonfire Shelter. The key tenets of geoarchaeology are: to create detailed models of site stratigraphy and chronology, to evaluate natural and anthropogenic site formation processes and their impact on the archaeological record, and to reconstruct past landscapes and track their changes over time (Waters 1992:4-13) . To that end, these methods are designed to develop geological profiles for each Bone Bed 1 stratum and build a coherent picture of Bonfire Shelter in the Late Pleistocene.

Geoarchaeological data are useful not only to describe the composition of each stratum, but also to provide relative temporal context in the absence of directly datable material. Tracking sedimentological changes over time can tie Bone Bed 1 to key Late Glacial climatic events (i.e.: the Younger Dryas or Bølling–Allerød) and refine expectations for archaeological material despite the sparse radiocarbon record.

Identifying the geological processes contributing to each stratum can elucidate biases and extenuating circumstances that can impact archaeological interpretations. Geoarchaeology can provide indicators that the observed archaeological picture is incomplete.

This project is fundamentally concerned with determining how humans were interacting with the Late Pleistocene landscape, including local flora and fauna. Given the antiquity of Bone Bed 1, confirming the presence of humans at Bonfire Shelter would be significant in its own right. The geoarchaeological data gleaned from these methods aim to go beyond this baseline, contextualizing the Late Pleistocene landscape at Bonfire Shelter, how humans and animals utilized it, and how those use-cases changed over time.

Even if Bone Bed 1 is determined to be non-cultural, the geological profiles developed here paint a valuable portrait of Bonfire Shelter prior to human exploitation. Identifying conditions inhospitable to the utilization of Bonfire Shelter provides a critical perspective on human ecology that cannot be derived from artifacts alone.

Methods used to assess these deposits include: particle size analysis, carbon content, carbon content, stable carbon isotopic composition, mineralogy, and magnetic susceptibility. Each provides valuable information regarding the environment and conditions associated with sampled stratum.

Particle size analysis was used to determine how sediment was entering the shelter. Transport and depositional processes are tied directly to local environmental conditions, which

can help to pin strata in geological time. Further interpretation can determine if conditions were conducive to human activity and/or in situ artifact recovery.

Carbon content breaks down the ratio of organic carbon to inorganic carbon within each stratum. Given the limestone parent material of Bonfire Shelter is almost entirely calcium carbonate, inorganic carbon is associated with endogenic deposition within the shelter. Organic carbon, derived from living organisms, originates outside the shelter and accumulates as a byproduct of exogenic processes including human or animal activity.

Loss-on-Ignition techniques were utilized to calculate preliminary organic and inorganic carbon content. Inorganic carbon content was refined using a volumetric calcimeter method (Chittick Apparatus). Samples of < 2.0 mm (0.08 in) sediment were submitted for detailed organic carbon analysis to the University of Kansas's KPESIL elemental analyzer service. After removing the acid-soluble inorganic carbon component, the organic carbon residual from these samples, the stable carbon and nitrogen isotopic composition was measured. The fractionation of carbon and nitrogen isotopes was used as a measure changing plant and animal communities overtime, contributing to the correlation of stratigraphy with geological events.

Semiquantitative X-ray diffraction was used to measure the mineralogical composition of each stratum. The constituent components of each stratum were compared to a limestone parent material control sample to identify exogenic material. The composition of these strata can indicate sources of exogenic material, especially where unique trace minerals are identified. The proportion of exogenic material to endogenic material provides insight into the rate of sediment deposition, with potentially significant implications for preservation conditions and shelter habitability.

Magnetic susceptibility measures the proportion of magnetic minerals within the deposits. Due to parent limestone's low susceptibility, elevated levels can be indicative of

exogenic deposition and/or human activity. Human activity, especially high temperature burn events, can dramatically increase the magnetism of nearby sediments. Dispersion of burned sediments across the shelter can increase the magnetic susceptibility of entire strata. Comparison against known cultural strata, such as Bone Bed 2, can highlight potentially diagnostic anomalies in culturally undefined strata.

The deposits examined in Column Sample 5 extend from the lower strata of Bone Bed 2 through Bone Bed 1. By including Bone Bed 2 strata, the ambiguous Bone Bed 1 strata are assessed against geological profiles of definitively cultural “control” samples. The limestone control sample was tested to control for Bonfire Shelter’s underlying geology. Considering the dramatic climatic fluctuations at the end of the Pleistocene, any assumptions regarding environmental consistency between Bone Beds 1 and 2 are precarious at best. Despite this, comparison may provide insight into the changing role of Bonfire Shelter (and rockshelters in general) over time.

Climate instability may be a driving factor behind the paucity of Late Pleistocene cultural material at Bonfire Shelter and in the Lower Pecos. Unpredictable food resources are not compatible with highly mobile hunter-gatherers subsistence strategies (Kelly 1983). As Robinson (1997) speculated of Bone Bed 2, the expansion of grasslands southward into the Lower Pecos opened new rangeland for bison and the pursuing hunter-gatherers. A similar pattern of inconsistent cultural occupation may explain the sparse nature of Bone Bed 1.

ASWT analysis determined that Late Glacial deposits at Eagle Cave, while largely endogenic limestone, included a notable aeolian sediment mineralogically similar to Rio Grande alluvium (Koenig, Nielsen, et al. 2017:99-100). Intuitively, Late Glacial strata at Bonfire Shelter should maintain a similar profile. However, significant morphological differences between Eagle Cave and Bonfire Shelter result in unique depositional patterns that limit the suitability of direct sedimentological comparisons.

Bonfire Shelter's notch and obstructed entrance, illustrated in **Figure 5-4** and **Figure 5-5**, result in sedimentation patterns unlike any other Mile Canyon shelter. During heavy rainstorms the notch becomes a waterfall, funneling water and upland sediments directly into the shelter. The boulders obstructing the entrance inhibit runoff, further channeling sediments into the shelter interior. In addition to sheet wash, the boulders help to create a wind eddy, trapping aeolian sediments and contributing to Bonfire Shelter's detailed palynological record (Robinson 1997:40-41).

Dibble argued that Bonfire's sloped floor topography would cause runoff to pool near the rear wall of the shelter (Bement 1986a:20; Dibble and Lorrain 1968:28). Considering the unconsolidated nature of the shelter's Holocene deposits, this scenario seems unlikely. Water should quickly infiltrate the deposits, limiting its capacity to pool in any meaningful way. It is unclear if "silty trough" described within Bone Bed 1 reflects actual pooling water, or the sediments left behind following the rapid infiltration of sheetwash. Given the thickness of Stratum E/F/G, it may be possible that enough sediment accumulated to slow infiltration and allow water to pool at the surface. However, additional testing may be necessary to evaluate this hypothesis.



Figure 5-4. View east towards Bonfire Shelter from the western rim of Mile Canyon. Note the iconic notch above the southern shelter entrance as well as the deeply incised Rio Grande in the background. The notch, formed at a gradually eroding joint in the Devils River Formation limestone bedrock, presents a direct vector for the introduction of exogenic sediment to the shelter interior. Immediately below the notch, over-rim sheetwash accumulates to form the Talus Cone. Photo courtesy of Texas Beyond History: <http://www.texasbeyondhistory.net/bonfire/images/aerial-closeup.html>



Figure 5-5. Modern photo of the Bonfire Shelter notch.

5.4.2 *Geoarchaeological Sample Preparation*

Aliquots for the geoarchaeological analyses described below were prepared for each bulk matrix sample retained from UC1.PS06.CS05. Before splitting, each sample was assigned a Laboratory Number (LN) (reported in **Table 5-2**) to simplify workflow tracking. The total mass of each matrix sample was recorded to the nearest gram. The bulk sample was then separated into coarse (>2.0 mm) and fine (<2.0 mm) fractions using a standard 2.0 mm (1 ϕ) geological sieve. The split mass of each fraction was again recorded to the nearest gram. The fine fraction was roughly homogenized by repeatedly transferring back and forth between large beakers and manually agitating. Subsamples of the homogenized matrix, detailed in **Table 5-3**, were split from the fine fraction and set aside for analysis.

Table 5-2. Geoarchaeological sample Field Numbers and Lab Identifiers.

Lab Sample ID Key				
LS#	PS06.CS05 ID	Bement ID	Lot FN	Matrix Sample FN
LS001	S19	A	60250	60258
LS002	S20	B	60251	60259
LS003	S21	C	60252	60260
LS004	S22	D	60253	60261
LS005	S23	EFG	60254	60262
LS006	S24	H	60274	60275

Table 5-3. Geoarchaeological Subsamples

Geoarchaeological Subsamples	
Analysis	Mass (g)
<2mm Particle Size (hydrometer)	60
Loss-on-Ignition	15
Gypsum Determination	20
Chittick Carbonate	2
Magnetic Susceptibility	10
XRD	100
Carbon Analyzer	100
Curated Geomatrix	200
Total	507

5.4.3 Particle Size

Particle size distribution calculations for the Bone Bed 1 strata required a combination of several methods due to the wide range of particles represented in each stratum spanning very large spalls and cobbles to very fine clays. Coarse fractions, including gravels and sands, were processed using nested geological sieves to grade sediments into size classes. The hydrometer method (ASTM-International 2017), which exploits the differential settling velocities of different particle sizes, was used to determine the relative proportion of silt and clay.

The phi-scale (ϕ), a logarithmic scale developed by Udden (1898) and modified by Wentworth (1922), is the most common metric for quantifying sediment particle size (Gale and

Hoare 1991:57). The logarithmic base facilitates the expression of large boulders well over 1.0 m (3.28 ft) in diameter and sub-micrometer clays a single functional scale. **Table 5-4**, below, summarizes the Phi Scale and Wentworth classifications as reported in Gale and Hoare (1991:58-59). Conversion from ϕ to mm is calculated using the formula $D = 2^{-\phi}$. Conversion from mm to ϕ is calculated using the formula $\phi = -\log_2(D)$ where D is the diameter in mm and ϕ is the reported phi value (Gale and Hoare 1991:57). Distributions are plotted as histograms classified by the measured ϕ intervals and relative sediment mass each class (see **Appendix A: Particle Size Distributions**). A corresponding cumulative percentage curve is presented with the histogram illustrating the percent mass of each ϕ class.

Descriptive statistics summarizing the central tendencies and range of particle size variation were calculated for each stratum. Sediments, including those from Bone Bed 1, are rarely normally distributed. Statistical methods that account for the increased variability spread across broader bands of the cumulative curve have been described by Folk and Ward (1957) including: Graphic Mean (M_z), Inclusive Graphic Standard Deviation (σ_I), Inclusive Graphic Skewness (Sk_I), and Graphic Kurtosis (K_G) (Gale and Hoare 1991:65).

Mean and median particle size can be used to infer transport vectors; high energy transport processes move larger average particle sizes than low energy processes. The standard deviation of particle sizes is a measure of sorting. Well sorted sediments include a smaller range of sediments than poorly sorted sediments. Poorly sorted sediments are expected to have larger standard deviations, representing higher energy depositional environments. Multi-modal distributions may represent multiple transport vectors contributing sediment to the stratum (Leigh 2001).

Table 5-4. Wentworth Phi Classifications

Wentworth Scale (1922)			
Phi Value (ϕ)	mm	μm	Particle Description
-10.00	1024.00	1024000.000	Large Boulder
-9.00	512.00	512000.000	Boulder
-8.00	256.00	256000.000	Large Cobble
-7.00	128.00	128000.000	Cobble (-6.75)
-6.00	64.00	64000.000	Gravel (-5.75)
-5.00	32.00	32000.000	Coarse Pebble
-4.00	16.00	16000.000	Pebble (-3.75)
-3.00	8.00	8000.000	Fine Pebble
-2.00	4.00	4000.000	Very Fine Pebble
-1.00	2.00	2000.000	Very Coarse Sand
0.00	1.00	1000.000	Coarse Sand
1.00	0.50	500.000	Sand
2.00	0.25	250.000	Medium Sand
3.00	0.125	125.000	Fine Sand
4.00	0.0625	62.5000	Very Fine Sand
5.00	0.03125	31.2500	Coarse Silt
6.00	0.015625	15.6250	Silt
7.00	0.007813	7.8130	Fine Silt
8.00	0.003906	3.9060	Coarse Clay
9.00	0.001953	1.9530	Medium Clay
10.00	0.000977	0.9770	Clay (9.75)

The distribution and relative sorting of sand, silt, clay, and gravel provide reflect the depositional processes contributing to each stratum. Aeolian processes transport narrow particle size bands (Waters 1992:186-187). These sediments are typically very well sorted and consist of very fine sands and silts. Alluvial processes are typically more turbulent, yielding less well-sorted particle distributions. Faster moving water carries greater potential energy and the capacity to move increasingly large particles (Waters 1992:120-122). As alluvial energy decreases, particles fall out of suspension according to Stokes Law: larger particles settle first, followed by smaller particles that require less energy to entrain often resulting in distinctive, relatively well sorted, fining upward sequences (Waters 1992:36-40).

At archaeological sites, transport processes can modify context including the artificial introduction, deletion, or redeposition of artifacts and faunal remains (Schiffer 1983). Experimental studies at the Colby Mammoth Site found that even relatively low-speed currents could redeposit, reorient, and size-grade large faunal elements (Frison and Todd 1986). Stratigraphic discontinuities and flood deposits at Skiles Shelter illustrate that artifacts and features exposed in surface contexts or due to erosion are also susceptible to the effects of water moving through archaeological deposits (Koenig, Black, et al. 2017). While both of these examples are very different from Bonfire Shelter’s geography, they illustrate the potential impacts that transport processes on archaeological deposits.

5.4.3.1 Coarse Fraction Particle Size

Coarse-fraction particle size was calculated using the sieving method outlined by Gale and Hoare (1991:83-86). All gravels retained from the initial sample split were rinsed with water to remove adhering sediments and dried at 100° C (212° F) overnight. Adhering sediments were captured in a 53 µm sieve and retained. A series of nested geological sieves at whole-φ intervals (-1φ through -6φ) was attached to a Tyler Sonic Sieve Shaker. Gravels were added to the stack and agitated in an orbital motion for 120 seconds (reduced from the recommended five-minute agitation cycle due to abrasion of the soft limestone) on the “coarse” setting (approximately 30-40 RPM). Gravels were processed in 1-liter batches due to the large volume of some samples. The gravels remaining on each sieve were weighed to the nearest 1/100th gram and bagged by sample number and size fraction. The masses from each batch were tabulated to calculate the total mass of each fraction for each sample. These totals were converted to percentages using the equation:

$$\frac{\textit{Fraction Mass}}{\textit{Total Sample Mass}} \cdot 100$$

The calculated percentages were combined with the <2.0 mm (0.08 in) fraction percentages to construct a cumulative curve encompassing the full range of particle sizes for each Bone Bed 1 stratum.

5.4.3.2 *Silt and Clay Fraction Particle Size – Hydrometer*

A 60 g sample of <2.0 mm (0.08 in) homogenized matrix was prepared to calculate silt and clay particle size distributions using the hydrometer method outlined in the American Society for Testing and Materials fine-grained soils methodology (ASTM-International 2017). Samples were pretreated to remove gypsum salts by washing sediments with 1 liter of distilled water, soaking overnight, and decanting the dissolved gypsum solution (repeated four times) (Pearson et al. 2015). The significant quantities of gypsum in the Bone Bed 1 sediments caused initial trials to flocculate and prematurely drop out of suspension, yielding inaccurate hydrometer readings. Pretreating the samples in this manner removed enough of the water-soluble salts to mitigate the flocculation effect.

Pretreated sediments were transferred to a stainless-steel dispersion cup with 50 ml of Sodium Hexametaphosphate, a deflocculant agent ($(\text{NaPO}_3)_6$), and distilled water. The sample was agitated for 5 minutes on the dispersion mixer's medium setting. The agitated sample was then transferred to a 1-liter graduated cylinder and topped with distilled water to 1000 ml. The graduated cylinder was capped with a rubber stopper and repeatedly inverted for 1 minute to ensure all sediment particles were suspended. After one minute, the cylinder was uncapped and an ASTM 152-H hydrometer was inserted and allowed to settle. The hydrometer reading (g/l of sediment in suspension), elapsed time (t , in minutes), and ambient temperature ($^{\circ}\text{C}$) were recorded for each sample and the control sample. The control sample consisted of a 950 ml distilled water, 50 ml Sodium Hexametaphosphate solution. The control was used to calculate the correction factor for each sample reading. Hydrometer measurements were recorded at exponentially increasing time intervals for the control sample and each experimental sample.

Table 5-5 outlines the timing and corresponding particle size for each measurement. **Figure 5-6** illustrates the suspended sediment samples during the hydrometer-based particle size analysis. **Figure 5-7** illustrates the fining upward sequence that develops as coarse particles settle to the cylinder's base, reducing the overall density of the suspension.

Table 5-5. Hydrometer sampling regimen and equivalent phi values

Hydrometer Measurement Intervals	
Time (t) (Minutes)	Phi Interval (ϕ)
1	4.5
3.5	5.5
15	6.5
45	7.5
300	8.5
1440	9.5



Figure 5-6. Fine-fraction sediment samples settling in graduated cylinders during hydrometer-based particle size analysis.



Figure 5-7. Detail photo of sediments settling at base of graduated cylinder. Note the fining upward sequence that develops as coarse particles fall out of suspension.

5.4.3.3 Sand Fraction Particle Size – Sieve

After recording the 1440-minute reading, the sediment suspension was decanted from the 1-liter graduated cylinder into a 53 μm sieve and rinsed with distilled water to separate the sand from the silt and clay fraction. The sand remaining on the sieve was transferred to a 250 ml beaker, filled with distilled water, and allowed to settle for two minutes. The water was then decanted, separating residual silts and clays. The remaining sand fraction was dried in an oven at 150°x`C (302° F) overnight.

Calculating the particle size distributions for the sand fraction followed a procedure similar to the coarse gravel calculations. The sand was passed through a set of nested geological sieves at $\frac{1}{2} \phi$ intervals ranging from -1ϕ through 4ϕ . Samples were agitated for five minutes using the Tyler Sonic Sieve Shaker machine's "fine" setting. The sediment mass remaining on each sieve was measured to the nearest 1/100th of a gram. The relative percentages of each size class were calculated by dividing the mass from each sieve by the hygroscopic moisture adjusted sample mass (see below) and multiplying by 100. These percentages were used in conjunction

with gravel and silt/clay percentages to construct particle size distribution histograms and cumulative curves for each sample

5.4.3.4 Particle Size Distributions

Data from the three methods described above were aggregated in a Hydrometer-Sieve Calculation spreadsheet programmed by Paul Lehman (University of Texas at Austin, Department of Geography and the Environment) to calculate the particle size distribution curve for each sample. Provided with the starting masses and measurements relevant to each sample, the software efficiently normalized and calculated percentages, cumulative curves, ϕ values, and descriptive statistics.

The software was modified to account for the significant quantity and excessive coarseness (small ϕ value) of gravels in Bone Bed 1. The software was originally designed to calculate intermediate ϕ value percentages at the sand-silt boundary (between 4ϕ and 5ϕ) which yielded negative values and cumulative percentages greater than 100% when extremely coarse sediments were encountered. To ensure accurate ϕ_{16} , ϕ_{50} , and ϕ_{84} values were obtained, cumulative percentages were exported, recalculated, and manually graphed and used to plot intercepts for the relevant percentiles.

The cumulative curve was constructed by adding the percentage by mass of sediment remaining on each sieve (or calculated equivalent for silt and clay fractions) to the running total percentage of all preceding classes. The cumulative percentages were plotted against ϕ value on the x-axis, beginning with the coarsest (-8ϕ) gravel fraction. Subsequent classes were added to the total percentage and plotted until 100% of the sample was graphed. The curve was interpolated by connecting the data points using straight lines to facilitate the graphic estimation of percentile ranks for any intermediate particle size.

5.4.3.5 Descriptive Statistics – Graphic Values derived from Cumulative Curve

- **Graphic Mean**

- Graphic mean is a measure of the average particle size useful for general comparisons of coarseness between samples (Folk 1980:41). On its own, mean particle size provides limited insight into the formation processes impacting a deposit. However, excessively coarse, excessively fine, or multi-modal distributions may skew the average in a manner that does not reflect the actual sedimentary constituents.

$$M_z = \frac{(\varphi15 + \varphi50 + \varphi84)}{3}$$

- **Median**

- Median particle size represents the 50th percentile ($\varphi50$), as measured on the cumulative curve. Half of all particles in the sample are greater than this value and half are smaller. Median particle size does not address the tails of a distribution and provides limited insight into the formation processes contributing to a deposit. This is especially important in non-normally distributed sediments (as is the case with the Bone Bed 1 sediments), where diagnostic patterns are observed in the tails of the distribution curve (Folk 1980:41).

- **Mode**

- Particle size distribution modes represent the size class with the greatest number of observations; the most common particle size in a sample. Modes were identified as points of inflection in particle size histograms. Bi- and poly-modal samples suggest that multiple transport vectors contributed to the formation of a sediment. The apex of each mode represents the average particle size contributed by that vector and may provide significant insight into the responsible transport

mechanism (aeolian particles can entrain only a narrow band of fine particles while fluvial processes can mobilize a broader range of larger particles) (Folk 1980:41).

- **Graphic Standard Deviation (σ_G)**

- Graphic Standard Deviation measures deviation from the mean particle size, identifying the ϕ range of the most abundant 68% of particles by mass. Computed using the ϕ_{16} and ϕ_{84} x-intercepts on the cumulative curve, graphic standard deviation approximately corresponds with the 1σ confidence interval in traditional statistics. Inclusive Graphic Standard Deviation (σ_I) includes the extremes (tails) of the distribution curve (5ϕ and 95ϕ) and approximately corresponds with the 2σ confidence interval at 90% (Folk 1980:42).
- Graphic standard deviation is a measure of particle sorting. Sorting indicates the range of particle sizes present in a sediment. Well-sorted sediments (i.e.: beach sands) are homogenous, consisting of a narrow band of particle sizes. Poorly sorted sediments (i.e.: glacial deposits) include a broad spectrum of particle sizes.

Table 5-6 outlines Folk’s classification scheme for sorting in particle size distributions (Folk 1980:42)

$$\sigma_G = \frac{(\phi_{84} - \phi_{16})}{2}$$

Table 5-6. Sorting Classification Scheme after Folk (1980)

Folk’s Sorting Classification Scheme	
.35 ϕ	Very well sorted
.35-.50 ϕ	Well sorted
.50-.71 ϕ	Moderately well sorted
.71-1.0 ϕ	Moderately sorted
1.0-2.0 ϕ	Poorly sorted
2.0-4.0 ϕ	Very poorly sorted
>4.0 ϕ	Extremely poorly sorted

- **Graphic Skewness (Sk_G)**

- Folk describes skewness as the symmetry of a particle size distribution, measured as “the displacement of the median” within 1σ of the mean particle size (i.e.: excluding the tails of the curve) (Folk 1980:43). In distribution histograms, skewness manifests as the disproportional exaggeration of either the positive (right) or negative (left) tail of the curve. Positively skewed distributions include a greater proportion of fine sediments, while negatively skewed curves have an abundance of coarse sediments.
- Outlined in **Table 5-7**, skewness statistics range between +1.00 (strongly fine-skewed) and -1.00 (strongly coarse-skewed). A symmetrical curve should yield a skewness value of 0.00 (Folk and Ward 1957:12). Skewness is calculated from the ϕ_{16} , ϕ_{84} , and ϕ_{50} cumulative curve x-intercepts measured using the equation below. Inclusive Graphic Skewness can be used to account for a larger proportion (ϕ_5 and ϕ_{95}) of the distribution tails (Folk 1980:43-44).

$$Sk_G = \frac{[\phi_{16} + \phi_{84} - 2(\phi_{50})]}{\phi_{84} - \phi_{16}}$$

Table 5-7. Skewness Classification Scheme after Folk (1980)

Folk Skewness Classifications	
+1.00 to +.30	Strongly fine-skewed
+.30 to +.10	Fine-skewed
+.10 to -.10	Nearly symmetrical
-.10 to -.30	Coarse-skewed
-.30 to -1.00	Strongly coarse-skewed

- **Graphic Kurtosis (K_G)**

- Kurtosis measures the difference between the tails and peaks of a distribution. This manifests sedimentologically as the relative sorting of coarse and fine particles versus mean particle size. Steeply peaked, or leptokurtic ($K_G > 1.10$), histogram curves have significantly more area under the curve peak than under

the tails. Leptokurtic sediments are generally better sorted near the mean than in the tails. Weakly peaked, or platykurtic ($K_G < 0.90$), curves exhibit less variation between the area under the curve peak and the area under the tails. In platykurtic particle size distributions, the tails of the curve are better sorted. **Table 5-8** summarizes Folk and Ward's kurtosis classification scheme for sediment particle size distributions. 0.41 is the minimum limit for platykurtic values; there is no maximum leptokurtic limit. Sediment sample kurtosis values typically range between 0.50 and 8.00 (Folk and Ward 1957:15).

$$K_G = \frac{\phi_{95} - \phi_5}{2.44 (\phi_{75} - \phi_{25})}$$

Table 5-8. Kurtosis Classification Scheme after Folk and Ward (1957:15)

Folk & Ward Kurtosis Classifications	
<0.67	Very Platykurtic
0.67 - 0.89	Platykurtic
0.90 - 0.1.10	Mesokurtic
1.11 - 1.49	Leptokurtic
1.50 - 2.99	Very leptokurtic
>3.00	Extremely leptokurtic

Due to the extreme coarseness of the sediments, inclusive graphic statistics and kurtosis could not be calculated for all Bone Bed 1 strata. The minimum phi class measured for most samples contained greater than 5% of the samples mass (ϕ_5). The resolution of the hydrometer method was not sensitive high enough to detect variation in particle sizes $>\phi_{10}$. These calculations are reported here to facilitate the description of the few strata where these statistics *could* be calculated, even if trends cannot be compared across the full column sample. While not statistically robust, kurtosis and skewness can still be qualitatively assessed from curves where ϕ_5 and ϕ_{95} values are not valid. These relative assessments may still provide insight into the characteristics of the Bone Bed 1 strata. If nothing else, it is an indication that those strata are incredibly coarse.

5.4.4 *Carbon Content*

Determining the ratio of organic to inorganic carbon can help resolve the sedimentation vectors contributing to each stratum. Averaging over 97% calcium carbonate (CaCO_3), Devils River Formation limestone is almost entirely inorganic carbon (Frederick 2017b:12). Sediments derived exclusively from this parent material are expected to have a similar composition. Deviations from this ratio suggest that other formation processes are contributing sediment to the tested stratum. Tracking changes in the ratio of organic to inorganic carbon over time illustrates broader climatic trends and guide expectations for other analyses. Beyond the ratio of organic to inorganic carbon, the composition of organic carbon provides a broader overview of the regional ecosystem.

Elevated organic carbon levels not correlated with environmental change (as identified in parallel geoarchaeological analyses) may indicate human or animal activity within Bonfire Shelter. Humans introduce organic carbon in the form of food stuffs, fuel, craft material, excrement, and their passive presence in the shelter. The decomposition of organic matter, including human and animal remains, can further concentrate organic carbon. Decomposition has the secondary effect of altering sediment chemistry by, depending on the source, significantly acidify soil and destabilizing associated remains.

In pedogenically active environments, organic carbon and decomposition byproducts can percolate through the sediment column influencing preservation well below the source (Gale and Hoare 1991:232-233). The dense bone accumulations at Bonfire Shelter suggest that a significant organic component may be present in the sampled sediments, potentially contributing to the adverse preservation conditions. Like the ambiguous faunal remains themselves, elevated organic carbon levels remain circumstantial without confirmation with artifacts and strong supporting evidence.

Loss-on-Ignition (LOI) provides a relatively simple and cost-effective method for determining the organic and inorganic carbon content in a sediment sample. Several known sources of error can skew mass calculations derived from loss-on-ignition procedures. Particularly, the presence of hydrated non-carbon minerals or combustible material may artificially inflate the mass lost at a given firing temperature (Rosenmeier 2005:2, 4). Inconsistent sample placement, firing time, or temperature instability in the muffle furnace can further distort results (Heiri et al. 2001).

For this reason, measures of both organic and inorganic carbon were verified using secondary analyses. A volumetric calcimeter method using a Chittick apparatus was used to measure the volume of CO₂ evolved from digesting a sediment sample in a strong acid. The Keck-NSF Paleoenvironmental and Environmental Laboratory's (KPESIL) elemental analyzer service at the University of Kansas was contracted to evaluate the specific quantity and isotopic composition of organic carbon.

5.4.4.1 *Loss-on-Ignition (LOI)*

Sequential differential weight loss methods were used to estimate the hygroscopic moisture, gypsum content, percent organic carbon, and percent inorganic carbon for each Bone Bed 1 stratum. Differential weight loss methods exploit the variable combustion and dehydration points of sediment constituents by comparing the pre- and post-firing sample masses. Gypsum content and hygroscopic moisture determinations are conducted at relatively low temperatures, measuring water evolved during the firing process. Loss-on-ignition refers specifically to the combustion of organic carbon and calcium carbonate at much higher temperatures. These analyses measure the *equivalent* proportions of gypsum and carbon in sediments using known thermogravimetric properties and combustion points of the target minerals. The release of mineral-held water and the conversion of carbon to ash and evolved CO₂ are measured directly; the actual gypsum and carbon content is inferred from the results (Artieda et al. 2006:1932)

As noted above, LOI results (particularly for the determination of organic and inorganic carbon) are readily distorted by sediments holding significant quantities of structural water (Schulte and Hopkins 1996:21-22). Gypsum is ubiquitous in the rockshelters of the Lower Pecos and readily incorporates atmospheric moisture as structural water. The presence of other hydrated salts and minerals (including clays) can cause similar inconsistencies. Unexpectedly high LOI results should be validated using alternative methods.

5.4.4.2 Hygroscopic Moisture

Hygroscopic moisture is the water retained by fine-grained sediment particles via capillary action and negative surface charges (Prakash et al. 2016:1). It is used as a correction factor in calculations for fine silt/clay hydrometer-based particle size and gypsum content.

Approximately 15 g of homogenized <2.0 mm (0.08 in) sediment were pulverized to a fine powder using a ceramic mortar and pestle. A ceramic crucible was marked with the appropriate LN and weighed to the nearest .0001 gram. The pulverized sample was then added to the crucible and reweighed to the nearest .0001 gram. The precise sample mass was obtained by subtracting the mass of the crucible from the combined crucible + sample mass.

To determine hygroscopic moisture content, samples were placed in a 105° C (221° F) oven to dry overnight. The dry samples were immediately transferred to a vacuum desiccator to cool. Once cooled, oven-dry sample mass was recorded to the nearest .0001g. Hygroscopic moisture was calculated as:

$$\text{Hygroscopic Moisture} = \left[\frac{\text{Mass Air Dry} - \text{Mass } 105^{\circ} \text{ C}}{\text{Mass Air Dry} - \text{Mass Crucible}} \right] \cdot 100$$

The percent hygroscopic moisture was then used to calculate the hygroscopic correction factor:

$$\text{Hygroscopic Correction Factor} = 1 - \left[\frac{\% \text{ Hygroscopic Moisture}}{100} \right]$$

The hygroscopic correction factor was used to correct the sediment sample mass in hydrometer particle size analyses:

Adjusted Sample Mass

$$= \text{Hygroscopic Correction Factor} * \text{Hydrometer Sample Mass}$$

5.4.4.3 Organic Carbon and Inorganic Carbon Determination

LOI methods and equations adapted from Heiri et al. (2001) were used to calculate equivalent organic carbon and inorganic carbon content. After recording the hygroscopic moisture mass, samples were returned to the 105° C (221° F) oven overnight to drive off any reaccumulated moisture and reach a constant stable mass. To determine the proportion of organic matter, samples were fired in a 500° C (932° F) muffle furnace for two hours. After the first firing, samples were cooled in a desiccator for 20 minutes, weighed to the nearest .0001g. To determine inorganic carbon content, the same samples were returned to the muffle furnace at 1000° C (1832° F) for one hour, cooled, and weighed again. **Figure 5-8** illustrates the sediment samples emerging from the 1000° C (1832° F) muffle furnace prior to cooling.

$$\text{Percent Organic Matter (LOI}_{500}) = \left(\frac{DW_{105} - DW_{500}}{DW_{105}} \right) \cdot 100$$

Where DW_{105} = pre-firing dry weight; DW_{500} = post-500° C firing dry weight; and LOI_{500} = percent organic matter converted to ash or evolved as CO₂.

$$\text{Percent Carbonate (LOI}_{1000}) = \left(\frac{DW_{500} - Dw_{1000}}{Dw_{105}} \right) \cdot 100$$

Where DW_{105} = pre-firing dry weight; DW_{500} = post-500°C firing dry weight; Dw_{1000} = post-1000°C firing dry weight; and LOI_{1000} = percent CO₂ evolved from calcium carbonate

Mass lost after heating to 500° C (932° F) represents the combustion of organic carbon derived from plant and animal material to carbon dioxide and ash. Weight lost after heating the

same sample a second time to 1000° C (1832° F) represents the combustion of calcium carbonate (CaCO_3) to carbon dioxide (CO_2) (Heiri et al. 2001). Drying samples prior to firing helps to mitigate error from hydrated minerals (such as gypsum). However, other hydrated compounds may release their molecular water at various temperatures greater than 105° C (221° F), introducing an unknown amount of error.

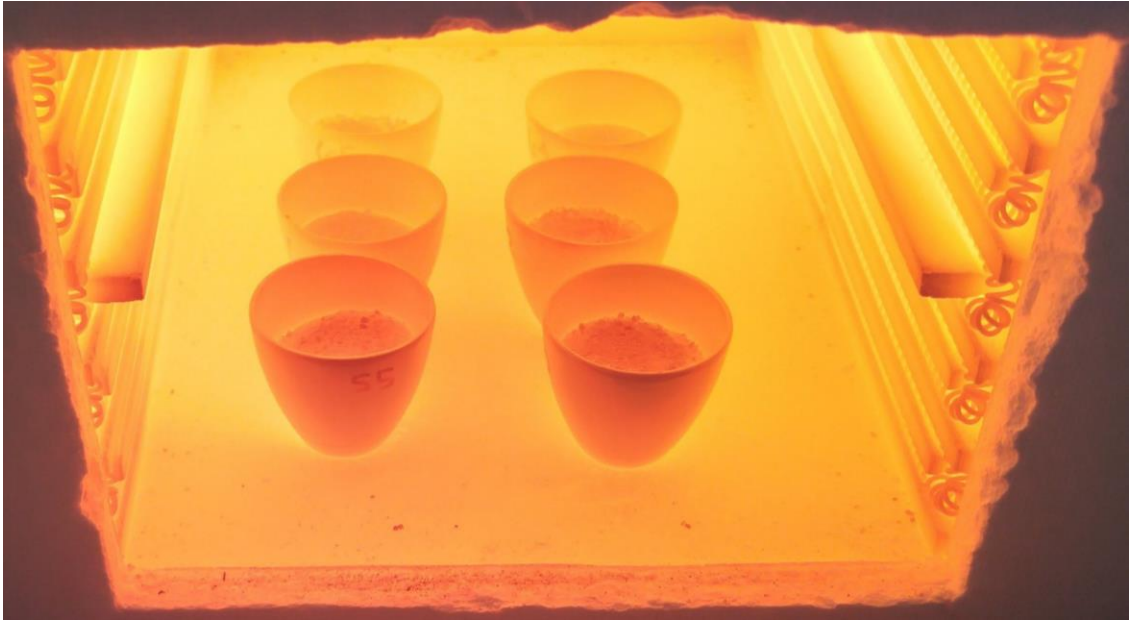


Figure 5-8. Preparing to remove sediment samples from the muffle furnace after firing at 1,000° C

5.4.4.4 Gypsum Determination

Flocculation during initial hydrometer particle size trials and discrepancies between LOI and Chittick carbonate content calculations suggested that significant quantities of ionically charged mineral salts retaining structural water were present in the sediment samples. Gypsum was inferred as the likely mineral candidate due to its abundance at Eagle Cave and other Lower Pecos rockshelters (Frederick 2017b; Nielsen 2017).

Equivalent gypsum content was determined using a differential water loss method exploiting the thermogravimetric dehydration of gypsum ($\text{CaSO}_4 \cdot 2\text{H}_2\text{O}$) to anhydrite (CaSO_4) between 70° C and 90° C (158° - 194° F) (Artieda et al. 2006). A 20 g aliquot of <2.0 mm (0.08

in) sediment matrix was weighted with a porcelain crucible prepared following the LOI procedures described above. The sample was dried in a 70° C (158° F) oven until a stable mass was achieved (non-gypsum held water was driven off), approximately 24 hours. The oven-dry sample was cooled in a desiccator for 20 minutes then weighed on a high-precision balance (.0001 g). The sample was returned to the oven set at 90° C (194° F) for an additional 24 hours. The samples were again cooled in the desiccator and weighed to the nearest .0001 g. Equivalent gypsum content was calculated using the equation below, as presented by Artieda et al. (2006:1933):

$$\% \textit{Gypsum} = \frac{ws - wf}{ws - wt} \cdot 100 \cdot \left(\frac{100}{14.95} \right) = \frac{ws - wf}{ws - wt} \cdot 669$$

Where: **ws** = Mass Sample + Vessel (g) at 70° C; **wf** = Mass Sample + Vessel (g) at 90° C; **wt** = Vessel Mass (g); 14.95 = Gypsum Recovery Factor between 70° C and 90° C as determined by Artieda et al. (2006).

5.4.4.5 Chittick Volumetric Calcimeter

A volumetric calcimeter method was used to reconcile discrepancies in the LOI carbonate determination data. Sediment samples were digested in an abundance of concentrated acid. The volume of CO₂ evolved from the reaction was measured in a closed-loop system known as a Chittick Apparatus, illustrated in **Figure 5-9**. This method provides a more precise measure of calcium carbonate in a sediment than LOI techniques. The residual mass represents organic carbon content plus any acid-insoluble minerals in the deposits. Devils River limestone is almost entirely calcium carbonate with a very small insoluble component. The limited quantity of undigested residual illustrates the significant volume of endogenic material within the shelter and can be used to estimate exogenic deposition. The methods described below were adapted from Dreimanis's (1962) workflow for the *Quantitative Gasometric Determination of Calcite and Dolomite by Using Chittick Apparatus*, Loepfert and Suarez (1996), and Gale and Hoare (1991).

Precisely 0.85 g of <2.0 mm (0.08 in) sediment was pulverized to a talc-like consistency using a ceramic mortar and pestle to ensure complete and rapid chemical digestion. The pulverized sample was added to an Erlenmeyer flask and sealed with a rubber stopper. The sliding reservoir of the apparatus was raised to -10 mL position and the system closed to create a vacuum loop. 10 mL of hydrochloric acid (HCL) was added to the sample flask via graduated burette. The sample was agitated until the reaction was complete and no longer effervesced; approximately two minutes. The reservoir elevation was equalized with the measurement burette meniscus and evolved CO₂ volume was recorded in milliliters. A Garmin GPS unit equipped with a barometric altimeter and digital thermometer was used to record the local atmospheric pressure in millibars (mb) and temperature in °C.

The calcium carbonate equivalent percentage was calculated using the formula:

$$CCE\% = \left(\frac{1.7}{\text{sample mass (g)}} \right) (\text{volume } CO_2 \text{ (ml)}) \left[0.0706 + (0.00143 \cdot \text{pressure(mb)}) - (0.00527 \cdot \text{temperature (} ^\circ C)) \right] \cdot 0.227$$

Where 0.00143 is the correction factor for barometric pressure, 0.00527 is the correction factor for temperature (Chemists 1950:118-119).

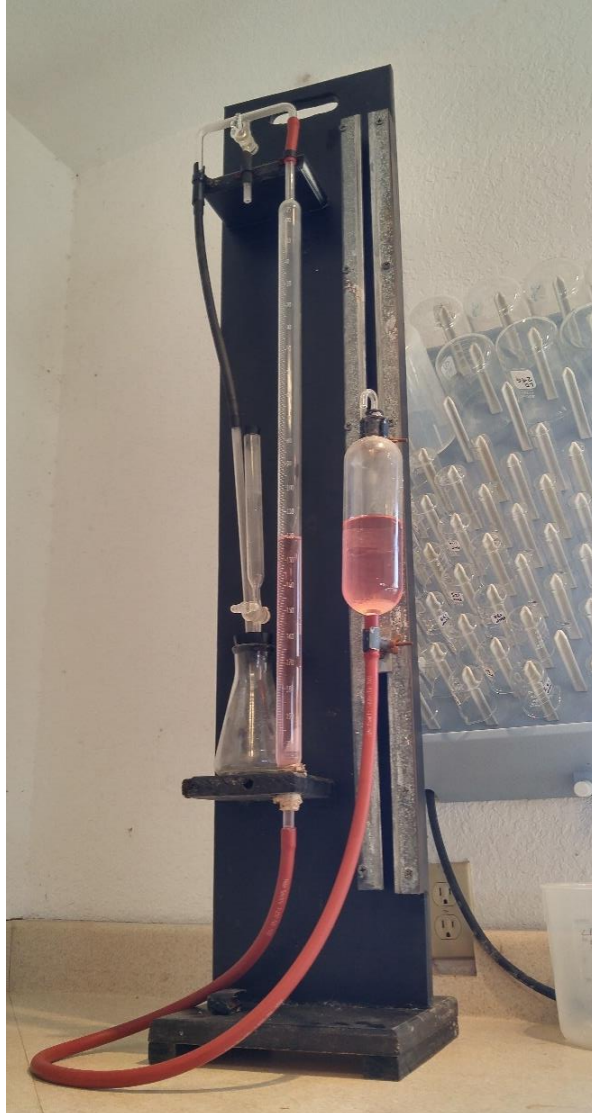


Figure 5-9. Chittick Apparatus used to determine calcium carbonate content in sediment. The pulverized sample reacts with HCL in the sealed Erlenmeyer flask. The displacement of the pink liquid by evolved CO₂ is measured on the large, graduated burette in the center of the system.

5.4.5 *Organic Carbon Content and Stable Isotopic Composition*

The significant organic carbon and structural water component in the Bone Bed 1 sediment samples yielded conflicting results between Chittick Apparatus and LOI methods. To gain a more accurate understanding of the Bone Bed 1 organic carbon composition, splits of the <2.0 mm (0.08 in) fraction sediment samples were sent to the University of Kansas Keck-NSF Paleoenvironmental and Environmental Stable Isotope Laboratory (KPESIL). In addition to the

accurate determination of organic carbon in each stratum, a Stable Isotope Ratio Mass Spectrometer and coupled elemental analyzer measured the carbon and nitrogen isotopic fractionation of that organic material.

5.4.5.1 Implications of Stable Isotope Fractionation

The ratio of ^{13}C to ^{12}C is an important proxy for paleoenvironmental reconstruction of regional plant communities, diet reconstruction, and as temporal marker for atmospheric CO_2 concentrations (Ehleringer and Monson 1993:411-414; Nordt 2001). C3 plant communities adapted to temperate climates have more efficient photosynthetic pathways that fix less atmospheric carbon resulting in lower concentrations of ^{13}C isotopes in their biomass. A typical $\delta^{13}\text{C}$ for predominantly C3 plant communities, as were common in the Pleistocene is approximately $-27\pm 3\text{‰}$ (Lohse et al. 2014:15). C4 plants are adapted to more arid climates with less efficient photosynthetic pathways, fixing greater quantities of CO_2 per cell respiration cycle resulting in a higher ^{13}C concentrations. A typical $\delta^{13}\text{C}$ for C4 plants is approximately $-13\pm 2\text{‰}$ (Ehleringer and Monson 1993).

A trophic level or food-web effect occurs as animals consume plants, integrating the $\delta^{13}\text{C}$ ratios from the environment into their bones (particularly bone collagen) and tissue (Nordt et al. 1994). Due to the volume of plant matter consumed by herbivores, the concentration of heavier isotopes becomes enriched, typically around 5-6‰ (Lohse et al. 2014:15). Tissues from Pleistocene bison consuming entirely C3 plants could be expected to yield a $\delta^{13}\text{C}$ vs. VPDB between -23.7‰ and -17.7‰ , while bison consuming exclusively C4 might yield between -8.7‰ and -4.7‰ . Carnivores who consume those herbivores further concentrate the heavier isotopes into their tissues. As plants and animals decompose, the residual organic matter and associated isotopic fractionation becomes integrated with the local soils (Nordt et al. 2002). Thus, analyzing the isotopic fractionation of soil organic carbon can provide insight into the origins of the organic matter, their trophic level, and the environmental conditions at their time of death.

In south-central Texas, geoarchaeological investigations at Applewhite Terrace identified very deeply stratified alluvial deposits chronicling over 15,000 years of changing environmental conditions (Nordt et al. 2002). Located on the Balcones Escarpment, analysis of organic carbon collected from a 20.0 m (65.6 ft) deep profile illustrates the local manifestations of broader Late Glacial and Holocene climatic shifts.

Broadly speaking, Late Pleistocene plant communities was composed of over half C3 plants (Nordt et al. 1994). Climatic fluctuations during the Pleistocene-Holocene transition resulted in a gradual increase in the proportion of C4 plants to C3 plants. Ever increasing aridity led to the dominance of C4 grasses at the expense of C3 plants by the Middle Holocene. However, geological and environmental changes on the global scale had significant local impacts detectable in the Applewhite alluvium.

Late Glacial meltwater pulses drove significant climatic instability in the timeframes relevant to Bone Beds 1 and 2 at Bonfire Shelter (Nordt et al. 2002:185-186). As massive quantities of cold water from the receding Laurentide Ice Sheet reached the Gulf of Mexico between 13,000 and 11,000 RCYBP, around the time of Bone Bed 1's accumulation, dropping regional temperatures by approximately 2°C (3.6°F). The climate swing had substantial repercussions for plant communities, with C4 plants all but disappearing and C3 filling the void, dropping soil $\delta^{13}\text{C}$ levels to approximately -25.0‰ 11,000 RCYBP; the lowest levels in the last 15,000 years. From 11,000 to 10,000 RCYBP, the meltwater runoff to the Gulf slowed and local conditions began to warm facilitating a resurgence of C4 plants coinciding with the events of Bone Bed 2. $\delta^{13}\text{C}$ levels from this period reached -19.0‰, marking the end of the Pleistocene with the permanent replacement of many C3 plants with C4 grasslands as conditions stabilized through the Holocene. This dramatic swing also coincides with the extinction of the Pleistocene megafauna that characterized Bone Bed 1 as their primary fodder sources dwindled. Organic

carbon samples from Bonfire Shelter should reflect these Late Glacial climate trends, regardless of the organic source material.

$\delta^{15}\text{N}$ in the atmosphere has been spatially and temporally relatively constant (Mariotti 1983). It is often used as a proxy measure for rainfall (which accumulates additional ^{15}N isotopes as droplets pass through the atmosphere (Kendall 2006; Weiner 2010c). Ratios derived from this rainfall provide a baseline for soil ecosystems. Soil $\delta^{15}\text{N}$ is elevated through microorganism respiration during pedogenesis and further concentrated by the preferential selection of ^{14}N by nitrogen fixing plant roots (Tiunov 2007). Plants in arid environments tend to have higher $\delta^{15}\text{N}$ values than those in temperate environments (Price 2014:75). Like ^{13}C , ^{15}N isotope concentrations are amplified farther up the food chain. Herbivores inherit and concentrate isotopic ratios from the autotrophic plants they consume, which are further enriched in carnivores (Brault et al. 2014) (Schoeninger and DeNiro 1984).

The decomposition of plant and animal matter by microorganisms reduces ^{13}C levels (and overall organic carbon content), concentrating ^{15}N and skewing the C/N ratio in the soils (Bonn and Rounds 2010). Warmer environments increase ^{15}N concentrations as photosynthesis accelerates and carbon is consumed. Plants and bacteria preferentially select lighter isotopes, concentrating of ^{15}N in the remaining material. It is also possible for this to trigger a feedback loop, as ^{15}N -rich plant matter accumulates and begins to decompose.

Peaks in organic carbon content are often associated with cultural activity, derived from the artificial concentration of foodstuffs, livestock, waste, associated pests, and microorganisms which can heavily influence ^{13}C and ^{15}N concentrations. This effect may be exacerbated in rockshelter settings where decomposition is limited (Weiner 2010b:57-58). However, retarded pedogenic activity and the absence of nitrogen fixing plants may limit the efficiency of concentration effects observed in other settings (Tiwari et al. 2015).

5.4.5.2 *KPESIL Procedures*

Inorganic carbon and other acid-soluble minerals were removed during a decalcification pretreatment process (conducted by KPESIL prior to analysis). Without pretreatment, the abundance of inorganic carbonate in a sample masks variation in the organic carbon component, ultimately measuring isotopic fractionation in the parent material rather than the organic matter of interest. Acid pretreatments impact carbon and nitrogen isotope ratios, but the effects are often less than the expected analytical precision at 0.2 - 0.5‰ (Schlacher and Connolly 2014; Tiunov 2007:395).

KPESIL's elemental analyzer procedure uses two main pieces of equipment: a Costech Elemental Analyzer 4010 paired with a continuous flow ThermoFinnigan MAT253 IRMS (Isotope Ratio Mass Spectrometer). Following decalcification pretreatments, the sample is incinerated at temperatures up to 1,800° C (3,272° F) in a reactor chamber filled with an inert gas. In the reactor, the sample decomposes into simple compounds including N₂, CO₂, H₂O, and SO₂. The gasses are separated by atomic mass in gas chromatography cylinder after which their relative abundance by mass is measured using a Thermal Conductivity Detector (TCD) (Costech 2005).

The gasses are then exported to the ThermoFinnigan MAT253 Isotope Ratio Mass Spectrometer. The MAT253 ionizes the gas molecules with a focused electron beam, exciting them to an electrically charged state. The ions are then drawn through a magnetic field towards a sensor. Heavier ions (those with an extra electron - ¹³Carbon and ¹⁵Nitrogen - are of interest in this study) follow a broader arc through the magnetic field towards the sensor than lighter ions (¹²Carbon and ¹⁴Nitrogen) (Carter and Barwick 2011:5-6). The ion detectors, known as Faraday cups measure the relative frequencies of each isotope.

Quantifying the ratio of ¹²C/¹³C and ¹⁴N/¹⁵N can elucidate the paleoenvironmental landscape at time sediments were deposited (Weiner 2010c:28-29). KPESIL's report for the Bone

Bed 1 samples included the relative abundance of carbon and nitrogen, $\delta^{15}\text{N}$ vs. Air ratio, $\delta^{13}\text{C}$ VPDB, N%, C%, and C/N (King 1997). C/N describes the ratio of carbon to nitrogen stable isotopes. Changes in ^{13}C , ^{15}N , and C/N ratio are often correlated; decreases in ^{13}C are correlated with a proportional ^{15}N increase, thus a lowering the C/N ratio. C/N ratio is also a useful indicator of distortions derived from the decalcification process (Bonn and Rounds 2010:7).

Stable isotope ratios are typically expressed in terms of parts per mille (‰) deviations from an internationally accepted reference material baseline (Ryabenko 2013). VPDB, Vienna Pee Dee Belemnite, is the carbon stable isotope standard derived from a Cretaceous Period fossil belemnite formation identified in South Carolina. All of the naturally occurring Pee Dee Belemnite reference material was consumed, but the International Atomic Energy Agency established the standard $^{12}\text{C}/^{13}\text{C}$ ratio at 0.01123720 (Iaea 1993; Kendall 2006). Atmospheric nitrogen is the accepted standard for $^{14}\text{N}/^{15}\text{N}$ at 272 ± 0.03 ‰ (Coplen et al. 1992; Ryabenko 2013:2).

The modern interior of Bonfire Shelter is shaded throughout most of the day, inhibiting plant growth and microbial activity. Most, if not all, organic carbon detected in the sediments should be attributable to exogenic sources. Increasing aridity from the Late Pleistocene into the Holocene should be reflected in the Bonfire organic carbon profiles with increasing ^{13}C concentrations as the climate dries and C4 grasses expand. ^{15}N levels may vary based on state of organic decomposition prior to redeposition Bonfire Shelter (decomposition within the shelter itself is limited).

Organic matter derived from slowly decaying animal remains may be detectable at Bonfire Shelter, particularly in the Bone Bed strata. As noted above, herbivores concentrate heavy carbon and nitrogen isotopes from their food sources. Carnivores further concentrate these isotopes, particularly nitrogen. If live animals were in the shelter for extended periods of time, the accumulation of excrement would likely cause a significant spike in ^{15}N , potentially without a

corresponding ^{13}C increase. If the decomposition of faunal organic matter is similar to plant decomposition, ^{15}N should be concentrated while organic carbon is depleted. In hydrologically active settings, it is possible for organic carbon to move through the profile. Increasing gypsum content with depth suggests that some moisture may percolate through the column, but stratum breaks are generally abrupt and inter-stratum bioturbation is limited so there is little reason to expect illuvial organic horizons.

5.4.6 *X-Ray Diffraction*

X-Ray Diffraction (XRD) was used to determine the mineral composition of sediment from each Bone Bed 1 stratum. Bulk and Detailed Clay Mineral XRD analysis was conducted by KT GeoServices in Gunnison, Colorado. Approximately 20 g of <2.0 mm (0.08 in) sediment from each stratum was allocated for XRD and shipped to KT GeoServices. XRD is particularly useful for its ability to identify unknown samples at the compound or mineral level, rather than at the elemental level (i.e.: X-Ray Fluorescence or chromatographic methods that require a baseline array of expected minerals) (Sparkman et al. 2011). Additionally, XRD can resolve the composition of extremely small particles (such as clay minerals) beyond the resolving power of typical desktop microscopes (Boggs 2012:126)

A limestone roof spall derived from Bone Bed 1 Stratum 24 (LS006) was submitted as a control sample. Previous studies report that Devils River limestone is approximately 97% acid-soluble calcium carbonate. However, the composition of the acid-insoluble 3% has never been evaluated within the context of the archaeological investigations at Mile Canyon. Deviations from the limestone mineral profile in the column sample sediments can be interpreted as exogenic deposition.

KT GeoServices conducted bulk sediment mineralogical analysis using a pulverized subsample of <2.0 mm (0.08 in) matrix. Detailed clay analysis utilized a further subsample of the <4 μm fraction separated via centrifuge and mounted to a nylon membrane filter and glass slide.

A Siemens D500 automated powder diffractometer equipped with a copper X-ray source (operated at 40 kV and 30mA) and a scintillation X-ray detector scanned the samples. Bulk samples were analyzed at angles from $5-60^{\circ} \cdot 2\theta$ at one degree per minute. Detailed clay samples were analyzed at angles from $2-35^{\circ} \cdot 2\theta$ at one degree per minute (Talbot 2019).

XRD measures the scattering effect of an X-ray impacting a crystal lattice and “diffracting” at a predictable angle. The X-ray detector scans over a range of angles to account for the random orientation of the sample particles (Poppe 2001). A Whole Pattern Fitting (WPF) software tool is used to interpret the scattering profile of complex samples to determine the relative proportion of minerals contributing to the observed pattern. WPF compares the unknown diffraction patterns to a library of known mineral standards to develop a diffraction model. KT GeoServices uses a Rietveld refinement, a sensitive statistical model that accounts for environmental and physical variables to determine what minerals under what conditions could create the observed diffraction pattern (Talbot 2019). The results are “semi-quantitative”, reporting the relative abundance of clay minerals as a percentage representing the area under the corresponding diffraction curve rather than a finite mass. Absolute values are not reported due to naturally occurring imperfections in mineral crystalline structures and XRD measuring environment variability (Biscaye 1965:805-809; Poppe 2001).

Robinson’s 1997 XRD study at Bonfire Shelter also used limestone cobbles as control samples (Robinson 1997). The study emphasizes “whole rock” mineralogy, but the specific control sample compositions are not reported. The experimental XRD assemblage included a small subset (10) of the 150 1983-1984 column sample levels, two of which are associated with Bone Bed 1 (Samples 125 and 150). The qualitative XRD method utilized in the study reports the presence/absence of minerals in the sediment samples but not their relative proportions. Robinson correlates the XRD results with larger scale sedimentological and palynological studies to place the Bonfire Shelter bone beds in a broader paleoenvironmental context.

5.4.6.1 XRD Mineral Classes

Table 5-9 summarizes the XRD-detected minerals and their properties relevant to Bone Bed 1 formation processes. Clay minerals were a major component of the samples. In addition to describing generic sediment particles below 10 ϕ , clay minerals refer to a specific group of phyllosilicates that incorporate various combinations of aluminum, calcium, iron, magnesium, potassium, and sodium ions into a crystalline lattice forming layered sheets (Kolb 2017:121). Organic matter, water, and other minerals can be incorporated into clay sheets. Beyond altering the color of the sediment, these incorporated materials have the potential to skew radiometric dates and organic carbon studies (Kolb 2017:121; Weiner 2010a:95).

Table 5-9. Bone Bed 1, Bonfire Shelter - XRD Mineral Components

Mineral	Chemical Formula	Notes	References
Quartz	SiO ₂	Stable, weathering resistant silicate mineral. Most common component of sandstones. Cherts are composed primarily of SiO ₂ and may appear as Quartz in XRD profiles.	(Boggs 2012:120-121) (Folk 1980:89)
K-Feldspar	KAlSi ₃ O ₈	Alkali/Potassium feldspar is an abundant aluminum silicate mineral formed in igneous rock, but also occurs in sedimentary formations. Relatively unstable, weathers to kaolinite or smectite via potassium leaching. Useful as post-depositional disturbance indicator due to susceptibility to weathering and mechanical alteration (especially when compared to co-occurring quartz) May occur naturally in marine limestones (such as the Devils River Formation)	(Boggs 2012:120-121) (Folk 1980:83-85) (Robinson 1997:40)
Plagioclase	(Na, Ca)(Al, Si)Si ₂ O ₈	Non-Alkali (non-potassium) feldspar variety	(Boggs 2012:120-121)
Calcite	CaCO ₃	Crystalline carbonate; Highly soluble in slightly acidic environments; Concentration potential increases with temperature and atmospheric CO ₂ ; Buffers soil/sediment pH, increasing organic preservation potential; Often derived from the weathering of limestone or combustion of organic material; Principle cementing agent in limestone	(Boggs 2012:126) (Karkanas 2017:131) (Loeppert and Suarez 1996:437-438)

Table 5-9. Continued

Mineral	Chemical Formula	Notes	References
Apatite	$\text{Ca}_5(\text{PO}_4)_3(\text{F},\text{Cl},\text{OH})$	Calcium phosphate; predominantly occurs as hydroxyapatite. Most common phosphate required by plants (phytoliths). Mineral component of animal bones/teeth. May remain at site if organic carbon components fully degrade or under acidic conditions	(Boggs 2012:224-229) (Weiner 2010b:59-67)
Anhydrite	CaSO_4	Dehydrated form of gypsum. Readily incorporates water into atomic structure. Crystal growth in rock or bone pore-space can be corrosive, contributing to exfoliation	(Loeppert and Suarez 1996:470-447)
Bassanite	$\text{CaSO}_4 \cdot 0.5\text{H}_2\text{O}$	Partially dehydrated gypsum. Uncommon in pedogenic/surface soils except in extremely arid and saline conditions. Readily hydrates to gypsum.	(Loeppert and Suarez 1996:470-471)
Hematite	Fe_2O_3	Antiferromagnetic iron oxide. Can formed from oxidation of magnetite; magnetic susceptibility may be between 3×10^{-7} and $6 \times 10^{-6} \text{ g}^3\text{kg}^{-1}$	(Gale and Hoare 1991:203)
R0 M-L I/S (90%S)*		Mixed layer clays - Illite/Smectite - 90% Smectite	
R1 M-L I/S (30%S)**		Mixed layer clays - Illite/Smectite - 30% Smectite	
Illite & Mica	$(\text{K},\text{H}_3\text{O})(\text{Al},\text{Mg},\text{Fe})_2(\text{Si},\text{Al})_4\text{O}_{10}[(\text{OH})_2,(\text{H}_2\text{O})]$ (highly variable)	Mixed layer clay mineral: Illite-micaceous clays. Potassium-rich clay mineral also referred to as hydromica. Secondary precipitate derived from weathering of other phyllosilicate clays, feldspars, muscovite (mica variety). Differentiated by the partial substitution of aluminum for silicon in the crystal lattice and/or incorporation of potassium ions. Limited water retention/swelling capacity.	(Boggs 2009:296, 210) (Folk 1980:89-94)
Kaolinite	$\text{Al}_2\text{Si}_2\text{O}_5(\text{OH})_4$	Phyllosilicate clay mineral derived from chemical weathering of smectite, illite, and other aluminum silicates including feldspars. Common karstic weathering product, especially in absence of magnesium and potassium. Relatively stable molecule, limited water-retaining potential.	(Folk 1980:40) (Nelson 2014) (Robinson 1997:40)
Chlorite	$(\text{Mg},\text{Fe})_3(\text{Si},\text{Al})_4\text{O}_{10}(\text{OH})_2 \cdot (\text{Mg},\text{Fe})_3(\text{OH})_6$ (Mg, Fe, Ni, Mn - $\text{O}_{10}(\text{OH})_8$) (variable)	Phyllosilicate clay mineral with variable composition. Potential secondary weathering product of smectite clays. Common component of sedimentary rock as well as some metamorphic and igneous rocks	(Boggs 2012:126, 148, 154) (Poppe 2001)

Table 5-9. Continued

Mineral	Chemical Formula	Notes	References
Gypsum	$\text{CaSO}_4 \cdot 2\text{H}_2\text{O}$	Highly soluble, extensive evaporative precipitation may be indicator drying climates. Can occur diagenetically where sulfates oxidize in presence of calcium (may be primary source at Bonfire Shelter). Crystallization may contribute to poor preservation. Dehydrates to anhydrite at approximately 200° C (392° F). See also: Anhydrite and Bassanite	(Bain 1990) (Loeppert and Suarez 1996) (Paz and Rossetti 2006)
Smectite	$0.5(\text{Ca},\text{Na})_{0.7}(\text{Al},\text{Mg},\text{Fe})_4[(\text{Si},\text{Al})_8\text{O}_{20}](\text{OH})_4n\text{H}_2\text{O}$ (variable)	Phyllosilicate clay mineral weathered from limestone in presence of magnesium, especially formations in poorly drained environments. Retains significant quantities of water between atomic layers causing swelling and high plasticity. Readily incorporated into mixed layer clays due to abundant exchangeable ions	(Boggs 2012:140-154) (Folk 1980) (Poppe 2001) (Severin 2004)
Montmorillonite	$(\text{Na},\text{Ca})_{0.33}(\text{Al},\text{Mg})_2(\text{Si}_4\text{O}_{10})(\text{OH})_2 \cdot n\text{H}_2\text{O}$	Phyllosilicate clay mineral, common variety of smectite clay. Often forms in magnesium rich environments	(Boggs 2012:126, 140-154) (Poppe 2001)

The clay minerals observed in a sediment profile can originate from several sources. Weathering can free clay minerals incorporated in sedimentary rock formations directly into a sediment system which “inherits” the clay profile of the parent material (Boggs 2012:126-127). Due to their extremely large surface area (a function of their small size) and strong ionic charge, clay minerals are highly reactive, readily weathering to form profiles unique from their source material (Folk 1980:91). The newly formed clays may be just as susceptible to secondary weathering as inherited clays (Galán and Ferrell 2013:92). With limited evidence of in situ weathering at Bonfire Shelter, clays are more likely to retain the characteristics of the source material.

Smectite, illite, and kaolinite are the most common groups of clay minerals, classified in part by number of atomic layers and the distance between them (Weiner 2010a:92-94). Kaolinite clays may form from the weathering of feldspar-rich limestones or as a secondary weathering product of illite and smectite clays in the absence of charged ions (Boggs 2012:160-161; Folk

1980:85, 90). Kaolinite's low reactivity results in a more stable molecule with a simplified construction that absorbs less water than smectite and illite clays (Nelson 2014; Velde and Meunier 2008:160-161). At Bonfire Shelter, higher proportions of kaolinite may indicate periods of instability preceding increasingly stable conditions. However, the parent material's clay profile with limited opportunities for in situ weathering should also be considered.

Smectite and Illite often occur in "mixed layers" of variably stacked clay molecules. Mixed layer clays form from ion exchange between layers catalyzed by weathering, oxidation, thermal processes, or other environmental changes (Galán and Ferrell 2013; Poppe 2001). The proportion of illite to smectite (often reported as I/S 60% , I/S 90%, etc.) is measurable using XRD and can provide insight into a deposit's weathering history. The ratio of smectite to illite can be a function the geological conditions at the time of crystallization: smectites form at temperatures below 100° C (212° F), illites form at greater than 200° C (392° F), and mixed-layer smectite and illite layers may form between 100° and 200° C (Boggs 2012:586). The formation of illite or smectite requires the presence of environmental potassium and magnesium, respectively. Post-depositional weathering may strip away ions from homogenous deposits to form mixed-layers or entirely different minerals (Folk 1980:83, 90-91). Clay minerals other than smectite and illite can form mixed layers, but smectite-illite sheets are among the most common and are the only mixed layers reported by KT GeoServices.

5.4.7 *Magnetic Susceptibility*

Magnetic susceptibility describes the relative ability of a material to become magnetized. When heated to temperatures as low as 100° C (212° F), magnetic minerals undergo chemical changes that increase their magnetic potential. An oxygen-deficient combustion atmosphere (reducing) facilitates the relatively rapid conversion of hematite to magnetite, becoming increasingly efficient to 800° C (1,472° F). This magnetite-rich soil exhibits much higher magnetic susceptibilities than unfired soils with hematite alone (Gale and Hoare 1991:214-215).

When hearths or other thermal features heated beyond this point are cleaned out the enhanced magnetic minerals are scattered, elevating magnetic susceptibilities over a broad area. Natural environmental processes also enhance magnetic susceptibility. The intrinsic magnetism of the underlying parent material, the presence of organic matter, groundwater interactions, and pedogenesis (via magnetotactic bacteria) may all concentrate magnetic minerals (Gale and Hoare 1991; Yan et al. 2012).

In this study, magnetic susceptibility was used to identify strata with elevated magnetic mineral concentrations. On its own, Mile Canyon limestone has a very low susceptibility. Sediments derived from the Rio Grande have elevated susceptibility values due to the accumulation of magnetic minerals in sediments washing out of the Rocky Mountains, Sierra Madre Oriental, and the volcanic deposits of the Trans-Pecos many miles upstream from Mile Canyon. Redeposition of these sediments can contribute to significant deviations in magnetic susceptibilities. Unlike other Mile Canyon shelters, spikes in magnetic susceptibility at Bonfire Shelter cannot be attributed to large burned rock features. In the Holocene strata, the incinerated bison bone beds and isolated surface hearths likely contribute to magnetic susceptibilities. No similar features or evidence of discrete living surfaces have been identified in association with Bone Bed 1, suggesting exogenic deposition may be the primary source of magnetic minerals in the Late Pleistocene. However, the presence of unidentified features and periodic small-scale human occupation cannot be wholly discounted.

5.4.7.1 Magnetic Susceptibility Procedure

Magnetic susceptibility was measured using a Bartington MS2 Magnetic Susceptibility Meter and paired sensor. Approximately 10.0 g of <2.0 mm (0.08 in) sediment was packed into a 1.0 cm³ plastic cube designed to fit the sensor apparatus. The sensor was zeroed using an empty cube before and after sediment readings and between high- and low-frequency readings. Each sample was measured twice in low-frequency magnetic fields and twice in high-frequency

magnetic fields. The average high-frequency reading and low frequency reading were used to calculate kappa (volume susceptibility, K) and chi (mass-corrected volume susceptibility, χ) values. Low and high frequency K values were calibrated against the zero readings using by subtracting the average zero readings from the average sample readings using the formula:

$$(\mathit{Avg Sample}) - (\mathit{Avg Zero}) = K$$

χ was calculated by dividing K by sample mass in kilograms:

$$\frac{K \cdot .01}{\mathit{Sample Mass (g)}} = \chi$$

The magnetic susceptibility meter applies a relatively weak magnetic field to the sample. The degree to which the material's electrons are excited when exposed to this magnetic field is known as "initial low-field reversible susceptibility" (or simply "susceptibility"), meaning that the induced magnetic response is not permanent (Gale and Hoare 1991:202-203). Magnetic susceptibility can be expressed as κ : volumetric susceptibility measured in dimensionless SI units; or χ : mass-specific susceptibility measured in $\text{m}^3 \text{kg}^{-1}$. Mass-corrected χ values are generally preferred, as they do not vary with sample density.

Due to the relatively low expected susceptibility of the Devils River limestone parent material, all measurements were recorded using the Bartington's more precise 0.1 SI sensor setting (as opposed to the less sensitive 1.0 SI setting). Magnetic susceptibility was measured in both high- (~4.6 Hz) and low-frequency (~0.46 kHz) fields. Discrepancies between high- and low-frequency K (specifically, lower K -values at high-frequency than low-frequency) can indicate the presence of ultrafine (<0.03 μm) superparamagnetic ferrimagnetic minerals within the sample. Consistent K -values in high- and low- frequency fields indicates that superparamagnetic minerals are not present (Dearing 1999:17).

In smaller particles, magnetic potential and the ability retain magnetic properties is limited by the degree to which their electrons can become excited and aligned to a magnetic pole

(Single-domain magnetism). Larger particles can absorb the elevated energy levels available at higher frequencies and retain their magnetism for longer periods of time (Superparamagnetism) (Gale and Hoare 1991:204-205).

The difference between high-frequency mass susceptibility (χ_{HF}) and low-frequencies mass susceptibility (χ_{LF}) is referred to as the Coefficient of Frequency Dependency (χ_{FD}) (Gale and Hoare 1991:207). Larger χ_{FD} values may indicate smaller magnetic particles. Smaller magnetic particles may reflect sediment transport mechanisms that size-sort particles. Aeolian processes typically carry finer particles than fluvial or colluvial processes, potentially resulting in higher χ_{FD} (Gale and Hoare 1991:209-210).

The Coefficient of Frequency Dependency was calculated using the formula:

$$\left(\frac{\chi_{LF} - \chi_{HF}}{\chi_{HF}} \right) \cdot 100 = \chi_{FD}$$

5.4.7.2 *Interpreting Magnetic Susceptibility*

Magnetic susceptibility provides a relative measure of magnetic mineral concentrations that must be contextualized with additional geoarchaeological data (Dalan 2006, 2008; Dearing 1999). Mile Canyon rockshelters accumulate sediment derived from a diverse array of sources and transport mechanisms. Sediments derived from Rio Grande alluvium likely contain elevated magnetic mineral concentrations compared to locally weathered soils and sediments (Frederick 2017b). Upland sediments introduced via sheetwash can also increase magnetic susceptibilities within the shelter.

It is impossible to determine the source of magnetism from magnetic susceptibility readings alone. Supplemented with particle size distributions (providing insight into transport vectors contributing to a sediment) and XRD (providing qualitative and semiquantitative measures of magnetic minerals), magnetic susceptibility can provide a more complete picture of a deposit. Samples with χ_{LF} lower than $0.1 \times 10^{-6} \text{m}^3 \text{kg}^{-1}$ are likely the result of paramagnetic

minerals or very limited quantities of ferrimagnetic minerals within the sediment samples. Samples with χ_{LF} greater than $100 \times 10^{-6} \text{m}^3 \text{kg}^{-1}$ likely contain more substantial concentrations of ferrimagnetic minerals such as Magnetite or Maghemite (Dearing 1999:40-41).

Ferromagnetic minerals spontaneously produce their very strong magnetic fields with very high mass susceptibilities (i.e.: Iron = $\sim 0.2 \text{m}^3 \text{kg}^{-1}$) (Gale and Hoare 1991:203-204). Ferrimagnetic mineral spontaneously produce relatively weak magnetic fields with lower mass susceptibilities (i.e.: Magnetite and Maghemite = $\sim 4-6 \times 10^{-4} \text{m}^3 \text{kg}^{-1}$). Antiferrognetic materials do not produce their own magnetic fields; magnetic responses induced by the presence of another magnetic field typically are very weak with low mass susceptibilities (i.e.: Hematite = $\sim 3 \times 10^{-7}$ to $\sim 6 \times 10^{-6}$). Hematite forms where iron (or magnetite) oxidizes in an oxygen-rich environment, often associated with higher moisture levels. Magnetite is more likely to form in oxygen-poor environments. If limited evidence of exogenic deposition is observed in Bone Bed 1 in conjunction with elevated magnetic susceptibilities associated with magnetite, it may be indicative of surface-hearth detritus scattering across the shelter interior.

Magnetic susceptibility measurements are sensitive to interference from electronic sources and magnetic materials in the laboratory environment (Dearing 1999:20). Analysis must be conducted in a magnetically stable setting. Higher ambient temperatures can decrease the superparamagnetic boundary, causing superficially high χ_{FD} values. Nearby ferrous objects, including furniture hardware and laboratory equipment may be detected by the sensor and artificially inflate susceptibilities. Electromagnetic radiation from microwave ovens and Wi-Fi routers as well as appliances containing electronic motors generate fields that interfere with the sensor. To ensure the testing environment was magnetically stable, the sensor was allowed to run continuously with no sample and observed for a ten-minute warmup period before measurements were collected.

6. INTERPRETIVE FRAMEWORK: CLASSIFYING BONE BED 1

This thesis was designed to identify evidence of human activity associated with some, all, or none of the Bone Bed 1 strata. Considering every possible contingency explaining the introduction of faunal remains to Bonfire Shelter is not possible. A functional model was developed to examine four plausible scenarios that could account for the Bone Bed 1 assemblages:

1. Null Hypothesis – The Bone Bed 1 assemblage was deposited in Bonfire Shelter via natural geological processes
2. Alternative Hypothesis¹: The Bone Bed 1 assemblage is the result of human activity
3. Alternative Hypothesis²: The Bone Bed 1 assemblage is the result of carnivore activity
4. Alternative Hypothesis³: The Bone Bed 1 fauna died of natural causes in Bonfire Shelter

To assess these hypotheses, three lines of evidence were evaluated: geological, faunal, and cultural. **Table 6-1** outlines the evidence expected in each scenario. This model is not meant to be exhaustive. Aspects of each hypothesis likely contributed to Bone Bed 1 resulting in a palimpsest of superimposed hunting, scavenging, and depositional events. The objective is to establish key *identifiable* processes that can be confidently attributed to a specific source explaining the origins of the Bone Bed 1 faunal material.

The bulleted points in each **Table 6-1** field establish baseline expectations for each potential source of faunal material. Several sources share overlapping criteria, reflecting the complex formation processes contributing to the Lower Pecos rockshelters. Multiple criteria must be satisfied for a stratum to be ascribed to a particular source. Based on a preponderance of the available evidence, hypotheses will be accepted or rejected based on a best fit alignment with the criteria outlined here.

Table 6-1. Simplified model explaining the origins of faunal material identified in Bone Bed 1 at Bonfire shelter. Site origin sources will be accepted or rejected based on a preponderance of available evidence and a best-fit alignment with this model.

		Site Origins			
		Geological	Ecological	Carnivore	Cultural
Evidence	Description	Faunal remains were introduced to the shelter via geological processes	Fauna entered shelter alive under their own power	Faunal remains introduced to shelter/impacted by carnivores	Faunal remains are result of human activity
	Geological	<ul style="list-style-type: none"> • Significant high-energy exogenic deposition • Poorly sorted sediments 	<ul style="list-style-type: none"> • Limited low-energy exogenic sediments • Evidence of standing water or significant mineral concentrations attractive to megafauna • Well sorted sediments 	<ul style="list-style-type: none"> • Stable – Limited exogenic and endogenic deposition • Moderate organic carbon • Moderate magnetic susceptibility 	<ul style="list-style-type: none"> • Stable – Limited exogenic and endogenic deposition • High organic carbon • High magnetic susceptibility
	Faunal	<ul style="list-style-type: none"> • Whole, possibly disarticulated carcasses • Patterned/size sorted distribution • Variable number of individuals represented • Variable taxonomic diversity • No age bias 	<ul style="list-style-type: none"> • Whole, partially articulated carcasses • Many Individuals represent • High taxonomic diversity • No age bias 	<ul style="list-style-type: none"> • Isolated, robust, high-utility elements • High Disarticulation • Many individuals represented • Moderate taxonomic diversity • Bias juvenile/weak individuals • Assemblage includes carnivore remains 	<ul style="list-style-type: none"> • High utility “sections” of carcasses including rider elements • Few individuals represented • Low taxonomic diversity • Bias juvenile/weak individuals
	Cultural	<ul style="list-style-type: none"> • None, unless redeposited with exogenic sediment <p>Limited abrasion, polish, or striations from transport</p>	<ul style="list-style-type: none"> • No cultural Material • Possible trampling damage 	<ul style="list-style-type: none"> • No cultural material • Extensive tooth marks/gnawing 	<ul style="list-style-type: none"> • Microartifacts present • Very limited numbers of formal/expedient tools • Cut marks and/or spiral fractures • Cultural features

6.1 *Geological Circumstances*

The null hypothesis for the origins of Bone Bed 1 is that the observed faunal assemblage is a product of its geological context; the same forces that contributed sediment to each stratum also introduced the megafauna remains. Given the large size of many elements observed in Bone Bed 1, high-energy transport processes manifesting as poorly sorted exogenic deposits would be required to introduce the remains to the shelter (Waters 1992:232, 241). An assemblage derived from geological processes is expected to represent a random sample of the local faunal population (Haynes 1991b); all age classes of all taxa have a relatively equal chance of appearing within the shelter. Specific element frequencies should not exhibit a utility bias. However, disarticulation of an existing skeleton and size sorting/linear distribution of elements in the direction of transport flow may occur. Limited abrasion, polish, or striations may occur on cortical bone surfaces from particles entrained with the faunal remains, but green breaks and cut marks are not expected (Haynes and Krasinski 2010). No cultural material should occur in sediments derived solely from geological processes unless redeposited from an occupation area outside the shelter.

Over-rim sheet wash and intense alluvial activity are two geological scenarios that could result in the faunal patterns observed in Bone Bed 1. Despite the reduced distance from the Pleistocene canyon floor to the shelter interior, a flood level of several meters would be required to breach the shelter (Byerly et al. 2005:624). Geological evidence of a major flood event might include massive, homogenous alluvial deposits exhibiting a fining upward sequence, increased magnetic susceptibility, increased organic carbon, and the detection of exogenic minerals through XRD (Patton and Dibble 1982; Robinson 1997). Faunal remains may be oriented and size-graded in the direction of water flow with larger elements concentrated upstream and smaller elements carried downstream (Frison and Todd 1986). At present, there is no evidence that such an event has occurred. However, alluvial deposition is included as a contingency outcome that may be detected in the geoarchaeological analysis.

Sediments derived from sheet wash may not accumulate in the thick, homogenous deposits associated with large-scale flooding (Farrand 2001:547). Sheet wash strata may be discontinuous with the densest accumulation concentrated immediately below the spillways (i.e.: the Bonfire notch) diffusing outward to form thinner deposits across the shelter interior. Larger debris (such as megafauna elements or large cobbles) may be more susceptible to colluvial redeposition, settling in lower lying areas of the shelter if the initial point of introduction is on a steep slope (i.e.: the talus cone).

6.2 *Ecological Causes*

Fauna entering the shelter under their own power and expiring there provides an alternative explanation for the accumulation of remains in Bone Bed 1. Subsistence resources including fresh water, mineral salts, and food stuffs or simply shelter from the elements could be contributing factors drawing fauna into the shelter (Ayotte et al. 2008; Hadjisterkotis and Reese 2008; Haynes 1985). In this scenario, faunal remains could accumulate independently of the ongoing shelter formation processes. However, pooling water or other fauna-attracting resources in the shelter may be detectable geoarchaeologically.

Dibble suggests that the silty trough observed in Bone Bed 1 is derived from ponding water within Bonfire Shelter in the Late Pleistocene (Dibble and Lorrain 1968:28). Compositional analysis of these sediments may clarify the depositional origins of the strata. Elevated proportions of exogenic material with a variably sorted coarse component may represent sheet wash redirected by the boulder field into the shelter interior in low-lying areas (Bement 1986a:2; Robinson 1997:36). Alternatively, well sorted endogenic sediments and minerals could be a sign of spring activity feeding small pools within the shelter, which Dibble notes are present at the base of the slopes below Bonfire Shelter (Dibble and Lorrain 1968:13).

If Bone Bed 1 represents the natural mortality of fauna within Bonfire Shelter, the assemblage should consist of relatively complete skeletons (Graham et al. 2013:24). If animals are returning to the shelter to access seasonal resources, once articulated skeletons may be damaged and dispersed by trampling (Haynes 1991b; Haynes and Krasinski 2010). Predators and scavengers attracted to accumulating carrion can exacerbate this effect, causing additional bite and gnawing damage. The deletion of less robust elements from the faunal record via weathering and attrition can mimic utility biases in natural mortality scenarios (Binford 1981:217). Regardless of dispersion, a preponderance of low-utility elements including cranial fragments, vertebrae, tarsals, and phalanges (among others) should be represented in the assemblage (Binford 1981:198-202). Rapid burial may mitigate some of these impacts, resulting in more complete assemblages (Haynes 1985; Rogers et al. 2008:293)

Natural faunal accumulations, especially those associated with scarce resources, should feature a broad sample of the local animal community (Rogers and Kidwell 2008). High taxonomic diversity is expected (Haynes 1991b:152). Likewise, the assemblage is not expected to bias very old or very young individuals to the extent observed in predation deposits (Castaños et al. 2017). Older individuals may be more likely to die in the shelter under normal circumstances. However, all members of the community require access to resources and may have reason to enter the shelter. In times of hardship or catastrophic resource scarcity, a broader spectrum of individuals including otherwise healthy adults may be represented in the faunal assemblage (Rogers and Kidwell 2008:7).

Even small, ephemeral water accumulations may have been enough to draw fauna into the shaded interior of Bonfire Shelter (Hadjisterkotis and Reese 2008). Gypsum salts, calcium carbonate, and other trace minerals may have been very attractive to herbivores across the landscape (Ayotte et al. 2008). In the wetter conditions of the Pleistocene, the moisture driving

cryoclastic spalling may have been extensive enough to accumulate as droplets providing water and minerals to desperate animals.

While anecdotal and speculative, these scenarios provide potential explanations for the natural accumulation of megafauna remains within Bonfire Shelter. Large fauna frequently expire near resource loci due to starvation, dehydration, entrapment, and predation (Haynes 1985, 1991b; Rogers and Kidwell 2008). Bonfire's modern morphology is not particularly trap-like, but three additional meters of steep boulders may have inhibited the rapid egress of larger animals. Natural accumulations are expected to yield taxonomically and agedly diverse assemblages with limited disarticulation. However, the dynamic nature of rockshelter settings may complicate differentiation from other sources. Post-depositional modification via geological, predator, or human vectors may obscure key archaeological evidence. As such, Bone Bed 1 strata will not be classified as natural accumulations unless other contributing factors can be ruled out as sources of the faunal assemblage.

6.3 *The Elephant in the Shelter*

Nearly all assumptions regarding the behavior and ecology of Pleistocene megafauna are derived from studies of related modern species (Haynes 1985, 1988, 1991a). These proxy taxa, including American bison and African elephants, provide valuable insight into group dynamics, migration, and resource consumption. Similar ethnoarchaeological studies, analysis of predator scavenging behavior, and the effects of post-depositional faunal assemblage modification function as comparative samples for the impacts observed at archaeological sites (Binford 1978b, 1981). It is impossible to verify the transferability of modern observations to past species, but they provide the only tangible reference points to Pleistocene. The discussion below is a detailed consideration of ecological scenarios that could account for the Bone Bed 1 assemblage. These studies of modern ungulate behavioral ecology were largely conducted by archaeologists for the explicit purpose of developing a model of expectations for extinct species.

Despite the geomorphological changes at Mile Canyon since the Pleistocene, the relatively lush micro-ecosystems that exist along the modern canyon margins may have existed in the past (Bush and Hanselka 2017). Spring seeps and pooling water in tinaja and among the boulders of the upper canyon may have attracted the attention of large mammals, drawing them into the vicinity of Bonfire Shelter. Bement suggests that a coordinated effort could plausibly divert animals present in the upper canyon towards Bonfire Shelter, utilizing the confined quarters as a natural trap (Bement 1986a:64)

Modern ungulates supplement their herbaceous diets through geophagia: the active consumption of sediments and minerals (Ayotte et al. 2008). Carbonates and potassium (both of which are present in the Bonfire clay minerals and limestone-derived sediments) are particularly attractive to balance gastrointestinal pH levels during transitions between seasonal fodder sources. African elephants have been documented traveling significant distances to consume sediments rich in carbonates, trace minerals, and salts. Salts have the added benefit of increasing water retention during dry periods. Elephants have also been documented seeking shade in caves, rockshelters, and wooded areas to further mitigate water loss (Hadjisterkotis and Reese 2008:126-127).

African elephants are known to return to seasonal watering holes that have sustained them through previous dry seasons (Haynes 1988, 1991a). As surface water runs dry, elephants may dig wells up to 3m deep with their tusks to access residual seeps (Haynes 1991a). These playas and tinaja may concentrate salts and minerals as they dry, serving the dual function of saltlick and water source (Haynes 1985).

Extended droughts or cold periods may tether ungulates to shrinking water sources. Mass die-offs due to starvation and dehydration in the vicinity of watering holes are well documented (Burke 2013:66-68; Haynes 1988, 1991b). Competition for access to water and resources may

drive fauna to seek increasingly isolated or otherwise risky resources, potentially raising the likelihood of falling into a natural trap (Hadjisterkotis and Reese 2008).

The drying water sources that sustain them also pose a serious threat (Haynes 1985). Muddy playas become natural traps, potentially miring animals until they succumb to dehydration and the elements (Haynes 1988). In addition to mass die-offs, these stressed populations tethered to fixed resources are susceptible to large-scale predation (at the peril of becoming mired themselves, RE: La Brae tar pits) (Haynes 1991a). A study of sea-cliffs in Cyprus suggests numerous Pleistocene fauna, including elephant taxa, met their demise attempting to reach fresh water and mineral deposits within the rockshelters (Hadjisterkotis and Reese 2008). Frequent traverses of the unstable cliffs left the animals exposed to collapse events, sink holes, entrapment, and falls on the steep slopes.

The massive accumulations of animal remains around scarce resources are susceptible to wide-spread secondary modification including scavenging, trampling, and hydrological activity (Haynes 1985; Haynes and Klimowicz 2015). Modern elephants have been documented moving and digging through the remains of other elephants to reach water resources (Haynes and Krasinski 2010:192). Desperate excavation to revitalize wells and seeps may render the features traps themselves, causing cave-ins and collapses that can entomb calves and juveniles. Haynes cites accidental death via mud mires, drowning, collapses, and falls from height as significant sources of natural mortality (Haynes 1991a)

6.4 Carnivore Activity

The mammoth long bone fragment pierced by what appears to be a *Homotherium* tooth indicates that the Bone Bed 1 strata were impacted, to at least some degree, by carnivores (Bement 1986a:51-54). Beyond this example, the extent of carnivore activity at Bonfire Shelter is unknown. The criteria for ascribing a site to “carnivore origins” were primarily based on

generalized descriptions of carnivore denning behavior by Binford (1981). However, reports from Friesenhahn Cave (described in **Chapter 3**) illustrate local adaptations that may diverge from these expectations in terms of taxonomic diversity and the state of carcasses in the shelter (Evans and Meade 1961; Graham 1976; Graham et al. 2013; Marean and Ehrhardt 1995; Martin 1968).

Dens are burrows, crevices, caves or other protected features seasonally occupied by animal family units for birthing and raising young (Binford 1981:202-205). Predators and scavengers often returned an ad hoc assemblage of elements to their dens to mitigate competition for direct access to a kill site, supporting cubs unable to hunt/defend themselves. The duration and intensity of denning behavior is largely a function of structural stability; permanent landscape features including caves and rockshelters may be continuously utilized as dens.

The geoarchaeological profile of a carnivore den should reflect this stability. Evidence of high-energy exogenic deposition is expected to be low, with relatively low spall exfoliation reducing the risk of injury from falling debris. Extended occupations by family units are expected to elevate organic carbon and levels due to the continuous influx of carrion and the accumulation of shed fur, excrement, and other biological material.

This secondary accumulation of faunal remains is a key attribute differentiating dens from other carnivore activity sites (Binford 1981:198-200). Den assemblages are expected to exhibit broad taxonomic diversity, with a preference towards species and individuals of a size that the predator can successfully hunt. Prey species are likely to be represented by disarticulated individual elements, with high frequencies of high caloric yield upper limb elements and marrow bones and limited specimens from the axial skeleton (Binford 1981:226-228). Cranial fragments, pelvises, scapulae, vertebra, and ribs are more likely to remain behind at the kill site (Binford 1981:222-223). Elements returned to the shelter are often subjected to intense gnawing, manifesting as extensive tooth and epiphyseal destruction (Haynes 1985:54-57).

As such, many individuals are expected to be represented in the assemblage by small number of elements from any one individual (Binford 1981:226-228; 236). The range of represented elements is partially limited by the predator's ability to disarticulate, manipulate, and transport individual specimens back to the den. The age range of prey species is likely to be biased towards juvenile, very old, other otherwise weakened individuals opportunistically targeted by predators (Graham et al. 2013; Haynes 1988). The assemblage is further biased by the differential preservation of robust elements which can withstand the intense gnawing (Castaños et al. 2017:375).

Juvenile predators have been documented introducing individual long bones, sticks/branches, and stone cobbles into dens (Binford 1981:208). These materials were used as "play" items, replicating the competition for preferential access to kills observed among adults. This behavior could account for the anomalous presence of some materials within the shelter if other evidence of denning activity is observed (Binford 1981:203).

Direct evidence of carnivores within the shelter is necessary to classify a site as a den; tooth marks, breakage patterns, and bone distributions are circumstantial (Binford 1981:207-208). Dens typically contain the bones, teeth, and coprolites of carnivores themselves. Deaths from miscarriage, childbirth, youth illness, wounds, or cave-ins result in the deposition of predator remains among the prey. Ethnoarchaeological and experimental studies suggest that carnivores frequently represent over 20% of the faunal assemblage at den sites (Castaños et al. 2017:374). In contrast, carnivores typically comprise <10% of the faunal assemblage at known archaeological sites.

6.5 *Human Activity*

Baseline expectations for human activity are modeled after a secondary processing location, as a discrete site-type from a kill site or a habitation site (Haynes and Klimowicz

2015:34). Humans typically follow a strategic kill disarticulation process facilitating transportation to where it will be consumed (Binford 1981:233-234). If the consumption site is a significant distance away from the kill site, an intermediate processing station may be established. If the kill site and the consumption site are close by, processing and consumption could occur at the same location. This strategic behavior is unique from carnivores, where prey is typically consumed within a few meters of the actual kill with a small number of individual elements are returned to denning locations (Binford 1981:207, 224).

During initial butchering at kill sites, easily transportable “sections” (i.e.: limb quarters, entire halves, etc.) are removed from the carcass (Binford 1978b:64). These sections include sets of high-utility elements and associated very low-yield “riders”. The incidental removal of these tarsals, meta-tarsals, phalanges, and other small bones from the kill site is known as the “Schlepp Effect” (Daly 1969:149). At processing sites, these large sections are broken down further into smaller, more manageable pieces for long-distance transport. At consumption sites, sections are further broken down to consumable pieces, extraneous riders removed, and bones cracked to extract marrow (Binford 1981:157-162).

Following this pattern, processing site assemblages should be marked by a high frequency of mixed-utility limb elements that were removed from a kill (Binford 1981:234). High-utility elements may be separated from one another, but riders are expected to remain intact. Kill sites should feature a notable absence of limb elements and the relatively complete and articulated elements from the axial skeleton that were left behind. Consumption sites should feature the highest degree of disarticulation, including riders . Disarticulation may occur on a sliding scale based on the specific needs and circumstances of the hunting party (Binford 1978b:62-64). Patterns can be further complicated by secondary scavenging activity and any of these site types.

Consistent with the high degree of disarticulation, higher cut mark frequencies are expected at processing sites. Cut and tool marks are more likely to occur as limbs and smaller joints are separated prior to cooking and consumption. Spiral fractures and green breaks may occur at processing sites, but are more commonly associated with marrow processing at consumption sites (Binford 1981:151-160).

It is important to note that butchering processes are culturally informed. The presence of cut marks may be minimal if elements are not completely defleshed, disarticulation is limited, or the butchers are very skilled (Haynes and Klimowicz 2015:28). Haynes argues that even very low cut mark frequencies (present on <1% of elements) are sufficient to attribute a site to human agents, especially if those marks are present on high-utility elements (Haynes and Klimowicz 2015:34). Ambiguous cut marks should be assessed within the context of the broader site.

Attrition from secondary carnivore scavenging can often resemble human modification patterns (Haynes 1988:152-155). The presence of cut marks and tooth marks on the same element is not uncommon. Striations from transverse molars dragging across a bone surface can resemble stone tool cut marks, but are often accompanied by other pits, punctures, furrows, and chipping from nearby teeth (Diedrich and McFarlane 2017). Human cut marks typically occur in strategic sets (Binford 1981:107-143)

Intense epiphyseal gnawing to access the marrow cavity can result in spiral fractures similar to human marrow extraction (Binford 1981:152-155). Carnivore induced spiral fractures are typically confined to the proximal or distal end and accompanied by tooth marks along bone shafts (Castaños et al. 2017:375). Humans typically use tools to crack the medial portions of long bones to access the marrow cavity, resulting in impact damage in addition to green breaks.

Human processing sites are expected to have relatively low taxonomic diversity compared to natural death sites and sites of geological origin (Waguespack and Surovell 2003).

Humans are more likely to target prey species with higher caloric returns, whereas natural accumulations may include a broader cross-section of the local faunal community. That is not to say that humans were not consuming lower yield organisms, but their representation at a processing site is likely to be low and difficult to disentangle from the background “noise” of non-prey species utilizing the shelter (Haynes and Klimowicz 2015:26). Like carnivores, humans opportunistically target juvenile or otherwise weakened individuals (Haynes and Klimowicz 2015:24), increasing the likelihood of a successful hunt and reducing the risk of bodily injury while engaging their prey. Sites of human origin reflect this bias in the faunal assemblage.

Extensive processing sites and consumption sites may include surface hearths or similar features. Features are critical diagnostic components of archaeological sites, both for ascribing them to human activity and validating their temporal association. During processing activity, elements may accumulate in Binford’s “toss-zone” model where smaller fragments are dropped in the immediate vicinity of the worker while larger pieces are tossed the perimeter of the work area. In some ethnoarchaeological studies, these work areas were organized around hearths (Binford 1978a). This size sorting effect contrasts the ad hoc nature of carnivore scattering and the linear distributions of geological transport mechanisms.

The presence of unambiguous artifacts is the key component for defining sites of human origin (Haynes and Klimowicz 2015:28, 32). The extensive disarticulation that characterizes human processing localities suggests that significant quantities of debitage, both as expedient tools and from tool resharpening, should be present. The razor-sharp edge of flake tools makes them well suited for butchering activity. Their expedient nature increases the probability of discard at the site. Formal tools are also useful butchering implements, but require time, energy, and resources to produce and are more likely to be curated and removed from the site for future use. Bifacial and unifacial tools require regular edge-rejuvenation resulting in microartifact concentrations in the vicinity of activity areas (Frison 1986:128-134; 1989). In contrast, kill site

lithic assemblages may be limited to lost, broken, worn, or discarded hunting implements. Functional tools are unlikely to be intentionally left at the site. Very small quantities of debitage are expected due to the limited extent of initial disarticulation at many kill sites. In both scenarios, macro-flakes are expected to remain concentrated in their primary context in the immediate vicinity of activity areas. Excavations into the Pleistocene strata at Eagle Cave reinforce this model, where a juvenile mammoth mandible bearing possible cut marks was found in association with several pieces of chert debitage (Koenig, Nielsen, et al. 2017:89).

Microdebitage and shatter may become scattered across the shelter interior due to ongoing human and animal activity as well as geological processes (Homsey-Messer and Ortmann 2016). Numerous taphonomic factors can result in patterns that resemble bone tools (Haynes and Krasinski 2010). For the purposes of this thesis bone tools and modification are considered supplemental evidence that must be supported by additional data.

Geological evidence for a site of human origin is expected to be comparable to carnivore dens. Humans would probably be inclined to utilize relatively stable rockshelters with limited high-energy exogenic deposition and reduced spalling frequency. As environmental conditions change, rockshelters may become more or less suitable for exploitation. In addition to their significance as markers of human activity, the presence of surface hearths and the subsequent dispersal of heated sediments is expected to yield elevated magnetic susceptibilities across the living surfaces. Similarly, the introduction and accumulation of food, fuel stuffs, animal remains, and refuse is expected to result in elevated organic carbon levels. Ongoing human activity has the potential to elevate these levels beyond those expected for carnivore dens, facilitating the differentiation of living surfaces. The intensity and duration of site use can further elevate these signatures.

6.6 *Considerations for Bone Bed 1*

These expectations were used to evaluate each stratum in the 2017-2018 Bone Bed 1 sampling column. Stratum 19, 20, and 21 correspond with Bone Bed 2, a definitively cultural Late Paleoindian component. Some debate regarding the nature of Bone Bed 2 as a primary kill site or secondary processing locality remains outstanding. However, much of the discussion focuses on resolving if the bison were dispatched *and* processed within the shelter or killed elsewhere and introduced to the shelter for processing (Bement 2007; Byerly, Cooper, et al. 2007; Prewitt 2007). In either scenario, Bonfire Shelter is a processing locality and should satisfy many of the criteria established for cultural sites in this model. The fact that artifacts were from these strata make them valuable comparative samples.

As noted above, it is unlikely that the Bone Bed 1 strata will fit perfectly into one of these categories. However, these scenarios provide a model that facilitates the comparison of Bone Bed 1 to other archaeological examples, including Bone Bed 2. Mass death scenarios resulting from drought, starvation, or predation provide ample scavenging opportunities for humans and carnivores alike (Haynes 1985, 1991b; Villa and Soressi 2000). The excesses of these events may result less intense or incomplete usage of any one individual. Bonfire Shelter forms a bottleneck that could function as an ambush point, a common Paleoindian hunting strategy, or a well-protected den or campsite (Bement and Carter 2010; Frison 1974). Other than logistical strategy and mitigating competition from scavengers, there is nothing preventing hunters from processing their kills at the same location they were taken (Bement 2007; Byerly, Cooper, et al. 2007; Prewitt 2007). Especially for large animals, such as the megafauna present in Bone Bed 1, require some degree of processing prior to transport; only relatively small game or juveniles could be feasibly transported any significant distance without some degree of pre-processing (Binford 1978b:62-63). Differential preservation of faunal remains due to geological attrition or scavenging activity can have a significant impact on site interpretations, giving the appearance

that the surviving robust marrow-yielding elements were the only elements brought to the site (Marean and Cleghorn 2003). The nature of Bone Bed 1 will be interpreted based on the best fit of the available data to the criteria outlined in **Table 6-1**, with the understanding that the picture is ultimately incomplete.

7. EXCAVATION RESULTS

Chapter 7 reports the results of the 2017-2018 Block C and Block D, illustrated in **Figure 7-1** excavations across the intact portions of Bone Bed 1 at Bonfire Shelter. The chapter presents observations by stratigraphic context within each excavation block. Stratigraphic descriptions, faunal remains, and radiocarbon data are compared against the results of the 1980's Bonfire expedition to present a more complete picture of Bone Bed 1. Where possible, data from the 1963-1964 expedition was included. Due to limited stratigraphic differentiation within Bone Bed 1 in the 1960s, comparisons are typically generalized.

Stratum 23 and 24 (Bement's E/F/G and H), the bone-bearing units associated with Dibble's Bone Bed 1, are the primary focus of this chapter. Excavations in Stratum 19, 20, and 21 (Dibble's Bone Bed 2 and Bement's Stratum A, B, and C) were restricted to a small portion of Unit C1 and the associated Column Sample 5. Data from these non-Bone Bed 1 strata are primarily geoarchaeological in nature and presented in **Chapter 8**. Stratum 22 is associated with Dibble's culturally "sterile" Zone 2 and is similarly only represented in Unit C1. Observations from these strata cautiously acknowledge this sampling bias.

In general, results from the 2017-2018 field season are consistent with previous reports from Dibble and Bement. The stratigraphic sequence presented in Bement (1986a) was readily reidentified and consistent with the findings reported here. **Table 7-1** outlines the relationship between Dibble and Bement's stratigraphic designations and the ASWT designations. The table also includes Bement's (1986a) stratigraphic descriptions that were used to reidentify the Bone Bed 1 strata in the field. Updated descriptions based on 2017-2018 excavations and analysis are presented in **Table 7-4**. **Table 7-2** provides additional information regarding the Bone Bed 1 strata identified within each unit, their layer designations, and lot numbers.

The faunal assemblage was consistent in terms of the Pleistocene taxa reported by Bement (1986a) but differed in relative frequencies. This may be a function of selection bias, where the majority of well-preserved or diagnostic elements were recovered from the partially excavated strata in the 1980s, with the elements left behind comprising the 2017-2018 assemblage. A formal faunal analysis remains to be completed and may supersede the preliminary findings and field identifications reported here. As noted previously, new findings were not directly compared to Dibble and Lorrain (1968) due to the limited stratigraphic differentiation reported in 1968. However, the 2017-2018 assemblage was consistent with the taxonomic classes described by Lorrain. Across 11 excavation units and one column sample, no definitively cultural material was identified. Despite inspection for cut marks and spiral fractures, no evidence of cultural modification was observed. This is likely in-part due to the extremely poor preservation documented in the Block C. Preservation was better in Block D, and fragmented faunal remains were identified. However, patterns were inconsistent with green breaks and other modification patterns.

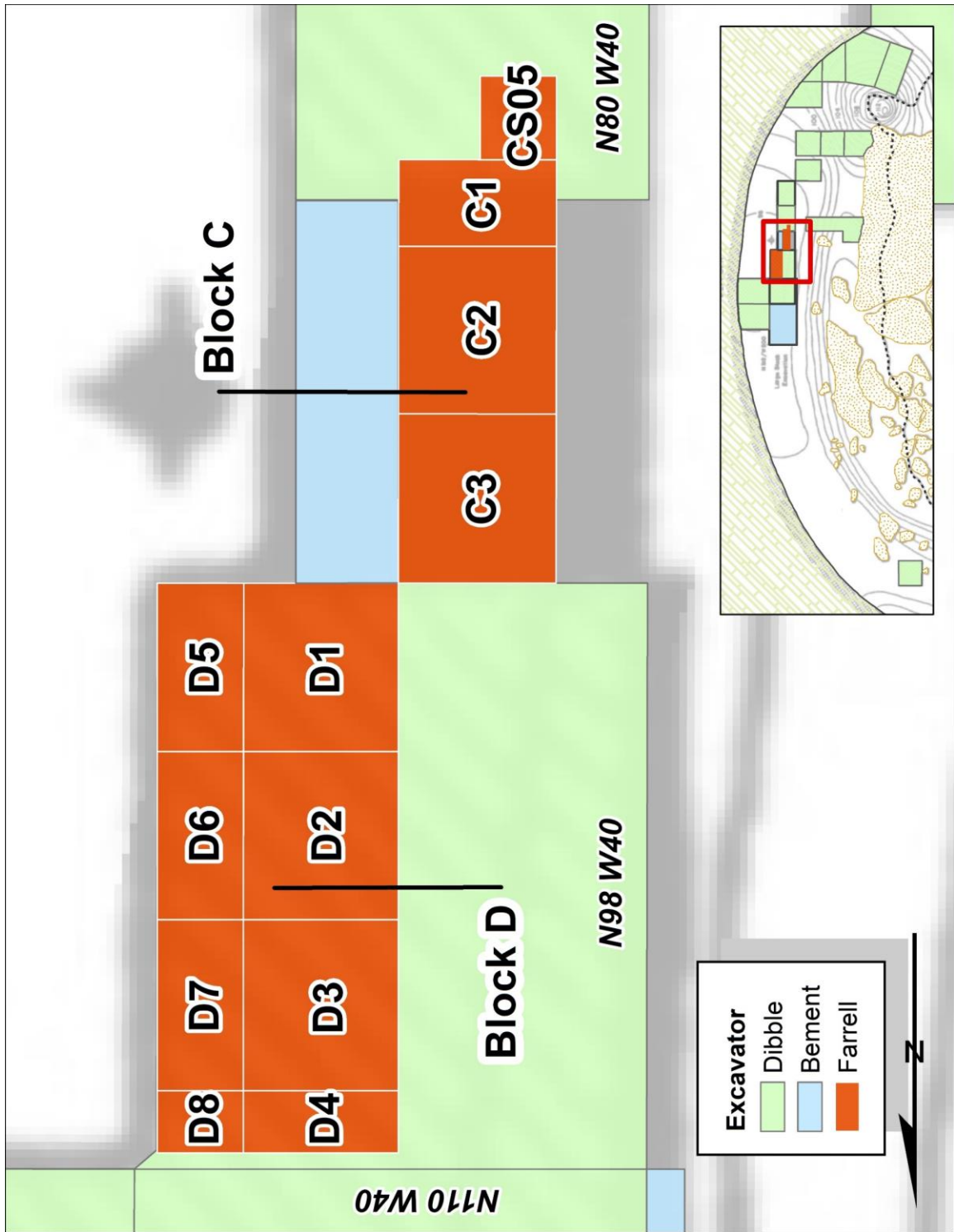


Figure 7-1. Planview layout of Block C and Block D Bone Bed 1 excavation units

Table 7-1. 41VV218 – Main Trench Stratigraphic Alignment. Aggregated sediment descriptions, fauna, artifact content, and radiocarbon dates from the 1963-1964 and 1983-1984 Bone Bed 1 excavations used to identify specific stratigraphic units in 2017-2018. Descriptions after Bement (1986).

41VV218 - Main Trench Stratigraphy Alignment												
Dibble	Bement	Kilby (CS05)	Farrell (UC1)	Farrell (UC 2)	Farrell (UC 3)	CS05 Depth (cmts)	Farrell (UD)	1983-1984 Sediment Description (Bement 1986)	1983-1984 Fauna (Bement 1986)	Artifacts (Bement 1986; Dibble 1968)	Date (Bement 1986; Dibble 1968)	Notes
Bone Bed 2	Stratum A	19	L1	-	-	29.1	-	Brown silty trough	Bison antiquus	Plainview	10,280+/-430 (TX-153)	
Bone Bed 2	Stratum B	20	L2	-	-	34.1	-	Gray powder with small limestone spalls; Shallow central trough	Bison antiquus, (3) Horse (1)	-	-	Bones at B/C interface - extend upward into B; smaller elements contained in B likely result of redeposition
Bone Bed 2	Stratum C	21	L3	-	-	38.7	-	Reddish brown clayey silt; Shallow trough	Bison antiquus	Folsom Point	-	No artifacts in 1980s
Zone 2	Stratum D	22	L4	-	-	47.1	-	Gray limestone powder with small rounded limestone spalls	Gray Fox	-	-	
Bone Bed 1	Stratum E/F/G	23	L5/5B	L1/2	L1/2	62.17	-	Brown silty clay; variable thickness; homogenous	Bison antiquus, Horse (3), Camel, Mammoth	-	-	
Bone Bed 1	Stratum H-1	24	L6	L3	L3	71.8	L1 – 7	Gray powder with numerous small limestone spalls (<1cm); Occasional large limestone boulders and tabular spalls	Bison (Dibble?), Horse (2), Mammoth	-	12,460+/-490 (AA-344)	Bement - no bison recovered. Dibble reports? Excavation incomplete - UC1 & UC2
Bone Bed 1	Stratum H-2	n/a	Not Exc	Not Exc	Not Exc	n/a	Son-dage	Increased spall size and density;; decreased gray powder	Antelope	-	Extinct by end of Pleistocene	
Bone Bed 1	Stratum H-3	n/a	Not Exc	Not Exc	Not Exc	n/a	Son-dage	No Description	Unknown	-	-	Not discussed in Bement's stratigraphic descriptions but illustrated on profile of record.
Bone Bed 1	Stratum I	n/a	Not Exc	Not Exc	Not Exc	n/a	Son-dage	Fine gray powder with small limestone detritus; Large +1m limestone boulders	Bison antiquus (1), Horse (1)	-	-	Parallel BB2 definitive cultural patterns - Bone/block association with V-Shaped incised bones

Table 7-2. Unit Layers and associated Lot FNs for each Block C and Block D excavation Unit. *Indicates arbitrary 5cm level. All others excavated in 10cm levels except column sample (PS06.CS05), which was excavated by natural stratigraphy. **Note that Unit C3 Layer 4 is only associated with mammoth element pedestal excavation.

41VV218 - Block C and Block D - Unit Provenience (Lot Number) Tracker												
Lot FN#s	Block C				Block D							
	PS06 CS05	Unit C1	Unit C2	Unit C3	Unit D1	Unit D2	Unit D3	Unit D4	Unit D5	Unit D6	Unit D7	Unit D8
Layer 1	60249 (Disturbed)	60024 (S19)	60076 (S23)	60023 (S23)	60412 (S24)	60413 (S24)	60361 (S24)	60316 (S24)	60457 (S24)	60458 (S24)	60477 (S24)	60490 (S24)
Layer 2	60250 (S19)	60034 (S20)	60099 (S23)	60028 (S23)	60423 (S24)	60426 (S24)	60363 (S24)	60318 (S24)	60459 (S24)	60460 (S24)	60485 (S24)	60531 (S24)
Layer 3	60251 (S20)	60059 (S21)	60294 (S24)	60030 (S24)	60444 (Disturbed); 60445 (Intact) (S24)	-	60392 (S24*)	60322 (S24*)	60462 (S24)	60463 (S24)	60489 (S24)	60535 (S24)
Layer 4	60252 (S21)	60060 (S22)	-	60278** (S24)	60447 (Disturbed); 60448 (Intact) (S24)	-	60442 (S24*)	60349 (S24*)	60464 (Disturbed); 60484 (Intact) (S24)	60465 (S24*)	60498 (Intact); 60509 (Disturbed) (S24*)	60537 (S24)
Layer 5	60253 (S22)	60061 (S23a)	-	-	-	-	-	-	-	-	-	60548 (Intact); 60554 (Disturbed) (S24*)
Layer 5B	60253 (S23)	60117 (S23b)	-	-	-	-	-	-	-	-	-	-
Layer 6	60274 (S24)	60248 (S24)	-	-	-	-	-	-	-	-	-	60567 (Sondage)
Layer 7	-	-	-	-	-	-	-	-	-	-	-	60583 (Sondage)

7.1 Block C Results

A total of 2.75m² were excavated in Block C, including Unit C3 (1.0 x 1.0 m [3.28 x 3.28 ft]), Unit C2 (1.0 x 1.0 m [3.28 x 3.28 ft]), Unit C1 (1.0 x 0.5 m [3.28 x 1.64 ft]), and Column Sample 5 (0.5 x 0.5 m [1.64 x 1.64 ft]). Units were excavated in natural stratigraphic layers, except where strata exceeded 10.0 cm (3.9 in). Due to the confined space and overlapping arrangement of faunal remains in Block C, units could not be excavated simultaneously. This method limited the exposure of faunal remains across the surface but protected elements from accidental trampling and degradation upon exposure to the atmosphere.

Stratigraphy was correlated across Block C, Column Sample 5 (PS06.CS05), and Block D using sediment attributes and total station measurements. Strata were generally traceable around the perimeter of the main block, except where profile walls were undercut and eroded. In these instances, measurements below the last intact stratum location were used to estimate the deposit's position. The identified strata were then correlated with Dibble's and Bement's stratigraphic units based on sediment composition and faunal assemblages. The relationship between these designations is reported in **Table 7-1** and illustrated in **Figure 7-5**.

7.1.1 *Unit C – Stratum 23*

Stratum 23 was first encountered in Unit C3L1 and Unit C2L1, marking the first Bone Bed 1-related context excavated. Described in detail in **Table 7-4**, below, Stratum 23 is uniquely recognizable as a thick (>15.0 cm, 5.9 in) 10YR6/4 (light yellowish brown) horizon with an abrupt increase in clay content (+10% vs. Stratum 22), decrease in limestone gravel and spall content (-15% vs. Stratum 22), and the appearance of Pleistocene megafauna other than bison. Excavation of Stratum 23 is illustrated in **Figure 7-2** below. Both Dibble and Bement described this layer as a dense, silty trough, which proved to be an apt assessment. Stratum 23's textural classification as a silt loam fails to adequately describe the dense sediments, especially contrasted against the gravel-dominated, relatively unconsolidated sediments present in Strata 22 and 24. Stratum 23 also included increasingly large gypsum nodules (up to ~1.0 cm, 0.4 in) throughout the matrix and adhering to spalls/elements. Overall gypsum content was lower in Stratum 22 and 24, where the salts appeared to be incorporated throughout the matrix, but the presence of large nodules was unique to Stratum 23. Discussion of the Stratum 23 geoarchaeological results continues in **Chapter 8**.



Figure 7-2. Overview of Stratum 23 excavation in Block C.

Stratum 23 was first encountered in Unit C3L1 and Unit C2L1. The layer was initially interpreted as part of Bement's Stratum D (S22). The exposure of large mammoth elements in the dense matrix quickly refuted this hypothesis, as Bement characterized Stratum D as "gray limestone powder" with isolated gray fox (*Urocyon cinereoargenteus*) remains (Bement 1986a: 20, 22). Unit C3L1 and C3L2, Unit C2L1 and L2, and Unit C1 L5 and L5B were subsequently reassigned to Stratum 23, Bement's Stratum E/F/G.

After removing wall slump from the block, two partially buried mammoth ribs (FN60009 and 60010) and pelvis (FN60011) were identified in the Block C floor. It appears that the upper portion of Stratum E/F/G was excavated in the 1980s. After determining that the ribs extended an unknown distance into the western wall, the ribs were left in situ and the trench was abandoned by the Bement team. An undercut corner in the eastern profile of Block C suggests that an effort

was made to extract the pelvis segment, but the attempt was also abandoned leaving the element in place. **Figure 7-3** illustrates the reexposed mammoth elements at the base of the 1983-1984 excavations, prior to the excavation of Unit C3.

Like previous excavators, Stratum 23 was excavated in two layers divided at a natural break between layers of mammoth ribs roughly 10.0 cm (3.9 in) below the initial excavation surface. The color and texture shifts between Layers 1 and 2 may have been a result of trampling or sediment packing in the upper centimeters of the stratum to rebury the mammoth elements. The full extent of previous excavations in UC2 L1 and UC3 L1 during the 1980s was difficult to discern, but the remains extending into unit sidewalls and intact underlying spall deposits suggest that the elements remaining in the unit were in situ.

Mammoth elements extending more than approximately five centimeters into the western profile of Block C (the already significantly under-cut and eroded wall of the main trench open in parts since 1963) were truncated at the wall to prevent further destabilization of block. This primarily impacted mammoth rib FN60009, the first major element identified upon reopening the trench in the winter of 2017 and one of the elements abandoned in the 1980s. The rib was carefully cut off as close to the wall as possible using a fine-tooth saw and razor blade, taking care to minimize disturbance to neighboring elements. It was decided that that more could be learned from the truncated element in the lab if it was extracted with some remaining integrity than could be gained from the element turning to dust in situ.

While this adverse effect was unfortunate, it highlights the poor faunal preservation observed in the Bone Bed 1 strata, particularly in Unit C. Nearly all identified elements quickly deteriorated upon exposure. The combined effects of the elevated gypsum levels (both in the sediment matrix and adhering to bone surfaces) and increased sediment moisture content in Stratum 23 and 24 are thought to contribute to this destabilization, exacerbated by gypsum's proclivity for absorbing atmospheric moisture. The role of gypsum in the formation of Bone Bed

1 is further explored in **Chapter 8.4.1**. As noted in **Chapter 5**, many elements were treated with a B-72 and acetone solution to consolidate and stabilize the bone. Relatively stable elements and a sample of the more delicate specimens were intentionally not treated with B-72 to facilitate ^{14}C dating; these elements are specifically marked as such in the Field Number catalog and **Appendix C: Faunal Assemblage**.

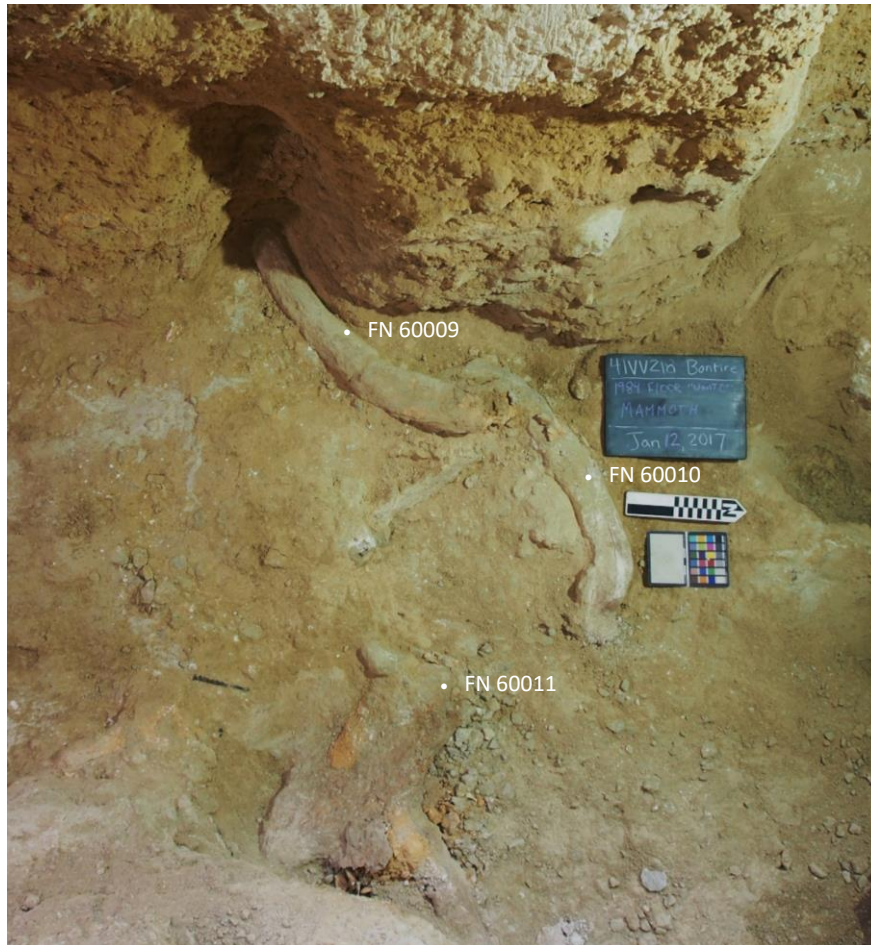


Figure 7-3. Exposure of partially excavated mammoth elements in UC1 L1 at the base of 1983-1984 excavations.

7.1.2 Unit C – Stratum 24

UC1L3, UC2L3 and UC3L6 were associated with Stratum 24, Bement’s Stratum H. Stratum 24 was characterized by an enormous increase in gravel content (+40% vs. Stratum 23) in a relatively fine-grain (mean $<2.0\text{ mm} = 4.6\phi$) 10YR8/2 (very pale brown) matrix. Stratum 24

is somewhat similar to Stratum 22, but with larger, more abundant gravel (exceeding -7.0φ [5.0 in]) and the presence of Pleistocene fauna. A more complete discussion of the Stratum 24 geoarchaeological results is presented in **Chapter 8**. The transition from Stratum 23 to Stratum 24 was abrupt and unambiguous, occurring immediately below a second set of Stratum 23 mammoth elements and marked by the exposure of a third set of remains including FN60247, the largest mammoth rib identified, in the southern portion of Unit C2 and C3.

Excavation of Stratum 24 in Block C continued to completely expose and extract these remains (approximately 10.0 cm [3.9 in]). The level was terminated upon the exposure of a relatively uniform spall surface below all identified faunal remains. This spall zone may represent a southern extension of the spall “pavement” observed at the base of Block D (described below).

The three Stratum H subdivisions reported by Bement (1986b) were not readily identifiable in Block C. The spall zone observed beneath the faunal remains may represent the interface between Bement’s Stratum H1 and H2, however this cannot be confirmed with certainty. Further excavation to explore the internal stratigraphy of Stratum 24 was precluded by limited time in the field. No additional faunal remains were observed at the termination of Units C1 L3, C2 L3, or C3 L6.

7.2 Column Sample 5 (PS06.CS05)

Following the excavation of Units C1, C2, and C3, the southern profile section of Unit C1 (PS06) was cleaned, mapped, and annotated. Column Sample CS05 (one of six column samples excavated across the shelter during the 2017/2018 field seasons) was excavated through the intact baulk as a 50.0 x 50.0 cm (19.7 x 19.7 in) continuous vertical sampling unit. The six intact stratigraphic units identified, illustrated in **Figure 7-4** were assigned shelter-wide stratigraphic identifiers S19 through S24 and were used to track stratigraphy across the shelter

interior. **Table 7-3** presents the relative depth and thickness of each strata as measured from the main site datum as well as below the local excavation surface at the top of PS06.

Stratum 19 through 24 correspond with Bement's Stratum A through H, encompassing the lower portion of Dibble's Bone Bed 2 and Bone Bed 1. These strata remain readily identifiable around the entire perimeter of the main excavation block and were well correlated with test unit layers excavated in Blocks C and D. **Figure 7-5** highlights the relationship between the 1983-1984 stratigraphic units, as illustrated in Bement's profile of record on the southernmost face of the main block, and the 2017-2018 units.

The intact Block C stratigraphy was overlain by a significant amount of disturbed sediment slumping from a side-wall blowout near the southern terminus of the 1980s catwalk. The disturbed sediment was recorded as Stratum 0, a generic catch-all designation for disturbed contexts. The disturbed sediments extended approximately 25.0 cm (9.8 in) from the top of the profile to a bent aluminum marker presumably buried in 1984 to mark the start of intact Bone Bed 2 deposits. Stratum 0 sediment was utilized for trial runs of geoarchaeological procedures but otherwise not analyzed. **Table 7-4** reports field descriptions for each stratum identified in Column Sample 5. These descriptions were used to define stratigraphic units in the field and correlate them with the results of previous investigators. A more refined, laboratory-based characterization of each stratum is reported in **Chapter 8: Geoarchaeological Results**.



Figure 7-4. Profile view of Block C, south wall: PS06-CS05 stratigraphic units prior to column sample excavation. White features in Stratum 20 highlight bison bone associated with Bone Bed 2. Sediments overlying Stratum 19 are disturbed slump and fill. Note the white gypsum nodules (visible white flecks) throughout Stratum 22 and 23.

Table 7-3. Vertical extent of stratigraphic units documented in CS05. Depths measured via TDS from shelter-wide survey datum.

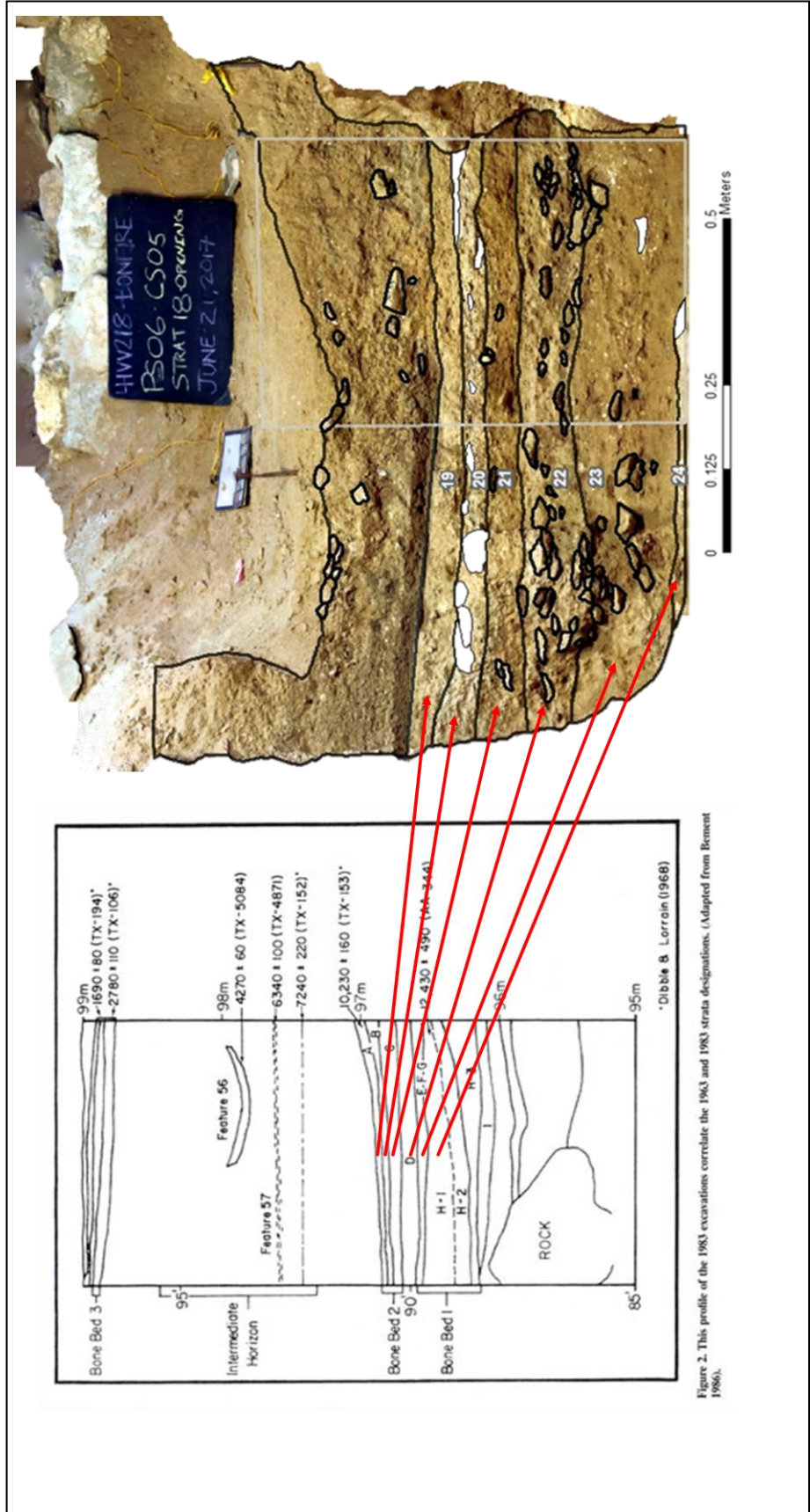
Column Sample 5 Stratigraphic Units					
Stratum	Top of Strat	Center of Strat	Bottom of Strat	Thickness (cm)	Depth below CS Surface (cm)
S0	497.772	497.6202	497.516	25.6	25.6
S19	497.516	497.4914	497.481	3.5	29.1
S20	497.481	497.4553	497.431	5	34.1
S21	497.431	497.4034	497.385	4.6	38.7
S22	497.385	497.3305	497.301	8.4	47.1
S23	497.301	497.1769	497.1503	15.07	62.17
S24	497.1503	497.1503	497.054	9.63	71.8

Table 7-4. 2017 – 2018 Excavation Results – Stratigraphic Field Descriptions derived from Column Sample 5 (PS06.CS05).

Strat	Center of Stratum (mbd)	Thickness (cm)	Depth below CS05 Surface (cm)	Munsell	Munsell Color Name	Texture (USDA)	Inclusions	Comments
S0	497.62	25.6	25.6	10YR6/4 mottled with 10YR7/3	Light yellowish brown with many coarse very pale brown mottles	Unconsolidated Slump – Not Processed in Lab	Few coarse-very coarse bone fragments; Very few channers	Disturbed; Unconsolidated slump; Lower ~5 cm possibly screened 1983-1984 backdirt; 2cm aluminum strip marking the start of intact sediments. Excavated as single layer; samples retained
S19	497.49	3.5	29.1	10YR7/4	Very pale brown	Channery clay loam; Weak massive structure, soft	~30% coarse gravel and channers (avg -4.4φ); Occasional gravels/channers ≥ -7φ; Extremely poorly sorted (7.2φ); Significant clay component (~20%) vs. S20.	Very thin; Potential partial excavation in 1983-84; Terminated at top of bone-bearing stratum and transition to lighter sediment
S20	497.46	5	34.1	10YR7/3	Very pale brown	Channery loam; Weak massive structure, soft	~30% fine gravel and channers (avg -2.6φ); Extremely poorly sorted, though much better sorted than S19 (4.9φ); Notable decrease in clay content vs. S19.	Very thin; Largely differentiated from S19 by appearance of Bison bone in profile
S21	497.40	4.6	38.7	10YR5/4	Yellowish brown	Very channery loam; Weak massive structure, slightly hard	~50% medium gravel and channers (avg -3.0φ); ~5% more clay than S20; Extremely poorly sorted (5.9φ)	Gravel/channer content appears to increase with depth; Faunal remains concentrated at S20/21 interface
S22	497.33	8.4	47.1	10YR7/3	Very pale brown	Extremely channery silt loam; Weak massive structure, soft	~60% medium gravel and channers (avg -3.1φ); Extremely poorly sorted (5.1φ), but better than S21 and S23; Few fine (≤2 mm) gypsum nodules throughout	Relatively loose; Noticeable increase in gravel/channer content; Brown silt/clay component found in S21/23 absent

Table 7-4. Continued

Strat	Center of Stratum (mbd)	Thickness (cm)	Depth below CS05 Surface (cm)	Munsell	Munsell Color Name	Texture (USDA)	Inclusions	Comments
S23	497.18	15.07	62.17	10YR6/4	Light yellowish brown	Very channery silt loam; Moderate massive, slightly hard; Slightly sticky	~45% medium gravel and channers (avg - 3.42φ); Extremely poorly sorted (6.1φ); nearly 10% increase in clay content; Common medium-coarse gypsum nodules throughout; fine (fine silt texture) gypsum powder adhering to gravel and bone surfaces.	Abrupt decrease in gravel; Very thick and dense, slightly sticky; Textural class does not adequately reflect clay-ey attributes observed in field. Better defined structure, approaching medium subangular blocky; Well-preserved Equus bone and ~ 1 cm charcoal sample collected above S23/S24 interface.
S24	497.15	9.63	71.8	10YR8/2	Very pale brown	Extremely channery loam; Weak massive structure, loose-soft	~85% coarse gravel and channers (avg -4.2φ), with individual spalls/cobbles exceeding ~7.0φ; Very poorly sorted (2.6φ), increasingly dominated by coarse fraction with decreasing matrix; Few fine-medium gypsum nodules throughout; fine gypsum powder adheres to gravel and bone surfaces, also appears incorporated into matrix	Unconsolidated, extremely fine-grained matrix surrounding large spalls; gravel size and density increases with depth; Stratum terminated at very dense spall accumulation; Lacks excessive clay observed in S23; Very few trace charcoal fragments throughout



7.3 *Block D Results*

Block D consisted of three complete 1.0 x 1.0 m (3.28 x 3.28 ft) excavation units and five partial units placed to maximize coverage over the intact “bench” immediately northeast of Block C. Units were initially excavated in 10.0 cm (3.9 in) arbitrary levels, with the intention of breaking levels at natural stratigraphic interfaces. Unit D4, located along the northwestern edge of the bench, was excavated first to explore stratigraphy within the block and create a guide for excavating the remaining units. The excavation interval was reduced to 5.0 cm (1.9 in) arbitrary levels when in situ faunal remains were encountered. **Table 7-2** reports the specific units and layers with the reduced 5 cm (1.9 in) interval.

Illustrated in **Figure 7-8**, Block D was protected under a layer of geotextile cloth and sheet of plywood installed following the 1980s excavation to limit damage to the intact sediments. Prior to excavation, it appeared that portions of Bement’s Stratum D, E/F/G, and H (S22, S23, and S24) remained intact in Block D. After removing the protective layers, two distinct stratigraphic zones were observed: A zone of very dense spall (up to approximately -7.0 φ [5.0 in]) in a very fine-grained, light gray (10YR7/2), loamy matrix consistent with Stratum 24 as observed in Block C and Bement’s Stratum H; and a pale brown (10YR6/3) silty loam sediment with abundant charcoal, bone, and shell fragments < 6.4 mm (0.25 in) and very little gravel.

The 10YR6/3 silty sediment was thought to be an intact component of Stratum 23 and was excavated separately under a unique FN (noted in **Table 7-2**). At least three pin-flags, rusted nail fragments, and a rusted dental pick among other modern debris were subsequently recovered from the darker areas, indicating that the context was disturbed. The conspicuous absence of gravel and larger bone fragments from the disturbed areas suggests that screened fill was used to pad partially excavated portions of Block D to create the level the bench.

The disturbed sediments were carefully excavated to expose the intact Stratum 24 contact, which revealed a substantial depression near the center of the block. **Figure 7-7** illustrates the initial exposure of the Block D sediment cap beneath the plywood. **Figure 7-8** highlights the contours of the intact portions of Stratum 24 within Block D. Previous excavators appear to have chased out faunal remains in this area, encompassing much of modern Units D2 and D6. The depression was subsequently leveled with sieved sediments and capped. It is unclear what elements were previously identified in the vicinity of Block D, as the 1983-1984 expedition published maps do not extend to this portion of the shelter (Bement 1986a). Based on the size of the depression and proximity to other elements, a moderately sized mammoth element could reasonably be imagined.



Figure 7-6. Oblique view east of Block D bench with protective plywood immediately prior to excavation.



Figure 7-7. View south of initial backfill clearing beneath Block D plywood. Material above the geotextile cloth was shovel-skimmed and screened.



Figure 7-8. Oblique view southeast of Block D test units immediately prior to excavation. Note the uneven surface near the center portion of the block where the 1980s excavators appear to have excavated into Stratum 24. Also note the darker brown sediments along the southwestern margin of the block (background right of this photo). These sediments were initially thought to be intact portions of Stratum 23, but were determined to be disturbed fill after modern excavation refuse was recovered while screening.

Intact portions of Stratum H in the northern portion of Block D extended approximately 45.0 cm (17.7 in). Intact sediments in the southern portion of Block D were variable and thinner due to the partial excavation in the 1980s. Block D was terminated at a layer of very large (>20.0 cm, 7.9 in), slightly overlapping spalls slightly angled towards the rear wall of the shelter that formed a “spall pavement”. **Figure 7-9** illustrates the large interlocking spalls concentrated in the northern Block D Units (D3, D4, D7, and D8). This pavement may represent the natural break between Bement’s Stratum H-2 and H-3. Confirmation of this theory is limited by the lack of published information regarding the attributes of H-3.



Figure 7-9. View east of "spall pavement" exposed across Block D.

A roughly 1.0 x 0.5 m (3.28 x 1.9 ft) sondage, illustrated in **Figure 7-10**, was excavated in the northern portion of Block D to explore sediments up to approximately 37.0 cm (14.6 in)

beneath the spall pavement. Two minor stratigraphic units were observed and assigned to Unit D8, Layers 6 and 7.

Unit D8 L6 extended approximately 20.0 cm (9.8 in) below the spall zone. D8 L6 sediments were very similar to those observed S24 above the spall pavement, consisting of abundant spalls surrounded by a very fine-grained, light gray (10YR7/2), loamy matrix. The spall to fine matrix ratio appeared to increase, suggesting the sediments included >85% coarse gravels and spall. An average D8 L6 spall was much smaller than the large slabs observed in the “pavement”, but were slightly larger than the average -4.2ϕ (1.8 cm, 0.7 in) spalls documented in Unit D8 L5 and the upper portions of S24. Unit D8 L7 marks an arbitrary subdivision within this stratum. Gravel size decreased slightly with depth. Examples of “lithifying” gravels forming concretions cemented with what appeared to be crystalline gypsum were observed near the base of excavation approximately 17.0 cm (6.7 in) below D8 L6.

Unit D8 L7 was terminated at an abrupt transition into a stratum of relatively small, extremely compact, medium-coarse limestone gravels coated in limited quantities of pale yellow, nearly white (2.5Y8/2) very fine silty matrix texturally similar to S24. Gravels were sub-rounded, roughly ranging from -3.3ϕ to -4.6ϕ (1.0 – 2.5 cm). Voids between the spalls appeared to be almost entirely filled with hardened, gypsum-based matrix, forming a broad concreted surface. This contact plane was exposed on last day of excavations in 2018, precluding further exploration.

Spot samples were collected from each sondage context, but limited geoarchaeological analysis was conducted. The samples were discontinuous from Column Sample 5 and collected in a judgmental and arbitrary manner as a representative sample of materials, limiting their viability for direct comparison. Basic interpretations in the field suggest that sediments below the Unit D8 L5 spall pavement are correlated with Bement’s Stratum H-2/H-3, while the very pale sediments exposed at the base of Unit D8 L7 represent Bement’s Stratum I.

The correlation of the sondage strata with Bement's results is highly speculative. The sondage was characterized by the abrupt absence of all faunal and botanical material, confirmed up to 3.2 mm (0.125 in) via field screening. Even the microfauna remains, snail shell fragments, and hackberry seedpods observed throughout Stratum 19 through Stratum 24 were absent. Bement's Stratum H-2/H-3 and I are characterized by the presence of Pleistocene fauna, justifying their inclusion in Bone Bed 1. Given the sparse distribution of remains in these strata, it is entirely possible that megafauna elements present below the spall "pavement" were not captured within the small sondage sample. Fossil shell fragments were the only faunal material documented among the sondage's limestone gravels. It is unclear if these specimens are derived from the fossiliferous Devils River Formation or are components of a discrete assemblage.

The nature of the rounded gravels observed at the base of excavation merits further analysis. Spalls and gravels observed in the overlying Late Pleistocene strata (S19 – S24) were distinctly angular and generally larger. Cryoturbation may play significant role, particularly if the sediments were impacted by the colder and wetter conditions earlier in the Pleistocene. As noted in **Chapter 4**, cyclical freezing and thawing can cause substantial in situ weathering via abrasion and frost-wedging (Lautridou and Ozouf 1982; Laville et al. 1980). The absence of faunal and botanical material from these strata limits viable direct dating options. Additional data is needed to thoroughly evaluate these deposits.



Figure 7-10. View east of Sondage excavated beneath the “spall pavement” extending through Unit D8 Layers 6 and 7.

7.4 *Faunal Remains*

A total of 86 new faunal elements were recovered during the 2017-2018 Bone Bed 1 excavations. Forty-six (46) new elements were recovered from Stratum 23 (Bement's Stratum E/F/G); forty (40) additional elements were recovered from Stratum 24 (Bement's Stratum H). **Table 7-5** and **Table 7-7** present the relative frequencies of each taxonomic class observed in Stratum 23 and Stratum 24 respectively, with comments describing the specific elements recovered (where identifiable). **Figure 7-13** through **Figure 7-15** illustrate the faunal material observed during the excavation of Stratum 23; **Figure 7-19** through **Figure 7-26** illustrate the faunal material observed in Stratum 24, Block C and Block D.

Many of the elements recovered in 2017-2018 were extremely deteriorated or were only represented by small fragments with few (if any) diagnostic attributes. Fields marked with an asterisk (*) in **Table 7-5** and **Table 7-7** below indicate that the count includes a tentative identification. The corresponding asterisk in the "Notes" field indicates whether the uncertainty is associated with the taxonomic classification (i.e.: mammoth* rib) or with the element classification (i.e.: mammoth rib*). Elements too degraded or fragmented to posit any type of taxonomic classification were assigned to "Unidentified" (UID). Additional zooarchaeological analysis may be able to resolve some of these missing data. However, these analyses were beyond the scope and time constraints of this thesis.

All elements were inspected for cut marks, green breaks, and other evidence of modification in the field. Cut mark identification on many elements was precluded by poor preservation. Where present, cortical surfaces were extremely eroded or disintegrated immediately upon exposure. The fragmentary nature of other elements further limited the potential for cut mark identification. High-potential, well preserved elements (especially those recovered from Block D where conditions were more favorable) were examined under low-power magnification. No cut marks or other evidence of cultural modification was observed during this

assessment. Significantly, no new evidence of carnivore gnawing or tooth marks were observed either.

The summarized results of the 1983/1984 University of Texas faunal assemblage are reported as a comparative sample for each stratum (Bement 1986b). The aggregate 1983-1984 and 2017-2018 assemblages for each stratum are illustrated in **Figure 7-16** and **Figure 7-27**. The 1963-1964 Bone Bed 1 assemblage was not quantified in the 1968 Bonfire Shelter report (Dibble and Lorrain 1968); qualitative descriptions of the assemblage were not broken down by the briefly referenced substrata. As such, the Amistad assemblage was not integrated with the main Stratum 23 and Stratum 24 assessment.

Section 7.4.3 presents a reconstruction of the Amistad-era Bone Bed 1 assemblage based on Dibble's field notes and TARL's internal inventory of Bonfire Shelter materials. Several discrepancies between the inventory, Dibble's notes, and the report limit the utility of the reconstructed assemblage, but the sample provides a slightly more detailed overview of the initial documentation of Bone Bed 1. An in-person assessment of the Bone Bed 1 collection held by TARL and the University of Texas Vertebrate Paleontology Laboratory is necessary to resolve these issues. The full catalogs of all faunal material recovered in 2017-2018, 1983-1984, and 1963-1964 are included in **Appendix C: Faunal Assemblage**.

7.4.1 *Faunal Remains – Stratum 23*

Illustrated in **Figure 7-11** and **Figure 7-12**, A total of 46 new faunal elements were recovered from Stratum 23 (Bement's Stratum E/F/G) in 2017/2018. **Table 7-5** summarizes the taxonomic and elemental classifications for remains recovered from each provenience. **Figure 7-16** illustrates the composition of the 2017-2018 Stratum 23 assemblage compared to the 1983/1984 expedition's results. Pleistocene horse remains, identified by Bement as *Equus francisci*, dominate Stratum 23 comprising over 50% of the assemblage. Mammoth (*Mammuthus sp.*) and Pleistocene camel (*Camelops hesternus*) are also well represented.

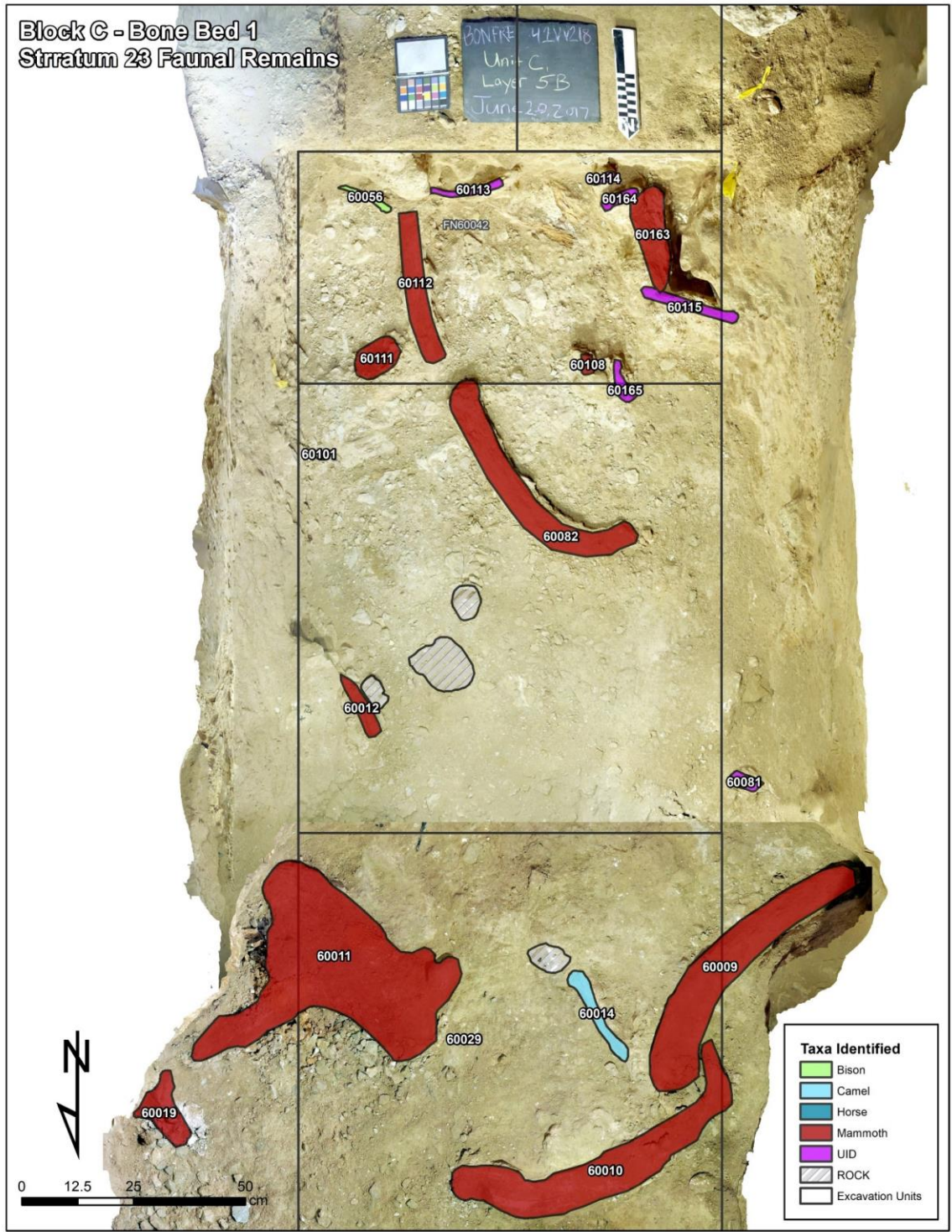


Figure 7-11. Planview illustration of Bone Bed 1 - Stratum 23 (E/F/G) exposed across Block C, Units C1, C2, and C3.

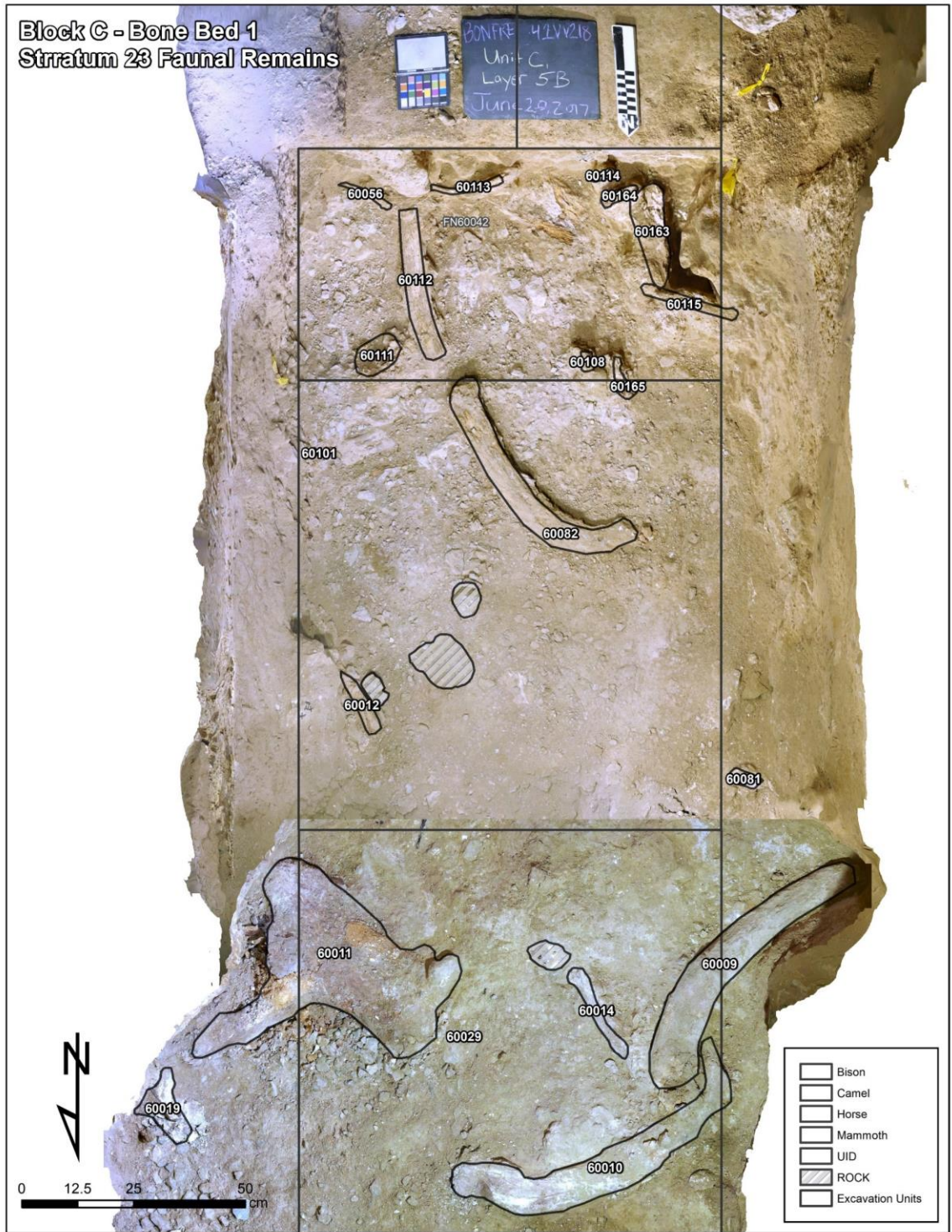


Figure 7-12. Unclassified planview map of Bone Bed 1 - Stratum 23 (E/F/G) highlighting Structure from Motion orthophoto of Units C1, C2, and C3.

The mammoth ribs (FN60009 and 60010 - right) and mammoth pelvis (FN60011 – left) illustrated in **Figure 7-13** were the first indicators that Bone Bed 1 sediments remained intact in Trench C. These elements appear to have been partially excavated in the 1980s and left in situ (note the partial exposure of FN60009 in the upper right of the frame). An element partially encased in a plaster jacket (FN60019) was identified immediately northeast (**Figure 7-14**, also left edge of **Figure 7-13**) of the pelvis, confirming these suspicions. They also provided the first indication that preservation in Trench C was extremely poor; rib 60010 was almost entirely disintegrated by the time it was pedestaled and extracted.

Figure 7-15 depicts additional mammoth ribs (FN60112 – upper and FN60082 – lower) recovered from Unit C1 L5B and C2 L2. These elements were initially thought to mark the start of Stratum 23, with the elements pictured in **Figure 7-13** associated with Stratum 22. However, the thickness of Stratum 23, the partial excavation of Unit C3, and Bement's reported faunal assemblage for Stratum 22 (D) indicate that these mammoth remains are all associated with Stratum 23 and likely related. All Stratum 23 elements were recovered from Block C units. No intact portions of Stratum 23 were observed in Block D.



Figure 7-13. Mammoth ribs (FN60009 and 60010) and pelvis (FN60011) prior to extraction at base of Unit C3 L1, planview - south.



Figure 7-14. In situ plaster-jacketed element (FN60019) in northeast corner of Unit C3 L1.



Figure 7-15. Pedestalled mammoth ribs (FN60112 and 60082) and major elements at Stratum 23/24 interface. Unit C1 L5B and C2 L2, planview - south.

Table 7-5. Summary of faunal remains recovered from each Stratum 23 (E/F/G) provenience. Elements recovered during the 1980s excavation are provided as a single record for comparison. Counts and notes marked with an asterisk (*) represent tentative taxonomic or element-level identification.

Stratum 23 (E/F/G) Faunal Remains									
Provenience	Bison	Camel	Horse	Mammoth	Microfauna	Snake	UID	Total	Notes
1983 Elements	2	12	24	3	0	0	0	41	-
Unit C3 L1	-	-	-	3	4	-	2	9	3 mammoth (2 rib, 1 pelvis); 3 additional microfauna recovered during unit C3 cleanup
Unit C3 L2	-	1*	1	1	-	-	3	6	1 camel rib*, 1 horse tooth fragment, 1 mammoth long bone fragment (plaster jacket), 3 UID elements
Unit C2 L1	-	-	-	1	-	1	3	5	1 mammoth rib, 1 snake vertebra
Unit C2 L2	1*	-	-	1	-	-	1	3	1 mammoth rib, 1 bison rib*; (1 additional mammoth rib (FN60089) determined to be part of rib FN60247).
Unit C1 L5	2	-	1	-	-	-	-	3	1 horse metapodial, 2 bison ribs
Unit C1 L5B	1	-	-	5*	-	-	11	17	5 mammoth elements (1 rib, 3 rib fragments*, 1 tusk segment*); 1 bison rib; 11 unidentifiable elements/fragments (including 1 UID long bone segment and 1 UID epiphyseal)
PS06.CS05.S23	-	-	1	1	-	-	1	3	1 mammoth rib segment*, 1 UID horse element, 1 UID fragment.
2017/2018 Total	4	1	3	12	4	1	21	46	-
Grand Total	6	13	27	15	4	1	21	87	-

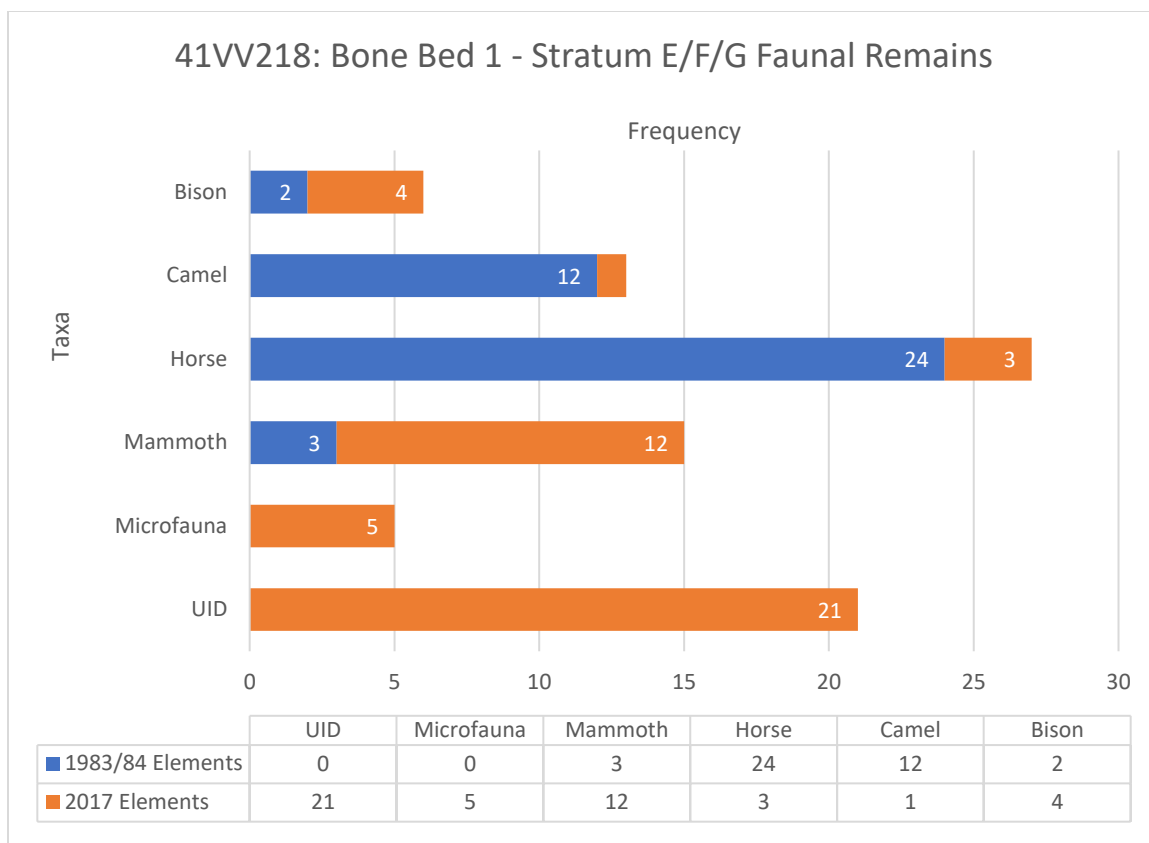


Figure 7-16. Graphic comparison of Stratum 23 elements recovered in 1983/84 to the 2017/2018 assemblage.

Based on the combined 1983-1984 and 2017-2018 assemblages reported in **Table 7-5** and **Figure 7-16** as well as the detailed specimen catalogs presented in **Appendix C: Faunal Assemblage**, the minimum number of individuals (MNI) was calculated for each taxa represented in Stratum 23. The MNIs reported in **Table 7-6** are based on the duplication of elements derived from the same species, accounting for the newly identified 2017-2018 specimens. Bement's 1986 MNIs (1986: 33-34, 38-39) were utilized as a starting point and are accounted for in these estimates. Due to the substantial number of unidentified elements in the 2017-2018 assemblage, the MNI estimates reported here are subject to revision based on future research.

A minimum of three Pleistocene horse (*Equus francisci*), one Pleistocene camel (*Camelops hesternus*), one Pleistocene bison (*Bison antiquus* or *occidentalis*), and one mammoth (*Mammuthus* sp.) are represented in Stratum 23. Estimates for Pleistocene horse are based on the

duplication of radii and the duplication of a metapodial; Bement identified a third individual based on epiphyseal closures and age at death estimations (Bement 1986a:33-34). No elements with intact diagnostic age-at-death features were identified in the 2017-2018 assemblage. No duplicate camel or bison elements were identified within or between the 1983-1984 and 2017-2018 assemblage. Mammoth pelvis fragments were reported in both the 1983-1984 assemblages. Due to the absence of photographs of the 1983-1984 Stratum 23 mammoth pelvis fragments, it was not possible to confirm if the pelvis fragment left behind in the shelter is accounted for in the 2017-2018 assemblage. Regardless, the 2017-2018 mammoth pelvis fragment is incomplete and all fragments could be accounted for by one individual. Multiple mammoth ribs were identified in the 2017-2018 Stratum 23, but these could similarly be attributed to a single mammoth.

Table 7-6. Minimum number of individuals represented in Stratum 23 for each identified taxa. Calculated based on the duplication of elements or diagnostic attributes across the 1983-1984 and 2017-2018 assemblage.

Stratum 23: Minimum Number of Individuals (MNI)		
Species	MNI	Determination
Horse	3	Duplicated left radius, differential epiphyseal closure (Bement); Duplicate metapodial (Farrell)
Camel	1	No duplicate elements; Cannot confirm >1 individual represented (Bement/Farrell)
Bison	1	No duplicate elements; Cannot confirm >1 individual represented (Bement/Farrell)
Mammoth	1	Multiple pelvis fragments (Farrell/Bement); Multiple ribs (Farrell); Insufficient duplication to confirm >1 individual represented

7.4.2 Faunal Remains – Stratum 24

Illustrated in **Figure 7-17** and **Figure 7-18** the 40 new elements recovered from Stratum H are summarized in **Table 7-7**. **Figure 7-27** compares the relative frequencies of taxa identified during the 2017-2018 excavations to the results of the 1983-1984 expedition. The stratigraphic differentiation of Stratum H-1, H-2, and H-3 described in Bement (1986a:20-22) was not

observed during the current excavations. As such, the three isolated *Capromeryx* elements recovered from Stratum H-2 were combined with Stratum H-1 for reporting purposes.

In Stratum 24 - Block D, faunal remains were only recovered from the norther half of the block in Units D3, D4, D7, and D8. All of these elements were recovered from above the spall pavement marking the primary base of excavation. No bone was observed in the exploratory sondage excavated beneath this layer. The depression near the center of the excavation block and undercut sidewalls suggest that if faunal remains were present in the southern half of Block D, they were likely chased out and excavated during the 1980s. Unfortunately, plan maps illustrating excavations in this portion of the shelter were not available for review to confirm this.

The Block D assemblage was limited to eight ribs/identifiable rib fragments, seven additional bone fragments likely derived from the ribs, one likely Pleistocene antelope (*Capromeryx sp.*) scapula fragment, one long bone end fragment, and two small mammal/rodent bone fragments. Illustrated in **Figure 7-19**, **Figure 7-20**, and **Figure 7-21**, a small grouping of ribs and rib fragments associated with the antelope scapula in Unit D4 L3 is the only multi-element cluster observed in Block D. Other elements were observed as isolated specimens.

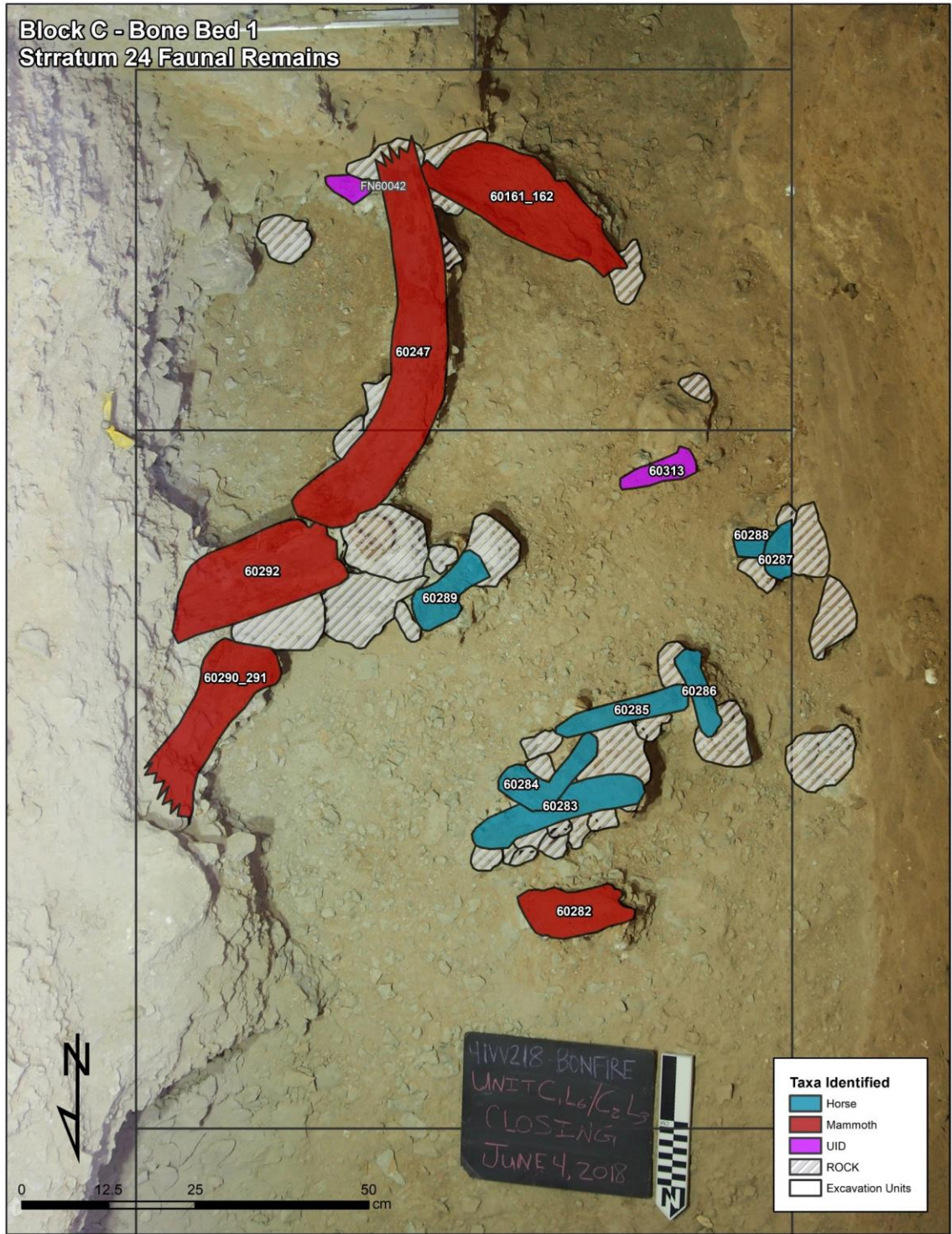


Figure 7-17. Planview map of Bone Bed 1 - Stratum 24 (H), faunal remains, Block C, Units C1 and C2. No orientable elements were recovered from Stratum 24 in Unit C3.



Figure 7-18. Unclassified planview map of Bone Bed 1 - Stratum 24 (H) faunal remains, Unit C1 and C2. No orientable elements were recovered from Stratum 24 in Unit C3.



Figure 7-19. Bone cluster at base of Unit D4 L3 including scapula (FN60333) and several ribs/fragments (FN60323, 60334 - 60338, 60345), planview - east.

The macrofauna remains recovered in Block D were much smaller than the mammoth and horse remains observed in the Block C units. If the spall pavement observed at the base of Block D represents the Stratum H-2/H-3 interface referenced by Bement, it is possible that the Block D remains may all be antelope; the only species reported in Stratum H-2 and the only provenience where Pleistocene antelope was reported. If these remains are derived from H-1, they may be associated with Pleistocene horse or a small/juvenile camel. Given the relatively gracile nature of the ribs, it is unlikely that they are bison.

The Block C Stratum 24 assemblage is more diverse than Block D, including numerous horse and mammoth elements as well as examples of rodent and bird taxa. The mammoth elements included several ribs/rib fragments and a scapula segment. FN60247 (**Figure 7-22**) was

the largest element observed during the excavations, extending over 100 cm (39.4 in) before becoming inaccessible beneath the south wall of Unit C3. Horse elements were clustered together with several cobbles in the central portion of Unit C2 L3, illustrated in **Figure 7-23** and **Figure 7-24**. These elements were highly degraded and began to crumble upon exposure limiting anatomical identification. Several ^{14}C samples were collected from amongst these cobbles and elements, the results of which are described in **Dating Stratum 24**, below. **Figure 7-23** illustrates the location of spot samples collected from Unit C1 L6 and C2 L3 and highlights the significant number of cobbles associated with the faunal remains.

FN60292 (**Figure 7-25**) appears to be the left scapula from a juvenile mammoth, inferred from its relatively small size. The scapula included semi-intact processes and a portion of the blade. While the processes were robust and relatively well preserved, the blade was extremely delicate, resting on several unstable spalls and extending beneath the eastern profile. The scapula was left in situ rather than risking total destruction during extraction and transport. FN60290 was a very robust mammoth long bone segment immediately south of FN60292. Its proximity to the scapula suggests that it may be a portion of a humerus, but this diagnosis requires further verification. Partially articulated rodent remains (FN60222 - **Figure 7-26**) were recovered from within the exposed interior cavity of FN60161, a robust and broad mammoth element recovered from the southwestern margin of Unit C1 L6. The presence of these rodent remains highlights potential adverse effects from bioturbation. While no clear krotovina were observed in Stratum 24, burrowing animals have the potential to displace datable materials. Rodent gnawing or undermining also has the potential to further destabilize the larger megafauna remains



Figure 7-20. Planview map of faunal remains recovered from Bone Bed 1 - Stratum 24 (H), Block D, Unit D4.



Figure 7-21. Unclassified planview map of faunal remains recovered from Bone Bed 1 – Stratum 24 (H), Block D, Unit D4.



Figure 7-22. Initial exposure of FN60161 (Unconfirmed mammoth element), FN60247 (mammoth rib - center), and FN60292 (mammoth scapula - lower left) at the Stratum 23/24 interface. Planview - south.

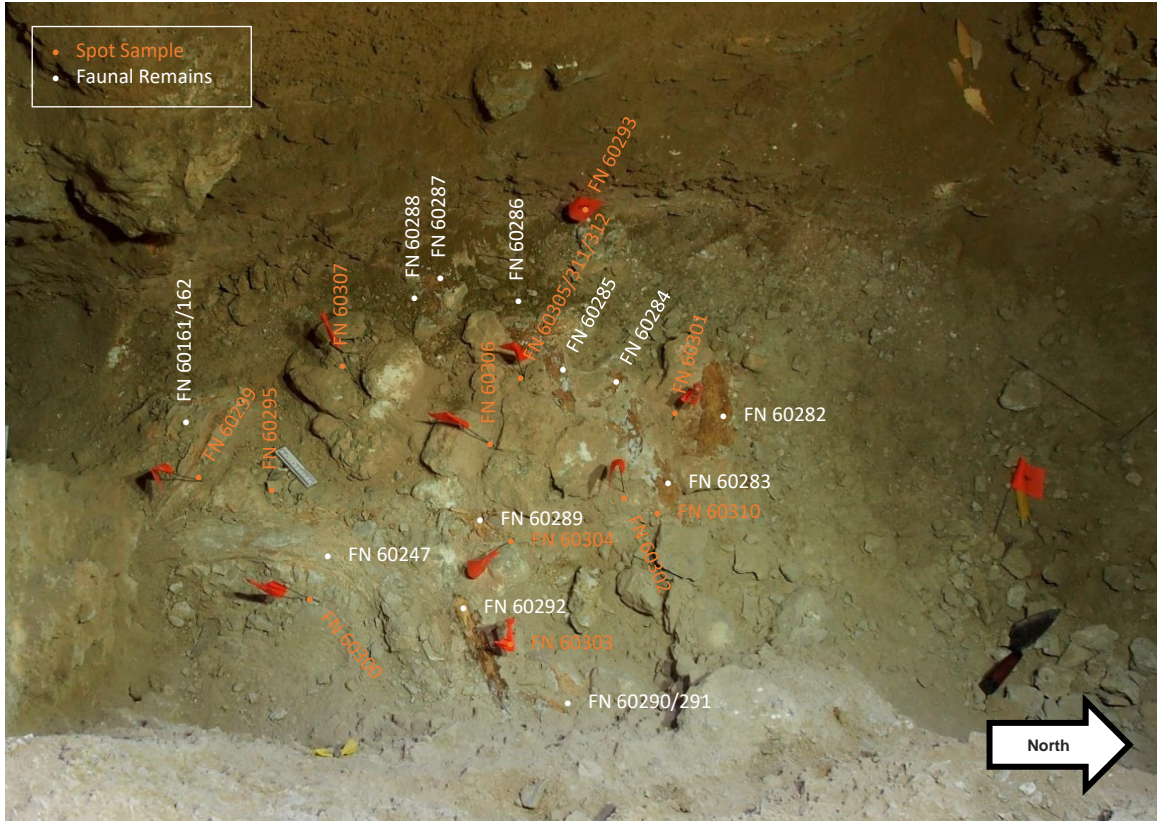


Figure 7-23. Spot samples and fauna remains recovered from Unit C1 L6 and C2 L3. Note the significant number of cobbles associated with the faunal remains near the center of the frame, planview - west.

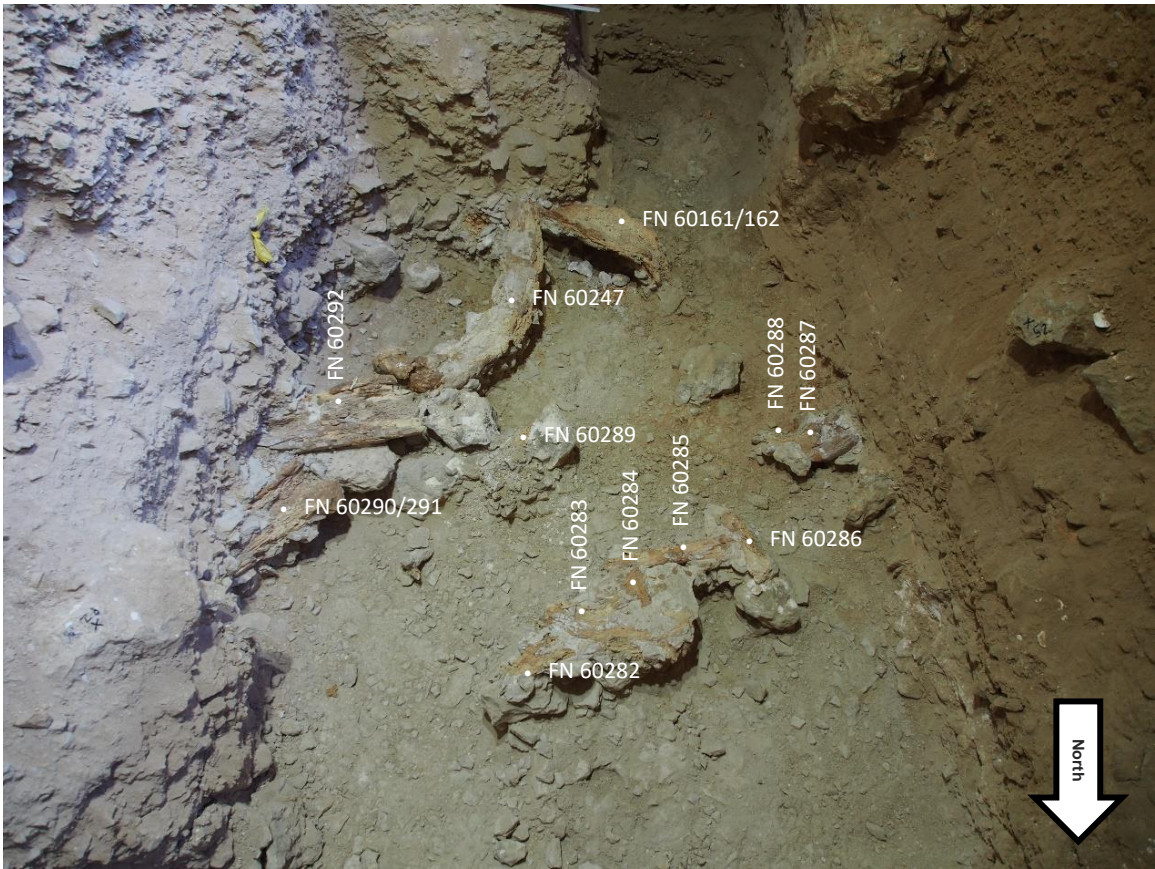


Figure 7-24. Closing photo of Unit C2 L3 and Unit C1 L6, view south. Note the cluster of horse elements in the foreground and mammoth elements in the background. Oblique view - south.



Figure 7-25. FN60292, mammoth scapula, extending beneath the eastern profile of Unit C2 L3, view east.



Figure 7-26. Partially articulated rodent remains (FN60222) within mammoth element (FN60161), view east.

Table 7-7. Summary of faunal remains recovered from each Stratum 24 (H) provenience. Elements recovered during the 1980s excavations are provided as a single record for comparison. Capromeryx elements assigned to Stratum H-2 in the 1980s are included here as the Stratum H-1/H-2 interface could not be re-identified in the field. Counts and notes marked with an asterisk (*) indicate tentative taxonomic or element level classifications.

Stratum 24 (H) - Faunal Remains									
Provenience	Bison	Antelope	Horse	Mammoth	Rodent	Bird	UID	Total	Notes
1983 Elements	1	3*	26	6	0	0	0	36	*Includes Capromeryx from Stratum H2.
Unit C3 L3	-	1	-	-	-	-	2	3	1 Capromeryx rib/toothlike fragment; 1 UID fragment; 1 UID screen lot fragment
Unit C2 L3	-	-	7	4	-	-	1	12	7 horse elements (1 tibia, 1 long bone segment*, 1 vertebra, 4 badly degraded UID); 4 mammoth (1 scapula [includes FN60290 and 291], 1 long bone segment* (possible humerus), 2 badly degraded and UID).
Unit C3 L6	-	-	-	2	1	1	-	4	2 mammoth (1 rib, 1 long bone segment* similar to FN60292 -- FN60162 determined to be portion of 60161); 1 partially articulated mouse; 1 small bird long bone
PS06.CS05.S24	-	-	-	1	-	-	-	1	1 UID mammoth fragment within column sample
Unit D3 L2	-	-	-	-	-	-	1	1	-
Unit D3 L3	-	-	-	-	-	-	1	1	1 UID rib fragment (FN60408 – possibly Capromeryx, does not appear robust enough for bison)
Unit D3 L4	-	-	-	-	-	-	1	1	1 very fragmented rib section
Unit D4 L2	-	-	-	-	-	-	1	1	Unidentifiable bone dust
Unit D4 L3	1*	1*	-	-	-	-	6	8	1 Capromeryx scapula; 1 bison rib*, 1 UID Rib, 5 UID bone fragments (appear to be derived from ribs).
Unit D4 L4	-	-	1*	-	-	-	-	1	1 horse rib*
Unit D7 L4	-	2*	-	-	1	-	3	6	2 Capromeryx* ribs; 1 UID rib, 1 UID long bone fragment, 1 UID fragment; 1 UID small mammal fragment
Unit D8 L5	-	-	-	-	1	-	-	1	1 UID small mammal fragment
2017/2018 Total	1	4	8	7	3	1	16	40	-
Grand Total	2	7	34	13	3	1	16	76	-

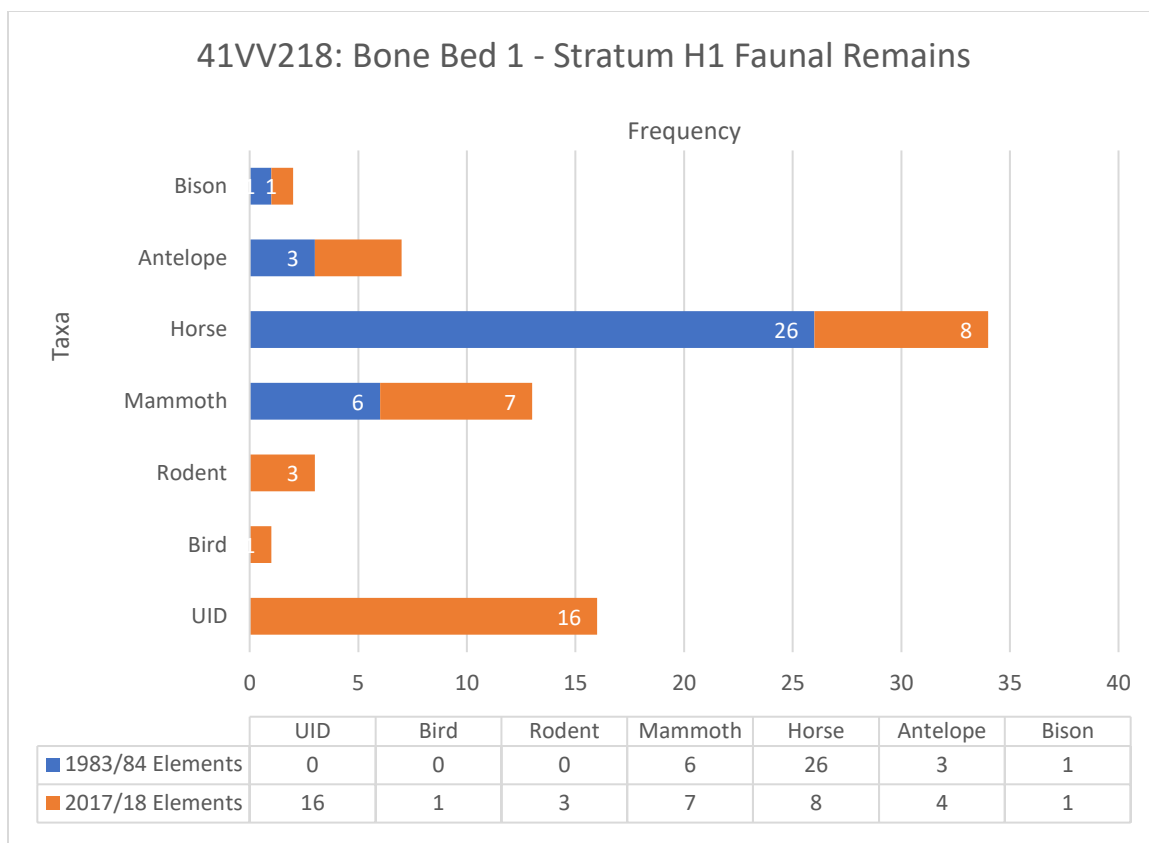


Figure 7-27. Graphic comparison of Stratum 24 elements recovered in 1983/84 to the 2017/2018 assemblage.

Based on the combined 1983-1984 and 2017-2018 assemblages reported in **Table 7-7**, **Figure 7-27**, and the detailed specimen catalogs presented in **Appendix C: Faunal Assemblage**, the minimum number of individuals (MNI) was calculated for each taxa represented in Stratum 24. The MNIs reported in **Table 7-8** are based on the duplication of elements derived from the same species, accounting for the newly identified 2017-2018 specimens. Bement's 1986 MNIs (Bement 1986a:38-39) were utilized as a starting point and are accounted for in these estimates. Due to the substantial number of unidentified elements in the 2017-2018 assemblage, the MNI estimates reported here are subject to revision based on future research.

A minimum of two Pleistocene horse (*Equus francisci*), one Pleistocene bison (*Bison antiquus* or *occidentalis*), one mammoth (*Mammuthus* sp.), and one Pleistocene antelope (*Capromeryx* sp.) are represented in Stratum 23. Estimates for Pleistocene horse are based on the

duplication of right ulna and differential epiphyseal closure (Bement 1986a) and possibly duplicated tibia between the 2017-2018 and 1986-1987 assemblage. No duplicate were present that could confirm the presence of more than one bison or mammoth. Duplicate antelope ribs were observed but could not be attributed to multiple individuals.

Potentially significantly, it was also not possible to confirm that more than one mammoth is represented across Stratum 23 and Stratum 24. The pelvis fragment photographed in Bement 1986:48 appears to be similar in size and does not duplicate the fragment documented in Stratum 23. Other mammoth elements across the 1983-1984 and 2017-2018 Stratum 23 and Stratum 24 assemblages are not duplicated (other than non-diagnostic ribs/rib fragments) and appear to be derived from a juvenile. It is possible that this is coincidental, but could also be an indication of post-depositional movement via carnivores or another taphonomic process. For reference, **Figure 7-28** and **Figure 7-29** illustrates the Stratum 23 and Stratum 24 faunal assemblages together across Block C.

Table 7-8. Minimum number of individuals represented in Stratum 23 for each identified taxa. Calculated based on the duplication of elements or diagnostic attributes across the 1983-1984 and 2017-2018 assemblage.

Stratum 24: Minimum Number of Individuals (MNI)		
Species	MNI	Determination
Horse	2	Duplicate right ulna, differential epiphyseal closure (Bement); Possible duplicate tibia (Bement/Farrell)
Bison	1	No duplicate elements; Cannot confirm >1 individual represented (Bement/Farrell)
Mammoth	1	No duplicate elements; Cannot confirm >1 individual represented (Bement/Farrell)
Antelope	1	Multiple ribs, insufficient duplication to confirm >1 individual represented (Farrell)

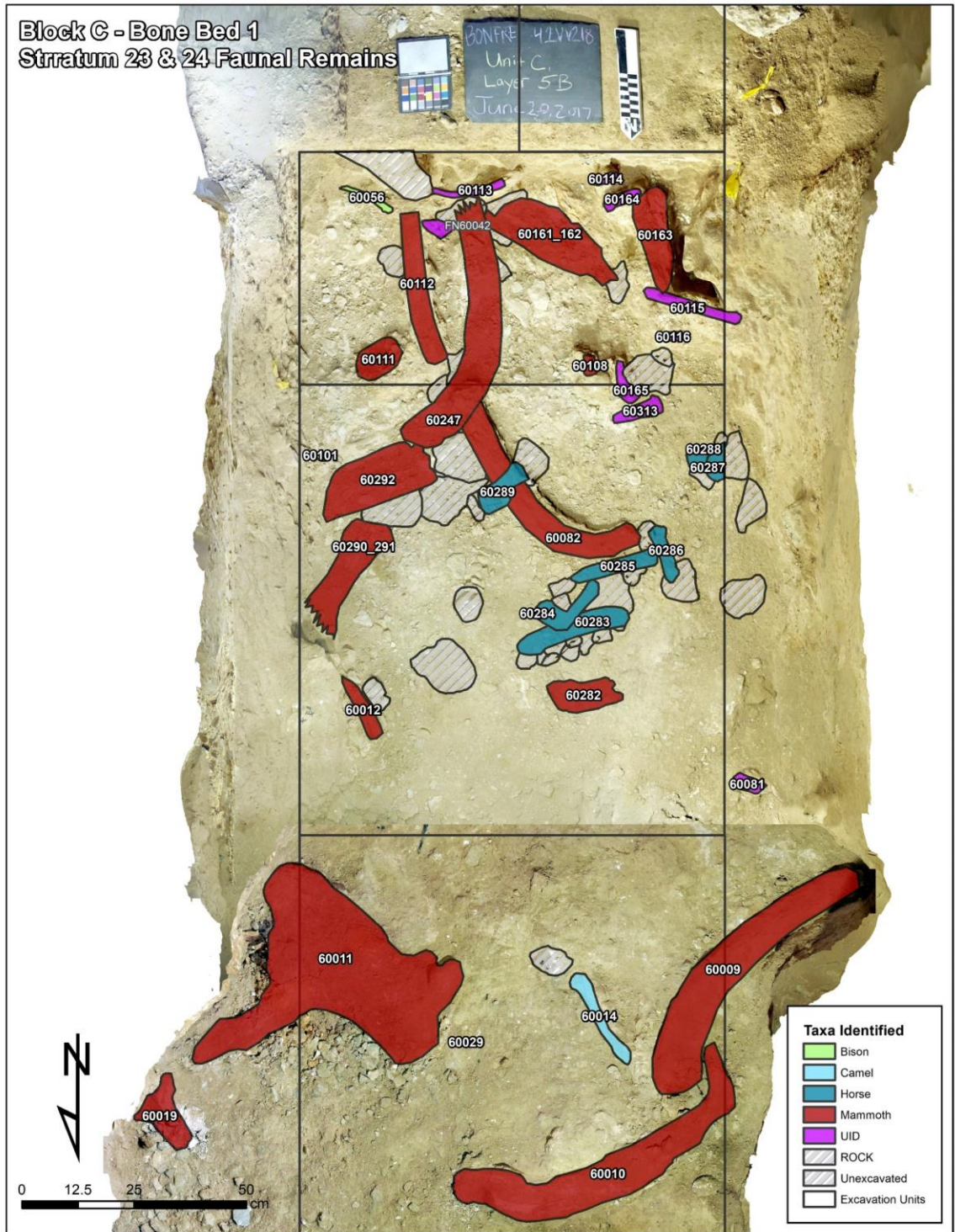


Figure 7-28. Planview illustration of superimposed Stratum 23 and 24 faunal assemblages.

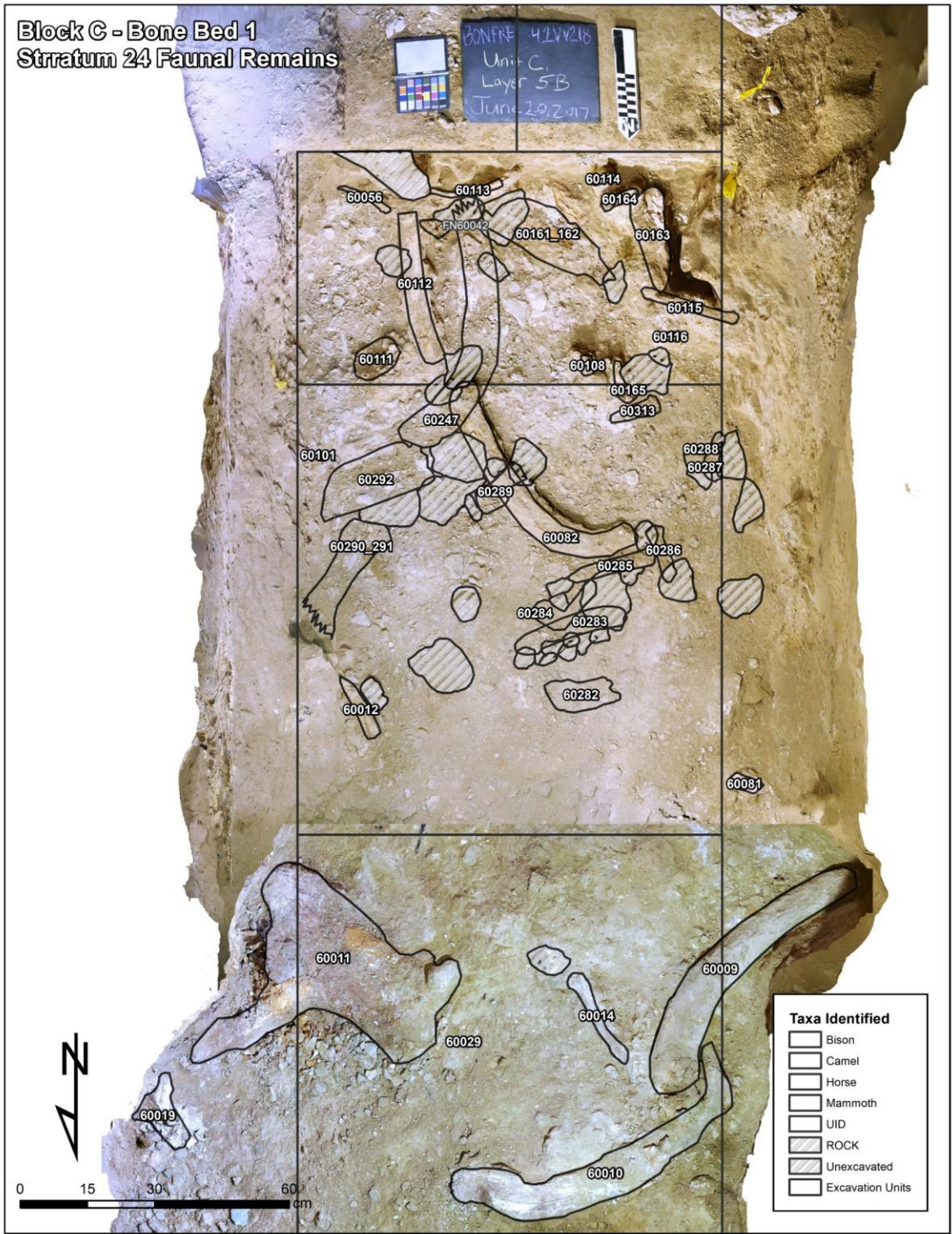


Figure 7-29. Unclassified plan map of superimposed Stratum 23 and 24 faunal assemblages.

7.4.3 *Faunal Remains – 1963-1964*

The Bone Bed 1 assemblage received extremely limited attention in the 1968 Bonfire Shelter report (Dibble and Lorrain 1968). Dibble briefly cites several smaller concentrations of Pleistocene Horse, Camel, Mammoth, and Bison remains beneath the Folsom-aged Bone Bed 2, but the specifics of the assemblage not discussed (Dibble and Lorrain 1968:28). Lorrain's detailed faunal analysis primarily addresses the robust Bone Bed 2 and Bone Bed 3 bison-kill assemblages. Bone Bed 1 is mentioned in passing on the very last page of the report, where the Pleistocene taxa are marked on a presence-absence table (Dibble and Lorrain 1968:134). To gain a better understanding of the specific materials recovered from Bone Bed 1 during the Amistad expedition, Bonfire Shelter records on file at TARL were reviewed.

Dibble's field notes shed additional light on early conceptions of Bone Bed 1's structure and composition (Dibble 1964). Of the 29 features Dibble defined at Bonfire Shelter, three are related to Bone Bed 1: Feature 4, Feature 12, and Feature 16. In this context, "Feature" was rather loosely defined and utilized to track significant bone concentrations. These features are roughly correlated with Bement's Stratum E/F/G, Stratum H, and possibly Stratum I and 2017-2018 Stratum 23 and Stratum 24; an equivalent of Bement's Stratum I was not identified during the 2017-2018 excavations. No Pleistocene horse or mammoth specifically reported in TARL catalog.

As noted in **Chapter 2**, portions of the Bonfire Shelter records at TARL are unaccounted for including scaled plan and profile drawings. Dibble specifically references additional description and 1-foot:1-inch scaled maps prepared for Features 4 and 12, but the records could not be located. The assemblage reported here is derived from TARL's inventory of the Bonfire Shelter collection. The catalog has been modified to account all elements specific cited in Dibble's Feature descriptions, but many specimens lack species or specific element

designations. Additionally, only elements that were unambiguously attributed to Bone Bed 1 (i.e.: clearly marked Feature 4, 12, or 16) are included here.

Confidence in the TARL inventory's taxonomic classifications is low, particularly for "Bison" bone lacking specific element designations. "Bison Bone" and "Misc Bison Bone" may serve as a catch-all for generic bone fragments in the AMIS database system. Additional in-person consultation with TARL and the Texas Vertebrate Paleontology Lab is necessary to resolve these discrepancies and compile a more complete inventory of the Amistad-Era Bone Bed 1 assemblage.

7.4.3.1 Bone Bed 1 - Feature 4

Feature 4 was the densest component of Bone Bed 1, approximately 0.7 – 1.0 ft (21.3 - 30.5 cm) below Feature 3 (Bone Bed 2) in units N110 E40 and N98 W40, approximately 88.5 ftbd (27.0 mbd). The deposits appeared to be discontinuous, extending an unknown distance south (but not so far as the southern excavation units or talus cone). Sediments associated with Feature 4 were distinct from surrounding strata, described as a "a yellowish brown or 'chestnut' silt with a high proportion of spall and occasional large limestone cobbles" (Dibble 1964:Feature 4, 2).

Feature 4 consisted of at least two mammoth femur fragments and one camel mandible with intact teeth among additional fragmentary remains. Dibble also describes a concentration of burned bone, trace charcoal, and decomposing organic matter in the northwestern quadrant of N98 W40 that were retained for radiocarbon dating (though the samples apparently did not survive the assay or were not processed; they are not mentioned in E. Mott Davis's 1964 letter on file at TARL reporting the Amistad-era radiocarbon results). Dibble argues that the trace charcoal and fragmentary remains suggest human activity, but no unambiguous evidence was identified describing Feature 4 as "a damn frustrating thing!" (Dibble 1964:Feature 4, 3).

Dibble's Feature 4 faunal assemblage and sediment descriptions are consistent with Bement's Stratum 23 and 2017-2018 Stratum 23. The presence of Pleistocene camel and mammoth in the same stratum is unique to Stratum 23, as is the unmistakable "chestnut-brown" silty matrix. TARL inventory data for Feature 4 indicates a much larger faunal assemblage than observed in subsequent excavations. It is likely that the inventory includes smaller bone fragments not attributable to a single element towards the total. Additionally, the TARL inventory does not include the mammoth elements Dibble explicitly mentions in the Feature 4 report. It is likely that the 1963-1964 Feature 4 assemblage is more diverse than indicated by these records.

7.4.3.2 Bone Bed 1 - Feature 12

Feature 12 was reported as a discrete concentration of large mammal bones stratigraphically below Feature 4 in units N110 W40 and N98 W40, approximately 87.5 ftbd (26.7 mbd). Dibble describes the Feature 12 sediments as "primarily gray or buff colored spall with a small percentage of fine-grained silt or 'limestone dust'" (Dibble 1964:Feature 12), similar to Bement's description of Stratum H and I as well as Dibble's underlying Feature 16. No specific species or elements are reported on the feature form beyond "large mammal". However, Dibble notes the bones are more scattered than overlying bone beds, with several specimens "cracked in a manner suggesting human – rather than carnivore – modification) (Dibble 1964:Feature 12, 12).

The TARL catalog for Feature 12 is generally consistent with Dibble's description, including one lot of fragmentary bison bone and several unidentified individual bison elements. Feature 12 is stratigraphically and geologically consistent with Bement's Stratum H and 2017-2018 Stratum 24. However, the faunal assemblage deviates from the primarily Pleistocene horse and mammoth remains reported by subsequent excavators. Only two bison elements were recovered from Stratum H/24; a significant deviation from the 37 reported in the TARL inventory. Based on the other similarities between Feature 12 and Stratum 24, the "Bison"

designation reported here should be treated with moderate skepticism until the TARL and Vertebrate Paleontology assemblages can be reviewed in person.

7.4.3.3 *Bone Bed 1 – Feature 16*

Feature 16 was identified approximately 1.0 ft below Feature 12 in Unit N110 W40 (86.44 – 86.79 ftbd; 26.4 – 26.5 mbd) in units N110 W40 and N98 W40 (Dibble 1964:Feature 16). Dibble describes the stratum as light gray silt or “limestone dust” with a very high percentage of tabular limestone spalls up 15.24 cm (6.0 in); very similar to the Feature 12 matrix and consistent with Bement’s descriptions of Stratum H and I. Dibble specifically reports three Feature 16 elements, including a well-preserved ulna fragment, a mandible fragment, and a very poorly preserved large mammal bone fragment, none of which are attributed to a specific species. In N98 W40, Feature 16 yielded a single large rib and an unidentified deeply buried element before excavations were abandon at the end of the field session in February 1964. The TARL inventory identifies several additional elements (calcaneum, sesamoids, and teeth) in Feature 16, all of which are attributed to Bison. The N98 W40 rib is not specifically identified. No charcoal or other evidence of human activity beyond general fragmentation was reported.

The relationship between Feature 16 and the 1983-1984/2017-2018 strata is unclear. By depth alone, Feature 16 is probably within the range of Bement’s H-2 or H-3 substrata. However, no Pleistocene antelope, horse, or mammoth are present in the assemblage. Bement’s Stratum I included a variety of Bison limb elements, including additional ulna and calcaneum, consistent with Feature 16 as reported in the TARL inventory. Stratum I was not reidentified in 2017-2018

7.5 *Dating Stratum 24*

Table 7-9 summarizes the results of three successful AMS dates recovered from Bone Bed 1 during the 2017-2018 field season. As reported by previous excavators, charcoal and organic material was extremely uncommon in the deeper deposits of Bonfire Shelter. Trace

charcoal flecks were occasionally observed and collected, but did not survive chemical pretreatment in the AMS lab. Examples of mammoth and horse bone from Bone Bed 1 were submitted to Dr. Raymond Mauldin at the University of Texas – San Antonio for XAD/ultrafiltration collagen extraction and dating, but no viable organic material was recovered.

A cluster of hackberry seeds (FN60295), illustrated in **Figure 7-30** below, was recovered in situ beneath the large mammoth rib (FN60247) and an UID mammoth segment (FN60161) extending from the southern wall of UC1 L6. Seeds from this sample yielded an AMS date of 12,112±69 BP.

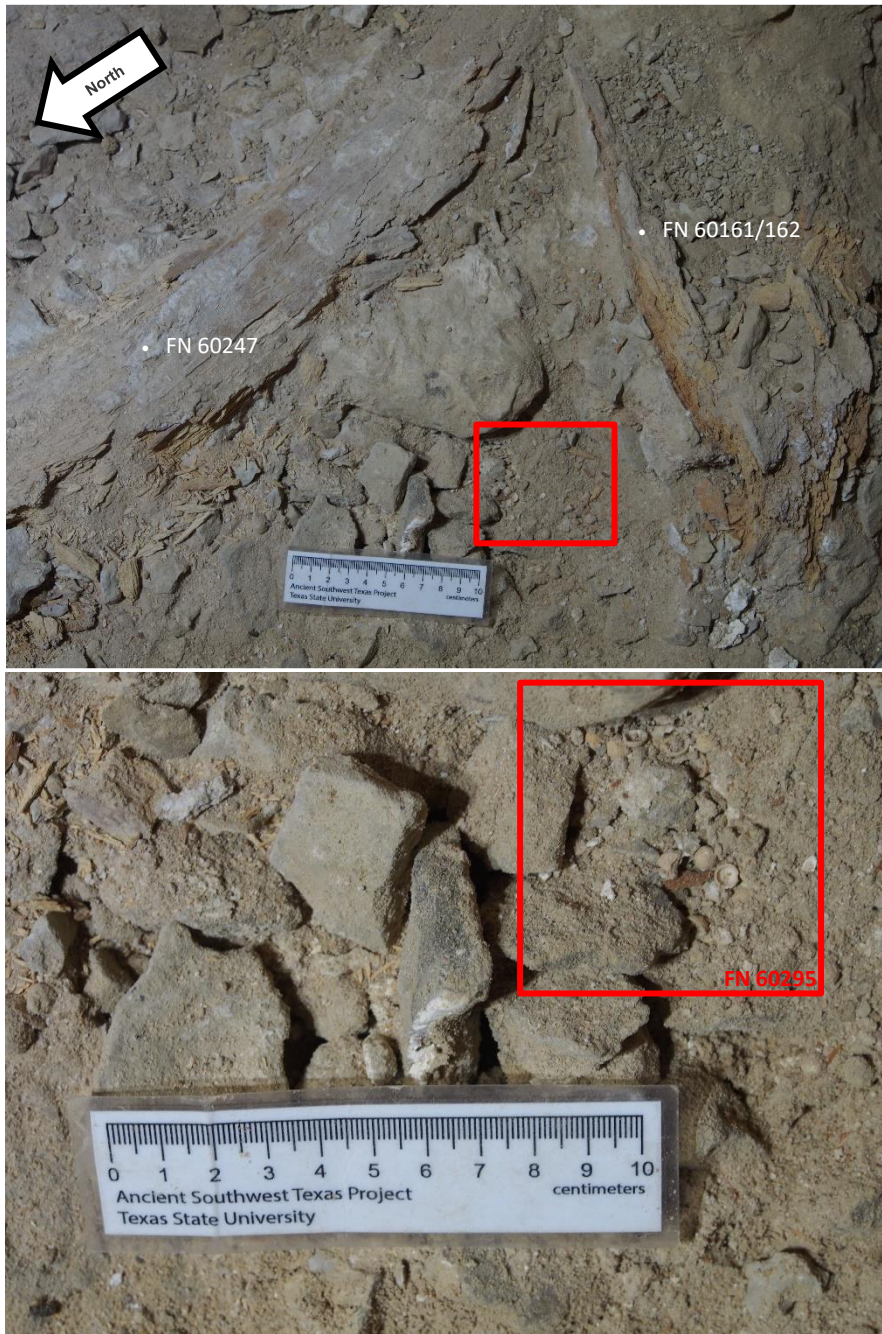


Figure 7-30. Detail photo of FN60295 showing in situ exposure of hackberry seeds (lower – red outline) and context photo illustrating the relationship between FN60295 and mammoth elements (FN60247 and 60161) (upper). View southeast.

FN60312 (**Figure 7-31**) and FN60329 (**Figure 7-32**) were recovered from a cluster of badly degraded horse elements near the center of UC2 L3. FN60312 consisted of a small amount of charcoal/organic material recovered from beneath a spall immediately south of a badly degraded horse tibia (FN60285) near the center of the bone concentration. FN60329 included a patch of trace charcoal recovered as a sediment sample along the northern edge of the bone concentration, immediately north of an unidentifiable horse element (FN60283). FN60312 yielded an AMS date of 12189±48 RCYBP. FN60329 yielded a date of 9834±46. Provenience information and calibrated dates are summarized in **Table 7-9**, below.

Table 7-9. Provenience and results for three viable radiocarbon dates recovered from Bone Bed 1.

2017-2018 AMS Dates - Bone Bed 1										
Direct AMS Sample ID	FN	Dibble Stratum	Bement Stratum	ASWT Stratum	Unit	Material	RCYBP	Cal BP 2σ	Cal Median Probability	Note
D-AMS 034547	60295	Bone Bed 1	H	S24	UC1 L6	Botanical	12112 ± 69	12194-11822	13971	Hackberry seeds recovered in situ beneath spall along margin of mammoth rib (FN60247)
D-AMS 034548	60312	Bone Bed 1	H	S24	UC2 L3	Charcoal	12189 ± 48	12289-11976	14080	Charcoal/organic material beneath spall within concentration of badly degraded horse elements. Immediately south of horse tibia (FN60285)
D-AMS 034549	60329	Bone Bed 1	H	S24	UC2 L3	Sediment	9834 ± 46	9374-9236	11239	Charcoal rich sediment along north edge of degraded horse bone concentration; immediately north of unidentifiable horse element (FN60283)



Figure 7-31. Initial exposure of ^{14}C sample FN60312 (upper) and association with cluster of horse remains (lower).



Figure 7-32. Initial exposure of ^{14}C sample FN60329 beneath element FN60282 and FN60283.

Prior to these new dates, Bement's Stratum H-1 date at $12,460 \pm 490$ RCYBP was the only chronometric verification of Bone Bed 1. The sample was derived from trace charcoal collected from across the stratum rather than a single source or concentration (Bement 1986b:58). Combining multiple sources provides an average date for the surrounding sediment matrix, but

the direct association of the dated material with the megafauna remains is tenuous at best. Interpretation was further muddled by potential “old wood” contamination, reflected in the nearly 1000-year standard deviation.

Ideally, the mammoth and horse remains would be dated directly. Dating the surrounding sediment matrix requires significant logical assumptions, particularly that the charcoal was deposited at or around the same time as the fauna. Given the dynamic formation processes that characterize rockshelter settings, limited confidence can be ascribed to those assumptions. Several specimens derived from Bone Bed 1 and Bone Bed 2 were submitted to The Paleo-Research Laboratory at UTSA’s Center for Archaeological research for collagen extraction, purification, and dating by Dr. Ray Mauldin, but the specimens failed to yield datable material. Ongoing technological developments in bone collagen dating may make direct fauna dating a possibility at Bonfire Shelter in the not so distant future. With this in mind, additional well-preserved elements from Block D were retained with consolidant treatment to specifically to facilitate future collagen dating campaigns. Bone apatite dating has not been attempted at Bonfire Shelter but may provide additional opportunities to refine the age of Bone Bed 1.

New dates FN60295 and FN60312 confirm Turpin and Bement’s Late Pleistocene age for Stratum H obtained in the 1980s. The increased precision of the new dates confirms that Stratum H falls on the younger end of the 1000-year window established by the 1980s date; much closer to the age window for Clovis than the initial ± 490 year range suggests.

FN60329 is anomalous, post-dating all other Bone Bed 1 dates by nearly 2000 years. FN60329 specifically targeted sediment containing trace charcoal, while FN60295 and FN60312 consisted of discrete individual samples of organic materials. The early date from FN60329 may be the result of contamination from overlaying Bone Bed 2 deposits. It is also possible that this much earlier date reflects the differential accumulation of sediment and bone across the stratum. Faunal remains may have been deposited first then gradually infilled with sediment.

Radiocarbon dates recovered from other Bone Bed 1/Column Sample 5 strata were not viable. The next available bounding date, $10,230 \pm 160$, was recovered from Bone Bed 2 Stratum A in the 1960s. Nearly 300 years earlier than the FN60329 date. It is unlikely that this isolated portion of Stratum H remained exposed and accumulating sediment throughout the deposition of four intervening strata. It is more likely that this result represents the effects intrusive rodent burrowing and the introduction of more recent sediment.

8. GEOARCHAEOLOGICAL RESULTS

As stated in **Chapter 6**, three primary criteria must be satisfied to classify Bone Bed 1 as an archaeological site: artifacts must be **unambiguously cultural, chronometrically verified,** and recovered from an **undisturbed provenience**. The data presented in **Chapter 8** comprise geological profiles of the strata sampled in Column Sample 5. These profiles are compared against the site-type expectations model outlined in **Table 6-1**. Combined with the cultural and faunal assemblage, these data are used to assess the origins of material recovered from each stratum. Even if the Bone Bed 1 strata are not cultural deposits, attributing the Pleistocene fauna of Bonfire Shelter to natural death events, carnivore activity, or geological formation processes provides useful insight relevant to otherwise opaque very early Paleoindian sites.

Specifically, these data are used to validate the provenience of recovered materials. Sedimentary composition and depositional origins are considered to determine if strata may have been compromised by post-depositional processes or are otherwise in secondary context. Geological processes can redeposit, scour, invert, or otherwise modify the stratigraphic position of archaeological materials; buried materials are subjected to the same geological impacts as the sediments that surround them. If a stratum has been compromised, the provenience of associated artifacts, radiocarbon dates, or other materials of interest cannot be confidently established, and the stratum cannot satisfy the criteria for classification as an archaeological deposit.

Environmental interpretations of geoarchaeological data are a critical check on the radiocarbon ages of deposits and provide more information regarding the provenience of recovered materials. It is essential to determine if artifacts, faunal remains, radiocarbon dates, and the sediment can be attributed to contemporary events. For example, if Pleistocene fauna are found in association with very young radiocarbon dates or sediments inconsistent with an extended cold, wet, climatic interval, the provenience of the dates or recovered materials should

be carefully scrutinized. Very old archaeological material recovered in very young deposits (or vice-versa) may be indicative of redeposition or contamination.

Landscape reconstruction provides insight into the habitability of the site/region for both humans and local fauna. If climatic changes are correlated with changes in the faunal or artifact assemblage, it may be indicative of the landscape becoming incompatible with the subsistence practices of the incumbent inhabitants. Relatively rapid climatic fluctuations suggest landscape instability, which may be a physical deterrent to utilizing a landscape feature (i.e.: frequent rockfalls and spalling turning rockshelters into dangerous traps). Any uncertainty that a location would not be able to consistently provide the necessary seasonal and annual resources would probably be cause for avoidance by high-mobility hunter-gatherers dependent upon the seasonal replenishment of food and materials. Migratory fauna dependent on the seasonal renewal of fodder sources might be similarly risk averse. If game animals avoid an area, the hunter-gatherers and predators who depend on them as a roaming source of protein are unlikely to be drawn to an area.

Three of the strata sampled in Column Sample 5 are associated with Bone Bed 2: Stratum 19 (Stratum A), Stratum 20 (Stratum B), and Stratum 21 (Stratum C). These samples provide baseline geological profiles for Late Pleistocene, high-mobility, hunter gatherer horizons. Known environmental and material culture differences between the Early and Late Paleoindian periods across Texas make this an imperfect comparison. However, the ephemeral signatures of human occupation and the conditions that sustain them remain useful for differentiating cultural from non-cultural strata. Deviations from the expected patterns may provide further insight into unique adaptations to local conditions.

Clearly, not all of the analyses outlined in **Chapter 5** are direct measures of human activity. Human or animal activity can enrich sediments with organic carbon and elevate magnetic susceptibility, but natural processes can result in equifinality. An organic carbon or

magnetic susceptibility peak accompanied by an influx of fine-grained exogenic material is less intriguing than an anomalous peak that lacks an apparent geological explanation. The geoarchaeological results are considered here as a whole for each stratum, rather than discrete data points. The results of geoarchaeological analyses derived from Column Sample 5 Stratum 19 through Stratum 24 are presented below. Results are organized by stratum with subsections for summarizing results for specific analytical classes highlighting general trends and outliers. Strata are organized from oldest to youngest, beginning with Stratum 24.

Data for each analysis are plotted as a function of depth/time. In-text figures are included to highlight key data. Lab Sample (LS) and stratum designations corresponding with each data point can be reviewed in **Table 5-2**

Stratum 19, 20, and 21 are primarily represented by geoarchaeological data collected from Column Sample 5. These layers were only present in the southernmost 50cm of Unit C1, biasing the 2017-2018 faunal assemblage and limiting the area available for microartifact sampling. Geoarchaeological sampling was intentionally consistent and continuous throughout the column sample strata to facilitate direct comparisons over time. However, comparisons of faunal and non-column sample microartifact data between Bone Bed 1 (Stratum 24 and Stratum 23) and the overlying deposits (Zone 2a – Stratum 22; Bone Bed 1 – Stratum 21 – Stratum 19) should cautiously acknowledge this sampling bias.

8.1 Overview

Figure 8-1 presents the compiled results of six key analyses illustrating the changing conditions at Bonfire Shelter spanning the period from Bone Bed 1 to Bone Bed 2. New radiocarbon dates with refined standard error (**Table 7-9**) place Stratum 24, the deepest sampled deposit, at 14,080 cal BP ($12,189 \pm 48$ RYBP). Stratum 19, the youngest Bone Bed 2 stratum (and best dated deposit in the shelter), dates to 12,006 cal BP ($10,230 \pm 160$ RYBP) (Bement

1986a:8; Dibble and Lorrain 1968:33). This roughly 2,000-year period coincides with highly volatile climatic swings of the Terminal Pleistocene.

Based on data from the Greenland Ice Core Project, the Bølling-Allerød interstadial extends from 14,642 to 12,846 cal BP. This roughly 1,800-year period is generally characterized by relatively warm global temperatures gradually cooling over time. The episode is interrupted by alternating warm and cold sub-periods before the onset of the Younger-Dryas. Extending from 12,896 to 11,650 cal BP, the Younger-Dryas stadial is marked by a relatively abrupt return to the cold, wet conditions of the Last Glacial Maximum. Part way through the Younger Dryas, conditions gradually begin warming with an abrupt jump in global temperatures near the end of the stadial. The end of the Younger Dryas marks the last gasp of the Pleistocene and the onset of the nearly continuous warming and drying trend that characterizes the Holocene around 11,650 cal BP (Bousman and Vierra 2012; Rasmussen et al. 2006).

Table 8-1. Timing of Late Pleistocene interstadials and their correlation to relevant Bonfire Shelter radiocarbon dates.

Period	cal BP	Years	Description	Bonfire Strat	Bonfire Date (cal BP median)
Bølling	14,642 - 14,025	617	Warm Interstadial		
GI-1d	14,025 - 13,905	120	Cool Interstadial	Stratum 24 (H)	14,080-13971
Allerød	13,905 - 12,846	1178	Warm, Moist Interstadial Trending to Cold		
Younger Dryas	12,846 -11,650	1196	Cold Stadial - Return to Glacial Conditions		
				Stratum 19 (A)	12,006
Holocene	11,650 - Present				

Table 8-1 illustrates the relationship of radiocarbon dates from Bonfire Shelter to these Late Pleistocene episodes. Dates derived from the ice cores represent broad global phenomena.

The trends illustrated in **Figure 8-1** appear to be well correlated with these climatic fluctuations. Beginning in Stratum 24, sediments exhibit a general fining trend that continues through the Late Paleoindian Bone Bed 2 (Stratum 19). The extremely coarse gravel deposits and low $\delta^{13}\text{C}$ found in Stratum 24 appear to be consistent with the cold interstadial occurring between the Bølling and Allerød periods (Dibble and Lorrain 1968:21). An abrupt reversal of this trend was observed in Stratum 22, Dibble's intermediate Zone 2a which separates Bone Beds 1 and 2. While no datable material was recovered from this stratum, the absence of megafauna, spike in spall content, and slight reversion in the rapidly declining $\delta^{13}\text{C}$ trend appear to be consistent with the onset of the Younger Dryas. The overlying strata 21, 20, and 19 are characterized by a dramatic shift in sedimentation patterns. The decrease in gravel proportion and rapidly increasing organic carbon and $\delta^{13}\text{C}$ values coincide with the global warming trends as the Younger Dryas begins to give way to the Holocene.

The following sections explore the nuances and anomalies of these patterns. With the expectations set forth in **Table 6-1** in mind, the remainder of this chapter presents the geological data collected from Bonfire Shelter. Particular attention will be allocated to the discussion of trends and anomalies that appear to deviate from the **Table 8-1** timeline. Anomalies that cannot be attributed to geological formation processes may be influenced by cultural or faunal activity within the shelter.

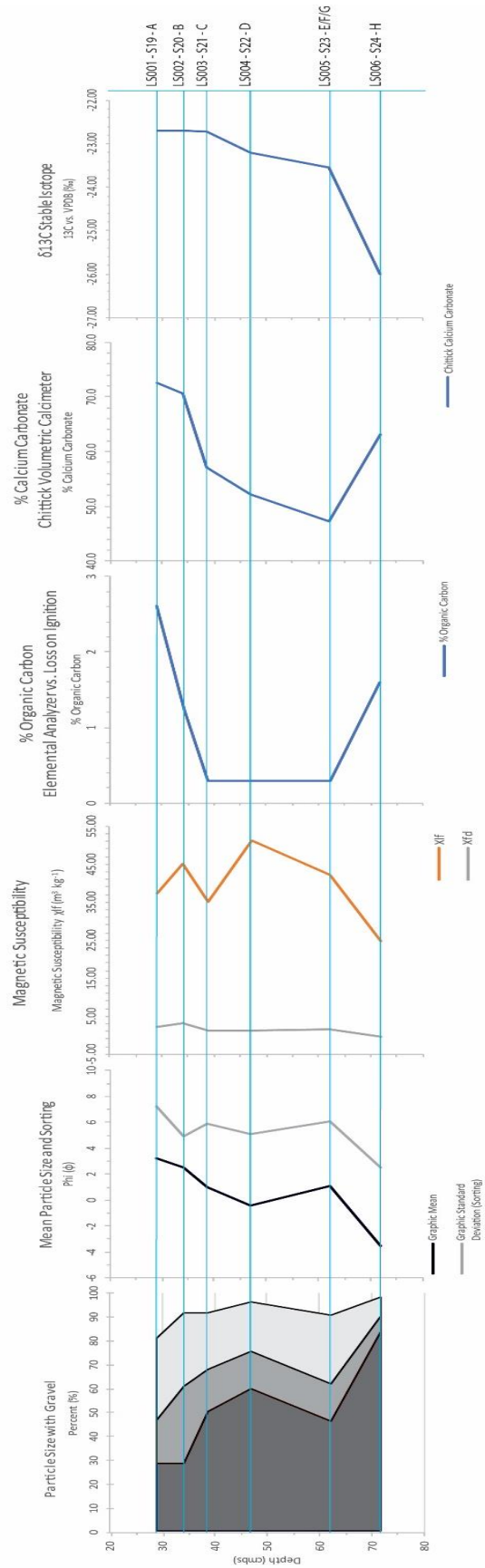


Figure 8-1. Column Sample 5 compiled geochronological results and stratigraphic correlations. Illustrated analyses from left to right include: particle size distribution (with gravel - ϕ), mean particle size and sorting (ϕ), magnetic susceptibility (χ_{fd} & $\chi_{fd} - m.3kg-l$), calcium carbonate content (%), and $\delta^{13}C$ (vs. VPDB ‰). Overlaid horizontal lines mark stratigraphic breaks added for clarity across the plate.

8.2 Particle Size

Significant quantities of gravel were present in all excavated strata, skewing particle size distribution to the coarse end of the spectrum. To identify nuances in the fine fraction, cumulative percentages and graphic statistics were calculated with and without the gravel fraction.

Cumulative percentages for each size (ϕ) class were plotted as a cumulative curve, which was used to measure the 16 ϕ , 50 ϕ , and 84 ϕ intercepts (used to calculate graphic mean, standard deviation, and skewness statistics) as well as the -1 ϕ , 4 ϕ , and 9 ϕ intercepts (used to calculate the compositional proportions of gravel, sand, silt, and clay) for each stratum. The cumulative curves, histograms, and raw particle size data sets presented in **Appendix A: Particle Size Distributions** provide graphic representations of particle size distributions for each Column Sample 5 stratum. These figures were interpreted to identify transport processes contributing to Bone Bed 1.

8.2.1 Coarse Fraction Distribution

All strata were composed of at least 25% endogenic limestone spall. The proportion of gravel in each stratum is interpreted as a relative climatic indicator. More gravel appears to correspond with colder climatic conditions. Sub-round gravels were observed at the Block D base of excavation suggesting extended freeze-thaw cycling, but sampling, excavation, and analysis of this stratum was very limited. PS06 exhibits a general fining trend beginning in the earlier Pleistocene continuing through the Late Paleoindian Bone Bed 2 strata.

Figure 8-1 plots mean particle size (graphic mean) and sorting (graphic standard deviation) in phi units (ϕ) for each stratum. These descriptive statistics were calculated including the gravel fraction and limited to graphic statistics. Inclusive statistics for several strata could not be calculated due to the excessively coarse distributions; the ϕ_5 and ϕ_{95} distribution tails could not be measured with confidence due to the unexpectedly high proportions of extremely coarse and/or extremely fine particles.

The shift in mean particle size between Stratum 24 and Stratum 19 is substantial: from ϕ -4 coarse gravel (16mm) to ϕ 3 fine sand (0.125 mm). This decrease corresponds with a significant increase in the proportion of silt-size particles in each stratum, which jumps from 8.1% in Stratum 24 to 34.2% in Stratum 19. As nearly all coarse fraction gravels were endogenic, the decrease appears to correspond with a simultaneous decrease in spall exfoliation and an increase in exogenic fine-fraction accumulation as the climate approaches Holocene conditions.

8.2.2 *Fine Fraction Distribution*

The enormous amount of gravel present in the Bone Bed 1 sediments tends to mask subtle variations in the fine fraction distribution. Sand, silt, and clay are much more susceptible to exogenic transport and introduction to the shelter. Outlined in **Table 8-2**, **Figure 8-2**, and **Figure 8-3**, sand and silt fractions in all strata are relatively equally distributed, representing between 30 and 40% of the total fine fraction respectively. Clay typically comprises 10 to 15% of the fine fraction.

The Graphic Standard Deviation trend illustrated in **Figure 8-4** indicates that all strata were “extremely poorly sorted” based on Folk’s classification scheme except for Stratum 24, which was “very poorly sorted”. With the gravel fraction included, Stratum 19 through Stratum 23 are “extremely poorly sorted” with σ_G values ranging from 4.92 (S20) to 7.225 (S19). This inverse relationship between particle size and sorting was unexpected but appears to reflect the influence of external transport vectors rather than intensity variation within any one source. In Stratum 24, 80% of sediments are derived from endogenic frost spalling and thus more consistently (large) sized than the overlaying strata with variable proportions of sand, silt, and clay.

Table 8-2. Calculated particle size analysis results of <2mm sediment fraction. USDA textural class based on percent sand, silt, and clay without out gravel fraction. Rock fragment modifier derived from gravel tabulations.

<2mm Particle Size								
Stratum	Sand	Silt	Clay	Graphic Mean	Graphic Sorting (Std Dev)	Graphic Skewness	USDA Texture	USDA Rock Fragment Modifier
S19	25.3	47.6	27.1	6.82	4.17	0.0360	Clay Loam	Gravelly
S20	45.2	43.8	11.1	4.54	3.42	0.0292	Loam	Gravelly
S21	35.8	47.6	16.6	5.21	4.045	-0.1422	Loam	Very Gravelly
S22	39.3	51.8	9.0	4.65	3.305	-0.0530	Silt Loam	Very Gravelly
S23	29.5	53.7	16.8	5.60	3.645	-0.1029	Silt Loam	Very Gravelly
S24	41.5	48.4	10.2	4.60	3.8	-0.2053	Loam	Extremely Gravelly

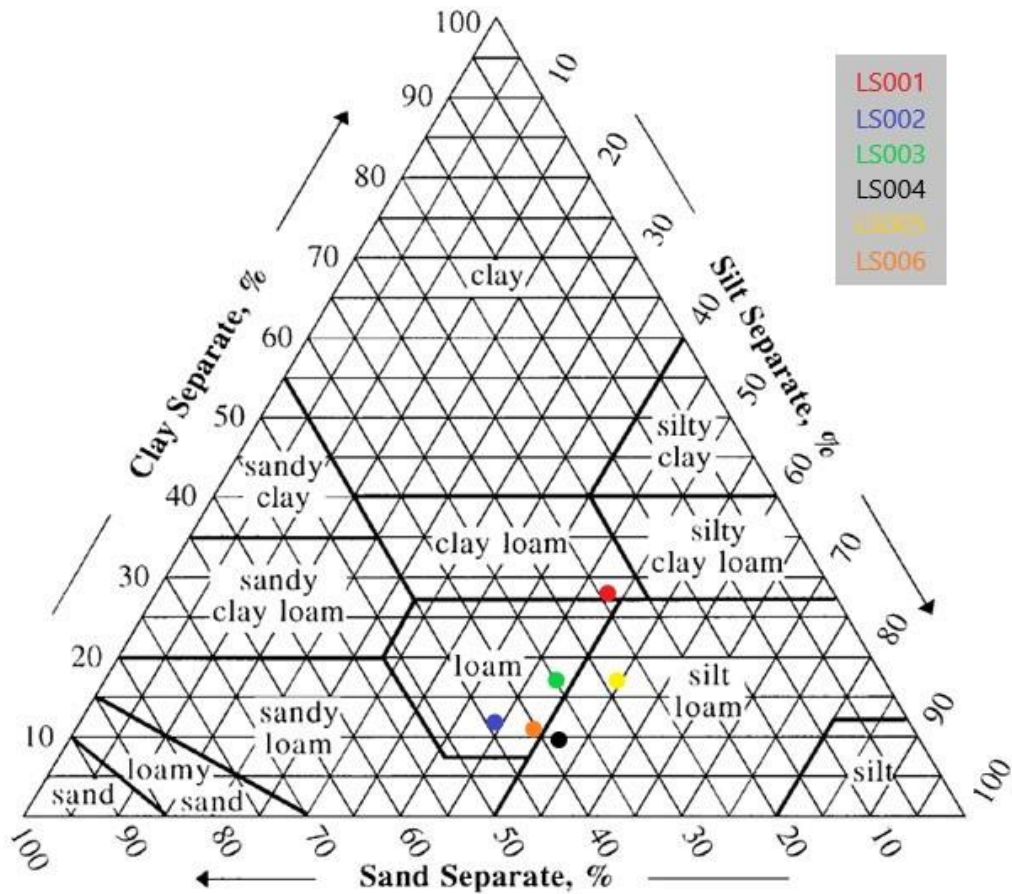


Figure 8-2. Graphic representation of PS06.CS05 <2mm-fraction USDA sediment texture classification.

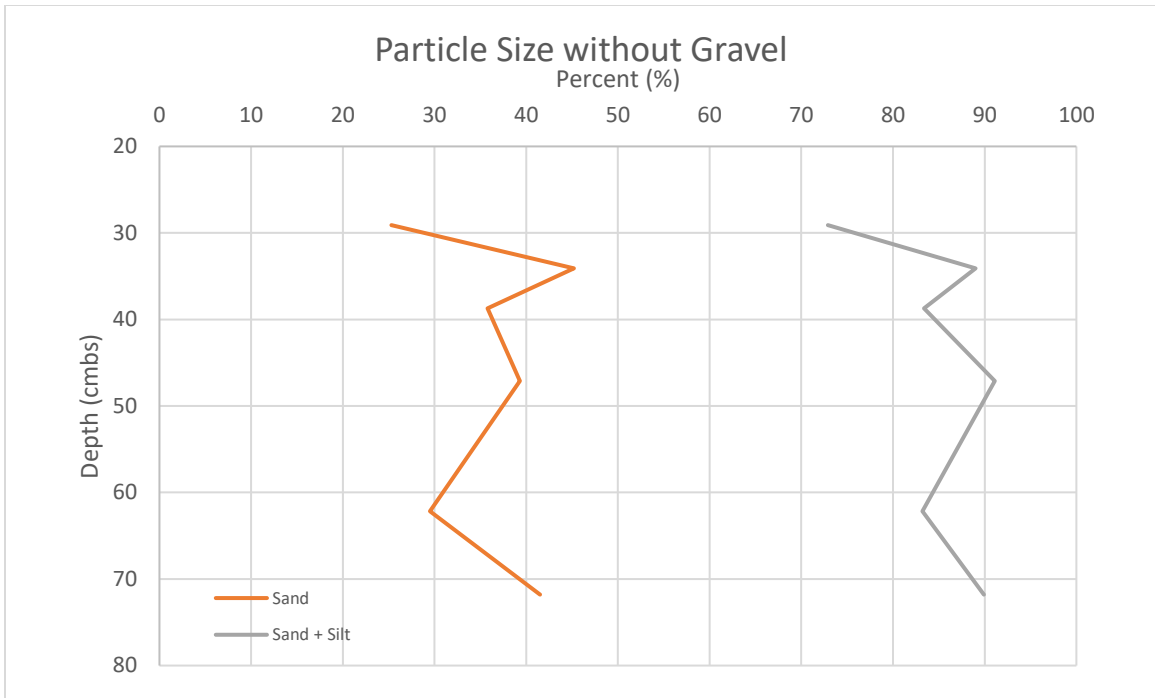


Figure 8-3. Proportional sand, silt, and clay components of each PS06.CS05 column sample stratum.

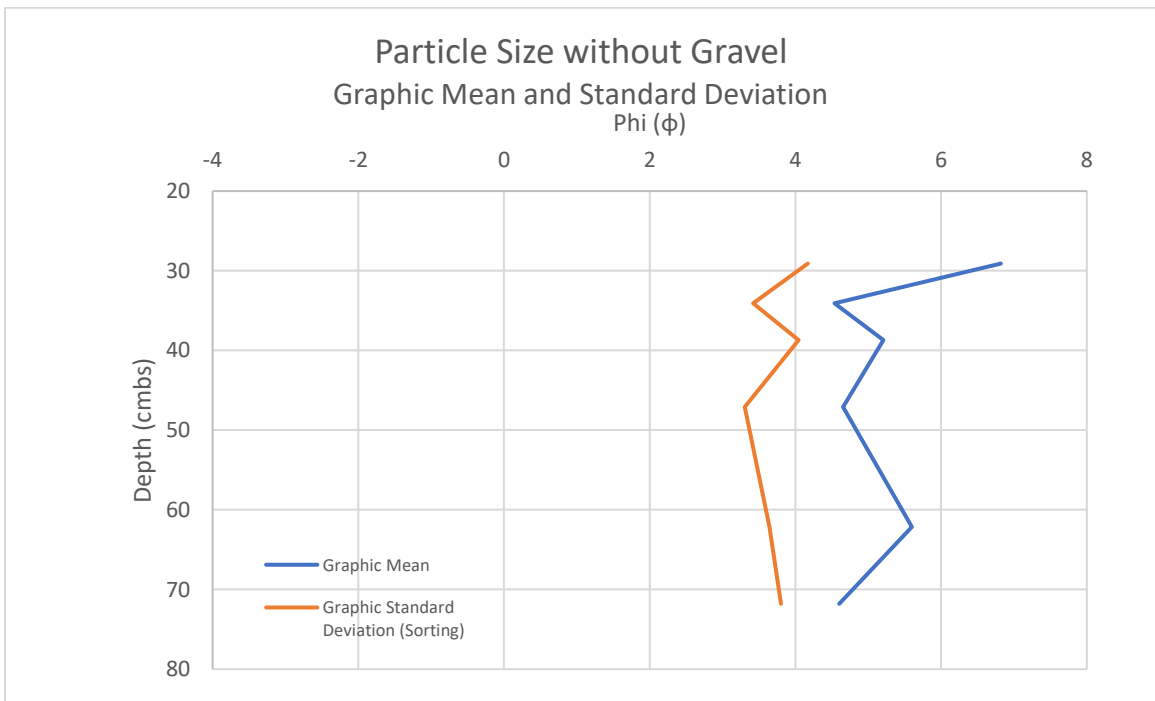


Figure 8-4. Graphic Mean and Standard Deviation of each PS06.CS05 column sample stratum excluding gravel fraction.

Illustrated in **Figure 8-4**, mean fine-fraction particle size varies between 5ϕ (coarse silt) and 6ϕ (medium silt), decreasing abruptly to approximately 7ϕ (fine silt) in Stratum 19. Fine

fraction sorting varies between 3ϕ and 4ϕ (very poorly sorted) and increases slightly in Stratum 19 to just beyond the threshold for “extremely poorly sorted”. This increasingly poor sorting trend is not proportional to the decrease in average particle size.

Coarse-fraction composition is consistent through the profile, varying only in the size and frequency of roof spalls; variations in color and texture are derived entirely from the sand, silt, and clay component.

The gray fine silt-based strata (S20, S22, and S24 -described by previous investigators as “gray powder” and “cave dust”) are relatively better sorted with larger mean particle sizes than the interbedded brown clayey deposits (S19, S21, and S23). These alternating bands represent pulses of exogenic material while the intervening “cave dust” strata are interludes dominated by endogenic deposition. This pattern indicates that bone deposition is not inherently tied to depositional mechanism. Potentially modified (per Bement 1986) faunal remains were recovered from both endogenic and exogenic strata.

8.2.3 *Distributional Modes*

Normal distribution modes are identifiable in both coarse- and fine- fraction particle size histograms illustrated in **Appendix A: Particle Size Distributions**. In coarse-fraction inclusive histograms, three modes are commonly expressed. **Table 8-3** reports the approximate distributional modes observed in each stratum. Modal peaks in the gravel fraction cluster around 4ϕ but become increasingly fine over time, trending towards -2ϕ in Stratum 20 and Bone Bed 2.

Secondary fine-fraction modes varied between 5ϕ (medium silt, 0.03 mm) and 6ϕ (fine silt, 0.016 mm). Distributions in this portion of the curve approached normal bell curves, with outliers regularly occurring around 8ϕ and 14ϕ . Sediments contributing to these curves are interpreted as aeolian deposition, though somewhat finer than the “ideal” aeolian particle size

between 3ϕ and 4ϕ (fine sand, 0.08mm) (Muhs 2014). “Noisy” sediments (i.e.: not normally distributed) and populations outside the aeolian band are thought to be the result of sheet wash.

Table 8-3. Modes visually estimated from parabolic distribution peaks in particle size histograms. Nothing approaching a normal distribution was observed in the S19 coarse gravel fraction.

Distributional Modes			
Stratum	Primary	Secondary	Tertiary
S19	–	6ϕ	0ϕ
S20	-2ϕ	5ϕ	0ϕ
S21	-3ϕ	6ϕ	0ϕ
S22	-4ϕ	5ϕ	0ϕ
S23	-4ϕ	5ϕ	0ϕ
S24	-4ϕ	6ϕ	0ϕ

The finer average aeolian particle size appears to be a function of the available source material. Rio Grande alluvium is the only significant sediment source in the vicinity of Mile Canyon (even earlier in the Holocene, the rocky regional uplands were likely denuded). The disaggregation of silt and clay aggregates during hydrometer particle size analysis may account for some of the “noise” in otherwise “normal” distribution patterns (Gale and Hoare 1991:71). Alternatively, the anomalous spikes may represent an influx of poorly sorted sheetwash material. However, in this scenario the very fine sediment spikes should be accompanied by additional evidence of poorly sorted material in the slightly coarser channels

Tertiary modes were present at 0ϕ (coarse sand, 1 mm) in all strata, typically presenting as well-defined, normal bell curves. Sediments associated with this population are attributed to water-borne transport mechanisms. Given the significant elevation of Bonfire Shelter, it is unlikely that any significant portion of these sediments entered the shelter via direct flooding from the Mile Canyon floor.

The recovery of rounded, exogenic coarse sand particles during microartifact processing reinforces the interpretation of tertiary modes as sheetwash events. The frequency of these particles is consistent with the low volumes indicated in the particle size histograms. It is

important to note that the majority of particles in this size range were angular limestone fragments, a reflection of the overlapping nature of these sediment populations. The consistent presence of 0ϕ modes all samples highlights the suitability of the 0ϕ class for microartifact analysis, providing a representative sample from the average particle size in this portion of the distributions while simultaneously capturing subsets of multiple sediment populations.

A single mode was observed in the gravel fraction in each stratum. The homogeneity of this material observed in the lab suggests that coarse fraction modal distributions represent endogenic roof spalling with limited post-depositional modification. Average spall size and the overall proportion of gravel in each stratum generally increases with depth. This increased exfoliation intensity is interpreted as increasingly cold and wet conditions during the Pleistocene. The habitability of the shelter during this period of shelter expansion was probably limited. However, the rapid accumulation of sediment and limited exogenic deposition suggests that faunal remains and other materials in these strata could become buried relatively quickly, limiting their susceptibility to scattering.

8.3 Carbon Content

Table 8-4 presents the results of the various carbon determinations used to evaluate the Column Sample 5 strata. Organic carbon and calcium carbonate (CaCO_3) were measured using Loss on Ignition. Devils River Formation limestone is composed of 98% calcium carbonate. CaCO_3 detected in the sediment samples is likely directly exfoliated from this parent material. Organic carbon measures the amount of carbon-based plant, animal, and microorganism matter present in a soil or sediment.

The proportion of calcium carbonate measured using Loss on Ignition is likely skewed due to significant gypsum and smectite clay in each stratum. Gypsum is a hydrated mineral that readily binds water molecules to its base CaSO_4 base. Despite drying samples overnight and

cooling in a moisture-free desiccator, the samples immediately began reabsorbing water when exposed to the atmosphere while weighing. The presence of unknown quantities of other hydrated, combustible, or otherwise volatile at low temperature minerals compounds potential Loss on Ignition error.

CaCO₃ content was verified using a volumetric calcimeter method (Chittick apparatus) as well as XRD, which reports the proportion of calcite in each sample among other detected minerals. Percent CaCO₃ derived from Chittick and XRD are very similar in the Bone Bed 1 strata with some divergence in Bone Bed 2 (0.5% in S24 to 9.1% in S19). LOI determination follows a somewhat similar curve trajectory, but at significantly lower percentiles than XRD and Chittick methods. Values ranged from nearly 25% at the base of excavation, dropping below 20% in the intermediate horizons, and increasing back to approximately 25% CaCO₃ in the upper strata of Bone Bed 2. The XRD CaCO₃ measurements ranged from over 60% in S24 and the upper Bone Bed 2 strata (S19 and S20) but drop below 50% in the intermediate horizons. The implications of these data are discussed on a stratum by stratum basis in **Section 8.9**, below. As a direct, quantitative measure, Chittick CaCO₃ content is utilized as the more precise measure.

Table 8-4. Compiled results of carbon content determinations calculated using differential weight loss methods (LOI), volumetric calcimeter (Chittick), X-ray diffraction - calcite content, and KEPSIL Elemental Analyzer.

Carbon Content							
Stratum	Differential Weight Loss (LOI)			Chittick	XRD	KEPSIL EA	
	% Organic Carbon	% Carbonate	% Gypsum	CaCO3 Equivalent	Calcite	% Organic Carbon	13C VPDB (Organic Carbon Stable Isotope)
S19	3.5934	26.1156	2.4713	72.6	63.5	2.6	-22.70
S20	2.7932	24.6841	4.2447	70.6	60.3	1.3	-22.71
S21	2.8806	20.1812	4.2367	57.0	48.1	0.3	-22.72
S22	2.4052	19.7444	5.9944	52.1	44.9	0.3	-23.20
S23	2.7399	17.3068	5.8873	47.2	41.4	0.3	-23.55
S24	3.3519	24.0629	8.1377	63.1	62.6	1.59	-25.99

8.4 Gypsum Determination

Gypsum (CaSO_4) is a commonly observed trace mineral in the Mile Canyon rockshelter deposits. The white (10YR8/1) to very pale brown (10YR8/2) fine silt coating observed adhering to gravel, faunal remains, and as nodules up to 1.0 cm (0.4 in) in diameter in the Bone Bed 1 strata. The powder and nodules were initially thought to be precipitated calcium carbonate. Using the Differential Water Loss (DWL) method outline by Artieda et al. (2006), the nodules were determined to be over 50% gypsum. **Figure 8-5** illustrates the percentage of gypsum in each stratum. Sample LS005a represents a large (approximately 1.0 cm [0.4 in], 19.1996 g) gypsum nodule identified in S23. Using this method, gypsum content consistently increases with depth, with S24 containing nearly four times the amount of gypsum as S19. This pattern is clearly visible in the profile illustrated in **Figure 7-4**, above.

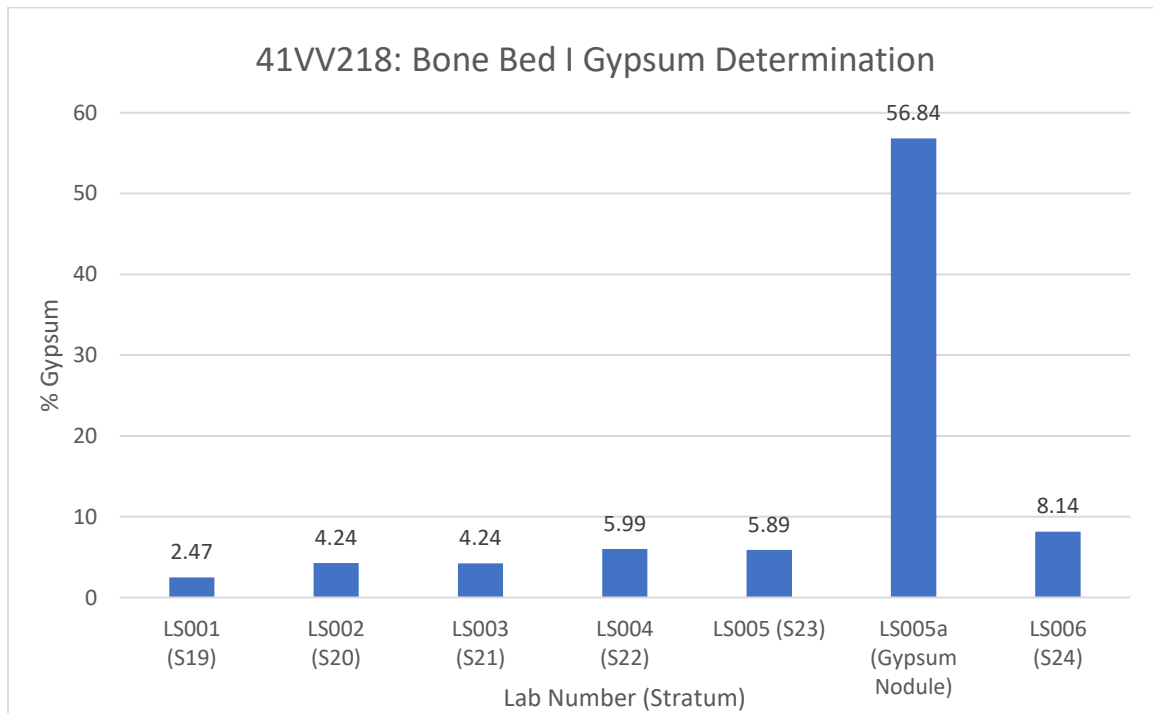


Figure 8-5. Gypsum content of Bone Bed 1 strata calculated using the Differential Water Loss method (Artieda et al. 2006).

To assess error from unknown hydrates, the proportion of calcium sulphate minerals detected during XRD analysis were compared to the calculated DWL gypsum content. **Figure 8-6** and **Table 8-5** illustrate the percentage of anhydrite, bassanite, anhydrite + bassanite (via XRD), and gypsum (via differential water loss). Gypsum, anhydrite, and bassanite share a common CaSO_4 base. Anhydrite holds no molecular water, but readily hydrates when exposed to environmental moisture. Gypsum holds two water molecules ($\text{CaSO}_4 \cdot 2\text{H}_2\text{O}$) while bassanite splits one water molecule with another base calcium sulphate ($\text{CaSO}_4 \cdot \frac{1}{2}\text{H}_2\text{O}$). The quantity of bassanite plus anhydrite was expected to approach the DWL calculated gypsum content.

Table 8-5. Comparison of XRD and Differential Weight Loss methods for gypsum determination in Column Sample 5 strata.

Gypsum Content					
Stratum	LOI	XRD (% Mass)			% Difference
	% Gypsum	% Anhydrite	% Bassanite	% Anhydrite + Bassanite	
S19	2.4713	0.3	0.6	0.9	1.57
S20	4.2447	0.3	0.6	0.9	3.34
S21	4.2367	0.4	0.9	1.3	2.94
S22	5.9944	0.8	2.2	3	2.99
S23	5.8873	0.4	1.3	1.7	4.19
S24	8.1377	0.6	2.2	2.8	5.34

Both XRD and DWL methods show a general increase in gypsum content with depth. However, discrepancies are apparent, with XRD measuring between 1.5 and 5% and increasing with depth. The presence of unknown materials that evolve water, combust, or otherwise change state at temperatures similar to gypsum can skew DWL measures. XRD is a semiquantitative method with results reported relative to the other minerals detected in the samples, which may not be precise for trace minerals.

Despite these discrepancies, the trend observed in both methods suggests that the gypsum may be post-depositional in nature. Evaluated from another perspective, the linear DWL trend indicates gypsum content decreases with distance above the bedrock. As a water-soluble mineral,

elevated gypsum levels indicate higher moisture content and/or repeated exposure over time. The correlation of gypsum with depth suggests that moisture content or hydrological activity is confined to the deeper strata. It is possible for gypsum to percolate through the sediment column in-solution. However, its concentration at depth suggests that the source moisture may be derived from seeps along the underlying bedrock. Combined with the corrosive effect of gypsum itself, increased moisture content would also account for the poor condition of faunal remains in this stratum.

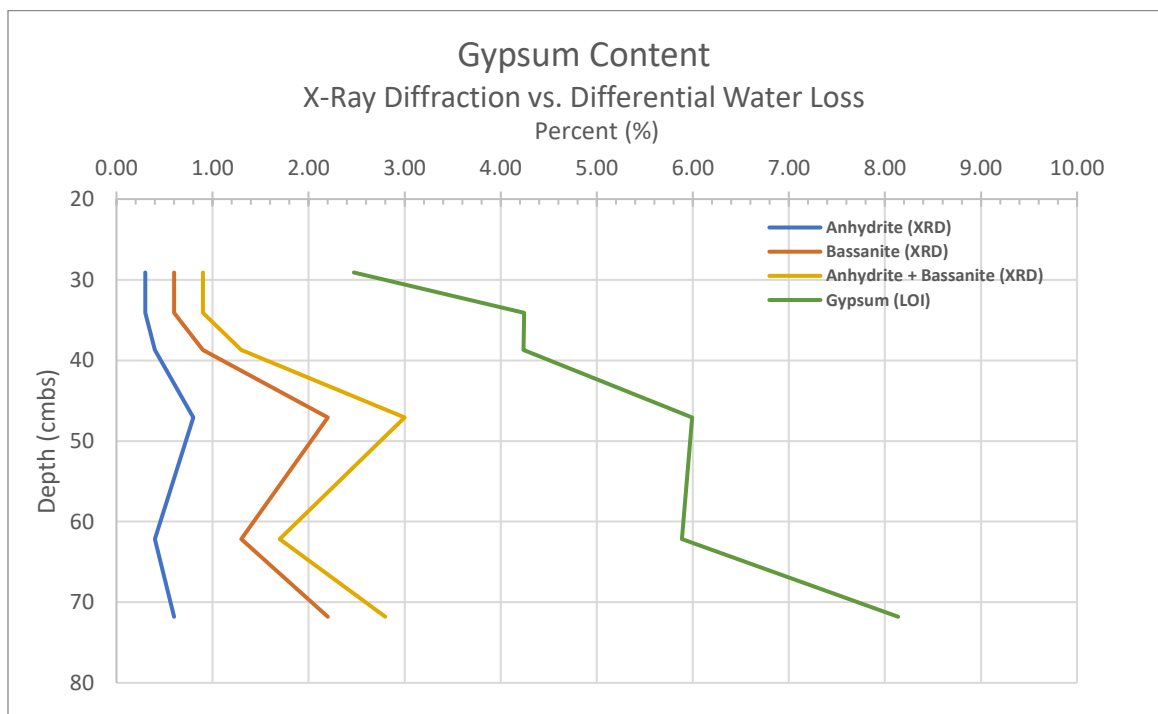


Figure 8-6. Gypsum Content: XRD (Anhydrite & Bassanite) vs. Differential Water Loss.

8.4.1 *Gypsum Sources*

The Cretaceous limestone bedrock of the Lower Pecos is overlain in many areas by Eagle Ford Shale. In addition to its valuable oil and gas resources, the deposit is rich in sulfide minerals. The weathering of Eagle Ford Shales in the presence of calcium, a major component of the underlying limestone in the form of calcium carbonate (CaCO_3), may lead to the formation of gypsum (Frederick 2017b:10-13; Harbor 2011; Lock and Wawak 2010).

Gypsum salt weathering is thought to play a significant role in the formation of the Mile Canyon rockshelters. As gypsum precipitates out of solution across the karstic parent material, crystals begin to form in crevices and irregularities. Gypsum crystal formation (in addition to cryoclastic activity, karstic dissolution, and aeolian scouring) forces spalls from canyon facies and contributes to dynamic shelter morphologies. Tafoni, the characteristic honeycombed or sponge-like pores on the surface of rock outcrops, are clearly visible at many of the region's rockshelters. **Figure 8-7**, below, illustrates tafoni weathering features at the White Shaman Site near the confluence of the Pecos River and the Rio Grande a short distance downstream from Mile Canyon, Val Verde County, Texas.



Figure 8-7. Example of Tafoni weathering features at the White Shaman Site, Val Verde County, Texas.

Increased gypsum precipitation in the deeper Bonfire Shelter strata also contributes to the poor faunal preservation. Abundant tafoni features clearly illustrate the mineral's corrosive capabilities. Gypsum's crystalline structure has been described as "fang-" or "lath-like", potentially contributing to the cortical exfoliation observed in the Bone Bed 1 faunal assemblage (High et al. 2018; Paz and Rossetti 2006). The elements exposure to the atmosphere subsequent

drying upon excavation catalyzes further precipitation, exacerbating damage to the materials. The presence of gypsum precipitates also suggests hydrological activity within the deposits. Gypsum-saturated water entering the shelter via the notch and canyon rim may percolate through the sediments and precipitate out in the low-lying Bone Bed 1. Additional analysis of the Holocene-age deposits is necessary to confirm this. Gypsum saturated ground water infiltrating the deposits via the bedrock from below could also account for the patterns observed in Bone Bed 1.

8.5 Organic Carbon

Table 8-6 and **Figure 8-8** illustrate the results of LOI- and KPESIL Elemental Analyzer-based organic carbon determinations in across the Column Sample 5 strata. Like other differential weight-loss methods, LOI yields a proxy measure of the organic component that is readily skewed by the inclusion of hydrated minerals. The KPESIL analysis is a direct measure of the organic component and is considered the more reliable dataset. The parabolic curve clearly illustrates much higher organic carbon levels in bone bed strata than non-bone bed strata

Table 8-6. Comparison of Column Sample 5 organic carbon content as determined via loss on ignition and KEPSIL Elemental Analyzer.

Organic Carbon Content			
Stratum	LOI	KPESIL	Organic Carbon % Difference
	% Organic Carbon	% Organic Carbon	
S19	3.59	2.6	0.98
S20	2.79	1.3	1.54
S21	2.88	0.3	2.59
S22	2.41	0.3	2.11
S23	2.74	0.3	2.44
S24	3.35	1.59	1.76

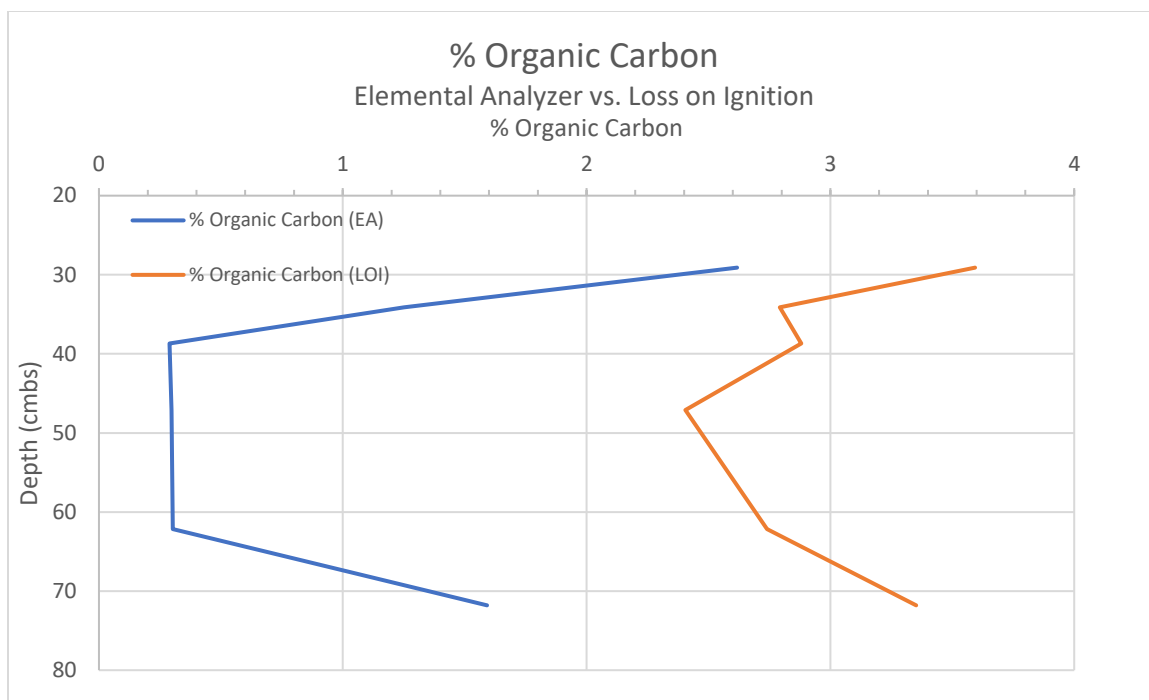


Figure 8-8. Comparison of Organic Carbon Determination Methods: Elemental Analyzer vs. Loss on Ignition.

As a protected rockshelter with limited internal plant growth or pedogenic activity, all organic carbon should be derived from exogenic processes. The organic carbon trend illustrated here roughly correlates with estimates for exogenic deposition reported in **Section 8.7**, below. However, this model does not appear to account for all variables. Based on its elevated clay content, Stratum 23 and the similarly clayey Stratum 21 were expected to yield the highest organic carbon levels in the column sample. This was based on the expectation that organic carbon would largely be derived from plant matter introduced via wind or sheet wash and contributing to the melanization of the sediments (Birkeland 1999).

The highest organic carbon levels were detected in Stratum 24 and 19, which also had the lowest estimated exogenic deposition and were among the lightest colored sediments. This suggests that the organic matter is not derived from plant matter. The large-scale bison harvest provides a clear source for the influx of organic matter in Bone Bed 2. Especially considering the subsequent decomposition and incineration of the remains as well as the human activities associated with the kill. The accumulation of megafauna remains in Stratum 24 provides a

potential source of organic matter independent of exogenic transport processes. Scavenging and scattering of the remains, by humans or carnivores, could distribute organic residues across the shelter. Like human habitations, carnivore denning behavior may further enrich sediments via the ongoing introduction of animal remains and the accumulation of excrement. This theory does not account for the abrupt organic carbon decrease in Stratum 23, which is also associated with a substantial accumulation of Pleistocene fauna.

8.6 $\delta^{13}\text{C}$ Stable Isotopes

In addition to calculating the proportion of organic carbon in each sample, KEPSIL measures $^{12}\text{C}/^{13}\text{C}$ fractionation in the CO_2 evolved from organic residuals following the chemical dissolution of calcium carbonate from the specimens. **Table 8-7** and **Figure 8-9** summarize the results of this analysis. As discussed in **Chapter 5** $\delta^{13}\text{C}$ is generally associated with changes in the regional plant community contributing organic carbon to the local ecosystem: lower $\delta^{13}\text{C}$ values indicate a greater proportion of C3 plants, while higher $\delta^{13}\text{C}$ values reflect growing numbers of C4 grasses (Ehleringer and Monson 1993). Even if plant matter is not directly incorporated into a sediment, the incorporation of faunal organic residues can impact stable isotope concentrations. Herbivores inherit the isotope ratios of the plant communities they consume, elevating overall isotope concentrations but maintaining the same ratios. Carnivores that subsequently consume those herbivores further concentrate the heavier isotopes in their bodies (Nordt 2001; Schoeninger and DeNiro 1984).

Table 8-7. Tabularized Column Sample 5 Stable Isotope Ratios.

Stable Isotope Analysis					
Stratum	$\delta^{15}\text{N}$ vs. Air	$\delta^{13}\text{C}$ vs. VPDB	N%	C%	C/N
Stratum 19	10.57	-22.70	0.31	2.6	8.5
Stratum 20	12.16	-22.71	0.17	1.3	7.6
Stratum 21	10.65	-22.72	0.05	0.3	5.7
Stratum 22	11.50	-23.20	0.05	0.3	6.3
Stratum 23	9.97	-23.55	0.05	0.3	6.1
Stratum 24	13.65	-25.99	0.13	1.59	12.3

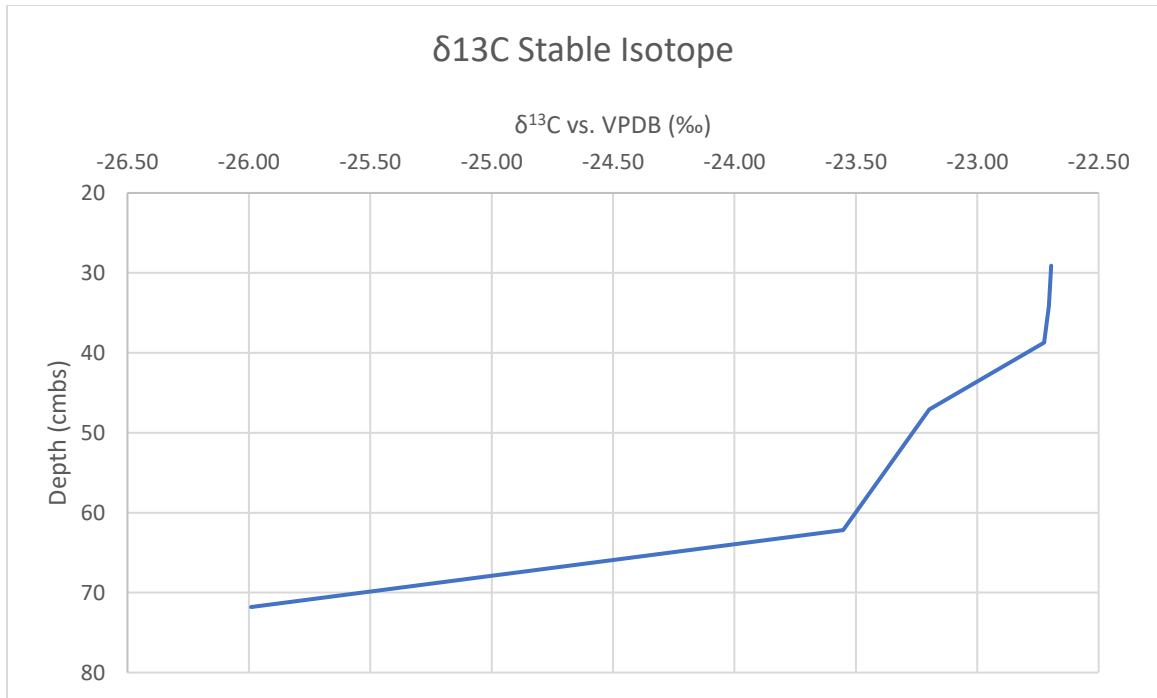


Figure 8-9. $\delta^{13}\text{C}$ versus Vienna Pee Dee Belemnite (parts per thousand (‰)) as determined by the University of Kansas KEPSIL for each PS06.CS05 stratum.

The $\delta^{13}\text{C}$ values increase consistently from Stratum 24 at approximately -26‰ through Stratum 19 at around -23‰. This pattern is generally consistent with other paleoenvironmental studies conducted throughout Southcentral Texas. Nordt's analysis of soil organic carbon at Applewhite Reservoir (Nordt et al. 2002) correlated $\delta^{13}\text{C}$ values with key climatic events over the past 15,000 years. Stratum 24 (~14,000 cal BP) coincides with the lowest $\delta^{13}\text{C}$ levels measured at the reservoir (~-25‰), driven by a massive glacial meltwater pulse which lowered regional temperatures up to 2°C and caused a large-scale decline in C4 plant communities. $\delta^{13}\text{C}$ measured -25.99‰ at Stratum 24, somewhat lower than the Applewhite measurements.

The Bone Bed 2 strata (S19, S20, and S21) date to the Younger Dryas, roughly 12,000 cal BP. Nordt notes that on the South Texas Plains, the Younger Dryas was characterized by elevated temperatures and a substantial expansion of C4 grasses to near modern levels as glacial meltwater from the retreating Laurentide Ice Sheet was routed to the North Atlantic rather than

the Gulf of Mexico. $\delta^{13}\text{C}$ levels associated with the Younger Dryas measured roughly -19‰ at Applewhite Reservoir (Nordt et al. 2002:185-186) and roughly -22.7 at Bone Bed 2.

Stratum 22 falls between these two extremes at -23.2‰, possibly a local expression of a brief period of C4 decline visible in Nordt's $\delta^{13}\text{C}$ plot. Stratum 22 is the only stratum where actual carnivore remains were recovered at Bonfire Shelter. It is possible that the elevated $\delta^{13}\text{C}$ is the result of trophic-level heavy isotope concentration, however there is no evidence that would suggest wide-spread exploitation of Bonfire Shelter as a carnivore den.

This comparison is not perfect, Applewhite is located farther east than Bonfire Shelter and is derived from very different formation processes. Despite this, Applewhite provides a continuous organic carbon profile derived from environmental organic carbon that parallel's Bonfire Shelter's depositional history. The sequence provides a valuable comparative resource that can be used to help identify the source of Bonfire Shelter's organic carbon. Any organic carbon at Bonfire Shelter must be exogenic in origin. Comparing the Bonfire isotopic fractionation to Applewhite's profile can help to determine if the organic carbon within the shelter is derived from the deceased megafauna, secondary carnivores/scavengers, or plant matter. Assessing potential trophic level increases versus the expected C3/C4 plant community profiles from Applewhite may clarify the source of organic material in Bone Bed 1.

8.7 X-Ray Diffraction Mineralogy

X-ray diffraction (XRD) was used to determine to composition of sediments recovered from Column Sample 5. Based on the results of geoarchaeological assays described above, substantial quantities of calcium carbonate and gypsum were expected. Particle size distributions suggest that exogenic processes may contribute variable amounts of sediment to each stratum. By identifying specific exogenic minerals within each stratum, it may be possible to determine the source of those sediments.

Figure 8-10 and **Table 8-8** summarize the mineralogy of each Column Sample 5 stratum. **Figure 8-11** and **Table 8-9** specifically report the composition of the clay fraction (<4 μm , 8ϕ). **Figure 8-12** and **Table 8-10** summarize the composition of the Devils River Formation limestone parent material submitted as a control sample. The minerals identified within the limestone were used to roughly estimate the proportion of exogenic to endogenic sediment for each stratum in **Table 8-11**. XRD analyses are semi-quantitative measures of mineral composition. Results are reported as percent by mass of each constituent mineral.

Clay fraction results in **Table 8-9** and **Figure 8-11** are presented as relative proportions of the total sample mass (rather than the proportions of only the clay fraction mass) to facilitate direct comparison between the two data sets. Specific clay fraction minerals represent a very small portion of entire sample. Breaking these out into separate tables highlights variation within this size class that might be obscured on the overall composition chart.

Calcite is the primary mineral component of each analyzed stratum, ranging from 63.5% to 41.4 %. Other minerals comprise small percentages of the total sample mass. Quartz is the second most abundant single mineral, followed by kaolinite, chlorite, plagioclase and potassium feldspar, illite/smectite mixed-layer clays, bassanite and anhydrite, apatite, and hematite. Calcite content decreases proportionally with increases in quartz, feldspar/plagioclase, and clay minerals. This trend mirrors the results of carbonate determinations and particle size distributions. Gravel content is typically replaced with a proportional increase in fine fraction sediments. These minerals represent the mineral composition of those exogenic sediments.

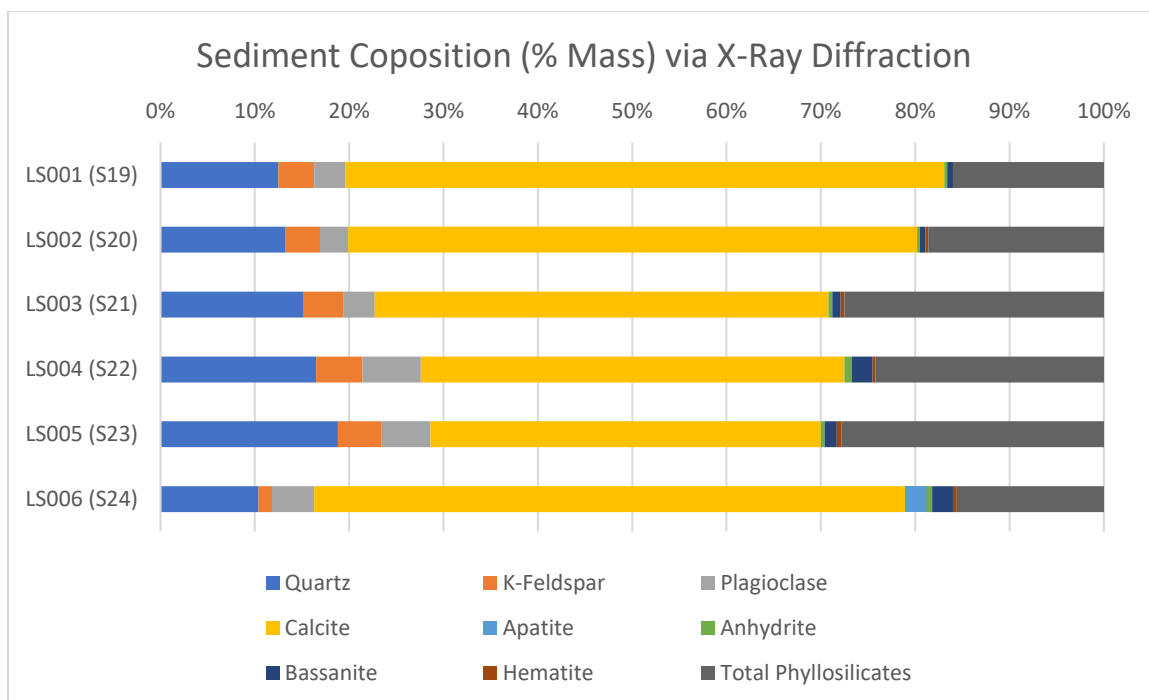


Figure 8-10. Column Sample 5 mineralogy by stratum, as determined by XRD. Reported values represent the relative proportions by mass of each constituent component.

Table 8-8. Column Sample 5 sediment mineralogy by stratum, as determined by XRD. Values represent the relative proportions of each constituent component.

Lab Sample	Quartz	K-Feldspar	Plagioclase	Calcite	Apatite	Anhydrite	Bassanite	Hematite	Total Phyllosilicates	Total
LS001 (S19)	12.5	3.8	3.3	63.5	0	0.3	0.6	0	16	100
LS002 (S20)	13.2	3.7	3	60.3	0	0.3	0.6	0.3	18.6	100
LS003 (S21)	15.1	4.3	3.3	48.1	0	0.4	0.9	0.4	27.5	100
LS004 (S22)	16.5	4.9	6.2	44.9	0	0.8	2.2	0.3	24.2	100
LS005 (S23)	18.8	4.6	5.2	41.4	0	0.4	1.3	0.5	27.8	100
LS006 (S24)	10.4	1.4	4.5	62.6	2.3	0.6	2.2	0.4	15.6	100

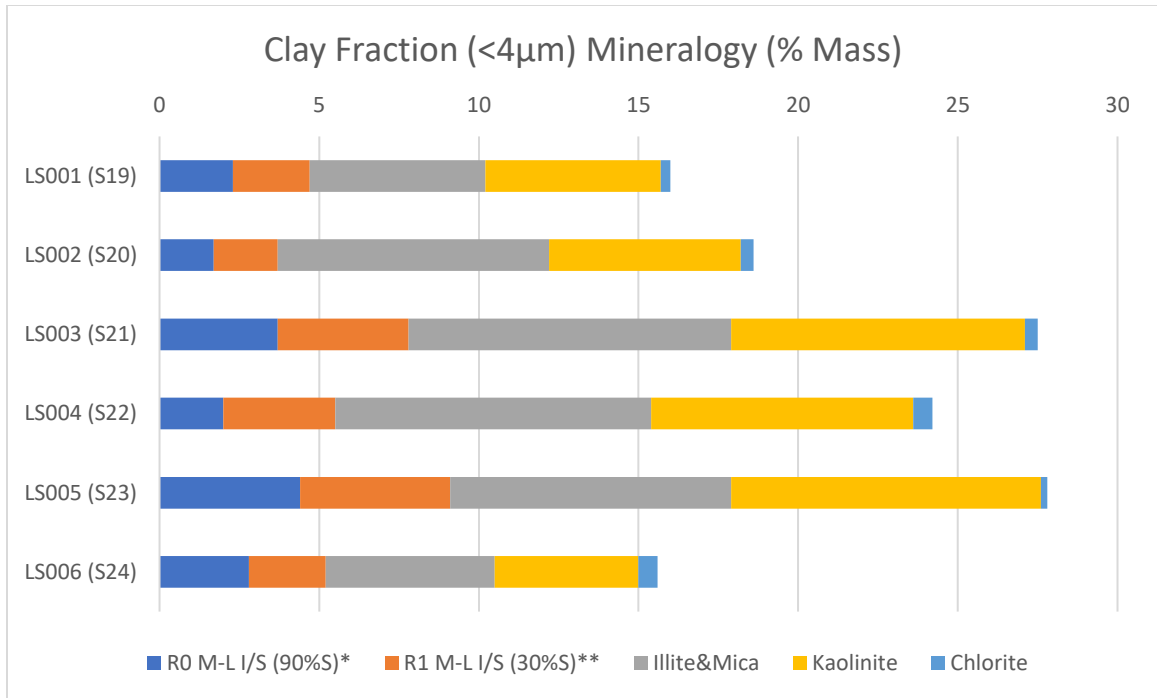


Figure 8-11. Column Sample 5 clay fraction (<4μm) mineralogy as a percentage of total sediment sample by mass. R0 M-L I/S (90%) represents the proportion of Mixed-Layer clays composed of 90% smectite/10% illite. R1 M-L I/S (30%S) represents Mixed-Layer clays composed of 30% smectite/70% illite.

Table 8-9. Column Sample 5 clay fraction (<4μm) mineralogy as a percentage of total sediment sample mass. R0 M-L I/S (90%) represents the proportion of Mixed-Layer clays composed of 90% smectite/10% illite. R1 M-L I/S (30%S) represents Mixed-Layer clays composed of 30%

Lab Sample	R0 M-L I/S (90%S)	R1 M-L I/S (30%S)	Illite & Mica	Kaolinite	Chlorite	Total
LS001 (S19)	2.3	2.4	5.5	5.5	0.3	16.0
LS002 (S20)	1.7	2.0	8.5	6.0	0.4	18.6
LS003 (S21)	3.7	4.1	10.1	9.2	0.4	27.5
LS004 (S22)	2.0	3.5	9.9	8.2	0.6	24.2
LS005 (S23)	4.4	4.7	8.8	9.7	0.2	27.8
LS006 (S24)	2.8	2.4	5.3	4.5	0.6	15.6

8.7.1 Limestone Control Sample

At 98.2%, calcite dominates the limestone mineral profile. The remainder (1.8%) is composed of trace quantities (<1%) of acid-insoluble quartz, kaolinite, illite/mica, and hematite. As a marine sedimentary stone, quartz, illite, and/ kaolinite were not unexpected components of the Devils River Formation limestone. Clay minerals incorporated into the bedrock may have

been subjected to in situ weathering and modification prior to sedimentation. K-Feldspar (potassium feldspar) and plagioclase (another variety of feldspar) are volcanic minerals not found in the Devils River formation and clear markers for exogenic deposition. As noted in **Chapter 5.4**, outwash from the volcanic formations of the Trans-Pecos and the Rocky Mountains on the Upper Rio Grande are an abundant source of non-local material in Lower Pecos rockshelters. The origins of other apatite, anhydrite, bassanite, mixed-layer clays, and chlorite are more ambiguous.

Hematite was an unexpected limestone mineral and appears to be somewhat problematic; it was only detected in the acid insoluble fraction. At 0.8% (9.9 mg) of the acid insoluble fraction, it is possible that hematite was below the minimum detection threshold or overshadowed by the comparatively enormous curves for calcite and other mineral components in the bulk limestone analysis. Hematite would only represent 0.014% of the bulk limestone sample mass (70.34 g). Illite/mica, the next smallest mineral component, represents 0.2% of the bulk limestone sample and 3.3% of the acid insoluble fraction.

If all illite/mica, kaolinite, and hematite and 1% of all quartz (per the control sample) are derived from the limestone parent material, an average of 69.1% of all <2mm sediment within each stratum is endogenic while 30.9% originates from exogenic sources. **Figure 8-13** and **Table 8-11** summarize the proportion of endogenic vs. exogenic material from each stratum. The presence of more quartz in the sediment samples than could be derived exclusively from limestone degradation highlights that “endogenic” minerals may be supplemented with mineralogically similar exogenic material, resulting in a known degree of error in these estimations. Despite this, the estimates provide a rough quantification for the exogenic material suggested by the other geoarchaeological methods. Deviations from the mineral. Deviations from the mineral profile observed in the limestone control sample can generally be attributed to exogenic formation processes.

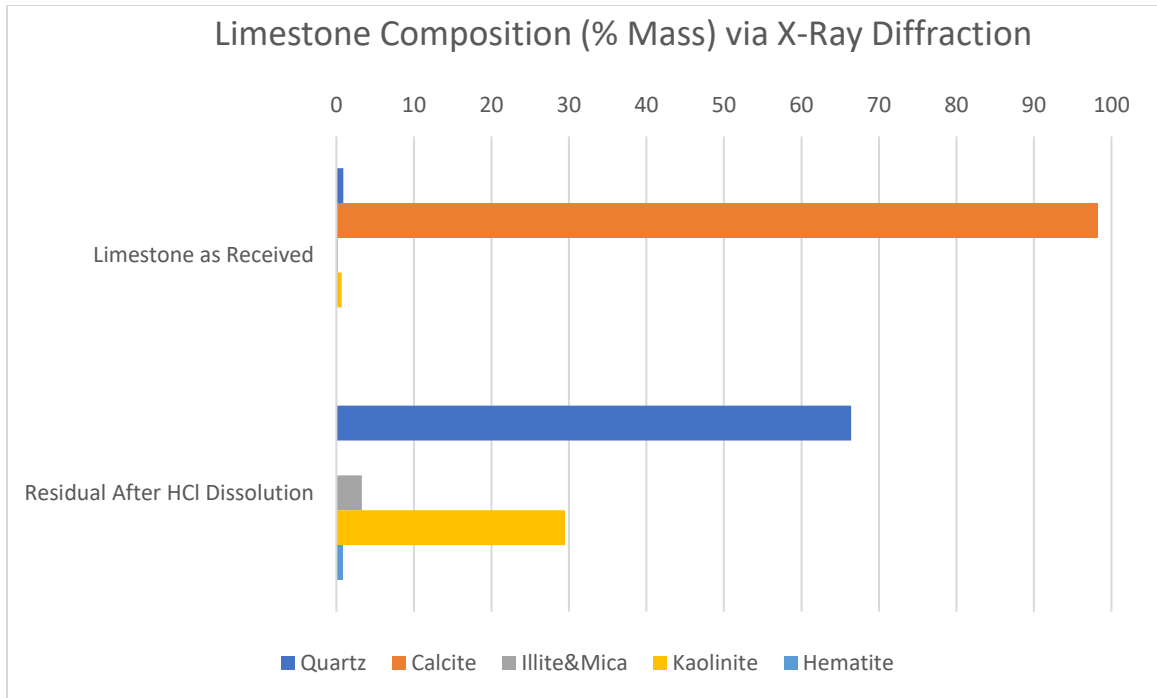


Figure 8-12. Limestone Mineralogy pre- and post-dissolution in HCl

Table 8-10. Limestone and HCl insoluble residual mineralogy.

Mineral	Bulk Limestone (% Mass)	HCl Insoluble Residual (% Mass)
Quartz	0.9	66.4
Calcite	98.2	0
Illite & Mica	0.2	3.3
Kaolinite	0.7	29.5
Hematite	0	0.8
Total %	100	100
Total Mass (g)	70.34g	1.24g

Table 8-11. Proportion of Endogenic vs. Exogenic <2 mm sediments assuming all calcite, illite/mica, kaolinite, hematite, and 1% of all quartz are derived from limestone parent material.

Lab Sample	% Endogenic	% Exogenic
LS001 (S19)	74.625	25.375
LS002 (S20)	75.232	24.768
LS003 (S21)	67.951	32.049
LS004 (S22)	63.465	36.535
LS005 (S23)	60.588	39.412
LS006 (S24)	72.904	27.096
Average Composition	69.1275	30.8725

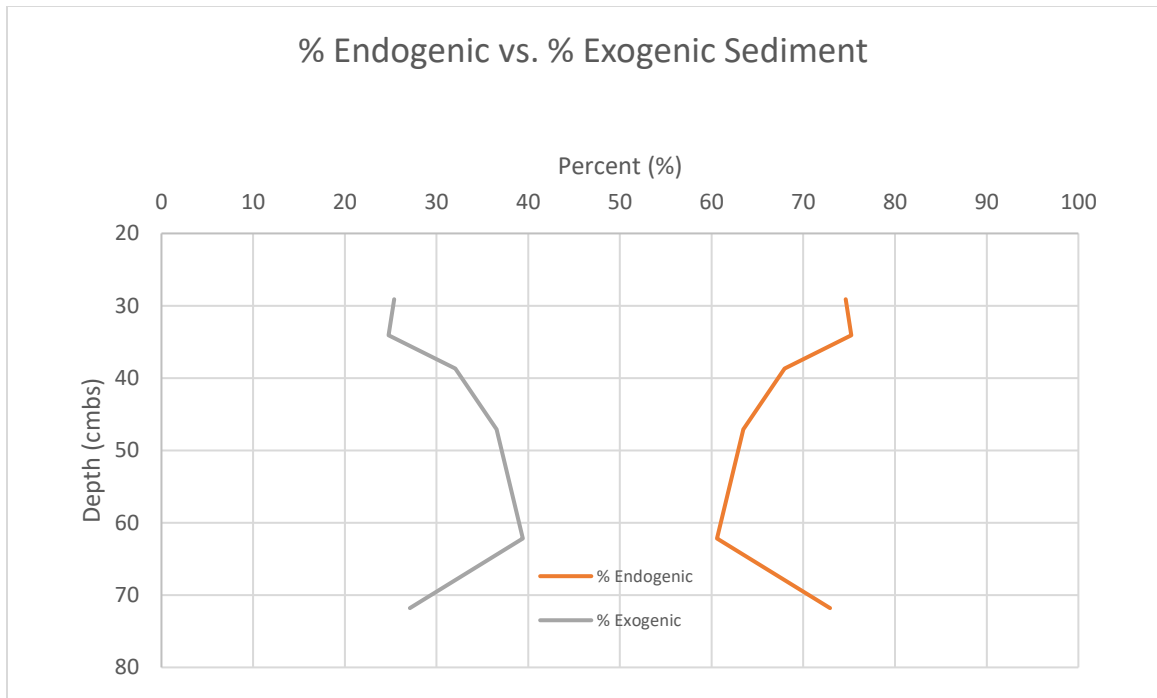


Figure 8-13. Proportion of Endogenic vs. Exogenic <2.0 mm sediment. Calculations assume all calcite, illite/mica, kaolinite, hematite, and 1% of quartz is derived from limestone parent material.

8.8 *Magnetic Susceptibility*

Figure 8-14 illustrates the change in χ_{LF} and χ_{HF} through the PS06.CS05 strata. **Figure 8-15** illustrate the χ_{FD} , variation between χ_{LF} and χ_{HF} , for the same samples. **Table 8-12** presents these data in tabular form. χ values and χ_{FD} are both lowest in Stratum 24. χ values are highest in Stratum 22, while χ_{FD} is highest in Stratum 20. **Figure 8-16**, **Figure 8-17**, and **Figure 8-18** illustrate the relationship between magnetic susceptibility and key site formation process proxy measures including carbonate content, particle size, particle sorting, and diagnostic exogenic minerals.

Hematite, the only antiferromagnetic mineral detected during the XRD study, was detected at consistently low levels throughout the column sample (Gale and Hoare 1991). The minor variations in hematite concentration do not follow the mass susceptibility trends presented below. However, magnetic susceptibility appears to be generally well correlated with other exogenic mineral accumulations detected via XRD including feldspars and phyllosilicate clay minerals.

8.8.1 *Mass Susceptibility*

Illustrated in **Figure 8-16**, mass susceptibilities are inversely related to calcium carbonate content (plotted versus volumetric calcimeter results). This relationship indicates that the accumulation of magnetic (or magnetically susceptible) minerals is independent of the endogenic processes that drive carbonate accumulation within the shelter. Feldspars (k-feldspar and plagioclase), illustrated in **Figure 8-17** and **Figure 8-18**, follow the same trend as mass susceptibilities: increasing from Stratum 24 to Stratum 22 and decreasing from Stratum 22 to Stratum 19. Feldspars were not detected in the limestone control sample, suggesting a positive relationship between exogenic material and magnetic susceptibility. As noted in the carbon and compositional analyses above, endogenic and exogenic processes appear to vary independently

based on different environmental conditions; a shift in endogenic deposition does not necessarily receive an equal and opposite exogenic counterpoint.

8.8.2 *Frequency Dependent Susceptibility*

Figure 8-18, below, provides a higher resolution comparison of <2mm particle size and sorting to feldspar content and χ_{FD} . At a smaller scale, the well-defined inverse relationship between χ and sorting becomes clear. This is slightly confusing in that larger ϕ values correspond with smaller actual particle sizes, while larger χ values represent actual increases in susceptibility.

In terms of Column Sample 5, particle size (increasing ϕ) generally decreases with χ_{FD} . Better sorted strata (decreasing ϕ) correspond with higher χ_{FD} . The relationship between sorting and χ_{LF}/χ_{HF} follows a similar pattern but is not as tightly correlated. Generally, χ values decrease as ϕ values increases for both sorting (more poorly sorted) and mean particle size (smaller particles). The relationship becomes skewed approaching Stratum 24, where χ_{LF}/χ_{HF} decrease significantly and χ_{FD} drops below zero in conjunction with increasing particle size, substantially increased gravel content, and significant decreases in the amount of exogenic material.

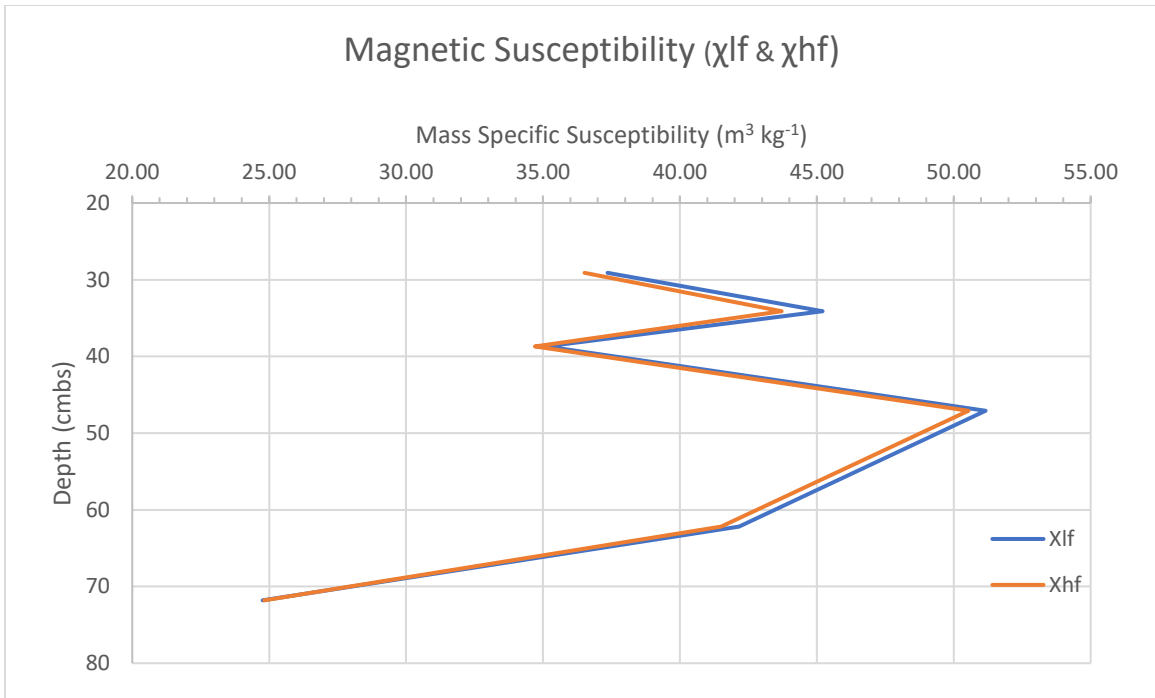


Figure 8-14. Column Sample 5 Mass Specific Magnetic Susceptibilities (χ_{lf} & χ_{hf}).

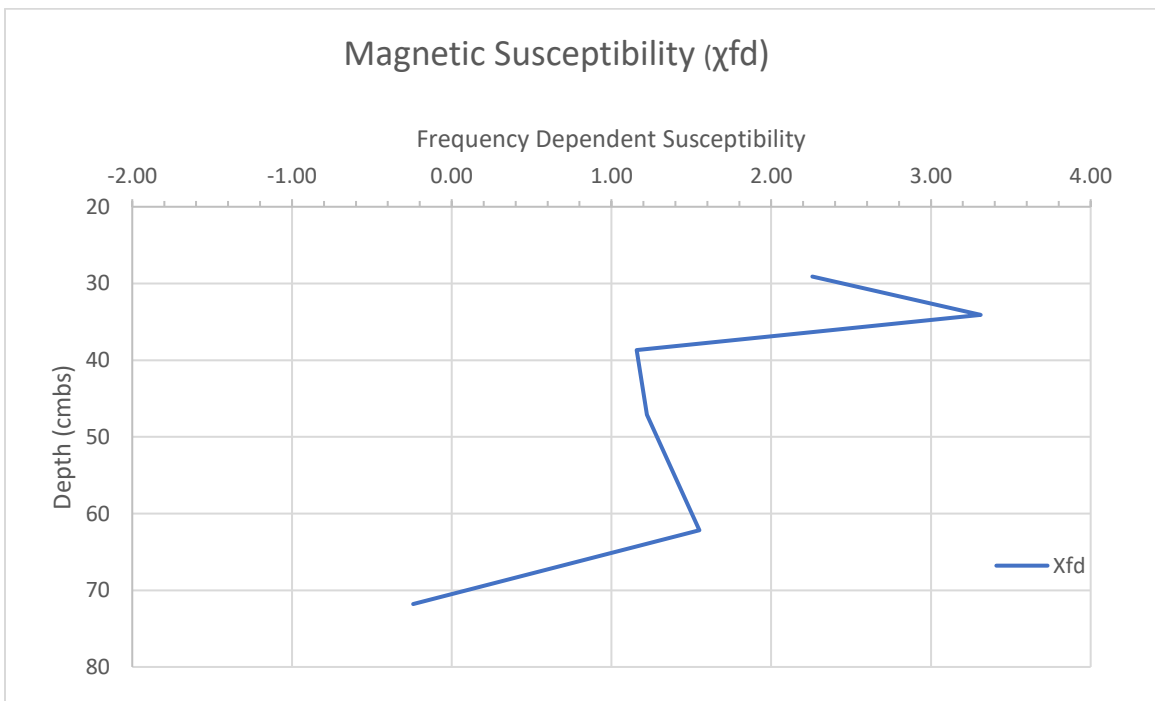


Figure 8-15. Column Sample 5 Mass Corrected/Frequency Dependent Magnetic Susceptibilities (χ_{fd})

Table 8-12. Column Sample 5 Mass Specific Magnetic Susceptibilities and Coefficient of Frequency Dependency

Lab Sample	χ_{LF} ($m^3 kg^{-1}$)	χ_{HF} ($m^3 kg^{-1}$)	X_{FD}
LS001 (S19)	37.36	36.51	2.26
LS002 (S20)	45.21	43.71	3.31
LS003 (S21)	35.11	34.71	1.16
LS004 (S22)	51.16	50.54	1.22
LS005 (S23)	42.16	41.51	1.55
LS006 (S26)	24.76	24.82	-0.24

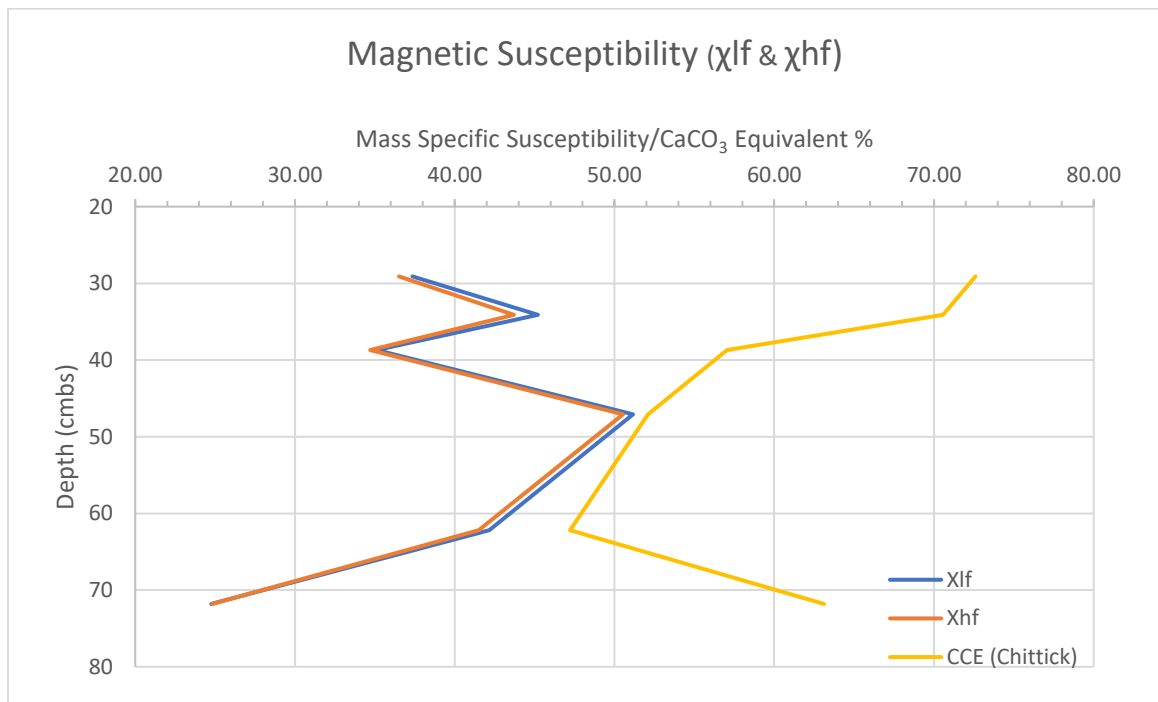


Figure 8-16. Column Sample 5 Mass Corrected Susceptibility versus Volumetric Calcimeter Calcium Carbonate Content (calcium carbonate equivalent).

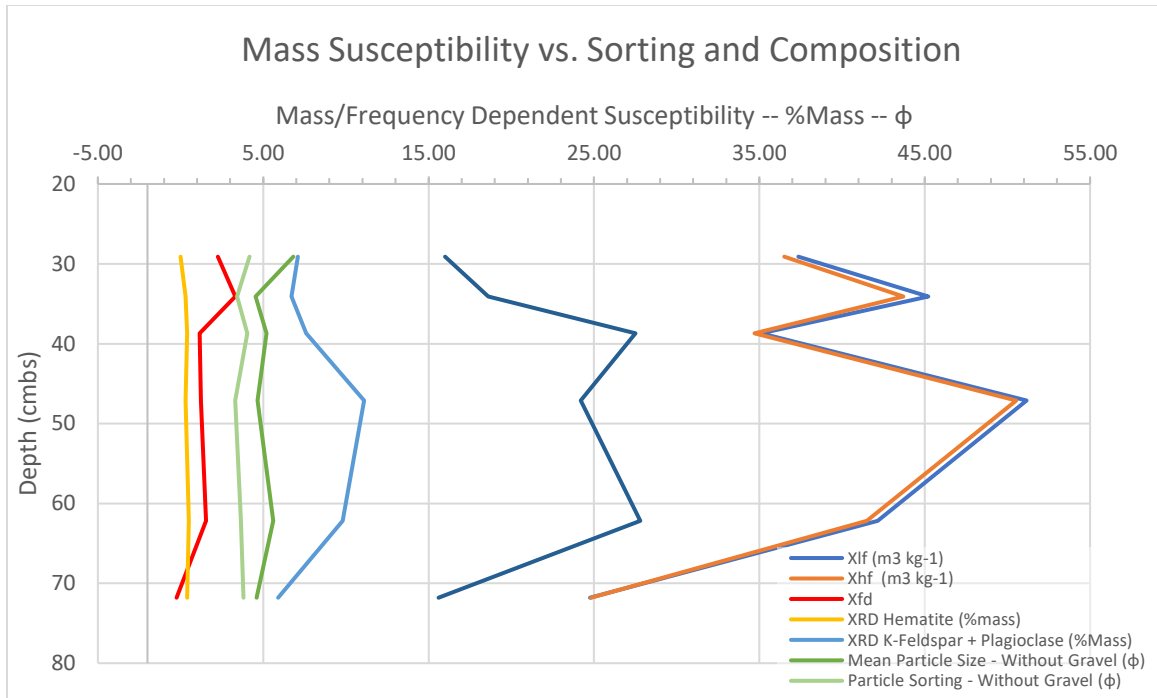


Figure 8-17. Column Sample 5 Mass Susceptibility versus Sorting and Composition. Variables include feldspars (k-feldspar and plagioclase) and total clay minerals (via XRD -- %mass), <2mm mean particle size and sorting (ϕ), and coefficient of frequency dependency. X-axis units vary by data series. Figure designed to illustrate curve variation and relationships.

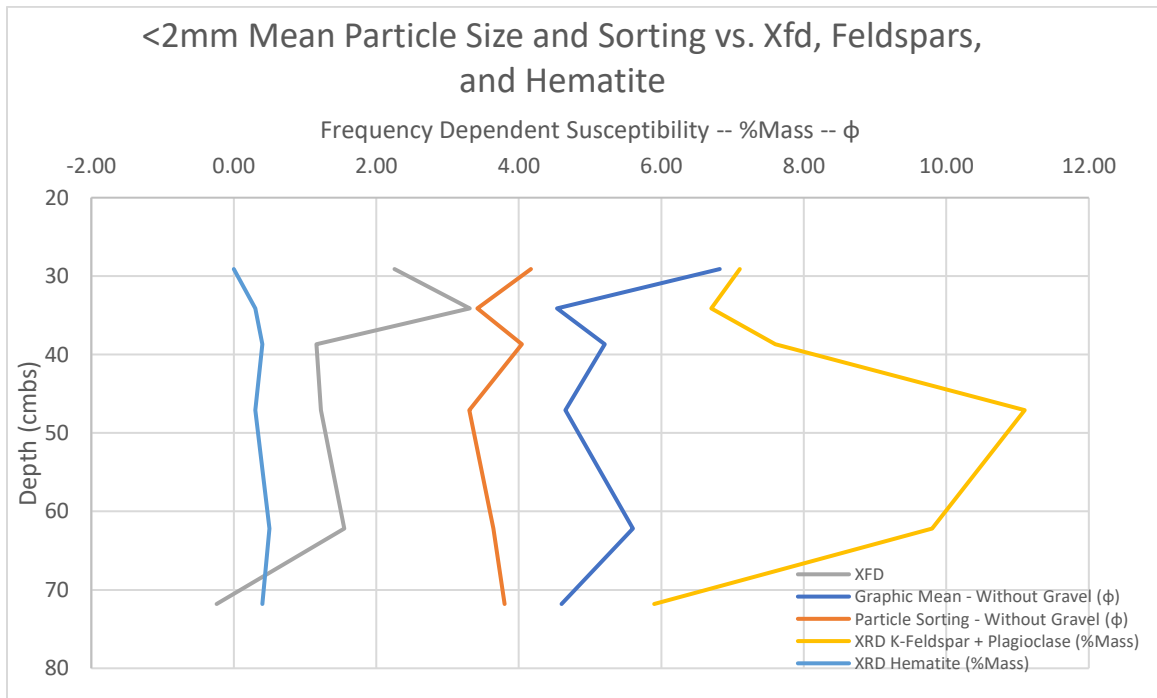


Figure 8-18. Higher resolution comparison of Column Sample 5 χ_{FD} , <2mm particle size and sorting, and feldspar content. X-axis units vary by data series. Figure designed to illustrate curve variation and relationships at smaller scale than Figure 8-17.

8.9 *Stratigraphic Details*

8.9.1 *Stratum 24*

8.9.1.1 *Stratum 24 - Particle Size*

Illustrated in **Figure A-11**, at over 80% gravel with a mean of $-3.5 \pm 2.5 \phi$, Stratum 24 is simultaneously the coarsest and best sorted (though still classified as “very poorly sorted” under Folk’s classification scheme) stratum sampled in Column Sample 5. The fine fraction is predominately sand and silt with a well-defined peak at 0ϕ and a poorly defined peak at 8.5ϕ . Stratum 24 sedimentation is driven by endogenic processes, resulting in a fairly homogenous profile with the majority of accumulated sediment originating from within the shelter.

New radiocarbon dates at 14,080 cal BP (**Table 7-9**) place Stratum 24 at the end of a cold interstadial period, contributing to increased bedrock exfoliation and in situ frost weathering (Nordt et al. 2002). This relative instability may have limited Bonfire Shelter’s habitability. No depositional vectors that could account for the geological deposition of the megafauna remains was observed. The combined impact of substantial debris falling from the ceiling combined at least some degree of cryoturbation may contribute to the stratum’s poor faunal preservation.

8.9.1.2 *Stratum 24 – Calcium Carbonate*

Volumetric calcimeter methods determined the <2.0 mm component of Stratum 24 was over 60% CaCO_3 , clearly derived from the 80% Devils River limestone gravel component. With cold conditions driving this much exfoliation, attrition from general spall detachment and cryoturbation-based abrasion may account for the limited amount of fine fraction (fine silt sized) matrix that surrounds the gravels.

With no evidence of exogenic calcium carbonate deposition, geological processes can be discounted as sources of faunal material. The fauna must have entered the shelter under their own power or were introduced by predators and/or humans. Any artifacts deposited in the shelter at

this time are likely to remain in situ (or very close to it). As noted above, the detachment of individual spalls weighing over 1.0 kg (2.2 lbs.) could cause significant damage to osseous material exposed on the shelter surface. The repeated association of large spalls and cobbles with fragmentary remains is suspicious. In Block D, the fragmented ribs and scapula were directly overlain by large spalls up to 30.0 cm (11.8 in). Even if not completely destroyed, cosmetic damage to cortical surfaces further complicates already ambiguous faunal interpretation.

8.9.1.3 Stratum 24 - Organic Carbon

The KPESIL elemental analysis determined organic carbon comprises 1.6% of the Stratum 24 fine-fraction sediment, second only to Stratum 19 in Bone Bed 2. This was much higher than expected given the limited evidence of exogenic deposition documented in particle size and carbonate determinations. This association suggests that the organic carbon is derived from the Pleistocene megafauna remains, rather than plant matter from the rich Rio Grande alluvium as initially thought.

At -25.99‰ vs. VPDB, Stratum 24 has the lowest $\delta^{13}\text{C}$ levels observed in Column Sample 5 and is within the expected range of C3 dominated plant communities ($-27.0\pm 3\text{‰}$) (Lohse et al. 2014). Herbivores with ^{13}C -enriched tissues consuming an entirely C3 diet could be expected yield $\delta^{13}\text{C}$ levels up to roughly -24‰ to -18‰ for bison. The large volume of plant matter consumed by mammoth and other Pleistocene taxa could account for this deviation. As the only stratum with clear evidence of carnivore activity (Bement 1986b:55-58), $\delta^{13}\text{C}$ enriched carnivore tissues or the ongoing introduction of large volumes herbivore remains in a den environment could further inflate values. Direct testing of the faunal remains could provide additional insight.

8.9.1.4 Stratum 24 – Gypsum

At 8.14%, as determined using differential water loss methods, Stratum 24 has the highest gypsum content detected Column Sample 5. The gypsum manifests as a very fine silt-size

white coating adhering to bone and gravel, as nodules (though not to the same extent as Stratum 23), and throughout the sediment matrix. As a water-soluble salt, gypsum entered the matrix via saturated ground water from bedrock seeps, accounting for the linear gypsum increase with depth (additional sampling is necessary to assess the potential for downward percolation from surface contexts). Gypsum is a substantial factor contributing to Stratum 24's poor faunal preservation. Bones coated with gypsum began degrading almost immediately upon exposure to the atmosphere as structural changes and further precipitation within pore-spaces exacerbated extant damage.

8.9.1.5 Stratum 24 – XRD Mineralogy

Stratum 24 is dominated by calcite, consistent with the substantial limestone component documented above. The ratio of k-feldspar to plagioclase is significantly lower, whereas in overlying strata the ratio is more balanced. This shift may reflect shifts in exogenic sediment origins from the Pleistocene into the Holocene. Stratum 24 is also the only tested stratigraphic unit where apatite was detected. Frequently associated with the inorganic mineral fraction of bone, it is possible that the XRD sediment aliquot included debris from the substantial faunal assemblage. Elevated anhydrite and basanite content are consistent with high gypsum levels and poor faunal preservation reported above.

8.9.1.6 Stratum 24 – Magnetic Susceptibility

Stratum 24 features the lowest χ_{FD} and $\chi_{HF/LF}$ levels documented in Column Sample 5. This relationship is consistent with Stratum 24's status as the coarsest deposit with the highest proportion of endogenic limestone carbonate, and the lowest levels of exogenic deposition. With nearly negligible endemic magnetic minerals, the Devils River Limestone comprises over 80% Stratum 24 and contributes to its very low χ values. The presence of somewhat elevated organic carbon levels may be the only factor contributing to non-negligible χ scores.

8.9.2 *Stratum 23*

8.9.2.1 *Stratum 23 - Particle Size*

Gravel content decreases by nearly 40% in Stratum 23, with a corresponding increase in the proportion of fine fraction sediments, including a 5% increase in clay content. Average spall size decreases suggesting an overall decline of cryoclastic intensity; consistent with a return to the global warming trend of the Allerød interstadial. Despite these decreases, deposits are increasingly poorly sorted at $1.0 \pm 6.2 \phi$. The substantial influx of clay and uptick in rounded <1.0 mm (0.04 in) gravel content suggests over-rim sheetwash as the source of exogenic material. Illustrated in **Appendix A: Particle Size Distributions Figure A-9** and **Figure A-10**, limited aeolian deposition appears to overshadowed by “noise” from the less well-sorted water-borne deposits. The disaggregation of clays during hydrometer analysis also appears to contribute to fine-fraction outlier bands.

No evidence of fluvial introduction or redeposition of faunal material was observed. As illustrated in **Figure 3-4**, large-scale flood waters in Mile Canyon remain 10.0 – 20.0 m (32.8 – 65.6 ft) below Bonfire Shelter and no massive alluvial deposits have been identified. Despite its smaller size in the Pleistocene, the talus cone and surrounding boulders serves as a break water dissipating much of the energy from sheetwash events before waters reach the shelter interior.

8.9.2.2 *Stratum 23 – Calcium Carbonate*

CaCO_3 content, based on volumetric calcimeter methods, drops approximately 16% from Stratum 24 to Stratum 23, the largest percent-change observed between any two strata. This decrease is associated with a substantial decrease in limestone gravel content, mean particle size (with and without gravel), and organic carbon as well as increases in magnetic susceptibility. This trend appears to represent simultaneous decreases in endogenic formation processes and increases in exogenic sedimentation, likely in the form of over-rim sheetwash carrying significant quantities of clay-rich sediment.

8.9.2.3 Stratum 23 – Organic Carbon

The decrease in organic carbon content from 1.6% in Stratum 24 to 0.3% in Stratum 23 is unexpected considering the significant influx of exogenic material. Stratum 23 provides the best indication that organic carbon accumulation is not tied directly to exogenic formation processes. The drop in organic carbon content is also not reflected in the faunal assemblage, which increases slightly from Stratum 24 to 23. However, this observation does not account for the total mass of the assemblage, which would vary based on taxa and age/size of the individuals represented.

The $\delta^{13}\text{C}$ shift from Stratum 24 to Stratum 23 is the most dramatic observed in Column Sample 5, dropping 2.44‰ from -25.99‰ to -23.55‰. This change represents a substantial step in the transition from Pleistocene to Holocene ecology. It also highlights the deepening plight of Pleistocene fauna remaining in the area as the C3 plants that sustained them gave way to a C4-dominant landscape.

8.9.2.4 Stratum 23 – Gypsum Content

Both XRD and DWL methods measure a steep decline in gypsum content from Stratum 24 to Stratum 23, dropping from 8.1% to 2.8% and 5.9% to 1.7% respectively. The decline coincides with decreased coarse fraction deposition and increases in exogenic sedimentation. Stratum 23 also featured an abundance of rounded gypsum nodules up to 1.0 cm (0.4 in) in diameter; other strata featured smaller nodules in lower quantities. Differential water loss measurements indicate the nodules were composed of nearly 60% gypsum

The nodules appear to form around individual sand, bone, or spall fragments of varying sizes. In strata with limited exogenic deposition, gypsum is better integrated with the sediment matrix with some mineral coatings adhering to bone and (to a lesser degree) spall surfaces and fewer large nodules. In primarily exogenic strata, particularly those with elevated silt and clay fractions, gypsum precipitation appears to occur via a different process more conducive to nodule formation.

8.9.2.5 Stratum 23 – XRD Mineralogy

The composition of Stratum 23 initiates a divergent compositional trajectory from Stratum 24, exhibiting a decrease in calcite, and increases in quartz, k-feldspar, and clay minerals. Stratum 23 is compositionally more similar to Stratum 22 and Stratum 21, exhibiting lower calcite levels and elevated quartz, k-feldspar, plagioclase, and clay minerals. Stratum 23 has the highest concentration of clay minerals observed in Column Sample 5. Combined with the elevated feldspars, the clay mineral peak is consistent with the influx of exogenic fine-fraction sediment identified in the particle size distribution and carbonate analyses. Though present in small quantities in the Devils River limestone sample, elevated quartz (the highest observed) and hematite content appears to be tied to the influx of exogenic material.

8.9.2.6 Stratum 23 – Magnetic Susceptibility

Magnetic susceptibility increases approximately 17 points from Stratum 24 to 23. Like the several other measures described in this chapter, this represents the single largest susceptibility change observed in Column Sample 5. The influx of fine grain exogenic material combined with the decreasing carbonate content appears to have played a substantial role. Given Stratum 23's very low organic carbon content, elevated susceptibility cannot be attributed to human or animal activity within the shelter. Rather, the increase appears to be a function of the influx of fine-grained exogenic material.

8.9.3 *Stratum 22*

8.9.3.1 Stratum 22 – Particle Size

Stratum 22 marks an abrupt reversal in the ongoing fining trend from Stratum 24 to Stratum 19. Gravel content increases from 45% (S23) to 60% (S22) with a corresponding increase in mean particle size from approximately $1 \pm 6\phi$ to $-1 \pm 5\phi$. The cumulative curve plotted in **Appendix A: Particle Size Distributions Figure A-7** is very similar to the Stratum 24 curve in **Figure A-11** suggesting similar depositional patterns. In **Figure A-8**, a well-defined

mode at 5φ indicates an uptick in aeolian deposition coinciding with the decreased gravel exfoliation; suggesting an abrupt cooling event during a longer warming sequence.

8.9.3.2 Stratum 22 – Calcium Carbon

<2.0 mm (0.08 in) fine fraction CaCO₃ content increases approximately 5% vs. Stratum 22 but decreases 11% from Stratum 24. This shift reinforces limestone gravels as the primary source of CaCO₃ for the fine fraction. Cryoclastic activity including overall rate of spall detachment and in situ frost-weathering have far reaching implications beyond generic particle size/gravel content, influencing the fully spectrum of particle sizes.

8.9.3.3 Stratum 22 - Organic Carbon

Organic carbon remains consistently very low from Stratum 23 to 22 and from Stratum 22 into 21. Despite the slight uptick in aeolian deposition, organic carbon remains at 0.3% and does not appear to trend with exogenic sediment deposition. Bement (1986) reports that the Stratum 22 faunal assemblage abruptly decreases to a single fox; a significant contrast to the large quantities of megafauna that characterize Bone Beds 1 and 2. Stratum 22 supports the hypothesis that organic carbon levels are tied to the accumulation of organic faunal material.

Inverse spikes in particle size, magnetic susceptibility, and mineral composition observed in Stratum 22 also suggest an environmental shift, which is reflected in the organic carbon stable isotope profile. Dipping to -23.2‰ vs. VPDB, δ¹³C indicates a brief resurgence of the previously waning C3 plant communities in Stratum 22, indicative of a temporary return to somewhat colder and wetter conditions in the midst of a longer aridization trend. This pattern appears to be consistent with the δ¹³C profile from Applewhite Terrace (Nordt et al. 2002:185), which illustrates a brief resurgence of C3 plants at approximately 12,000 cal BP in the midst of a large-scale shift towards C4 plant dominance during the Younger Dryas.

8.9.3.4 Stratum 22 – Gypsum

Based on the results from the DWL analysis, Stratum 22 exhibited the second highest gypsum content observed in Column Sample 5, exceeded only by Stratum 24; based on the semi-quantitative XRD analysis Stratum 22 exhibited the highest gypsum content. By either measure, this abrupt reversal mirrors the coarse-fraction particle size distribution and $\delta^{13}\text{C}$ profile's indication of a brief return to cold, wet conditions. This relationship between gypsum and climate is also consistent with the hypothesis that gypsum enters the profile via saturated groundwater seeps. Increased groundwater availability during wetter periods could allow gypsum to be drawn higher into the profile, accumulating in greater concentrations in Stratum 22.

In contrast to Stratum 24, no faunal remains were recovered from Stratum 22 precluding the comparison of elevated gypsum concentrations on bone degradation. The fine silty gypsum coating adhering to spall and bone in Stratum 23 and 24 was not present in appreciable quantities, nor were the larger gypsum nodules. This trend may be a further indication that gypsum content is tied to soil moisture content, possibly originating at depth rather than infiltrating from the surface.

8.9.3.5 Stratum 22 - XRD Mineralogy

Stratum 22 exhibits compositional similarities to both Stratum 23 and 21 with generally increased quartz, feldspars, and clay minerals and lower calcite levels. As illustrated in the carbon and stable isotope analyses, Stratum 22 deviates from this trend and with a partial resurgence of Pleistocene formation processes observed in Stratum 24. Anhydrite/bassanite and chlorite content are nearly identical to Stratum 24 (a pattern present but not as pronounced in the DWL data, possibly a function of anhydrite's dehydrated state). Clay minerals drop abruptly compared to Stratum 23, but not to the same minimum observed in the largely endogenic Stratum 24.

Plagioclase and K-feldspar reach the highest levels measured in Column Sample 5 in Stratum 22. Quartz content decreases slightly from Stratum 23 but remains significantly higher

than Stratum 24. This pattern indicates that exogenic processes contributed more sediment to Stratum 22 than Stratum 24, but the material appears to be derived from a different source than Stratum 23. The absence of Stratum 23's very high clay content supports this hypothesis, suggesting that the exogenic material may be of aeolian origin. This combination of exogenic and endogenic processes is consistent with the brief resurgence of Pleistocene conditions in the midst of an ongoing warming trend.

8.9.3.6 *Stratum 22 – Magnetic Susceptibility*

Stratum 22 marks the largest peak in mass susceptibility, which corresponds with the highest feldspar levels and a slight increase in mean particle size and sorting (both with and without >2.0 mm fraction). A closer look at the particle size distributions illustrated in **Figure 8-1** and **Figure 8-3** reveals a significant increase in the proportion of gravel at the expense of silt and (to a lesser degree) clay. If magnetic susceptibility is tied to exogenic deposition, Stratum 22 may represent a shift in the source and/or composition of material transported and retained within the shelter.

This pattern may reflect an increase in aeolian deposition at the expense of over-rim sheetwash. Increased outwash from the Trans-Pecos on the Rio Grande may have elevated concentrations of magnetic minerals in the vicinity of Mile Canyon. The slight increase in mean particle size from 3.6 ϕ in Stratum 23 to 3.3 ϕ in Stratum 22 (5.6 ϕ to 4.6 ϕ without gravel) is accompanied by improved particle sorting and decreases in the fine silt and clay fractions. The shift to favor coarser sands is still within the range of aeolian transport, but may reflect increasing windspeeds transporting heavier particles or an increase in the availability of coarser sediments. Increased aeolian deposition and reduced cryoclastic intensity also account for improved overall sorting in Stratum 23.

8.9.4 *Stratum 21*

8.9.4.1 *Stratum 21 – Particle Size*

The general fining/warming trend resumes in Stratum 21, marked by a decrease in mean particle size to approximately $1 \pm 6\phi$; similar to Stratum 23. Gravel content, illustrated in **Figure 8-1** and **Figure A-5**, is moderately reduced from approximately 60% in Stratum 22 to just over 50% in Stratum 21, with a reduction in average spall size to -3ϕ . As illustrated in **Figure 8-3** and **Figure A-6**, The fine fraction is characterized by and uptick in the proportion of silts and clays, with distributional modes at 0ϕ and around 6ϕ . The increased silt and clay content combined with the sediments 10YR5/4 yellowish brown color (similar to the clayey 10YR6/4 Stratum 23) suggests that a combination of aeolian deposition and over-rim sheetwash (though not to the same extent as Stratum 23) contributed to Stratum 21.

8.9.4.2 *Stratum 21 – Carbon Content*

Carbonate levels continue on a somewhat positive trajectory from Stratum 22 to 21, increasing from 52.1% to 57.0% (per volumetric calcimeter measurements reported in **Table 8-4** and **Figure 8-1**). This shift corresponds with a decrease in average particle size and a 10% decrease in gravel content, suggesting increasingly temperate environmental conditions. The effects of a possible exogenic carbonate source observed in the other Bone Bed 2 strata becomes initially detectable in Stratum 22 as calcite content increases without a corresponding increase in the size or proportion of gravel. This shift appears to represent broader ecological changes, including significant modifications to shelter weathering and bedrock attrition patterns as well as a potentially significant shift in the composition of Rio Grande alluvium.

8.9.4.3 *Stratum 21 – Organic Carbon*

As illustrated in **Figure 8-8**, Organic carbon remains constant at 0.3% (EA) from Stratum 22 into Stratum 21. However, Stratum 22 marks a significant inflection point as organic matter increases by nearly 10x through Bone Bed 2. Bement reports that most of the faunal remains

associated with these horizons were recovered from the Stratum B/C (Stratum 21/20) interface (Bement 1986b:28-35). Due to the lack of intra-stratum geoarchaeological samples, it was not possible to confirm the distribution of organic carbon over the depositional history of Stratum 21. Based on the available data, the increase in organic carbon likely coincides with the bison kill events of Bone Bed 2.

Following the $\delta^{13}\text{C}$ spike in Stratum 22, the pattern of expanding C4 grasses resumes but begins to stabilize. **Figure 8-9** illustrates the $\delta^{13}\text{C}$ increase from -23.2‰ to -22.72‰, approximately 0.5‰. The characteristic fauna of the Pleistocene (mammoth, horse, and camel) never return to Bonfire Shelter as food sources dwindle and grasslands expand. The expansion of *Bison antiquus*, previously a minor component of the Bone Bed 1 faunal assemblage, into these new rangelands coincides with the first concrete evidence of human site-use at Bonfire Shelter. As Robinson (1997) notes, bison hunters of the plains likely followed the migratory herds southward across the newly opened southern rangeland.

8.9.4.4 *Stratum 21 – Gypsum*

Illustrated in **Figure 8-5**, Gypsum content decreases and appears to stabilize in Stratum 21. Due to the limited Bone Bed 2 area excavated in Blocks C and D a comparison of faunal preservation with Bone Bed 1 is limited. General observations from previous excavations suggests that preservation conditions dramatically improved in Bone Bed 2 compared to the Bone Bed 1 assemblage. The combined variables of time, gypsum exposure, and exposure to the processes that precipitate gypsum appear to play an important role in faunal preservation.

8.9.4.5 *Stratum 21 – XRD Mineralogy*

Stratum 21's composition exhibits additional evidence of a warming trend with increased exogenic deposition initiated in Stratum 23 while the evidence of a cold-snap in Stratum 22 falls away. Quartz, k-feldspar, and clay mineral content is somewhat decreased but remains above Stratum 24 levels. Calcite content begins to increase, potentially marking the introduction of

exogenic calcium carbonate to the shelter and/or a shift in the composition or source of Rio Grande alluvium as endogenic limestone gravel decreases substantially. The small uptick in clay mineral content appears to support this. However, the trend drops off in Stratum 20 and 19. It is also possible that warmer conditions yielded finer-grain bedrock attrition particles and the accumulation of non-spall endogenic limestone.

8.9.4.6 *Stratum 21 – Magnetic Susceptibility*

Figure 8-14 illustrates a dramatic decrease in $\chi_{HF/LF}$ in Stratum 21 to below levels observed in Stratum 23, following the magnetic susceptibility apex in Stratum 22. This first stratum in Bone Bed 2 is characterized by a 10% decrease in gravel content, the start of an ongoing mean particle size fining sequence, an increase silt and clay content, and a general decrease in exogenic minerals. These impacts appear to be driven by generalized climatic stabilization extending through Stratum 19. Organic carbon content possibly associated with Bone Bed 2 cultural activity begins to increase in Stratum 21, however the effects are not realized in terms of magnetic susceptibility until Stratum 22.

8.9.5 *Stratum 20*

8.9.5.1 *Stratum 20 – Particle Size*

Stratum 20 is characterized by an influx of sand-size particles ($-0.5\phi - 3.5\phi$) and a substantial decrease in overall gravel content from approximately 50% in Stratum 21 to just under 30% in Stratum 20 (**Figure A-3**). The resulting Stratum 20 fine fraction is somewhat better sorted (3.42ϕ) than Stratum 21 (4.045ϕ) and Stratum 19 (4.17ϕ) but includes an increase in coarser sand at the expense of silt and clay. Based on observations in the field, Stratum 20 is a very pale brown (10YR7/3) unconsolidated loam similar to the largely endogenic Stratum 24 and 22 rather than the darker brown exogenic Stratum 23 and 21.

Irregular increases in the particle bands associated with aeolian deposition at Bonfire Shelter suggest that the composition of the Rio Grande alluvium has shifted to include additional

aggregate silt particles and an abundance of calcium carbonate or that an irregular transport processes is contributing sediment. If Bone Bed 2 is in fact a Bison Jump, significant quantities of sediment would likely have been introduced to the shelter as the herd tumbled over the cliff. These peaks and irregularities could represent the literal settling dust from such an event and the subsequent human processing activity.

8.9.5.2 *Stratum 20 – Calcium Carbonate*

From Stratum 21 to Stratum 20, calcium carbonate content increased nearly 15% to levels exceeding Stratum 24 (as calculated using all three carbonate determination methods). This increase somewhat counterintuitively coincides with an influx of fine material sediment particles and a decrease in overall gravel content (**Figure 8-1**). This may be a function of a shift in endogenic limestone deterioration processes, favoring smaller granules rather than large spalls thereby accounting for the simultaneous decrease in gravel and increase in carbonate.

These carbonate level fluctuations suggest that endogenic and exogenic sedimentation processes vary independently. Increasing aridity with time ultimately results in less water within bedrock pore spaces and less intense freeze thaw cycles, shifting the endogenic particle size profiles away from the larger spalls observed in the underlying strata associated with colder Pleistocene conditions. Changing or decreased ground cover as the climate warms also changes the nature of exogenic sediment deposition as uplands become denuded and the composition of the Rio Grande alluvium shifts.

8.9.5.3 *Stratum 20 – Organic Carbon*

At 1.3% organic carbon (per KPESIL-EA, **Figure 8-8**) Stratum 20 is consistent with the pattern of increasing organic carbon through Bone Bed 2, and the elevated organic carbon content observed in Bone Bed 1 Stratum 24. At roughly 25% exogenic sediment (as calculated in **Table 8-11**), the lowest proportion observed in Column Sample 5, increasing organic carbon content

appears to be tied to the mass accumulation of bison remains and associated human/scavenger activity surrounding Bone Bed 2.

As a major component of the unambiguously cultural Bone Bed 2, human activity cannot be ruled out as a source organic material enrichment. At -22.71‰ vs. VPDB, the organic carbon stable isotope profile (**Figure 8-1**) is within the expected range for bison tissue derived from individuals subsisting on a diet of largely C3 plants, likely incorporating an increasing proportion of C4 plants. If heavier isotopes are concentrated based on trophic level, a phenomenon that should be occur in herbivores but is not readily disentangled from the background C3 plant communities associated with underlying Pleistocene strata, this could reflect an herbivore diet shifting to include more C4 plants (Lohse et al. 2014; Nordt et al. 2002). If organic matter derived from humans or other carnivores contributed to Stratum 20, the ratio could be further enriched by trophic level indicating the broader expansion of C3 plants. It is unclear if the intense burning associated with parts of Bone Bed 2 impacted organic carbon content, as Stratum 20 continues the increasing linear trend from Stratum 21 to Stratum 19.

8.9.5.4 *Stratum 20 – Gypsum*

Gypsum content, illustrated in **Figure 8-5** and **Figure 8-6**, decreases slightly from Stratum 21 to 20, though the change is relatively negligible compared to the dramatic swings observed between deeper strata. This pattern is consistent with other geoarchaeological analyses indication of stabilizing environmental conditions approaching the end of the Pleistocene. Particularly, increasing aridity may decrease the ability of gypsum-saturated water to move through the sediment profile. Alternatively, gypsum-saturated groundwater entering the sediment column from underlying bedrock seeps may evaporate before reaching the Bone Bed 2 strata via capillary action, concentrating precipitates in lower levels. Based on the association of decreased gypsum content with Bone Bed 2, the environmental conditions limiting gypsum accumulation may be more suitable for cultural activity within or in the vicinity of Bonfire Shelter.

8.9.5.5 *Stratum 20 – XRD Mineralogy*

Based on the XRD profile reported in **Figure 8-10**, Stratum 20 and Stratum 19 very mineralogically similar, with less than 1% variation in every class except for calcite and illite/mica. Calcite content rises substantially from 48% to 60% from Stratum 21 to 20. As noted in the Stratum 21 XRD observations, this pattern may reflect new endogenic limestone weathering patterns related to the ongoing warming trend as all other exogenic sedimentation markers decrease from Stratum 21 to 20. All other mineral concentrations drop slightly from Stratum 21 to 20. This pattern reflects the low level of exogenic sediment expected based on the very pale brown, unconsolidated nature of the sediments (described in greater detail in **Table 7-4**) observed in the field. The increased in organic carbon content is unaccounted for except for the cultural activities associated with the Bone Bed 2 bison kill.

8.9.5.6 *Stratum 20 – Magnetic Susceptibility*

Stratum 20 features an abrupt χ spike, illustrated in **Figure 8-16**, slightly higher than levels observed in Stratum 23, a silt and clay dominated, largely exogenic deposit featuring abundant extinct fauna and possible evidence of human modification. The Stratum 20 χ peak coincides with an increase in mean <2.0 mm (0.08 in) particle size and sorting (decreased ϕ value) while the Stratum 21 χ valley aligns with a decrease in <2.0 mm particle size and sorting (increased ϕ value). The relationship between χ values, <2.0 mm particle size, and relevant XRD mineral proportions is illustrated in **Figure 8-17**.

Stratum 20 also aligns with Bement's Stratum B: the middle layer of burned and calcined bone within Bone Bed 2 assemblage (Dibble and Lorrain 1968:29). High-temperature firing and the subsequent oxidation of iron-rich minerals in the underlying sediments could elevate the stratum's magnetic susceptibility without a corresponding increase in particle size, carbonate content, or exogenic sediment deposition. Based on the calculations summarized in **Table 8-10** and **Figure 8-11**, Stratum 20 features the lowest proportion of exogenic sediment of all Column

Sample 5 strata. In Stratum 20, elevated magnetic susceptibility appears to be directly tied to human activity. Specifically, the accumulation and incineration of faunal remains. Strata 19 and 21, the overlaying and underlying Bone Bed 2 horizons, do not feature the same peak despite their association with the cultural event, suggesting that the burn feature plays an important role in susceptibility.

8.9.6 *Stratum 19*

8.9.6.1 *Stratum 19 – Particle Size*

Unlike the underlying strata, Stratum 19 gravels are not normally distributed within the sampled size classes (**Figure A-1**). Nearly 10% of the stratum is comprised of two very large ($>6\phi$) spalls recovered from the column sample that were lumped into the -7ϕ , the largest size class quantified, for analysis purposes. Even excluding these outliers, the $<1\phi$ fraction lacks a clearly defined mode. With a mean particle size of 3.22 ± 7.23 , Stratum 19 is simultaneously the finest and most poorly sorted stratum sampled in Column Sample 5. Interestingly, Stratum 19 and Stratum 20 included identical proportions of gravel by mass at 28.8%. This was initially attributed to a calculation or laboratory error, but both strata have very different gravel fraction (and fine fraction) distributions. It is possible that this coincidence represents stabilizing environmental conditions.

In addition to the anomalous gravel distribution, Stratum 19 exhibits an abrupt 16% increase in clay content to nearly 30% of the total sample mass. This spike is correlated with a decrease in the sand fraction, which drops to 25% while the silt fraction remains relatively constant at 47% (**Table 8-2** and **Figure 8-3**). Combined with the rounded gravel increase observed in the Stratum 19 microartifact sample reported in **Table 8-14**, this increase in clay content appears to be derived from an influx of over-rim sheetwash. An increase in sand and silt-size particles indicates aeolian processes also contributed exogenic sediment.

Despite this, the overall proportion of exogenic sediment remains low at approximately 25% (**Table 8-11** and **Figure 8-13**). Superficially, Stratum 19's poorly defined structure and pale color (10YR7/4) is consistent with other endogenic-dominant strata (i.e.: Stratum 24 and Stratum 22). Yet exogenic processes appear to have contributed sufficient material to classify the sediments as a clay loam without altering the overall appearance of the sediment matrix. As noted in Stratum 20, changes in endogenic weathering patterns as environmental aridity increase could result in the increased exfoliation of sand and silt size particles. This alternative to aeolian deposition would account for the low proportion of exogenic material in the XRD profile. Changes in the source and/or composition of aeolian sediments to include non-local calcite could also account for this pattern. Because Stratum 19 is associated with Bone Bed 2, human activity cannot be ruled out as a source of some these anomalous sediments.

8.9.6.2 *Stratum 19 – Carbonate Content*

Calcium carbonate content continues to increase, though less dramatically, from Stratum 20 to 19. At approximately 73% (per volumetric calcimeter measurements reported in **Table 8-4**). As noted in Stratum 20, this increase in CaCO_3 is associated with a substantial decrease in gravel content from the Bone Bed 1 strata (the proportion of gravel remains constant from Stratum 20 to 19). The particle size profile discussed above suggests sheetwash and aeolian processes contribute exogenic material to Stratum 19, one of which may include an exogenic source of CaCO_3 . It is difficult to determine if the fine-fraction CaCO_3 component was present in the underlying Bone Bed 1 strata due to the abundance of clearly endogenic limestone overshadowing potential secondary sources.

8.9.6.3 *Stratum 19 – Organic Carbon*

Illustrated in **Figure 8-1**, Stratum 19 contained the highest organic carbon content observed in Column Sample 5 at 2.6%; the relative peak of a trend spanning the Bone Bed 2 strata. Based on observations throughout this profile, the influx of organic matter appears to be

derived from the large-scale bison harvest that characterizes Bone Bed 2. The accumulation of decomposing and incinerated bison carcasses combined with increased sheetwash, as evidenced by the elevated clay and rounded coarse sand described above, could create an outwash of organic-rich debris from the talus cone that subsequently settled in the shelter interior. If not the bison carcasses themselves, associated human and scavenger activity following the events of Bone Bed 2 could also enrich and/or scatter organic material across the shelter. Shifting exogenic sediment sources could provide a secondary source of organic carbon, but given the low overall proportion of exogenic material calculated in **Table 8-11** it is unlikely that this could account for the very high organic component observed in Stratum 19.

Stratum 19 also marks the peak $\delta^{13}\text{C}$ ratio observed in Column Sample 5, with a slight increase from -22.71‰ in S20 to -22.70‰ illustrated in **Table 8-7**. As observed of other analyses, it is not clear if this is due to the rapid sequential deposition of these three strata or a long-term trend towards environmental stability beginning in Stratum 21. Like Stratum 20, -22.70‰ is within the range of variation for organic matter derived from bison tissue subsisting on a diet of largely C3 grasses or trophic-level enrichment of a diet with an increasing proportion of C4 plants. An expansion of C4 grasses is consistent with the increased warming and aridity observed in the palynological record as well as the particle size distributions conducted in this study (Bryant and Holloway 1985; Scott-Cummings 1992).

8.9.6.4 *Stratum 19 – Gypsum*

Based on DWL methods, gypsum content decreases from 4.24% in Stratum 20 to 2.47% in Stratum 19; the lowest levels observed in Column Sample 5 and a 58% decrease. Measured via XRD, Stratum 19 and Stratum 20 exhibit duplicate gypsum levels. While it is possible that samples were contaminated in the field or lab, the significant variation in other analyses suggest this is unlikely. The relationship between gypsum and gravel content illustrated in Stratum 24, 22, and 19 demonstrates that gypsum accumulation is tied to endogenic formation processes.

Decreasing gypsum content through Bone Bed 2 is consistent with warming temperatures, increasing aridity, and decreasing cryoclastic activity. If gypsum is primarily introduced via saturated groundwater seeps, Stratum 19 is at the highest elevation above bedrock and consistent with the relatively linear decrease through the profile illustrated in **Figure 8-6**. Regardless of the nature of Bone Bed 2 as a single tripartite event or three separate events in relatively rapid succession, consistent formation processes would be expected.

8.9.6.5 *Stratum 19 – XRD Mineralogy*

Illustrated in **Table 8-8** and **Figure 8-10**, the mineralogical composition of Stratum 19 is extremely similar to Stratum 20. Key differences include a 3.2% increase in calcite content and a 2.6% decrease in clay minerals. Feldspars remain nearly constant at the lowest levels observed in the column sample. Hematite is not present in Stratum 19; the only stratum where it is completely absent. Quartz content remains elevated slightly above Stratum 24 levels. Despite superficial similarities between Stratum 19 and Stratum 24, the units appear to be derived from very different formation processes.

At 63.5% Stratum 19 is the only position in Column Sample 5 where calcite content exceeds Stratum 24 levels (62.4%). Based on the volumetric calcimeter analysis reported in **Table 8-4**, both Stratum 19 and 20 exceed Stratum 24's calcium carbonate content at 72.6% and 70.6% versus 63.1% respectively. This pattern is consistent with the higher proportion of endogenic sediment estimated in **Table 8-11**. This pattern is somewhat unexpected based on Stratum 19 and 20's much lower gravel content.

Quartz and clay minerals, while identified in the limestone control sample (**Table 8-10** and **Figure 8-12**) are also introduced via exogenic vectors. K-feldspar and plagioclase were not detected in the control sample but occur at higher levels in Stratum 19 than Stratum 24 despite elevated calcium carbonate and a lower estimated exogenic sediment. This reinforces the hypothesis that some proportion of calcium carbonate is introduced via exogenic processes, at

least in the Bone Bed 2 strata. This would result in the underestimation of exogenic sediments in **Table 8-11**, since calcite was considered an endogenic mineral component in the calculation. Variable weathering processes under the more arid environmental conditions also undoubtedly play a role in this discrepancy. Despite this, finer-grain exfoliation of the Devils River Limestone still appears to be the dominant component of Stratum 19.

8.9.6.6 *Stratum 19 – Magnetic Susceptibility*

In Stratum 19, $\chi_{LF/HF}$ and χ_{FD} abruptly decrease approximately 8 points and 1 point from the mid-Bone Bed 2 peak in Stratum 20. The nearly duplicate measurements between Stratum 19 and 20, particularly in gravel content, carbonate content, and exogenic mineral content, indicates that some factors are held constant between the strata. The complete absence of hematite may play a role in declining susceptibility. However, hematite concentrations varied through the entire Column Sample profile without a significant effect on magnetic susceptibility.

The most significant differences exist between specific particle size distributions and the extent of cultural activity (which may be reflected in the particle size distribution, as noted above). Stratum 19 appears to be dominated by aeolian deposition, which biases the maximum size and mass of particles introduced. Without supplemental water-driven deposition, maximum magnetic capacity appears to be limited. Additionally, the stratum 21/20 interface comprises the densest portion of Bone Bed 2 and encompasses the most significant burning damage observed in the horizon. The absence of burning and associated sediment oxidation likely plays the most significant role in the decreasing susceptibility. Variability in the introduction of excess organic matter and colluvium associated with falling bison or extensive human processing activity may be contributing factors.

8.10 Microartifact

A total of 58 spot samples collected across eight test units were evaluated for the presence of microartifacts. Samples were floated to separate heavy and light fractions, and further processed to isolate the 1-2 mm fraction for analysis. Due to limited laboratory access and time constraints, detailed spot sample analysis was limited to 13 specimens. The fully processed samples were selected to provide the maximum horizontal and vertical coverage across Blocks C and D possible while still targeting high-probability proveniences associated with faunal remains. The remaining 45 spot samples were qualitatively evaluated to identify the components present in each sample, including potential microartifacts.

No definitive microdebitage was observed in these samples. Two likely chert fragments, illustrated in **Figure 8-25**, were recovered from FN60092 (Unit C2 L1), collected along the margin of a Stratum 23 mammoth rib. These specimens lack the diagnostic attributes expected in cultural debitage, but appear to be derived from an appropriate exogenic lithic material. However, the fragments are very angular and lack the rounded morphology associated with the rounded gravels also identified in the matrix. The isolated nature of these specimens in a stratum with a significant exogenic component demands further validation before their presence can be attributed to human agents. Other “possible chert” fragments were determined to most likely be fossil shell fragments derived from the local Devils River limestone. Despite the limited quantity of lithic material identified, processing the samples yielded significant insight into the formation processes contributing to the Bone Bed 1.

For the fully sorted samples, each sediment particle was manually separated by material type. Each of the 13 material classes were quantified by mass (to the nearest .01g) rather than count due to the large volume of material. Some error is associated with the measurements due to the limited accuracy of the balanced used for this analysis (roughly +/- .03g). This is most problematic in low frequency or low density classes weighing <0.03 g. In several samples, the

sum of all sorted classes appeared to be larger than the starting sample mass. This may be due to the gradual loss of dust and residual material during processing compounded by balance error. The residual material classes was utilized to quantify fine sand-sized particles unidentifiable under low-power magnification or too small to physically sort.

Table 8-13 reports the results of fully sorted microartifact samples broken down by constituent component mass (g) and percent mass of each sample. Initially, a 50.0 g aliquot from each spot sample was processed for microartifacts. Subsample mass was reduced to a 20.0 g target after determining that the time required to process each sample was much greater than anticipated. The smaller sample size helped to reduce the range of variation between small and large samples as well as analyst selection bias. Many samples remained smaller than the 20.0 g threshold after geomatrix samples were separated for curation. The percent mass value was included to facilitate comparison between samples of various sizes.

To further expand the sample size, a 20.0 g aliquot from 45 additional samples was thoroughly scanned to determine which materials were present. This qualitative assessment particularly emphasized microartifacts and rounded gravel. Due to the generally small number present in each sample, rounded gravel and (if present) debitage was separated and tallied.

Appendix B: Raw Microartifact - Table reports the results of the qualitative analysis. Despite the expanded sample size, no further microartifacts were identified

Table records highlighted in light blue indicate samples that were also quantified. Fields marked with an “X” indicate that a material was present in the sample while “-“ indicates the material was not identified. No definitive examples of chert were identified beyond FN60092 (described above), though fossil gravel was fairly ubiquitous. Rounded gravel content, also highlighted in light blue, is presented as a raw count as well as a frequency of gravel fragments per analyzed gram.

Table 8-14 is an excerpt from **Table** presenting the qualitative results of microartifact samples associated with Column Sample 5. Illustrated in **Figure 8-19**, round gravel counts and frequency generally mirror influxes of exogenic sediment as estimated in **Table 8-11** and **Figure 8-13**, above. Strata with limited exogenic deposition (broadly interpreted as low clay content), were expected to have low incidence of rounded gravel. While this pattern generally holds true in Stratum 20 and 24, rounded gravel frequency is higher than expected in Stratum 22. This is particularly notable compared to the underlying Stratum 23, which was estimated to include the highest proportion of exogenic material of all sampled strata. Across all samples, rounded gravel was approximately 19% more abundant in Stratum 23 than in Stratum 24. However, this figure is biased by the increased number of overall Stratum 23 samples that were fully processed.

Table 8-13. Microartifact (1-2mm Fraction) Processing Results

Provenience		Sample Mass		Limestone	Bone		Shell		Charcoal		Botanical (Hackberry)		Botanical (other)		Rounded		Quartz Crystal		Gypsum Crystal		Chert		Fossil		Concretion/ Gypsum Nodule		Other		Unsorted Residual		Total Sorted		Notes				
		Lot	Unit		Strat	Total 1mm Mass	Analyzed 1mm Mass	Mass %	Mass %	Mass %	Mass %	Mass %	Mass %	Mass %	Mass %	Mass %	Mass %	Mass %	Mass %	Mass %	Mass %	Mass %	Mass %	Mass %	Mass %	Mass %	Mass %	Mass %	Mass %	Post Sort %	Total %						
60299	60248	C1	L6		37.25	12.97	9.28	71.55	3.01	23.21	0.08	0.62	0	0.00	0.15	1.16	0	0.00	0.09	0.69	0.04	0.31	<0.01	0.00	0.1	0.77	0.18	1.39	0	0	0.14	1.08	12.97	100.77	Induces 1 whole & 4 ~half hackberry		
60167	60248	C1	L6		6.14	6.14	4.22	74.30	0.84	14.79	0.16	2.82	0	0.00	<0.01	0.00	<0.01	0.00	0.08	1.41	0.03	0.53	0.16	2.82	0	0.00	0.32	5.63	0.23	4.05	0	0	0.12	2.11	5.88	108.45	Float light <0.01; 15 round gravel
60094	60076	C2	L1		7.36	7.12	5.4	75.84	0.96	13.48	0.28	3.93	<0.01	0.00	<0.01	0.00	0	0.00	0.05	0.70	0.09	1.26	0	0.00	<0.01	0.00	0.05	0.70	0.15	2.11	0	0	0.19	2.67	7.12	100.70	<0.01 - insect carapice fragment
60092	60076	C2	L1		17.42	17.42	13.46	81.23	0.86	5.19	0.3	1.91	0	0.00	0.01	0.06	0	0.00	0.42	2.53	0.00	0	0.00	<0.01	0.00	0.6	3.62	0.19	1.15	0	0	1.33	8.03	16.57	103.62	2 small "fossil" vertebra. Black and atleast somewhat mineralized. 2 Possible chert frags photographed	
60062	-	C3	Pelvis Ped L1		-	20.7	11.27	54.44	3.83	18.50	0.09	0.43	0	0.00	0.04	0.19	0	0.00	0.28	1.35	0.06	0.29	0	0.00	0.07	0.34	0.08	0.39	0.25	1.21	0	0	4.81	23.24	20.7	100.39	Large amount of bone, heavily degraded and unsortable. "Chert" likely fossil shell frags
60054	-	C3	Rib Ped L2		-	20.02	18.36	91.71	0.18	0.90	0.12	0.60	0	0.00	0.17	0.85	0	0.00	0.68	3.40	0.12	0.60	0	0.00	0.13	0.65	0.19	0.95	0.26	1.30	0	0	0	0.00	20.02	100.95	1 mandible, 1 small vert. bagged separately. Chert frags likely mostly fossil, require closer inspection. Unclear if shell frags are fossil
60038	-	C3	Rib Ped Residua I		94.4	16.31	13.82	84.73	1.57	9.63	0.04	0.25	0	0.00	0.02	0.12	<0.01	0.00	0.13	0.80	0.07	0.43	0	0.00	0.01	0.06	0	0.00	0	0.00	0	0	0.65	3.99	16.31	100.00	Check rounded for mineral. Contained several quartz-like grains. Maybe Gypsum frags? 3 possible chert - examine under high power. Excessive bone frags, long time to sort.
60051	-	C3	Rib Ped L3		-	20.03	18.42	91.96	0.16	0.80	0	0.00	0	0.00	0.11	0.55	0	0.00	0.42	2.10	0.13	0.65	0	0.00	0.11	0.55	0	0.00	0	0.00	0	0	0.68	3.39	20.03	100.00	Several possible chert frags - need closer look -- Whole hackberry seed; lig amount of rounded gravel - try to ID
60409	60392	D3	L3		19	19	16.97	98.09	0.09	0.52	0.09	0.52	0	0.00	0	0.00	<0.01	0.00	0.05	0.29	0	0.00	0.04	0.23	0	0.00	0.06	0.35	0	0	0	0.00	17.3	100.00			
60510	60498	D7	L4		57.4	20	19.69	99.29	<0.01	-	0.06	0.30	0	0.00	<0.01	0.00	0.00	0.04	0.20	0	0.00	<0.01	0.00	0	0.00	0.04	0.20	0	0.00	0.00	0.00	19.83	100.00	Reduced sorting sample to 20g - 50 too large and inefficient.			
60523	60498	D7	L4		21.5	21.5	20.71	98.01	0.27	1.28	0.06	0.28	<0.01	0.00	0	0.00	<0.01	0.00	0.04	0.19	0	0.00	<0.01	0.00	0.05	0.24	0.05	0.24	0	0	0	0.00	21.13	100.24			
60540	60537	D8	L4		17.66	17.66	17.66	100.00	0	0.00	0	0.00	0	0.00	0	0.00	0	0.00	0	0.00	0	0.00	0	0.00	0	0.00	0	0.00	0	0.00	0	0	0.00	17.66	100.00	miniscule hackberry fragment; 3 black grains, possibly charcoal; Possible chert fragment - PHOTO; Includes semi-mineralized vertebra ~1mm - mammal?	
60552	60548	D8	L5		33.2	20	19.74	100.00	<0.01	0.00	<0.01	0.00	0	0.00	0	0.00	0	0.00	<0.01	0.00	0	0.00	0	0.00	0	0.00	0	0.00	0	0.00	0	0	0.00	19.74	100.00	Notable decrease in non-limestone material	

Table 8-14. Column Sample 5 - Qualitative Microartifact Results

Column Sample 5 - Qualitative Microartifact Results															
FN	Lot	Unit	Level	Stratum	Analyzed Mass (g)	Lime-stone	Bone	Char-coal	Shell	Gypsum Nodule	Round Gravel	Round Gravel (per g)	Quartz	Hack-berry Seed	FN Comment
60258	60250	CS5	1	S19	20.41	X	X	X	X	X	22	1.08	X	X	PS06.CS05.S19; LS001
60259	60251	CS05	2	S20	17.02	X	X	X	X	X	5	0.29	X	-	PS06.CS05.S20; LS002
60260	60252	CS05	3	S21	20.53	X	X	-	-	X	10	0.49	X	X	PS06.CS05.S21; LS003
60261	60253	CS05	4	S22	17.85	X	X	-	X	X	25	1.40	X	-	PS06.CS05.S22; LS004
60262	60254	CS05	5	S23	19.68	X	X	X	X	X	24	1.22	X	-	PS06.CS05.S23; LS005
60275	60274	CS05	6	S24	18.45	X	X	-	X	X	20	1.08	X	X	PS06.CS05.S24; LS006

Table 8-15. Summary of rounded gravel recovered from Bone Bed 1 strata.

Bone Bed 1 - Overall Rounded Gravel Summary									
Stratum	Total Gravel (count)	Total Analyzed Mass (g)	Gravel (per gram)	Block C Gravel (count)	Block C Analyzed Mass (g)	Block C Gravel (per gram)	Block D Gravel (count)	Block D Analyzed Mass (g)	Block D Gravel (per gram)
Stratum 23 Round Gravel	494.00	351.19	1.41	494.00	351.19	1.41	n/a	n/a	n/a
Stratum 24 Round Gravel	442.00	460.80	0.96	407.00	325.36	1.25	35.00	135.44	0.26
Total	936.00	811.99	2.37	901.00	676.55	2.66	35.00	135.44	0.26
% Stratum 24	52.78%	43.25%	59.46%	54.83%	51.91%	52.93%	-	-	-
% Stratum 23	47.22%	56.75%	40.54%	45.17%	48.09%	47.07%	-	-	-
% Difference	5.56%	-13.50%	18.91%	9.66%	3.82%	5.86%	-	-	-

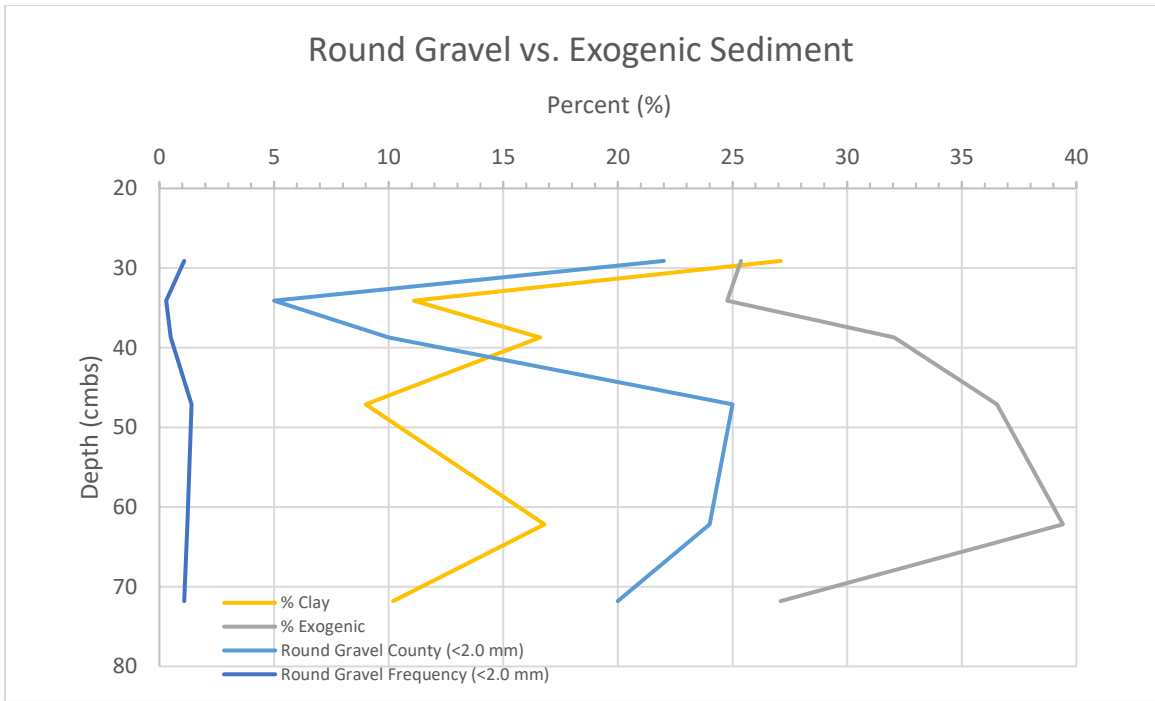


Figure 8-19. Column Sample 5: Round Gravel Count and Frequency vs. Exogenic Sediment.

8.10.1 *Limestone*

Limestone gravel was the primary constituent component of all microartifact processed samples, often representing over 90% of the total sample mass. Limestone was generally very flat with angular facets. Black mineral deposits thought to be manganese pyrolusite were infrequently observed on the surface individual fragments. This mineral was observed on large spalls and some bone specimens during the excavation of Blocks C and D. No variation in gravel morphology was observed across the analyzed samples; limestone fragments remained flat and angular throughout suggesting limited post-depositional cryoturbation, fluvial action, or otherwise displacing mechanisms that might compromise the stratigraphic integrity of associated materials. The proportion of limestone was reduced in samples associated with large faunal elements, where bone fragments and splinters represented a larger proportion of the total sample mass. It does not appear that this represents a shift in the geological processes contributing the limestone.



Figure 8-20. Limestone gravel was the primary component of all analyzed microartifact samples. A sample of the gravel from FN60092, Unit C2 L1, is illustrated here at approximately 31x magnification; 1 Cell = 2.5 mm (0.1 in)

8.10.2 *Faunal Remains – Bone*

Bone fragments were the second most abundant material observed in the microartifact samples. **Figure 8-21** and **Figure 8-22** illustrate the diverse array of faunal material recovered. Deteriorating megafauna elements, especially mammoth ribs, contributed significant quantities of cortical bone splinters and fragments of cancellous material. However, microfauna remains from small rodents, reptiles, and birds were also observed. Due to their highly fragmentary nature and the emphasis of this study on microdebitage recovery, no attempt was made to further identify or quantify faunal remains. Vertebrae and other potentially diagnostic elements were bagged separately and noted in the sample comments after weighing.

The significant quantity of osseous material remaining in these samples was unexpected and slowed progress considerably. Bone fragments were expected to separate out from lithic

material during floatation for capture as part of the light fraction. Unfortunately, the osseous material remained with the heavy fraction and was ultimately sorted manually. The unexpected density of these bone fragments may be a function of their Pleistocene megafauna origins. Alternatively, it could be a function of the partial mineralization of the osseous Bone Bed 1 materials. The significant quantities of gypsum detected within the sediment, both as nodules and adhering to the surface of larger elements, may have begun to penetrate the interior of the bone decreasing its buoyancy. Gypsum nodules were also not buoyant and did not dissolve in any appreciable manner during the floatation process. The weight of gypsum or other minerals (manganese pyrolusite is visible on the surface of several fragments in the **Figure 8-21** and **Figure 8-22**) adhering to the surface of the bone fragments may have been sufficient to weigh them down.



Figure 8-21. Examples of osseous material recovered from FN60092. Unit C2 L1, at approximately 37x magnification; 1 Cell = 2.5 mm (0.1 in).



Figure 8-22. Bone fragments recovered from FN60092. Unit C2 L1, at approximately 37x magnification.; 1 Cell = 2.5 mm (0.1 in). Several highly deteriorated mammoth rib sections were recovered from this layer, the primary source of long bone splinters illustrated here.

8.10.3 *Faunal Remains – Shell*

Land snail shell fragments were sorted independently of vertebrate osseous material recovered from microartifact samples. Extremely small, fine sand grain size, intact snail shells were observed in the light fraction and unsorted residual fraction of the samples, but no intact shells were identified in the 1-2mm target range. This may partially be a function of the delicate nature of these specimens, which easily fractured when manipulated. Given the significant baseline calcium carbonate content from the limestone parent material and the small quantity of snail shells present, shell content does not appear to be a significant variable in Bone Bed 1 sediment composition.

Nine terrestrial snail taxa and two aquatic snail taxa were identified in a microfauna column sample collected during the 2004 Southern Methodist University expedition. The column sample does not extend into the Bone Bed 1 strata, but several lots were collected from the Late

Pleistocene Bone Bed 2 strata. Byerly did not publish the entire invertebrate data set, but summarized the assemblage noting that *Succineidae* was the most abundant taxa with minor components of *Helicodiscus*, *Hawaiiia*, *Gastrocopta*, and *Rabdotus*. Byerly suggests that the snails likely lived within the moist shaded interior of the shelter, sustained by organic-rich sheetwash from the uplands. Variation in the frequency of these invertebrate taxa can provide more information on the environmental conditions at the time of deposition. However, little elaboration regarding the implications of specific invertebrates is provided in Byerly's preliminary synopsis (Byerly, Meltzer, et al. 2007:134-135).

In the Bone Bed 1 microartifact samples, the extremely small intact shells appear to be consistent with *Hawaiiia miniscula* or *Helicodiscus singleyanus* (Nickels 2014:135). Other specimens recovered from the spot samples were too fragmentary to identify beyond general invertebrate shell fragment. However, Byerly notes that *Rabdotus*, the ubiquitous land snail of Texas, was only observed in later Holocene deposits (Byerly, Meltzer, et al. 2007:135). Evidence of snail consumption is relatively common across Texas, with human refuse deposits typically biasing larger adult specimens that may accumulate in conspicuous middens or concentrations. Unfortunately, the Bone Bed 1 specimens appear to represent natural environmental background noise (Brown 2015).



Figure 8-23. Snail shell fragments recovered from FN60092. Unit C2 L1, at approximately 37x magnification; 1 Cell = 2.5 mm (0.1 in)

8.10.4 *Fossil Shell*

Figure 8-24 below illustrates examples of fossilized shell fragments recovered from microartifact samples. These fragments generally had smooth, glassy textures and were partially encased in limestone/calcite. The Devils River Formation is a well-documented marine limestone. Shell reef fossils, particularly rudistid bivalves, are visible on exposed rockfaces and boulders throughout Mile Canyon and Bonfire Shelter (Frederick 2017b:12).

Due to their concave profile, tapering angular facets, and chert-like texture, fossil fragments were often mistaken for microdebitage both in the field and during microartifact processing. The opaque color, adhering stone, and shell-like surface textures often found on at

least one face of the specimens allowed them to be easily differentiated once recognized. However, several samples have outstanding questionable specimens that could not be confidently assigned to a processing class.



Figure 8-24. Examples of fossil shell fragments recovered from FN60092. Unit C2 L1, at approximately 37x magnification; 1 Cell = 2.5 mm (0.1 in)

8.10.5 *Possible Chert Fragments*

Possible microartifacts and fragments of likely exogenic lithic material were sorted into this category for closer examination. These fragments were very uncommon and often determined to be fossil shell fragments or limestone upon further inspection. The remaining specimens could not be definitively identified as microartifacts and often could not be positively identified as chert.

Long wavelength ultraviolet light was used in an attempt to induce the orange fluorescence characteristic of Edwards Plateau cherts with limited results. While sorting batches, the white shells and light-colored limestone fragments brightly reflected large amounts of the light washing out the muted glow observed in the Bone Bed 2 and 3 test specimens. Specimens assessed in isolation did not exhibit any notable fluorescence. It is possible that these small specimens contained insufficient quantities of requisite minerals to emit a detectable fluorescence. However, this does not disqualify them as chert or another cryptocrystalline lithic raw material.

Figure 8-25, below, illustrates two possible chert fragments recovered from a spot sample collected along the northwest margin of mammoth rib FN60082 Unit C2 L1 (Stratum 23). These specimens appear to be a chert like material and are semi-translucent with surface striations reminiscent of conchoidal fracture ripples. However, they are uncharacteristically chunky and exhibit no other characteristics associated with lithic debitage. Examples identified in other microartifact samples are more akin to fossil shell fragments without the limestone rind than to chert. All of the suspected chert specimens lack multiple key diagnostic features to confirm with certainty that they are microartifacts or (more frequently) that they are in fact chert.



Figure 8-25. Possible chert fragments observed in spot sample FN60092, Unit C2 L1. Collected from the northwest margin of mammoth rib FN60082. Approximately 90x magnification; 1 Cell = 2.5 mm (0.1 in)

8.10.6 *Quartz Crystal*

Crystal quartz grains were identified in small quantities in nearly all analyzed microartifact samples. These fragments were often much smaller than the surrounding material and difficult to identify due to their transparent color. While not assessed under a high-power microscope, the quartz grains did not exhibit any obvious signs of rounding or weathering. Nearly all examples were angular with well-defined facets.

As illustrated in **Figure 8-12** above, the control sample of Devils River limestone consisted of nearly 1% quartz. Quartz represented the largest component of acid-insoluble material at over 60%. It is possible that the quartz observed in these microartifact samples is entirely endogenic. But given the generally smaller grain size, it is also possible that some quartz entered the shelter via aeolian processes.



Figure 8-26. Quartz crystal fragments recovered from FN60092. Unit C2 L1, at approximately 56x magnification; 1 Cell = 2.5 mm (0.1 in)

8.10.7 *Rounded Gravel*

A significant number of rounded very coarse sand/very fine gravel ($-1\phi - 0\phi$, 1 – 2mm) particles were observed in nearly all analyzed samples. Illustrated in **Figure 8-27** below, the rounded gravels were composed of a variety of lithic materials, the majority of which were non-limestone. Specific rock types were not differentiated. However, the assemblage appears similar to the alluvial gravels observed in the vicinity of Mile Canyon.

Dibble noted that hydrological activity appeared to play a direct role in the sedimentation of Bonfire Shelter (Dibble and Lorrain 1968:27). The presence of these gravels confirms his hypothesis, demonstrating that fluvial processes contribute exogenic material to Bone Bed 1. No larger rounded gravels or cobbles were observed during excavation or while processing sediment samples. This narrow sorting band may be indicative of relatively low-energy water action within the shelter. Given the location of these units well into the interior of the shelter, it is possible that these gravels are the remnants of sheet wash entering over the canyon rim and dissipating across the shelter interior.

Figure 8-27 clearly illustrates the size variation observed within this class, even within the confines of the 1-2 mm graded fraction. The range of variation in both size and material may be more in line with dissipated sheetwash than the well-sorted deposits typically associated with standing water. These rounded grains were observed in greater quantities in Block C than in Block D. This may be a function of its lower elevation near the deepest part of the shelter and the subsequent concentration of waterflow and sediments in that area.



Figure 8-27. Examples of rounded gravel observed in FN 60299. Unit C1 L6, at approximately 57x magnification; 1 Cell = 2.5 mm (0.1 in). Note the varied lithic materials and size range within the 1-2mm fraction.

8.10.8 *Gypsum Crystal*

In addition to the powdered gypsum nodules observed throughout Bone Bed 1, fragments of crystalline gypsum (illustrated in **Figure 8-28** below) were observed throughout fine fraction sediments. During initial spot sample processing, fragments of gypsum and quartz were sorted into a single “crystal” category under the assumption that they were derived from the same processes with similar compositions. As processing continued, gypsum crystals were sorted into a unique category.

Gypsum crystals were primarily differentiated from quartz by color and morphology. Gypsum crystals were a pale yellow brown or tan color with many intersecting sheet-like plains

or “blades” (reminiscent of the lathe-like crystal growths described by (Paz and Rossetti 2006). Quartz crystals were differentiated by their clear or opaque white color and flat, angular facets.

Calcium sulphate minerals, including gypsum, anhydrite, and bassanite, were detected in all strata using XRD and LOI analyses. Because the crystals were only differentiated in a small proportion of samples, it is not possible to define a relationship between the geoarchaeological analyses and this microartifact class. However, the presence formation of these crystals suggests an arid environment where gypsum-saturated water was able to evaporate quickly and stable conditions conducive to crystal growth.



Figure 8-28. Crystalline gypsum fragments observed in FN60092. Unit C2 L1, at approximately 57x magnification; 1 Cell = 2.5 mm (0.1 in)

8.10.9 *Gypsum Concretion*

Rounded aggregate nodules of an extremely fine white powder up to 1cm in diameter were observed throughout Bone Bed 1. LOI testing suggests that these nodules were nearly 60% gypsum. Smaller rounded nodules, illustrated in **Figure 8-29** below, with similar color, texture, and morphology were observed in the 1-2mm fraction during microartifact processing. These nodules were extremely friable and readily crumbled or disintegrated when manipulated.

Much like the rounded gravels described above, gypsum nodule size varied greatly within the 1-2mm range. Gypsum powder with a similar color and texture was observed adhering to bone and spall during excavation. It is possible that these nodules were formed from precipitating gypsum adhering to sand grains within the fine fraction. It is unknown if these nodule form under the same conditions as the gypsum crystals.

Precipitates simultaneously require significant quantities of super-saturated water and an arid environment driving evaporation. Byerly's description of a "carbonate-like mineral" adhering to snail shells observed in the upper strata are attributed to "a very moist environment" and likely refers to these gypsum precipitates (Byerly, Meltzer, et al. 2007:135). Seasonal variation between wet and dry seasons could be sufficient to drive the accumulation of these coatings, resulting in the accumulation of new mineral layers like tree rings. However, the long term drying trend through the Holocene might also cause the continuous long-term precipitation and accretion of gypsum.

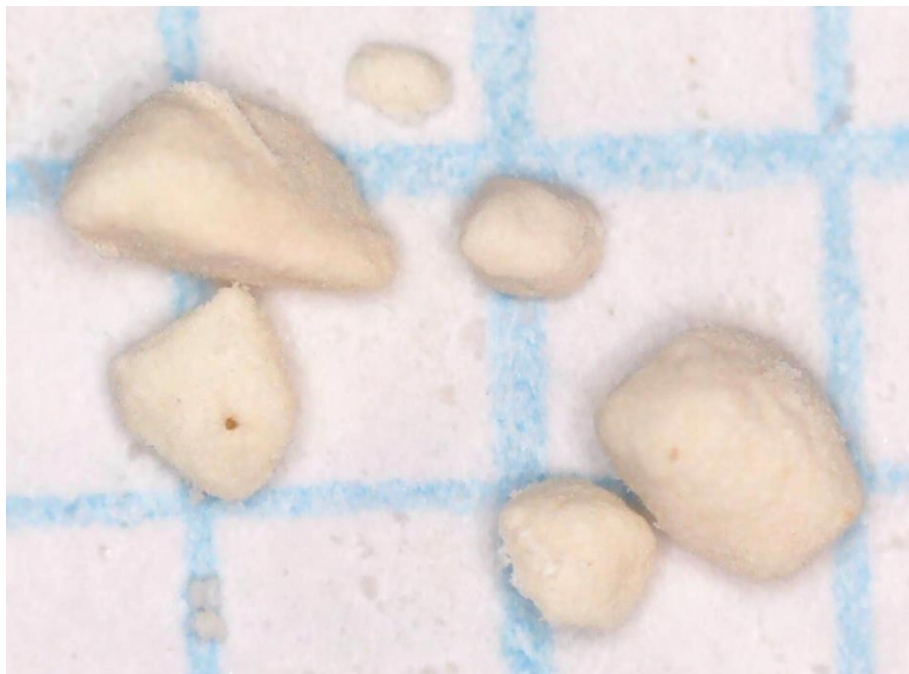


Figure 8-29. Rounded gypsum nodules observed in FN60092. Unit C2 L1, 1 Cell = 2.5 mm (0.1 in)

8.10.10 *Botanical Material*

Heavy-fraction microartifact samples occasionally yielded seeds and seed fragments in the 1-2mm range not separated out during floatation. Small quantities of organic material recovered with the light fraction were retained for future research but were not processed as part of this study. Hackberry seeds (*Celtis sp.*), illustrated in **Figure 8-30** and **Figure 8-31**, were the predominant botanical specimen recovered. Small flecks of charcoal and other unidentifiable seed fragments were occasionally observed, but constituted a very small portion of the assemblage.

Initially, hackberry seeds observed in the field were thought to be intrusive, the result of bioturbation and rodent caching behavior. However, several concentrations of hackberry seeds were documented in situ during excavation and collected for ^{14}C dating. A specimen recovered from Unit C1 Layer 6 in association with mammoth remains yielded an AMS date of 12,112 +/- 69 RYCBP (13,971 cal BP), consistent with the previous date obtained from Bone Bed 1 in the 1980s. Given the paucity of charcoal and limited success of bone collagen dating efforts,

hackberry seeds recovered from other microartifact samples may be a valuable source of datable material. These samples are well provenienced and selected specifically for their proximity to key faunal remains and points of interest for microartifacts making them well suited for chronometric analysis.



Figure 8-30. Nearly intact hackberry (*Celtis* sp.) seeds and hemispheres recovered from FN60299. Unit C1 L6, at approximately 34x magnification; 1 Cell = 2.5 mm (0.1 in)



Figure 8-31. Hackberry (*Celtis* sp.) seed fragments recovered from FN60299. Unit C1 L6, at approximately 34x magnification; 1 Cell = 2.5 mm (0.1 in)

9. DISCUSSION & CONCLUSION

The primary goal of this thesis was to sample the Late Pleistocene Bone Bed 1 strata at Bonfire Shelter to determine if any or all components comprise a very early Paleoindian archaeological site. The deposits were evaluated against three main criteria: Do the deposits contain artifacts and/or features of unambiguously human origin? Are those artifacts or features in well-documented, undisturbed, primary context? Is there stratigraphic and temporal control over those proveniences verified using multiple chronometric methods?

These criteria were used to develop a model classifying the strata comprising Bone Bed

1. These site types were used as null and alternative hypotheses:

- Faunal remains were geologically redeposited in Bonfire Shelter
- Faunal remains were introduced through human activity
- Faunal remains were introduced through carnivore activity
- Fauna died of natural causes in Bonfire Shelter

Strata were classified based on evidence collected during the 2017 and 2018 field seasons supplemented by analyses reported by (Bement 1986a, 1986b). Results from (Dibble and Lorrain 1968) were considered but not specifically integrated due to their limited stratigraphic differentiation. Expectations for each site type were broken down into three main categories: Faunal, Geological, and Cultural. **Table 9-1** summarizes classifications for each sampled stratum and the key data points from each analytical category.

Table 9-1. PS06.CS05 - Bone Bed 1 - Final Classification based on 2017-2018 site data.

		Stratum					
		Bone Bed 2			Zone 2a	Bone Bed 1	
		S19	S20	S21	S22	S23	S24
Evidence	Geological	Most stable; limited low-energy exogenic	Ongoing warming; High MagSus & $\delta^{13}\text{C}$; Sand anomaly	Begin warming trend, stabilization	Extremely unstable	Pooling Water, Environmental Stress	Extensive Endogenic
	Faunal	Low taxa diversity;	With S21; Low taxonomic diversity; Bias young individuals		Sparse, single fox fragment	Diverse Assemblage, Limited age bias	Age and Taxa Bias, mixed utility
	Cultural	None; Extensive disarticulation; isolated high yield	Extensive disarticulation; Sectional utility bias with riders; 1963-1964 Folsom & Plainview		Carnivore Remains	None; Extensive disarticulation	Carnivore Damage
	Classification	Cultural (Carnivore)	Cultural	Cultural	Carnivore	Ecological	Carnivore

9.1 Stratigraphic Classification

Using the site-type model developed for this thesis, Stratum 19, 20, and 21 were classified as cultural, Stratum 22 and 24 were classified as carnivore impacted assemblages, and Stratum 23 was classified as natural death/ecological assemblages. However, most of these strata did not satisfy all of the expected criteria. Classification was assigned based on a best fit and preponderance of evidence.

Based on the 2017-2018 data reported here alone, the Bone Bed 2 strata would appear to be consistent with natural accumulations. Artifacts were recovered from column samples on the talus cone (Kilby and Hamilton 2018), but no cultural material was recovered from the shelter interior. Even integrating the 1980s data, arguments for cultural origins remain unconvincing. Cut marks and spiral fractures were identified, but cultural material reported by (Dibble and Lorrain 1968) could not be verified.

9.2 *Stratigraphic Narrative*

9.2.1 *Stratum 24*

9.2.1.1 *Geological*

Geologically, persistent endogenic deposition dominates Stratum 24 characterized by extensive accumulations of large, tabular limestone spalls. While an estimated 27% of sediments are derived from exogenic processes, these sediments are nearly all within the range of aeolian or low-energy fluvial mechanisms. This pattern suggests that larger non-local materials (i.e.: megafauna remains) were introduced to Bonfire Shelter through some form of animal activity. Detected organic carbon levels cannot be attributed geological formation processes. Relatively low $\delta^{13}\text{C}$ levels indicate that the organic matter is derived from a mix of C3 and C4 plants. This pattern is consistent with the four radiocarbon dates available for Stratum 24, dating the material to around 14,080 cal BP.

9.2.1.2 *Faunal*

The Stratum 24 faunal assemblage is consistent with the expected characteristics of carnivore-derived sites outlined in **Table 6-1**. Direct evidence of carnivore activity is limited to the scimitar-toothed cat (*Homotherium serum*) -pierced mammoth bone fragment identified by Bement during the 1983-1994 excavation (Bement 1986b:53-58). However, the composition of the faunal assemblage provides additional supporting evidence.

The size of newly documented mammoth elements is consistent with the juvenile specimens reported by Bement (1986). No clear developmental indicators were recovered with the new horse specimens, however both previously recovered individuals were also juveniles. Studies of modern carnivore proxies and paleontological assemblages, as reviewed in **Chapter 6**, demonstrate a clear bias towards juvenile or otherwise weakened individuals as prey targets.

Taxonomic diversity was dominated by Pleistocene horse and mammoth, verifying the 1980s findings. The Pleistocene antelope (*Capromeryx sp.*) specimens were associated with Stratum H-2 in 1983, which could not be differentiated from Stratum 24 in the field, so are included here. *Capromeryx* and bison are represented by a small number of isolated elements.

The presence of disarticulated cranial and axial skeletal elements in addition to high-utility limb elements is similar to the *Homotherium* den assemblage at Friesenhahn cave, where the nearly complete carcasses were of juvenile animals were brought to the site. The Stratum 24 assemblage diverges somewhat from Binford's characterization of denning behavior where individual elements were brought to the den. However, his observations were based on modern wolves and may not translate directly to extinct big cat behavior. The limited number of antelope and bison elements suggests that components of both behaviors may be present. Combined with the preponderance of two taxa, bias towards juvenile individuals, mixed-utility assemblage, extensive disarticulation, the Stratum 24 assemblage is consistent with the carnivore denning behavior

9.2.1.3 Cultural

No new evidence of human activity was detected in Stratum 24 during the 2017-2018 excavations. The faunal assessments conducted with this thesis were not able to verify the presence of spiral fractures or V-shaped incisions reported by Bement in the newly excavated assemblage (Bement 1986b:41-58). Many of the reported cut-marks occurred in tandem with parabolic or U-shaped incisions, further elevating the ambiguity of the findings. The extremely deteriorated condition of nearly all newly recovered elements severely limited our ability to detect additional evidence of human or carnivore modification.

Several large limestone cobbles, visible in **Figure 7-23** and **Figure 7-24**, were identified in the newly excavated portions of Stratum 24, however faunal remains appeared to be scattered among or supported underneath from these cobbles rather than arranged or stacked around them.

Some of these faunal elements were fragmentary while others appeared to be mostly intact, but none exhibited spiral fractures or impact damage. The bone fragments identified in Block D are tightly clustered and well preserved but are not associated with any cobbles nor do they exhibit evidence of butchery or direct impact. Their position immediately beneath several large spalls suggests they may have been fractured by falling debris.

No microartifacts were identified in Stratum 24. Samples from this horizon exhibited among the lowest levels of (possible) chert fragments of the samples processed. Low levels of rounded exogenic material indicate that exogenic processes contributed to the formation of Stratum 24, but not in a capacity that could introduce the remains of Pleistocene fauna or scour away artifacts. No microartifacts or unambiguous bone tools were recovered from Stratum 24 during the 2017-2018 field season or previous expeditions.

9.2.1.4 Conclusion

Stratum 24 is consistent with the criteria established for carnivore denning activity at Bonfire Shelter. This conclusion was drawn primarily from geoarchaeological evidence and the combined 1983-1984 and 2017-2018 faunal assemblage. The anomalous accumulation of organic carbon without a corresponding exogenic depositional force appears to be a key indicator. If intact or nearly intact megafauna carcasses were introduced to the shelter or carnivores exploited Bonfire Shelter for substantial periods of time, the accumulation of faunal material could account for these elevated levels. While significant quantities of falling debris are not particularly conducive to human or animal activity, geological assessments indicate that conditions at Bonfire Shelter were consistent and predictable during this time period; a valuable attribute of any lair.

9.2.2 *Stratum 23*

9.2.2.1 Geological

The extensive spall deposits of Stratum 24 give way to a dense accumulation of silt and clay in Stratum 23 that appears to represent ongoing low-energy fluvial activity or sheetwash,

potentially forming ephemeral puddles in the shelter interior. Statistically, the deposits are poorly sorted; a function of the influx of exogenic material and broadened range of transport mechanisms contributing sediment. Other than the outlying clay peaks, curves interpreted as specific processes appear to approach normal distributions. The clean curve associated with the gravel fraction further suggests that the coarse fraction deposition was derived from a single consistent source and not influenced by high-energy exogenic forces.

Organic carbon content decreases dramatically from Stratum 24 despite the influx of exogenic sediments. This suggests that organic carbon accumulation is not inherently tied to exogenic geological processes. The $\delta^{13}\text{C}$ shift indicates an ecological transition towards C4 grasses and the expansion of Holocene ecological conditions. Forage-range depletion combined with increasing aridity and warmer temperatures may have driven increasingly stressed Pleistocene fauna to seek alternative water sources within, or in the vicinity of Bonfire Shelter. If conditions were dire enough, it could account for their expiration within the shelter. Overall, Stratum 23 geoarchaeological data aligns most closely with the ecological formation model outlined in **Table 6-1**.

9.2.2.2 *Faunal*

The increased taxonomic diversity observed in the 1983-1984 assemblage was verified in the 2017-2018 assemblage is also consistent with the ecological formation model. MNI and age estimates derived from the 1983-1984 assemblage includes three horse of varying ages are represented, in addition to one adult camel, one likely juvenile mammoth, and one bison of unknown age. Bement notes that the assemblage includes a preponderance of limb elements. However, elements from the cranial anatomy and axial skeleton are also present for several individuals (Bement 1986b:35-38). The 2017-2018 excavations added additional elements that support this distribution, including mammoth (including possible mammoth tusk fragments),

horse, and camel, and bison axial anatomy as well as supplemental horse limb elements detailed in **Table 7-5** and **Appendix C: Faunal Assemblage**.

Bement reports two modified bone specimens: a spiral fractured horse tibia and a spiral fractured camel tibia exhibiting polish and striations (Bement 1986b:39). No similar examples or spiral fractures, cut marks, or tooth marks were identified in the 2017-2018 assemblage. However, very poor preservation may have limited the effectiveness of the examinations. Trampling in muddy sediments around a potential water source, abrasion from the coarse sediments, and post-depositional carnivore scavenging cannot be ruled out at sources of equifinality.

Faunal remains were recovered in relatively tight clusters in 2017-2018 but were not articulated in anatomical position, consistent with the 1983-1984 findings. This extensive disarticulation diverges from the ecological formation criteria established for this project. Based on the taxa and elements represented and limited age bias, this disarticulation is interpreted as post-depositional modification and scattering of fauna that perished within the shelter.

9.2.2.3 Cultural

No unambiguous micro- or macro- artifacts were recovered from Stratum 23 during the 2017-2018 or during previous expeditions. Several possible chert fragments were identified during microartifact processing, most of which were determined to be fragments of fossil shells endemic to the Devils River limestone. Two specimens, illustrated in **Figure 8-25**, were recovered from spot sample FN60092 collected along the northwest margin of mammoth rib FN60082. The semi-translucent material observed in FN60092 was distinct from any other stone identified in other microartifact samples and unambiguously derived from outside of Bonfire Shelter. While these specimens lack the morphological attributes typically associated with stone tool debitage, they also lack the rounded morphology associated with other exogenic specimens observed throughout the <2.0 mm (0.08 in) fraction.

Stratum 23 microartifact samples consistently exhibited the highest levels of rounded exogenic sand specimens illustrated in **Figure 8-27**. The frequency of these particles is consistent with the exogenic formation processes that dominate this stratum. The grain's rounded morphologies suggest over-rim sheetwash was the source of much of these sediments.

The high incidence of rounded sands and exogenic material complicates the provenance of the potential microartifacts. The semi-translucent material and angular morphology of the fragments was distinct from any of the rounded sands, suggesting the specimens entered the shelter via a different process. Their association with large mammoth elements is consistent with the expectations established for the presence of microartifacts. Due to the substantial influx of exogenic material in Stratum 23 and isolated nature of the FN60092 specimens, additional confirmation is necessary to assert the presence of a Very Early Paleoindian component at Bonfire Shelter. Analysis of the reserved portions of microartifact samples collected from similar proveniences present a valuable opportunity for future research.

9.2.2.4 *Conclusion*

Substantial exogenic deposition and associated particle size distributions suggest pooled and/or low-energy water play a significant role in the formation of Stratum 23. The faunal assemblage generally satisfies the criteria for ecological origins, with the exception of articulated skeletons. Changing ecological conditions in the terminal Pleistocene may have driven poorly adapted fauna to the isolated water source. The variety of skeletal elements suggests that the animals expired within the shelter. While many elements are missing, only a small sample of the bone bed has been excavated. The broader age and taxa range does not exhibit the biases typically associated with opportunistic predation.

It is possible that disarticulation and damage, including spiral fractures, to the faunal assemblage is the result of post-depositional trampling; a commonly observed phenomenon in experimental and modern proxy studies (Haynes 1988, 1991b). The effects of post-depositional

carnivore modification also cannot be ruled out. But poor preservation has precluded the positive identification of tooth marks. Both of these scenarios are not uncommon at watering hole sites (Haynes and Krasinski 2010).

9.2.3 *Stratum 22*

9.2.3.1 *Geological*

Subjectively, Stratum 22 appears to be the most unstable period represented in the Column Sample 5 series. Both exogenic and endogenic depositional processes abruptly increase in intensity, a function of abruptly shifting climatic conditions. Nordt et al.'s (2002) correlation of Late Glacial geological events with southcentral Texas $\delta^{13}\text{C}$ levels suggest that these changes may reflect a cold snap in the midst of a general warming trend preceding the Younger Dryas as glacial meltwater was gradually directed away from the Gulf of Mexico. $\delta^{13}\text{C}$ levels measured in Stratum 22 reflect this trend, exhibiting a moderate resurgence of C3 plants in the midst of a longer term warming trend. However, the amount of organic material recovered from this stratum is very low. In terms of particle size, sediments do not appear to be particularly poorly sorted but this is a function of the simultaneous uptick in gravel exfoliation (versus Stratum 23) and fine aeolian deposition with decreasing intermediate particle sizes. No "high-energy" deposits were identified, but the intensity of the observed processes increases.

9.2.3.2 *Faunal*

Excavation of Stratum 22 was limited to Column Sample 5 and the southern half of Unit C1. No faunal remains were recovered from either provenience. Bement reports a similarly sparse assemblage consisting of a single gray fox mandible fragment with two intact molars. This jaw represents the only actual carnivore remains documented at Bonfire Shelter. Low organic carbon levels are consistent with the limited faunal assemblage, with no indication that the shelter functioned as a fox den or hosted other substantial animal populations at this time. Given the paucity of faunal material, limited inferences can be drawn regarding presence of fox cranial

anatomy within the shelter or predator-prey relationships that may have existed. Whether Bonfire Shelter was systematically avoided due to geological instability or rapidly changing ecological conditions (including depletion of C3 plant communities) forced megafauna to abandon the region entirely is unknown.

9.2.3.3 *Cultural*

No cultural material or potentially modified faunal remains were observed in Stratum 22.

9.2.3.4 *Conclusion*

Stratum 22 is associated with Bement's Stratum D and Dibble's Zone 2a, previously reported as a culturally sterile intermediate horizon between Bone Beds 1 and 2. This interpretation is consistent with the results of the 2017-2018 excavations. Based on Robinson's 1997 argument that Late Paleoindian bison hunters followed the expanding grasslands and migrating herds the Bone Bed 2 period, it is possible that the Pleistocene fauna and any dependent predators modified their range as C3 grasslands receded, in effect abandoning the Lower Pecos to better adapted species with less specialized dietary requirements. The subsequent warming trend may have opened an environmental niche allowing the settlement of the area (Robinson 1997).

The absence of cultural material and any significant accumulation of faunal remains limits the classification of Stratum 22 in this model. Based on the geoarchaeological profile, it is plausible that the fox entered Bonfire Shelter seeking small prey or shelter and died of natural causes. The remainder of the fox's generally gracile skeletal anatomy may not have survived in the archaeological record or was scattered into unexcavated portions of the shelter. No evidence of predation by larger species was observed, but due to the sparse assemblage post-mortem scavenging cannot be ruled out.

9.2.4 *Strata 21 & 20*

9.2.4.1 *Geological*

Stratum 21 marks a return to the warming trajectory initiated in Stratum 23 generally characterized by fining sediments, decreasing bedrock exfoliation, and an influx of silts and clays. The yellowish brown (10YR5/4) loamy matrix suggests some degree of low-energy water-borne deposition, but not to the extent observed in Stratum 23. Magnetic susceptibility drops abruptly from a significant peak at Stratum 22 to levels similar to the measurements observed in Stratum 23. Organic carbon also remains anomalously low. The volume of rounded gravel identified in microartifact samples also drops abruptly. These attributes indicate an increasingly stable shelter environment lacking powerful depositional forces with exogenic sediments largely derived from aeolian processes. Without prior knowledge of the cultural nature of Bone Bed 2, these conditions fit the established criteria for ecological/natural death or carnivore origins of the faunal assemblage. However, the fit is not particular good.

Stratum 20 highlights the ongoing environmental stabilization beginning in Stratum 21. Gravel content decreases dramatically and sand content increases, consistent with warming and drying trend indicated in $\delta^{13}\text{C}$ levels.

Stratum 20 is associated with Bement's Stratum B, the heavily burned bison bone bed within Dibble's. The counterintuitive decrease in gravel, increase in CaCO_3 , increase in organic carbon, and influx of irregularly distributed silt-size particles indicates that abnormal formation processes are contributing to Stratum 20. The limited spall activity and apparent lack of water-borne deposits suggest a high stability and 'habitability' of the shelter. If Bone Bed 2 was the result of a Bison Jump, significant quantities of otherwise endogenic material would have been dislodged in unusual patterns while simultaneously introducing vast quantities of organic matter to the shelter. The fallout from such an event could account for many of the Stratum 20 particle size anomalies. Organic carbon content and magnetic susceptibility increase substantially,

consistent with the expectations for exogenic aeolian deposition but not reflected in the previous examples observed in PS06.CS05. These increases are interpreted with as cultural phenomena associated with the Bone Bed 2 bison kill and subsequent incineration, as well as the expectations established for sites of cultural origin.

9.2.4.2 *Faunal*

The 2017-2018 faunal assemblage for Stratum 21 is again limited remains observed in the CS05 and the southern portion of UC1 including: 5 unidentifiable bone fragments and one bison vertebra. The 1983-1984 assemblage consisted of nearly 100 bison elements and five Pleistocene horse fragments. The bison assemblage consisted primarily of limb elements, vertebra, and ribs, with several examples of “riding” elements. The horse assemblage included a single radius shaft and several mandible/tooth fragments. Remains were concentrated at the Stratum 21/20 (Bement’s C/B) contact. Due to the limited excavated area, it is difficult to determine if this provenience is consistent with the 2017-2018 elements as no faunal remains were recovered from Stratum 20. Taxonomic diversity was very low in both assemblages and a limited number of individuals were represented. Bement’s age estimations indicate individuals were generally young, but not exclusively calves or juveniles.

The overall assemblage is consistent with the expectations established for a human modified assemblage separating transportable, high-yield limb sections from larger carcass halves and quarters. The details of the unresolved “to jump or to drag” debate will not be addressed here other than to highlight the clearly cultural nature of the assemblage.

9.2.4.3 *Cultural*

No artifacts were recovered from Stratum 20 or 21 during the 1983-1984 expedition or the 2017-2018 expedition. Without the recovery of Late Paleoindian projectile points and other stone artifacts during the 1963-1964 excavations, portions of Bone Bed 2 within the shelter

interior would remain just as equivocal as Bone Bed 1. The patterned distribution of bison remains around the limestone cobble is similarly equivocal without supporting evidence.

9.2.4.4 *Conclusion*

Stratum 21 and 20 are reported together to facilitate direct comparison with Bement's data set. Both strata are components of Dibble's Paleoindian Bone Bed 2. Despite the unresolved debate regarding the nature of the Bone Bed 2 strata as redeposition events or multiple bison kill events (Prewitt 2007), Stratum 20 may be the least ambiguous regarding cultural origins. However, the cumulative effects of large-scale incineration on the geoarchaeological data set may render it not the best representative sample. However, the elevated magnetic susceptibility and organic carbon levels among the relatively stable Stratum 21, 20, and 19 is a clear indication of an occupational surface.

The fine-fraction particle size anomalies discussed in Section 8.9.5.1 appear to be unique to Bone Bed 2, potentially associated with falling debris from a jump-kill event. The limited number of individuals identified in the shelter interior clearly highlights excavation bias effects when compared to the dozens of estimated individuals identified in the 1963-1964 assemblage. The age bias expected for a small scale kill or predation event has similarly limited applicability for a mass kill event. Even without artifacts, the preponderance of evidence suggests Stratum 20 and (to a lesser degree) Stratum 21 are cultural horizons.

9.2.5 *Stratum 19*

9.2.5.1 *Geological*

Stratum 19 is associated with Bement's Stratum A, the uppermost component of Dibble's Bone Bed 2. Geoarchaeological data highlight the increasing environmental and depositional stability at Bonfire shelter. Substantial increases in the clay and silt fraction suggest low-energy water deposition similar to stratum 23 supplemented with aeolian deposition are the primary sediment contributors to Stratum 19. Overall, Stratum 19 appears to be one of the most stable and

habitable levels in Column Sample 5 despite the limited fluvial activity, consistent with its temporal association on the cusp of the Holocene.

Organic carbon content peaks while magnetic susceptibility decreases to near Stratum 20 levels. These elevated levels are generally in line with the expectations for culturally influenced sites, but the ongoing warming trend observed through Bone Bed 2 and Column Sample 5 suggests that organic carbon varies independently from exogenic sediment deposition and may be influenced to a greater extent by the presence of faunal material. Compared to the Stratum 20 levels, the magnetic susceptibility level may be a result of the exogenic sediment influx rather than cultural activity. However, the intense burning associated with parts of Stratum 20 may render it a poor baseline comparative sample.

9.2.5.2 *Faunal and Cultural*

Faunal remains recovered from Stratum 19 in 2017-2018 were very limited: one small bison rib fragment was recovered from Unit C1. The assemblage is similarly sparse in the 1983-1984 assemblage which includes four juvenile Pleistocene bison elements (one rib, one humerus, one mandible fragment, and one tibia epiphysis) (Bement 1986b:27). This small assemblage is consistent with archaeological expectations for a site of human origin including: the limited number of individuals represented, low taxonomic diversity, and bias towards juvenile individuals. The utility of these elements is debatable, but several limb elements are present. No cultural material was recovered from either excavation and nor was evidence of cultural modification observed.

9.2.5.3 *Conclusion*

Without the results of Dibble's excavations on the talus cone, it would be impossible to attribute Stratum 19 to human activity. The presence of isolated, relatively high-yield elements biasing juvenile individuals in a stable shelter environment with moderately elevated magnetic susceptibility and high organic carbon levels better aligns with the expectations for carnivore

denning behavior. The only attributes missing are extensive bone damage and the presence of carnivore remains themselves.

9.3 *Post-Mortem*

This project was conducted to determine if humans contributed to the accumulation of Bone Bed 1 at Bonfire Shelter, a series of stratified deposits containing the remains of extinct Pleistocene fauna. As outlined in **Chapter 2**, previous researchers Dibble and Lorrain (1968) and Bement (1986a) cautiously argued that humans were at least partially responsible for the breakage patterns and distribution of remains across the shelter interior approximately 14,000 years ago. Despite their extensive excavations no unambiguous evidence of intervention was identified. While no conclusive evidence of human intervention was identified during the 2017-2018 excavations, this thesis contributes significant new information regarding the depositional history of Bonfire Shelter and the Late Pleistocene environmental conditions that set the stage for the events of Bone Bed 2.

Bona fide Early Paleoindian sites are uncommon; sites minimally problematic earlier than Clovis sites are particularly rare. Over 10,000 years of geological activity have undoubtedly destroyed many of the earliest sites in North America and rendered others very difficult to access beneath meters of sediment or miles offshore. Clovis and earlier than Clovis sites offer brief, invaluable, glimpses of human adaptation to a Pleistocene landscape alien to modern observers. Set against the dynamic environmental upheaval of the Late Pleistocene, these early sites tell the story of human migration into North America and their strategies for survival on a previously unknown landscape (Buchanan et al. 2019; Kelly and Todd 1988; Meltzer 2009b). In recent decades, evidence from Clovis and potential earlier than Clovis sites challenged traditional “Clovis-First” via the ice-free corridor models (Braje et al. 2019).

The hunt for Clovis and (more recently) Clovis antecedents dominated Paleoindian archaeology for much of the 20th and early 21st century (Meltzer 1983, 1993, 2009a). The allure of identifying the oldest sites on the continent and disrupting the archaeological status quo has led to numerous premature or otherwise unsubstantiated claims of pre-Clovis origins. Conflicting dates, potential contamination from overlying strata, or ambiguous artifacts that cannot be unequivocally attributed to human actors plague many would-be earlier than Clovis sites. As noted in **Chapter 1**, earlier than Clovis sites are generally met with a justifiable degree of skepticism from the archaeological community.

In part due to Bone Bed 2's notoriety as a large-scale Folsom bison kill, Bone Bed 1 at Bonfire Shelter did not fade from archaeological memory as other tenuous earlier than Clovis sites (Haynes 2015; Meltzer 2009a). As in the case with Southern Methodist University's return to Bonfire Shelter early in the early 2000s (Byerly et al. 2005), that attention was sometimes to categorically exclude Bone Bed 1 from analysis (Grayson and Meltzer 2002:328-329; Wyckoff 1999:349). Others expressed a more optimistic assessment, but acknowledge the assemblage was inconclusive and more data was needed (Johnson 1989:443). The growing corpus of evidence supporting very early Paleoindian and earlier than Clovis occupations across North America resurrected lingering questions regarding Bone Bed 1. The emergence of the Gault and Debra L. Friedkin sites of central Texas in the early 2010s as one of the best documented earlier than Clovis sites was a major catalyst for reassessing other potential early sites across the state (Collins and Bradley 2008; Michael R. Waters et al. 2011; Waters et al. 2018; Williams et al. 2018).

As noted in **Chapters 2 and 3**, very few Paleoindian-age sites have been identified and the Lower Pecos. Turpin's Aurora sub-phase (14,500 – 11,900 RCYBP) is particularly poorly represented (Turpin 2004). Bone Bed 1 at Bonfire Shelter and the similarly ambiguous Late Pleistocene deposits at Arenosa Shelter (Dibble 1967; Jurgens 2005) and Cueva Quebrada

(Lundelius 1984) until recently represented the few pre-Bone Bed 2 deposits of potential cultural origin. All three components are characterized by ambiguous potential cut marks and spiral fractures. Of these, Bone Bed 1 is the best documented and best candidate to yield additional supporting evidence of human intervention. Technological and methodological developments since their initial documentation highlight analytical gaps that, given the antiquity and scarcity of sites from this period, warrant modern reevaluation.

Recent ASWT findings at Eagle Cave gave cause for the serious reconsideration of Bone Bed 1. Beneath what was reported in the 1960s as the culturally sterile base of excavation (Ross 1965), excavators identified unambiguous stone tools associated with butchered *Bison antiquus* remains and a small surface hearth dating to approximately 10,250 cal BP (Koenig, Nielsen, et al. 2017:86); roughly contemporary with Bone Bed 2 at Bonfire Shelter. Beneath the bison feature, a small cluster of debitage, expedient tools, and exogenic cobbles associated with mammoth remains overlaid a narrow band of organic matter dating to approximately 13,070 cal BP (Koenig, Nielsen, et al. 2017:89-92). The parallels with Bonfire Shelter were striking and reinvigorated the search for Early Paleoindian activity in Bone Bed 1.

Acknowledging the scarcity of artifacts in Bone Bed 1, the model outlined in **Chapter 6** was designed to evaluate the geological, faunal, and potentially cultural components of each substratum. Data from the 1963-1964, 1983-1984, and 2017-2018 excavations was integrated and compared against expectations for a series of scenarios that could account for the patterns observed in the field. These expectations were based on findings at sites of similar antiquity, ethnoarchaeological and experimental replications, and studies of modern proxies for Pleistocene fauna. The conclusions reached from these comparisons are summarized in **Table 9-1**.

While no direct evidence of cultural activity was identified in association with Bone Bed 1, this thesis contributes significant new information towards understanding the Late Pleistocene landscape of the Lower Pecos. Since the conclusion of the Amistad excavations, Bonfire Shelter

has played a critical role in Paleoenvironmental reconstructions of southwest Texas (Bryant 1969; Bryant and Holloway 1985; Robinson 1997; Scott-Cummings 1992). The geoarchaeological data reported in **Chapter 8**, particularly the results of particle size analyses in **Section 8.2** and the organic carbon profile in **Section 8.6**, illuminate the Late Glacial conditions at Bonfire Shelter from a new perspective. Previous studies have primarily emphasized palynological analysis and in many cases are based on only include a small component of the Bone Bed 1 strata. Prior to this study, sediment organic carbon stable ^{13}C and ^{15}N isotope analysis was not conducted at Bonfire Shelter. Sampling all strata associated with Bone Bed 1 provides a higher resolution profile of the turbulent environment surrounding the exodus and extinction of many Pleistocene megafauna species in the Lower Pecos, setting the stage for the mass bison kill event(s) of Bone Bed 2.

Bonfire Shelter's chronology, particularly in Pleistocene strata, was largely unverified and based on radiocarbon dates unreliable by modern standards (McCuistion 2019). The 2017-2018 excavations yielded three new radiocarbon dates, reported in **Table 7-9**, associated with Stratum 24. Two of these dates (FN60295: $13,966 \pm 103$; FN60312: $14,079 \pm 76$) overlap with Bement's AA-344 $14,754 \pm 725$ cal BP ($12,460 \pm 490$ RCYBP) date in the 2σ range at approximately 14,000 cal BP. These new dates verify Bement's findings and refine Stratum 24's dating precision from an unacceptably large nearly 1,000-year window to less than ~ 150 years. These dates confirm the earlier than Clovis age of Stratum 24 (H-1), suggesting slightly younger overlying deposits more consistent with "traditional" Paleoindian timelines and better aligned with the new Paleoindian features at Eagle Cave. Improving dating technologies facilitate the analysis ever smaller quantities of carbon. Further processing of additional samples may yield opportunities to directly date faunal remains and materials from other Bone Bed 1 strata. The future publication of dates from overlying components at Bonfire Shelter and additional Late Pleistocene dates present exciting new opportunities to evaluate Paleoindian activity in Mile Canyon.

The data reported in **Chapters 7 and 8** provide a more detailed overview of the taphonomic agents and variability contributing to Bone Bed 1. The substantial concentrations of gypsum (**Section 8.4**), particularly in Stratum 23 and 24, may in part explain the differential preservation of faunal remains observed between strata as well as across northern and southern excavation blocks. On a larger scale, if similar processes are active in other Lower Pecos rockshelters, the physical preservation of faunal remains may be partially responsible for the scarcity of Aurora-Phase archaeological sites.

Bone Bed 1 remains enigmatic. The new data reported in this thesis contributes to the long history of Paleoindian research at Bonfire Shelter. The new dates and paleoenvironmental data from this analysis contextualize the landscape of the Lower Pecos preceding Bone Bed 2 and the exciting new finds at Eagle Cave. Exploring the differential site use patterns and human activities across the Late Pleistocene Mile Canyon presents valuable new research opportunities. Determining why a site was avoided may prove to be just as important as the identification of artifacts themselves. As additional research emerges from the ASWT's excavations, outstanding questions regarding the nature of Bone Bed 1 may be cast in new light to form a more coherent picture of the least understood period in Lower Pecos prehistory.

9.3.1 *Future Research*

Much like Robinson's 1997 pilot study, this thesis establishes a framework for future investigations at Bone Bed 1 and Bonfire Shelter. Many of the samples and data from the 2017-2020 Bonfire Shelter field work remains to be processed. Two column samples on the talus cone and two additional columns from the shelter interior traverse Bonfire Shelter's entire depositional sequence. These data will provide abundant opportunities to validate the findings reported here and to answer new questions regarding the rich prehistory of the Lower Pecos. The methods utilized here can be readily adapted to analyze the composition and formation processes contributing to other Bonfire Shelter strata.

More specifically, samples from these columns -may help to resolve the specific origins of the two 1.0 mm chert fragments identified in Stratum 23 (**Figure 8-25**). As noted in **Section 8.10**, the initially proposed quantitative microartifact analysis was transitioned to a qualitative analysis due to the time constraints of this thesis. Further investigation of the remaining 1.0 mm fraction and reserved, unprocessed geomatrix aliquots (including <1.0 mm material) may yield additional specimens. Samples from the as yet unprocessed Bonfire Shelter column samples may provide further context. If similar materials are recovered from other definitively cultural horizons, the nature of the currently isolated Stratum 23 specimens may need to be reevaluated.

Curated samples from the 1963-1964 and 1983-1984 expeditions also have the potential to yield significant new information for Bone Bed 1 and Bonfire Shelter as a whole. Aliquots from retained soil samples analyzed using the methods outlined in this thesis could be utilized as an unambiguous geoarchaeological and microartifact comparative sample. With the advances in radiocarbon dating technology since these samples were collect, organic material previously passed over could help to further refine the chronology of Bonfire Shelter and further validate newly reported dates. Better preserved faunal specimens held by TARL and the University of Texas Vertebrate Paleontology Laboratory (if untreated with consolidants or stabilizers) may now be viable for collagen dating. If the original plan maps and scaled diagrams from these excavations can be recovered, integrating the legacy faunal assemblage into the GIS database developed for this thesis could help identify broader spatial patterns across all three Bonfire Shelter bone beds.

In the winter of 2020, final micromorphology samples were embedded and the final backfilling of excavation units open since 1963 commenced. The stabilization of this invaluable archaeological site ultimately catalyzed ASWT's current field work. This conservation effort aims to return the Shelter to as close to pre-Amistad conditions as possible, preserving the remaining intact deposits for future generations. As new technologies emerge and new research

questions arise from the data gathered during the ASWT expedition, conservation minded archaeologists may be able to seek answers in the unexplored northern reaches of Bonfire Shelter.

9.3.2 *Lessons Learned*

One of the critical lessons learned from this undertaking was that real-world data does not fit neatly into idealized categories. It is impossible to model every possible scenario and depositional contingency that could occur at an archaeological site. Some degree of simplification is necessary for a model to be a useful, functional analytical tool without becoming unwieldy. Implementing the model, it is more than possible that that some, all, or none of the expectations will be satisfied. Accepting a “best fit” rather than attempting to expand the model was an important cross-roads.

Selecting appropriate case studies and comparative samples greatly improved the functionality of the model. Despite extensive preparation, the data were not always a good fit. It was difficult to define the expected geological conditions for cultural phenomenon. This was compounded by the highly variable environmental conditions of the Terminal Pleistocene as well as the limited number of explicitly cultural sites from this time period, particularly in the Lower Pecos. Modern proxies and later comparisons are imperfect, especially where environmental conditions are alien and the species in question are extinct.

The usefulness of the model is only as good as the data collected in the field. Data collected with an explicit purpose in mind proved more valuable and provided clearer interpretations than data collected for contingency purposes. Implementing a more refined model earlier in the planning process would have made this research even more productive.

If this project were repeated, establishing a smaller sampling interval in Column Sample 5 would help to address outstanding questions. As implemented, matrix samples were collected by natural stratigraphy, leaving depositional variation within those strata was unaddressed.

Considering the significant differences between strata, it is extremely unlikely that conditions remained static for the hundreds or thousands of intervening years.

This higher resolution column sample strategy would be traded off for a more restrained and explicit microartifact sampling strategy. The number of samples collected was over ambitious and the timeline for processing those samples was naively short. Dedicating time to sorting and analyzing a targeted small number of samples instead of preprocessing a large, broad swath of samples would have been more efficient. Further quantitative analysis of these microartifact samples will be a component follow up research to this thesis.

Similarly, methods implemented for extracting, processing, and analyzing faunal remains should have been more explicitly established before fieldwork commenced. The limited facilities to safely clean, process, stabilize, and store significant numbers of mammoth remains greatly impacted the trajectory of this project. Extremely poor preservation made extraction of the remains, let alone the identification of cut marks and evidence of modification, an exercise in frustration. Restructuring this study to include additional photography and in-field cleaning/assessment would have yielded more functional dataset than counting on time, resources, and facilities to become available in the future.

Despite these preservation and logistical issues, a formal faunal analysis is needed for Bone Bed 1. Attempting to integrate this procedure into an already overly broad research design was irresponsible, unrealistic, and short sighted given the timeline and logistical issues. I hope that a future archaeologist will be able to afford the remains their due diligence.

Bone collagen dating efforts related to Bone Bed 1 have thus far proved unsuccessful. Well preserved specimens from Stratum 23 and 24 were submitted to UTSA for XAD Ultrafiltration collagen extraction, but no viable material was recovered. To date, specimens submitted from Bone Bed 2 have been similarly unsuccessful. Perhaps future technological

developments will provide new, innovative, or refined dating opportunities. Further processing of sediment samples and untreated faunal specimens may continue to yield viable material for traditional AMS dating. Until then, several of the Bone Bed 1 strata remain unverified.

It is my hope that this thesis has the groundwork for future research and evaluation of Bone Bed 1 and Bonfire Shelter as a whole. While all microartifact samples were reviewed in some capacity, only a subset were fully processed and quantified. Raw portions of all spot samples and column sample material were retained for verification and supplemental testing. Integrated with the new column samples excavated on the Talus Cone and elsewhere on the main block, these data can form a cohesive and more complete depositional history of Bonfire Shelter for future archaeologists working to resolve the many outstanding questions at Bonfire Shelter.

APPENDIX SECTION

Appendix A: Particle Size Distributions

Table A-1. LS001 (S19) Particle Size Distribution: Cumulative Curve Data Tabulation

LS001 (S19) - Particle Size Distribution				
Phi (ϕ) Class	Mass % With Gravel	Cumulative % With Gravel	Mass % Without Gravel	Cumulative % Without Gravel
-7	9.39	9.39	9.39	-
-6	0	9.39	0	-
-5	5.55	14.94	5.55	-
-4	3.06	18	3.06	-
-3	3.04	21.04	3.04	-
-2	3.84	24.88	3.84	-
-1	3.92	28.8	3.92	-
-0.5	1.19	29.99	1.67	1.67
0	1.49	31.48	2.09	3.76
0.5	1.36	32.84	1.91	5.67
1	1.48	34.32	2.07	7.74
1.5	1.54	35.86	2.17	9.91
2	1.66	37.52	2.33	12.24
2.5	1.83	39.35	2.57	14.81
3	2.09	41.44	2.94	17.75
3.5	2.08	43.52	2.92	20.67
4	3.28	46.8	4.61	25.28
5.403	6.53	53.33	9.18	34.48
6.388	7.84	61.17	11.01	45.49
7.125	7.19	68.36	10.1	55.59
8.467	10.45	78.81	14.69	70.28
9.528	3.92	82.73	5.51	75.79
14	17.27	100	24.21	100

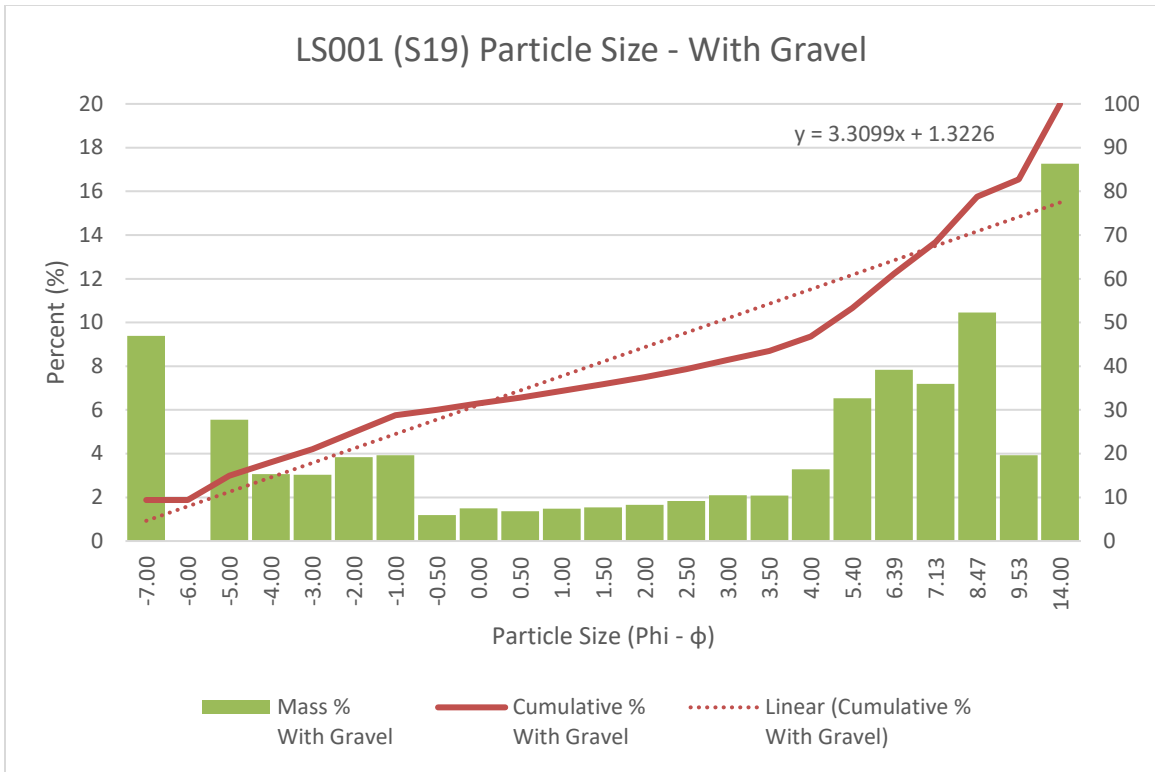


Figure A-1. LS001 (S19) Particle Size Distribution with Gravel: Histogram and Cumulative Curve

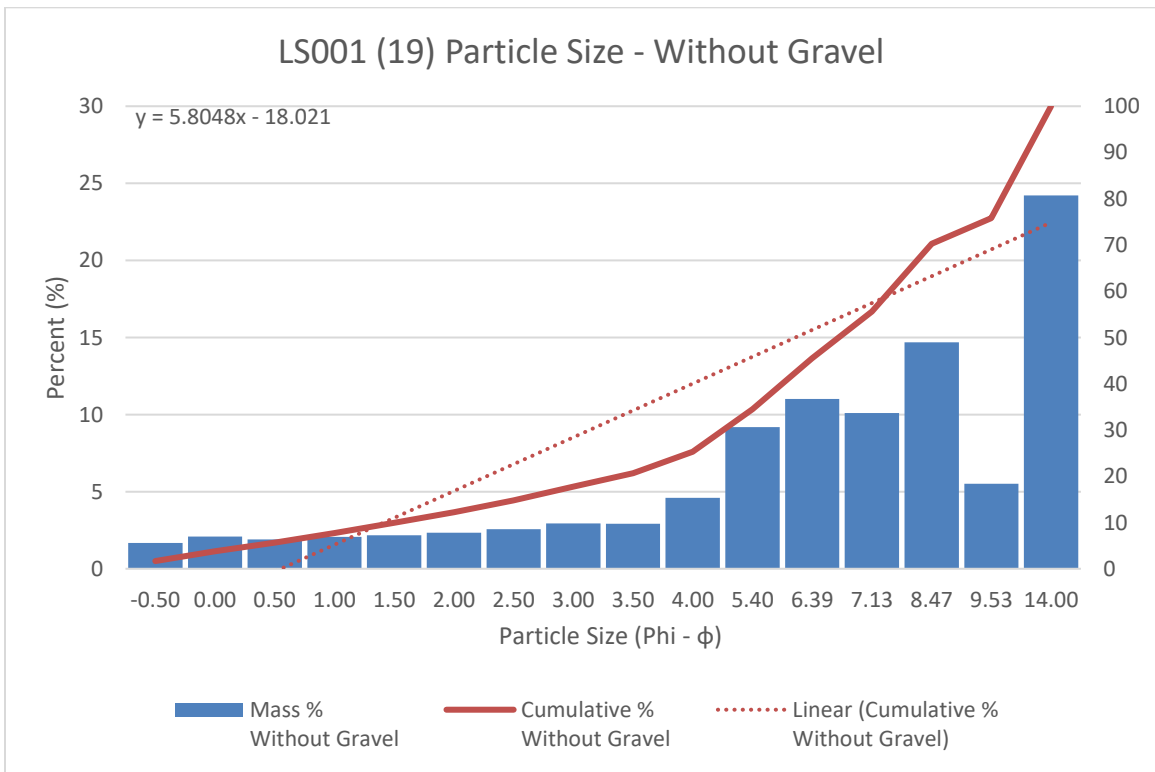


Figure A-2. LS001 (S19) Particle Size Distribution without Gravel: Histogram and Cumulative Curve

Table A-2. LS002 (S20) Particle Size Distribution: Cumulative Curve Data Tabulation

LS002 (S20) - Particle Size Distribution				
Phi (ϕ) Class	Mass % With Gravel	Cumulative % With Gravel	Mass % Without Gravel	Cumulative % Without Gravel
-5.00	3.6	3.6	3.6	-
-4.00	3.3	6.9	3.3	-
-3.00	7.0	13.9	7.0	-
-2.00	8.3	22.2	8.3	-
-1.00	6.7	28.8	6.7	-
-0.50	2.3	31.1	3.2	3.2
0.00	3.0	34.1	4.2	7.4
0.50	2.8	36.9	4.0	11.4
1.00	2.5	39.5	3.6	14.9
1.50	2.5	41.9	3.5	18.4
2.00	2.5	44.4	3.5	21.9
2.50	2.5	46.9	3.5	25.4
3.00	2.9	49.8	4.1	29.5
3.50	3.0	52.8	4.2	33.7
4.00	8.1	61.0	11.4	45.2
5.30	9.5	70.5	13.3	58.5
6.31	6.3	76.8	8.9	67.4
7.07	7.1	83.9	10.0	77.3
8.45	7.1	91.0	10.0	87.3
9.52	2.4	93.4	3.3	90.6
14.00	6.6	100.0	9.4	100.0

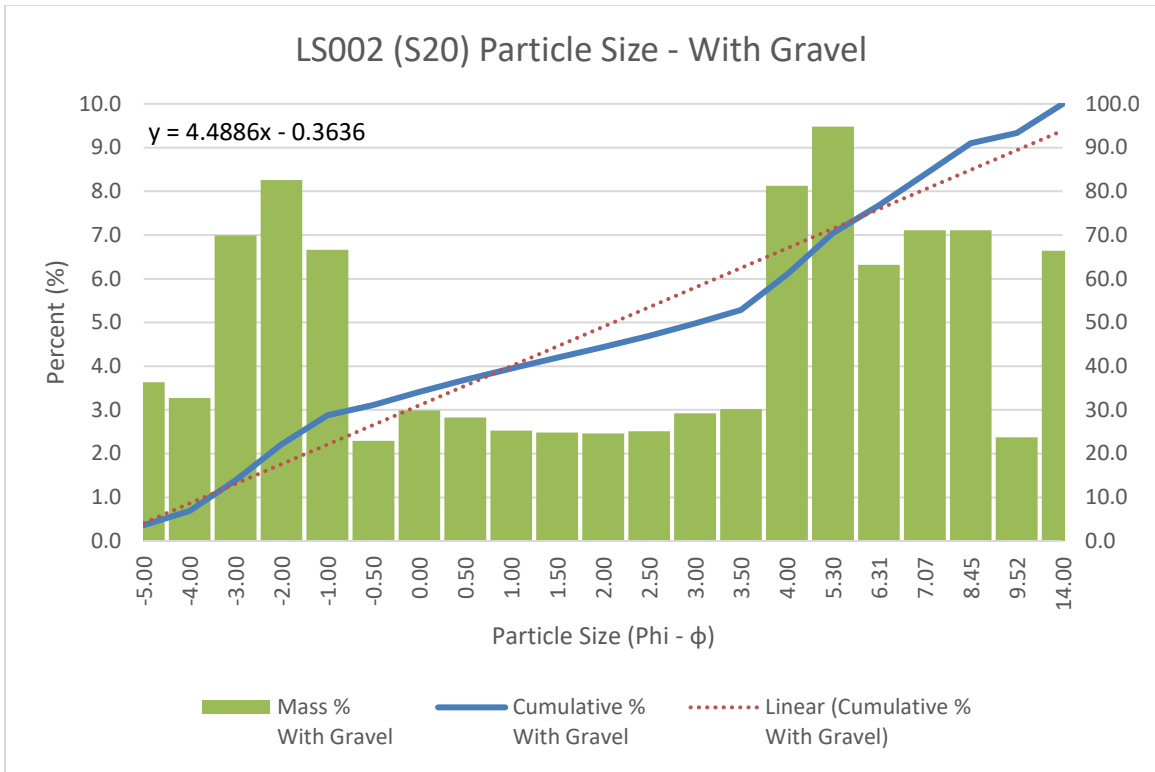


Figure A-3. LS002 (S20) Particle Size Distribution with Gravel: Histogram and Cumulative Curve

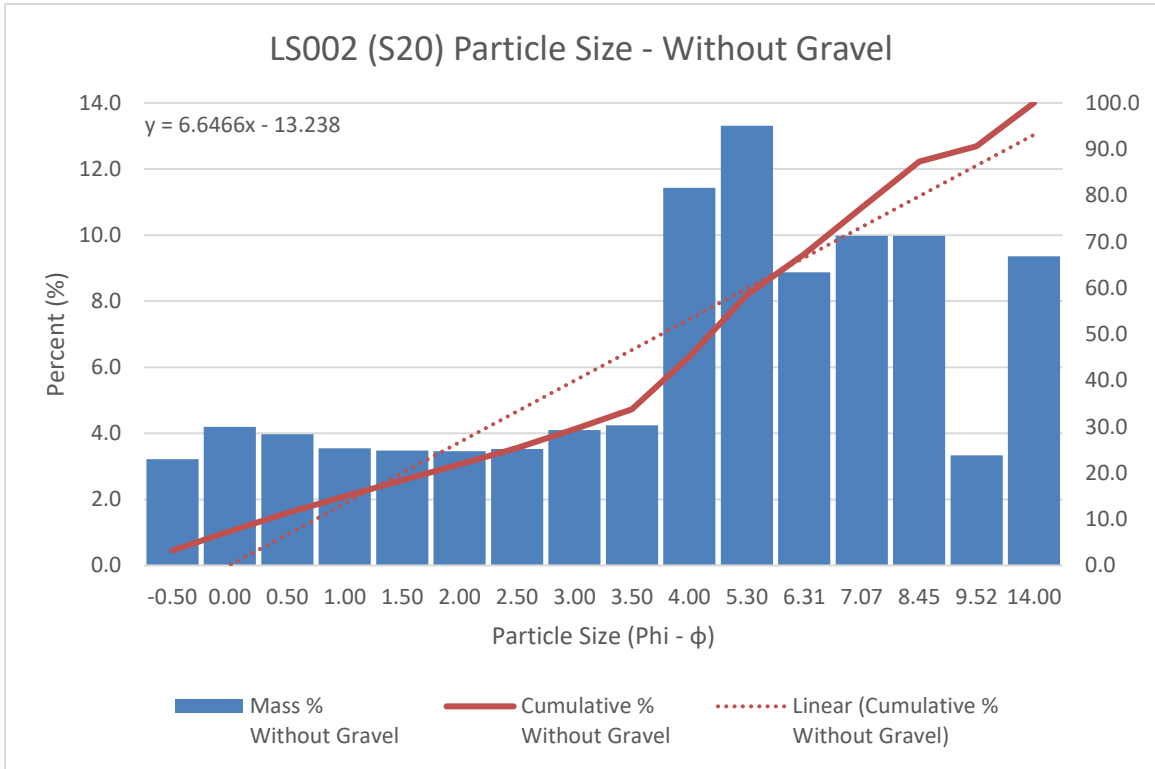


Figure A-4. LS002 (S20) Particle Size Distribution without Gravel: Histogram and Cumulative Curve

Table A-3. LS003 (S21) Particle Size Distribution: Cumulative Curve Data Tabulation

LS003 (S21) - Particle Size Distribution				
Phi (ϕ) Class	Mass % With Gravel	Cumulative % With Gravel	Mass % Without Gravel	Cumulative % Without Gravel
-6	1.24	1.24	1.24	-
-5	2.64	3.88	2.64	-
-4	13.72	17.6	13.72	-
-3	15.07	32.67	15.07	-
-2	11.42	44.09	11.42	-
-1	6.58	50.67	6.58	-
-0.5	1.62	52.29	3.27	3.27
0	2.3	54.59	4.66	7.93
0.5	2.1	56.69	4.25	12.18
1	2.02	58.71	4.09	16.27
1.5	1.78	60.49	3.62	19.89
2	1.44	61.93	2.91	22.8
2.5	1.13	63.06	2.3	25.1
3	1.12	64.18	2.27	27.37
3.5	1.28	65.46	2.59	29.96
4	2.89	68.35	5.87	35.83
5.343	5.61	73.96	11.37	47.2
6.342	5.61	79.57	11.37	58.57
7.097	4.49	84.06	9.1	67.67
8.463	6.17	90.23	12.51	80.18
9.524	3.37	93.6	6.82	87
14	6.4	100	13	100

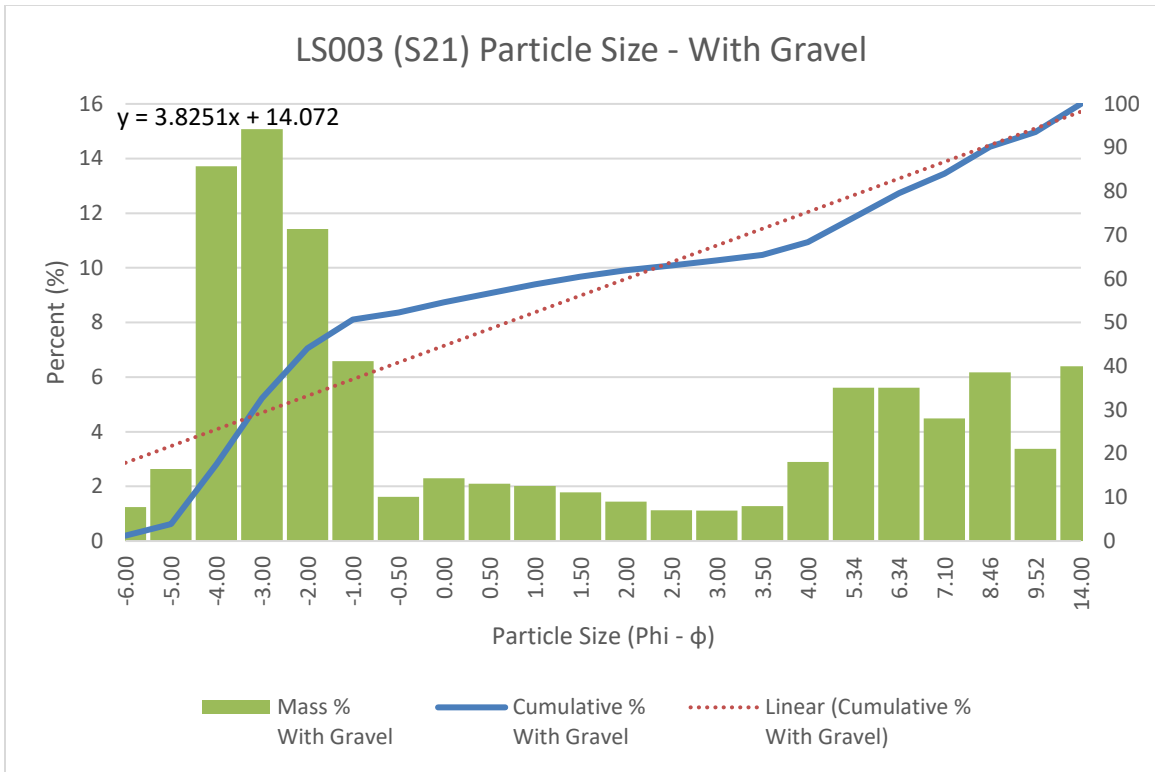


Figure A-5. LS003 (S21) Particle Size Distribution with Gravel: Histogram and Cumulative Curve

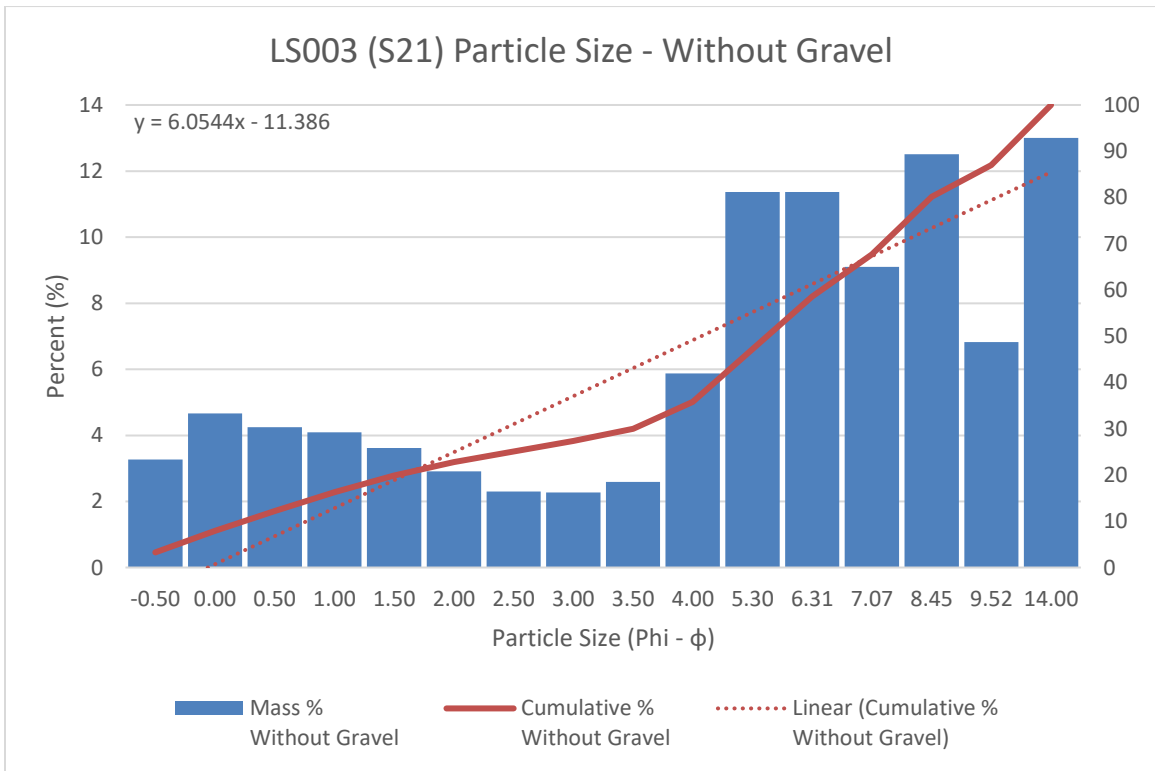


Figure A-6. LS003 (S21) Particle Size Distribution without Gravel: Histogram and Cumulative Curve

Table A-4. LS004 (S22) Particle Size Distribution: Cumulative Curve Data Tabulation

LS004 (S22) - Particle Size Distribution				
Phi (ϕ) Class	Mass % With Gravel	Cumulative % With Gravel	Mass % Without Gravel	Cumulative % Without Gravel
-5	5.62	5.62	5.62	-
-4	19.85	25.47	19.85	-
-3	17.44	42.91	17.44	-
-2	10.85	53.76	10.85	-
-1	6.48	60.24	6.48	-
-0.5	1.5	61.74	3.78	3.78
0	1.75	63.49	4.41	8.19
0.5	1.36	64.85	3.42	11.61
1	1.14	65.99	2.88	14.49
1.5	1.02	67.01	2.56	17.05
2	0.92	67.93	2.32	19.37
2.5	0.98	68.91	2.47	21.84
3	1.37	70.28	3.44	25.28
3.5	1.79	72.07	4.5	29.78
4	3.77	75.84	9.49	39.27
5.288	7.15	82.99	17.99	57.26
6.291	4.47	87.46	11.24	68.5
7.052	3.13	90.59	7.87	76.37
8.421	4.92	95.51	12.37	88.74
9.491	1.79	97.3	4.5	93.24
14	2.7	100	6.76	100

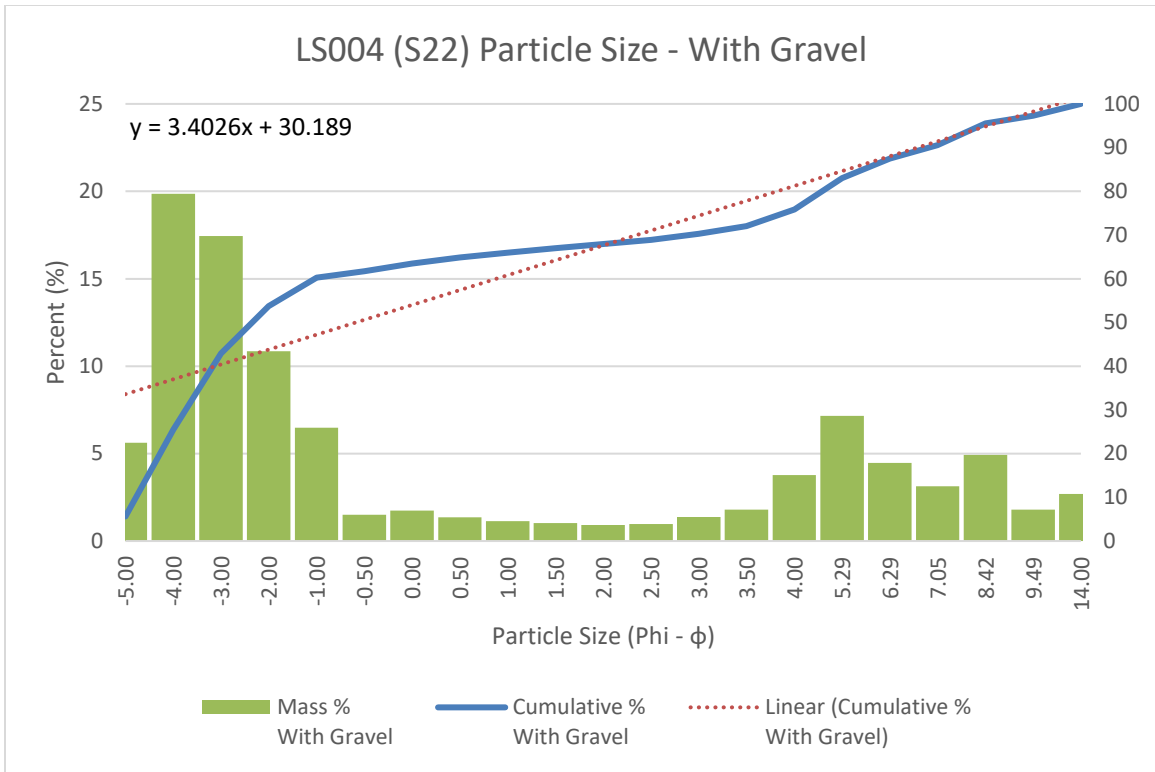


Figure A-7. LS004 (S22) Particle Size Distribution with Gravel: Histogram and Cumulative Curve

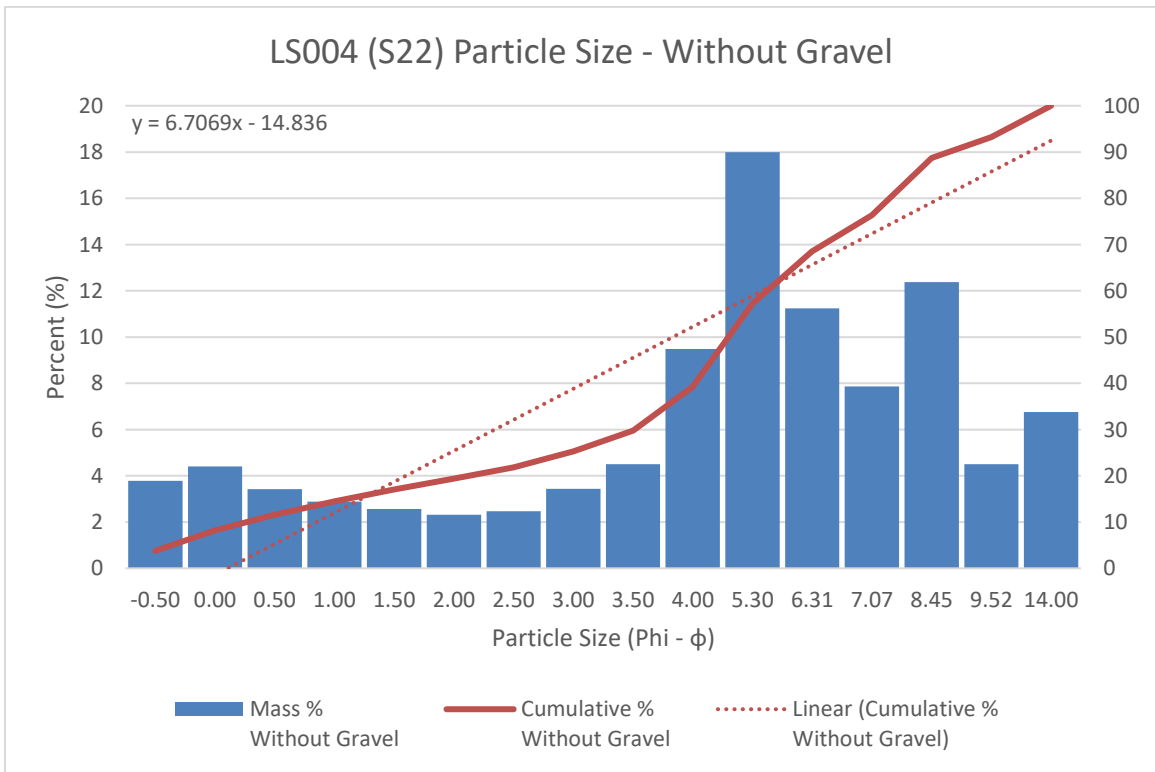


Figure A-8. LS004 (S22) Particle Size Distribution without Gravel: Histogram and Cumulative Curve

Table A-5. LS005 (S23) Particle Size Distribution: Cumulative Curve Data Tabulation

LS005 (S23) - Particle Size Distribution				
Phi (ϕ) Class	Mass % With Gravel	Cumulative % With Gravel	Mass % Without Gravel	Cumulative % Without Gravel
-5	6.82	6.82	6.82	0
-4	18.75	25.57	18.75	0
-3	11.34	36.91	11.34	0
-2	6.14	43.05	6.14	0
-1	3.3	46.35	3.3	0
-0.5	1.4	47.75	2.61	2.61
0	2.06	49.81	3.84	6.45
0.5	1.54	51.35	2.87	9.32
1	1.51	52.86	2.82	12.14
1.5	1.29	54.15	2.4	14.54
2	1.18	55.33	2.2	16.74
2.5	1.05	56.38	1.96	18.7
3	1.24	57.62	2.31	21.01
3.5	1.45	59.07	2.7	23.71
4	3.1	62.17	5.78	29.49
5.333	7.44	69.61	13.87	43.36
6.328	6.82	76.43	12.71	56.07
7.088	4.34	80.77	8.09	64.16
8.441	8.68	89.45	16.18	80.34
9.507	3.1	92.55	5.78	86.12
14	7.45	100	13.88	100

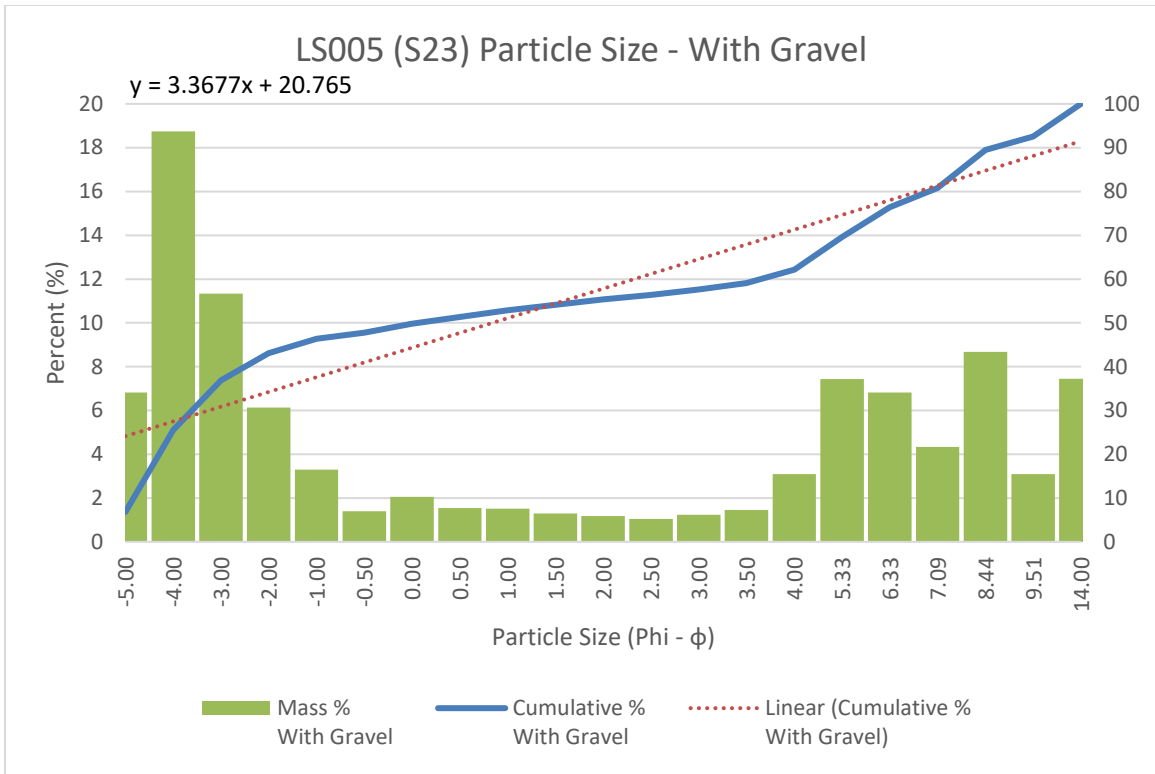


Figure A-9. LS005 (S23) Particle Size Distribution with Gravel: Histogram and Cumulative Curve

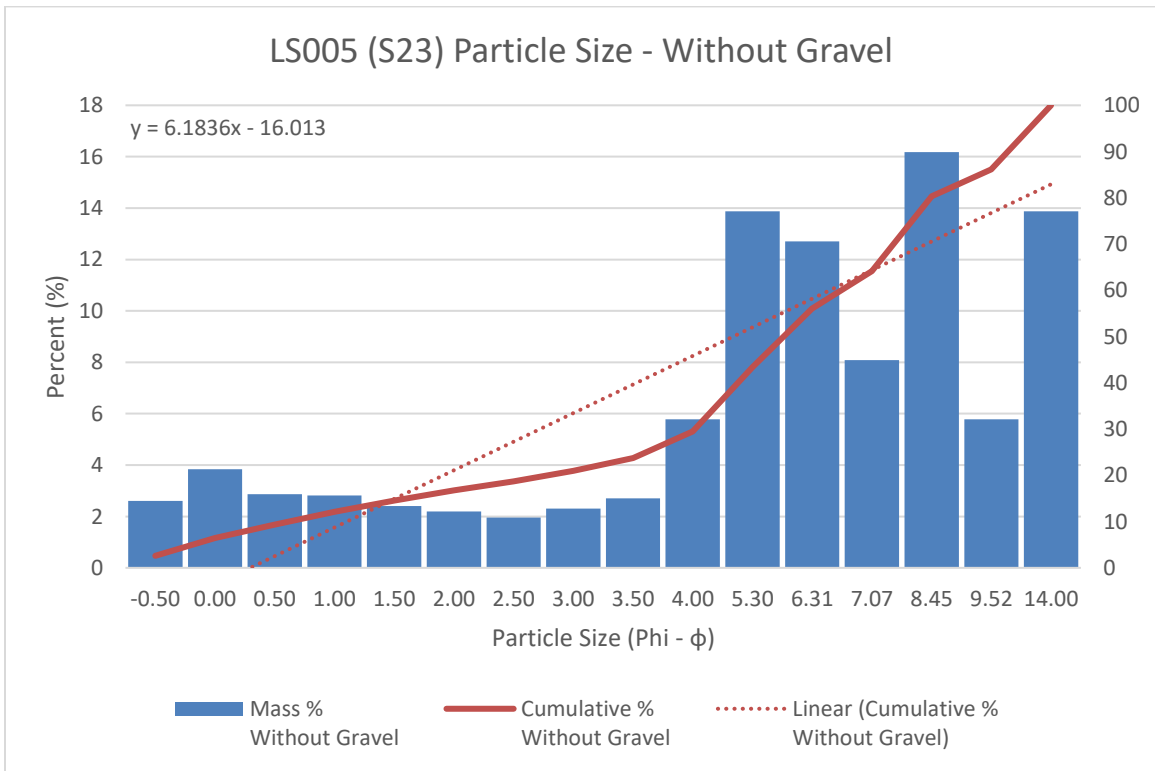


Figure A-10. LS005 (S23) Particle Size Distribution without Gravel: Histogram and Cumulative Curve

Table A-6. LS006 (S24) Particle Size Distribution: Cumulative Curve Data Tabulation

LS006 (S24) - Particle Size Distribution				
Phi (ϕ) Class	Mass % With Gravel	Cumulative % With Gravel	Mass % Without Gravel	Cumulative % Without Gravel
-7	9.38	9.38	9.38	-
-6	0	9.38	0	-
-5	20.91	30.29	20.91	-
-4	32.88	63.17	32.88	-
-3	13.04	76.21	13.04	-
-2	5.09	81.3	5.09	-
-1	2.31	83.61	2.31	-
-0.5	0.72	84.33	4.42	4.42
0	0.97	85.3	5.93	10.35
0.5	0.87	86.17	5.28	15.63
1	0.72	86.89	4.39	20.02
1.5	0.61	87.5	3.72	23.74
2	0.51	88.01	3.13	26.87
2.5	0.42	88.43	2.58	29.45
3	0.5	88.93	3.08	32.53
3.5	0.59	89.52	3.57	36.1
4	0.88	90.4	5.36	41.46
5.297	1.63	92.03	9.92	51.38
6.309	1.63	93.66	9.92	61.3
7.065	1.63	95.29	9.92	71.22
8.425	2.64	97.93	16.12	87.34
9.495	0.81	98.74	4.96	92.3
14	1.26	100	7.7	100

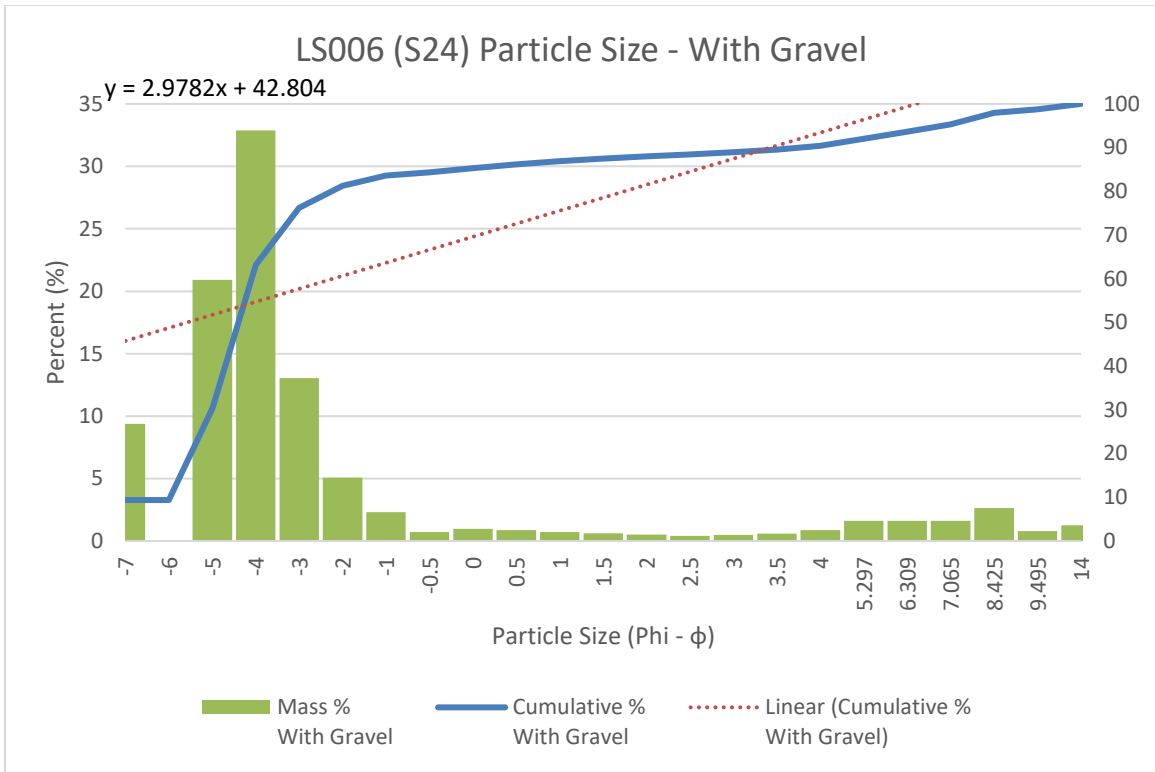


Figure A-11. LS006 (S24) Particle Size Distribution with Gravel: Histogram and Cumulative Curve

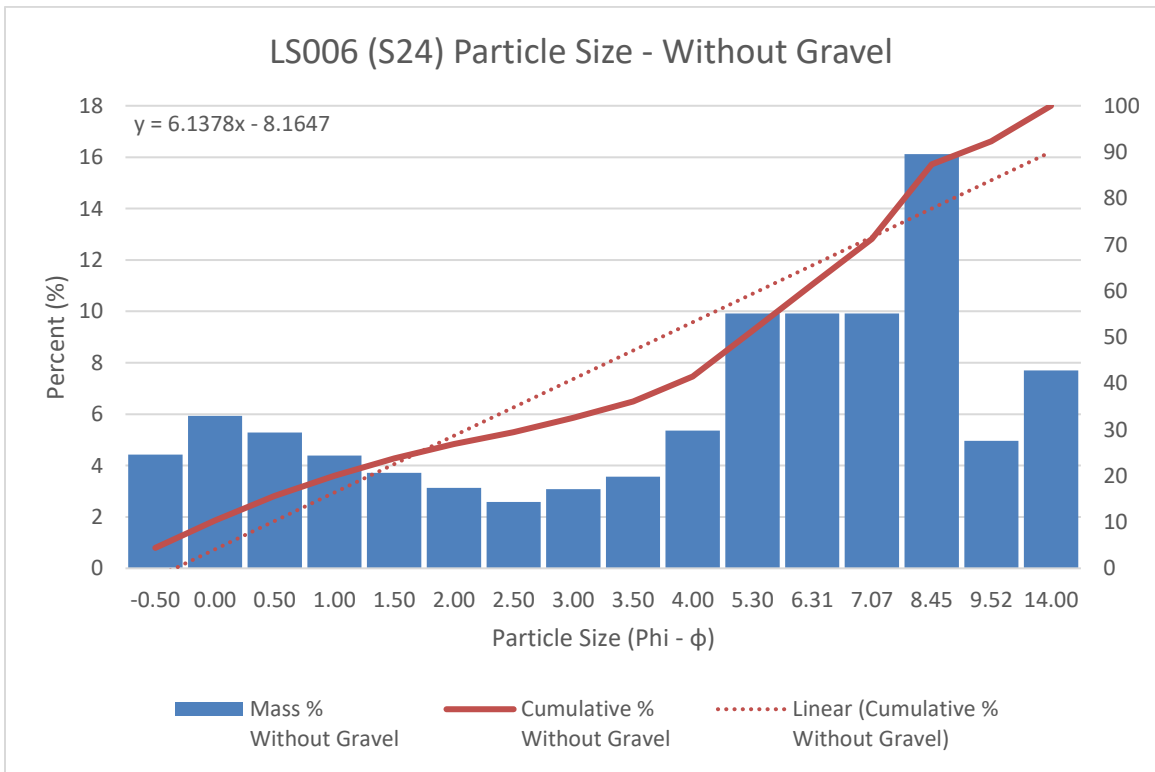


Figure A-12. LS006 (S24) Particle Size Distribution without Gravel: Histogram and Cumulative Curve

Appendix B: Raw Microartifact

Table B-1. Bone Bed 1: Qualitative Microartifact Results

Bone Bed 1 - Qualitative Microartifact Results 2017-2018																	
FN	Lot	Unit	Level	Stratum	Analyzed Mass (g)	Limestone	Bone	Charcoal	Shell	Gypsum Nodule	Round Gravel	Round Gravel (per g)	Quartz	Hackberry Seed	Fossil	Possible Chert	FN Comment
60057	60061	C1	5	S23a	12.28	X	X	-	X	X	11	0.90	-	-			With horse metapodial (60055)
60279	60061	C1	5	S23a	7.95	X	X	X	X	X	3	0.38	X	-			Below mammoth ribs (60056 & 60227)
60082	60076	C1	5B	S23b	20.39	X	X	-	-	X	5	0.25	X	-			Beneath mammoth rib (60082)
60104	60117	C1	5B	S23b	10.59	X	X	-	X	X	4	0.38	-	X			Near south end of mammoth rib (60082)
60109	60117	C1	5B	S23b	11.85	X	X	-	X	X	5	0.42	X	-			Margin of mammoth rib (60108)
60111	60117	C1	5B	S23b	10.97	X	X	-	X	-	17	1.55	-	-			Adjacent to mammoth rib (60112); Lots of bone
60112	60117	C1	5B	S23b	20.73	X	X	-	X	-	8	0.39	X	-			Beneath mammoth rib (60112); Lots of bone
60121	60117	C1	5B	S23b	13.64	X	X	-	X	X	7	0.51	X	-			Margins of cobble in NW profile
60144	60117	C1	5B	S23b	9.2	X	X	X	-	X	7	0.76	X	-			Below UID bone (60113)
60163	60117	C1	5B	S23b	11.47	X	X	X	X	X	8	0.70	X	-			Beneath possible mammoth tusk segment (60163); Mostly Bone
60166	60117	C1	5B	S23b	19.04	X	X	X	-	X	15	0.79	X	-			Behind possible tusk segment
60174	60117	C1	5B	S23b	17.42	X	X	-	X	X	14	0.80	X	-			Southern half of mammoth rib (60108), pedestal
60229	60248	C1	6	S24	8.21	X	X	-	X	X	7	0.85	X	X			Beneath 60114 pedestal
60300	60248	C1	6	S24	19.82	X	X	-	-	X	10	0.50	X	X			Inside bend of mammoth rib (60247)
60167	60248	C1	6	S24	6.14	X	X	-	X	X	16	2.61	X	X	X	-	Between mammoth ribs (60082 & 60112) at stratum interface
60299	60248	C1	6	S24	12.97	X	X	-	X	X	30	2.31	X	X	X	X	Between mammoth rib (60247) and UID bone (60161)
60084	60076	C2	1	S23	9.6	X	X	-	X	X	3	0.31	-	X			Inside margin of mammoth rib (60082)
60087	60076	C2	1	S23	18.81	X	X	-	X	X	22	1.17	X	-			Inside margin of mammoth rib (60082), beneath sample 60084
60090	60076	C2	1	S23	17.98	X	X	X	X	X	11	0.61	X	-			Above mammoth rib fragment (60088)
60092	60076	C2	1	S23	17.42	X	X	-	X	X	68	3.90	X	X	X	X	NW margin of mammoth rib (60082); 2 possible chert flakes
60094	60076	C2	1	S23	7.12	X	X	X	X	X	18	2.53	X	X	X	X	Margin of UID bone (60081)

Table B-1. Continued

FN	Lot	Unit	Level	Stratum	Analyzed Mass (g)	Limestone	Bone	Charcoal	Shell	Gypsum Nodule	Round Gravel	Round Gravel (per g)	Quartz	Hackberry Seed	Fossil	Possible Chert	FN Comment
60095	60076	C2	1	S23	10.36	X	X	X	X	X	2	0.19	X	-			Near UID bone (60026)
60097	60076	C2	1	S23	6.93	X	X	-	X	X	11	1.59	X	-			North margin of mammoth rib (60082)
60301	60294	C2	3	S24	14.44	X	X	-	-	X	9	0.62	X	X			Between UID mammoth element (60282) and possible horse element (60283)
60302	60294	C2	3	S24	4.44	X	-	-	X	X	2	0.45	X	-			SE margin of possible horse element (60283)
60303	60294	C2	3	S24	17.58	X	X	-	X	X	13	0.74	X	X			North of possible horse longbone (60292)
60304	60294	C2	3	S24	20.9	X	X	-	X	X	11	0.53	X	-			North margin of possible horse vertebra (60289)
60305	60294	C2	3	S24	19.04	X	X	-	X	-	16	0.84	X	X			Inside articulation of possible horse tibia (60285) & possible horse UID (60286)
60306	60294	C2	3	S24	15.2	X	X	-	X	X	11	0.72	X	X			Between two cobbles near south-central edge of unit
60307	60294	C2	3	S24	17.35	X	X	X	X	X	5	0.29	X	X			Beneath cobbles at SW margin of unit
60391	60294	C2	3	S24	18.23	X	X	-	-	X	18	0.99	X	-			Pedestal below two poorly preserved possible horse elements (60283 & 60286)
60676	60294	C2	3	S24	21.68	X	X	-	X	X	21	0.97	X	-			Below UID mammoth element (60282)
60677	60294	C2	3	S24	13.72	X	X	-	-	X	21	1.53	X	X			Below possible horse vertebra (60289)
60063	60023	C3	1	S23	16.61	X	X	-	X	X	0	0.00	-	-			Within mammoth pelvis pedestal (60011)
60065	60028	C3	2	S23	20.43	X	X	-	X	X	17	0.83	X	-			Within mammoth pelvis pedestal (60011)
60062	60023	C3	Pelvis Ped L1	S23	20.7	X	X	-	X	X	88	4.25	X	X	X		Within mammoth pelvis pedestal (60011)
60054	60278	C3	Rib Ped L2	S23	20.02	X	X	-	X	X	126	6.29	X	X	X		Mammoth rib pedestal (60009 & 60010)
60064	60023	C3	Pelvis Ped Slump	S23/24	17.97	X	X	-	-	X	21	1.17	X	X			Mammoth pelvis pedestal (60011) slump
60031	60030	C3	3	S24	23.67	X	X	-	X	X	5	0.21	X	X			Darker matrix NW of mammoth rib (60009)
60032	60030	C3	3	S24	2.92	X	X	X	-	X	7	2.40	X	-			Light matrix NE quadrant of unit
60068	60030	C3	3	S24	16.47	X	X	-	-	X	27	1.64	X	X			Within mammoth pelvis pedestal (60011)

Table B-1. Continued

FN	Lot	Unit	Level	Stratum	Analyzed Mass (g)	Limestone	Bone	Char-coal	Shell	Gypsum Nodule	Round Gravel	Round Gravel (per g)	Quartz	Hack-berry Seed	Fossil	Possible Chert	FN Comment
60071	60278	C3	4	S24	17.79	X	X	-	-	X	22	1.24	-	X			Within mammoth pelvis pedestal (60011)
60051	60030	C3	Rib Ped L3	S24	20.03	X	X	-	-	-	101	5.04	X	X	-	X	Mammoth rib pedestal (60009 & 60010)
60038	60030	C3	Rib Ped L3	S24	16.31	X	X	-	X	-	35	2.15	X	X	-	X	Immediately beneath mammoth rib (60010)
60258	60250	CS05	1	S19	20.41	X	X	X	X	X	22	1.08	X	X			PS06.CS05.S19; LS001
60259	60251	CS05	2	S20	17.02	X	X	X	X	X	5	0.29	X	-			PS06.CS05.S20; LS002
60260	60252	CS05	3	S21	20.53	X	X	-	-	X	10	0.49	X	X			PS06.CS05.S21; LS003
60261	60253	CS05	4	S22	17.85	X	X	-	X	X	25	1.40	X	-			PS06.CS05.S22; LS004
60262	60254	CS05	5	S23	19.68	X	X	X	X	X	24	1.22	X				PS06.CS05.S23; LS005
60275	60274	CS05	6	S24	18.45	X	X	-	X	X	20	1.08	X	X			PS06.CS05.S24; LS006
60370	60263	D3	2	S24	11.77	X	X	X	X	X	11	0.93	X	X			Generic sediment sample
60452	60442	D3	4	S24	18.4	X	X	-	-	X	0	0.00	-	-			Below UID rib fragments (60449)
60409	60392	D3	3	S24	19	X	X	-	X	X	8	0.42	X	-	-	X	Below UID rib (60408)
60511	60509	D7	4	S24	7.11	X	X	-	-	X	1	0.14	X	-			Disturbed sediment in southern portion of unit, near flagging tape
60510	60498	D7	4	S24	20	X	<0.01	-	X	X	5	0.25	X	-	-	X	Between possible antelope ribs (60499 & 60506)
60523	60498	D7	4	S24	21.5	X	X	<0.01	X	X	10	0.47	X	-	X	X	Beneath possible antelope rib (60506)
60540	60537	D8	4	S24	17.66	X	-	-	-	-	0	0.00	-	-	-	-	North of UID bone fragment
60552	60548	D8	5	S24	20	X	<0.01	-	<0.01	-	0	0.00	<0.01	-	-	-	NE corner of unit, above "spall pavement"

Appendix C: Faunal Assemblage

Table C-1. 1963-1964 Bone Bed 1 Faunal Assemblage - Reconstructed from TARL Records

AMIS ID	N (ft)	W (ft)	Depth (ftbd)	Zone (Dibble)	Stratum* (Bement)	Stratum* (Farrell)	Species	Element	Count	Comment
43501				F4	E/F/G	S23	Bison	Unlisted	34	
43508	98	40		F4	E/F/G	S23	Bison	Unlisted	89	
43909	98	40		F4	E/F/G	S23	Unlisted	UID	1	
43914	50	70		Zone 4, Below 7	E/F/G	S23	Unlisted	Unlisted	4	
43926	98	40		F4	E/F/G	S23	Bison	Unlisted	5	
43947	98	40		F4	E/F/G	S23	Bison	Unlisted - Fragments of single bone	12	
43975	98	40		F4	E/F/G	S23	Bison	Unlisted	1	
43975				F4	E/F/G	S23	Bison	Unlisted	1	
44036	98	40		F4	E/F/G	S23	Unlisted	Mandible	1	
44036	98	40		F4	E/F/G	S23	Bison	Mandible	1	
44215	110	40		F4	E/F/G	S23	Unlisted	Unlisted	3	
44216	98	40		F4	E/F/G	S23	Unlisted	Unlisted	1	
44217	98	40		F4	E/F/G	S23	Non-Bison	Unlisted	2	
44235	110	40	88.66	F4	E/F/G	S23	Camel	Unlisted	1	
44264	110	40		F4	E/F/G	S23	Non-Bison	Unlisted	1	
44265	98	40		F4	E/F/G	S23	Non-Bison	Unlisted	1	
44269	110	40		F4	E/F/G	S23	Bison	Unlisted	1	
44312	110	40		F4	E/F/G	S23	Non-Bison	Unlisted	2	
44313	110	40		F4	E/F/G	S23	Camel	Jaw with Teeth	1	
44412	98	40		F4	E/F/G	S23	Non-Bison	Unlisted	1	
44414	110	40	88.66	F4	E/F/G	S23	Bison	Unlisted	14	
44416	110	40		F4	E/F/G	S23	Bison	Unlisted	1	
44422	98	40		F4	E/F/G	S23	Bison	Tibia	1	
44432	98	40		F4	E/F/G	S23	Bison	Unlisted	1	
44432				F4	E/F/G	S23	Bison	Unlisted	4	
44432				F4	E/F/G	S23	Bison	Unlisted	14	
44432				F4	E/F/G	S23	Bison	Unlisted	1	
44432				F4	E/F/G	S23	Bison	Unlisted	1	
44433				F4	E/F/G	S23	Bison	Unlisted	1	
44433				F4	E/F/G	S23	Bison	Unlisted	3	
44475	98	40		F4	E/F/G	S23	Bison	Ribs	2	
44476				F4	E/F/G	S23	Bison	Unlisted	8	
44476				F4	E/F/G	S23	Bison	Unlisted	1	

Table C-1. Continued

AMIS ID	N (ft)	W (ft)	Depth (ftbd)	Zone (Dibble)	Stratum* (Bement)	Stratum* (Farrell)	Species	Element	Count	Comment
44476				F4	E/F/G	S23	Bison	Unlisted	3	
44476				F4	E/F/G	S23	Bison	Unlisted	1	
44478	98	40		F4	E/F/G	S23	Bison	Unlisted	1	
44491	110	40	88.66	F4	E/F/G	S23	Unlisted	Unlisted - Fragments	26	
44491				F4	E/F/G	S23	Bison	Unlisted	1	Likely gypsum
44491				F4	E/F/G	S23	Bison	Unlisted	1	
44491				F4	E/F/G	S23	Bison	Unlisted	1	
44491				F4	E/F/G	S23	Bison	Unlisted	1	Non-bison bone in plaster cast
44491				F4	E/F/G	S23	Bison	Unlisted	2	
44491				F4	E/F/G	S23	Bison	Vertebra	1	
44491				F4	E/F/G	S23	Bison	Vertebra	1	
44491				F4	E/F/G	S23	Bison	Unlisted	1	
44491				F4	E/F/G	S23	Bison	Unlisted	1	
44491				F4	E/F/G	S23	Bison	Vertebra	9	Likely gypsum
44494	98	40		F4	E/F/G	S23	Bison	Unlisted	2	
44497	98	40		F4	E/F/G	S23	Bison	Unlisted	6	Previously inventoried as UID bone.
43076	110	40		F4	E/F/G	S23	Botanical	Leaves	1	
43107	98	40		F4	E/F/G	S23	Botanical	Wood	1	
43119	110	40	88.59	F4	E/F/G	S23	¹⁴ C	-	1	
43209	98	40		F4	E/F/G	S23	¹⁴ C	-	2	
43336	98	40		F4	E/F/G	S23	Geological	Quartz Crystal	6	
44363	110	40	88	F4	E/F/G	S23	Soil Sample	Unknown Powder	1	
44403	98	40		F4	E/F/G	S23	Soil Sample	Soil	1	
44410	110	40		F4	E/F/G	S23	Geological	Unlisted - Stone	1	
43946	98	40		F12	H	S24	Bison	Unlisted - Fragments	33	
44488				F12	H	S24	Bison	Unlisted	1	
44489				F12	H	S24	Bison	Unlisted	2	
44493	98	40		F12	H	S24	Bison	Unlisted	1	
43755	80	42		F16	I	-	Bison	Calcaneum	3	
43771	80	47		F16	I	-	Bison	Sesamoids	3	
43973			86.63	F16	I	-	Bison	Ulna	1	

Table C-1. Continued

AMIS ID	N (ft)	W (ft)	Depth (ftbd)	Zone (Dibble)	Stratum* (Bement)	Stratum* (Farrell)	Species	Element	Count	Comment
44480				F16	I	-	Bison	Teeth	1	
44492	110	40	86.46	F16	I	-	Bison	Unlisted	1	
43121	98	40	95-97	-	-	-	¹⁴ C		1	
43360	110	40		-	-	-	Geological	Unlisted - Stone	68	Stone - Associated with deep bone deposit
43365	110	40		-	-	-	Geological	Quartz Crystal	2	Likely gypsum
43401	50	70		-	-	-	Shell	Snail Shell	1	Deep Test, Zone 4
43484	98	40	95-94	-	-	-	Bison	Unlisted	29	
44440	98	40		-	-	-	Bison	Radius	1	
44481	-	-	86.61	-	-	-	Bison	Teeth Plates	4	Bison Antiquus or Occidentalis

Table C-2. 1983-1984 Faunal Assemblage - Reconstructed from TARL Records and Bement (1986)

TMM #	Stratum (Bement)	Stratum (Farrell)	Depth	Species	Element	Side	End	Count	Modified
40806-275	A	19	96.75	Bison	Rib Tuberculum	R		1	
40806-337	A	19		Bison	Humerus Epiphyses	L	D	1	
40806-338	A	19		Bison	Horizontal Ramus			1	
40806-339	A	19		Bison	Tibia Epiphyses	R	P	1	
40806-276	B/C	20/21	96.79	Bison	Lumbar Vertebrae			1	
40806-277	B/C	20/21		Bison	Lumbar Vertebrae			1	
40806-278	B/C	20/21		Bison	Lumbar Vertebrae			1	
40806-279	B/C	20/21	96.74	Bison	Humerus Epiphyses	R	D	1	
40806-280	B/C	20/21	96.76	Bison	Lumbar Vertebrae			1	
40806-281	B/C	20/21		Bison	Lumbar Vertebrae			1	
40806-282	B/C	20/21		Bison	Lumbar Vertebrae			1	
40806-286	B/C	20/21	96.8	Bison	Lumbar Vertebrae			1	
40806-287	B/C	20/21		Bison	Humerus Fragment	L	D	1	
40806-288	B/C	20/21		Bison	Lumbar Vertebrae			1	
40806-294	B/C	20/21		Bison	Atlas			1	
40806-295	B/C	20/21		Bison	Mandible	R		1	
40806-296	B/C	20/21		Bison	Humerus Epiphyses	L	D	1	
40806-298	B/C	20/21		Bison	Tarsal	L		1	
40806-328	B/C	20/21		Bison	Phalanx, Second	L		1	
40806-330	B/C	20/21		Bison	Metacarpal Fragment			1	
40806-331	B/C	20/21		Bison	Lumbar Vertebrae			1	
40806-332	B/C	20/21		Bison	Vertebrae Fragment			1	
40806-336	B/C	20/21		Bison	Rib Tuberculum	L		1	
40806-345	B/C	20/21		Bison	Horizontal Ramus Fragment	L		1	
40806-346	B/C	20/21		Bison	Radius Fragment	R	D	1	
40806-347	B/C	20/21		Bison	Metacarpal	L		1	
40806-348	B/C	20/21		Bison	Tibia Shaft Fragment	L		1	
40806-349	B/C	20/21	96.8	Bison	Tibia Shaft Fragment	R		1	
40806-350	B/C	20/21		Bison	Axis			1	
40806-351	B/C	20/21		Bison	Cervical Vertebrae			1	
40806-352	B/C	20/21		Bison	Radius Fragment	R	P	1	
40806-353	B/C	20/21		Bison	Vertebrae Fragment			1	
40806-354	B/C	20/21		Bison	Radius Fragment	R	D	1	
40806-355	B/C	20/21		Bison	Lumbar Vertebrae			1	
40806-356	B/C	20/21		Bison	Lumbar Vertebrae			1	

Table C-2. Continued

TMM #	Stratum (Bement)	Stratum (Farrell)	Depth	Species	Element	Side	End	Count	Modified
40806-357	B/C	20/21		Bison	Cervical Vertebrae			1	
40806-358	B/C	20/21		Bison	Ulna Fragment	R	P	1	
40806-359	B/C	20/21		Bison	Radius Fragments	L	P	1	
40806-360	B/C	20/21		Bison	Radius Fragment	R	P	1	
40806-361	B/C	20/21		Bison	Tarsal	L		1	
40806-362	B/C	20/21		Bison	Thoracic Vertebrae			1	
40806-363	B/C	20/21		Bison	Cervical Vertebrae			1	
40806-364	B/C	20/21		Bison	Cervical Vertebrae			1	
40806-365	B/C	20/21		Bison	Tarsal	L		1	
40806-366	B/C	20/21		Bison	Tarsal	L		1	
40806-367	B/C	20/21		Bison	Tibia Epiphyses	L	P	1	
40806-368	B/C	20/21		Bison	Radius Epiphysis	L	D	1	
40806-369	B/C	20/21		Bison	Lumbar Vertebrae			1	
40806-370	B/C	20/21		Bison	Phalanx, First	L		1	
40806-371	B/C	20/21		Bison	Tibia Epiphyses	L	P	1	
40806-285	B/C	20/21	96.65	Horse	Mandibular Tooth Fragment			1	
40806-297	B/C	20/21		Horse	Mandible Ramus	L		1	
40806-344	B/C	20/21		Horse	Radius Shaft	L		1	
40806-372	B/C	20/21		Horse	Maxillary Tooth Fragment	L		1	
40806-373	B/C	20/21		Horse	Maxilla Fragment	L		1	
40806-314	D			Gray Fox	Horizontal Ramus with M/1 & M/2 (rootless)	R		1	
40806-318	E/F/G	23		Bison	Vertebrae Fragment			1	
40806-324	E/F/G	23	96.57	Bison	Tibia Shaft Fragment	L		1	
40806-290	E/F/G	23		Camel	Phalanx, First			1	
40806-291	E/F/G	23		Camel	Phalanx, Second			1	
40806-292	E/F/G	23	96.52	Camel	Phalanx, Second			1	
40806-299	E/F/G	23	96.51	Camel	Pelvis Fragment			1	
40806-303	E/F/G	23		Camel	Tibia Shaft Fragment	L		1	
40806-316	E/F/G	23		Camel	Femur Fragment + Head	R	P	1	
40806-374	E/F/G	23		Camel	Calcaneus	R		1	
40806-376	E/F/G	23		Camel	Tarsal	R		1	
40806-377	E/F/G	23		Camel	Metatarsal	L		1	
40806-378	E/F/G	23		Camel	Radius Fragment	R	D	1	
40806-379	E/F/G	23		Camel	Pelvis Fragment			1	

Table C-2. Continued

TMM #	Stratum (Bement)	Stratum (Farrell)	Depth	Species	Element	Side	End	Count	Modified
40806-385	E/F/G	23		Camel	Astragulus	L		1	
40806-289	E/F/G	23	96.55	Horse	Mandibular Tooth Fragment			1	
40806-293	E/F/G	23	96.52	Horse	Metacarpal Splint Fragment	R		1	
40806-300	E/F/G	23		Horse	Metatarsal	R		1	
40806-302	E/F/G	23	96.52	Horse	Thoracic Vertebrae			1	
40806-305	E/F/G	23		Horse	Tibia Epiphysis	L	P	1	
40806-306	E/F/G	23		Horse	Tibia Fragment	L	P	1	
40806-308	E/F/G	23		Horse	Metacarpal Splint Fragment	R		1	
40806-311	E/F/G	23		Horse	Radius Shaft	L		1	
40806-312	E/F/G	23		Horse	Astragulus	L		1	
40806-315	E/F/G	23		Horse	Metapodial Splint Fragment			1	
40806-317	E/F/G	23		Horse	Interparietal			1	
40806-322	E/F/G	23	96.51	Horse	Radius Shaft Fragment	R		1	
40806-325	E/F/G	23		Horse	Calcaneum	L		1	
40806-326	E/F/G	23		Horse	Phalanx, First	L		1	
40806-327	E/F/G	23		Horse	Metacarpal Fragment	L	D	1	
40806-329	E/F/G	23		Horse	Radius Epiphysis	L	P	1	
40806-333	E/F/G	23		Horse	Mandibular Tooth Fragment			1	
40806-375	E/F/G	23		Horse	Metatarsal Fragment	L	P	1	
40806-380	E/F/G	23		Horse	Metacarpal Fragment	R	D	1	
40806-382	E/F/G	23		Horse	Coccyx Vertebrae			1	
40806-383	E/F/G	23		Horse	Ulna Fragment	R	P	1	
40806-384	E/F/G	23		Horse	Radius	L		1	
40806-386	E/F/G	23		Horse	Vertebra Fragment			1	
40806-401	E/F/G	23		Horse	Sesamoid			1	
40806-304	E/F/G	23		Mammoth	Pelvis Fragment			1	
40806-307	E/F/G	23		Mammoth	Skull Fragment			1	
40806-381	E/F/G	23		Mammoth	Pelvis Fragment			1	
40806-403	H-1	24	96.41	Bison	Sesamoid			1	
40806-273	H-1	24	96.29	Horse	Metatarsal Fragment	L	D	1	
40806-273	H-1	24		Horse	Metatarsal Shaft Fragment	L		1	
40806-273	H-1	24		Horse	Metatarsal Shaft Fragment	L		1	

Table C-2. Continued

TMM #	Stratum (Bement)	Stratum (Farrell)	Depth	Species	Element	Side	End	Count	Modified
40806-334	H-1	24		Horse	Atlas			1	
40806-335	H-1	24		Horse	Palate with Both Maxillae			1	
40806-343	H-1	24		Horse	Tibia	L		1	
40806-389	H-1	24		Horse	Ulna Fragment	R	P	1	
40806-390	H-1	24		Horse	Calcaneus	L		1	
40806-391	H-1	24		Horse	Naviculo-cuboids	L		1	
40806-392	H-1	24	96.39	Horse	Metatarsal Fragment	L	P	1	
40806-393	H-1	24		Horse	Metatarsal Splints	L		1	
40806-394	H-1	24		Horse	Astragalus	L		1	
40806-395	H-1	24		Horse	Radius Fragment	R	P	1	
40806-395	H-1	24		Horse	Ulna Fragment	R	P	1	
40806-396	H-1	24		Horse	Naviculo-cuboids	L		1	
40806-397	H-1	24		Horse	Lower Lumbar Vertebrae			2	
40806-398	H-1	24		Horse	Phalanx, First	L		1	
40806-399	H-1	24		Horse	Femur Fragment	L	D	1	Spiral Fracture; U & V Incision
40806-400	H-1	24		Horse	Humerus Fragment	L	P	1	
40806-404	H-1	24		Horse	Femur Fragment	R	P	1	
40806-405	H-1	24		Horse	Skull Fragment			1	
40806-406	H-1	24		Horse	Thoracic Vertebrae			1	
40806-407	H-1	24		Horse	Sacrum Fragment			1	
40806-408	H-1	24		Horse	Rib Tuberculum	L		1	
40806-409	H-1	24		Horse	Sacrum Fragment			1	
40806-309	H-1	24		Mammoth	Mandible Fragment	L	P	1	
40806-341	H-1	24		Mammoth	Lumbar Vertebra			1	
40806-342	H-1	24	96.44	Mammoth	Pelvis Fragment			1	
40806-387	H-1	24		Mammoth	Rib Fragment			1	
40806-402	H-1	24		Mammoth	Tibia Shaft Fragment			1	Incision, green break
40806-444	H-1	24		Mammoth	UID Long Bone Fragment			1	
40806-319	H-2	24		Antelope	Mandible Fragment	L		1	
40806-320	H-2	24		Antelope	Maxillary Fragment	L		1	
40806-388	H-2	24		Antelope	Humerus, End	L	D	1	
40806-410	I	Unknown		Bison	Sacrum Fragment			1	
40806-411	I	Unknown		Bison	Astragalus	R		1	

Table C-2. Continued

TMM #	Stratum (Bement)	Stratum (Farrell)	Depth	Species	Element	Side	End	Count	Modified
40806-412	I	Unknown		Bison	Thoracic Vertebrae			1	
40806-413	I	Unknown		Bison	Thoracic Vertebrae			1	
40806-414	I	Unknown		Bison	Calcaneus	L		1	
40806-415	I	Unknown		Bison	Tibia Shaft Fragment	R		1	
40806-416	I	Unknown		Bison	Tibia Shaft Fragment	R		1	
40806-417	I	Unknown		Bison	Phalanx, First	R		1	
40806-418	I	Unknown		Bison	Thoracic Vertebrae			1	
40806-419	I	Unknown		Bison	Thoracic Vertebrae			1	
40806-420	I	Unknown		Bison	Tibia Fragment	R	P	1	Spiral break w. step fracture; V-shaped groove
40806-421	I	Unknown		Bison	Thoracic Vertebrae			1	
40806-422	I	Unknown		Bison	Rib Tuberculum	R		1	
40806-423	I	Unknown		Bison	Femur Shaft Fragment	L		1	
40806-425	I	Unknown		Bison	Ulna Fragment	L	P	1	Tangent V-shaped incisions
40806-426	I	Unknown		Bison	Phalanx, Second	R		1	
40806-427	I	Unknown		Bison	Scapula Blade Fragment	L		1	
40806-428	I	Unknown		Bison	Pelvis Acetabular Fragment	R		1	
40806-430	I	Unknown		Bison	Mesocuneiform	R		1	
40806-431	I	Unknown		Bison	Patella	R		1	
40806-432	I	Unknown		Bison	Phalanx, Third	R		1	
40806-434	I	Unknown		Bison	Rib Shaft	R		1	
40806-438	I	Unknown	95.8	Bison	Naviculo cuboid - Tarsal	L		1	
40806-424	I	Unknown		Horse	Mandibular M/3	L		1	
40806-429	I	Unknown		Horse	Coccyx Vertebrae			1	
40806-433	I	Unknown		Horse	Maxillary Fragment	L		1	
40806-284	Unlisted	Unknown		Bison	Humerus Fragment	L	D	1	
40806-297	Unlisted	Unknown		Bison	Mandible	L		1	
40806-321	Unlisted	Unknown		Bison	Tibia Shaft Fragment	R		1	
40806-340	Unlisted	Unknown		Bison	Lumbar Vertebrae			1	
40806-436	Unlisted	Unknown		Bison	Tibia Fragment	R	P	2	
40806-437	Unlisted	Unknown		Bison	Phalanx, Third	L		1	
40806-283	Unlisted	Unknown	96.69	Horse	Basioccipital			1	

Table C-2. Continued

TMM #	Stratum (Bement)	Stratum (Farrell)	Depth	Species	Element	Side	End	Count	Modified
40806-284	Unlisted	Unknown		Horse	Naviculo-cuboids	R		1	
40806-301	Unlisted	Unknown		Horse	Metatarsal Splints	L		1	
40806-310	Unlisted	Unknown	96.62	Horse	Radius Shaft	L		1	
40806-313	Unlisted	Unknown		Horse	Metapodial Splint Fragment			1	
40806-435	Unlisted	Unknown	96.78	Horse	Mandible Fragment	R		1	
40806-439	Unlisted	Unknown	96.65	Horse	Mandible	L		1	
40806-440	Unlisted	Unknown	96.68	Horse	Maxilla	R		1	
40806-441	Unlisted	Unknown	96.61	Horse	Ascending Ramus	R		1	
40806-323	Unlisted	Unknown		Mammoth	Rib Fragment			1	
40806-442	Unlisted	Unknown	NOT IN LOG	Mammoth	Rib Fragment			1	
40806-443	Unlisted	Unknown		Mammoth	Tooth Fragment			1	

Table C-3. 2017-2018 Bonfire Shelter Assemblage - Bone Bed 1

Field Number (FN)	TDS Shot	Unit	Layer	Stratum (Farrell)	Stratum (Bement)	Stratum* (Dibble)	Species	Element	Count	Comment
FN60037	1146	C1	L1	19	A	F3	Bison*	Rib	1	Fragment
FN60044	1149	C1	L2 (B)	20	B	F3	Bison	Thoracic Vertebra	1	
FN60041	1163	C1	L2 (B)	20	B	F3	UID	UID	1	
FN60042	1152	C1	L2 (B)	20	B	F3	UID	UID	1	
FN60043	1153	C1	L2 (B)	20	B	F3	UID	UID	1	
FN60045	1151	C1	L2 (B)	20	B	F3	UID	UID	1	
FN60046	1150	C1	L2 (B)	20	B	F3	UID	UID	1	
FN60056	1186	C1	L5	23	E/F/G	F4	Bison*	Rib	1	
FN60227	1304	C1	L5	23	E/F/G	F4	Bison*	Rib	1	
FN60055	1185	C1	L5	23	E/F/G	F4	Horse	Metapodial	1	
FN60228	1305	C1	L5B	23	E/F/G	F4	Bison*	Rib	1	
FN60108	1228	C1	L5B	23	E/F/G	F4	Mammoth	Rib	1	
FN60112	1232	C1	L5B	23	E/F/G	F4	Mammoth	Rib	1	
FN60163	1282	C1	L5B	23	E/F/G	F4	Mammoth	Tusk*	1	Broad, flat mammoth element below 60115. Distinct play structure
FN60111	1231	C1	L5B	23	E/F/G	F4	Mammoth	UID	1	Flat mammoth bone between 60110
FN60110	1230	C1	L5B	23	E/F/G	F4	Mammoth	UID Fragmentary	1	Determined to be part of 60247
FN60143	1265	C1	L5B	23	E/F/G	F4	UID	Epiphyseal	1	Collected for ¹⁴ C
FN60115	1235	C1	L5B	23	E/F/G	F4	UID	Long Bone*	1	
FN60113	1233	C1	L5B	23	E/F/G	F4	UID	UID	1	
FN60114	1234	C1	L5B	23	E/F/G	F4	UID	UID	1	
FN60116	1236	C1	L5B	23	E/F/G	F4	UID	UID	1	
FN60125	-	C1	L5B	23	E/F/G	F4	UID	UID	1	
FN60164	1283	C1	L5B	23	E/F/G	F4	UID	UID	1	Determined to be part of 60229
FN60165	1284	C1	L5B	23	E/F/G	F4	UID	UID	1	Flat bone beneath 60108
FN60225	1302	C1	L5B	23	E/F/G	F4	UID	UID	1	
FN60226	1303	C1	L5B	23	E/F/G	F4	UID	UID	1	In 60114 pedestal

Table C-3. Continued

Field Number (FN)	TDS Shot	Unit	Layer	Stratum (Farrell)	Stratum (Bement)	Stratum* (Dibble)	Species	Element	Count	Comment
FN60229	1306	C1	L5B	23	E/F/G	F4	UID	UID	1	In 60114 pedestal
FN60230	1307	C1	L5B	23	E/F/G	F4	UID	UID	1	
FN60377	-	C1	L6	24	H	F12	Bird	Long Bone*	1	
FN60247	-	C1	L6	24	H	F12	Mammoth	Rib	1	Very large, incorporates FN60086, 60089, and 60110
FN60222	1299	C1	L6	24	H	F12	Rodent	Multiple	1	Articulated mouse
FN60161	1280	C1	L6	24	H	F12	UID	UID	1	
FN60162	1281	C1	L6	24	H	F12	UID	UID	1	
FN60082	1206	C2	L1	23	E/F/G	F4	Mammoth	Rib	1	Fragment - L3/L4 interface
FN60086	-	C2	L1	23	E/F/G	F4	Mammoth	Rib	1	Determined to be part of 60247
FN60093	1214	C2	L1	23	E/F/G	F4	Mammoth	Rib	1	Determined to be part of rib 60082
FN60053	-	C2	L1	23	E/F/G	F4	Rodent*	Vertebra	1	Cadual vertebra
FN60026	1114-1116	C2	L1	23	E/F/G	F4	UID	UID	1	
FN60081	-	C2	L1	23	E/F/G	F4	UID	UID	1	
FN60098	1219	C2	L1	23	E/F/G	F4	UID	UID	1	
FN60101	-	C2	L2	23	E/F/G	F4	Bison*	Rib	1	
FN60089	1210	C2	L2	23	E/F/G	F4	Mammoth	Rib	1	Determined to be part of 60247
FN60088	1209	C2	L2	23	E/F/G	F4	Mammoth	Rib Fragment	1	Fragment
FN60100	-	C2	L2	23	E/F/G	F4	UID	UID	1	Gypsum coating
FN60287	1402	C2	L3	24	H	F12	Horse*	Long Bone*	1	Poorly preserved
FN60292	1407	C2	L3	24	H	F12	Horse*	Long Bone*	1	Robust, well preserved cortical surface
FN60285	1400	C2	L3	24	H	F12	Horse*	Tibia	1	Poorly preserved
FN60283	1398	C2	L3	24	H	F12	Horse*	UID	1	Poorly preserved

Table C-3. Continued

Field Number (FN)	TDS Shot	Unit	Layer	Stratum (Farrell)	Stratum (Bement)	Stratum* (Dibble)	Species	Element	Count	Comment
FN60284	1399	C2	L3	24	H	F12	Horse*	UID	1	Poorly preserved
FN60286	1401	C2	L3	North of UID bone fragment	H	F12	Horse*	UID	1	Poorly preserved
FN60288	1403	C2	L3	24	H	F12	Horse*	UID	1	Poorly preserved
FN60289	1404	C2	L3	24	H	F12	Horse*	Vertebra	1	
FN60290	1405	C2	L3	24	H	F12	Mammoth	Scapula	1	Includes 60291
FN60282	1397	C2	L3	24	H	F12	Mammoth	UID	1	Poorly preserved
FN60291	1406	C2	L3	24	H	F12	Mammoth	UID	1	Determined to be part of 60290
FN60281	1396	C2	L3	24	H	F12	Mammoth*	UID Fragmentary	1	Poorly preserved
FN60313	1424	C2	L3	24	H	F12	UID	UID	1	Poorly preserved, beneath spalls
FN60009	1081	C3	L1	23	E/F/G	F4	Mammoth	Rib	1	
FN60010	1082	C3	L1	23	E/F/G	F4	Mammoth	Rib	1	
FN60048	1165	C3	L1	23	E/F/G	F4	Microfauna	UID	1	In mammoth rib pedestal L1
FN60025	1117	C3	L1	23	E/F/G	F4	UID	UID	1	
FN60049	1166	C3	L1	23	E/F/G	F4	UID	UID	1	In mammoth rib pedestal L1, possibly same element as 60014
FN60074	-	C3	L1 - 4	S0	x	Bone Bed I	Microfauna	UID	1	In mammoth pelvis pedestal slump
FN60075		C3	L1 - 4	S0	x	Bone Bed I	Microfauna	UID	1	In unit wall cleanup
FN60014	1086	C3	L2	23	E/F/G	F4	Camel?	Rib	1	
FN60029	1142	C3	L2	23	E/F/G	F4	Horse*	Tooth	1	
FN60019	1087	C3	L2	23	E/F/G	F4	UID	Long Bone*	1	Plaster jacket
FN60012	1084	C3	L2	23	E/F/G	F4	UID	UID	1	South of pelvis
FN60067	1192	C3	L2	23	E/F/G	F4	UID	UID Fragmentary	1	Only bone dust
FN60069	1194	C3	L3	24	H	F12	Antelope*	Tooth*	1	
FN60036	1145	C3	L3	24	H	F12	UID	UID	1	Fragment
FN60073	-	C3	L3	24	H	F12	UID	UID	1	Screen lot
FN60011	1083	C3	L1	23	E/F/G	F4	Mammoth	Pelvis	1	
FN60013	1085	C3	L2	23	E/F/G	F4	UID	Long Bone*	1	
FN60039	-	C3	L2/3	24	H	F12	Microfauna	UID	1	In mammoth rib pedestal

Table C-3. Continued

Field Number (FN)	TDS Shot	Unit	Layer	Stratum (Farrell)	Stratum (Bement)	Stratum* (Dibble)	Species	Element	Count	Comment
FN60298	1410	CS5	L6	24	H	F12	Mammoth	UID	1	
FN60263	-	CS5	Strat 23	23	E/F/G	F4	Horse*	UID	1	
FN60270	1368	CS5	Strat 23	23	E/F/G	F4	Mammoth	Rib*	1	
FN60269	1367	CS5	Strat 23	23	E/F/G	F4	UID	UID	1	
FN60376	1511	D3	L2	24	H	F12	UID	UID		
FN60408	1527	D3	L3	24	H	F12	UID	Rib	1	
FN60449	1568	D3	L4	24	H	F12	UID	Rib	1	Highly fragmented
FN60317	1450	D4	L2	24	H	F12	UID	UID		
FN60333	1482	D4	L3	24	H	F12	Antelope*	Scapula	1	
FN60323	1480	D4	L3	24	H	F12	Bison*	Rib	1	
FN60334	1483	D4	L3	24	H	F12	UID	Rib	1	
FN60335	1484	D4	L3	24	H	F12	UID	UID	1	Fragment
FN60336	1485	D4	L3	24	H	F12	UID	UID	1	
FN60338	1487	D4	L3	24	H	F12	UID	UID	1	Fragment
FN60345	1491	D4	L3	24	H	F12	UID	UID	1	Fragment
FN60337	1486	D4	L3	24	H	F12	UID	UID Fragmentary	1	Fragment
FN60354	1495	D4	L4	24	H	F12	Horse*	Rib	1	Uncertain if horse of camel
FN60499	-	D7	L4	24	H	F12	Antelope*	Rib	1	Uncertain if horse of antelope
FN60506	-	D7	L4	24	H	F12	Antelope*	Rib	1	Uncertain if horse of antelope
FN60518	-	D7	L4	24	H	F12	Rodent	UID	1	Fragment
FN60516	-	D7	L4	24	H	F12	UID	Long Bone*	1	Long bone termination fragment
FN60517	-	D7	L4	24	H	F12	UID	Rib	1	
FN60519	-	D7	L4	24	H	F12	UID	UID	1	Fragment
FN60546	1599	D8	L5	24	H	F12	Rodent	UID	1	Fragment

WORKS CITED

- Adovasio, J. M., J. Donahue, and R. Stuckenrath
1990 The Meadowcroft Rockshelter Radiocarbon Chronology 1975-1990. *American Antiquity* 55(2):348-354.
- Adovasio, J. M., J. D. Gunn, J. Donahue, and R. Stuckenrath
1977 Progress Report on the Meadowcroft Rockshelter -- A 16,000 Year Chronicle. *Annals of the New York Academy of Sciences* 288(1):137-159.
- Agisoft
2020 Agisoft Metashape User Manual: Professional Edition, Version 1.6. Agisoft, LLC, St. Petersburg, RU.
- Amick, Daniel S.
2017 Evolving Views on the Pleistocene Colonization of North America. Article. *Quaternary International* 431:125-151.
- Anderson, David G., D. Shane Miller, Stephen J. Yerka, J. Christopher Gillam, Erik N. Johanson, Derek T. Anderson, Albert C. Goodyear, and Ashley M. Smallwood
2010 PIDBA (Paleoindian Database of the Americas) 2010: Current Status and Findings. *Archaeology of Eastern North America* 38:63-89.
- Andrefsky, William
2005 *Lithics: Macroscopic Approaches to Analysis*. Cambridge Manuals in Archaeology. Cambridge University Press, Cambridge, UK.
- Artieda, O., J. Herrero, and P. J. Drohan
2006 Refinement of the Differential Water Loss Method for Gypsum Determination in Soils. *Soil Science Society of America Journal* 70(6):1932-1935.
- ASTM-International
2017 *ASTM D7928-16 e1: Standard Test Method for Particle-Size Distribution (Gradation) of Fine-Grained Soils using the Sedimentation (Hydrometer) Analysis*. American Society for Testing Materials International, West Conshohocken, PA.
- Ayotte, Jeremy B., Katherine L. Parker, and Michael P. Gillingham
2008 Use of Natural Licks by Four Species of Ungulates in Northern British Columbia. *Journal of Mammalogy* 89(4):1041-1050.
- Bahm, Matt A., and James M. Mueller
2011 The Mammals of Amistad National Recreation Area, Texas, edited by Ann Lewis, and M. Hildegard Reiser. Natural Resource Technical Report. National Park Service - US Department of the Interior, Fort Collins, CO.
- Bain, Roger J.
1990 Diagenetic, Nonevaporative Origin for Gypsum. *Geology* 18(5):447-450.

- Barnes, V.E., Noel Waechter, G.R. Pinkley, R.G. Martin, J.C. Wyeth, J.A. Knupke, J.F. Sulik, W.G. Ellis, G.B. Bowman, R.H. Sams, and E.C. Roy
1977 *Geological Atlas of Texas: Del Rio Sheet*, 1:62,500. University of Texas at Austin, Bureau of Economic Geology. Austin, TX.
- Basham, G. Matt
2015 Subsistence Strategies and Landscape Use in the Canyon Edge Zone: Eagle Nest Canyon, Langtry, Texas. Master of Arts, Department of Anthropology, Texas State University, San Marcos, TX.

2017 Canyon Edge Archaeology. In *Lower Pecos Canyonlands Academy Guidebook*, edited by Ken Lawrence, pp. 19-21. Texas Archeological Society, San Marcos, TX.
- Bates, Lennon N., Amanda M. Castaneda, Carolyn E. Boyd, and Karen L. Steelman
2015 A Black Deer at Black Cave: New Pictograph Radiocarbon Date for the Lower Pecos, Texas. *Journal of Texas Archeology and History* 2:45-57.
- Beck, Charlotte, and George T. Jones
2010 Clovis and Western Stemmed: Population Migration and the Meeting of Two Technologies in the Intermountain West. *American Antiquity* 75(1):81-116.
- Bell, Wayne, and David S. Dibble
1970 Mile Canyon (Eagle Nest Canyon) National Register of Historic Places Nomination. United States Department of the Interior - National Park Service.
- Bement, Leland C.
1985 Spray Foam: A New Bone Encasement Technique. *Journal of Field Archaeology* 12(3):371.

1986a *Excavation of the Late Pleistocene Deposits of Bonfire Shelter, 41VV218, Val Verde, Texas, 1983-1984*. Archeology Series, Vol. 1. Texas Archeological Survey, University of Texas at Austin, Austin, TX.

1986b Mammalian Faunal and Cultural Remains in the Late Pleistocene Deposits of Bonfire Shelter, 41VV218, Southwest Texas, University of Texas at Austin, Austin, TX.

2007 Bonfire Shelter: A Jumping Off Point for Comments for Byerly Et Al. Article. *American Antiquity* 72(2):366-372.
- Bement, Leland C., and Brian J. Carter
2010 Jake Bluff: Clovis Bison Hunting on the Southern Plains of North America. *American Antiquity* 75(4):907-933.
- Binford, Lewis R.
1978a Dimensional Analysis of Behavior and Site Structure: Learning from an Eskimo Hunting Stand. *American Antiquity* 43(3):330-361.

1978b *Nunamiut Ethnoarchaeology*. Studies in Archaeology. Academic Press, New York, NY.

1981 *Bones: Ancient Men and Modern Myths*. Academic Press, New York, NY.

- Birkeland, Peter W.
 1999 The Soil Profile, Horizon Nomenclature, and Soil Characteristics. In *Soils and Geomorphology*. 3 ed. Oxford University Press, New York, NY.
- Biscaye, Pierre E.
 1965 Mineralogy and Sedimentation of Recent Deep-Sea Clay in the Atlantic Ocean and Adjacent Seas and Oceans. Article. *Bulletin of the Geological Society of America* 76(7):803-832.
- Black, Stephen L.
 2001a Bonfire Shelter: A Tour of Mile Canyon. In *Texas Beyond History*, edited by Texas Beyond History Web Team. Texas Archaeological Research Laboratory, University of Texas at Austin, Austin, TX.
 2001b Bonfire Shelter: The Archeologists. In *Texas Beyond History*, edited by Texas Beyond History Web Team. Texas Archaeological Research Laboratory, University of Texas at Austin, Austin, TX.
 2001c Bonfire Shelter: The Investigations. In *Texas Beyond History*, edited by Texas Beyond History Web Team. Texas Archaeological Research Laboratory, University of Texas at Austin, Austin, TX.
 2013 Archaeologists of the Lower Pecos Canyonlands. In *Painters in Prehistory: Archaeology and Art of the Lower Pecos Canyonlands*, edited by Harry J. Shafer, Al Rendon, and Susan Toomey Frost. Trinity University Press, published in association with the Witte Museum, San Antonio, TX.
 2017 Introduction to Ancient Southwest Texas (ASWT) Investigations. In *Lower Pecos Canyonlands Academy Guidebook*, edited by Ken Lawrence, pp. 7-9. Texas Archeological Society.
- Black, Stephen L., and Phil Dering
 2008 Lower Pecos Canyonlands: Archaeology. In *Texas Beyond History*, edited by Texas Beyond History Web Team. Texas Archaeological Research Laboratory, University of Texas at Austin, Austin, TX.
- Black, Stephen L., and Charles W. Koenig
 2018 Sand, Chute, Carts, and Waddles: Eagle Cave and Bonfire Shelter Restoration Project. Paper presented at the 82nd Annual Meeting of the Society for American Archaeology, Washington, DC.
- Blair, W. Frank
 1950 The Biotic Provinces of Texas. *Texas Journal of Science* 93:3-117.
- Boggs, Sam
 2009 *Petrology of Sedimentary Rocks*. Book. Cambridge University Press, Cambridge.
 2012 *Principles of Sedimentology and Stratigraphy*. 5th ed. ed. Pearson Prentice Hall.

- Bonn, Bernadine A., and Stewart A. Rounds
 2010 *Use of Stable Isotopes of Carbon and Nitrogen to Identify Sources of Organic Matter to Bed Sediments of the Tualatin River, Oregon*. Scientific Investigations Report 2010-5154. Copies available from U. S. Geological Survey, Reston, VA.
- Bonnichsen, Robson
 1979 *Pleistocene Bone Technology in the Beringian Refugium*. Archaeological Survey of Canada, Vol. Paper No. 89. National Museums of Canada, Ottawa.
- Bousman, C. Britt, Barry W. Baker, and Anne C. Kerr
 2004 Paleoindian Archeology in Texas. In *The Prehistory of Texas*, edited by Timothy K. Pertulla, pp. 15-97. Texas A&M University Press, College Station, TX.
- Bousman, C. Britt., and B. J. Vierra
 2012 Chronology, Environmental Setting, and Views of the Terminal Pleistocene and Early Holocene Cultural Transitions in North America. In *From the Pleistocene to the Holocene: Human Organization and Cultural Transformations in Prehistoric North America*, edited by C. B. Bousman, and B. J. Vierra, pp. 1-15. Vol. 9781603447782. Texas A&M University.
- Boyd, Carolyn E.
 1996 Shamanic Journeys into the Otherworld of the Archaic Chichimec. *Latin American Antiquity* 7(2):152-164.
- 2003 *Rock Art of the Lower Pecos*. Texas A&M University Press, College Station, TX.
- Boyd, Carolyn E., and Kim Cox
 2016a Archaic Codices. In *The White Shaman Mural*, edited by Carolyn E. Boyd, and Kim Cox, pp. 1-11. An Enduring Creation Narrative in the Rock Art of the Lower Pecos. University of Texas Press, Austin, TX.
- 2016b The Painted Landscape. In *The White Shaman Mural*, edited by Carolyn E. Boyd, and Kim Cox, pp. 12-30. An Enduring Creation Narrative in the Rock Art of the Lower Pecos. University of Texas Press, Austin, TX.
- 2016c *The White Shaman Mural: An Enduring Creation Narrative in the Rock Art of the Lower Pecos*. University of Texas Press, Austin, TX.
- Boyd, Carolyn E., and James Philip Dering
 1996 Medicinal and Hallucinogenic Plants Identified in the Sediments and Pictographs of the Lower Pecos, Texas Archaic. *Antiquity* 70(268):256-275.
- Braje, Todd, Jon Erlandson, Torben Rick, Loren Davis, Tom Dillehay, Daryl Fedje, Duane Froese, Amy Gusick, Quentin Mackie, Duncan McLaren, Bonnie Pitblado, Jennifer Raff, Leslie Reeder-Myers, and Michael Waters
 2019 Fladmark + 40: What Have We Learned about a Potential Pacific Coast Peopling of the Americas? *American Antiquity*:1-21.

- Brault, Emily K., Paul L. Koch, Elizabeth Gier, R. I. Ruiz-Cooley, Jessica Zupcic, Kwasi N. Gilbert, and Matthew D. McCarthy
2014 Effects of Decalcification on Bulk and Compound-Specific Nitrogen and Carbon Isotope Analyses of Dentin. *Rapid Communications in Mass Spectrometry* 28:2744-2752.
- Bronk Ramsey, Christopher
2009 Bayesian Analysis of Radiocarbon Dates. *Radiocarbon* 51(1):337-360.
- Brown, A. G.
1997 *Alluvial Geoarchaeology: Floodplain Archaeology and Environmental Change*. Cambridge University Press, Cambridge, UK.
- Brown, Kenneth M.
2015 Archeomalacology: What We Can Learn from Snails. In *Texas Beyond History*, edited by Texas Beyond History Web Team. Texas Archaeological Research Laboratory, University of Texas at Austin, Austin, TX.
- Bryant, Vaughn M.
1969 Late Full-Glacial and Postglacial Pollen Analysis of Texas Sediments. Doctoral dissertation, Department of Anthropology, Doctoral Dissertation, University of Texas at Austin, Austin, TX.
- Bryant, Vaughn M., and Richard G. Holloway
1985 A Late-Quaternary Paleoenvironmental Record of Texas: An Overview of the Pollen Evidence. In *Pollen Records of late-Quaternary North American Sediments*, edited by Vaughn M. Bryant, and Richard G. Holloway, pp. 39-70. American Association of Stratigraphic Palynologists, Dallas, TX.
- Buchanan, B., B. Andrews, J. D. Kilby, and M. I. Eren
2019 Settling into the Country: Comparison of Clovis and Folsom Lithic Networks in Western North America shows Increasing Redundancy of Toolstone Use. *Journal of Anthropological Archaeology* 53:32-42.
- Burke, Chrissina Coleen
2013 A Study of Carnivore Modification in North American Archaeology: Perspectives on Neotaphonomy, Carnivore Use of Carrion, and Great Plains Bison Bonebeds. Ph.D. Dissertation, Department of Anthropology, University of Nevada, Reno, Reno, NV (<http://hdl.handle.net/11714/3054>).
- Bush, Leslie L.
2015 Appendix A: Plants Observed in Eagle Nest Canyon. In *Patterns in the Use of the Rockshelters of Eagle Nest Canyon, Langtry, Texas*, edited by Daniel P. Rodriguez. Texas State University, San Marcos, TX.
- Bush, Leslie L., and J. Kevin Hanselka
2017 Plants and Plant Remains at Eagle Nest Canyon. In *Lower Pecos Canyonlands Academy Guidebook*, edited by Ken Lawrence, pp. 23-30. Texas Archeological Society.
- Byerly, Ryan M., Judith R. Cooper, and David J. Meltzer
2007 A Further Assessment of Paleoindian Site-Use at Bonfire: A Response to Leland C. Bement. *American Antiquity* 72(2):373-381.

- Byerly, Ryan M., Judith R. Cooper, David J. Meltzer, Matthew E. Hill, and Jason M. LaBelle
2005 On Bonfire Shelter (Texas) as a Paleoindian Bison Jump: An Assessment Using GIS and Zooarchaeology. *American Antiquity* 70(4):595-629.
- Byerly, Ryan M., David J. Meltzer, Judith R. Cooper, and Jim Theler
2007 Exploring Paleoindian Site-Use at Bonfire Shelter (41VV218). *Bulletin of the Texas Archeological Society* 78:125-147.
- Carter, Jim, and Vicki Barwick
2011 *Good Practice Guide for Isotope Ratio Mass Spectrometry*. 1st ed. FIRMS, United Kingdom.
- Castañeda, Amanda M.
2015 The Hole Story: Understanding Ground Stone Bedrock Feature Variation in the Lower Pecos Canyonlands. Master of Arts, Department of Anthropology, Texas State University, San Marcos, TX.
- Castañeda, Amanda M., Charles W. Koenig, and Charles D. Frederick
2017 Horse Trail Shelter (41VV166). In *Lower Pecos Canyonlands Academy Guidebook*, edited by Ken Lawrence, pp. 65-72. Texas Archeological Society.
- Castaños, Jone, Pedro Castaños, and Xabier Murelaga
2017 Imanolen Arrobia: A New Upper Pleistocene Carnivore Den in the North of the Iberian Peninsula (Deba, Spain). *Ameghiniana* 54(4):370-389.
- Chadderdon, Mary Frances
1983 *Baker Cave, Val Verde County, Texas: The 1976 excavations*. Center for Archaeological Research, University of Texas at San Antonio, San Antonio, TX.
- Chemists, Association of Official Agricultural
1950 *Official Methods of Analysis*, edited by Association of Official Agricultural Chemists, Washington D.C.
- Collins, M. B., and B. A. Bradley
2008 Evidence for Pre-Clovis Occupation at the Gault Site (41BL323), Central Texas. *Current Research In the Pleistocene* 25:70-72.
- Collins, Michael B.
1991 Rockshelters and the Early Archaeological Record in the Americas. In *The First Americans: Search and Research*, edited by Tom D. Dillehay, and David J. Meltzer, pp. 157-182. CRC Press, Boca Raton, FL.
- Collins, Michael B., and Pamela Headrick
1990 Fluorescent Properties of "Edwards" and Related Cherts of Central Texas. *Submitted to Journal of Field Archaeology*.
- Collins, Michael B., Dennis J. Stanford, Darrin L. Lowery, and Bruce A. Bradley
2014 North America Before Clovis: Variance in Temporal/Spatial Cultural Patterns, 27,000–13,000 cal yr BP. In *Paleoamerican Odyssey*, edited by Kelly E. Graf, Caroline V. Ketron, and Michael R. Waters, pp. 521-539. Center for the Study of the First Americans - Texas A&M University Press, College Station, TX.

- Collinson, J.D.
1996 Alluvial Sediments. In *Sedimentary Environments: Processes, Facies and Stratigraphy*, edited by Harold G. Reading, pp. 37-82. John Wiley & Sons, Hoboken, UK.
- Coplen, T. B., J. K. Böhlke, and H. R. Krouse
1992 Reporting of Nitrogen-Isotope Abundances (Technical Report). *Pure and Applied Chemistry* 64(6):907-908.
- Costech
2005 ECS 4010 CHNSO Analyzer - Innovation in Elemental Analysis.
- Cotter, John Lambert
1937 The Occurrence of Flints and Extinct Animals in Pluvial Deposits near Clovis, New Mexico. Part IV: Report on Excavation at the Gravel Pit, 1936. *Proceedings of the Academy of Natural Sciences of Philadelphia* 89:1-16.
- Dalan, Rinita A.
2006 Magnetic Susceptibility. In *Remote Sensing in Archaeology: An Explicitly North American Perspective*, edited by Jay K. Johnson, pp. 161-204. University of Alabama Press, Tuscaloosa, AL.

2008 A Review of the Role of Magnetic Susceptibility in Archaeogeophysical Studies in the USA: Recent Developments and Prospects. *Archaeological Prospection* 15(1):1-31.
- Daly, Patricia
1969 Approaches to Faunal Analysis in Archaeology. *American Antiquity* 34(2):146-153.
- Davenport, J. Walker
1938 *Archaeological Exploration of Eagle Cave, Langtry Texas*. Papers of the Witte Memorial Museum. The Witte Museum, San Antonio, TX.
- Davis, Owen K.
1990 Caves as Sources of Biotic Remains in Arid Western North America. *Palaeogeography, Palaeoclimatology, Palaeoecology* 76(3):331-348.
- Dean, Glenna W.
2006 The Science of Coprolite Analysis: The View from Hinds Cave. *Palaeogeography, Palaeoclimatology, Palaeoecology* 237(1):67-79.
- Dearing, John A.
1999 *Environmental Magnetic Susceptibility: Using the Bartington MS2 System*. 2nd ed. Bartington Instruments Ltd, London, UK.
- Dering, James Philip
1979 Pollen and Plant Macrofossil Vegetation Record Recovered from Hinds Cave, Val Verde County, Texas. Master of Science, Botany, Texas A&M University, College Station, TX.

- 2002 Amistad National Recreation Area: Archeological Survey and Cultural Resources Inventory. In *Intermountain Cultural Resources Management Anthropology Projects*. No. 68. National Park Service, Santa Fe, NM.
- Dibble, David S.
 1964 Bonfire Shelter Field Documents - Daily Journal & Feature Log, Records of the Amistad Reservoir Salvage Project, Held in trust at the Texas Archeological Research Laboratory, Austin, TX.
 1967 *Excavations at Arenosa Shelter, 1965-66*. National Park Service, Austin, TX.
 1970 On the Significance of Additional Radio-Carbon Dates from Bonfire Shelter, Texas. *Plains Anthropologist* 15(50-1):251-254.
 1975 Archaeological Investigations at Bonfire Shelter, Texas. Ph.D., Department of Anthropology, Washington State University., Pullman, WA.
- Dibble, David S., and Dessamae Lorrain
 1968 *Bonfire Shelter: A Stratified Bison Kill Site, Val Verde County, Texas*. A Publication of the Texas Memorial Museum. Miscellaneous papers, No. 1. University of Texas, Texas Memorial Museum, Austin, TX.
- Diedrich, Cajus. G., and Donald. A. McFarlane
 2017 Homotherium from Middle Pleistocene Archaeological and Carnivore Den Sites of Germany – Taxonomy, Taphonomy and a Revision of the Schöningen, West Runton and Other Saber-Tooth Cat Sites. *Quaternary International* 436:76-83.
- Donahue, Jack, and James M. Adovasio
 1990 Evolution of Sandstone Rockshelters in Eastern North America; A Geoarchaeological Perspective. In *Archaeological Geology of North America*, edited by Norman P. Lasca, and Jack Donahue, pp. 231-251. Vol. 4. Geological Society of America.
- Dreimanis, Aleksis
 1962 Quantitative Gasometric Determination of Calcite and Dolomite by Using Chittick Apparatus. *Journal of Sedimentary Petrography* 32(3):520-529.
- Dreybrodt, Wolfgang
 2004 Carbonate Minerals: Precipitation. In *Encyclopedia of Caves and Karst Science*, edited by John Gunn, pp. 383-387. Fitzroy Dearborn, New York, NY.
- Ehleringer, James R., and Russell K. Monson
 1993 Evolutionary and Ecological Aspects of Photosynthetic Pathway Variation. *Annual Review of Ecology and Systematics* 24:411-439.
- Evans, Glen L., and Grayson E. Meade
 1961 *Friesenhahn Cave: The Saber-Toothed Cat Dinobastis*. Bulletin of the Texas Memorial Museum: No. 2. The Texas Memorial Museum, Austin, TX.

- Farrand, William R.
 1975 Sediment Analysis of a Prehistoric Rockshelter: The Abri Pataud. *Quaternary Research* 5(1):1-26.
- 2001 Sediments and Stratigraphy in Rockshelters and Caves: A Personal Perspective on Principles and Pragmatics. Article. *Geoarchaeology* 16(5):537-557.
- Fernandez-Jalvo, Yolanda, and Peter Andrews
 2016 *Atlas of Taphonomic Identifications: 1001 Images of Fossil and Recent Mammal Bone Modification*. Vertebrate Paleobiology and Paleoanthropology. Springer, Dordrecht, Netherlands.
- Ferring, C. Reid
 2017 Alluvial Settings. In *Encyclopedia of Geoarchaeology*, edited by Allan S. Gilbert, pp. 4-14. Springer, Dordrecht, Netherlands.
- Figgins, J. D.
 1927 Antiquity of Man in America. Article. *Natural History* 27(3):220-239.
- Fladmark, K. R.
 1982 Microdebitage Analysis: Initial Considerations. *Journal of Archaeological Science* 9(2):205-220.
- Folk, Robert L.
 1980 *Petrology of Sedimentary Rocks*. Hemphill, Austin, TX.
- Folk, Robert Louis, and William C. Ward
 1957 Brazos River Bar: A Study in the Significance of Grain Size Parameters. *Journal of Sedimentary Research* 27(1):3-26.
- Ford, Derek
 2004 Karst. In *Encyclopedia of Caves and Karst Science*, edited by John Gunn, pp. 1017-1020. Fitzroy Dearborn, New York, NY.
- Forti, Paolo, and Carol A. Hill
 2004 Speleothems: Evaporite. In *Encyclopedia of Caves and Karst Science*, edited by John Gunn, pp. 1481. Fitzroy Dearborn, New York, NY.
- Frederick, Charles D.
 2017a Eagle Nest Canyon: Flooding the Canyon. In *Lower Pecos Canyonlands Academy Guidebook*, edited by Ken Lawrence, pp. 109-112. Texas Archeological Society.
- 2017b Eagle Nest Canyon: Landscapes and Uplands. In *Lower Pecos Canyonlands Academy Guidebook*, edited by Ken Lawrence, pp. 10-17. Texas Archeological Society.
- Frederick, Charles D., Michael D. Glascock, Hector Neff, and Christopher M. Stevenson
 1994 Evaluation of Chert Patination as a Dating Technique: A Case Study from Fort Hood, Texas, edited by Department of the Army. Archeological Resource Management Series: Research Report No. 12. Fort Hood Directorate of Engineering and Housing, Fort Hood, TX.

- Freeman, Val L.
1964 *Geological Map of the Langtry Quadrangle, Val Verde County, Texas*, 1:62,500. U.S. Geological Survey. Washington, D.C.
- Frison, George C.
1974 *The Casper Site: A Hell Gap Bison Kill on the High Plains*. Studies in Archeology. Academic Press, New York, NY.

1986 Mammoth Hunting and Butchering from a Perspective of African Elephant Culling. In *The Colby Mammoth Site: Taphonomy and Archaeology of a Clovis Kill in Northern Wyoming*, edited by George C. Frison, and Lawrence C. Todd, pp. 115-134. University of New Mexico Press, Albuquerque, NM.

1989 Experimental Use of Clovis Weaponry and Tools on African Elephants. *American Antiquity* 54(4):766-784.

1991 *Prehistoric Hunters of the High Plains*. 2nd ed. New World Archaeological Record. Academic Press, San Diego, CA.
- Frison, George C., and Lawrence C. Todd
1986 *The Colby Mammoth Site: Taphonomy and Archaeology of a Clovis Kill in Northern Wyoming*. University of New Mexico Press, Albuquerque, NM.
- Galán, E., and R. E. Ferrell
2013 Genesis of Clay Minerals. In *Handbook of Clay Science*, Vol 5, edited by Faïza Bergaya, and Gerhard Lagaly, pp. 83-126. Developments in Clay Science. Elsevier.
- Gale, Stephen. J., and Peter. G. Hoare
1991 *Quaternary Sediments: Petrographic Methods for the Study of Unlithified Rocks*. Belhaven Press, London, UK.
- Gines, Angel
2004 Karren. In *Encyclopedia of Caves and Karst Science*, edited by John Gunn, pp. 1010-1016. Fitzroy Dearborn, New York, NY.
- Goldberg, Paul, and Richard I. Macphail
2013 *Practical and Theoretical Geoarchaeology*. Interdisciplinary Contributions to Archaeology. John Wiley & Sons, Inc, Hoboken, UK.
- Goldberg, Paul, Vance T. Holliday, and C. Reid Ferring
2001 *Earth Sciences and Archaeology*. Kluwer Academic - Plenum, New York, NY.
- Golden, Michael L., Wayne J. Gabriel, and Jack W. Stevens
1982 Soil Survey of Val Verde County, Texas. United States Department of Agriculture, Soil Conservation Service, Washington, DC.
- Gonzalez, Juan L., James R. Hinthorne, Russell K. Skowronek, Thomas Eubanks, and Don Kumpe
2014 Characteristics and Genesis of El Sauz Chert: An Important Prehistoric Lithic Resource in South Texas. *Lithic Technology* 39(3):151-161.

- González Rul, Francisco
 1990 *Reconocimiento Arqueológico en la Parte Mexicana de la Presa de la Amistad*. Serie Arqueología (Mexico City, Mexico); Colección Científica, No 203. Instituto Nacional de Antropología e Historia, México City, MX.
- Goodyear, Albert C, and Kenn Steffy
 2003 Evidence of a Clovis Occupation at the Topper Site, 38AL23, Allendale County, South Carolina. *Current Research in the Pleistocene* 20:23-25.
- Goodyear, Albert C.
 2005 Evidence for Pre-Clovis Sites in the Eastern United States. In *Paleoamerican Origins: Beyond Clovis*, edited by Robson Bonnicksen. Peopling of the Americas Publication. Center for the Study of the First Americans: Distributed by the Texas A&M University Press, College Station, TX.
- Graham, John Allen, and William A. Davis
 1958 *Appraisal of the Archeological Resources of Diablo Reservoir, Val Verde County, Texas*. Archeological Salvage Field Office, Austin, TX. Submitted to US National Park Service.
- Graham, Russel W.
 1976 Pleistocene and Holocene Mammals, Taphonomy, and Paleoecology of the Friesenhahn Cave Local Fauna, Bexar County, Texas. Ph.D., Geological Sciences, The University of Texas at Austin, Austin, TX. ProQuest Dissertations & Theses Global.
- Graham, Russel W., Ernest L. Lundelius, and Laurence Meissner
 2013 Friesenhahn Cave: Late Pleistocene Paleoecology and Predator-Prey Relationships of Mammoths with an Extinct Scimitar Cat. In *GSA Field Guides*, pp. 15-31. Vol. 30. Geological Society of America.
- Grayson, Donald K., and David J. Meltzer
 2002 Clovis Hunting and Large Mammal Extinction: A Critical Review of the Evidence. *Journal of World Prehistory* 16(4):313-359.
- 2015 Revisiting Paleoindian Exploitation of Extinct North American Mammals. *Journal of Archaeological Science* 56:177-193.
- Gustafson, Carl E., Delbert W. Gilbow, and Richard D. Daugherty
 1979 The Manis Mastodon Site: Early Man on the Olympic Peninsula. *Canadian Journal of Archaeology* (3):157-164.
- Hadjisterkotis, E., and D. S. Reese
 2008 Considerations on the Potential Use of Cliffs and Caves by the Extinct Endemic Late Pleistocene Hippopotami and Elephants of Cyprus. *European Journal of Wildlife Research* 54(1):122-133.
- Halligan, Jessi J., Michael R. Waters, Angelina Perrotti, Ivy J. Owens, Joshua M. Feinberg, Mark D. Bourne, Brendan Fenerty, Barbara Winsborough, David Carlson, Daniel C. Fisher, Thomas W. Stafford, Jr., and James S. Dunbar
 2016 Pre-Clovis Occupation 14,550 Years Ago at the Page-Ladson Site, Florida, and the Peopling of the Americas. *Science Advances* 2(5):e1600375.

- Hannus, L. Adrien, Eric Christopher Grimm, Glen Fredlund, C. Vance Haynes, Manuel R. Palacios-Fest, A. Byron Leonard, Pat Shipman, and Marvin Kay
2018 *Clovis Mammoth Butchery: The Lange/Ferguson Site and Associated Bone Tool Technology*. L. Adrien Hannus. 1st ed. Texas A&M University Press, College Station, TX.
- Harbor, Ryan Lee
2011 Facies Characterization and Stratigraphic Architecture of Organic-Rich Mudrocks, Upper Cretaceous Eagle Ford Formation, South Texas. Masters of Science, Geological Sciences, University of Texas at Austin, Unpublished.
- Hassan, Fekri A.
1978 Sediments in Archaeology: Methods and Implications for Paleoenvironmental and Cultural Analysis. Article. *Journal of Field Archaeology* 5(2):197-213.
- Haynes, C. Vance, Jr., and George A. Agogino
1986 *Geochronology of Sandia Cave*. Smithsonian Contributions to Anthropology: Number 32. Smithsonian Institution Press, Washington, DC.
- Haynes, Gary A.
1985 On Watering Holes, Mineral Licks, Death, and Predation. In *Environments and Extinctions: Man in Late Glacial North America*, edited by J. I. Mead, and David J. Meltzer, pp. 53-71. Center for the Study of Early Man, University of Maine, Orono, ME.

1988 Longitudinal Studies of African Elephant Death and Bone Deposits. Article. *Journal of Archaeological Science* 15(2):131-157.

1991a *Mammoths, Mastodons, and Elephants: Biology, Behavior, and the Fossil Record*. Cambridge University Press, Cambridge, NY.

1991b Noncultural Modifications to Mammalian Bones in Sites of Mass Deaths and Serial Predation. *Anthropologie, Brno* 29(3):151-156.

2015 The Millennium Before Clovis. *PaleoAmerica* 1(2):134-162.
- Haynes, Gary A., D. G. Anderson, C. R. Ferring, S. J. Fiedel, Donald K. Grayson, C. Vance Jr. Haynes, Vance. T. Holliday, B. B. Huckell, M. Kornfeld, David J. Meltzer, J. Morrow, Todd A. Surovell, N. M. Waguespack, P. Wigand, and R. M. Yohe, 2nd
2007 Comment on "Redefining the Age of Clovis: Implications for the Peopling of the Americas". *Science* 317(5836):320b.
- Haynes, Gary A., and Janis Klimowicz
2015 Recent Elephant-Carcass Utilization as a Basis for Interpreting Mammoth Exploitation. *Quaternary International* 359-360:19-37.
- Haynes, Gary A., and Kathryn Krasinski
2010 Taphonomic Fieldwork in Southern Africa and its Application in Studies of the Earliest Peopling of North America. *Journal of Taphonomy* 8(2-3):181-202.

- Heiri, Oliver, André F. Lotter, and Gerry Lemcke
 2001 Loss on Ignition as a Method for Estimating Organic and Carbonate Content in Sediments: Reproducibility and Comparability of Results. *Journal of Paleolimnology* 25(1):101-110.
- Heisinger, Bryan E.
 2019 The Archaeology of Skiles Shelter (41VV165): A Long-Term Rockshelter Plant Baking Facility in the Lower Pecos Canyonlands of Texas. Master of Arts, Department of Anthropology, Texas State University, San Marcos, TX.
- Hester, Thomas R.
 2010 Center for Archaeological Research. In *Handbook of Texas Online*, edited by Laurie E. Jasinski, and Katherine K. Walters. Texas State Historical Association, Austin, TX.
- Hevly, Richard H.
 1966 A Preliminary Pollen Analysis of Bonfire Shelter. In *A Preliminary Study of the Paleoecology of the Amistad Reservoir Area*, edited by Dee Ann Story, and Vaughn M. Bryant, pp. 165-178. National Science Foundation Research Report (GS-667). Department of Anthropology, University of Texas at Austin, Austin, TX.
- High, Kirsty, Kirsty Penkman, Nicky Milner, Steve Boreham, Julie Boreham, Andy Needham, Ian Panter, Margrethe Felter, Becky Knight, Ben Elliott, Michael Bamforth, Maisie Taylor, Charlotte Rowley, Chantal Conneller, and Barry Taylor
 2018 Deterioration and Conservation. In *Star Carr: Studies in Technology, Subsistence, and Environment*, Vol 2, edited by Nicky Milner, Chantal Conneller, and Barry Taylor, pp. 175-192. Studies in Technology, Subsistence and Environment. White Rose University Press.
- Hill, Carol A., and Paolo Forti
 2004 Speleothems: Carbonate. In *Encyclopedia of Caves and Karst Science*, edited by John Gunn, pp. 1476-1480. Fitzroy Dearborn, New York, NY.
- Hofman, Jack L., Robert L. Brooks, Joe S. Hays, Douglas W. Owsley, Richard L. Jantz, Murray K. Marks, and Mary H. Manhein
 1989 *From Clovis to Comanchero: Archeological Overview of the Southern Great Plains*. Arkansas Archeological Research Series: No. 35. Arkansas Archeological Survey, Fayetteville, AR.
- Hofman, Jack L., Lawrence C. Todd, and Michael B. Collins
 1991 Identification of Central Texas Edwards Chert at the Folsom and Lindenmeier Sites. *Plains Anthropologist* 36(137):297-308.
- Holen, Steven R., Thomas A. Deméré, Daniel C. Fisher, Richard Fullagar, James B. Paces, George T. Jefferson, Jared M. Beeton, Richard A. Cerutti, Adam N. Rountrey, Lawrence Vescera, and Kathleen A. Holen
 2017 A 130,000-Year-Old Archaeological Site in Southern California, USA. *Nature* 544(7651):479-483.

- Holliday, Vance T.
 1997 *Paleoindian Geoarchaeology of the Southern High Plains*. Texas Archaeology and Ethnohistory. University of Texas Press, Austin, TX.
- 2000 The Evolution of Paleoindian Geochronology and Typology on the Great Plains. *Geoarchaeology* 15(3):227-290.
- 2009 Geoarchaeology and the Search for the First Americans. *CATENA* 78(3):310-322.
- Homsey-Messer, Lara, and Anthony Ortmann
 2016 Microartifact Analysis: Recent Applications in Southeastern Archaeology. *Southeastern Archaeology* 35(1):1-7.
- Homsey-Messer, Lara, Anthony Ortmann, Lori Roe, and Howard Cyr
 2016 Taphonomy and the Role of Experimentation in Microartifact Analysis. *Southeastern Archaeology* 35(1):65-69.
- Huggett, J. M.
 2015 Clay Minerals. In *Reference Module in Earth Systems and Environmental Sciences*. Elsevier.
- Hull, Kathleen L.
 1987 Identification of Cultural Site Formation Processes through Microdebitage Analysis. *American Antiquity* 52(4):772-783.
- Iaea
 1993 Reference and Intercomparison Materials for Stable Isotopes of Light Elements, edited by the International Atomic Energy Agency Isotope Hydrology Section, Vienna, Austria.
- Jackson, A. T.
 1938 *The Picture-Writing of Texas Indians*. Anthropological Papers. The University of Texas at Austin, Austin, TX.
- Jenkins, D. L., L. G. Davis, T. W. Stafford, P. F. Campos, B. Hockett, G. T. Jones, L. S. Cummings, C. Yost, T. J. Connolly, R. M. Yohe, S. C. Gibbons, M. Raghavan, M. Rasmussen, J. L. A. Paijmans, M. Hofreiter, B. M. Kemp, J. L. Barta, C. Monroe, M. T. P. Gilbert, and E. Willerslev
 2012 Clovis Age Western Stemmed Projectile Points and Human Coprolites at the Paisley Caves. Article. *Science* 337(6091):223-228.
- Johnson, D. L.
 2002 Darwin Would Be Proud: Bioturbation, Dynamic Denudation, and the Power of Theory in Science. *Geoarchaeology* 17:7-40.
- Johnson, E. H.
 2010 South Texas Plains. In *Handbook of Texas Online*, edited by Laurie E. Jasinski, and Katherine K. Walters. Texas State Historical Association, Austin, TX.

- Johnson, Eileen
 1982 Paleoindian Bone Expediency Tools: Lubbock Lake and Bonfire Shelter. *Canadian Journal of Archaeology* 2:145-157.
- 1989 Human-Modified Bones from Early Southern Plains Sites. In *Bone Modification*, edited by Robson Bonnichsen, and Marcella H. Sorg, pp. 431-471. Center for the Study of the First Americans, Orono, ME.
- Johnson, LeRoy
 1964 *The Devil's Mouth Site: A Stratified Campsite at Amistad Reservoir, Val Verde County, Texas*. Department of Anthropology, University of Texas, Austin, TX.
- Jonathan, A. Burns, and A. Raber Paul
 2010 Rockshelters in Behavioral Context: Archaeological Perspectives from Eastern North America. *North American Archaeologist* 31(3):257-285.
- Joyce, Daniel J.
 2006 Chronology and New Research on the Schaefer Mammoth (*Mammuthus primigenius*) Site, Kenosha County, Wisconsin, USA. *Quaternary International* 142-143:44-57.
- Jull, Thomas
 1983 Results of 1983-1984 Radiocarbon Dates from Bonfire Shelter. Official letter from the University of Arizona to Dr. Turpin dated November 1, 1983. Letter on file at TARL. In *University of Arizona Department of Physics, Radiocarbon Laboratory*, edited by Solveig A. Turpin. Texas Archeological Research Laboratory, University of Texas, Austin, TX.
- Jurgens, Christopher James
 2005 Zooarcheology and Bone Technology from Arenosa Shelter (41VV99), Lower Pecos Region, Texas. Ph.D. Dissertation, Department of Anthropology, The University of Texas at Austin, Austin, TX.
- Karkanas, Panagiotis
 2017 Chemical Alteration. In *Encyclopedia of Geoarchaeology*, edited by Allan S. Gilbert, pp. 129-138. Springer, Dordrecht, Netherlands.
- Karkanas, Panagiotis, and Paul Goldberg
 2017 Cave Settings. In *Encyclopedia of Geoarchaeology*, edited by Allan S. Gilbert, pp. 108-118. Springer, Dordrecht, Netherlands.
- Kelley, J. Charles
 1932 Area Investigations. *Field Notes - Langtry, Val Verde County, Southwest Texas*
 On file, J. Charles Kelley and Ellen A. Kelley Memorial Library, Center for Big Bend Studies, Sul Ross State University, Alpine, TX.
- Kelley, J. Charles, T. N. Campbell, and Donald J. Lehmer
 1940 The Association of Archaeological Materials with Geological Deposits in the Big Bend Region of Texas. *Sul Ross State Teachers College Bulletin* (21).

- Kelly, Robert L.
 1983 Hunter-Gatherer Mobility Strategies. *Journal of Anthropological Research* 39(3):277-306.
- 1988 The Three Sides of a Biface. *American Antiquity* 53(4):717-734.
- Kelly, Robert L., and Lawrence C. Todd
 1988 Coming into the Country: Early Paleoindian Hunting and Mobility. *American Antiquity* 53(2):231-244.
- Kendall, Carol
 2006 Interpreting the Data: Isotope Terminology. United States Geological Survey.
- Kilby, J. David
 2008 An Investigation of Clovis Caches: Content, Function, and Technological Organization. Ph.D. Dissertation, Anthropology, The University of New Mexico, Albuquerque, NM.
- 2014 A Regional Perspective on Clovis Blades and Caching Behavior. In *Clovis: On the Edge of a New Understanding*, edited by Ashley M. Smallwood, and Thomas A. Jennings, pp. 145 - 159. Texas A&M University Press, College Station, TX.
- Kilby, J. David, Sean P. Farrell, and Marcus J. Hamilton
 2020 New Investigations at Bonfire Shelter, Texas Examine Controversial Bison Jumps and Bone Beds. *Plains Anthropologist* Manuscript in Review.
- Kilby, J. David, and Marcus J. Hamilton
 2018 New Investigations at Bonfire Shelter: A Consideration of Bison Jumps and Their Implications for Paleoindian Social Organization. Paper presented at the 83rd Annual Meeting of the Society for American Archaeology, Washington, DC.
- Kilby, James David
 1998 A Geoarchaeological Analysis of Ten Pueblo III Pit Structures in the Sand Canyon Locality, Southwest Colorado. Master of Arts Unpublished Master's Thesis, Anthropology, Eastern New Mexico University, Portales, NM.
- King, Angela
 1997 Organic Chemistry 223L - Table of Common Fragment Ions. Wakeforst University, Winston-Salem, NC.
- Kirkland, Forrest
 1937 A Study of Indian Pictures in Texas. *Bulletin of the Texas Archeological and Paleontological Society* 9:89-119.
- 1938 A Description of Texas Pictographs. *Bulletin of the Texas Archeological and Paleontological Society* 11:9-20.
- 1939 Indian Pictures in the Dry Shelters of Val Verde County, Texas. *Bulletin of the Texas Archeological and Paleontological Society* 11:47-76.

- Koenig, Charles W., and Stephen L. Black
 2014a The Canyon Runs Deep. Texas State University. ASWT Blog Post - June 20, 2014 - 2014 Historic Flooding in Mile Canyon, <https://aswtproject.wordpress.com/category/flooding-in-the-canyon/>, accessed 2/21/2019, 2019.
- 2014b The Canyon Transformed. Texas State University. ASWT Blog Post - June 24, 2014: 2014 Historic Flooding in Mile Canyon, <https://aswtproject.wordpress.com/category/flooding-in-the-canyon/>, accessed 2/21/2019, 2019.
- 2015 *Eagle Nest Canyon 2016: Eagle Cave Investigations*. Ancient Southwest Texas Project, Texas State University.
- Koenig, Charles W., Stephen L. Black, and Charles D. Frederick
 2017 Skiles Shelter (41VV165). In *Lower Pecos Canyonlands Academy Guidebook*, edited by Ken Lawrence, pp. 40-48. Texas Archeological Society, San Marcos, TX.
- Koenig, Charles W., Christina Nielsen, Charles D. Frederick, Stephen L. Black, Victoria Roberts, Jerod Roberts, and Eva Panagiotakopulu
 2017 Eagle Cave (41VV167). In *Lower Pecos Canyonlands Academy Guidebook*, edited by Ken Lawrence, pp. 73-105. Texas Archeological Society, San Marcos, TX.
- Koenig, Charles W., Mark D. Willis, and Stephen L. Black
 2017 Beyond the Square Hole: Application of Structure from Motion Photogrammetry to Archaeological Excavation. *Advances in Archaeological Practice* 5(1):54-70.
- Kolb, Charles C.
 2017 Ceramics. In *Encyclopedia of Geoarchaeology*, edited by Allan S. Gilbert, pp. 118-128. Springer, Dordrecht, Netherlands.
- Lautridou, J. P., and J. C. Ozouf
 1982 Experimental Frost Shattering: 15 Years of Research at the Centre de Géomorphologie du CNRS. *Progress in Physical Geography: Earth and Environment* 6(2):215-232.
- Laville, Henri, Jean Philippe Rigaud, and James Sackett
 1980 *Rock Shelters of the Périgord: Geological Stratigraphy and Archaeological Succession*. Studies in Archaeology. Academic Press, New York, NY.
- Leigh, David S.
 2001 Buried Artifacts in Sandy Soils: Techniques for Evaluating Pedoturbation versus Sedimentation. In *Earth Sciences and Archaeology*, edited by Paul Goldberg, Vance T. Holliday, and C. Reid Ferring, pp. 269-293. Kluwer Academic - Plenum, New York, NY.
- Lock, B. E., L. Peschier, and N. Whitcomb
 2010 The Eagle Ford (Boquillas Formation) of Val Verde County, Texas-A Window on the South Texas Play. *Transactions* 60:419-434.

- Lock, B.E., and B. Wawak
 2010 Eagle Ford (Boquillas) Formation and Associated Strata in Val Verde County, Texas. In *South Texas Geological Society Guidebook 2010-1*. South Texas Geological Society, San Antonio, TX.
- Loeppert, R. H., and D. L. Suarez
 1996 Carbonate and Gypsum. In *Methods of Soil Analysis. Part 3 - Chemical Methods.*, edited by D. L. Sparks, A. L. Page, P. A. Helmke, R. H. Loeppert, P. N. Soltanpour, M. A. Tabatabai, C. T. Johnston, and M. E. Sumner, pp. 437-474, Vol. 3. Soil Science Society of America Inc., Madison, WI.
- Lohse, Jon C., David B. Madsen, Brendan J. Culleton, and Douglas J. Kennett
 2014 Isotope Paleoecology of Episodic Mid-to-Late Holocene Bison Population Expansions in the Southern Plains, U.S.A. *Quaternary Science Reviews* 102:14-26.
- Lorrain, Dessamae
 1965 Aboriginal Exploitation of Bison at Bonfire Shelter in Trans-Pecos Texas. Master of Arts, Department of Anthropology, University of Texas at Austin, Austin, TX.

 1966 Bonfire Shelter Fauna. In *A Preliminary Study of the Paleoecology of the Amistad Reservoir Area*, edited by Dee Ann Story, and Vaughn M. Bryant Jr, pp. 221-226. National Science Foundation Research Report (GS-667). The National Science Foundation, University of Texas at Austin.
- Lundelius, E. L.
 1984 *A Late Pleistocene Mammalian Fauna from Cueva Quebrada, Val Verde County, Texas*. Special Publications of the Carnegie Museum of Natural History. University of Texas at Austin. Geology Foundation.
- Marean, Curtis W., and Naomi Cleghorn
 2003 Large Mammal Skeletal Element Transport: Applying Foraging Theory in a Complex Taphonomic System. *Journal of Taphonomy* 1(1):15-42.
- Marean, Curtis W., and Celeste L. Ehrhardt
 1995 Paleoanthropological and Paleoecological Implications of the Taphonomy of a Sabertooth's Den. *Journal of Human Evolution* 29(6):515-547.
- Marean, Curtis W., L. M. Spencer, R. J. Blumenshine, and S. D. Capaldo
 1992 Captive Hyaena Bone Choice and Destruction, the Schlepp Effect and Olduvai Archaeofaunas. *Journal of Archaeological Science* 19(1):101-121.
- Mariotti, A.
 1983 Atmospheric Nitrogen is a Reliable Standard for Natural ¹⁵N Abundance Measurements. *Nature* 303(5919):685-687.
- Martin, George C.
 1932 The Big Bend Basket Maker. Big Bend Basket Maker Papers 1, Bulletin 1. In *Bulletin of the Witte Memorial Museum*. Southwest Texas Archaeological Society, San Antonio, TX.

- 1933 Archaeological Exploration of the Shumla Caves. Big Bend Basket Maker Papers 3, Bulletin 3. In *Bulletin of the Witte Memorial Museum*. Southwest Texas Archaeological Society, San Antonio, TX.
- Martin, George C., and David Dorchester
1941 Unpublished Photographic Record of the Material Culture of the Big Bend Basket-maker, Parts I-III. On file at the Texas Archeological Research Laboratory, University of Texas at Austin.
- Martin, Robert A.
1968 Further Study of the Friesenhahn Cave Peromyscus. *The Southwestern Naturalist* 13(3):253-266.
- McAvoy, Joseph M., and Lynn D. McAvoy
1997 *Archaeological Investigations of Site 44SX202, Cactus Hill, Sussex County, Virginia*. Nottoway River Survey Archaeological Research Report No. 2, Vol. IX. Department of Historic Resources, Richmond, VA.
- McCuiston, Emily R.
2019 The Camel of Time: Radiocarbon Dating the Lower Pecos Canyonlands. Master of Arts, Department of Anthropology, Texas State University, San Marcos, TX.
- Mear, Charles E.
1949. Unpublished Field Notes at Texas Archeological Research Laboratory. University of Texas at Austin, Austin, TX.
- Meltzer, David J.
1983 The Antiquity of Man and the Development of American Archaeology. In *Advances in Archaeological Method and Theory*, Vol 6, edited by Michael B. Schiffer, pp. 1-51. Academic Press, San Diego, CA.

1993 *Search for the First Americans*, Vol. Book, Whole. St. Remy Press, Washington, DC; Montreal, Canada.

2006a *Folsom: New Archaeological Investigations of a Classic Paleoindian Bison Kill*. University of California Press, Berkeley, CA.

2006b History of Research on the Paleo-Indian. In *Handbook of North American Indians*, Vol 3, edited by D.H. Ubelaker, pp. 110-129, William C. Sturtevant, general editor. Smithsonian institution, Washington, DC.

2009a The Pre-Clovis Controversy and Its Resolution. In *First Peoples in a New World: Colonizing Ice Age America*, pp. 95-136. 1 ed. Colonizing Ice Age America. University of California Press, Berkeley, CA.

2009b What Do You Do When No One's Been There Before? In *First Peoples in a New World : Colonizing Ice Age America*, pp. 209-238. University of California Press, Berkeley, CA.

- Meltzer, David J., Ryan M. Byerly, and Judith R. Cooper
 2007 On an Alternative Interpretation of Paleindian Site Use at Bonfire Shelter. *Bulletin of the Texas Archeological Society* 78:159-160.
- Mentzer, Susan M.
 2017 Rockshelter Settings. In *Encyclopedia of Geoarchaeology*, edited by Allan S. Gilbert, pp. 725-743. Springer, Dordrecht, Netherlands.
- Muhs, D. R.
 2014 Overview of Paleosols and Wind Blown Sediments☆. In *Reference Module in Earth Systems and Environmental Sciences*. Elsevier.
- Nelson, Stephen A.
 2014 Weathering and Clay Minerals. In *EENS 2110 - Mineralogy*. Tulane University, New Orleans, LA.
- Nickels, David
 2014 *Archaeological Data Recovery at Fish Creek Slough Site (41DL436)*. Index of Texas Archaeology: Open Access Gray Literature from the Lone Star State. Submitted to Texas Department of Transportation, Austin, TX.
- Nielsen, Christina
 2017 A Microstratigraphic Approach to Evaluating Site Formation Processes at Eagle Cave (41VV167). Master of Arts, Department of Anthropology, Texas State University, San Marcos, TX.
- NOAA, and NWS
 2019 NOAA Online Weather Data: Langtry, TX (1969 - 2018). *Austin/San Antonio Weather Forecast office*. accessed March 1, 2019.
- Nordt, Lee C.
 2001 Stable Carbon and Oxygen Isotopes in Soils: Applications for Archaeological Research. In *Earth Sciences and Archaeology*, edited by Paul Goldberg, Vance T. Holliday, and C. Reid Ferring, pp. 419-448. Kluwer Academic - Plenum, New York, NY.
- Nordt, Lee C., Thomas W. Boutton, Charles T. Hallmark, and Michael R. Waters
 1994 Late Quaternary Vegetation and Climate Changes in Central Texas Based on the Isotopic Composition of Organic Carbon. *Quaternary Research* 41(1):109-120.
- Nordt, Lee C., Thomas W. Boutton, John S. Jacob, and Rolfe D. Mandel
 2002 C4 Plant Productivity and Climate-CO2 Variations in South-Central Texas during the Late Quaternary. *Quaternary Research* 58(2):182-188.
- Nunley, J. P., L. F. Duffsfeld, and Edward B. Jelks
 1965 *Excavations at Amistad Reservoir, 1962 Season*. Miscellaneous Papers, No. 3. Submitted to University of Texas at Austin, Austin, TX.
- Overstreet, David F., and Michael F. Kolb
 2003 Geoarchaeological Contexts for Late Pleistocene Archaeological Sites with Human-Modified Woolly Mammoth Remains in Southeastern Wisconsin, USA. *Geoarchaeology* 18(1):91-114.

- Pagano, Victoria C.
2019 Stories in the Sand: Excavation and Analysis of the Sayles Adobe Terrace (41VV2239) in Eagle Nest Canyon, Langtry, Texas. Master of Arts, Department of Anthropology, Texas State University, San Marcos, TX.
- Panagiotakopulu, Eva, and Paul Buckland
2017 A Thousand Bites – Insect Introductions and Late Holocene Environments. *Quaternary Science Reviews* 156:23-35.
- Panagiotakopulu, Eva, Buckland C, and Kemp B
2010 Underneath Ra-Nefer's House Floors: Archaeoentomological Investigations of an Elite Household in the Main City at Amarna, Egypt. *Journal of Archaeological Science* 37:474-481.
- Parsons, Mark L.
1962 41VV218 - Amistad Bone Cave Archeological Site Form. Texas Historical Commission - Texas Archeological Sites Atlas. Submitted to Texas Archeological Research Laboratory University of Texas At Austin, Austin, TX.
- Patton, Peter. C., and David S. Dibble
1982 Archeologic and Geomorphic Evidence for the Paleohydrologic Record of the Pecos River in West Texas. *American Journal of Science* 282:97-121.
- Paz, J. D. S., and D. F. Rossetti
2006 Petrography of Gypsum-Bearing Facies of the Codo Formation (Late Aptian), Northern Brazil. *Anais Da Academia Brasileira De Ciencias* 78(3):557-572.
- Pearce, James Edwin, and A. T. Jackson
1933 A Prehistoric Rockshelter in Val Verde County, Texas. Bureau of Research in the Social Sciences Study No. 6, Anthropological Papers, Vol. 1, No. 3. The University of Texas at Austin, Austin, TX.
- Pearson, F. J., E. Mott Davis, Murray A. Tamers, and Robert W. Johnstone
1965 University of Texas Radiocarbon Dates III. *Radiocarbon* 7:296-314.
- Pearson, M. J., S. E. Monteith, R. R. Ferguson, C. T. Hallmark, W. H. Hudnall, H. C. Monger, T. G. Reinsch, and L. T. West
2015 A Method to Determine Particle Size Distribution in Soils with Gypsum. *Geoderma* 237-238:318-324.
- Pelletier, J. D., P. A. Kapp, J. Abell, J. P. Field, Z. C. Williams, and R. J. Dorsey
2018 Controls on Yardang Development and Morphology: 1. Field Observations and Measurements at Ocotillo Wells, California. *Journal of Geophysical Research: Earth Surface* 123(4):694-722.
- Pentecost, Allan
2005 Travertine Dating. In *Travertine*, pp. 243-251. Springer, Neatherlands.
- Poppe, Lawrence J.
2001 A Laboratory Manual for X-Ray Powder Diffraction. USGS Open-File Report: 01-41. USGS, Coastal and Marine Geology Program.

- Prakash, K., A. Sridharan, and S. Sudheendra
2016 Hygroscopic Moisture Content: Determination and Correlations. *Environmental Geotechnics* 3(5):293-301.
- Prewitt, Elton R.
2007 To Jump or to Drag: Reflections on Bonfire Shelter. *Bulletin of the Texas Archeological Society* 78:149-458.
- Price, T. Douglas
2014 An Introduction to the Isotopic Studies of Ancient Human Remains. *Journal of the North Atlantic*:71-87.
- Rasmussen, M., S. L. Anzick, Michael R. Waters, P. Skoglund, M. DeGiorgio, T. W. Stafford, S. Rasmussen, I. Moltke, A. Albrechtsen, S. M. Doyle, G. D. Poznik, V. Gudmundsdottir, R. Yadav, A. S. Malaspina, S. S. White, M. E. Allentoft, O. E. Cornejo, K. Tambets, A. Eriksson, P. D. Heintzman, M. Karmin, T. S. Korneliusson, D. J. Meltzer, T. L. Pierre, J. Stenderup, L. Saag, V. M. Warmuth, M. C. Lopes, R. S. Malhi, S. Brunak, T. Sicheritz-Ponten, I. Barnes, Michael B. Collins, L. Orlando, F. Balloux, A. Manica, R. Gupta, M. Metspalu, C. D. Bustamante, M. Jakobsson, R. Nielsen, and E. Willerslev
2014 The Genome of a Late Pleistocene Human from a Clovis Burial Site in Western Montana. *Nature* 506(7487):225-239.
- Rasmussen, S. O., K. K. Andersen, A. M. Svensson, J. P. Steffensen, B. M. Vinther, H. B. Clausen, M. L. Siggaard-Andersen, S. J. Johnsen, L. B. Larsen, D. Dahl-Jensen, M. Bigler, R. Röthlisberger, H. Fischer, K. Goto-Azuma, M. E. Hansson, and U. Ruth
2006 A New Greenland Ice Core Chronology for the Last Glacial Termination. *Journal of Geophysical Research: Atmospheres* 111(D6).
- Rawn-Schatzinger, Viola
1992 *The Scimitar Cat, Homotherium serum Cope: Osteology, Functional Morphology, and Predatory Behavior*. Reports of Investigations of the Illinois State Museum 0360-0270, No. 47. Illinois State Museum, Springfield, IL.
- Reimer, Paula J., Edouard Bard, Alex Bayliss, J. Warren Beck, Paul G. Blackwell, Christopher Bronk Ramsey, Caitlin E. Buck, Hai Cheng, R. Lawrence Edwards, Michael Friedrich, Pieter M. Grootes, Thomas P. Guilderson, Haflidi Haflidason, Irka Hajdas, Christine Hatté, Timothy J. Heaton, Dirk L. Hoffmann, Alan G. Hogg, Konrad A. Hughen, K. Felix Kaiser, Bernd Kromer, Sturt W. Manning, Mu Niu, Ron W. Reimer, David A. Richards, E. Marian Scott, John R. Southon, Richard A. Staff, Christian S. M. Turney, and Johannes van der Plicht
2013 IntCal13 and Marine13 Radiocarbon Age Calibration Curves 0-50,000 Years cal BP. *Radiocarbon* 55(4):1869-1887.
- Robinson, David G.
1997 Stratigraphic Analysis of Bonfire Shelter, Southwest Texas: Pilot Studies of Depositional Processes and Paleoclimate. *Plains Anthropologist* 42(159):33-43.
- Rodriguez, Daniel P.
2015 Patterns in the Use of the Rockshelters of Eagle Nest Canyon, Langtry, Texas. Master of Arts, Department of Anthropology, Texas State University, San Marcos, TX.

- Rodriguez, Daniel P., and Stephen L. Black
 2017 Kelley Cave (41VV164). In *Lower Pecos Canyonlands Academy Guidebook*, edited by Ken Lawrence, pp. 57-64. Texas Archeological Society, San Marcos, TX.
- Rogers, Raymond R., David A. Eberth, and Anthony R. Fiorillo
 2008 *Bonebeds: Genesis, Analysis, and Paleobiological Significance*. University of Chicago Press, Chicago, IL.
- Rogers, Raymond R., and Susan M. Kidwell
 2008 A Conceptual Framework for the Genesis and Analysis of Vertebrate Skeletal Concentrations. In *Bonebeds: Genesis, Analysis, and Paleobiological Significance*, edited by Raymond R. Rogers, David A. Eberth, and Anthony R. Fiorillo, pp. 1-64. University of Chicago Press, Chicago, IL.
- Rosenmeier, Abbot
 2005 Loss on Ignition (LOI) Procedures. In *Geology 3931: Paleoenvironmental Analysis - Laboratory Standard Operating Procedures*. University of Pittsburgh, Department of Geology and Environmental Science, Pittsburgh, PA.
- Ross, Richard E.
 1965 *The Archaeology of Eagle Cave*. Papers of the Texas Archaeological Salvage Project, No. 7. Texas Memorial Museum, Austin, TX.
- Ryabenko, Evgenia
 2013 Stable Isotope Methods for the Study of the Nitrogen Cycle. In *Topics in Oceanography*, edited by Enrico Zambianchi, pp. 1-40. Research Center for Environmental Health - Institute of Groundwater Ecology, Munchen, Germany.
- Sayles, E. B.
 1935 *An Archaeological Survey of Texas*. Medallion Papers. Book, Globe, AZ.
- Schick, Kathy Diane, and Nicholas Patrick Toth
 1994a Dawn Breaks: The First Stone Tool Makers. In *Making Silent Stones Speak: Human Evolution and the Dawn of Technology*, pp. 77-103. 1st ed. Simon & Schuster, New York, NY.
- 1994b The Role of Rock: Uses of Early Stone Tools. In *Making Silent Stones Speak: Human Evolution and the Dawn of Technology*, pp. 147-186. 1st ed. Simon & Schuster, New York, NY.
- Schiffer, Michael B.
 1972 Archaeological Context and Systemic Context. *American Antiquity* 37(2):156-165.
- 1983 Toward the Identification of Formation Processes. *American Antiquity* 48(4):675-706.
- 1987 *Formation Processes in the Archaeological Record*. University of New Mexico, Albuquerque, NM.

- 1995 *Behavioral Archaeology: First Principles*. Foundations of Archaeological Inquiry. University of Utah Press, Salt Lake City, UT.
- Schlacher, Thomas A., and Rod M. Connolly
2014 Effects of Acid Treatment on Carbon and Nitrogen Stable Isotope Ratios in Ecological Samples: A Review and Synthesis. *Methods in Ecology and Evolution* 5(6):541-550.
- Schmidt, Robert H.
2010 Trans-Pecos. In *Handbook of Texas Online*, edited by Laurie E. Jasinski, and Katherine K. Walters. Texas State Historical Association, Austin, TX.
- Schoeninger, Margaret J., and Michael J. DeNiro
1984 Nitrogen and Carbon Isotopic Composition of Bone Collagen from Marine and Terrestrial Animals. *Geochimica et Cosmochimica Acta* 48(4):625-639.
- Schulte, E. E., and B. G. Hopkins
1996 Estimation of Soil Organic Matter by Weight Loss-on-Ignition. In *SSSA Special Publication No. 46*, edited by F. R. Magdoff, E. A. Hanlon Jr., and A. Tabatabai, pp. 21-31. Soil Science Society of America, Madison, WI.
- Scott-Cummings, Linda
1992 *Stratigraphic Pollen Analysis at Bonfire Shelter, 41VV218, Southwest Texas*. Texas Archeological Research Laboratory, University of Texas at Austin, Austin TX.
- Scott, Robert W.
2002 Albian Caprinid Rudists from Texas Re-Evaluated. *Journal of Paleontology* 76(3):408-423.
- Sealy, Judith, Malia Johnson, Michael Richards, and Olaf Nehlich
2014 Comparison of Two Methods of Extracting Bone Collagen for Stable Carbon and Nitrogen Isotope Analysis: Comparing Whole Bone Demineralization with Gelatinization and Ultrafiltration. *Journal of Archaeological Science* 47:64-69.
- Setzler, Frank M.
1934 Cave Burials in Southwestern Texas. In *Explorations and Fieldwork of the Smithsonian Institution, Publication 3235*, edited by The Smithsonian Institution, pp. 35-37. The Lord of Baltimore Press, Baltimore, MD.
- Severin, Kenneth P.
2004 *Energy Dispersive Spectrometry of Common Rock Forming Minerals*. Kluwer Academic, Dordrecht, Netherlands.
- Shafer, Harry J., and Vaughn M. Bryant Jr
1977 *Archeological and Botanical Studies at Hinds Cave, Val Verde County, Texas*. Special Series, No 1. Submitted to Texas A&M University, Anthropology Laboratory, College Station, TX.

- Shafer, Harry J., and Vaughn M. Bryant Jr.
1977 *Archeological and Botanical Studies at Hinds Cave, Val Verde County, Texas*. Special Series, No 1. Submitted to Texas A&M University, Anthropology Laboratory, College Station, TX.
- 1988 Notes on Hinds Cave, Val Verde County, Texas. *North American Archaeologist* 8(3):249-254.
- Sherwood, Sarah Catherine
2001 Microartifacts. In *Earth Sciences and Archaeology*, edited by Paul Goldberg, Vance T. Holliday, and C. Reid Ferring, pp. 327-352. Kluwer Academic - Plenum, New York, NY.
- Shott, Michael J.
1994 Size and Form in the Analysis of Flake Debris: Review and Recent Approaches. *Journal of Archaeological Method and Theory* 1(1):69-110.
- Smallwood, Ashley Michelle
2011 Clovis Technology and Settlement in the American Southeast. Ph.D. Dissertation, Department of Anthropology, Texas A&M University, College Station, TX.
- Smart, Chris, and Stephen R. H. Worthington
2004 Springs. In *Encyclopedia of Caves and Karst Science*, edited by John Gunn, pp. 1495-1505. Fitzroy Dearborn.
- Sparkman, O. David, Zelda E. Penton, and Fulton G. Kitson
2011 Introduction and History. In *Gas Chromatography and Mass Spectrometry*, edited by O. David Sparkman, Zelda E. Penton, and Fulton G. Kitson, pp. 2-13. 2nd ed. Academic Press, Amsterdam, Netherlands.
- Steuber, Thomas
2002 An Introduction to the Palaeontology of Rudist Bivalves. In *PaleoTax Database*. July 1, 2002 ed.
- Story, Dee Ann
2010 Texas Archeological Research Laboratory. *The Handbook of Texas Online*.
- Story, Dee Ann, and Vaughn M. Bryant
1966 *A Preliminary Study of the Paleoecology of the Amistad Reservoir Area*. National Science Foundation Research Report (GS-667). The National Science Foundation, Department of Anthropology, University of Texas at Austin, Austin, TX.
- Straus, Lawrence Guy
1990 Underground Archaeology: Perspectives on Caves and Rockshelters. *Archaeological Method and Theory* 2:255-304.
- Talbot, James
2019 Whole Rock and Clay Fraction (<4 micron) XRD Analysis: Sample Preparation and Analytical Procedures. KT GeoServices, Gunnison, CO.

- Tamers, Murray A., and F. J. Pearson
1965 Validity of Radiocarbon Dates on Bone. *Nature* 208(5015):1053-1055.
- Tamers, Murray A., F. J. Pearson, and E. Mott Davis
1964 University of Texas Radiocarbon Dates II. *Radiocarbon* 6(1):138-159.
- Taylor, Herbert C.
1948 An Archaeological Reconnaissance in Northern Coahuila. *Bulletin of the Texas Archeological and Paleontological Society* 19:74-87.

1949 A Tentative Cultural Sequence for the Area About the Mouth of the Pecos. *Bulletin of the Texas Archeological and Paleontological Society* 20:73-88.
- Taylor, R. E., and Ofer Bar-Yosef
2014 *Radiocarbon Dating: An Archaeological Perspective*. 2nd ed. Left Coast Press, Walnut Creek, CA.
- Team, Texas Beyond History Web
2001 Before Amistad. The University of Texas at Austin
<https://www.texasbeyondhistory.net/pecos/before.html>, accessed April 4, 2018.
- Texas Water Science Center, (USGS TWSC)
2014 Geologic Database of Texas, 2014-02-01. Texas Natural Resources Information System (TNRIS), Austin, TX.
- Texier, J., Pascal Bertran, J. Coutard, Bernard Francou, Pierre Gabert, Jean-Luc Guadelli, J. Ozouf, Hugues Plisson, Jean-Paul Raynal, and Dominique Vivent
1998 TRANSIT, An Experimental Archaeological Program in Periglacial Environment: Problem, Methodology, First Results. *Geoarchaeology* 13:433-473.
- Tiner, Ralph W.
1991 The Concept of a Hydrophyte for Wetland Identification. *BioScience* 41(4):236.
- Tiunov, A. V.
2007 Stable Isotopes of Carbon and Nitrogen in Soil Ecological Studies. *Biology Bulletin* 34(4):395-407.
- Tiwari, Manish, Ashutosh K. Singh, and Devesh K. Sinha
2015 Stable Isotopes: Tools for Understanding Past Climatic Conditions and Their Applications in Chemostratigraphy. In *Chemostratigraphy: Concepts, Techniques, and Applications*, edited by Mu Ramkumar, pp. 65-92. Elsevier, Oxford, UK.
- Turpin, Solveig A.
1982 *Seminole Canyon: The Art and the Archeology*. Texas Archeological Survey Research Report No. 83. Texas Archeological Survey, University of Texas at Austin, Austin, TX.

1990 Rock Art and Hunter-Gatherer Archaeology: A Case Study from SW Texas and Northern Mexico. *Journal of Field Archaeology* 17(3):263-281.

- 1992 More about Mortuary Practices in the Lower Pecos River Region of Southwest Texas. *Plains Anthropologist* 37(138):7-17.
- 1994a Lower Pecos Prehistory: The View from the Caves. In *The Caves and Karst of Texas*, edited by W. R. Elliott, and G. Veni, pp. 69-84. National Speleological Society, Huntsville, AL.
- 1994b The Were-Cougar Theme in Pecos River Style Art and Its Implications for Traditional Archeology. In *New Light on Old Art: Recent Advances in Hunter-Gatherer Rock Art Research*, Vol 36, edited by Lawrence L. Loendorf, and David S. Whitley, pp. 75-80. Institute of Archaeology, University of California, Los Angeles, Los Angeles, CA.
- 1996 Painting on Bones and Other Unusual Media in the Lower and Trans-Pecos Region of Texas and Coahuila. *Plains Anthropologist* 41(157):261-272.
- 2004 The Lower Pecos River Region of Texas and Northern Mexico. In *The Prehistory of Texas*, edited by Timothy K. Perttula, pp. 266-280. 2 ed. Texas A&M Anthropology Series, Vol. 9, D. Gentry Steele, general editor. Texas A&M University Press, College Station, TX.
- Turpin, Solveig A., and Leland C. Bement
1988 The Site and Its Setting. *Plains Anthropologist* 33(122):1-18.
- Turpin, Solveig A., Leland C. Bement, T. M. Byrd, M. K. Marks, and J. C. Rose
1988 Seminole Sink: Excavation of a Vertical Shaft Tomb Val Verde County, Texas. Memoir 22. *Plains Anthropologist* 33:122.
- Turpin, Solveig A., Maciej Henneberg, and David H. Riskind
1986 Late Archaic Mortuary Practices of the Lower Pecos River Region, Southwest Texas. *Plains Anthropologist* 31(114):295-315.
- Udden, Johan August
1898 *The Mechanical Composition of Wind Deposits*. Augustana Library Publications, No. 1. Lutheran Augustana, Rock Island, IL.
- Velde, Bruce, and Alain Meunier
2008 Clay Mineral Formation in Weathered Rocks: Water/Rock Interaction. In *The Origin of Clay Minerals in Soils and Weathered Rocks*, edited by Bruce Velde, and Alain Meunier, pp. 143-239. Springer Berlin Heidelberg, Berlin, Germany.
- Villa, Paola, and Marie Soressi
2000 Stone Tools in Carnivore Sites: The Case of Bois Roche. *Journal of Anthropological Research* 56(2):187-215.
- Waguespack, Nicole M.
2012 Early Paleoindians, from Colonization to Folsom. In *The Oxford Handbook of North American Archaeology*. Oxford University Press.
- Waguespack, Nicole M., and Todd A. Surovell
2003 Clovis Hunting Strategies, or How to Make out on Plentiful Resources. *American Antiquity* 68(2):333-352.

- Waters, M. R., T. W. Stafford, H. G. McDonald, C. Gustafson, M. Rasmussen, E. Cappellini, J. V. Olsen, D. Szklarczyk, L. J. Jensen, M. T. P. Gilbert, and E. Willerslev
2011 Pre-Clovis Mastodon Hunting 13,800 Years Ago at the Manis Site, Washington. *Science* 334(6054):351-353.
- Waters, Michael R.
1992 *Principles of Geoarchaeology: A North American Perspective*. University of Arizona Press, Tucson, AZ.
- Waters, Michael R., S. L. Forman, Thomas A. Jennings, Lee C. Nordt, S. G. Driese, J. M. Feinberg, J. L. Keene, J. Halligan, A. Lindquist, J. Pierson, C. T. Hallmark, Michael B. Collins, and James E. Wiederhold
2011 The Buttermilk Creek Complex and the Origins of Clovis at the Debra L. Friedkin Site, Texas. *Science* 331(6024):1599-1603.
- Waters, Michael R., Joshua L. Keene, Steven L. Forman, Elton R. Prewitt, David L. Carlson, and James E. Wiederhold
2018 Pre-Clovis Projectile Points at the Debra L. Friedkin Site, Texas: Implications for the Late Pleistocene Peopling of the Americas. *Science Advances* 4(10).
- Waters, Michael R., and Thomas Wier Stafford
2007 Redefining the Age of Clovis: Implications for the Peopling of the Americas. *Science* 315(5815):1122-1126.
- Weiner, Stephen
2010a Common Mineral Components of the Archaeological Record. In *Microarchaeology: Beyond the Visible Archaeological Record*, pp. 68-98. Cambridge University Press, New York, NY.
2010b Completeness of the Archaeological Record. In *Microarchaeology: Beyond the Visible Archaeological Record*, pp. 46-67. Cambridge University Press, New York, NY.
2010c Information Embedded in the Microscopic Record. In *Microarchaeology: Beyond the Visible Archaeological Record*, pp. 13-45. Cambridge University Press, New York, NY.
2010d *Microarchaeology: Beyond the Visible Archaeological Record*. Book. Cambridge University Press, New York, NY.
- Wentworth, Chester K.
1922 A Scale of Grade and Class Terms for Clastic Sediments. *The Journal of Geology* 30(5):377-392.
- Whelan, Carly, and Stephen L. Black
2008a Arenosa Shelter: Arenosa Through Time. In *Texas Beyond History*, edited by Texas Beyond History Web Team. Texas Archaeological Research Laboratory, University of Texas at Austin, Austin, TX.
2008b Arenosa Shelter: Investigations. In *Texas Beyond History*, edited by Texas Beyond History Web Team. Texas Archaeological Research Laboratory, University of Texas at Austin, Austin, TX.

- Williams, Paul W.
2004 Karst Evolution. In *Encyclopedia of Caves and Karst Science*, edited by John Gunn, pp. 1020-1026. Fitzroy Dearborn.
- Williams, Thomas J., Michael. B. Collins, Kathleen Rodrigues, William Jack Rink, Nancy Velchoff, Amanda Keen-Zebert, Anastasia Gilmer, Charles D. Frederick, Sergio J. Ayala, and Elton R. Prewitt
2018 Evidence of an Early Projectile Point Technology in North America at the Gault Site, Texas, USA. *Science Advances* 4(7):1-7.
- Word, James H., and Charles L. Douglas
1970 *Excavations at Baker Cave, Val Verde County, Texas*. Bulletin of the Texas Memorial Museum: No. 16. The Texas Memorial Museum, Austin, TX.
- Wyckoff, Don G.
1999 The Burnham Site and Pleistocene Human Occupation of the Southern Plains of the United States. In *Ice Age People of North America: Environments, Origins, and Adaptations*, edited by Robson Bonnichsen, and Karen L. Turnmire, pp. 340-361. 1st ed. Oregon State University Press for the Center for the Study of the First Americans, Corvallis, OR.
- Yan, Lei, Shuang Zhang, Peng Chen, Hetao Liu, Huanhuan Yin, and Hongyu Li
2012 Magnetotactic Bacteria, Magnetosomes and Their Application. *Microbiological Research* 167(9):507-519.